Shear Strength of Full-Scale Prestressed Lightweight Concrete Girders with Composite Decks

Bernard Leonard Kassner

Dissertation submitted to the faculty of the
Virginia Polytechnic Institute and State University
in partial fulfillment of the requirements for the degree of

Doctor of Philosophy
In
Civil Engineering

Tommy E. Cousins, Co-Chair
Carin L. Roberts-Wollmann, Co-Chair
Michael C. Brown
W. Samuel Easterling

December 4, 2012
Blacksburg, VA

Keywords: lightweight, concrete, prestress, shear, reliability

Shear Strength of Full-Scale Prestressed Lightweight Concrete Girders with Composite Decks

Bernard Leonard Kassner

ABSTRACT

Although design codes have accepted lightweight concrete as a suitable structural material for nearly 50 years, there is still a good deal of uncertainty as to how to calculate the strength of this material when designing for shear in beams. Design codes tend to penalize lightweight concrete due to its lower tensile strength and smoother interface along the shear cracks. In this study, there were twelve tests on six full-scale, prestressed girders with composite decks designed to provide answers to some of those uncertainties. The variables considered were concrete density, concrete compressive strength, effective shear depth, shear span-to-effective depth ratio, the amount of shear reinforcement, and the composite cross-sectional area. Results show that the sand-lightweight concrete girders exceeded the expected shear strength according to the 2010 AASHTO LRFD Bridge Specifications. Compared to normal weight concrete, sand-lightweight concrete performed reasonably well, and therefore, does not need a lightweight modifier when designing for shear. However, a reliability analysis of the sand-lightweight girders in this study as well as twelve previous experiments indicate that there should be two different strength reduction factors for the shear design of sand-lightweight concrete depending on which shear design procedures are used in the 2010 AASHTO LRFD Bridge Design Specifications. For the *General Procedure* as well as the guidelines outline in *Appendix B5*, the strength reduction factor should be increased from 0.70 to 1.00. For the *Simplified Procedure*, that factor should be 0.75.

Acknowledgements

I would like to thank the following for their support and guidance throughout this journey:

- Dr. Carin Roberts-Wollmann, my co-chair who opened up this path for me to travel on by asking me to join the research team for the lightweight concrete project and who helped me wade through the intricacies of shear design.
- Dr. Tommy Cousins, also my co-chair who taught me the first rule of electricity as well as provided valuable experience in conducting the load tests for this project.
- Dr. Michael Brown (and Dr. Jose Gomez), who exhibited great patience with my odyssey to the finish line, even though there was plenty of other innovating and researching to be done.
- Dr. Sam Easterling, who challenged my initial assessment of resistance factors, which resulted in a more credible, statistically-based analysis of my results.
- The Charles E. Via, Jr. family for generously granting me funding for not one, but two civil engineering degrees.
- Jon Emenheiser, without whom I would likely still be out in the lab trying to build formwork and setting up the load tests.
- Brett Farmer and Dennis Huffman for all of their expertise in the laboratory and for arranging the installation and removal of the full-sized composite concrete girders.
- Dr. David Mokarem, who encouraged me to trust him simply because he was a "doctor," and who provided a roof over my head during the waning months of my time in Blacksburg. Brenna and Katy also thank Baxter, Emma, Benson and Eli for being great hosts.
- Jana Scott and Dr. Ben Cross for being my teammates in the lightweight concrete research, as well as the numerous other students who assisted with concrete placement and load tests.
- Michael Lineberry, amicus magnificus who managed deep discussions about the world outside of my research despite our busy schedules – sapere aude, Broski!
- My parents, Dennis and Jo Anne Kassner for their love and support through the years.
- Most importantly, Dr. Laura Kassner, my true companion and best friend without whom this adventure would not have been imaginable. In the words of Blaaze and Wendy Parr, "You are my waking dream. You're all that's real to me. You are the magic in the world I see … You are the spark of dawn. You are where I belong." Now, let's continue going down the road of life as we watch our family grow. GOMFLLTT.

Table of Contents

List of Figures

List of Tables

Notation

$A.B5$ = shear strength calculations following Appendix B5.2 of the 2010 AASHTO LRFD Bridge Design Specifications

A_c = area of concrete on the flexural tension side of a member

A_{comp} = composite cross-sectional area

A_g = cross-sectional area of the girder by itself

A_{ps} = area of the prestressing steel

A_s = area of non-prestressed longitudinal reinforcement

A_v = cross-sectional area of a stirrup

$A_{v\,min}$ = required minimum area of shear reinforcement

a = maximum aggregate size; shear span

a_i = coefficient associated with an uncorrelated random variable X_i

a/d = shear span-to-effective shear depth ratio, shear span-to-effective depth ratio

b = width of a rectangular section or the width of the flange of a T-section

b' = width of the web (see also b_w); width of the web of a flanged member

$b_{barrier}$ = width of the guard rails at the sides of the deck

b_{bridge} = width of the bridge, from edge of deck to edge of deck

b_w = width of the web of a concrete girder (see also b')

C = coefficient used for calculating E_c according to ACI's *Guide for Structural Lighweight-Aggregate Concrete*

CoV = coefficient of variation

CoV_i = coefficient of variation for a given variable i

D_1 = dead load of factory-made components

D_2 = dead load of cast-in place members

D_3 = dead load of the asphalt wearing surface

DC = dead load of the structural components and non-structural attachments

DC_{NCHRP} = sum of the structural dead load components, as given in *NCHRP Report 368*

DW = dead load of the wearing surface

d = effective depth, measured from the extreme compression fiber to the centroid of the tensile reinforcement; overall beam depth (see also d_e)

d_e = effective depth from extreme compression fiber to the centroid of the tensile force in the tensile reinforcement (see also d_e)

d_p = distance from the extreme compression fiber to the centroid of the prestressing tendons

d_s = distance from extreme compression fiber to the centroid of the nonprestressed tensile reinforcement.

d_v = effective shear depth, taken as the distance between the resultant compressive and tensile forces due to flexure, but need not be less than $0.9d_e$ or $0.72h$

e = eccentricity of the centroid of the strands from the centroid of the girder, taken as positive when the strand centroid is below the girder centroid

E_c = elastic modulus of concrete

E_{ps} = modulus of elasticity of the prestressing tendons, assumed to be 28,500 ksi

E_s = modulus of elasticity of the mild reinforcement, assumed to be 29,000 ksi

F = force in the compressive strut

F_{sp} = splitting ratio of f'_{sp} versus $\sqrt{f'_c}$

$\mathrm{F_X}$ = cumulative distribution function

f_1 = principal tensile stress in the concrete

f_2 = principal compressive stress in the concrete

f'_c = 28-day specified compressive strength; the maximum stress observed in a cylinder compressive test, taken as a negative quantity

$f'_{c\,deck}$ = 28-day compressive strength of the deck concrete

f'_{ci} = specified compressive strength at the time of release of the prestressing strands

f_{2max} = the diagonal crushing strength of the concrete

f_c = concrete compressive strength

f_{ci} = local compressive stresses normal to a crack plane

f_{cpe} = stress in the concrete due to the effective prestressing force, at the extreme fiber location where externally applied loads cause tensile stress

f_{cr} = cracking strength of concrete

f_{ct} = splitting tensile strength (see also f'_{sp} and f_t)

f_{cx} = stress in the concrete in the x-direction

f_{cy} = stress in the concrete in the y-direction

f_d = stress due to unfactored dead loads, at the extreme fiber of the cross-section where external loads cause tension

f_{pc} = compressive stress due to prestressing, computed at the centroid using f_{pe} (for a composite section, f_{pc} is calculated at the centroid of the composite section using both f_{pe} and the stress due to the dead load acting on the beam by itself)

f_{pe} = effective stress in the prestressing steel after losses

f_{po} = parameter calculated as E_{ps} multiplied by the locked-in difference in strain between the prestressing tendons and the surrounding concrete; for typical levels of prestressing, a value of $0.7\,f_{pu}$ is used for this parameter.

f_{ps} = average stress in the prestressing steel

f_{pt} = stress in the prestressing steel immediately after transfer

f_{pu} = yield strength of prestressing steel

f_r = modulus of rupture

f'_{sp} = splitting tensile strength (see also f_{ct} and f_t)
f_{sx} = average stress in the x-reinforcement
f_{sxcr} = stress in the x-reinforcement at the cracked surface
f_{sy} = average stress in the y-reinforcement
f_{sycr} = stress in the y-reinforcement at the crack surface
f_t = splitting tensile strength (see also f_{ct} and f'_{sp})
f_v = compressive stress due to vertical loads on an arbitrary stress element
f_x = stress applied to an arbitrary element in the x- direction
f_X = probability density function
f_y = yield strength of the non-prestressed longitudinal reinforcement; stress applied to an arbitrary element in the y-direction
f_{yv} = yield strength of the shear reinforcement
Gen = shear strength calculations following the General Procedure in Article 5.8.3.4.2 of the 2010 AASHTO LRFD Bridge Design Specifications
H = annual average ambient mean relative humidity
h = overall depth of the member
h_c = overall depth of the composite section
I = moment of inertia of the composite cross section resisting the live loads; dynamic load allowance (see also *IM*)
I_g = moment of inertia of the girder by itself, neglecting the reinforcement
IM = vehicular dynamic load allowance (see also I)
j = ratio of the distance between the compression and tension centroids versus d
K_1 = correction for the aggregate source used in calculating E_c, generally taken as 1.0 unless determined by testing
K_L = factor accounting for the type of prestressing steel, taken as 30 for low relaxation strands unless more accurate manufacturer's data is available
k = number of standard deviations away from the mean value
L = live load according to the 1989 AASHTO Standard Specifications.
LL = vehicular live load
l = span length
LWC = lightweight concrete (see also *lwc*)
lwc = lightweight concrete (see also LWC)
M = total moment at a given section; moment at a given section due to unfactored live loads; total Green strain or a measure of the strain of a line in a given body, where the direction cosines of that line are l, m, and n
M_{cr} = cracking moment; moment to cause flexural cracking at a distance d away from the section in question, in the direction of decreasing moment
M_{cre} = moment causing flexural cracking at a given section due to externally applied loads
M_d = moment due to unfactored dead loads acting on both the composite and non-composite section

M_{deck} = dead load moment at the point in question along the longitudinal axis of the girder due the weight of the deck on the non-composite girder

M_{dnc} = total unfactored dead load moment acting on the monolithic or non-composite section

$\overline{M}_{fl}$ = flexural capacity

M_{max} = maximum moment at a given section due to the load combination causing that maximum moment to occur

M_{self} = dead load moment at the point in question along the longitudinal axis of the girder due the self weight of the beam

M_u = maximum bending moment in a given section at failure; moment due to factored loads at a given section

N = number of simulations

N_u = the factored axial force in the member, where tension is taken as positive

N_v = horizontal force resulting from V_f and carried by the longitudinal reinforcement

NWC = normal weight concrete (see also *nwc*)

nwc = normal weight concrete (see also NWC)

P_F = probability of failure

P_e = effective prestressing force of all of the strands

Q = sum of the load effects

R = design resistance; sum of the resistance effects

R_{HS20} = required resistance, assuming an HS20 truck model in the 1989 edition of the AASHTO Standard Specifications for Highway Bridges

R_{LRFD} = required resistance, as proposed in *NCHRP Report 368*

R_{lwc} = required minimum shear capacity for a lightweight concrete beam

R_n = nominal resistance

r = ratio of R_{LRFD} versus R_{HS20}

S = center-to-center girder spacing

S_c = composite section modulus for the extreme fiber where externally applied loads cause tensile stress

S_{nc} = monolithic or non-composite section modulus for the extreme fiber where externally applied loads cause tensile stress

s = stirrup spacing

s_{max} = maximum stirrup spacing

Sim = shear strength calculations following the Simplified Procedure for Prestressed and Nonprestressed Sections in Article 5.8.3.4.3 of the 2010 AASHTO LRFD Bridge Design Specifications

t_{deck} = design thickness of the deck, used for calculating the dead load on the girder

$t_{struct\ deck}$ = deck thickness used for determining the structural capacity of the composite section

t_{haunch} = maximum thickness of the haunch between the girder and the deck and used to provide a level riding surface

$t_{wearing\ surface}$ = thickness of the wearing surface

u = randomly generated, uniformly distributed number

V = total shear force at a given section; shear force at a given section due to unfactored live loads; or vertical component of the force in a compressive strut

V_c = nominal shear resistance provided by the concrete

$V_{c\ Exp}$ = concrete component of the shear resistance at the experimental failure load

V_{calc} = nominal shear strength calculated according to a given shear design method

V_{ci} = shear force at first inclined cracking that develops from a combination of shear stresses and tensile stresses due to the flexural moment, where the shear stresses increase in the region immediately above the flexural cracks

V_{cr} = shear force corresponding to M_{cr}

V_{cw} = shear force in the concrete at first diagonal cracking, where cracking is primarily due to excessive tensile stresses in the web as dictated by Article 5.8.3.4.3 of the 2010 AASHTO LRFD Bridge Design Specifications

$V_{cw\ Exp}$ = concrete component of shear resistance at first diagonal cracking in the web during experimentation

V_d = shear force due to non-composite dead loads at a given section; also the shear force due to unfactored dead loads acting on both the non-composite and composite section

V_{Exp} = ultimate failure load during experimentation

V_f = factored shear force at a given section

V_i = shear force corresponding to the load combination causing the maximum moment to occur at a given section

V_n = nominal shear strength

$V_{n\ A.B5}$ = calculated nominal shear strength following Appendix B5.2 of the 2010 AASHTO LRFD Bridge Design Specifications

$V_{n\ calc}$ = calculated nominal shear strength using one of three shear design models in the AASHTO specifications

$V_{n\ Gen}$ = calculated nominal shear strength following Article 5.8.3.4.2 of the 2010 AASHTO LRFD Bridge Design Specifications

$V_{n\ Sim}$ = calculated nominal shear strength following Article 5.8.3.4.3 of the 2010 AASHTO LRFD Bridge Design Specifications

V_p = vertical force component of harped prestress tendons

V_s = steel component of the shear resistance

V_u = total shear force at a given section at ultimate; shear force at a given section due to factored loads

v = shear stress on an arbitrary stress element

v_c = shear stress carried by the concrete at first diagonal cracking

v_{ci} = local shear stresses along a crack plane
$v_{ci\ max}$ = maximum local shear stress along a crack plane
v_{cxy} = shear strain in the concrete relative to the x- and y-axis
v_{cw} = web-shear cracking stress
v_f = shear stress in the beam at failure
v_u = ultimate shear stress in concrete
w = crack width
$w_{barrier}$ = linear weight of the guard rails at the sides of the deck
w_c = unit weight of concrete (see also γ_c)
w_u = factored uniformly-distributed load
X_i = a given load component; uncorrelated random variable
x^* = design point at which a limit state function is being evaluated
y = vertical distance from the composite cross-section's centroid to the point in question within the cross section, taken as positive when above the girder centroid
y_t = distance from the centroid of the gross composite section to the extreme tension fiber
Z = random variable converted into standard form
z = standard normal random value
α = angle of inclination of the shear reinforcement with respect to the horizontal, in degrees; angle of rotation to the principal stresses in an arbitrary stress element; sensitivity factors used in determining the reliability index
β = factor relating the effect of longitudinal strain to the ability of diagonally cracked concrete to transmit tension; reliability index
β_T = target reliability index
Δf_{pRI} = prestress loss due to relaxation of prestressings strands between time of transfer and deck placement
ε'_c = strain associated with f'_c, typically assumed to be –0.002
ε_1 = principle tensile strain in the concrete
ε_2 = principle compressive strain in the concrete
ε_{ab} = strain in the *ab*–plane
ε_R = prediction errors that factor into the variability of a given resistance model
ε_s = net longitudinal tensile strain in the section at the centroid of the tension reinforcement
ε_t = tensile strain in the concrete
ε_x = longitudinal strain at mid-depth of the member; strain in the x-axis
ε_y = strain in the y-axis
Φ = cumulative distribution function of a standard normal variable
Φ^{-1} = inverse of the standard normal cumulative distribution function

ϕ = resistance factor; capacity reduction factor equal to 0.85 and applied to the diagonal tensile strength; probability density function of a standard normal variable

ϕ_v = resistance factor for shear

γ = unit weight of lightweight concrete

γ_c = unit weight of concrete (see also w_c)

$\gamma_{c\ deck}$ = unit weight of the deck concrete

γ_i = load factor for a given load component X_i

γ_{xy} = shear strain relative to the x- and y-axis

$\gamma_{wearing\ surface}$ = unit weight of the wearing surface

λ = lightweight modification factor; lightweight modification factor for shear (see also λ_v)

λ_F = fabrication bias factor, calculated as the ratio of the average actual dimension versus the nominal cross-sectional properties

λ_{FM} = bias factors for materials and fabrication combined into a single bias factor

λ_M = material properties bias factor, mathematically is the ratio of the average actual material property to the nominal material properties

λ_P = modeling error or professional bias factor, calculated as the average ratio of the actual behavior to the strength predicted by the model

λ_R = bias factor for the design resistance

λ_i = the bias factor for a given load component X_i

λ_v = lightweight modification factor for shear (see also λ)

μ = mean value

μ^e = equivalent normal mean value

μ_Q = mean total load effect

$\mu_{Q\ lwc}$ = mean total load effect for lightweight concrete

θ = the angle of shear cracking; angle of inclination of principal stresses, relative to the horizontal, in an arbitrary stress element (see also θ_{prin})

θ_{calc} = the angle of diagonal compressive stresses in a concrete beam, calculated using one of the three shear design models in the 2010 AASHTO LRFD Bridge Design Specifications

$\theta_{crack\ med}$ = the median value of a given range of crack angles measured for a given test

θ_E = θ_{LVDT} for the East face of the girder web

$\theta_{prin\ last}$ = the last θ_{prin} that could be calculated due to an LVDT going offscale during testing

$\theta_{prin\ post\text{-}V_{cw}}$ = θ_{prin} calculated immediately after first web-shear cracking

$\theta_{prin\ pre\text{-}V_{cw}}$ = θ_{prin} calculated just before first web-shear cracking

θ_{LVDT} = the angle of inclination of principal stresses determined using an LVDT rosette

θ_{prin} = angle of inclination of principal stresses, relative to the horizontal, in an arbitrary stress element (see also θ)

θ_{SG} = the angle of inclination of principal stresses determined using a strain gauge rosette

θ_{Sim} = the angle of diagonal compressive stresses in a concrete beam, calculated using the *Simplified Procedure* in Article 5.8.3.4.3 of the 2010 AASHTO LRFD Bridge Design Specifications

θ_W = θ_{LVDT} for the West face of the girder web

ρ = longitudinal reinforcement ratio (see also ρ_w); density of lightweight concrete; diagonal matrix of correlation coefficients between variables

ρ_b = balanced longitudinal reinforcement ratio

ρ_o = percentage of longitudinal reinforcement

ρ_{sx} = reinforcement ratio in the *x*-direction

ρ_{sy} = reinforcement ratio in the *y*-direction

ρ_v = percentage of vertical reinforcement relative to the gross horizontal area of the web

$\rho_v f_{yv}$ = shear reinforcing index

ρ_w = longitudinal reinforcement ratio (see also ρ)

σ = standard deviation

σ_1 = principle tensile stress in an arbitrary stress element

σ_2 = principle compressive stress in an arbitrary stress element

σ^e = equivalent normal standard deviation

σ_P = standard deviation for the ratios of the experimental shear strength versus the calculated shear strength

σ_Q = standard deviation of the total load effect

Chapter 1

Introduction

1.1 Background

1.1.1 Assessment of the U. S. Bridge Inventory

According to the U.S. Department of Transportation's Federal Highway Administration (*1*), more than 11% of U.S. bridges were structurally deficient as of December 2010. In other words, at least one major component of 11% of the nation's bridges needed extensive maintenance, rehabilitation, or complete replacement. If none of these options were available, then transportation officials would need to either restrict traffic or close the bridge altogether until repairs could be performed.

In response to this data, Transportation for America (T4 America), a broad alliance of developers, conservationists, public health officials and urban transportation officials advocating responsible investment of federal funds into greener, smarter transportation systems that ensure the economic and physical security of the U.S., released a report entitled, *The Fix We're In For: The State of Our Nation's Bridges* (*2*). Sounding the alarm bell, this report informed readers that funding provided at the local, state, and federal level has been, and continues to be, woefully inadequate, and has barely put a dent in the number of deficient bridges over the last 20 years. This statistic is on top of the fact that a large number of bridges in this country are older than 50 years, which has been the typical design life for a bridge. Thus, the problem will only get worse as the aging bridge inventory accelerates at a time when difficult economic conditions further restrict the funds that government officials are willing to dedicate to replacing the dilapidated inventory.

As part of its answer to dwindling financial resources, T4 America has urged officials to make better use of available funds through improved bridge maintenance practices. Two other potential solutions are doubling the lifespan of a bridge from 50 years to 100 years and reducing the overall lifecycle costs of the bridge. Sand-lightweight concrete, produced with manufactured lightweight coarse aggregate and sand fine aggregate, is one means to achieving those solutions.

1.1.2 Historical Background of Lightweight Concrete

The Romans are the first known engineers to use lightweight aggregate on a massive scale. Lightweight material such as volcanic rock and crushed brick was instrumental in building such structures as the Pantheon and the Colosseum about 2000 years ago. After the demise of the Roman Empire, lightweight aggregate was not widely used until 1880 when porous clay pieces were produced in Germany through rapid water evaporation (*3*). In the U.S., the lightweight concrete industry got its start in 1918 when Stephen J. Hayde patented a rotary kiln process of expanding pieces of clay, shale, and slate (*4*).

Although lightweight concrete was not officially sanctioned by the American Concrete Institute (ACI) as an acceptable construction material until 40 years after Hayde's patent (*5*), this material was in use long before ACI's approval. The shipping industry was the first to use reinforced lightweight concrete during World War I (*6*), followed by the housing construction industry in the late 1940's. Lightweight concrete eventually made its way into multi-story buildings in the 1950's (*7*).

Even though the material did not achieve mainstream use in bridge applications until much later than other industries, lightweight concrete was placed in the upper deck of the San Francisco-Oakland Bay Bridge in the early 1930's. Another early use in bridge decking was the reconstructed Tacoma Narrows Bridge in 1950 following that bridge's collapse in 1940 (*7*). Going beyond mildly reinforced concrete, prestressed lightweight concrete has been in use since the early 1960's (*8*).

1.1.3 Economic Advantages of Lightweight Concrete

Due to the manufacturing process for lightweight aggregate, the material cost of lightweight concrete is typically greater than normal weight concrete. However, designing with lightweight concrete yields a 17 to 24% reduction in the structure's weight (*9*). This weight reduction results in construction cost savings that outweigh the added material cost. Such economies are actualized by:

- allowing for smaller footings or fewer piles and less steel reinforcement,
- reducing the inertial seismic demand on the structure,
- enabling wider deck widths in bridge rehabilitations without the need for additional superstructure or substructure,
- allowing for deeper deck thicknesses, thus enabling greater cover depths and protection for reinforcement,
- increasing the live load capacity of an existing bridge,
- using longer girder elements, thus needing fewer columns or piers, as well as fewer joints in the bridge deck
- enabling cantilevered construction through the combination of longer lightweight concrete beams on one side of a pier with normal weight concrete serving as a counterbalance on the other side,
- reducing the transportation costs of the concrete materials and elements to the job site,
- decreasing the crane capacity that would be required for installing the concrete elements.

In fact, a study performed in the late 1990's showed that the transportation costs alone realized a savings that averaged about seven times above and beyond the increase in cost of manufacturing lightweight aggregate. Of course, this analysis was done prior to the dramatic inflation of diesel fuel prices, where prices have tripled since 1999 (*10*).

In a more recent example, Castrodale stated that the premium for lightweight concrete ranged from $20 to $40 per cubic yard (*9*). In light of this premium, Castrodale calculated that a 150-ft lightweight girder had $1024 in additional material costs over that of traditional concrete. However, a precast company indicated to Castrodale that the shipping cost of the lightweight girder to the bridge site was $811 less than the normal weight beam. Furthermore, the

lightweight design required fewer prestressing strands, thus saving another $390. Therefore, there was a net savings of $177 just for using lightweight concrete in the beam itself. This savings would be even greater if the analysis accounted for the smaller foundation size and the reduction in steel required for that smaller foundation due to the lighter overall dead load.

1.1.4 Disadvantages of Designing with Lightweight Concrete

Despite the many aforementioned advantages discussed above, there are several disadvantages of lightweight concrete:

- the mix design is typically more expensive due to the need for a higher cement content to achieve the same compressive strengths as normal weight concrete (*11*).
- quality control issues arise in construction, such as proper preparation of the lightweight aggregate and pumping lightweight concrete without a decrease in slump.
- lightweight concrete tends to have lower material properties, such as elastic modulus, modulus of rupture, and splitting tensile strength, that can reduce the benefits of weight reduction.
- prestressed girders tend to have larger cambers due to the lower modulus of elasticity.
- prestress girders can have higher prestress losses, primarily due to the elastic shortening, which again is due to the lower elastic modulus.
- failure planes tend to form through the lightweight coarse aggregate, as opposed to around traditional gravel aggregate, resulting in a smoother crack interface, which reduces the structural shear strength of a member.
- uncertainty exists in how to model shear strength in light of the tensile strength of lightweight concrete and smoother shear crack interface.

For these reasons, engineers are reluctant to use lightweight concrete.

1.2 Objectives

To give engineers greater confidence in designing with lightweight concrete, the focus of this study is to alleviate some of the uncertainty mentioned above regarding calculating the shear strength of prestressed, lightweight concrete girders that would be found in a typical bridge. This goal has been achieved by:

- augmenting the existing database of full-scale prestressed lightweight girder tests,
- comparing various models for shear design with experimental results,
- examining the need to modify the tensile strength calculation when designing for shear in prestressed, lightweight concrete bridge girders,
- considering the reliability basis of the strength reduction factor, ϕ, used in the shear design of prestressed, lightweight concrete girders, and
- making recommended changes to the AASHTO LRFD Bridge Design Specifications for designing lightweight concrete girders for shear.

1.3 Scope

To fulfill the objectives above, there were a series of full-scale, prestressed lightweight concrete girders, each having a lightweight concrete deck cast on top. All of the girders were designed for both shear and flexure according to the procedures of the 2007 AASHTO LRFD Bridge Design Specifications (*12*). Note, however, that portions of the shear provisions in the 2007 edition that were used to design the beams were subsequently placed in the appendix of the 2008 interim revisions of the Specifications (*13*).

Also note that "full-scale" means that the experimental girder cross-sections are types commonly used in bridge construction in Virginia. These full-scale beams were designed with the number of prestressing strands needed for the flexural capacity of the longest span length possible for a given cross-sectional geometry. The shear design was then performed accordingly. However, because the purpose of this study focused on shear capacity, most of the original design between the two harping points for the prestressing tendons was deleted from the fabrication plans for the test beams. Doing so principally affected the region of the beam where the shear forces were low relative to the moment in the girder. All other aspects of the original design remained more or less the same, including stirrup size and spacing, number of strands, number and inclination of harped strands, and the deck design.

The experimental program comprised six beams, with two tests per beam, for a total of twelve shear tests, as indicated in Table 1-1. The numbers given in this table are nominal values. Note

Table 1-1. Planned testing matrix showing various variables under consideration.

Test ID	γ_c (pcf)	f'_c (ksi)	a/d	ρ_v (%)	d_v (in)	A_{comp} (in^2)
T2.8.Typ.1	125	8	1.5	0.75	40	1000
T2.8.Typ.2	125	8	3.0	0.75	40	1000
T2.8.Min.1	125	8	1.5	0.55	40	1000
T2.8.Min.2	125	8	3.0	0.55	40	1000
BT.8.Typ.1	125	8	2.0	0.65	49	1300
BT.8.Typ.2	125	8	3.5	0.65	49	1300
BT.8N.Typ.1	150	8	2.0	0.40	49	1300
BT.8N.Typ.2	150	8	3.5	0.40	49	1300
BT.10.Typ.1	125	10	2.0	0.60	49	1300
BT.10.Typ.2	125	10	3.5	0.60	49	1300
BT.10.Min.1	125	10	2.0	0.25	49	1300
BT.10.Min.2	125	10	3.5	0.25	49	1300

that the unit weight of concrete, γ_c, includes 5 pcf that was assumed to be the weight of steel reinforcement uniformly distributed throughout the concrete. Also note that one of those beams was constructed with normal weight concrete to make a comparison between the shear behavior of lightweight and normal weight concrete. All of the beams were simply supported during testing and subjected to two concentrated loads. The principal variables covered by these twelve tests were:

- unit weight, γ_c
- 28-day specified compressive strength, f'_c
- effective shear depth, d_v
- shear span-to-effective shear depth ratio, a/d
- shear reinforcing index, defined as the percentage of vertical reinforcement relative to the gross horizontal area of the web, ρ_v, multiplied by the yield strength of the shear reinforcement, f_{yv}.
- composite cross-sectional area, A_{comp}.

The analysis of data collected during these tests includes:

- comparing the ultimate shear strengths of the different beams with the strengths predicted by shear strength models provided in the AASHTO LRFD Bridge Design Specifications,

- determining the concrete contribution versus the steel contribution to overall shear strength, and comparing these results with those predicted by AASHTO,
- comparing the experimental cracking angles with those predicted by Article 5.8.3.4.2 and Appendix B5 of the AASHTO LRFD Bridge Design Specifications,
- determining the applicability of a modification factor for the $\sqrt{f'_c}$ term when designing for shear in prestressed, sand-lightweight concrete beams,
- developing a strength reduction factor that will result in a given prestressed, lightweight concrete girder having an acceptable degree of reliability.

The remainder of this document includes an in-depth literature review discussing the material characteristics of lightweight concrete as they pertain to shear strength, development of various methodologies for calculating shear capacity, and research into lightweight concrete. There are also details regarding the experimental program, including beam design and testing procedures. Next, the results are presented followed by the conclusions drawn from those results.

Chapter 2

Literature Review

2.1 Properties of Lightweight Concrete

2.1.1 Aggregate

While still available in the form of natural volcanic pumice, scoria, or tuff, most of today's lightweight aggregates are manufactured from shale, clay, slate, blast-furnace slag, fly ash, perlite, or vermiculite (*14*). There are a few countries where crushed palm oil shells also serve as lightweight aggregate (*3*).

The major manufactured lightweight aggregates are generally produced using one of three processes: the rotary kiln, where pieces of raw material are rotated in a heated drum that is lined with refractory materials; sintering, where the raw material is carried along a moving grate inside of an ignition hood; and the rapid agitation of molten slag (*8*). Any one of these processes result in a relatively lower density of the aggregate compared to regular gravel or sand. The reason is due to the cellular pore structures that form when the raw material is heated to between 1800 and 2200 ^{o}F, at which point gases generate within and cause the material to expand two to seven times its original volume (*6*, *9*). Upon cooling, the material contracts somewhat, yet retains much of its expanded shape as well as the air voids formed by the gases. These pores are typically on the order of 5μm to 300 μm in diameter and can fill with moisture that is 5—25% of the weight of the dry aggregate (*14*). Without the additional moisture, the expanded aggregate has a density that is roughly one-half of that of traditional gravel. This lower aggregate density results in the lower unit weight for lightweight concrete. However, the voided aggregate has a lower stiffness compared to normal weight aggregate.

2.1.2 Density

Typically, structural lightweight concrete has an equilibrium density ranging from 105 to 120 lb/ft^3 (*8*). However, the industry has suggested that the fresh density be used in final design calculations because water can be retained within the concrete for quite some time, particularly in those members with a high volume-to-surface area ratio. For clarity, the engineer should state whether or not the density includes an assumed unit weight of reinforcing steel (*9*). Those concretes on the lighter end of the density range tend to contain both lightweight coarse and fine aggregate, thus are termed "all-lightweight" concrete. On the other hand, the heavier "sand-lightweight" concretes contain sand as the fine aggregate.

2.1.3 Compressive Strength

Using similar mix designs with the exception of the type of aggregate, lightweight concrete tends to have a lower compressive strength, f_c, compared to its normal weight counterpart (*15*). However, mix design modifications, including admixtures and decreasing the nominal maximum coarse aggregate size, can increase the compressive strength of lightweight concrete up to 10 ksi or 12 ksi (*16*). On the other hand, the type of lightweight aggregate used will also affect f_c. Regardless of the type of aggregate, lightweight concrete does appear to have a compressive strength "ceiling" near 12 ksi, and in fact reaching consistent strengths above 8 ksi or 10 ksi can be problematic (*16, 17*). The reason is due to fractures occurring through the aggregate, similar to that observed in normal weight concrete with strengths upwards of 15 ksi.

2.1.4 Tensile Strength

Early work by Hanson (*18*) found that the diagonal tensile strength of lightweight concrete can be directly related to its splitting tensile strength, f_t. However, more recent research by Ramirez et al. (*19*) contradicted that observation.

Nevertheless, if the test specimen is continuously moist-cured, then the results of a splitting-tensile strength versus compressive strength graph fall within a relatively narrow band for lightweight concrete, while the strengths of comparable normal weight specimens will be within that band. However, if the specimen is cured according to the testing standard ASTM C496-04

(*20*), where the cylinder is moist-cured for 7 days and then air-cured for 21 days at 73.5 ± 3.5 ^{o}F and 50 ± 5% relative humidity, then the rate of moisture loss differs between the surface and the interior of the specimen. This difference results in tensile stresses at the specimen surface, and thus, reduced strength when subjected to loading, where the splitting tensile strength of lightweight concrete tends to be 0 to 30% below the strength of a comparable normal weight specimen (*8, 14*).

2.1.5 Modulus of Elasticity

The elastic modulus of concrete depends on the modulus of its constituent parts. Because lightweight aggregate is not as stiff as its normal weight counterpart, the modulus of elasticity of lightweight concrete tends to be 25 to 50% less than the modulus of normal weight concrete of the same compressive strength.

ACI's 2003 publication, *Guide for Structural Lighweight-Aggregate Concrete* (*8*), suggests that the equation for calculating the elastic modulus of lightweight concrete, E_c, should vary according to the concrete's compressive strength, such that

$$E_c = w_c^{1.5} C\sqrt{f'_c} \text{ [ksi]} \quad (1)$$

where w_c is the concrete unit weight in kip/ft^3 and f'_c is the design concrete compressive strength in ksi, while C = 31,000 when f'_c = 5 ksi and C = 29,000 when f'_c = 6 ksi.

In 2004, Kahn et al. (*16*) proposed another formula for the modulus of elasticity of high-performance lightweight concrete made with slate aggregate. This formula differs from that used by ACI or AASHTO such that

$$E_c = 44{,}000\sqrt{f'_c \frac{w_c}{145}} \text{ [psi]}$$

which, when using f'_c in ksi and w_c in kips/ft^3, becomes

$$E_c = 3654\sqrt{f'_c w_c} \text{ [ksi]} \quad (2)$$

Eq. (2) is different from the equation the authors first set out using. Prior to the inclusion of additional data from their experiments, the researchers considered the formula

$$E_c = \left(33{,}000\sqrt{f'_c} + 4{,}000{,}000\right)\left(\frac{w_c}{242}\right)^{0.9} \text{ [psi]} \quad (3)$$

where f'_c is in psi units and w_c is in lb/ft^3. Eq. (3) is itself a modification from a formula suggested by Slate et al. (*21*):

$$E_c = \left(40{,}000\sqrt{f'_c} + 1{,}000{,}000\right)\left(\frac{w_c}{145}\right)^{1.5} \text{ [psi]} \quad (4)$$

However, note that Eq. (4) is limited to 3 ksi $\leq f'_c \leq$ 9 ksi.

In 2005, Stiffey (*22*) analyzed 500 tests for modulus of elasticity to arrive at two additional equations for calculating this mechanical property of lightweight concrete:

$$E_c = 50 w_c^{1.7} \sqrt[3]{f'_c} \text{ [psi]}$$

and

$$E_c = \left(173{,}400\sqrt[3]{f'_c} + 1{,}000{,}000\right)\left(\frac{w_c}{145}\right)^{1.7} \text{ [psi]}$$

where w_c and f'_c are in units of lb/ft^3 and psi, respectively. When using kcf and ksi units, the two above equations become

$$E_c = 6.29\times10^4 w_c^{1.7} \sqrt[3]{f'_c} \text{ [ksi]} \quad (5)$$

and

$$E_c = \left(1734\sqrt[3]{f'_c} + 1000\right)\left(\frac{w_c}{0.145}\right)^{1.7} \text{ [ksi]} \quad (6)$$

However, Stiffey noted that Eqs. (5) and (6) do not apply to normal weight concrete. Thus, the author developed coefficients that accurately fit the data for normal weight concrete but were different from those in the two equations above.

There is one final equation developed by Cook (*23*) for use with normal weight concrete:

$$E_c = w_c^{2.55} f_c'^{0.315} \text{ [ksi]} \quad (7)$$

where w_c is 151 lb/ft^3. However, research by Dymond et al. (*24*) concluded that Eq. (7) reasonably predicts the modulus of elasticity of lightweight self-consolidating concrete, yielding results that are considerably closer than the traditional equation for the elastic modulus supported by the current AASHTO LRFD Bridge Design Specifications:

$$E_c = 33{,}000 K_1 w_c^{1.5} \sqrt{f'_c} \text{ [ksi]} \quad (8)$$

where w_c is in units of kip/ft^3 and K_1 is a correction for the aggregate source, but is taken as 1.0 unless determined by testing.

2.1.6 Modulus of Rupture

ACI 318-11 defines the modulus of rupture, f_r, as

$$f_r = 7.5\lambda\sqrt{f'_c} \text{ [psi]}$$

where λ is the lightweight modification factor discussed in Section 2.3.4.1. AASHTO, on the other hand, does not use a λ-factor. Instead, the rupture modulus is more explicitly listed as

$$f_r = \begin{cases} 0.20\sqrt{f'_c} \text{ [ksi]} & \text{for normal weight and sand-lightweight concrete} \\ 0.17\sqrt{f'_c} \text{ [ksi]} & \text{for all-lightweight concrete} \end{cases} \quad (9)$$

Note that f_r for normal weight concrete in Eq. (9) only applies to the cracking moment calculated for shear design in Article 5.8.3.4.3 of the 2010 AASHTO LRFD Bridge Design Specifications .

2.1.7 Prestress Losses

The Prestressed Concrete Institute suggests that the total prestress losses in typical beams be estimated between 30 and 55 ksi for lightweight members versus 25 to 50 ksi for normal weight members (*25*). Apart from higher short-term losses due to a lower modulus of elasticity, one possible reason for excess long-term losses in lightweight concrete is greater shrinkage. This

greater amount of shrinkage may be due in part to the large amount of carbon dioxide present in the aggregate due to the manufacturing process. Also known as the "carbonation" of concrete, the excess CO_2 decomposes the calcium silicate hydrates in the concrete, resulting in additional shrinkage on top of typical drying shrinkage (*26*). As for drying shrinkage, lightweight concrete can exhibit up to twice the shrinkage of normal weight concrete. Furthermore, lightweight aggregate is less rigid than gravel. As a result, lightweight concrete is more prone to cracking during drying because the aggregate cannot restrain the contraction of the paste (*26*). However, as compressive strength levels increase, the difference in shrinkage between the lightweight and normal weight concrete decreases. Compared to moist curing, steam curing can reduce shrinkage in lightweight concrete by as much as 10 to 40% after one year, similar to normal weight concrete. However, the higher strength lightweight concrete typically found in prestressed girders exhibits the lower percentage reduction in shrinkage. To a smaller degree, replacing lightweight fine aggregate with natural fines can also help reduce the amount of shrinkage (*8, 14*).

In addition to shrinkage, lightweight concrete has exhibited creep that is as much as two times the creep in normal weight concrete. However, replacing lightweight fine aggregate with natural fines as well as using higher strength concrete helps to reduce the amount of creep. Additionally, steam curing can reduce creep by 25—40% relative to moist-curing methods. Nevertheless, creep in high-strength lightweight concrete may still be 50% greater than creep in steam-cured high-strength normal weight concrete (*8, 14*).

2.1.8 Durability

Lightweight concrete tends to have better durability than normal weight concrete for several reasons. One is that there tends to be a greater degree of adhesion between the lightweight aggregate and the cement mortar as well as better elastic congruity between the two phases of concrete. Therefore, there is less microcracking at the interface transition zone between the aggregate and the hydrated cement phases (*27*). Furthermore, lightweight concrete tends to have a higher ultimate strain capacity and a better air-entrainment system due to the surface of the aggregate (*28*). Another factor is that lightweight concrete tends to have much lower permeability (*8*). As a result, freeze-thaw experiments have shown that lightweight concrete can

endure highly variable environments (*26*). Additionally, the lower permeability offers greater resistance to chloride intrusion compared to normal weight concrete, therefore providing better protection against corrosion of the reinforcing steel (*9*). One negative aspect with regards to durability is the abrasion resistance of the lightweight aggregate, although there have been contradicting views on that particular characteristic (*9, 27*).

2.2 Development of Shear Design for Concrete Beams

There are many factors that can affect the shear strength of concrete beams, such as (*29-36*):

- material properties of both the concrete and the reinforcing steel,
- the cross-sectional geometry,
- the percentage and distribution of longitudinal reinforcement,
- the amount and arrangement of the shear reinforcement,
- the shear span-to-effective depth ratio, *a/d*,
- arching action,
- shear in the compression zone,
- dowel action,
- aggregate interlock,
- type of loading and the ratio of applied sectional forces,
- prestressing conditions,
- residual tensile stresses across the cracks,
- nominal maximum aggregate size
- support conditions

Some of these factors are interdependent (*36*), and certainly, all of these influences together complicate the science of shear interaction. Over time, there has been a fair amount of disagreement regarding the importance of some of the above factors. For example, Moody et al. (*37*) found that the presence of vertical reinforcement does not appear to influence the beam behavior prior to diagonal cracking, nor does anchoring the tension reinforcement. These same researchers assumed that no stresses transfer across the diagonal tension crack and that dowel action is negligible. Instead, Moody et al. believed that all of the vertical shear stress is acting

through the uncracked concrete above the tip of the diagonal tension crack. On a different issue, some researchers firmly believed that the shear strength decreases as the depth increases (*38*), while others had results that showed little correlation (*39*). There is even disagreement over the relationship between f_c and the diagonal cracking load. Kani (*40*) determined that this load is independent of the concrete compressive strength; twenty years later, Elzanaty et al. (*36*) concluded that such a load increases as f_c increases. Yet, Elzanaty et al. also found that the presence of stirrups does not affect the diagonal cracking load.

In addition to the components that play a role in the design shear strength, there are also various failure modes that the engineer must consider, including (*37, 41*):

- Diagonal tension (or shear tension) failure, where a diagonal tension crack extends from the web towards both the top and bottom flanges, resulting in complete separation of two parts of the beam,
- Shear compression failure, where a diagonal crack extends into the top flange, reducing the compression zone, resulting in concrete crushing,
- web crushing in the form of concrete spalling in the web and crushing near the support,
- shear bond failure, where the tensile forces in the longitudinal reinforcement breaks the anchorage between the steel and concrete, resulting in slip of the longitudinal reinforcement within the concrete,
- Splitting failure, where horizontal splitting occurs along the longitudinal reinforcement. This failure is believed to be due primarily to dowel action and diagonal tension stresses resulting from transferring the stress in the tensile reinforcement to the surrounding concrete.

In an attempt to capture all of the various factors affecting shear strength and the variety of failure mechanisms, a number of engineering organizations have published guidelines and specifications that detail how to design concrete beams. As early as the 1951, ACI (*42*) guidelines for shear design consisted of a couple of pages, while the 1953 AASHTO code (*43*) needed less than a single page of equations. Today, engineers follow design codes such as those by ACI and AASHTO that are upwards of 13 and 30 pages long, respectively (*44, 45*).

2.2.1 Early Development of Shear Design Methods

The nascency of shear design came in 1899 with Ritter's (*46*) introduction of the 45° parallel chord truss model. In this model, a reinforced concrete beam behaves as a 45° truss, where the bottom chord consists of longitudinal steel reinforcement, the top chord forms from the compression zone in the concrete, discrete concrete struts act as the diagonal compression members, and the steel stirrups help to transmit the load vertically from the bottom of one concrete strut to the top of an adjacent strut. This transmission ultimately directs the forces from the load to the abutments or other girders supporting the loaded beam.

In 1902, Mörsch (*47*) modified Ritter's theory by configuring the concrete struts as a continuous field of diagonal compression instead of discrete compression members. Still, this modified 45° truss model assumes that the angle of the diagonal compression remains constant. Furthermore, Mörsch's theory neglects any tensile strength in the concrete; therefore, all of the vertical reinforcement provides the shear resistance. Assuming an effective shear area measuring b_w wide and jd deep, where b_w is the width of the web, d is the effective depth measured from the extreme compression fiber to the centroid of the tensile reinforcement, and j is the ratio of the distance between the compression and tension centroids versus d, the principal compressive stress in the concrete, f_2, is calculated as

$$f_2 = \frac{2V}{b_w jd} \qquad (10)$$

where V is the shear force in the beam at a given section. For a given stirrup spacing, s, the compressive strut would have a force

$$F = \frac{1}{\sqrt{2}} f_2 b_w s \qquad (11)$$

whose vertical component,

$$V = \frac{1}{2} f_2 b_w s \qquad (12)$$

would need to be resisted by the strength of the stirrup, $A_v f_{yv}$, where A_v is the cross-sectional area of a stirrup and f_{yv} is the yield strength of that stirrup. Combining Eqs. (10) and (12) along with the strength of the stirrup yields Mörsch's beam shear strength calculation as

$$V = A_v f_{yv} \frac{jd}{s} \qquad (13)$$

Mörsch did recognize that secondary cracks could form at angles that were shallower than 45°. While a shallower cracking angle would engage more stirrups, and thus require fewer stirrups for ultimate strength, Mörsch concluded that determining the angle of such secondary cracks is mathematically impossible. Thus, Mörsch proposed maintaining the conservative 45° angle as observed in the initial shear cracks (*48*). About the same time as Mörsch's work, however, Withey (*49, 50*) and Talbot (*29*) observed that the truss model is conservative compared to test results. Presumably, the reason for this conservatism is the absence of the contribution from the concrete, V_c, in the formulation.

2.2.2 Factors Influencing Concrete's Contribution to Shear Strength

Concrete is primarily composed of cement, aggregate, and water. The overall strength of the concrete tends to be weaker than its components because the weak link is the interface between the aggregate and the cement mortar. In flexural members, shear forces that cause vertical stresses combine with flexural forces that cause longitudinal stresses resulting in both compressive and tensile stresses in the web. The tensile stresses lead to diagonal tension cracking in concrete, where a diagonal tension crack has been defined as an inclined crack that causes significant redistribution of internal stresses. A diagonal tension crack generally forms above the tension reinforcement, gradually growing toward the load nearest the support on one end of the crack, while the other end extends down toward the tension reinforcement and then runs along the reinforcement.

Mörsch (*47*) had initially suggested that the ultimate shear stress in concrete, v_u, is a constant value that only depends on the concrete compressive strength, f_c. However, in 1909, Talbot (*29*) suggested that the shear span length also affects the shear strength. Yet Talbot's work appeared to go unrecognized until 1951 when Clark (*30*) incorporated an effective depth-to-shear span

ratio, *d/a*, into his formulation for shear strength. Clark also included the effect of longitudinal reinforcement on the concrete shear stress.

Separately, Moody et al. (*37*) agreed with Mörsch that f_c is a major factor in the cracking load. However, their research strongly suggested that the ratio v_c / f_c decreases as f_c increases from 3 ksi to 5 ksi. Furthermore, these scientists confirmed Talbot's concerns about shear span length, where the data showed that v_c / f_c increases with a decreasing a/d ratio.

Ten years later, Kani (*40*) showed results that agreed with Talbot and Clark regarding the shear span-to-effective depth ratio, a/d, and the longitudinal reinforcement ratio, ρ. Kani also disputed Mörsch's theory regarding a constant ultimate shear stress that is dependent on f_c. Instead, the researcher found that v_u could vary 700% when going from a/d = 5.0 to a/d = 1.0, and 100% when ρ changed from 0.80% to 2.80%. Given the influence of a/d and ρ, Kani suggested that the maximum bending moment at failure, M_u, serves as a major predictor of shear strength. Defining flexural capacity, $\overline{M}_{fl}$, as

$$\overline{M}_{fl} = A_s f_y jd \qquad (14)$$

where A_s is the area of longitudinal reinforcement and f_y is the yield strength of that reinforcement, the author found that the flexural capacity ratio, $M_u/\overline{M}_{fl}$, is about 1.00 for a/d = 1.0. Likewise, as a/d increases to about 2.5, $M_u/\overline{M}_{fl}$ decreases to some minimum value. Then, as a/d increases further to some transition point, $M_u/\overline{M}_{fl}$ returns to 1.0. Beyond that transition point, diagonal tension failure typically does not occur. The author termed this inverse peak of $M_u/\overline{M}_{fl}$ as the "valley of diagonal failure" and concluded that shear failure would only occur within this valley.

Kani also attempted to describe the internal mechanisms of shear resistance (*32*). In doing so, the author presented a comb analogy, where the compressive zone in the top of the beam forms the backbone of the comb and the concrete in between the cracks in the tensile zone forms the teeth of the comb. Kani concluded that the traditional assumption that plane sections remain plane is inaccurate, the reason being that because there is a bond between the longitudinal reinforcement and the concrete, the "teeth" in his analogy are acting as cantilevers subjected to

the incremental bond forces. The bending due to these bond forces causes tension in the concrete at the location where the "teeth" are connected to the "backbone." At the tensile stress limit in the concrete, an inclined crack would form, separating a "tooth" from the "backbone." Eventually, the "teeth" would no longer be able to provide resistance. At that point, the beam transforms into a tied-arch structure, where the load is transferred through the uncracked compression zone to the support.

While members containing less than a minimum amount of shear reinforcement are clearly affected by the depth of the member, where larger sections tend to have a lower shear stress at failure (*38, 51, 52*), the general consensus is that size has no effect on shear in members containing at least the minimum amount of shear reinforcement. However, Bažant (*53*) strongly disagreed with this consensus.

In 1981, Walraven (*33*) suggested that the concrete shear strength is also a function of the distribution and width of cracks, as well as the relative shear displacement between the two faces of a crack. As the two faces of a crack move relative to each other in shear, the surface of a given aggregate would come in contact with the cement mortar of the other surface, resulting in plastic deformation of that mortar. As the aggregate begins to slide further, the contact area on the mortar would be reduced, thus increasing the stress in this contact region. Additional plastic deformation would occur until the system reaches equilibrium. This action came to be known as aggregate interlock. Walraven's analysis concluded that concrete strength is the largest factor in resistance against shear displacements at the crack interface, while the aggregate size has a smaller importance.

As indicated by Walraven, the crack normally forms around the aggregate, thus forming a relatively rough surface. However, in both high-strength concrete and lightweight concrete, the tensile strength of the cement mortar is similar to the tensile strength of the aggregate. Therefore, cracks tend to form through the aggregate, thus creating a relatively smooth surface. This smoother crack surface may lead to reduced shear strength, particular in members where the slip resistance along the crack is the dominant resistance mechanism (*31*).

However, Hegger et al. (*54*) determined that the displacement perpendicular to the crack is much larger than the displacement along the crack. Because Walraven indicated that the displacement along the crack has a greater influence on shear stress than the displacement across the crack, the researchers concluded that shear friction has a negligible role in shear resistance. The authors did note that despite complete separation between the cracks, the beams continued to hold the load, and in some cases, had additional load-carrying capacity. The researchers concluded that this ability to increase the loading is due to the initial truss action being supplanted by arching action closer to failure, as suggested by Kani. These conclusions held for all levels of shear reinforcement.

2.2.3 V_c

As early as the 1920's, researchers began augmenting shear design with empirical equations to account for the additional capacity in the concrete. The first design calculation for the concrete contribution to shear strength, V_c, is

$$V_c = \begin{cases} 0.02 f'_c bjd \leq 59 \text{ psi (for non-anchored longitudinal reinforcement)} \\ 0.03 f'_c bjd \leq 90 \text{ psi (for anchored longitudinal reinforcement)} \end{cases} \quad (15)$$

where b is the width of a rectangular section or the width of the flange of a T-section.

The steel contribution, V_s, remained similar to Eq. (13), with minor modifications:

$$V_s = V_u - V_c = A_v f_{yv} \frac{jd}{s \sin\alpha} \quad (16)$$

where V_u is the total shear force at a given section and α is the angle of inclination of the shear reinforcement with respect to the horizontal.

At that time, the maximum allowable total shear stress at service was $0.06 f'_c \leq 180$ psi; if using anchored longitudinal reinforcement, then the limit was $0.12 f'_c \leq 360$ psi. These limits were instituted to avoid diagonal crushing failures prior to stirrup yielding (*55*). Both allowable stresses remained in place for the next thirty years until the advent of deformed reinforcement led ACI to drop the lower stress limits and simply state that all longitudinal reinforcement must

either be plain bar with adequate anchorage or deformed reinforcing bars. Still, the required amount of vertical steel was formulated using the 45° truss analogy that Ritter had originated in 1899.

Unfortunately, the 1955 failure at the Wilkins Air Force Depot brought to light the fact that shear and diagonal tension is more complicated and not fully captured in the original design equations. Thus, researchers reexamined Talbot's oft-ignored conclusion that shear strength is dependent on the amount of longitudinal reinforcement and the span-to-depth ratio. Further research determined that predicting the concrete contribution using the diagonal cracking strength provides a better fit to test data calculations instead of using the uniaxial compressive strength. Nevertheless, the diagonal cracking strength is a function of $\sqrt{f'_c}$. Thus, the concrete contribution in the 1963 ACI code (*56*) is calculated as

$$V_c = \left(\sqrt{f'_c\ [\text{psi}]} + 1300\rho_w \frac{Vd}{M}\right) b'd \ \ [\text{lb}] \qquad (17)$$

but is limited to

$$V_c = 1.75\sqrt{f'_c[\text{psi}]}b'd \ \ [\text{lb}] \qquad (18)$$

where b' is the width of the web, V and M are the total shear and bending moment, respectively, and ρ_w is the longitudinal reinforcement ratio.

In the 1971 edition of its *Building Code Requirements for Reinforced Concrete* (*57*), ACI increased the coefficient in Eq. (18) to 2. Additionally, Eq. (18) could be exceeded provided that additional analysis was done on members subjected only to shear and flexural forces. If so, then

$$V_c = \left(1.9\sqrt{f'_c\ [\text{psi}]} + 2500\rho_w \frac{V_u d}{M_u}\right) b_w d \ \leq\ 3.5\sqrt{f'_c\ [\text{psi}]}b_w d \ \ [\text{lb}] \qquad (19)$$

where b_w, V_u, and M_u are the same as b', V, and M, respectively.

AASHTO did not adopt some form of Eq. (18) until 1973 (*58*). However, there was never a rational explanation as to why the diagonal cracking load, combined with the transverse reinforcement contribution found from a constant 45° truss model, provided an acceptable estimate of the ultimate shear capacity. The reason may quite simply be the ease in understanding the model and the fact that the model fit the existing data fairly well (*59*).

2.2.4 V_{ci} and V_{cw}

As indicated in Eq. (15), the concrete contribution to the shear resistance was originally calculated as a fraction of the concrete compressive strength multiplied by the effective shear area of the beam. However, by the 1960's researchers had redefined the resistance provided by the concrete in prestressed beams as a factor of the diagonal cracking strength, which is the smaller of the web cracking strength, V_{cw}, and the flexural cracking strength, V_{ci}. ACI first introduced the terms V_{ci} and V_{cw} for prestressed concrete in the 1963 version of its *Building Code Requirements for Reinforced Concrete* (*56*). V_{ci} arises from a combination of shear stresses and tensile stresses due to the flexural moment, where the shear stresses increase in the region immediately above the flexural cracks. On the other hand, V_{cw} is defined as the shear force at first diagonal cracking, but that cracking is primarily due to excessive tensile stresses in the web. By definition, flexure-shear cracks initiate as flexural cracks in the bottom of the beam, while web-shear cracks initiate within the beam web.

2.2.4.1 V_{ci}

When ACI first formulated the flexure-shear concrete contribution in 1963, the equation was published as

$$V_{ci} = 0.6b'd\sqrt{f'_c} + \frac{M_{cr}}{\frac{M}{V} - \frac{d}{2}} + V_d \geq 1.7b'd\sqrt{f'_c} \qquad \textbf{(20)}$$

The middle term in Eq. (20) was rationally derived at a given section, where M and V are the moment and shear due to unfactored live loads. The term M_{cr} is the moment to cause flexural cracking at a distance d away from the section in question, in the direction of decreasing moment. M_{cr} is calculated as

$$M_{cr} = \frac{I}{y}\left(6\sqrt{f'_c} + f_{pe} - f_d\right)$$

where

I = the moment of inertia of the composite cross section resisting the live loads

y = distance from the composite cross-section's centroid to the extreme tension fiber

$6\sqrt{f'_c}$ = the modulus of rupture of the concrete

f_{pe} = compressive stress due to effective prestress, at the extreme fiber of the cross-section where external loads cause tension

f_d = stress due to unfactored dead loads, at the extreme fiber of the cross-section where external loads cause tension

At that time, ACI assumed that a flexural crack forming at a distance $d/2$ away from the section in question, as shown in Figure 2-1, is indicative of the formation of a flexure-shear crack. Using the term V_{cr}, which is the shear force corresponding to M_{cr}, ACI formulated the equation

$$M - M_{cr} = \frac{V + V_{cr}}{2}\frac{d}{2} \qquad (21)$$

which is simply the change in moment being related to the area underneath the shear diagram over distance $d/2$. Because the difference between V and V_{cr} over the distance $d/2$ can be dismissed, Eq. (21) becomes

$$M - M_{cr} = V\frac{d}{2}$$

which can be arranged such that

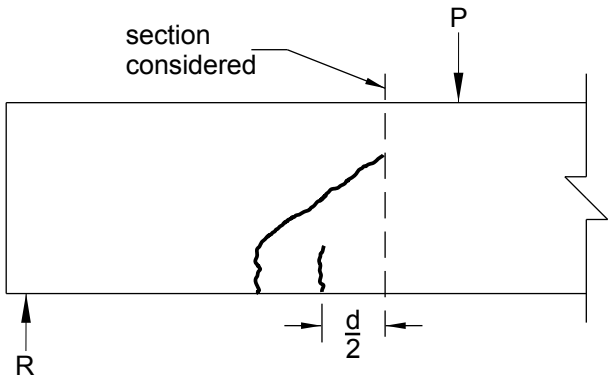

Figure 2-1. Sketch showing the formation of a theoretical flexure-shear crack.

$$V = \frac{M_{cr}}{\frac{M}{V} - \frac{d}{2}}$$

which matches the middle term in Eq. (20) and is essentially the shear due to live loads at the time flexural cracking occurrs. Meanwhile, V_d is the shear due to non-composite dead loads at the section in question and is separated from the applied loads for two reasons. First, dead loads are typically uniformly distributed, while live loads can have any distribution. Secondly, the majority of dead loads act on the prestressed girder alone while the live loads act on the composite section.

While the last two terms for V_{ci} in Eq. (20) have been derived rationally, the first term is an additional shear force required to transform a flexural crack into a diagonal tension crack. This additional shear has been observed during experimentation, and appears to be dependent on the cross-sectional geometry and the concrete strength. The lower limit in that equation was established in 1963 because the only beams that failed at loads below this limit were those with relatively small amounts of prestressing force (*60*).

The 1971 *Building Code Requirements for Reinforced Concrete (ACI 318-71)* slightly modified the equation for V_{ci} in composite sections to a form similar to the current equation:

$$V_{ci} = 0.6\lambda\sqrt{f'_c}b_w d_p + V_d + \frac{V_i M_{cre}}{M_{max}} \geq 1.7\lambda b_w d\sqrt{f'_c} \qquad \textbf{(22)}$$

where d_p is the distance from the extreme compression fiber to the centroid of the prestressing tendons, and

$$M_{cre} = \frac{I}{y_t}\left(6\lambda\sqrt{f'_c\ (\text{psi})} + f_{pe} - f_d\right) \qquad \textbf{(23)}$$

The shear force at the time of flexural cracking is then assumed to equal

$$\frac{V_i M_{cre}}{M_{max}}$$

In this case V_i and M_{max} are calculated as

$$V_i = V_u - V_d$$
$$M_{max} = M_u - M_d$$

where V_u and M_u are the respective shear and moment due to the total *factored* load, while V_d and M_d are due to the *unfactored* dead loads acting on both the non-composite *and* composite section. Note the λ-factor in Eq. (22) that allows for lightweight concrete. Also note that that any contribution from harped or draped prestressing tendons is ignored in the formula for V_{ci}.

2.2.4.2 V_{cw}

V_{cw} has been derived from an arbitrary stress element and Mohr's circle, as shown in Figure 2-2, where σ_1 and σ_2 are the principle tensile and compressive stresses, respectively, and θ is the angle of rotation to the principal stresses. According to Figure 2-2b, σ_1 can be calculated as

$$\sigma_1 = \frac{f_v + f_{pc}}{2} + \sqrt{v^2 + \left(\frac{f_v - f_{pc}}{2}\right)^2} \qquad (24)$$

where f_v is the compressive stress on the arbitrary element due to vertical loads, f_{pc} is the compressive stress due to prestressing, and v is the shear stress, as shown in Figure 2-2a. If

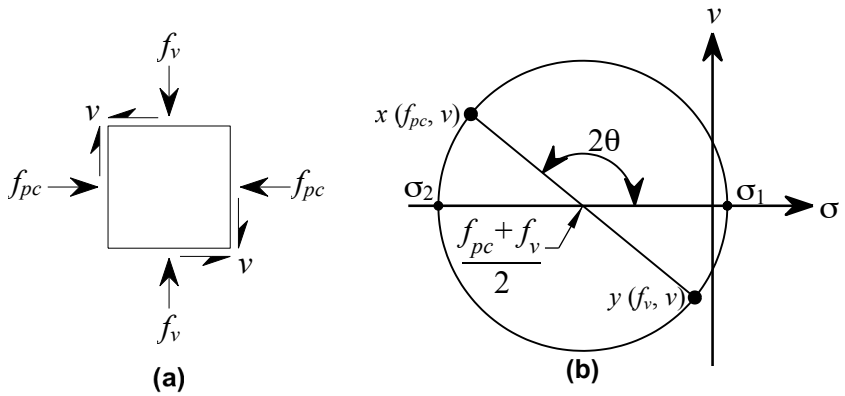

Figure 2-2. (a) Arbitrary stress element and (b) the corresponding Mohr's circle showing principle stresses.

assuming that f_v can be neglected, then Eq. (24) becomes

$$\sigma_1 = \frac{f_{pc}}{2} + \sqrt{v^2 + \left(\frac{f_{pc}}{2}\right)^2} \qquad (25)$$

Web-shear cracking is assumed to occur when the principal tensile stress reaches the concrete tensile stress, f_t. Therefore,

$$f_t = \frac{f_{pc}}{2} + \sqrt{v^2 + \left(\frac{f_{pc}}{2}\right)^2} \qquad (26)$$

Solving for v, which is the web-shear cracking stress, v_{cw}, yields

$$v_{cw} = f_t \sqrt{1 + \frac{f_{pc}}{f_t}} \qquad (27)$$

where f_{pc} is positive if in compression and is calculated using the full effective prestress force at a given section. Tests had shown that f_t is equal to $4\sqrt{f'_c}$. However, because v_{cw} is a nominal stress, ACI Committee 318 elected to equate f_t to $3.5\sqrt{f'_c}$. Thus, Eq. (27) becomes

$$v_{cw} = 3.5\sqrt{f'_c}\sqrt{1 + \frac{f_{pc}}{3.5\sqrt{f'_c}}} \qquad (28)$$

Because the plot of $f_{pc}/\sqrt{f'_c}$ versus $v_{cw}/\sqrt{f'_c}$ is approximately linear, Eq. (28) can be further simplified such that

$$v_{cw} = 3.5\sqrt{f'_c} + 0.3f_{pc} \qquad (29)$$

Because the nominal shear stress in the web is defined as

$$v_{cw} = \frac{V_{cw} - V_p}{b_w d} \qquad (30)$$

where V_p is the vertical force component of harped prestress tendons, the diagonal cracking strength in the beam web can be calculated as

$$V_{cw} = \left(3.5\sqrt{f'_c\ (\text{psi})} + 0.3f_{pc}\right) b_w d + V_p \qquad (31)$$

Because the first diagonal tension crack tends to occur at mid-depth of the web close to the support, the actual value for f_{pc} at mid-depth is typically lower than the calculated f_{pc}, which is computed at the centroid using the effective prestress force, f_{pe} (for a composite section, f_{pc} is calculated at the centroid of the composite section using both f_{pe} and the stress due to the dead load acting on the beam by itself). Nevertheless, tests had shown that the calculated V_{cw} is conservative, indicating that either the principal tensile strength, f_t, assumed in Eq. (27) is actually greater than $4\sqrt{f'_c}$ or that shear forces are being carried in the flanges, or both (*61*).

Previous testing had shown that the ACI model tends to be conservative; however, as f_c increases, the level of conservatism for the web-shear cracking loads increases, yet decreases for the flexural-shear cracking loads. The reason behind the increase in the test-to-predicted ratio for web-shear failure may stem from the average tensile strength being proportional to $f_c^{0.73}$, as Carino and Lew concluded for normal weight concrete up to 10 ksi compressive strength (*62*), not $f_c^{0.5}$ as implied by ACI. Furthermore, Elzanaty et al. (*35*) reasoned that as f_c increases in beams with the same amount of prestressing force, the ratio of the principal compressive force to uniaxial compressive strength, f_2 / f_c, decreases. This decrease would then result in a larger tensile splitting strength that ACI does not account for. On the other hand, the ratio of the test-to-predicted strength in flexure-shear decreases because ACI assumes that the load needed to transform a flexure crack into a diagonal crack remains constant. However, as f_c increases, aggregate interlock in normal weight concrete decreases due to the smoother surface along the fracture interface. The lower aggregate interlock resistance requires the uncracked compressive concrete zone to carry more load, resulting in higher stresses at the tip of the flexure-shear crack underneath the compressive zone (*35*).

Of course, relatively short spans or deep sections tend to have arching action, which increases the beam's ability to carry larger loads. However, Elzanaty et al. also found that the ratio of test-to-predicted values for both V_{cw} and V_{ci} decreases with an increase in *a/d*. With regards to V_{cw}, ACI considers the principal tensile stress at the centroid of the cross-section, which remains constant when varying *a/d*. However, the critical stress is typically at the web-bottom flange intersection, where an increase in *a/d* results in larger moments accompanied by greater tensile stresses. Therefore, the load to cause cracking in the web decreases as *a*/*d* increases, thus decreasing the experimental-to-theoretical shear strength ratio. The same effect occurs with V_{ci}, except that the moment in the flexure-shear region tends to be even greater. Therefore, there can be a shift in the neutral axis, meaning that the tension at the tip of a crack will be higher, enhancing the crack's development into an inclined one.

Regardless of whether V_{cw} or V_{ci} controls, Elzanaty et al. found that, for all beams with or without stirrups, the experimental concrete contribution to shear strength is proportional to f_c, instead of $\sqrt{f_c}$, as assumed under ACI 318. Therefore, the test-to-predicted ratio of the overall shear strength increases as the compressive strength increases.

In addition to V_{ci} and V_{cw}, ACI instituted one additional limitation for prestressed sections where the effective prestress force is at least 40% of the tensile strength of the flexural reinforcement. If such is the case, then

$$2\sqrt{f'_c\,(\text{psi})}\,b_w d \;\le\; V_c = \left(0.6\sqrt{f'_c\,(\text{psi})} + 700\frac{V_u d}{M_u}\right) b_w d \;\le\; 5\sqrt{f'_c\,(\text{psi})}\,b_w d \qquad (32)$$

where

$$\frac{V_u d}{M_u} \le 1.0$$

2.2.4.3 Reprised V_{ci} / V_{cw}

Up to and including the 1977 AASHTO Standard Specifications, AASHTO had a single equation for the concrete contribution to shear strength in prestressed concrete that was based on f'_c instead of $\sqrt{f'_c}$. AASHTO did not adopt the V_{ci} / V_{cw} methodology until the 13th edition of its

Standard Specifications for Highway Bridges (*63*), twenty years after ACI initially endorsed the concept. AASHTO's first formulas for these concrete contributions were basically the same as those published by ACI in 1971. Still, there had been debate regarding the level of accuracy that the V_{ci} / V_{cw} equations provided in matching the true behavior of actual concrete bridge girders. Therefore, Hawkins et al. conducted a study for the National Cooperative Highway Reserch Program (NCHRP), which also sought to unify the equations for both mild and prestressing steel (*59*). The modified formulations for V_{ci} and V_{cw} are stipulated in Article 5.8.3.4.3 of the 2010 AASHTO LRFD Bridge Design Specifications, and henceforth denoted as the *Simplified Procedure*.

2.2.4.3.1 Modified V_{ci}

In developing a new expression for V_{ci}, Hawkins et al. recognized that there are many factors in the concrete contribution to shear resistance. Because multiple components make determining a decisive diagonal cracking load complicated, the authors decided to take a lower bound estimate of that load. The resulting equation in the AASHTO LRFD Bridge Design Specifications, Eq. 5.8.3.4.3-1, is

$$V_{ci} = 0.02\sqrt{f'_c\ (\text{ksi})}\,b_v d_v + V_d + \frac{V_i M_{cre}}{M_{max}} \geq 0.06\sqrt{f'_c\ (\text{ksi})}\,b_v d_v \ (\text{kip}) \qquad (33)$$

where M_{cre} is slightly different from ACI's version of M_{cre} in Eq. (23) and is defined in Eq. 5.8.3.4.3-2 of the AASHTO LRFD Bridge Design Specifications as:

$$M_{cre} = S_c \left(f_r + f_{cpe} - \frac{M_{dnc}}{S_{nc}} \right) \qquad (34)$$

where

S_c = composite section modulus for the extreme fiber where externally applied loads cause tensile stress,

f_r = modulus of rupture, as determined in Section 5.4.2.6 of the AASHTO LRFD Bridge Design Specifications

f_{cpe} = stress in the concrete due to the effective prestressing force, at the extreme fiber location where externally applied loads cause tensile stress,

M_{dnc} = total unfactored dead load moment acting on the monolithic or non-composite section,

S_{nc} = monolithic or non-composite section modulus for the extreme fiber where externally applied loads cause tensile stress.

When converting to psi units, the coefficients 0.02 and 0.06 in Eq. (33) become 0.632 and 1.9, respectively. These values for the psi units compare to 0.6 and 1.7 in Eq. (22), which are not very different when considering $d_v = 0.9d$.

2.2.4.3.2 Modified V_{cw}

With regards to web-shear strength, Hawkins et al. recommended revising V_{cw} such that the result is more consistent with the ultimate state according to the crack model with the friction concept. As done originally in Eq. (27), the researchers derived v_{cw} using Mohr's circle such that

$$v_{cw} = f_t \sqrt{1 + \frac{f_{pc}}{f_t}}$$

However, the authors suggested that f_t could vary between $0.06\sqrt{f'_c}$ and $0.13\sqrt{f'_c}$, where f'_c is in ksi units. The lower bound is for beams with no or relatively low amounts of prestress, while the upper bound applies to fully prestressed sections. Therefore, the 2010 AASHTO LRFD Bridge Design Specifications formulation for the new V_{cw} is

$$V_{cw} = \left(0.06\sqrt{f'_c\ (\text{ksi})} + 0.3f_{pc}\right) b_v d_v + V_p \qquad \textbf{(35)}$$

If expressed in psi units, the coefficient 0.06 becomes 1.9, which compares to 3.5 in Eq. (31).

The reinstatement of V_{ci} and V_{cw} provides a means for assessing the probability of cracking under service loads, differentiating between the two types of cracking that will occur, as well as rating capacities of in-services girders (*59, 61*). From this point, the concrete contribution to shear resistance, V_c, is the lesser of V_{ci} and V_{cw}.

2.2.4.4 Designing for Shear Reinforcement Using V_{ci} / V_{cw}

Having determined the concrete contribution to shear strength, the engineer can then calculate the demand from the transverse reinforcement as:

$$V_s = \frac{V_u}{\phi} - V_c \qquad (36)$$

where ϕ is the strength reduction factor dictated in Article 5.5.4.2 of the 2010 AASHTO LRFD Bridge Design Specifications. The area of steel needed to provide V_s can be calculated from Eq. 5.8.3.3-4 of the AASHTO code:

$$V_s = \frac{A_v f_{yv} d_v (\cot\theta + \cot\alpha)\sin\alpha}{s} \qquad (37)$$

where

d_v = effective shear depth, taken as the distance between the resultant compressive and tensile forces due to flexure, but need not be less than $0.9d_e$ or $0.72h$

θ = the angle of shear cracking

where h is the overall depth of the composite cross-section and d_e is calculated as

$$d_e = \frac{A_{ps} f_{ps} d_p + A_s f_y d_s}{A_{ps} f_{ps} + A_s f_y}$$

where

A_{ps} = area of the prestressing steel

f_{ps} = average stress in the prestressing steel

d_s = distance from extreme compression fiber to the centroid of the nonprestressed tensile reinforcement.

Hawkins et al. indicated that θ in Eq. (37) could still be calculated using Mohr's circle in Figure 2-2:

$$\cot\theta = \sqrt{1 + \frac{f_{pc}}{f_t}} \qquad (38)$$

In predicting θ in their research on high-strength concrete girders, Hawkins and Kuchma (*61*) assumed f_t to be $4\sqrt{f'_c}$ and used the full effective prestress stress f_{pc}. The authors calculated θ in the first design region, which is approximately the section in between the distance d from the support and the point where the cracking transitions from web-shear to flexure-shear cracking. The analysis showed that the angle predicted by Eq. (38) is fairly close to the experimental cracking angle. Nevertheless, the AASHTO LRFD Bridge Design Specifications modified that calculation somewhat, depending on V_{ci} and V_{cw}. If $V_{ci} < V_{cw}$, then cotθ = 1.0. Otherwise,

$$\cot\theta = 1.0 + 3\left(\frac{f_{pc}}{\sqrt{f'_c}}\right) \leq 1.8 \qquad (39)$$

where f'_c is in ksi. Besides the debate over the concrete contribution to shear capacity, there is a small discrepancy in determining the shear reinforcement's contribution. While most models agree with ACI and AASHTO that cracks will intersect a certain number of stirrups based on the angle of inclination of the crack, other researchers have proposed that instead of crossing stirrups, cracks run from the top of one stirrup to the base of another. According to this theory, therefore, the number of stirrups contributing to the shear strength should be calculated as (*64*):

$$\frac{d_v \cot\theta}{s} - 1 \qquad (40)$$

There is one additional note regarding when shear reinforcement needs to be provided. At any point where

$$V_u > 0.5\phi\left(V_c + V_p\right) \text{ [2010 AASHTO LRFD Specifications]}$$

$$V_u > 0.5\phi V_c \text{ [ACI 318-11]}$$

then at least a minimum area of transverse reinforcement must be provided, as discussed in Section 2.2.7.

2.2.5 Sectional Design Model

Test results had essentially shown that the ACI equations are conservative for high-strength concrete, although the degree of safety depends on parameters such as f_c, a/d, P_e and the shear reinforcing index, $\rho_v f_{yv}$ (*36, 59*). Therefore, some academics began supporting the Sectional Design Model (SDM), which has evolved over a series of projects by Mitchell and Collins (*65*), Collins (*66*), Collins and Mitchell (*67, 68*), Vecchio and Collins (*69-71*), and Collins et al. (*72*). Ultimately, SDM is based on the Modified Compression Field Theory (MCFT), which was derived to capture the load-deformation response of diagonally cracked concrete subjected to normal and in-plane shear stresses (*45*).

2.2.5.1 Development of the Sectional Design Model (SDM)

2.2.5.1.1 Compression Field Theory

By 1964, researchers were proposing a variable angle truss model that included a concrete contribution (*73*). In the variable angle truss model, a beam subjected to a load has cracks that form at a fairly consistent angle of inclination except at the support and at the point load, or in the case of a uniformly distributed load, near mid-span. At those locations, the cracks converge, thus forming a "fan" pattern. If the length of the stirrup is approximated as d_v, and the cracking angle is defined as θ, then the horizontal projection of a given crack would be $d_v \cot\theta$ (*76*).

Despite its advances, the variable angle truss model does not include dowel action in the longitudinal reinforcement, aggregate interlock, or shear carried across uncracked concrete. Furthermore, the allowable stress in the diagonal compression struts is limited to a fraction of the concrete cylinder compressive strength. In attempting to establish a more rational procedure that overcame the shortcomings of the truss models, Mitchell and Collins (*65*) put forth their diagonal compression field theory (CFT) in 1974. This theory satisfies both equilibrium and compatibility requirements, yet still assumes that the concrete can carry no tension after cracking. Instead, the vertical steel in the beam transmits all of the shear.

CFT divides a section into horizontal layers, and within each layer, assumes that the longitudinal strain, normal shear stresses, and angle of inclination of principal stresses, θ, are constant, and that the principal stresses and the principal strains align in the same direction. Therefore, the principle compressive stress in the concrete can be related to the principle compressive strain by the formulation

$$f_2 = f_{2max}\left|2\left(\frac{\varepsilon_2}{\varepsilon'_c}\right) - \left(\frac{\varepsilon_2}{\varepsilon'_c}\right)^2\right| \qquad (41)$$

where

$$\frac{f_{2max}}{f'_c} = \frac{1}{0.8 - 0.34\frac{\varepsilon_t}{\varepsilon'_c}} \leq 1.0 \qquad (42)$$

and

f_{2max} = the diagonal crushing strength of the concrete.

f'_c = the maximum stress observed in a cylinder compressive test (negative quantity)

ε'_c = the strain associated with f'_c (negative quantity)

ε_t = the tensile strain

ε_2 = the principal compressive strain

If ε_t is defined as ε_1 and ε'_c is assumed to be –0.002, then Eq. (42) becomes

$$f_{2max} = \frac{f'_c}{0.8 + 170\varepsilon_1} \leq f'_c \qquad (43)$$

Eqs. (41) and (43) introduce the concept of concrete softening, where the compressive strength will decrease as the concrete is subjected to increasing tensile strains in the orthogonal direction. Because the largest crushing strength for concrete, f_{2max}, is related to ε_1, then a concrete beam that is severely cracked has a reduced ability in resisting any diagonal compressive forces.

If assuming that there are no tensile stresses, then the principle compressive stress in the concrete can be related to the shear stress using Mohr's circle, resulting in the equation

$$f_2 = \left(\tan\theta + \frac{1}{\tan\theta}\right)\frac{V_f}{b_v d_v}$$

where V_f is the factored shear force at a given section. Compatibility requires the principle tensile and compressive strains, ε_1 and ε_2, respectively, along with the longitudinal strain at mid-depth, ε_x, to be interrelated with θ. Thus,

$$\varepsilon_1 = \frac{\varepsilon_x + (\varepsilon_x + \varepsilon_2)}{\tan^2\theta}$$

where ε_2 is assumed to be 0.002.

Mitchell and Collins' theory continued with the premise that shear forces in the section are resisted by the vertical component of the diagonal compressive stress in the struts. Thus, the horizontal component of that diagonal stress must then be countered by a tensile force, which is carried by the longitudinal reinforcement. If the shear force is V_f, then the resulting force carried by the longitudinal reinforcement, N_v, would be

$$N_v = \frac{V_f}{\tan\theta}$$

The authors suggested selecting the smallest θ possible to minimize the amount of vertical reinforcement, thus making the beam more economical. Also, values for ε_x lower than 0.002 are possible if the section has high axial compressive forces, low moments, or relatively large amounts of longitudinal reinforcement because such a section is stiffer and would be able to withstand higher shear stresses. Of course, the ultimate goal is to select a combination of θ and ε_x such that the concrete does not crush prematurely and the vertical steel yields prior to failure. However, this requires a laborious iteration process. Furthermore, dividing a given section into multiple layers would require a tremendous amount of computing time. However, Mitchell and Collins indicated that the engineer could assume that the conditions at mid-depth of the beam are applicable to the entire beam depth, including the assumptions of constant shear stress and θ at that section.

2.2.5.1.2 Modified Compression Field Theory

Out of CFT evolved Vecchio and Collins' MCFT (*70*), which retains equilibrium and compatibility principles, as well as the constitutive properties that have been established using average stresses and strains. The major difference between the two theories is that the modified version takes into account the tensile stresses in the concrete that exist between the cracks, as well as the local stress conditions at the crack interface. The authors figured that although concrete may not carry tension across a crack, the material can transmit shear and compression where the two surfaces of the crack are in contact with each other. Additionally, under progressive loads, new cracks would form in the concrete, and existing cracks could either close or propagate further. However, the authors acknowledged that cracked concrete is "weaker" in compression when subjected to tensile strain in the direction normal to the compressive strain, as compared to concrete subjected to uniaxial compression.

So, to develop their theory, the researchers made a handful of assumptions:

- there is one and only one stress state for each corresponding strain state,
- stress and strain could be averaged when taken over an area that includes several cracks,
- no slip occurrs between the concrete and the steel reinforcement, hence allowing for compatibility,
- the reinforcement is evenly distributed in both the longitudinal and transverse directions,
- the axial stress in the reinforcement only depends on the axial strain in that reinforcement,
- the reinforcement does not provide any resistance to shear stresses on the plane normal to the reinforcement,
- plane sections remain plane.

From compatibility and Mohr's circle, shown in Figure 2-3, Vecchio and Collins developed several relationships for average strain:

$$\gamma_{xy} = \frac{2(\varepsilon_x - \varepsilon_2)}{\tan\theta}$$

$$\varepsilon_x + \varepsilon_y = \varepsilon_1 + \varepsilon_2$$

$$\tan^2\theta = \frac{\varepsilon_x - \varepsilon_2}{\varepsilon_y - \varepsilon_2} = \frac{\varepsilon_1 - \varepsilon_y}{\varepsilon_1 - \varepsilon_x} = \frac{\varepsilon_1 - \varepsilon_y}{\varepsilon_y - \varepsilon_2} = \frac{\varepsilon_x - \varepsilon_2}{\varepsilon_1 - \varepsilon_x}$$

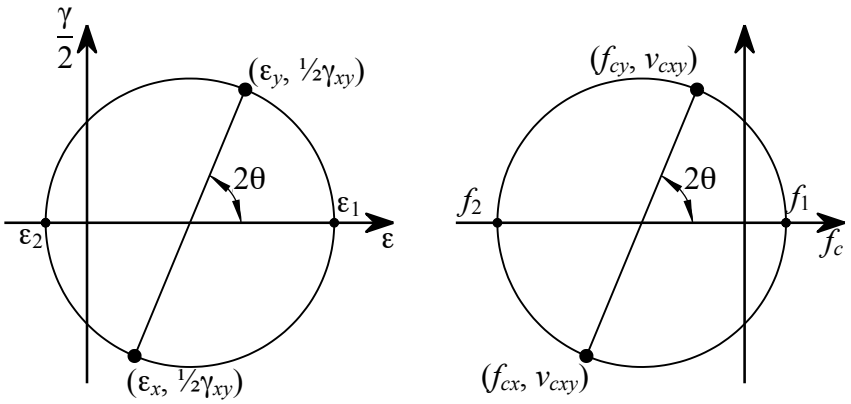

(a) average strains **(b) average stresses**

Figure 2-3. Mohr's circle depicting (a) average strains and (b) average stresses.

where

γ_{xy} = the shear strain relative to the *x*- and *y*-axis

ε_x, ε_y = the strain in the *x*- and *y*-axis, respectively

Likewise, the authors used equilibrium and Mohr's circle to formulate several average stress equations:

$$f_x = f_{cx} + \rho_{sx} f_{sx} \quad (44)$$

$$f_y = f_{cy} + \rho_{sy} f_{sy} \quad (45)$$

$$f_{cx} = f_1 - \frac{v_{cxy}}{\tan\theta}$$

$$f_{cy} = f_1 - v_{cxy} \tan\theta$$

where

f_x, f_y = the stress applied to the element in the *x*- and *y*-direction, respectively

f_{cx}, f_{cy} = stress in the concrete in the *x*- and *y*-direction, respectively

ρ_{sx}, ρ_{sy} = the reinforcement ratio in the *x*- and *y*-direction, respectively

f_{sx}, f_{sy} = the average stress in the *x*- and *y*-reinforcement, respectively

f_1 = the principal tensile stress in the concrete

v_{cxy} = shear strain in the concrete relative to the *x*- and *y*-axis

θ = the angle of inclination of principal stresses in the concrete, relative to the *x*-axis; assumed to equal the cracking angle.

To link the average stresses with the average strains, the researchers used constitutive relationships found from experiments of thirty concrete square panels. Using measured strains concurrent with known applied stresses, the researchers determined the average stresses in the reinforcement. From Eqs. (44) and (45), the authors calculated the average stresses in the concrete using the stresses in the reinforcement and the applied stresses. Having this information, the researchers created stress circles and strain circles for the concrete at each load stage, and then correlated the two sets of circles to come up with the constitutive relationships between the principal stresses and strains.

Prior to cracking, if the concrete is in tension, then the principal tensile stress in the concrete, f_1, is:

$$f_1 = E_c \varepsilon_1$$

where

$$E_c = \frac{2f'_c}{\varepsilon'_c}$$

Immediately after cracking, Collins et al. (*72*) suggested that the relationship between the principal tensile stress and the principal tensile strain is:

$$f_1 = \frac{f_{cr}}{1 + \sqrt{500\varepsilon_1}} \qquad \textbf{(46)}$$

where f_{cr} is assumed to be $0.13\sqrt{f'_c}$ (in ksi). Although the constitutive equations for both the concrete and the steel are not necessarily independent of each other, Vecchio and Collins (*71*) assumed as much to maintain simplicity in the model. In addition, the researchers assumed that the axes for the principal stress and principal strain have the same angle of rotation, θ. While not completely accurate, the authors deemed this assumption to be reasonable. With regards to the steel reinforcement, the authors assumed a bilinear stress-strain relationship.

Unfortunately, the above derivations do not take into account the effect of local stresses at the cracks. At a crack, the stress in the reinforcement should be higher and the stress in the concrete

should be zero compared to a location in between cracks, where the reinforcement stress will be lower and the concrete stress will be higher. Therefore, Vecchio and Collins considered two planes in a concrete element, one which is parallel to a crack but located in an uncracked area of concrete, and the other which is on the crack surface, as seen in Figure 2-4. The first plane, Figure 2-4(a), contains average stresses, while the second plane, Figure 2-4(b), contains local stresses. There are no average shear stresses along the first plane, but there are local shear stresses, v_{ci}, accompanied by small local compressive stresses, f_{ci}, on the second plane.

Because these two stress states are statically equivalent, any loss of tensile stress in the concrete at the crack interface must be compensated by the steel reinforcement or an increase in the interface shear stress, where the interface shear strength capacity will be limited by the width of the crack. Furthermore, the change in interface shear stress will necessitate a change in the angle of the principle stresses at the crack (*72*). Given that the external forces are the same for the two planes, the average principal stresses on the first plane must equal the local stresses on the second plane. Therefore, for the *x*-direction,

$$\rho_{sx} f_{sx} \sin\theta + f_1 \sin\theta = \rho_{sx} f_{sxcr} \sin\theta - f_{ci} \sin\theta - v_{ci} \cos\theta \qquad (47)$$

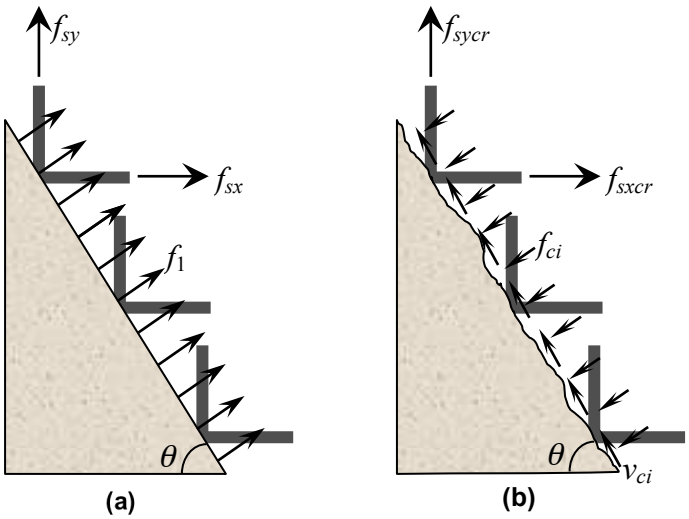

Figure 2-4. Comparison of (a) average stresses in uncracked concrete versus (b) local stresses at a crack. Note that f_{sxcr} and f_{sycr} are the stresses at the crack location in the *x*- and *y*-reinforcement, respectively.

Eq. (47) can be rearranged such that

$$\rho_{sx}\left(f_{sxcr} - f_{sx}\right) = f_1 + f_{ci} + \frac{v_{ci}}{\tan\theta} \qquad (48)$$

If one were to assume that there are no compressive or shear stresses on the crack, then

$$\rho_{sx}\left(f_{sxcr} - f_{sx}\right) = f_1 \qquad (49)$$

However, if the stress in the steel can not be greater than the yield stress, and if the average stress in the steel in the *x*-direction, f_{sx}, are large, then finding a solution for Eq. (49) may be impossible. A similar conclusion could be reached for the reinforcement in the y-direction. Therefore, Vecchio and Collins concluded that there must be shear stresses present at the crack. Using work by Walraven (*33*), the researchers determined that the relationship between v_{ci} and f_{ci} is:

$$v_{ci} = 0.18 v_{ci_{max}} + 1.64 f_{ci} - 0.82 \frac{f_{ci}^{\,2}}{v_{ci_{max}}} \qquad (50)$$

where

$$v_{ci_{max}} = \frac{0.38\sqrt{-f'_c\ (\text{ksi})}}{0.31 + \dfrac{24w}{a + 0.63}}$$

where *w* is the crack width and *a* is the maximum aggregate size, both in inches. The researchers simplified Eq. (50) by keeping only the first term of that equation. Therefore,

$$v_{ci} = \frac{0.068\sqrt{f'_c\ (\text{ksi})}}{0.3 + \dfrac{24w}{a + 0.63}} \qquad (51)$$

Note that f'_c in Eq. (51) is taken as a positive value in compression. Collins et al. suggested that as the cracks widen, f_1 would no longer follow Eq. (46). Instead, the cracks may begin to slip after the shear reinforcement yields. Thus, the principal tensile stress would be limited to

$$f_1 = v_{ci} \tan\theta \quad (52)$$

2.2.5.2 Designing with the Sectional Design Model Tables

Vecchio and Collins acknowledged that MCFT is iterative and can become a cumbersome process. Nevertheless, MCFT allows for a varying θ, strain softening of concrete in tension, as well as the stiffening effect of concrete in compression. As with CFT, the procedure for MCFT analysis includes dividing the beam into relatively short segments, with each segment then being divided into thin horizontal layers. Each segment/layer satisfies compatibility and equilibrium requirements. Therefore, the longitudinal strain along the depth of the section can be assumed as a linear interpolation between strains in the top and bottom fibers of the beam. For equilibrium, each segment needs to be balanced amongst the shear, bending and axial loads acting on the section. Additionally, each layer has to be balanced with the adjacent layers, meaning that the horizontal shear forces that exist between each layer of a section need to be in equilibrium.

Fortunately, Vecchio and Collins did offer a few additional assumptions that can be made to simplify the calculations. One is to assume that the shear flow distribution is fairly constant in between the top and bottom reinforcement. This approximation would lead to a slightly conservative strength calculation due to overestimating the shear stress in the tension region. An alternative would be to assume that the shear strain through the depth of the member follows a parabolic distribution. This approximation would give unconservative results because the assumption would overestimate the shear stress in the compression region. The authors acknowledged that the earlier assumption of plane sections remaining plane would result in underestimating the shear capacity when much of the force transfer from the load to the supports is due to direct strut action, because the plane section assumption does not account for any beneficial transverse compressive stresses arising in local zones. Otherwise, the researchers surmised that either of two alternative approximations would give fairly accurate results, particularly in regions of low flexural and axial loads.

In adopting MCFT, AASHTO made some additional simplifying assumptions. SDM deems that the shear stresses are uniformly distributed over the shear depth of the beam, and that the angle of rotation to the principal compressive stress is constant over that effective shear depth. Also,

SDM assumes that the shear strength of a given beam section could be calculated using the state of biaxial stress at a single point in the girder web (*45*).

To begin an analysis using MCFT, the designer needs to start with estimates for the longitudinal strain profile, the shear stress distribution through the depth of each section, as well as the angle of rotation to the principal stresses, θ. If the resulting shear strength agrees with the strength from the initial assumed stress distribution, then the engineer would have a satisfactory solution. However, such an agreement typically is not achieved until after multiple iterations, which can be a time-consuming process, especially in light of the need to reach a solution for each horizontal layer in each beam section (*71*).

As a starting point, Collins et al. (*72*) suggested using the largest longitudinal tensile strain, ε_x, to calculate the principal tensile strain, ε_1. Because ε_x is taken at the bottom flexural reinforcement, ε_x can be calculated from statics:

$$\varepsilon_x = \frac{\frac{|M_u|}{d_v} + 0.5N_u + 0.5|V_u - V_p|\cot\theta - A_{ps}f_{po}}{E_sA_s + E_{ps}A_{ps}} \quad (53)$$

where

N_u = the factored axial force in the member, where tension is taken as positive

f_{po} = a parameter calculated as E_{ps} multiplied by the locked-in difference in strain between the prestressing tendons and the surrounding concrete, in units of ksi; for typical levels of prestressing, a value of 0.7 f_{pu} is used for this parameter.

E_{ps} = the modulus of elasticity of the prestressing tendons, assumed to be 28,500 ksi

E_s = the modulus of elasticity of the mild reinforcement, assumed to be 29,000 ksi

Note that the initial value for ε_x should not be greater than 0.002. On the other hand, if ε_x from Eq. (53) is negative (i.e., compressive), then the longitudinal strain should be calculated as

$$\varepsilon_x = \frac{\frac{|M_u|}{d_v} + 0.5N_u + 0.5|V_u - V_p|\cot\theta - A_{ps}f_{po}}{E_cA_c + E_sA_s + E_{ps}A_{ps}} \quad (54)$$

where A_c is the area of concrete on the flexural tension side of the member as shown in Figure 5.8.3.4.2-1 of the AASHTO LRFD Bridge Design Specifications. Note that Eqs. (53) and (54) are divided by two in Appendix B5.2 of the AASHTO LRFD Bridge Design Specifications, because ε_x in the appendix is taken at mid-height of the web. From Mohr's circle in Figure 2-3, ε_1 can be calculated as

$$\varepsilon_1 = \varepsilon_x + (\varepsilon_x - \varepsilon_2)\cot^2\theta \quad (55)$$

From Eq. (41), ε_2 can be calculated as

$$\varepsilon_2 = \varepsilon'_c\left(1 - \sqrt{1 - \frac{f_2}{f_{2_{max}}}}\right) \quad (56)$$

where ε'_c can be taken as -0.002. If using the conservative assumption that the concrete could not withstand any tensile stresses, then the principal compressive stress, f_2, could also be found using Mohr's circle:

$$f_2 = v(\tan\theta + \cot\theta) \quad (57)$$

where

$$v = \frac{V_n - V_p}{b_v d_v} \quad (58)$$

Combining Eqs. (43) and (55) through (57) results in

$$\varepsilon_1 = \varepsilon_x + \left\{\varepsilon_x + 0.002\left[1 - \sqrt{1 - \frac{v}{f'_c}(\tan\theta + \cot\theta)(0.8 + 170\varepsilon_1)}\right]\right\}\cot^2\theta \quad (59)$$

Note that Eq. (59) contains ε_1 on both sides of the equation. Furthermore, the shear stress, v, depends on the nominal shear strength, V_n, in Eq. (58), which is comprised V_s and V_c. V_c is in turn directly related to the tensile stress in the concrete, f_1, such that

$$V_c = f_1 b_v d_v \cot\theta$$

where f_1 is defined in Eqs. (46) and (52), resulting in

$$V_c = \frac{0.13\sqrt{f'_c\,(\text{ksi})}}{1+\sqrt{500\varepsilon_1}} b_v d_v \cot\theta \le \frac{0.068\sqrt{f'_c\,(\text{ksi})}}{0.3+\frac{24w}{a+0.63}} b_v d_v \quad (60)$$

If β is defined as

$$\beta = \frac{4\cot\theta}{1+\sqrt{500\varepsilon_1}} \le \frac{2.16}{0.3+\frac{24w}{a+0.63}} \quad (61)$$

where β is a factor relating the effect of longitudinal strain to the ability of diagonally cracked concrete to transmit tension, then Eq. (60) can be simplified to

$$V_c = 0.0316\beta\sqrt{f'_c\,(\text{ksi})} b_v d_v \quad (62)$$

as written in Eq. 5.8.3.3-3 of the AASHTO LRFD Bridge Design Specifications (*45*). Note that the coefficient in front of β is for converting f'_c from psi units to ksi units, whereas the table for θ and β was originally created using psi units.

Nevertheless, Eqs. (60) through (62) make it clear that V_c is dependent on θ and ε_1, which are, in turn, partially dependent on V_c. As such, the engineer would need the aid of a computer to find a suitable and economical combination of θ and β. Therefore, Collins et al. devised a less rigorous solution using a table that listed these two variables as a function of the longitudinal strain, ε_x, and the shear stress, v. Although this table was formulated assuming a crack spacing of 12 in. and a nominal maximum aggregate size of ¾ in., the conclusion was that these assumptions would still give adequate results for the full range of designs if the beam contained the minimum amount of stirrups. For beams containing less than the minimum amount of required stirrups, Collins et al. provided a second table that the designer should use. Regardless, the tabular method typically still requires a number of iterations before arriving at an acceptable solution for V_c.

In addition to the complicated iterative process involved with finding β and θ using the table, there is some evidence that this method is inaccurate in predicting θ. Attempts to measure the concrete contribution to the shear strength requires knowing the angle of diagonal compression, which Hawkins et al. (*59*) indicated is not necessarily the same as the angle of diagonal cracking, especially near the end regions of the girder where large anchorage forces in the strands cause the angle of diagonal compression to be larger than the diagonal cracking. Still, other researchers suggested that the angle of diagonal compression is smaller than the angle of diagonal cracking because of the shear stress being transferred across the cracks.

Similar to their efforts discussed in Section 2.2.4.4, Hawkins and Kuchma compared the cotangent of the experimental cracking angles with the cotangent of the angles computed using the θ and β table. Assuming that the angle of diagonal compression and the angle of diagonal cracking are the same, the authors concluded that the predicted angle of web-shear cracks is typically smaller than the observed angle, resulting in unconservative predictions for V_s, described as:

$$V_s = \frac{V_u}{\phi} - V_c - V_p = \frac{A_v f_y}{s} d_v \cot\theta \qquad (63)$$

At any rate, Collins et al. recommended a five-step process for designing for shear at a given section:

(1) Calculate the shear stress, v, using Eq. (58) with an initially assumed V_n:

$$V_n = \frac{V_u}{\phi}$$

(2) Calculate the longitudinal strain, ε_x, using Eq. (53) with an initially assumed value for θ.

(3) Use the results from Steps (1) and (2) along with the provided table to find θ and β. A few iterations of Steps (2) and (3) may be required before reaching stable values for θ and β.

(4) Calculate the concrete contribution to the shear strength, V_c, using Eq. (62)

(5) For beams with vertical shear reinforcement, use Eq. (63) to find the amount of steel needed to meet the given shear demand.

Ultimately, the engineer will need to confirm that $\phi V_n \geq V_u$, where according to Eqs. 5.8.3.3-1 and 5.8.3.3-2 of the 2010 AASHTO LRFD Bridge Design Specifications, V_n is the lesser of

$$V_n = V_c + V_s + V_p \quad (64)$$

$$V_n = 0.25 f'_c b_v d_v + V_p \quad (65)$$

where Eq. (65) is designed so that the transverse reinforcement will yield prior to the concrete crushing in the web. V_p in the two equations above is determined by the effective prestress, the angle of the draped or harped tendons, the area of those strands, and the transfer length, where

$$V_p = f_{pe} A_{\text{harped strand}} \sin\theta_{\text{harped strand}} \quad (66)$$

or some fraction of Eq. (66) if the section is located less than the transfer length from the end of the beam.

2.2.5.3 Simplification of the Sectional Design Model

Despite the praise for the rationality behind SDM, as well as its flexibility in various applications, many engineers called into question the need for its complexity, including Shahawy and deV Batchelor (*74*), Ma et al. (*34, 75*), and Ma and Tadros (*41*). As discussed in Section 2.2.5.2, the complexity of the SDM shear calculations lies almost entirely in the calculation of V_c. Yet, most modern-day girders use thin webs; therefore, the effect of varying V_c is relatively small (*41*). In fact while V_c varied significantly amongst various design codes, the total cost of the beam associated with accommodating the concrete contribution varied only by about 1% (*34*).

In light of these findings, Hawkins et al. used the same *NCHRP Report 549* discussed in Section 2.2.4.3 to develop an alternative means of determining θ and β that are then used in the SDM. The results of this effort now appear in Article 5.8.3.4.2 of the 2010 AASHTO LRFD Bridge Design Specifications, henceforth labeled as the *General Procedure*. For both prestressed and non-prestressed girders containing at least the minimum reinforcement, the formulas for calculating θ and β are:

$$\beta = \frac{4.8}{1 + 750\varepsilon_s} \quad (67)$$

$$\theta = 29 + 3500\varepsilon_s \quad (68)$$

where ε_s is the net longitudinal tensile strain in the section at the centroid of the tension reinforcement and replaces ε_x in Eq. (53) such that

$$\varepsilon_s = \frac{\frac{|M_u|}{d_v} + 0.5N_u + 0.5|V_u - V_p| - A_{ps}f_{po}}{E_sA_s + E_pA_{ps}} \quad (69)$$

Note that Hawkins et al. derived Eq. (69) by assuming that $\theta = 30^o$ (*59*). Furthermore, like the tabular method for SDM, Hawkins et al. derived Eqs. (67) through (69) using MCFT. These equations mimic those formulas adopted in the 2004 Canadian Standards Association's *Design of Concrete Structures* (*CSA A23.3-04*) (*76*). Due to these formulations, Step (3) of the design process in Section 2.2.5.2 is no longer iterative, thus dramatically decreasing the computing time needed compared to using the tabular method, henceforth denoted as *Appendix B5* and presented in Appendix B5.2 of the AASHTO LRFD Bridge Design Specifications. However, the *General Procedure* still requires an iterative approach in shear analysis using SDM, because ε_s still depends on the shear capacity, and β and θ depend on ε_s (*59*).

If a member is not continuous nor is cast integrally with the support, and when the stress at the first critical section exceeds $0.18f'_c$, then Hawkins et al. suggested that the design of sections at the end of the beam follow the strut-and-tie approach. The reason for this suggestion is to avoid a diagonal compression failure in the critical section at a simple support.

The researchers used a subset of an available database to verify the effectiveness of the proposed changes. All beams in this subset have depths of at least 20 in., contain at least the minimum amount of shear reinforcement as prescribed by ACI, have a compressive strength of at least 4 ksi, and have been tested with a shear span-to-effective shear depth ratio of at least 1.7. Using this database, the authors found that tabular method for determining θ and β, presented in Appendix B5 of the 2010 AASHTO LRFD Bridge Design Specifications, and the *General*

Procedure had the best results for both reinforced concrete and prestressed concrete members, with mean V_{test}/V_{calc} values ranging from 1.1 to 1.24. While the *Simplified Procedure* was not as accurate, this modification of the AASHTO Standard Specifications proved to be more accurate than the original standard approach (*59*).

2.2.6 The Staggering Concept for Shear Reinforcement Design

The traditional approach to shear design involves dividing a beam into ten segments and then detailing the stirrups within a given segment using the design force that is at the end of the segment closest to the support (*45*). Collins et al. offered an alternative, albeit, slightly less conservative approach where beam segments could be of length $d_v\cot\theta$, because a shear failure resulting from yielding of the stirrups will have stirrups yielded along the length of that segment. However, when using segments of length $d_v\cot\theta$, the design force must be that force at the middle of the segment. As a simplification, Collins et al. indicated that the beam section could be d_v instead of $d_v\cot\theta$.

If the force is applied to the top of the girder, a third and even riskier option is the staggering concept, which Collins and Mitchell initially supported (*68*). The staggering concept is based on two assumptions, the first of which is the variable angle truss model mentioned in Section 2.2.5.1.1 . The second assumption is that the components in the beam follow the theory of plasticity, where the materials can deform freely and independently. Therefore, no forces transfer between the concrete compression struts and the vertical steel stirrups. Furthermore, the stress in each strut or stirrup must be uniform throughout the length of the element (*77*).

Using the two aforementioned assumptions, consider a uniformly-distributed load, w_u, on a beam that has a span, $l = 8d_v\cot\theta$, where again, d_v is the effective shear depth, and θ is the cracking angle. If the beam consists of 8 segments, then each segment would have a length of $d_v\cot\theta$. For the segment immediately to the left of mid-span, all of the diagonal compression struts that originate within that section would transfer a total force of $\frac{1}{8}w_u l$ from the top chord of that section down to the bottom chord of the adjacent section closest to the support. This flow of forces would mimic the arching action that occurs near the support, as originally proposed by Kani. The total force being transferred would be the same value as the shear force at the location

$d_v\cot\theta$ away from mid-span. The tension stirrups in this second segment would then uniformly transfer the force from the bottom of this second section to the top. However, due to the plasticity assumption, the stresses in all of the stirrups in this adjacent section would be the same. Thus, all of these stirrups could be designed for the same shear force located $d_v\cot\theta$ away from mid-span, i.e., $\frac{1}{8}w_u l$. Now, at the top of the second segment, there would an additional external force totaling $\frac{1}{8}w_u l$. Therefore, the diagonal compression struts originating in this second section would transfer a force equal to $\frac{1}{4}w_u l$. From there, the process would reiterate until reaching the support (*77*).

This staggering differs from the traditional concept of shear design in that the traditional design uses a triangular shear demand that merely follows the shear forces due to a distributed loading across the beam. On the other hand, the shear demand in the staggered concept is more of a "step" pattern. The problem with stepping the shear demand is that materials in reinforced concrete do not behave in a purely plastic fashion, particularly for uniformly loaded beams. Using equilibrium in an analysis, Hsu (*77*) showed that beams subjected to distributed loads have stirrups that vary in stress both vertically down the length of an individual stirrup as well as horizontally along the length of the beam. As would be the case for traditional design, the stirrups within a given section of staggered approach would have the same area, and the stirrups closest to the support in that particular section would see the highest stresses and yield first. However, the plasticity assumption in the materials dictates that the design load be set equal to the plastic load. Yet, plasticity within reinforced concrete is not guaranteed, so actual failure may occur prior to reaching the design load. Analysis by Hawkins and Kuchma (*61*) agreed with Hsu's conclusion.

Regardless of whether using the traditional approach for designing the transverse reinforcement, the staggering concept, or the force located at the middle of a given segment of a beam, the AASHTO LRFD Bridge Design Specifications dictate that the engineer must employ strut-and-tie modeling whenever the stress in the web of a top-loaded, simply supported beam exceeds $0.18f'_c$. The reason is that such conditions result in all of the load funneling down into the bearings, which could result in either localized diagonal compression in the web or horizontal shearing at the web-bottom flange interface.

2.2.7 Minimum Shear Reinforcement

As mentioned in Section 2.2.4.4, both the ACI code and the AASHTO LRFD Bridge Design Specifications require a minimum amount of vertical reinforcement when the shear demand in the steel exceeds a specified limit. The reasons for such minimum reinforcement are: to mitigate the formation of diagonal cracks at service loads, to provide reserve shear strength should the diagonal cracking load be exceeded, provide some degree of ductility against sudden shear failures, and to ensure that the stirrups yield prior to the concrete failing (*45, 61, 78*).

2.2.7.1 Research Regarding Minimum Reinforcement

2.2.7.1.1 Johnson and Ramirez

As discussed at the beginning of Section 2.2, one component of the concrete contribution to shear strength is aggregate interlock. However, as the compressive strength of concrete increases, the surface of the crack interface tends to become relatively smoother, thus reducing aggregate interlock and lowering the shear capacity upon cracking. For this reason, Johnson and Ramirez (*79*) examined a series of beams with rectangular cross-sections measuring 24 in. by 12 in. With the exception of one beam having none, the transverse reinforcement was spaced in such a manner that $\rho_v f_{yv}$ = 50 or 100 psi. The term ρ_v is defined as

$$\rho_v = \frac{A_v}{b_w s} \qquad (70)$$

Defining the reserve shear strength index as the ratio of the shear stress at failure, v_f, versus the shear stress carried by the concrete at first inclined cracking, v_c, the researchers found that the beam without any reinforcement failed in diagonal tension with v_f / v_c equal to 0.88. While most of the remaining beams containing a minimum amount of shear reinforcement of $\rho_v f_{yv}$ = 50 psi had reserve shear strength indices ranging from 1.24 to 1.35, there was one beam that failed almost immediately and only had a reserve strength index of 1.08. Additionally, there were two beams which had the same shear reinforcement ratio, but the beam with the greater compressive strength had a lower reserve shear strength index. The ratio of the experimental versus predicted shear strength, v_f / v_n, increased from 0.88 to 1.16 as the level of reinforcement increased from 0 psi to 100 psi, thus indicating that the ACI 318-83 code started out very unconservative but became conservative at higher levels of minimum reinforcement.

2.2.7.1.2 Roller and Russell

A year after Johnson and Ramirez, Roller and Russell (*80*) conducted two series of tests, with each series consisting of five beams designed according to ACI 318-83. The beams in the first series were 14 in. wide by 14 ft long and had a 22-in. effective depth; the *a/d* ratio was 2.5. The concrete compressive strength was about 17 ksi, and the amount of shear reinforcement varied from the minimum amount of steel, or

$$A_{v\,min} = 0.050 \frac{b_w s}{f_{yv}\,(\text{ksi})} \qquad (71)$$

to the maximum amount that can be assumed for shear capacity,

$$A_{v\,max} = 0.25\sqrt{f'_c\,(\text{ksi})} \frac{b_w s}{f_{yv}\,(\text{ksi})}$$

The second set of beams measured 18 in. wide by 16 ft long with an effective depth of 30 in., and *a/d* was 3.0. Two beams had f'_c of 10 ksi; the other three had f'_c of 18 ksi. These beams also varied in the amount of reinforcing steel, from the minimum amount in Eq. (71) to about three times that amount. All beams were designed to fail in shear under single-point loading at midspan under simply supported conditions.

Typically, the first diagonal tension crack was less than the calculated V_c, although the difference between the theoretical and the experimental load causing diagonal tension cracking decreased as the shear reinforcement increased. Three beams failed at a load less than the calculated V_n,; two contained the minimum amount of reinforcement, and in fact, failed at a load less than V_c, while the third had twice the amount required. These failures indicate that ACI overestimates V_c when the minimum amount of reinforcement is used. There were two sets of beams that had the same cross-sectional dimensions, same amount of reinforcement, and the same shear spans. The only difference within each set was f'_c, where the beams with the higher design compressive strength of about 18 ksi failed prior to the predicted failure load. These results suggest that minimum reinforcement requirements should be related to the compressive strength in some way. ACI

provisions (*81*) seem to take this into account by limiting $\sqrt{f'_c}$ to 100 psi unless additional shear reinforcement is included, and then by having $A_{v\,min}$ depend on $\sqrt{f'_c}$ (*82*).

2.2.7.1.3 Angelakos et al.

Angelakos et al. (*83*) also asked the question as to whether or not beams that contained the minimum amount of vertical reinforcement required by the ACI code would be safe. To answer this question, the authors tested six sets of paired beams with a rectangular cross-section measuring 39.4 in. deep by 11.8 in. wide, with a 17.75-ft span length. Within each set, one beam had near-minimum amounts of shear reinforcement, while the other beam had none. The amount of shear reinforcement for the six beams with transverse steel was equivalent to 58 psi. This reinforcement ratio was 16% more than the minimum requirement according to ACI 318-89 (*81*), which is calculated as

$$\frac{A_{v\,min} f_{yv}\ (\text{ksi})}{0.05 b_w s}$$

Amongst the six sets of beams, the compressive strength ranged from 3.0 to 11.6 ksi, while the longitudinal reinforcement ratio ranged from 0.50% to 2.09%. These twelve beams were also compared to nine beams from the Collins and Kuchma study (*84*) that were similar. All 21 beams were simply supported and loaded with a single point load at midspan.

Angelakos et al. found that there is very little effect of the concrete compressive strength on the shear failure load, although the roughness of the crack surface decreases as the compressive strength increases. While changing the compressive strength by a factor of 4 has little effect, increasing the longitudinal reinforcement ratio by roughly the same factor (from 0.50% to 2.09%) results in a 62% increase in the shear strength. As for the beams containing 16% more shear reinforcement than that required by ACI 318-89, none of the beams reached their predicted strengths, with the ratio of experimental versus calculated strength ranging from 0.68 to 0.92. Combining with the beams from the Collinis and Kuchma study, three of the 21 beams had less than half the shear capacity predicted by ACI 318-89.

2.2.7.1.4 Laskar et al.

As a part of their effort to develop an empirical formula for V_c and V_n, Laskar et al. (*85, 86*) conducted four tests where the transverse reinforcement ratio was 0.17%, which the researchers considered to be a minimum amount of reinforcement. The four beams were Texas Department of Transportation Type A prestressed beams that were 28-in. deep and had 24-ft span lengths. The concrete compressive strength ranged from about 9.4 ksi to 10.8 ksi. Each beam contained twelve ½-in. diameter, low-lax strands that had an ultimate strength of 270 ksi. All of the beams were subjected to two concentrated loads at the third points, resulting in two beams having a shear span-to-depth ratio of 1.61, while a/d for the other two was 4.29. One of these last two beams contained harped tendons.

Strains in the stirrups within the failure region were beyond yield at failure, with many stirrups going into strain hardening range. After some additional analysis, Laskar et al. concluded that, despite the changes made regarding minimum area of reinforcement, ACI 318-08 (*87*) was inadequate in terms of minimum vertical reinforcement requirements when a/d is between 2 and 4.

2.2.7.2 Minimum Shear Reinforcement Requirements for ACI

Even in the early days of its 318 code, ACI had a requirement pertaining to minimum reinforcement. The 318-56 code stipulated that a given beam had to have web reinforcement that was greater than or equal to 0.15% of the longitudinal area, which is calculated as the web width multiplied by the shear reinforcement spacing. Furthermore, the reinforcement spacing was limited such that every line extending from mid-depth to the depth of the longitudinal reinforcement at a 45^o angle had to be intersected by at least one stirrup. If the design stress was greater than $0.06f_c'$, then the required number of steel reinforcement crossing that theoretical crack doubled. By 1963, this stress limit requiring at least two lines of reinforcement was changed to $3\sqrt{f'_c}$. However, before 1971, all of these aforementioned requirements only needed to be met if the design shear stress exceeded the shear strength of the concrete, v_c.

The current minimum reinforcement requirements are much the same as they have been since 1971, where such reinforcement is needed whenever

$$V_u > 0.5\phi V_c \tag{72}$$

Furthermore, the calculation for the minimum area of reinforcement is:

$$A_{v\,min} = 0.024\sqrt{f'_c\ (\text{ksi})}\frac{b_w s}{f_{yv}} \geq 0.05\frac{b_w s}{f_{yv}\ (\text{ksi})} \tag{73}$$

where $A_{v\,min}$ is in units of in^2. Note that the first half of Eq. (73) was instituted in 2008. For prestressed applications where the effective prestress in the longitudinal reinforcement is at least 40% of its ultimate tensile strength, f_{pu}, then:

$$A_{v\,min} = \frac{A_{ps}}{80}\frac{f_{pu}}{f_{yv}}\frac{s}{d}\sqrt{\frac{d}{b_w}} \tag{74}$$

Furthermore, the maximum allowable spacing of the stirrups in non-prestress members is $0.5d \leq$ 24 in., and for prestressed members, $0.75h \leq 24$ in., where h is the overall depth of the member. However, if

$$V_s > 0.13\sqrt{f'_c\ (\text{ksi})}b_w d \tag{75}$$

then that spacing maximum is reduced by half. Note that according to ACI 318-11, Article 11.1.2, $\sqrt{f'_c}$ shall not exceed 0.100 ksi in Eqs. (73) and (75).

2.2.7.3 Minimum Shear Reinforcement Requirements for AASHTO

While ACI had begun instituting minimum reinforcement requirements by 1956, AASHTO did not do so until its 1969 Standard Specifications (*88*). Even then, the limits were only in terms of the maximum limit on stirrup spacing, s_{max}, which was $0.5d$ for vertical stirrups and $0.75d$ in the direction of the longitudinal axis if the stirrups were bent at an angle between 20^o and 45^o from the longitudinal axis. However, if the vertical stirrups were not required to carry shear forces, then that maximum spacing was $0.75d$, regardless of the orientation of the reinforcement. For

prestressed concrete, the maximum spacing was 0.75h. All of these limits applied to situations where the applied shear stress was greater than the design strength of the concrete.

Six years later, AASHTO (*58*) did call for a minimum area of reinforcement in reinforced concrete that was equivalent to the minimum instituted by ACI in 1956, that is:

$$A_{v\,min} = 0.0015 b_w s$$

For prestressed concrete, the minimum area was

$$A_{v\,min} = \frac{100 b' s}{f_{yv}}$$

where b' is the width of the web of a flanged member and f_{yv} is limited to 60 ksi. However, these minimums only applied to the Load Factor Design (LFD) methodology. Likewise, the stirrup spacing limitations were slightly different than under Allowable Stress Design (ASD), where

$$s_{max} = \frac{d}{2} \leq 24 \text{ in.} \qquad (76)$$

If the design shear stress, v_u, exceeded $6\phi\sqrt{f'_c}$, then the maximum spacing indicated in Eq. (76) was reduced by a half. For stirrups that were constructed at an angle, the only requirement was that every imaginary line at a 45^o angle to the horizontal be crossed by at least a single stirrup. Again, these limitations in the 1973 Specifications applied to cases where $v_u > v_c$.

In 1977, there were a number of significant changes to the minimum reinforcement requirements that remained in place through the printing of the last AASHTO Standard Specifications in 2002 (*89, 90*). First, a minimum amount of shear reinforcement was required whenever the design shear stress exceeded half of the allowable shear stress in the concrete. Secondly, the minimum area of transverse reinforcement was

$$A_{v\,min} = 0.05 \frac{b_w s}{f_{yv}\,(\text{ksi})} \qquad (77)$$

If using prestressed concrete, then

$$A_{v\,min} = 0.1\frac{b_w s}{f_{yv}\,(\text{ksi})} \qquad (78)$$

where f_{yv} was limited to 60 ksi. As for the maximum stirrup spacing, the limits remained the same as in the 1973 specifications, except that spacing was then reduced by half if the shear stress in the stirrups exceeded $2\sqrt{f'_c}$. If using LFD to design prestressed beams, that spacing only needed 50% reduction if the stress in the steel exceeded $4\sqrt{f'_c}$.

The introduction of LRFD into shear design in 1994 brought about another major shift in minimum shear reinforcement requirements, which increased the amount of steel compared to the AASHTO Standard Specifications (*91*). By unifying the design code for both non-prestressed and prestressed members, a minimum amount of shear reinforcement was then required if

$$V_u = 0.5\phi\left(V_c + V_p\right) \qquad (79)$$

Instead of Eqs. (77) and (78), there is now a single equation based on the concrete compressive strength:

$$A_{v\,min} = 0.0316\sqrt{f'_c\,(\text{ksi})}\frac{b_v s}{f_{yv}} \qquad (80)$$

which is slightly larger than ACI's minimum in Eq. (73). With regards to stirrup spacing restrictions,

$$s_{max} = \begin{cases} 0.8d_v \le 24 \text{ in. if } V_u < 0.1f'_c b_v d_v \\ 0.4d_v \le 12 \text{ in. if } V_u \ge 0.1f'_c b_v d_v \end{cases} \qquad (81)$$

Again, there were no separate requirements for prestressed concrete. The current AASHTO LRFD Bridge Design Specifications for minimum shear reinforcement are much the same as they were in 1994, except that Eq. (81) has been amended to

$$s_{max} = \begin{cases} 0.8d_v \leq 24 \text{ in. if } v_u < 0.125f'_c \\ 0.4d_v \leq 12 \text{ in. if } v_u \geq 0.125f'_c \end{cases} \quad (82)$$

where v_u is defined by AASHTO Eq. 5.8.2.9-1 as:

$$v_u = \frac{|V_u - \phi V_p|}{\phi b_v d_v} \quad (83)$$

2.3 Shear Behavior of Lightweight Concrete Beams

Despite the advantages to using lightweight concrete, Section 1.1.4 mentioned some of the disadvantages to designing with this material, including the potential for:

- lower elastic modulus
- lower modulus of rupture
- lower splitting tensile strength
- smoother crack interface

relative to normal weight concrete. In light of these drawbacks, there has been uncertainty in how to model the shear capacity of a given beam constructed with lightweight concrete. Even though modern development of this material began in 1880, research regarding shear strength did not appear in the U.S. until nearly 80 years later, beginning with reinforced concrete beams without stirrups.

2.3.1 Lightweight Beams without Shear Reinforcement

2.3.1.1 University of Texas

Some of the earliest research into the shear behavior of lightweight concrete beams was performed at the University of Texas in the late 1950's (*92-97*). These studies focused on sets of small beams that were generally 9.4 in. deep by 5.5 in. wide and had a clear span of 6 ft to 7 ft. The concrete mix design included expanded shale for both the fine and coarse aggregate, with a nominal maximum aggregate size of $^3/_8$ in. The design compressive strength in these studies ranged from 2.5 ksi to 7 ksi. None of the beams had shear reinforcement, but both compressive and tensile longitudinal reinforcement was anchored to prevent bond slippage. The beams were simply supported and loaded with two symmetric point loads. Some of the conclusions coming

out of these tests were as follows. As *a/d* became larger, the difference between lightweight and normal weight concrete with regards to the diagonal tension strength grew larger. In particular, $v / \sqrt[3]{f_c}$ was lower in lightweight concrete than normal weight concrete when *a/d* was greater than 2.5. Also, as f_c increased, the difference between the diagonal tension strength of the lightweight concrete and the normal weight concrete became larger. In some cases, the diagonal tensile strength was about 30% below that of normal weight concrete. However, an increase in f_c did result in an increase in the diagonal tension strength of the lightweight beams measured at ultimate load. Given that the longitudinal reinforcement ratio, ρ, was 3%, the results showed values for shear decreasing dramatically when *a/d* went from 2.5 to about 4 or 4.5, at which point, the shear tended to level off as *a/d* increased. This behavior was somewhat similar to tests performed on normal weight concrete specimens. There were no conclusive results regarding the angle of inclination of the cracks; some studies showed the crack angle in lightweight concrete to be shallower than their normal weight counterparts, while other tests resulted in steeper angles.

2.3.1.2 Hanson

Hanson (*18, 98*) followed this initial work with two separate studies comprising a total of 52 beams with compressive strengths ranging from 3.0 ksi to 9.0 ksi and concrete densities varying from 90 pcf to 113 pcf. All of the beams had an effective depth of 10.5 in., and a total length of either 6.5 ft or 10 ft. The simply-supported rectangular beams were loaded at two points, with *a*/*d* ranging from 2.5 to 4.8. The results from these investigations showed that the nominal shear capacity of lightweight concrete varied from 60% to 100% of that of the normal weight comparison beams, where Hanson limited the shear capacity to the diagonal tension cracking load. However, Hanson's comparisons with other studies using conventional aggregate showed that, given a similar compressive strength, the lightweight concrete beams had similar shear capacities of those of normal weight concrete beams. Nevertheless, the author pointed out that lightweight aggregates tend to result in higher shrinkage than conventional aggregates. Thus, restrained lightweight beams would experience greater axial tension, and therefore, lower shear capacity. So, the researcher developed an equation for designing the shear strength of lightweight concrete that was similar in form to that of normal weight concrete, but had different constants to reflect the lower diagonal tension strength. In the absence of necessary data, Hanson recommended the following formula:

$$v_c = 1.1\sqrt{f'_c\ (\text{psi})} + 3750\frac{\phi Vd}{M} \le 3.5\sqrt{f'_c\ (\text{psi})} \qquad (84)$$

or

$$v_c = 1.1\sqrt{f'_c\ (\text{psi})}\left(\frac{f_y}{f_y - 4280}\right) \le 3.5\sqrt{f'_c\ (\text{psi})} \qquad (85)$$

At the time, F_{sp} was known as the splitting ratio and was defined as the ratio of $f'_{sp} / \sqrt{f'_c}$, where f'_{sp} was also known as the splitting tensile strength, or f_{ct}. If the value of F_{sp} were known, then the coefficients in Eqs. (84) and (85) could vary according to a table that Hanson had established. Although Eq. (84) tended to be highly conservative, the calculation took care of any shrinkage and continuity effects on diagonal tension resistance. On a separate note, Hanson confirmed that the split-cylinder tensile test was a good relative measure of the shear resistance at diagonal cracking.

2.3.1.3 Ivey and Buth

In response to the work by Hanson, Ivey and Buth (*99*) set out to determine which of several design methods provided the most accuracy relative to experimental shear tests. Generally, the beams were 6 in. wide by 12 in. deep, although some were 9 in. and 18 in. deep. The experimental program varied the *a/d* ratio, the percentage of longitudinal steel, and the beam cross-section. While f_c was between 3 and 4 ksi, f_{ct} was in between 300 and 450 psi and concrete densities ranged from 94 to 126 pcf. The researchers noted that an *a/d* of 3.5 seemed to be the dividing line between shear compression failure and failure due to diagonal tension cracking. Ivey and Buth also found that there was little if any effect of the beam depth on the shear resistance of the beams. The results from this study averaged 14% below the strength predicted by Hanson (1961). The authors also compared their results to Eq. 17-9 in ACI's 318-63 Building Code (*56*), which was formulated as:

$$v_c = \phi\left(0.28F_{sp}\sqrt{f'_c\ (\text{psi})} + 2500\frac{\rho Vd}{M}\right) \qquad (86)$$

The shear stresses from the experiments averaged 21% higher than the ACI calculations when using the value for F_{sp} suggested by the manufacturer. Ivey and Buth also examined another approach by applying a 0.85 (for sand-lightweight concrete) or 0.75 (for all-lightweight concrete) correction factor to the original normal weight concrete equation for shear. In this case, the average test results were 36% higher than predicted, which the authors deemed highly conservative. However, the previous studies performed at the University of Texas and by Hanson seemed to provide data from low-tensile strength aggregate that fell below even this conservative design method. A third approach suggested by the researchers was to use f_{ct} determined a priori in substitution for $F_{sp}\sqrt{f_c'}$. In this case, the test results for shear stress were 18% higher than the predicted values. The researchers concluded that the f_{ct} method would be acceptable for high-tensile strength lightweight aggregates, albeit at a reduced factor of safety.

2.3.1.4 Taylor and Brewer

Taylor and Brewer (*100*) compared a series of 10-in. deep beams, some made with gravel and others constructed with lightweight aggregate. The compressive strengths of the concrete ranged from 3.2 to 4.1 ksi. The stress at failure of the expanded clay concrete beams averaged about 85% of the strength of the normal weight specimens.

2.3.1.5 Salandra and Ahmad

Research in the U.S. on high-strength, reinforced lightweight concrete beams began in the late 1980's. Salandra and Ahmad (*101*) published the test results of sixteen beams; eight had stirrups, as discussed in Section 2.3.2.6, while eight did not. All beams were 4 in. wide and 8 in. deep, with an effective depth of 6.75 in. The compression strength ranged in between 8 ksi and 10.5 ksi, and the average unit weight was 122.5 pcf. The lightweight aggregate was expanded slate, with a nominal maximum aggregate size of ½ in. All beams had the same longitudinal reinforcement ratio of 1.45%. The shear span-to-effective depth ratio varied from 0.52 to 3.63. ACI 318-83 Eq. 11-6 (*102*), as shown in Eq. (19) proved to be unconservative for beams with *a/d* of 2.59 and 3.63, and f_c' of 10 ksi. Furthermore, ACI 318-83 Eq. 11-3, written as

$$V_c = 2\sqrt{f'_c\,(\text{psi})}\,b_w d \qquad (87)$$

proved unconservative for beams without stirrups and with *a/d* of 3.63 and f_c' of 10 ksi. Additional analysis also suggested that the maximum limit of 100 psi for $\sqrt{f'_c}$ used in calculating the shear contribution from V_c may be unconservative for beams with strengths upwards of 10 ksi. The code also overestimated the diagonal tension parameter, defined as:

$$\frac{V_c}{b_w d\sqrt{f'_c}\ (\text{psi})}$$

for when the compressive strength was greater than 10 ksi and when *a/d* was greater than or equal to 2.59. Also, the researchers observed that as *a/d* increased, the angle of critical cracking decreased. Lastly, beams with a smaller *a/d* had more reserve capacity after cracking compared to beams with a larger *a/d*.

2.3.1.6 International Research

2.3.1.6.1 Evans and Dongre

Outside of the United States, early work included experiments in countries such as Great Britain, India, Japan, Netherlands and Australia. Evans and Dongre (*103*) investigated the tensile and compressive strength concrete made with a sintered clay material called Aglite, as well as its shear behavior at ultimate loads. There were 24 beams measuring 6.25 in. wide by 12 in. deep with an 8-ft span length. Concrete densities ranged from 90 pcf to 115 pcf, while the concrete compressive strength was between 3.1 ksi and 4.1 ksi. The reinforcement ratios for the tensile and compressive longitudinal steel were 5.7% and 1.9%, respectively. Half of the beams did not have shear reinforcement; those with vertical steel had a reinforcement ratio of 0.262%. All beams were tested with two concentrated loads spaced twelve inches apart, resulting in an *a/d* ratio of about 4.0. The researchers concluded that Aglite had a tensile strength that was about 75% of that of normal weight concrete. Furthermore, Evans and Dongre recommended that the allowable shear stress in Aglite concrete be 60 psi provided that the concrete cylinder compressive strength was at least 2.5 ksi. When shear reinforcement was present, Evans and Dongre suggested limiting the allowable stress in the concrete to 300 psi to prevent the cracks in the concrete from exceeding 0.01 in. in width. Results also showed that there was not much of an effect on the ultimate shear strength due to shrinkage cracking or shrinkage stresses in the

lightweight concrete, probably because of the presence of the shear stirrups that inhibited failure due to shrinkage. Thus, authors suggested that lightweight beams could use the typical stirrup designs found for traditional concrete.

2.3.1.6.2 Jindal

In 1966, Jindal (*104*) performed shear tests on lightweight concrete beams constructed with sintered fly ash. The beams were 9 in. wide with an effective depth of 13 in., and had a 9-ft span length. The lightweight coarse aggregate had a nominal size of $^3/_8$ in. to ¾ in., while the fine aggregate was either sand or sintered fly ash. The compressive strength for all of the beams was about 4.3 ksi to 4.7 ksi and the concrete density varied from 93 pcf to 106 pcf. During testing, the beams were simply supported and loaded under third-point loading. The shear strengths of the all-lightweight and sand-lightweight beams were 76% to 82% and 83% to 90%, respectively, of the strength of the normal weight beams.

2.3.1.6.3 Nishibayashi et al.

Researchers in Japan took a strong interest in lightweight concrete. Nishibayashi et al. (*105*) tested 16 beams for shear strength; the dimensions of these beams were 3.9 in. wide by 7.9 in. tall and 4.9 ft long. Pelletized expanded shale served as both the coarse and fine lightweight aggregate, with a nominal maximum aggregate size of 0.8 in. for the coarse aggregate. The two concrete densities used were about 98 pcf and 99 pcf, while the compressive strength was in between 3.1 ksi and 6.3 ksi. Longitudinal reinforcement consisted of either two 0.5-in. or 0.6-in. round or deformed bars on the tension side and two 0.4-in round bars on the compression side of the beams. The test results showed that the shear strength of the lightweight concrete was about 30% less than that of normal weight concrete. If plotting $V_c / bd\sqrt{\sigma_c}$ versus $\rho Vd / M\sqrt{\sigma_c}$, then the results match relatively closely with Eq. (84) proposed by Hanson.

2.3.1.6.4 Walraven

Having already studied aggregate interlock, Walraven (*106*) examined the effect of depth on the shear strength of beams made with lightweight concrete. As mentioned in Section 2.1.3, lightweight concrete tends to fracture through the aggregate, and therefore, has a reduced

aggregate interlock mechanism. Thus, while depth may affect the shear strength of a beam made with traditional aggregate because deeper beams result in wider cracks near the bottom of the beam and therefore, reduced aggregate interlock, Walraven hypothesized that depth might affect beams constructed with lightweight aggregate differently because the influence of aggregate interlock is somewhat less.

To test his hypothesis, Walraven experimented with three series of beams, where two series were the same with the exception of the concrete density, either normal weight or lightweight. The third series was also lightweight, but had a higher longitudinal reinforcement ratio compared to the first lightweight series. All three series had approximately the same compressive strength of 4.2 ksi and similar splitting tensile strengths ranging from 360 to 435 psi. Each series consisted of three beams, with depths of 6 in., 18 in., and 30 in. and corresponding *a/d* ratios of 2.5, 2.8, and 2.88. All of the tests were simply supported and loaded with two symmetrical concentrated loads.

As in previous tests, the lightweight beams had a lower shear capacity with all other parameters being similar. This lower shear strength was attributed to the reduced aggregate interlock in lightweight concrete. Furthermore, the results showed that depth definitely influenced the shear capacity of both the normal weight and lightweight beams. However, the author stated that the cause for this effect in lightweight concrete was not the decreasing ratio between the aggregate and the crack width, as was the case for the normal weight specimens. Walraven's reasoning was that even in the shallower beams, the cracks were still wide relative to the roughness of the crack surface. Thus, the differences with the crack widths of deeper sections were negligible. Furthermore, if the ratio of the aggregate size versus crack width were the main factor in the depth effect, then comparisons between the lightweight and normal weight beams would show major differences in behavior. However, the test data did not indicate that the relationship between the ultimate shear stress and beam depth was affected by the different types of aggregate.

Instead, the author proposed that the depth affect could be attributed to the concrete tensile strength. After combining the results from this investigation with the results by Hanson (*98*) and

Ivey and Buth (*99*), the author proposed the following equation for the shear capacity of lightweight concrete beams without shear reinforcement, where $a/d \geq 3.0$:

$$v_u = \frac{V_u}{bd_e} = 2.5 f_{ct} \rho_o^{0.3} d_e^{-0.4} \quad \textbf{(88)}$$

where:

d_e = effective depth of the beam (mm)

f_{ct} = concrete splitting tensile strength (N/mm^2)

ρ_o = percentage of longitudinal reinforcement

For d_e in inches, Eq. (88) becomes

$$v_u = \frac{V_u}{bd_e} = 0.69 f_{ct} \rho_o^{0.3} d_e^{-0.4} \quad \textbf{(89)}$$

where v_u has the same units as f_{ct}. For beams closer to the support, the author recommended multiplying Eq. (89) by $3h/a$ such that Eq. (89) becomes:

$$v_u = \frac{V_u}{bd_e} = 2.05 f_{ct} \rho_o^{0.3} d_e^{-0.4} \frac{h}{a} \quad \textbf{(90)}$$

2.3.1.6.5 Swamy and Bandyopadhyay

In 1979, Swamy and Bandyopadhyay (*107*) continued with past experiments from Great Britain regarding sintered pulverized fuel ash and expanded slate. The researchers examined 24 lightweight T-beams and compared them with companion normal weight T-beams. All beams had the same cross-sectional dimensions of 11.8 in. for the flange width, a flange thickness of about 2 in., a web width measuring 3.9 in. and an effective depth of 5.0 in. The span length of each member was 6.2 ft. The concrete compressive strength was around 5.5 ksi. As a second variable, the researchers varied the ratio of longitudinal reinforcement from 1.64% to 2.70%, which corresponded to being 55% to 91% of the balanced longitudinal reinforcement ratio, ρ_b. All of the steel had adequate anchorage to prevent bond slippage. The beams were simply

supported and loaded with two concentrated point loads, with the ratio of the shear span to the effective depth varying from 1.5 to 6.0. The mechanism for shear transfer through the compression zone was similar, regardless of the type of aggregate used.

While the formation and propagation of diagonal tension cracks was the same in lightweight concrete as for normal weight concrete, the lightweight members generally had wider crack widths than their normal weight counterparts. In this research, some tests of the expanded slate aggregate had comparable levels of shear cracking load as normal weight concrete, while other specimens actually had cracking strengths that were 10% to 17% greater than the normal weight specimens. On the other hand, the fuel ash aggregate had results that were 5% to 12% less than the normal weight concrete results.

Regarding ultimate shear strength, the ranges were 75% to 95% of normal weight concrete for the expanded slate and 83% to 95% for the fuel ash. Test results also revealed the significant effect of the amount of longitudinal reinforcing; for lightweight concrete, the dowel action of the longitudinal steel increased the shear resistance between 30% and 70%. However, this dowel effect appeared to be insignificant for lightweight beams with relatively short shear spans, whereas normal weight beams exhibited the influence of dowel action regardless of the span length. The authors postulated that the reason for the difference between the two concretes was that shorter spans seem to undergo both beam action and arch action, resulting in a combined state of stress. Hanson (*108*) had shown that lightweight concrete performs poorly compared to normal weight concrete under biaxial stresses.

2.3.1.6.6 Swamy and Lambert

Similar to the work by Swamy and Bandyopadhyay (*107*), Swamy and Lambert (*109*) studied T-beams constructed with sintered fuel ash. This time, the basic geometry was a 4-in. web, with 12 in. wide by 3 in. thick flanges, an effective depth of 7.1 in. and a length of 9.84 ft. The concrete strength ranged from 3.4 ksi to 7.0 ksi. The percentage of longitudinal reinforcement ranged from 0.29% to 3.01%. The beams were loaded with two concentrated point loads such that the a/d ratio varied from 1.5 to 6.0. For $a/d \leq 3.0$, the T-beams failed by diagonal tension cracking. Beams with $a/d \geq 4.5$ had flexural failures. For $3.0 \leq a/d \leq 4.5$ there was combination of arching

mechanism and flexural-type of failure. The researchers found that *a*/*d* and the percentage of longitudinal steel had a profound effect on the shear strength of lightweight concrete. On the other hand, f_c had a much smaller effect, where an 80% increase in compressive strength only yielded a maximum 21% increase in ultimate shear strength. The lightweight coarse aggregate combined with sand had about 75% to 85% of the strength of normal weight concrete. To account for *a/d*, longitudinal reinforcement ratio and f_c, the authors proposed a design equation to be used for the ultimate shear stress in all lightweight concrete beams as:

$$v_u = 0.292 f_{ct} + 31.83 \frac{\rho V d}{M}$$

However, this equation did not work well for beams with $a/d \leq 2.0$.

2.3.1.6.7 Hoff et al.

Pioneering efforts in high-strength lightweight concrete, Hoff et al. (*110*) tested six beams designed to fail in shear. The beams were 6 in. by 8 in. by 9.35 ft. The concrete compressive strength was about 10 ksi, the average splitting tensile strength was 540 psi, and the average density was 120 pcf. Although there was a lot of scatter in the results for ultimate shear strength, the lightweight concrete beams definitely had lower strengths than the normal weight counterparts. However, the ratio of measured to calculated shear strength was similar for lightweight concrete as it was for normal weight concrete, where the calculated shear strength was according to the Norwegian Code for Design of Concrete Structures, NS 3473.

2.3.1.6.8 Hoff

In looking at extreme weather applications, Hoff (*111*) studied the shear capacities of higher-strength lightweight concrete beams, with compressive strengths ranging from 8.7 to 11.7 ksi. The longitudinal reinforcement ratio was 4% to ensure shear failure prior to flexural failure. The 7.5-ft beams were simply supported and subjected to third-point loading, resulting in an a/d = 2.6. Test results showed that the ratio of shear stress to the square root of the compressive strength, $v_u / \sqrt{f_c}$, was similar for all beams, and furthermore, there was no apparent correlation

between the ultimate load capacity and f_c'. Nevertheless, all of the test specimens exceeded the inclined cracking stress calculated according to ACI 318-89.

2.3.1.6.9 Murayama and Iwabuchi

Researchers in Japan started their own program in high-strength lightweight concrete in the early 1980's. Murayama and Iwabuchi (*112*) published a paper examining the shear strength of eleven high-strength lightweight concrete beams that had cross-sectional dimensions of 8 in. wide by 9 in. tall, with span lengths being either 6.6 ft or 8.2 ft. The three lightweight concrete mixtures used sand as the fine aggregate; all mixes had a density of about 119 pcf. A second parameter, the longitudinal reinforcement ratio, ranged from 1.55% to 3.18%. The beams were simply supported and loaded with two concentrated point loads, where the shear span-to-effective depth ratio varied from 2.5 to 4.0.

Test results showed that the splitting tensile strength of lightweight concrete was about 15% less than that of normal weight concrete, while the shear transfer results showed that lightweight concrete had 30% less resistance than normal weight concrete. This result was possibly due to the smoother shear planes along the crack. Therefore, the authors suggested that the shear transfer strength of high-strength lightweight concrete be limited to 70% of that of normal weight concrete. Although the researchers found that, for *a/d* equal to 4.0, all of the beams had shear failures after diagonal cracks formed, but that lightweight beams had shear cracking strengths that were 30% less than the strengths of the normal weight beams. Murayama and Iwabuchi's research confirmed the guidance from the ASCE-ACI Task Committee 426 (*113*) that the lower tensile splitting strength and lower shear transfer strengths may reduce cracking strength of lightweight concrete.

For *a/d* equal to 3.0, the normal weight concrete beams failed immediately after the formation of a diagonal tension crack. On the other hand, the lightweight concrete beams actually exhibited higher reserve capacities after the first diagonal tension crack appeared, and had greater strengths than the normal weight beams. One possible reason for the differences in failure strengths was the difference in cracking patterns in the two beams. Diagonal cracks in the normal weight beams started in the upper half of the beam member and progressed to the top of the beam within

the shear span. On the other hand, cracks in the lightweight beams reached the top of the section within the constant moment region. For beams with *a/d* = 2.5, both the normal weight and lightweight aggregate beams failed in shear compression. Again, however, the lightweight beams failed at loads greater than the normal weight beams.

2.3.1.6.10 Funahashi et al.

While not necessarily high-strength, Funahashi et al. (*114*) ventured into beams constructed with super-lightweight aggregate (SLA). There were four smaller beams measuring 7.9 in. wide, 15.7 in. tall and 11.2 ft long beams, and ranging in concrete densities from 81.8 pcf to 107.4 pcf. Additionally, two larger-scale beams measuring 19.7 in. wide, 42.1 in. tall and 32.8 ft long had densities of 97.4 pcf and 113.0 pcf. The concrete mixes employed a combination of SLA, conventional lightweight aggregate, and sand. The compressive strength of the smaller beams ranged from 3.3 ksi to 6.5 ksi, while the compressive strength of the larger beams was about 5 ksi. The beams were simply supported, with a span length of 9.8 ft and 31.2 ft for the small-scale and large-scale beams, respectively. The loading consisted of two concentrated loads that were 4.1 ft away from the beam centerline, giving a shear span-to-effective depth ratio of 2.94.

Three of the smaller beams survived diagonal tension cracking on both sides of the beam before failing completely in shear compression. The normal weight beam failed at twice the load of the lightweight beams, but failed completely immediately at the formation of the first diagonal tension crack, as did the large-scale lightweight specimen with a density of 113 pcf. Although the 97.4 pcf large-scale beam also had a diagonal tension crack, this specimen formed a tied-arch mechanism before completely failing by concrete crushing. The authors stated that in general, the normal weight concrete beams transitioned from diagonal tension failure to shear compression failure when *a/d* was around 2.0. However, in the case of lightweight concrete, that value appeared to be about 3.5. For the SLA beams, the shear forces in the beams were 44% to 59% of the normal weight beams when diagonal tension cracking occurred. However, the ultimate shear capacity of the beams with densities of about 113.0 pcf was the same as what was predicted. On the other hand, the results for lower-density concretes were lower than what was predicted. Therefore, the methods used to calculate the shear capacity of normal weight concrete may only work for the higher range of lightweight concrete densities.

Furthermore, the shear capacity decreased as the concrete density decreased. The authors also noted that the bond strength between the rebar and concrete decreased as the concrete density decreased. Yet, the Japanese Society of Civil Engineers code specified that the shear strength of lightweight concrete should be calculated as 70% of that of normal weight concrete, regardless of the concrete unit weight. From this research, the authors proposed a conversion factor, η_s, in calculating the shear strength of lightweight concrete:

$$\eta_s = \left(\frac{\rho}{2300}\right)^{\frac{3}{2}}$$

where ρ is the density of the lightweight concrete and 2300 is the density of normal weight concrete (in kg/m^3). However, this factor only applies for values of *a/d* that are greater than or equal to 3.5. When *a/d* is equal to 3.0, i.e., the transition region between diagonal tension failure and the tied-arch mechanism, the conversion factor becomes

$$\eta_s = \left(\frac{\rho}{2300}\right)^{\frac{3}{2}} \left(\frac{3.5}{a/d}\right)^2$$

2.3.2 Lightweight Beams with Shear Reinforcement

2.3.2.1 Hamadi and Regan

Hamadi and Regan (*115*) also studied T-beams, but with an emphasis on the effects of shear reinforcement with lightweight concrete constructed with expanded clay as the coarse aggregate. The T-beams were 15.7 in. tall and 4.7 in. wide in the web; the top flange dimensions were 3.9 in. by 19.7 in. The compressive strength of the concrete in the lightweight beams was around 3 ksi, while the shear reinforcing index ranged from 92 psi to 493 psi. Loaded with a single concentrated load at the centerline, the beams had a shear span-to-effective depth ratio of 3.6.

The three lightweight beams with smaller reinforcing indices failed with an inclined shear crack going through the flange, while the more heavily-reinforced beams exhibited bond-splitting at failure. Given the same amount of shear reinforcement, the lightweight beams had higher stresses in the stirrups compared to the normal weight control beams, although, stirrup yielding occurred at loads that were well below the ultimate failure loads, regardless of the type of

aggregate used. Once the stirrups had yielded, there was a progressive decrease in the cracking angle, along with a realignment of the truss system to resist the additional load. However, this realignment appeared to be limited to the aggregate interlock at the crack interface. The reduced aggregate interlock in lightweight concrete resulted in the web compression strut being closer to the angle of inclination of the original shear crack. Thus, the angle of inclination was greater in lightweight beams than in normal weight beams. Compared to their normal weight counterparts, the lightweight beams exhibited greater displacements at the cracks, particularly in a direction parallel to the crack as opposed to normal to the crack.

Overall, both the V_c and V_s components of V_u were lower in the lightweight concrete beams compared to the normal weight beams. Furthermore, the lightweight beams did not show as much of an increase in shear strength as the amount of shear reinforcement increased.

2.3.2.2 Kirmair

Although the five beams in his study failed in flexure, Kirmair (*116*) published the results of these beams that were designed to fail at a range of low, medium, and high shear stresses. Kirmair made comparisons of the crack widths and crack patterns between the lightweight and normal weight concrete. The cross-sections were rectangular, T, and Bulb-T shapes, measuring either 19 or 26 in. tall and 14 or 17 ft long. The unit weight for the lightweight concrete was only 94 lb/ft^3. Due to lower tensile strength of the lightweight concrete, shear cracking started at a lower load and the cracks were wider and were spaced closer together compared to normal weight concrete. This was particularly the case for the beams designed for lower shear stresses, where the stirrups were spaced further apart. The author recommended either limiting the stirrup spacing or increasing the reinforcement.

2.3.2.3 Clarke

The 1985 British Standards Institution's code of practice for the structural use of concrete, BS 8110 required that the allowable shear stresses of structural lightweight concrete be 80% of the strength that was calculated assuming normal weight concrete (*117*), even though the steel reinforcement was designed in the same manner, regardless of aggregate type. Thus, Clarke (*118*) investigated the shear strength of beams constructed with lightweight aggregate, where the

density ranged from 109 lb/ft^3 to 128 lb/ft^3 and the compressive strengths ranged from 2.9 ksi to 7.4 ksi. The test specimens were 8-in. by 4-in. rectangular sections and contained either ¼-in. diameter 36-ksi bars, or ⅛-in. diameter 40-ksi rods spaced at 6 in. for shear reinforcement. The beams were loaded with a single point load, where *a*/*d* was about 2.8. Overall, the results from this analysis showed that some of the lightweight beams had shear strengths that were just above the design strength if the 0.8 reduction factor was removed from the calculation. Yet, in some cases, the normal weight concrete beams failed at loads less than the design strength. Thus, the author suggested that no reduction factor should be applied to lightweight concrete beams containing stirrups.

2.3.2.4 Ahmad et al.

Ahmad et al. (*119*) compared results to the BS 8110 Code in an experiment of lightweight concrete having normal and high strength. The researchers investigated 15 beams measuring 10 in. deep to determine the effects of f_c, *a/d*, and web reinforcement ratios. The normal compressive strength ranged from 4.4 to 6.5 ksi; the high compressive strength ranged from 11.9 to 13 ksi. The *a/d* ratio was typically 1, 2, or 3, although one high-strength beam had an *a/d* of 4. The shear reinforcement ratio varied from 0 to 0.78. The results showed that shear capacity decreases as *a*/*d* increases. In fact, the ACI 318-89 code overpredicts the shear capacity of a normal-strength lightweight beam with shear reinforcement that is loaded with an *a*/*d* of 3, and is only marginally conservative for the high-strength beams at the same *a*/*d* ratio, regardless of whether or not the beams have any shear reinforcement. While the authors agreed with Clarke in that the BS 8110 specification for a 0.80 reduction factor for shear strength of lightweight concrete is too conservative, the researchers concluded that there still needs to be a penalty. Instead, Ahmad et al. recommended a factor of 0.85.

2.3.2.5 Walraven and Al-Zubi

In 1995, Walraven and Al-Zubi (*120*) considered lightweight concrete beams with stirrups in conjunction with the variable strut inclination method of analysis. The test program involved testing three different types of lightweight aggregates in I-beams. The beams had an effective depth of about 30 in. and a cross-sectional area of 279 in^2, with a web thickness of 3.9 in. There were four series of lightweight beams cast using three types of lightweight aggregate: Lytag,

Liapor and Aardelite. The concrete cylinder compressive strengths and unit weights ranged from 2.4 ksi to 7.3 ksi and 108 pcf to 131 pcf, respectively. A fifth series was constructed with conventional aggregate. All of the beams used natural sand as fine aggregate.

The amount and spacing of longitudinal and vertical steel varied depending on the type of desired shear failure and design compressive strength. Within each series of beams, there were three levels of shear reinforcement ratios, 0.43%, 0.89%, and 1.45%. The medium ratio was selected so that the stirrups would yield just at the point of web crushing; the other two levels of reinforcement were designed to yield and not yield, respectively, prior to concrete crushing in the web.

The authors' conclusion from the results was that there was virtually no difference between the lightweight beams and their normal weight companions regarding the rotation of the principle stress angles. One possible explanation is that despite the reduced aggregate interlock from the lightweight aggregate, there is a sufficient amount of shear force being transferred due to the irregular shape of the crack faces. This reasoning was evidenced by the fact that the lightweight beams had regions with steeper cracks that exhibited concrete crushing. Analytically, the two different types of concrete had the same redistribution capacity and the same degree of strut rotation. The researchers did note, however, that the lightweight concrete beams had about twice the shear displacement along the crack interface as that of the normal weight beams.

2.3.2.6 High-Strength, Lightweight Concrete with Shear Reinforcement

2.3.2.6.1 Salandra and Ahmad

As mentioned in Section 2.3.1.5, Salandra and Ahmad (*101*) studied high-strength, reinforced lightweight concrete beams, half of which contained shear reinforcement. All beams were 4 in. wide and 8 in. deep, with an effective depth of 6.75 in. The compression strength ranged in between 8 ksi and 10.5 ksi, and the average unit weight was 122.5 pcf. The lightweight aggregate was expanded slate, with a nominal maximum aggregate size of ½ in. All beams with vertical reinforcement had the same longitudinal and web reinforcement ratios of 1.45 and 0.78%, respectively. The shear span-to-effective depth ratio varied from 0.52 to 3.63.

The results showed that both ACI 318-83 Eq. 11-6 [Eq. (19)] and ACI 318-83 Eq. 11-3 [(Eq. (90)] are unconservative for beams with *a/d* of 2.59 and 3.63 and f_c' of 10 ksi. The beams that had web reinforcement and *a/d* = 0.52 failed due to diagonal tension cracking and without any redistribution of concrete stresses to the stirrups. All of the other beams with *a*/*d* > 0.52 failed in flexure. Nevertheless, the calculated values for V_c in the shear-reinforced beams were similar to the beams without reinforcement. Additionally, beams with *a/d* of 2.59 and 3.63 exhibited ductile behavior. Like the beams without stirrups, the shear-reinforced beams exhibited a decrease in the angle of critical cracking as *a/d* increased. However, with the exception of *a*/*d* = 0.52, this critical cracking angle was greater for beams with web reinforcement than for beams without reinforcement. For *a*/*d* = 0.52, that angle was the same. The researchers also noted that beams with reinforcement had more inclined cracks than beams without web reinforcement.

2.3.2.6.2 Ramirez et al.

In 2004, Ramirez et al. (*19*) presented their research on high-strength lightweight concrete, which included tests of seven normal weight and five lightweight beams. The beams were 11.6 ft long and had 14 in. by 14 in. cross-section within the test region while being larger outside of the test region. The lightweight, regular strength beams had an average compressive strength of 6.4 ksi, while the lone lightweight, high-strength beam registered 10.5 ksi. In comparison, the average compressive strength of the regular and high-strength normal weight beams were 6.7 ksi and 9.8 ksi, respectively. The lightweight concrete beams contained expanded shale with a nominal maximum aggregate size of 0.37 in., which was half the size of the normal weight aggregate. The unit weight of the lightweight beams ranged from 106 pcf to 127 pcf.

Both the tension and compression reinforcement ratios were 2.35%, although the researchers did vary the distribution of the longitudinal reinforcement across the width of the beam. The shear reinforcing index varied between 157 psi and 236 psi, thus meeting or exceeding the minimum required amount of transverse reinforcement. Therefore, the maximum design limit on $\sqrt{f'_c}$, as stipulated by both the 1998 AASHTO LRFD Specifications (*121*) and ACI 318-02 code (*82*), could be exceeded. Beams were simply supported with one end of the beam overhanging the support. Load was applied with a spreader beam straddling the support with the overhang. This

condition provided a large shear force accompanied by a relatively large moment, which was a more critical shear condition than that created with a simply supported beam loaded at midspan.

All specimens failed in shear-compression and had yielding in the web reinforcement. The average experimental shear capacity of the lightweight, regular-strength concrete was 82% of the normal weight concrete. This percent is less than the 0.85 factor used in the codes, but is within the variation observed in previous studies. The authors also noted that the smaller aggregate in the lightweight concrete resulted in larger shear stresses in the concrete, which reduced the stress in the vertical reinforcement and contributed to the shear carrying mechanism, as suggested by Bhide and Collins (*122*). On the other hand, the lone lightweight, high-strength concrete beam was nearly the same as one of the normal weight, high-strength concrete beams and was 10% stronger than the other normal weight beam.

Additional detail to the paper by Ramirez et al. was given by Malone (*123*). Although the Simplified Procedure in the AASHTO LRFD Specifications predicted strengths that averaged 15% below the ACI-calculated values, General Procedure in the AASHTO LRFD Specifications predicted values that were roughly 8% higher than those predicted by ACI 318-95. Note that in the case of Malone's work, the "Simplified Procedure" applies only to non-prestressed members, while the "General Procedure" uses the tabular method for determining θ and β in prestressed sections. As another comparison, Table 2-1 shows that both codes yielded less conservative calculations for lightweight concrete versus normal weight concrete when considering moderate-strength concrete. However, when it came to high-strength concrete, both design codes proved to be more conservative in estimating the capacity of high-strength, lightweight concrete versus high-strength, normal weight concrete. In half of the twelve beams, the researcher determined

Table 2-1. Average ratios of experimental versus code-calculated shear capacities from the Malone study.

Density	f'_c (ksi)	$\frac{V_{exp}}{V_{LRFD\ Gen.}}$	$\frac{V_{exp}}{V_{LRFD\ Simp.}}$	$\frac{V_{exp}}{V_{ACI}}$
Lightweight	6	1.10	1.31	1.18
Normal	6	1.29	1.51	1.36
Lightweight	10	1.41	1.68	1.51
Normal	10	1.29	1.50	1.35

that the steel contribution to the shear strength was less than what was calculated using the AASHTO LRFD code, although this overprediction typically occurred in the normal weight beams. Meanwhile, the experimental concrete contribution was greater than the predicted results, regardless of which specification was used in the calculations, as seen in Table 2-2.

Table 2-2. Comparison of experimental versus code-predicted results for the steel and concrete contributions to shear capacity from Malone study.

Density	f'_c (ksi)	$\frac{V_{s\,exp}}{V_{s\,LRFD\,Gen.}}$	$\frac{V_{c\,exp}}{V_{c\,LRFD\,Simp.}}$	$\frac{V_{s\,exp}}{V_{s\,ACI}}$	$\frac{V_{c\,exp}}{V_{c\,ACI}}$
Lightweight	6	1.05	1.44	1.33	1.20
Normal	6	1.08	1.84	1.69	1.23
Lightweight	10	1.28	1.76	1.68	1.49
Normal	10	0.87	1.83	1.75	1.00

2.3.2.7 Super-Lightweight Concrete Beams with Shear Reinforcement

2.3.2.7.1 Kawaguchi et al.

Japanese researchers delved into the realm of super lightweight concrete (SLC) in the new millennium. Kawaguchi et al. (*124*) experimented with four beams that had cross-sections measuring 7.9 in. wide by 13.8 in. tall, with an effective depth of 11.8 in. and a span length of 7.9 ft. Concrete densities ranged from 74 pcf to 107 pcf due to the use of a combination of sand, conventional lightweight aggregate and super lightweight fine aggregate. The longitudinal reinforcement ratio was a constant 1.77%, while the shear reinforcement ratio was 0.15%, which was the minimum shear reinforcement required by the Japan Society of Civil Engineers (JSCE) code. All of the beams were simply supported and loaded with two concentrated loads that were about six inches away from the beam centerline, giving a shear span-to-effective depth ratio 3.5.

The beams failed in a relatively ductile manner and exceeded the shear strength predicted by the JSCE code. However, the results also showed that as the compressive strength increased, the ratio of the experimental to predicted shear strength decreased. The same was true for the ratio of f_t / f_c. Furthermore, the researchers found that the shear capacity of lightweight concrete was dependent on the unit weight of the concrete, and therefore, the concrete contribution to shear, V_c, should not be reduced to a constant factor of 70% of normal weight concrete beams.

2.3.2.7.2 Kobayashi et al.

Meanwhile, Kobayashi et al. (*125*) published an article that reported the development of ultra lightweight concrete which had concrete densities of 75 pcf and 105 pcf. The former concrete had a compressive strength of 4.4 ksi, while the latter had a compressive strength of 8.7 ksi. Nine lightweight concrete beams were tested along with four normal weight concrete beams, although three of the lightweight beams and one of the normal weight beams failed in flexure. The dimensions of the cross-sections were 7.9 in. wide by 10.6 in. tall, while the total length of each beam was 10.2 ft. The beams were reinforced longitudinally on both the compression and tensile faces of the beams, while the percentage of shear reinforcing varied between 0.13% and 1.20%. The shear span-to-effective depth ratio was 2.0.

The authors followed the guidelines set forth by the Architectural Institute of Japan (*126*) to predict the beam shear strengths. Shear capacities of the 4.4 ksi beams were 20% to 30% below what was predicted, while the 8.7 ksi beams were 10% below. In comparison, the normal weight beams exceeded their predicted strengths by as much as 15%. Furthermore, the shear force carried via arching mechanism in the lightweight concrete beams was less than the normal weight concrete beams. Relative to the normal weight concrete, the lightweight concrete had a lower elastic modulus, lower splitting tensile strength, and larger angle of inclination in the cracks. Consequently, the researchers modified the formula for estimating the arching mechanism by multiplying the formula by the ratio of the elastic moduli of the two different concretes, reducing the compressive strength by the ratio of the splitting tensile strength of the two different concretes, and using the crack angle observed during experimentation. Making these modifications to the equation for traditional concrete provided an adequate margin of safety.

2.3.3 Lightweight Prestressed Girders

As mentioned in Section 1.1.2, prestressed lightweight concrete has been in use since the early 1960's. While most of the research on the shear strength of lightweight concrete has focused on non-prestressed beams, there has been some attention paid to prestressed concrete.

2.3.3.1 Brettle

The first such research was actually done in Australia by Brettle (*127*). Using lightweight aggregate for both the coarse and fine aggregate, the density of this concrete was about 105 pcf and had a compressive strength ranging from 4.8 ksi to 6.4 ksi. While the beam width was held constant at 2 in., the depth varied from 6 in. to 18 in., and the length was in between 1.75 ft and 9 ft. There was a single 0.28 in.-diameter prestressing wire located in the bottom third point of the beam cross-section; the tensile strength of this prestressing wire was 220 ksi. Given the different cross-sectional dimensions, the percentage of longitudinal reinforcing steel varied from 1% to 1.5%. The beams were simply supported and loaded symmetrically with two concentrated loads, with *a/d* ranging from 1.0 to 8.5, where *d* was defined as the total depth of the beam. Overall, sixteen beams failed in shear without bond failures. Despite lacking quantifiable data at the time of publication of the article, the author concluded the quality of failure in prestressed lightweight concrete beams was similar to that of normal weight concrete.

2.3.3.2 Malone

In addition to his work on reinforced concrete, Malone (*123*) was the first to provide substantial information regarding the performance of prestressed lightweight concrete. The researcher evaluated four AASHTO Type I girders, all of which had 4-in. thick by 4-ft wide cast-in-place normal weight decks, giving a composite area of concrete of 469 in^2. Total length of each girder was 22 ft, while the span length was 16 ft. The mix design included a $^3/_8$-in. nominal maximum sized expanded shale with a natural sand fine aggregate. Two of the beams weighed 106 pcf and had compressive strengths measuring about 6.75 ksi. The other two beams had a unit weight of 127 pcf and a compressive strength of 10.1 ksi. Each beam had ten ½-in. special, Grade 270 steel strands providing the main longitudinal reinforcement, with two of those strands being three inches below the surface of the top flange. In addition, there was mild reinforcement in the middle portion of the beam to prevent flexural failures. For each of the two compressive strengths, one beam had no shear reinforcement, while the other had double-legged, No. 3 uncoated rebar stirrups spaced at 20 in., which resulted in a reinforcing index of 92 psi. The 20-in. spacing was near the maximum spacing allowed by the AASHTO LRFD code (*91*) and the ACI 318-02 (*82*) code. In the deck, No. 5 rebar ran longitudinally and transversely at a 5-in.

spacing. The beams were simply supported and loaded with a single concentrated load at midspan, giving a shear span-to-depth ratio of about 3.0.

All specimens suffered web-shear failures with smooth crack surfaces. When comparing the 6 ksi and 10 ksi beams without stirrups, a 44% increase in compressive strength resulted in a 28% increase in shear capacity. However, a similar comparison of the beams with shear reinforcement yielded only a 3% increase in shear strength for a 56% increase in compressive strength.

In a follow up to Malone's publication, Ramirez (*78*) noted that for the 10 ksi beams, the beam with stirrups only had a 15% increase in shear strength over the capacity of the beam without stirrups. Furthermore, the stirrups had yielded upon first cracking. These observations were in light of the fact that the stirrups actually had twice the minimum area of steel required. Because the amount of vertical reinforcement used in this project was actually dictated by the maximum stirrup spacing, Ramirez's concern was that the minimum reinforcement requirements did not truly affect the shear capacity of high-strength beams. Therefore, the researcher suggested that there might be a need to increase the amount of minimum reinforcement for higher strength concretes to ensure sufficient post-diagonal cracking reserve strength.

Comparisons between the measured shear strengths and those calculated using the AASHTO LRFD or the ACI 318-95 specifications are in Table 2-3. These comparisons used the experimental yield strength of the steel. Based on calculations, the experimental steel contribution to shear strength was about 30% less than the predicted result using the AASHTO LRFD method, but was 37% greater than the result predicted using the guidelines in ACI 318-95. The difference between the experimental and LRFD results is presumably due to the lower crack

Table 2-3. Comparative results between experimental and predicted shear tests of prestressed AASHTO Type I girders in Malone's study.

f'_c (ksi)	Stirrups?	$\frac{V_{exp}}{V_{LRFD\ Gen}}$	$\frac{V_{exp}}{V_{ACI}}$
6	No	1.18	1.13
6	Yes	1.19	1.32
10	No	1.44	1.32
10	Yes	1.08	1.25

angle predicted by the LRFD specifications. Table 2-4 gives the angle of the inclined crack that ultimately led to failure in the beam along with the predicted angle using the AASHTO LRFD General Method (*91*); there is no apparent pattern as to whether the predicted angle was less than or greater than the experimental result.

Table 2-4. Comparative results between experimental and predicted crack angles from prestressed beam tests in Malone's study.

f'_c (ksi)	Stirrups?	θ_{fail} (deg)	θ_{LRFD} (deg)
6	No	36	30
6	Yes	34	26
10	No	23	32
10	Yes	33	27

2.3.3.3 Kahn et al.

As part of a larger study on the performance of precast, prestressed high-performance, lightweight concrete (HPLC) bridge girders, Kahn et al. (*16*) constructed six beams to examine the shear strength, effect of shear reinforcement spacing on strand slippage, and transfer and development length.

All of the girders in this experiment were AASHTO Type II beams with a cast-in-place deck measuring 11.5 in. thick and 19 in. wide, giving a total composite area of 588 in^2. The concrete was made with 0.5-in. expanded slate coarse aggregate and natural sand fine aggregate, resulting in a unit weight that was between 118 pcf and 119 pcf. The girders were divided into two groups; the first series had a design compressive strength of 8 ksi, while the second series was designed for 10 ksi. However, the 8 ksi girders actually had compressive strengths that ranged from 8.7 ksi to 10.6 ksi, while the actual compressive strength of the 10 ksi girders was between 9.9 ksi and 11.4 ksi. For the deck, the strength ranged from 4.8 ksi to 6.1 ksi. Longitudinal reinforcement consisted of ten 0.6-in, Grade 270 low-relaxation strands, with eight strands in the bottom flange and two strands in the top. None of the strands were harped. For shear reinforcement, there were two No. 4, Grade 60 stirrups spaced at 3.5 in., 7 in., or 24 in. During testing, the beams were simply supported and loaded using a single point load. However, each beam was tested three times, with the location of the supports changing each time to avoid

damaged sections. Although there were 18 tests, only six of those tests resulted in shear failures. Of these six tests, the ratio of shear span-to-effective depth ranged from 1.5 to 2.4.

With one exception, the force to cause the initial experimental crack was greater than the force predicted using either the 1999 ACI code (*128*), 1996 AASHTO Standard Specifications (*129*), or 1998 AASHTO LRFD Specifications (*121*). The ACI calculations came in as the least conservative, with the shear strength being overpredicted by nearly 9% for one beam and from 2% to 17% higher for the remaining beams. The AASHTO Standard calculations provided more conservative results, with the experimental cracking load being 9% to 39% greater than that which was predicted. On the other hand, the LRFD methodology grossly underestimated the initial cracking strength, with the experimental results being 377% to 470% greater than the calculated strengths.

As for the ultimate shear strength, again both the AASHTO Standard and LRFD codes produced conservative results, with the ratio of experimental to predicted ultimate strengths ranging from 1.21 to 1.86 when using the Standard Specifications and 1.13 and 3.11 when using the LRFD specifications. ACI's alternative method for calculating shear netted several results that overestimated the ultimate shear strength. Thus, the authors recommended additional studies to determine the concrete contribution to the shear strength for beams constructed with concrete having a compressive strength greater than 10 ksi.

2.3.3.4 Watanabe et al.

As mentioned in Section 2.3.1.6.10 , the JSCE called for the shear strength of concrete containing lightweight aggregate to be calculated as 70% of that of normal weight concrete. However, there had been some debate as to whether or not this rate of reduction should be constant. In previous studies, factors used to determine the strength reduction ratio included the concrete density and the ratio of the tensile strength of lightweight concrete to normal weight concrete. One conclusion was these factors netted in a 30% reduction in shear capacity for lightweight concrete. However, much of the data used in reaching this conclusion were for compressive strengths less than 5.8 ksi. Other research had shown that prestressing significantly improved the shear cracking strength. However, this increase was typically underestimated by

formulations that multiplied the prestress by a correction factor that used the decompression moment, that is, the moment due to prestressing.

Therefore, Watanabe et al. (*130*) focused on the shear strength of lightweight prestressed, precast members with a compressive strength of about 8.7 ksi, as well as the influence of prestressing on shear cracking strength, and the behavior of lightweight concrete beyond shear cracking. There were three different combinations of aggregate: lightweight fine aggregate with normal weight coarse aggregate, lightweight coarse aggregate with sand fine aggregate, and lightweight coarse aggregate with lightweight fine aggregate. The lightweight coarse aggregate was granulated expansive shale, with a nominal maximum aggregate size of 0.31 in. The density of the lightweight concrete ranged from 106 pcf to 119 pcf. The slump was about 7.9 in., while the concrete compressive strength for all of the beams ranged from 8.6 ksi to 9.6 ksi.

Dimensions of the beams were 7.9 in. wide by 24.6 in. tall, and the span length was 14.1 ft. There were six 0.6-in. diameter prestressing strands in two layers of in the bottom of the members, with two additional strands at the top of the section. The prestressing strands were tensioned in such a manner that there were three cases of stress in the concrete: zero stress, that is no prestress forces; the top concrete fiber having zero stress and the bottom concrete fiber having 1.2 ksi of compressive stress, and then the top concrete fiber having zero stress and the bottom concrete fiber having 2.3 ksi of compressive stress. The prestressing steel had a tensile strength of 270 ksi, where the prestress force was transferred to the concrete four days after the beams were cast. Shear reinforcement consisted of No. 4 rebar spaced at 7.9 in. and had a tensile strength of 75 ksi. All of the beams were loaded with two point loads that were spaced about 19.7 in. away from the beam centerline. The shear span-to-effective depth ratio was 3.0.

The researchers concluded that the shear cracking strength declined as the concrete density decreased, with the super lightweight concrete having a shear cracking strength that was much less than typical 70% factor used in design. On the other hand, the concrete mix with lightweight fine aggregate and normal weight coarse aggregate had about the same value for V_c as normal weight concrete. The researchers considered using the reduction factor formulated as:

$$\lambda = 0.4 + 0.6\frac{\gamma}{147} \leq 1.0 \quad (91)$$

where 147 is the unit weight of normal weight concrete (in pcf) and γ is the density of the lightweight concrete. However, the results from the 106 pcf specimens had a greater reduction than suggested by this formulation, with one reason being the tensile strength that was about 50% of that of normal weight concrete. Because this concrete had a high brittleness factor, which was defined as the ratio of the compressive strength to tensile strength, the conclusion was that concretes with a high brittleness factor would have a much lower shear cracking strength than calculated.

Although previous research found that there was a linear relationship between shear cracking and the distribution of the prestressing force if the stress distribution is in a triangular fashion, the authors of this report found no relationship between the type of aggregate and the degree of increase in shear cracking strength due to prestressing. Post-cracking, the researchers observed that the normal weight concrete specimens had a one-to-one relationship between the increase in force in the transverse reinforcement, V_s, and the increase in the applied shear. This observation implied that the shear force resisted by the normal weight concrete remained constant after cracking had occurred. On the other hand, that ratio for lightweight concrete was somewhat greater than one, thus indicating that there was a decrease in the shear force carried by the lightweight concrete after cracking that was compensated for by the stirrups.

2.3.3.5 Dymond et al.

Taking lightweight concrete one step further to include self-consolidating concrete (SCC), Dymond et al. (*24*) experimented with a lightweight self-consolidating concrete (LWSCC) mix design. Ordinary SCC contains a higher percentage of fine aggregate relative to traditional slump-measured concrete, thus potentially reducing aggregate interlock in SCC. Given that ordinary lightweight concrete also has a reduced aggregate interlock compared to normal weight concrete, the combination of the two mix design concepts, that is LWSCC, could have entirely different structural behaviors altogether. Therefore, the researchers tested a prestressed Virginia PCBT-53 girder with a composite cast-in-place lightweight concrete deck to examine the beam's web-shear strength.

The test specimen was 65 ft long and 53 in. deep, with a cross-sectional area of 802.7 in^2. There were 32 pretensioned 0.5-in. diameter, 270 ksi low-relaxation strands. Six of those strands were harped at the end of the girder. Shear reinforcement consisted of No. 5 double-legged stirrups spaced at 7 in. within the shear span, as dictated by the 2006 AASHTO LRFD Bridge Design Specifications (*131*). The composite deck design was based on a 9-in. thick deck placed on girders that were spaced 9 ft on center, although the actual deck was only 7 ft wide due to the limits of the testing facility. The coarse aggregate for both the girder and the deck was ¾-in. expanded slate, while the unit weights of the girder and deck concrete were 118 and 125 pcf, respectively. At the time of testing, the girder compressive strength was 10.6 ksi, while the compressive strength of the deck was 7.6 ksi. Likewise, the splitting tensile strength was 800 psi and 680 psi for the girder and deck, respectively. For testing, the beam was simply supported and subjected to two concentrated loads located 7.5 ft and 10.5 ft away from the girder end, resulting in an a/d of 1.3.

The researchers were only able to get close to failure during the web-shear testing due to limits of the testing facility. Imminent failure was evidenced by concrete flaking in the web. In comparing the experimental web-shear results with predicted values, the authors considered four different models: the 17th edition of the AASHTO Standard Specifications (*90*), the Simplified Procedure, the General Procedure, and a stut-and-tie model (STM). The last three models were in or based on the in the 3rd edition of the AASHTO LRFD Specifications (*13*). All calculations were conducted using a strength reduction factor of 1.0 and the lightweight modifier for sand-lightweight concrete, 0.85, when required. Additionally, the location for these shear strength calculations was at one-half the shear span, because that location was generally where the initial web-shear cracks formed. The resulting ratios of experimental to calculated ultimate strengths are given in Table 2-5. Note that the calculations in Table 2-5 used measured material properties and crack angles where possible, as opposed to those assumed for design. However, separate calculations using only design material properties yielded smaller calculated shear strengths than the experimental shear strength in all cases except for the Simplified procedure. The authors indicated that the modification for lightweight concrete had a relatively minor impact on the calculated overall shear strength, ranging from 2 to 4% of the strength.

Table 2-5. Ratio of experimental to calculated ultimate strengths in Dymond et al. study.

Calculation Model	V_{exp} / V_{calc}
AASHTO Standard Specifications	1.42
Simplified AASHTO LRFD Specifications	1.38
General AASHTO LRFD Specifications	1.46
STM	1.18

As for the load to cause first cracking, both the AASHTO Standard Specifications and the Simplified Approach in the AASHTO LRFD Specifications calculations severely under-predicted the first cracking load. The ratio of $V_{crack\ exp}$ versus $V_{crack\ calc}$ was 1.78 using the Standard Specifications and was 2.46 when considering the LRFD Specifications. On the other hand, the approach using Mohr's circle proved to be closer but over-predicted the web-shear cracking strength. Thus, the ratio of $V_{crack\ exp}$ to $V_{crack\ calc}$ was 0.96.

In addition to the shear strengths, the authors compared the crack angle formed during testing with the angle predicted by the AASHTO LRFD Specifications, STM, and an approach using Mohr's circle. The results are in Table 2-6. Note that the smaller theoretical cracking angle found with the LRFD approach resulted in a higher theoretical steel contribution to the shear strength. Also note that the STM was a little bit on the conservative side in terms of actual shear strength, but the relative accuracy is not all that surprising because the prediction was formulated using the actual test geometry. Lastly, the Mohr's circle calculations were made by assuming the maximum principle stresses determined from the bi-axial failure criterion according to Kupfer and Gerstle (*132*).

Table 2-6. Comparison of web-shear cracking angles versus predicted values

Method of Calculation	θ_{exp} / θ_{calc}
LRFD	1.20
STM	0.98
Mohr's circle	1.05

2.3.4 Code Specifications for Lightweight Concrete

2.3.4.1 Modifications for Lightweight Concrete under ACI

The first appearance of lightweight concrete in the ACI 318 Building Code was in 1963, where the allowable stress in lightweight concrete was limited to

$$v_c = \phi\left(0.28F_{sp}\sqrt{f'_c\ (\text{psi})} + 2500\frac{\rho_w Vd}{M}\right) \le 0.3\phi F_{sp}\sqrt{f'_c(\text{psi})} \qquad (92)$$

where F_{sp} was limited to 4 unless determined using the actual aggregate source. The capacity reduction factor, ϕ, was equal to 0.85 and applied to the diagonal tensile strength regardless of the type of lightweight concrete used. The term ρ_w was defined as

$$\rho_w = \frac{A_s}{b_w d} \qquad (93)$$

The following design code, ACI 318-71, abandoned F_{sp}, and instead used the same equations as those for normal weight concrete, with coefficients in front of $\sqrt{f'_c}$ depending on the type of concrete. This format is basically still used today, with the minor change that the current ACI 318 code has a more general lightweight modification factor, λ, instead of the aforementioned coefficients. If f_{ct} is specified, then:

$$\lambda = \frac{f_{ct}}{6.7\sqrt{f'_c\ (\text{psi})}} \le 1.0 \qquad (94)$$

If the splitting tensile strength is not specified, then λ equals 0.85 for sand-lightweight concrete and 0.75 for all-lightweight concrete. According to the ACI 318-11 code, this λ-factor applies to:

- shear strength of concrete
- shear friction (where λ = 0.75 regardless of whether sand- or all-lightweight concrete is used)
- development length of reinforcement (again, where λ = 0.75 regardless of whether sand- or all-lightweight concrete is used)

- tensile stresses in concrete shell structures
- amount of reinforcement in seismic force-resisting systems
- coupling beams in seismic applications
- tension face of structural plain concrete in combined flexure and axial compression
- concrete compressive strength in the general zone of post-tensioned structures.

Note that λ does not apply to:

- minimum area of transverse reinforcement
- spacing limits on shear reinforcement
- maximum limit on the shear strength provided by the stirrups, V_s
- maximum limit on V_n in concrete slabs
- cross-section dimensions for torsion design

While there are numerous areas in shear design where the engineer must consider the impact of lightweight concrete on the overall strength, ACI 318-11 has only a single strength reduction factor for the nominal shear strength of a structural element, regardless of the concrete density. That reduction factor is $\phi = 0.75$.

2.3.4.2 Modifications for Lightweight Concrete under AASHTO

AASHTO first acknowledged the application of lightweight concrete in its 1973 Standard Specifications, but even then the discussion was limited to the modulus of rupture. By the following publication in 1977, AASHTO adopted the same modifications for lightweight concrete as did ACI in 1971. Those substitutions remained in place through the remaining publications of the AASHTO Standard Specifications.

The adoption of LRFD in 1994 brought about a minor change in the way AASHTO dealt with lightweight concrete, which is the same as the current 2010 AASHTO LRFD Bridge Design Specifications. While not specifically termed "λ," Article 5.8.2.2 calls for "substituting" $\sqrt{f'_c}$ with some calculation based on what is known about the concrete. This specification essentially applies the same lightweight concrete modification multipliers in front of $\sqrt{f'_c}$ as in ACI 318-11.

The one minor exception is the format of the case when the tensile strength is specified, where $\sqrt{f'_c}$ is replaced by

$$4.7f_{ct} \le \sqrt{f'_c}\ (\text{ksi}) \qquad (95)$$

where f_{ct} is also in ksi units. If f'_c is converted into ksi units and Eq. (94) is rearranged to the same format as Eq. (95), then Eq. (94) would become

$$4.72f_{ct} \le \sqrt{f'_c}\ (\text{ksi})$$

which, given the number of significant figures, is the same as Eq. (95).

The substitution accounting for lightweight concrete applies to wherever $\sqrt{f'_c}$ appears in Articles 5.8.2 and 5.8.3 of the 2010 AASHTO LRFD Bridge Design Specifications. Thus, like the ACI 318-11 code, the lightweight strength reduction occurs when designing for the shear strength of concrete following the SDM. However, unlike ACI, the AASHTO modification also applies to: the minimum area of transverse reinforcement, the shear resistance provided by the steel if that reinforcement consists of a single longitudinal bar or a group of longitudinal bars bent up at the same distance from the support, and the shear strength provided by the steel reinforcement following the Simplified Procedure for Prestressed and Nonprestressed Sections. As for development length, AASHTO does not require the engineer to modify the development length based on the concrete density. Additionally, AASHTO does not apply any sort of λ-factor in calculations for interface shear friction as in ACI 318-11; however, the factors limiting the interface shear resistance are fairly similar.

Another significant departure that the 2010 AASHTO LRFD Bridge Design Specifications makes from the ACI 318-11 code is the strength reduction factor in shear design, ϕ_v. First of all, AASHTO differentiates between normal weight and lightweight concrete. This differentiation was a change from all editions of the AASHTO Standard Specifications using LFD for shear design, where there was a single strength reduction factor regardless of the concrete density. The reason for the change was based on the data showing that the tensile strength of lightweight

concrete was a fixed fraction of the tensile strength of normal weight concrete. Secondly, ϕ_v is 0.70 for lightweight concrete, which is lower than the 0.75 factor for ACI, even though the AASHTO resistance factor was based on multipliers provided in the ACI 318-89 code. Note that for normal weight concrete, $\phi_v = 0.90$. Lastly, by differentiating between lightweight and normal weight concrete and applying the strength reduction factor to the overall nominal shear strength, the penalty for using lightweight concrete applies to both the concrete and the steel. This reduction to the steel strength is in spite of the fact that the same steel is going into either concrete design. Furthermore, past research has indicated that lightweight concrete can have as good, if not better, bond, with steel compared to normal weight concrete (*133-135*). Although Funahashi et al. (*114*) found that the bond strength decreased as concrete density decreased, that research team was experimenting with super lightweight concrete with concrete densities as low as 82 pcf, as discussed in Section 2.3.1.6.10 .

2.4 Reliability-based Strength Reduction Factors

2.4.1 The Underpinnings of Structural Reliability

The strength reduction factors mentioned in Section 2.3.4.2 stem from *NCHRP Report 368*, written by Nowak in 1999 (*136*). The author focused on calibrating the load and resistance factors to establish a consistent level of safety across the bridge design spectrum, measuring the level of safety in terms of the probability of failure. However, direct calculation of the probability of failure, $P_f = P(R - Q < 0)$, where R is the sum of the resistance effects and Q is the sum of the load effects, can be difficult given all of the factors that go into the resistance and loads. Instead, engineers can measure the safety of a structure using the reliability index, β (*137*).

Nowak found a base level of safety using the target reliability index, β_T, which he arbitrarily selected such that all structures had similar margins of safety. The range of bridges considered included steel girders with and without composite decks, reinforced concrete T-beams and prestressed concrete girders, with spans ranging from 30 ft to 200 ft and girder spacings ranging from 4 ft to 12 ft. However, the target reliability index also depends on the importance of the structure, the consequences of failure, and the marginal cost of increasing or decreasing the level

of safety (*138*). In surveying the myriad of combinations, Nowak found that the reliability index for the design moment in a simply-supported, 60-ft span for girders spaced at 6 ft was around 3.5, regardless of the structure type. Thus, β_T was defined as 3.5 and was deemed an acceptable level of reliability.

In conjunction with establishing the target reliability index, Nowak developed a statistical database of variables that went into calculating the load effects and strengths of structural members through both in-situ field measurements as well as numerical simulations. In terms of strength, the capacity of a bridge depends on the resistance of the components and the connections between those components. The uncertainty in that resistance primarily depends on the randomness of the material properties, the variability in fabrication or geometry, and the accuracy of the model used to design the member (*138, 139*). Therefore, the overall component resistance, *R*, is a random variable that is the product of these three bias factors along with the nominal strength (*136-138*):

$$R = R_n \lambda_M \lambda_F \lambda_P \quad (96)$$

where

R_n = nominal resistance

λ_M = material properties factor, mathematically is the ratio of the average actual material property to the nominal material property

λ_F = fabrication factor, calculated as the ratio of the average actual dimension versus the nominal cross-sectional property

λ_P = "professional" or modeling error factor

λ_P covers the engineer's design methodology, including analysis methods, assumed stress and strain distributions. This factor is defined as the average ratio of the actual behavior to the strength predicted by the model, where that prediction uses known material properties and member geometries. The material and fabrication parameters can be grouped together by performing thousands of Monte Carlo simulations (see Section 2.4.2.2) to develop the statistical variation in the calculated design strength of a given structure due to the variation in the materials and geometric properties (*139*). In the case of shear strength in *NCHRP Report 368*, the design model was the Modified Compression Field Theory (*70*).

Nowak followed a similar Monte Carlo process for the loads affecting the element. Having found the statistical parameters for each of the load components, the researcher determined the load factors, γ, such that the overall load had a predetermined probability of being exceeded. For every load component, X_i, there was a load factor, γ_i, calculated as

$$\gamma_i = \lambda_i(1 + kCoV_i) \quad (97)$$

where

γ_i = the load factor for a given load component

λ_i = the bias factor for a given load component

k = the number of standard deviations away from the mean value, which the author had taken to be 2 as a matter of good practice (*137*)

CoV_i = the coefficient of variation for the given load component

Nowak then used those load factors to select the resistance factors such that the reliability index was proximal to the target reliability index, where the structural reliability was calculated following the procedures outlined by Rackwitz and Fiessler, as discussed in Section 2.4.2.3. The resistance factor was also based on the minimum required resistance, which was defined as

$$R_{LRFD} = \frac{1.25DC + 1.50DW + 1.70(LL + IM)}{\phi} \quad (98)$$

where

DC = the dead load of the structural components and non-structural attachments

DW = the dead load of the wearing surface

LL = the vehicular live load

IM = vehicular dynamic load allowance

Note that the live load in Eq. (98) includes the 0.64 klf uniformly distributed lane load, which is not multiplied by the dynamic load allowance, *IM*. However, also note that the live load factor in Eq. (98) is 1.70, unlike the 2010 AASHTO LRFD Bridge Design Specifications (*45*), where the Strength I limit state has a factor of 1.75. Obviously, the nature of this calibration means that the resistance factors are not wholly independent of the load factors. Work by Ellingwood et al. reached a similar conclusion (*140*).

2.4.2 Reliability Calculation Procedures

2.4.2.1 Bias Factors

As mentioned in the section above, the bias factors for materials and fabrication can be combined into a single factor, λ_{FM}. Therefore, the bias factor and the coefficient of variation for the design resistance, R, become

$$\lambda_R = \lambda_{FM}\lambda_P \quad (99)$$

$$CoV_R = \sqrt{CoV_{FM}^2 + CoV_P^2} \quad (100)$$

where λ_P is defined in Eq. (96), and λ_{FM} is the average ratio of the tested material properties and element dimensions combined together versus the nominal material properties and geometrical dimensions combined together. CoV_P and CoV_{FM} are the coefficients of variation of the respective ratios used to calculate λ_P and λ_{FM} (*137*).

Separately, Ellingwood et al. (*141*) suggested that the variability in the professional factor actually comes from three sources:

- variability of the model itself, CoV_m
- uncertainties in the measured test load due to errors in the gages and readings, and definitions of failure, CoV_{test}
- differences in the strengths of material sample specimens versus the true strength of the material in the girder, as well as differences in the actual geometry versus what was recorded, CoV_{spec}

If $CoV_{T/C}$ is defined as the coefficient of variation obtained from comparisons between the tested and calculated strengths, then

$$CoV_{T/C} = \sqrt{CoV_m^2 + CoV_{test}^2 + CoV_{spec}^2} \quad (101)$$

Solving Eq. (101) for CoV_m yields:

$$CoV_m = \sqrt{CoV_{T/C}^2 - CoV_{test}^2 - CoV_{spec}^2} \quad (102)$$

Ellingwood et al. found that CoV_{test} was 2% – 4% and CoV_{spec} was about 4%. The researchers used CoV_m along with the average value of R_{test} / R_{calc} to randomly generate a professional variable that was multiplied by the randomly generated material and fabrication variables, which then in turn was multiplied by the nominal strength, R_n, to come up with a theoretical strength in a Monte Carlo simulation procedure.

2.4.2.2 Monte Carlo Simulation

Ideally, there would be a sufficiently sized database of actual tests of full-scale elements to generate the statistical parameters needed to conduct a reliability analysis. However, such a database is not economically practical. Therefore, researchers often times simulate the load effects and resistances; one numerical simulation solution is the Monte Carlo method. The Monte Carlo method uses a small sample of actual test results to generate a probability distribution of a given set of parameters, which in turn can be used to generate samples of numerical data that give theoretical test results (*137*).

Certainly, the variability in the Monte Carlo simulation results is influenced by the randomness of the basic variables going into the simulation. However, while Monte Carlo simulation can take into account such factors as the variability in the material or geometrical properties by comparing the calculated strength using randomly generated parametric values versus the calculated strength using nominal values for those parameters, the process does not account for incomplete or insufficient inputs or the error in the resistance equations predicting the actual strength of the member. Thus there is the need to formulate the professional factor, as discussed in Section 2.4.2.1. However, often times there is insufficient data available to generate the variability in λ_P. If so, then the parameters for the professional factor must be assumed (*142*).

Nevertheless, there are four basic steps to the Monte Carlo simulation process:

1. Generate random numbers for the basic variables
2. Convert those numbers from Step 1 to fit the appropriate statistical distribution for each variable

3. Evaluate the strength capacity using the results from Step 2 in the appropriate strength prediction model
4. Repeat the Steps 1 through 3 enough times to reach a desired level of uncertainty in the strength prediction model.

In Step 1, the generated number is of a uniformly distributed, random number, u, between 0 and 1. Then, in Step 2, u is translated into another number, x, that is between extreme values a and b for a given variable by using the formulation

$$x = a + (b - a)u$$

Given a uniformly distributed random value, u_i, the standard normal random value, z_i, can be calculated as

$$z_i = \Phi^{-1}(u_i)$$

where Φ^{-1} is the inverse of the standard normal cumulative distribution function (CDF). If a random value, g_i, is needed from some arbitrary normal distribution (as opposed to a standard normal distribution), then g_i can be calculated as

$$g_i = \mu_g + z_i \sigma_g \quad \textbf{(103)}$$

where

μ_g = the mean of g,

σ_g = the standard deviation of g, calculated as $\mu_g CoV_g$

where CoV_g = the coefficient of variation of g. If a random variable follows a lognormal distribution, one can generate a set of uniformly distributed values as done in Step 1 above, and then convert each number using the following:

$$x_i = e^{(\mu_{\ln X} + z_i \sigma_{\ln X})} \quad \textbf{(104)}$$

where

$$\sigma^2_{\ln X} = \ln\left(CoV_X^2 + 1\right) \approx CoV_X^2 \quad \textbf{(105)}$$

$$\mu_{\ln X} = \ln\left(\mu_X\right) - \frac{1}{2}\sigma^2_{\ln X} \approx \ln\left(\mu_X\right) \quad \textbf{(106)}$$

where

$$CoV_X = \frac{\sigma_X}{\mu_X} \qquad (107)$$

where σ_X and μ_X are the mean and standard deviation of the random variable, X. Note that the approximations in Eqs. (105) and (106) are valid only if $CoV_X < 0.20$ (*137*).

Typically, load parameters are assumed to have normal distributions while resistance parameters have lognormal distributions (*136*). Upon completion of the Monte Carlo process, one can plot the probability density function (PDF) and cumulative distribution function of the results and identify the type of distribution of the given strength model. Once the distribution is known, the researcher can calculate the mean and coefficient of variation for the model (*139*), which gives rise to λ_{FM} and CoV_{FM} as mentioned in Section 2.4.1.

Monte Carlo simulation can only provide an estimate for the probability of failure; however, the estimate improves as the number of simulations increase. If $\overline{P}$ is defined as a sample estimate, the value of $\overline{P}$ will vary from sample to sample, and therefore, can itself be considered a random variable with its own mean, variance, and coefficient of variation. If P_{true} is defined as the theoretically correct probability that is estimated by $\overline{P}$, then

$$\begin{aligned} \mu_{\overline{P}} &= P_{true} \\ \sigma^2_{\overline{P}} &= \frac{1}{N}[P_{true}(P_{true}\text{-}1)] \\ CoV_{\overline{P}} &= \sqrt{\frac{1\text{-}P_{true}}{N \cdot P_{true}}} \end{aligned} \qquad (108)$$

where N is the number of required simulations. Using the equations in (108), one can determine the number of samples needed to limit the uncertainty in the estimated probability. For example, if one needs to achieve a probability that is no greater than 0.01 and has a coefficient of variation less than or equal to 0.1, then N would be (*137*):

$$N = \frac{1 - P_{true}}{CoV^2_{\overline{P}}(P_{true})} = \frac{1 - 0.01}{0.10^2 \cdot 0.01} = 9900$$

2.4.2.3 Rackwitz-Fiessler Procedure

Having determined all of the statistical parameters for the load and resistance, one can calculate the reliability index, β, which again, is defined as a function of the probability of failure, P_F, or mathematically:

$$\beta = -\Phi^{-1}(P_F)$$

If the load and resistances are independent, normal random variables, then

$$\beta = \frac{(\mu_R - \mu_Q)}{\sqrt{\sigma_R^2 + \sigma_Q^2}} \qquad (109)$$

If Q and R are independent, lognormal random variables, then

$$\beta = \frac{\ln(\mu_R - \mu_Q)}{\sqrt{CoV_R^2 + CoV_Q^2}} \qquad (110)$$

If Q and R are not independent and normal or lognormal, then Eqs. (109) and (110) only give approximate reliability values. More accurate results can be obtained through alternative methods, including the First-Order, Second-Moment (FOSM) reliability index. If one has a linear limit state, such that

$$g(X_1, X_2, \ldots, X_n) = a_0 + a_1X_1 + a_2X_2 + \ldots + a_nX_n = a_0 + \sum_{i=1}^{n} a_iX_i$$

where the terms X_i are uncorrelated random variables and a_i are coefficients associated with X_i, then β can be expressed as:

$$\beta = \frac{a_0 + \sum_{i=1}^{n} a_i\mu_{X_i}}{\sqrt{\sum_{i=1}^{n}(a_i\sigma_{X_i})^2}} \qquad (111)$$

where μ_{Xi} and σ_{Xi} are the mean and standard deviations of the values for the variables X_i. However, the problem with the FOSM reliability index is that the results can be inaccurate if the

tails of the distribution functions are not normally distributed. Furthermore, this index depends on the form of the limit state function. As an answer to the two aforementioned shortcomings, the Hasofer-Lind reliability index was proposed in 1974 (*137*). The Hasofer-Lind method establishes an alternative definition of the reliability index, where β is the shortest distance from the origin between the reduced variables, Z_R and Z_Q, and the line $g(Z_R, Z_Q) = 0$ (see Figure 2-5).

If using the Hasofer-Lind method, all random variables should be converted into their "standard" form. For given variables, R for resistance and Q for load, the standard forms are

$$Z_R = \frac{R - \mu_R}{\sigma_R}$$
$$Z_Q = \frac{Q - \mu_Q}{\sigma_Q} \qquad (112)$$

where Eq. (112) can be written as

$$R = \mu_R + Z_R\sigma_R$$
$$Q = \mu_Q + Z_Q\sigma_Q \qquad (113)$$

Using Eq. (113), the failure limit state defined as $R - Q < 0$ can be written as

$$g(Z_R, Z_Q) = (\mu_R - \mu_Q) + Z_R\sigma_R - Z_Q\sigma_Q$$

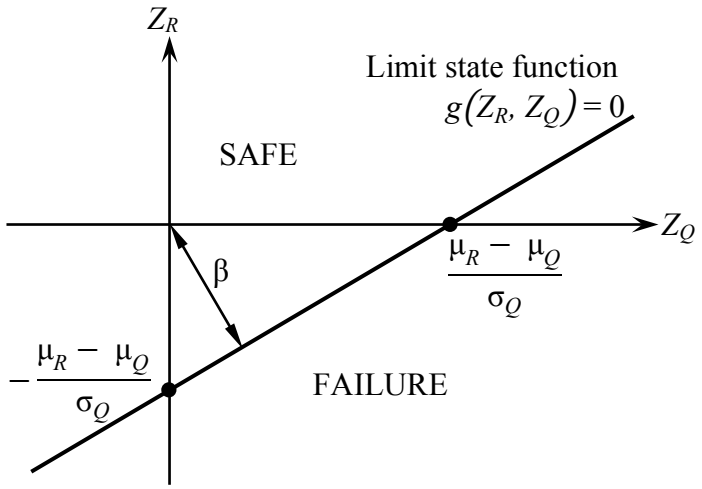

Figure 2-5. Reliability index in terms of the Hasofer-Lind definition.

where the above equation represents a straight line in the space of reduced variables, Z_R and Z_Q. However, this method is an iterative process because the limit state function is evaluated at a "design point," which is unknown a priori. Also, all of the variables in the limit state function must be uncorrelated, or converted into uncorrelated variables (*137*).

If the probability distributions for all of the variables are known, then the Rackwitz-Fiessler procedure can provide an even more accurate reliability index. The basic process makes use of the Hasofer-Lind definition and involves calculating an equivalent normal mean and standard deviation for all variables that do not follow a normal distribution. Thus, the CDF and PDF of these non-normal variables must be equal to the normal CDF and PDF at the boundary described as $g(Z_R, Z_Q) = 0$. In other words,

$$F_X(x^*) = \Phi\left(\frac{x^* - \mu_X^e}{\sigma_X^e}\right) \quad (114)$$

$$f_X(x^*) = \frac{1}{\sigma_X^e}\phi\left(\frac{x^* - \mu_X^e}{\sigma_X^e}\right) \quad (115)$$

where Φ and ϕ are the CDF and PDF of the standard normal distribution, respectively, and x^* is the design point at which the limit state function g is being evaluated. After rearranging Eqs. (114) and (115), one arrives at the equivalent normal mean and standard deviations:

$$\mu_X^e = x^* - \sigma_X^e\left[\Phi^{-1}\left(F_X(x^*)\right)\right] \quad (116)$$

$$\sigma_X^e = \frac{1}{f_{X(x^*)}}\phi\left(\frac{x^* - \mu_X^e}{\sigma_X^e}\right) = \frac{1}{f_{X(x^*)}}\phi\left[\Phi^{-1}\left(F_X(x^*)\right)\right] \quad (117)$$

The basic steps behind the Rackwitz-Fiessler procedure are as follows:

1. Formulate the limit state function (in the form of $g = 0$), with the distribution parameters (type of distribution, mean and standard deviation) for the various random variables.

2. Assume $n - 1$ of the random variables and solve for the remaining variable using the limit state function in Step 1, giving a set of x_i^* variables for an assumed design point.

3. For all variables x_i^* with non-normal distributions, find equivalent mean and standard deviations ($\mu^e_{X_i}$ and $\sigma^e_{X_i}$) using Eqs. (116) and (117).

4. Determine the reduced variables, z_i^* using the equation

$$z_i^* = \frac{x_i^* - \mu^e_{X_i}}{\sigma^e_{X_i}} \qquad \textbf{(118)}$$

5. Find the partial derivatives of the limit state function found in Step 1 with respect to the reduced variables from Eq. (118) using the equation

$$\frac{\partial g}{\partial Z_i} = \frac{\partial g}{\partial X_i}\frac{\partial X_i}{\partial Z_i} = \frac{\partial g}{\partial X_i}\sigma_{X_i} \qquad \textbf{(119)}$$

Place the results of Eq. (119) into a column vector multiplied by -1, such that

$$\{G\} = \begin{Bmatrix} G_1 \\ G_2 \\ \vdots \\ G_n \end{Bmatrix} \text{ where } G_i = -\left.\frac{\partial g}{\partial Z_i}\right|_{\text{evaluated at the design point}} \qquad \textbf{(120)}$$

where ∂Z_i is in terms of ∂X_i, as expressed in Eq. (119).

6. Calculate the reliability index as

$$\beta = \frac{\{G\}^T\{z^*\}}{\sqrt{\{G\}^T[\rho]\{G\}}} \qquad \textbf{(121)}$$

where

$$\{z^*\} = \begin{Bmatrix} z_1^* \\ z_2^* \\ \vdots \\ z_n^* \end{Bmatrix}$$

and where [ρ] is a diagonal matrix with the coefficients off of the diagonal being the correlation coefficients between the various variables. For example,

$$[\rho] = \begin{bmatrix} 1 & C_{X,Y} & C_{X,Z} \\ C_{X,Y} & 1 & C_{Y,Z} \\ C_{X,Z} & C_{Y,Z} & 1 \end{bmatrix} \qquad \textbf{(122)}$$

If the variables are uncorrelated, then [ρ] becomes the identity matrix.

7. Calculate the α_n sensitivity factors as

$$\{\alpha\} = \frac{[\rho]\{G\}}{\sqrt{\{G\}^T[\rho]\{G\}}} \quad \textbf{(123)}$$

8. Find the $n - 1$ reduced variables for a new design point using the equation

$$z_i^* = \alpha_i \beta \quad \textbf{(124)}$$

9. Calculate the $n - 1$ variables, x_i^*, using Eqs. (118) and (124).

10. Calculate the remaining random variable, x_n^* using the results from Step 9 in the limit state equation, $g = 0$.

11. Repeat Steps 3—10 until β and $\{x_i^*\}$ converge.

If the limit function is linear (such as $g = R - Q$), then β in Eq. (121) simplifies to something similar to Eq. (111):

$$\beta = \frac{a_0 + \sum_{i=1}^{n} a_i \mu_{X_i}^e}{\sqrt{\sum_{i=1}^{n} \left(a_i \sigma_{X_i}^e\right)^2}} \quad \textbf{(125)}$$

If a given variable is lognormal, then the equivalent mean and standard deviation in Eq. (125) can be calculated as

$$\sigma_X^e = x^* \sigma_{\ln X} \quad \textbf{(126)}$$

$$\mu_X^e = x^* \left[1 - \ln(x^*) + \mu_{\ln X}\right] \quad \textbf{(127)}$$

where $\sigma_{\ln X}$ and $\mu_{\ln X}$ are the parameters for a lognormal distribution, calculated using Eqs. (105) and (106). Note that the term σ_{X_i} in Eq. (119) must be replaced by $\sigma_{X_i}^e$ if the variable is a lognormal random variable. Also note that the CDF and PDF for a lognormal random variable are:

$$F_X(x^*) = \Phi\left(\frac{\ln(x^*) - \mu_{\ln X}}{\sigma_{\ln X}}\right) \quad (128)$$

$$f_X(x^*) = \frac{1}{x^*\sigma_{\ln X}}\phi\left(\frac{\ln(x^*) - \mu_{\ln X}}{\sigma_{\ln X}}\right) \quad (129)$$

where Φ and ϕ are the CDF and PDF for the standard normal random variable, respectively.

Often times, the function $g(R,Q) = R - Q$ defines a complex reliability problem. The resistance is typically considered to have a lognormal distribution while the load has a normal random distribution. If so, and if $CoV_R < 0.20$, then the reliability index in Eq. (121) becomes

$$\beta = \frac{\lambda_R R_n(1 - kCoV_R)[1 - \ln(1 - kCoV_R)] - \mu_Q}{\sqrt{[\lambda_R R_n(1 - kCoV_R)CoV_R]^2 + \sigma_Q^2}} \quad (130)$$

where

k = the number of standard deviations away from the actual mean value
λ_R = the bias factor
R_n = the nominal design value for the resistance (*137*)

2.4.3 Past Research on Reliability of Concrete Girders

2.4.3.1 NCHRP Report 368

In *NCHRP Report 368*, Nowak reported bias factors and the coefficients of variation for reinforced concrete (both with and without shear reinforcement) and prestressed concrete beams, listed in Table 2-7. The table gives the material/fabrication and professional statistics, along with the resulting overall factors for shear capacity. Presumably, these values are solely for normal weight concrete.

Table 2-7. Statistical parameters of shear resistance, published in *NCHRP Report 368*.

Element Type	FM		P		R	
	λ	CoV	λ	CoV	λ	CoV
Reinforced Concrete (no stirrups)	1.165	0.135	1.20	0.10	1.40	0.17
Reinforced Concrete (with stirrups)	1.13	0.12	1.075	0.10	1.20	0.155
Prestressed Concrete	1.07	0.10	1.075	0.10	1.15	0.14

In most cases, shear failures tend to occur after a flexural failure; therefore, the two failure modes are correlated in a statistical sense, where the shear strength will increase as the flexural strength increases (*137*). However, ordinarily, shear only governs in regions of low moment and high shear (*136*). Furthermore, there is not a lot of data available regarding the correlation between the strength parameters (*143*).

The statistical parameters listed in Table 2-7 stem from the work by Yamani (*139*), who developed the material/fabrication parameters using Monte Carlo simulations with girders designed according to the 1989 AASHTO LFD Specifications. As for the professional factors, Yamani collected those values for reinforced concrete from literature by Ellingwood et al. (*141*) and Vecchio and Collins (*69*); for prestressed concrete, Yamani used results published by Vecchio and Collins as well as Siriaksorn (*142*). The work by Ellingwood et al. calculated the professional factor using data provided by Mirza and MacGregor in 1979 (*144*). The Mirza and MacGregor data set consisted of 62 beams with and 96 beams without vertical shear reinforcement, all of which had rectangular cross-sections with webs ranging from 6 in. to 12 in. and d ranging from 10 in. to 18 in. The concrete compressive strength varied from 3.2 ksi to 7 ksi, while the shear reinforcing index varied from 0 psi to 290 psi. Shear span-to-depth ratios were between 2.3 and 4.9. Using the ACI 318-77 (*145*) standard to predict shear strengths, Ellingwood et al. found that the average ratio of test-to-theoretical strength and the corresponding coefficient of variation of the beams with "low" amounts of stirrups was 1.085 and 0.137, respectively, while beams with "large" amounts of stirrups had statistical values of 1.13 and 0.082, respectively. For beams with a "moderate" amount of shear reinforcement had a professional factor of 1.09 with a coefficient of variation of 0.17.

The 1982 Vecchio and Collins report was published four years before the two authors had introduced their Modified Compression Field Theory. Furthermore, the beam data in that analysis came from four different studies performed at the University of Toronto (*146-149*). The six reinforced concrete beams and six prestressed concrete beams in the Vecchio and Collins report had rectangular cross-sections measuring 24 in. tall by 12 in. wide. One of the six reinforced concrete beams was solid, while the other five were hollow box beams. The concrete compressive strength ranged from 3.6 ksi to 5.8 ksi, while the stirrup density ($\rho_v f_{yv}$) ranged from

135 psi to 520 psi. Additionally, the longitudinal steel density (ρf_y) ranged from 2.28 ksi to 4.2 ksi. Some of the specimens were simply supported continuous members, while others were loaded with fixed supports at each end. Nevertheless, in all cases, the test regions of interest had constant shear along the length of the test region. Of these six reinforced concrete beams, the average ratio of experimental to calculated shear strength was 1.03 with a coefficient of variation of 4.2%.

With regards to Siriaksorn's work, his research was published in 1980, fourteen years before Modified Compression Field Theory was used in the AASHTO code. As such, the design strength in that project was obtained using the ACI code, where the analysis only considered service loads. Furthermore, Siriaksorn's analysis only considered the flexural strength of prestressed beams, not shear strength. Lastly, the prestressed beams were only partially prestressed, as opposed to being fully prestressed.

Siriaksorn acknowledged that there were different factors that played into the variability of a given resistance model, which he termed as "prediction errors, ε_R." However, this researcher indicated that that there was insufficient data available to generate ε_R. Therefore, Siriaksorn assumed values for different sources in ε_R, as given in Table 2-8. The author indicated that results on tests on prestressed beams by Nawy and Huang (*150*) indicated that ε_R ranged from 0.15 to 0.23.

For the analysis in *NCHRP Report 368*, the total load, *Q*, was assumed to be a random normal variable and the resistance, *R*, was assumed to be a lognormal random variable. The live load parameters were based on a 1975 database consisting of 10,000 trucks as well as current legal

Table 2-8. Sources of model prediction errors, according to Siriaksorn

Limit State	ε_R
maximum crack width	0.1 or 0.2
allowable stress range, repeated service load	0.05
stress range in mild steel, repeated service load	0.05
stress range in prestress steel, repeated service load	0.05
live load deflection	0.05
additional deflection	0.1 or 0.2

load limits. If those limits were to increase, then the author acknowledged that the load factors would need to be revised upwards.

Having developed all of the necessary information regarding loads and resistances, Nowak narrowed down the number of reliability analyses to four combinations where the live load factor was either 1.6 or 1.7, and the strength reduction factor for shear was either 0.90 or 0.95. Regardless of which combination of factors was used in the reliability calculations, the results indicated that the reliability indices of the shear strengths calculated using these newly-calibrated load and resistance factors under the AASHTO LRFD code were more consistent across the range of girder type and span length when compared to the indices calculated under the 1992 AASHTO LFD code, where the resistance factors for shear in reinforced and prestressed concrete were 0.85 and 0.90, respectively, and the reliability index ranged from 1.91 to 3.98. For the AASHTO LRFD code, the recommended resistance factor was 0.90 regardless of whether or not the concrete was prestressed, and the reliability index ranged from 3.62 to 4.03 (assuming that the live load factor was 1.70). Furthermore, the author concluded that although varying slightly along the range of girder spacing, the reliability index did not depend greatly on that parameter for practical design purposes if following the AASHTO LRFD Bridge Design Specifications. The ratio of $V_{n\,LRFD}$ / $V_{n\,Std}$ for reinforced and prestressed concrete girders with 100-ft span lengths was about 1.2 to 1.35 (*136*), where $V_{n\,Standard}$ is the nominal shear strength calculated using the AASHTO Standard Specifications.

2.4.3.2 Statistical Reliability of Lightweight Concrete

More recently, Nowak has been involved in the reliability analysis of lightweight concrete. For one such project, the researcher investigated the statistical parameters for the compressive strength of lightweight concrete (*151*). Generally, Nowak and Rakoczy found that the material bias factor was larger for lightweight concrete compared to normal weight concrete, particularly for high-strength concretes. The authors recommended that the material bias factor for lightweight concrete be calculated as

$$\lambda_M = -0.07 f'_c + 1.634 \qquad \textbf{(131)}$$

On the other hand, the coefficient of variation was fairly similar to that of high-strength normal weight concrete. Thus, the authors recommended maintaining that value at 0.12.

At about the same time, Paczkowski and Nowak examined reliability models for shear in lightweight reinforced concrete bridges (*138*). As a part of that study, the researchers gathered a comprehensive data set of both lightweight and normal weight concrete. Their results showed that along with compressive strength, lightweight concrete had similar material statistics in terms of tensile strength and modulus of rupture. Naturally, because the elastic modulus of lightweight aggregate tended to be lower than its normal weight counterpart, the elastic modulus of lightweight concrete was lower.

As a part of their reliability analysis, Paczkowski and Nowak established a professional factor for lightweight concrete. However, the researchers only considered 13 lightweight tests in the analysis along with 10 normal weight companion tests collected from previous research by Hamadi and Reagan (*115*), Walraven and Al-Zubi (*120*), and Ramirez et al. (*152*). This data set included rectangular, T, and I-shaped cross-sections, measuring 14 in. to 32 in. high with a composite cross-sectional area varying from 132 in^2 to 279 in^2. The longitudinal reinforcement consisted of mild steel while the reinforcing index in the web was in between 87 psi and 467 psi. The span lengths in this data set ranged from 8.2 ft to 18.0 ft and loaded at a/d ranging from 2.2 to 3.6. While the five beams in the Hamadi and Regan study used all-lightweight concrete, the other two studies comprised sand-lightweight concrete. Of the 13 beams tested, only one had compressive strength that exceeded 8 ksi. The shear strength calculations followed the General Method in the 4^{th} edition of the AASHTO LRFD Bridge Design Specifications, retaining the lightweight modification factors as required.

The authors organized the available data into two sets, matching one beam in the lightweight set with one to three beams in the normal weight set, or vice versa. These pairings only matched beams that were in the same original study and attempted to match similar compressive strengths. The authors' analysis showed that more than a third of the lightweight tests had experimental strengths that were less than what was predicted, while all of the normal weight tests exceeded their predicted results. Furthermore, while the ratio of experimental versus expected strengths decreased as the amount of shear reinforcement increased regardless of the

concrete density, the rate of decrease for the lightweight beams was greater. This fact is in line with Hamadi and Reagan's hypothesis that lightweight concrete is not affected by an increase in steel reinforcement to the same degree as normal weight concrete. A second conclusion was that the level of conservatism in the design calculation increased as concrete compressive strength increased, regardless of the type of concrete. However, the rate of increase for lightweight concrete was higher than that of normal weight concrete, which suggests that lightweight concrete behaves more like high-strength normal weight concrete, where fracturing tends to occur within the aggregate.

Paczkowski and Nowak found the professional bias factor to be 1.2 for the normal weight beams in the analysis, with a coefficient of variation of 0.11. This value for λ_P is quite a bit larger than the value of 1.075 in *NCHRP Report 368*. On the other hand, λ_P for lightweight concrete was about 15% lower at 1.0, with a similar CoV_P of 0.10. Because the NCHRP study had set the professional bias factor for normal weight concrete bridge girders at 1.075 with a coefficient of variation of 0.10, the authors of this report concluded that the average λ_P for lightweight bridge girders should be 15% less, or 0.91 with the coefficient of variation equal to 0.10.

Using the above modeling bias factor and coefficient of variation, the researchers developed a resistance factor for the shear design of lightweight concrete T-sections following the 2007 AASHTO LRFD Bridge Design Specifications. The nominal resistance was expressed in terms of

$$R_n = \frac{1.25DC + 1.5DW + 1.75(LL + IM)}{\phi_v} \quad \textbf{(132)}$$

Having established that lightweight concrete had a similar material bias as its normal weight counterpart, and assuming that the fabrication uncertainty should be the same regardless of what type of concrete is in the member, the authors used the previously established λ_{FM} and CoV_{FM} parameters of 1.12 and 0.1, respectively, for reinforced concrete. However, note that λ_{FM} for shear in reinforced concrete was actually reported as 1.13 in NCHRP Report 368, and for prestressed concrete, λ_{FM} and CoV_{FM} were 1.07 and 0.10, respectively. Combining these parameters with the aforementioned λ_P and CoV_P, Paczkowski and Nowak calculated that λ_R was

equal to 1.02 and CoV_R was equal to 0.14 for lightweight concrete. The researchers used these statistical parameters to select a resistance factor that would result in the reliability index that was close to the target reliability index, which had already been established in *NCHRP Report 368*. In conclusion, the authors recommended using $\phi_v = 0.80$ for the shear design of lightweight concrete girders.

2.5 Literature Summary

Over the course of a century or more, modern shear design of concrete members has been evolving, with each evolutionary step bringing engineers closer to understanding the true behavior of concrete in shear. Yet, as advanced as the design profession has become, engineers have not mastered all of concrete's complexities. Nevertheless, the demand for this building material continues, and new technologies help to answer that demand. One improvement has been the introduction of lightweight aggregate in concrete, which provides both structural and economic benefits. However, after more than 50 years and nearly 400 tests, as summarized in Table 2-9, there is still some degree of uncertainty and even disagreement as to how to treat lightweight concrete relative to normal weight concrete, as seen in the differences in the ACI 318-11 code and the 2010 AASHTO LRFD Bridge Design Specifications.

Focusing on large-scale, prestressed lightweight concrete beams, the fact that there have only been 12 experimental shear tests conducted prior to this point has left gaps in the data when considering different parameters. In the case of Figure 2-6, these gaps exist for f_c between 7 and 9 ksi, the effective shear depth between 29 in. and 41 in. as well as 42 in. and 52 in., the area of the composite girder between 600 and 1600 in^2, the shear reinforcing index between 200 and 600 psi, among other parameters as well. Note that V_{calc} in Figure 2-6 is the theoretical shear strength according to Appendix B5.2 of the 2010 AASHTO LRFD Bridge Design Specifications. Also note that the data in this same figure does not include tests from Brettle and Watanabe et al. because those authors did not provide sufficient information needed to calculate the theoretical strength. Nevertheless, the goal is to help plug some of these gaps in an effort to provide guidance to engineers on how to better design for shear when building with lightweight concrete.

Table 2-9. Summary of reinforced and prestressed lightweight concrete beam shear tests

Researcher	Number of Tests	Unit Weight (pcf)	Compr. Strength (ksi)	Effective Depth (in)	*a/d*	Cross-Sectional Area (in^2)	ρ_w (%)	ρ_v (%)
University of Texas	27	—	2.9 - 7.1	6 - 8	1.4 - 5	27 - 44	0.75 - 5.4	0
Hanson	49	90 - 112	3.2 - 8.6	10.4	2.5 - 5.0	72	1.25 - 5.0	0
Ivey and Buth	26	94 - 126	2.8 - 4.7	7.4 - 15.6	2 - 5	38 - 160	1.0 - 2.3	0
Taylor and Brewer	24	94 - 102	3.1 - 4.8	9.5	3.4	75	1.1 - 1.7	0
Salandra and Ahmad	16	122.5	7.9 - 10.5	6.75	0.5 - 3.6	32	1.5	0 - 0.76
Evans and Dongre	10	90 - 115	3.1 - 4.9	—	—	56	5.7	0 - 0.26
Jindal	6	93 - 106	2.9 - 3.4	13	2.8	131	1.3	0
Nishibayashi et al.	16	98 - 99	3.1 - 6.3	6.0 - 6.5	2.1 - 2.9	31	1.6 - 2.6	0
Walraven	6	115 - 116	4.2 - 4.8	4.9 - 27.6	2.5 - 2.88	46 - 232	0.74 - 1.6	0
Swamy and Bandyopadhyay	16	—	4.4 - 4.9	5	1.5 - 6	41	1.6 - 2.7	0
Swamy and Lambert	28	—	2.9 - 5.8	7.1	1.5 - 6	62	0.29 - 3.0	0
Hoff et al.	14	120	9.9 - 10.3	6.2 - 6.5	2.5 -3.5	46.5	4.0 - 8.3	0 - 0.44
Hoff	9	112 - 128	8.3 - 11.1	10.0	2.6	72	4.0	0
Murayama and Iwabuchi	11	119	6.3 - 7.4	9.8	2.5 - 4	93	1.6 - 3.2	0
Funahashi et al.	5	82- 113	4.8 - 6.5	13.4 - 39.4	3 - 3.5	124 - 830	0.96 - 1.7	0
Hamadi and Regan	5	—	2.8 - 3.3	13.8	3.6	133	3	0.19 - 0.67
Kirmair	4	94	4.3	18 - 23	3.4 - 5.9	174 - 260	1.5 - 7.4	0.15 - 0.67
Clarke	36	104 - 128	3.4 - 8.8	7.1	2.8	31	1.7 - 2.5	0 - 0.45
Ahmad et al.	15	—	4.4 - 13.0	7.8 - 8.5	1 - 4	50	0.94 - 4.5	0 - 0.78
Walraven and Al-Zubi	12	108 - 131	2.9 - 7.0	28.9 - 30.1	2.2 - 2.3	279	3.2 - 5.4	0.43 - 2.7
Ramirez et al.	6	106 - 127	6.2 - 10.5	12.1	2.1 - 2.2	196	2.3 - 2.4	0.26 - 0.39
Kawaguchi et al.	9	74 - 107	2.7 - 6.8	11.8	3.5	109	1.8	0 - 0.15
Kobayahsi et al.	9	75 - 105	4.3 - 8.9	8.7	2	84	1.8	0.13 - 0.8
Brettle	16	105 - 115	4.8 - 6.4	—	1.0 - 4.4	12 - 36	1.0 - 1.5	0
Malone	4	106 - 127	6.5 - 10.1	28.9 - 29.1	3	469	1.4 - 2.1	0 - 0.18
Kahn et al.	6	118 - 119	8.9 - 11.0	44.5	1.4 - 3.3	369	0.7	0.28 - 1.9
Watanabe et al.	5	106 - 119	8.7 - 9.6	21.7	3	194	0.8	0.15
Dymond et al.	1	118	10.6	58.5	1.3	1559	1.2	1.3

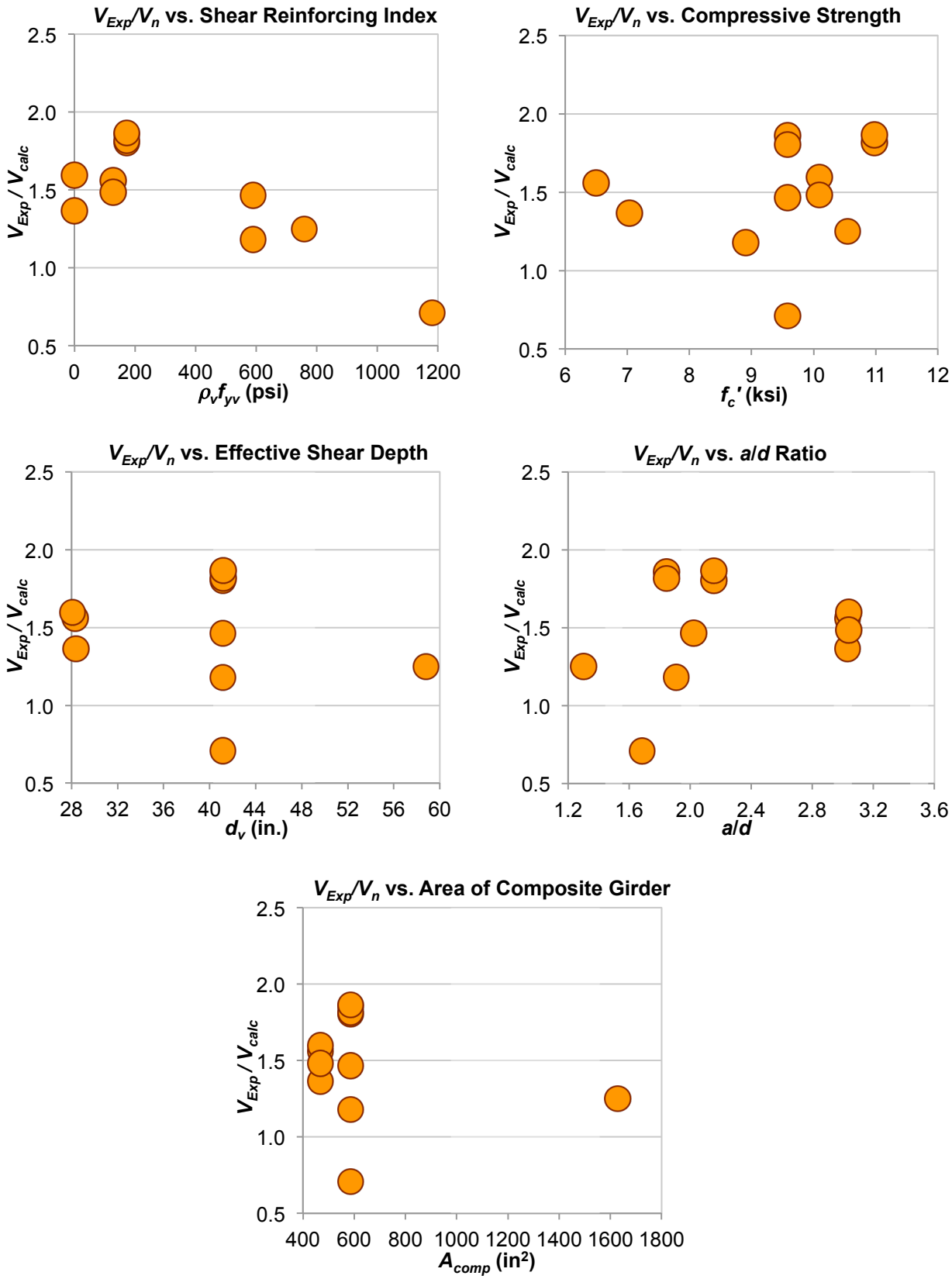

Figure 2-6. Comparison of V_{exp}/V_n versus various parameters from past research on prestressed lightweight concrete

Chapter 3

Experimental Program

3.1 Description of Test Girders

3.1.1 Nomenclature

Each beam and test in this study was assigned an alphanumeric identifier, where the first term in the designation represents either an AASHTO Type II beam (T2) or a PCBT-45 girder (BT), shown in Figure 3-1. The PCBT-45 is a standard section used by the Virginia Department of Transportation (VDOT). The second term indicates the design compressive strength of the girder, either 8 ksi (8) or 10 ksi (10). Note that the second term of one beam is (8N), indicating that this girder was constructed with normal weight concrete; all of the other girders contained sand-lightweight concrete. The third term describes the amount of shear reinforcement, either (Typ) for typical reinforcement or (Min) for minimum reinforcement, as prescribed by the 2007 AASHTO LRFD Specifications. The last term indicates the end of the girder being tested, either the first (1) or second (2) end. In all cases, the first end of the girder is the end with the smaller

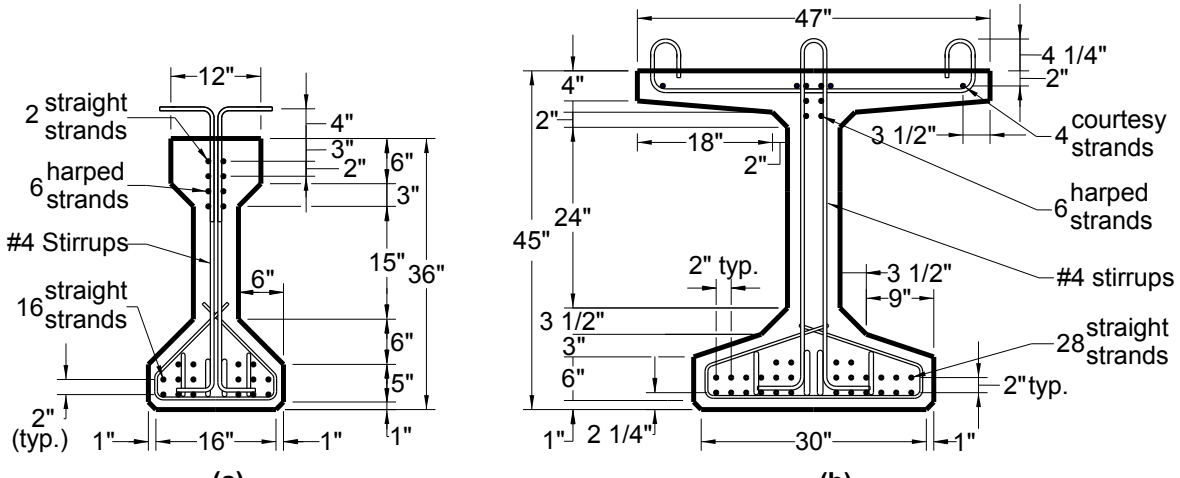

Figure 3-1. Cross-sectional geometry and reinforcement details for (a) AASHTO Type II girder and (b) PCBT-45 girder.

a/*d* ratio, that is, 1.5 or 2.0. The intended *a*/*d* for the second end of the beam was either 3.0 or 3.5, but this ratio was decreased to 3.0 or less, for reasons explained in Section 3.3.2. As an example, the experiment labeled BT.10.Min.2 represents a PCBT-45 girder with a 10-ksi design strength and containing a minimum amount of reinforcement, and is the second end of the girder that was tested.

3.1.2 Design

3.1.2.1 Girder Design

As mentioned in Section 1.3, the experimental program consisted of testing both ends of six beams, each having specific structural characteristics such as: γ_c, f_c, a/d, ρ_v, d_v, and A_c. In light of these parameters, two of the girders had AASHTO Type II cross-sections, while the other four were the PCBT-45 shape. Aside from Figure 3-1, additional details for each cross-section, including the longitudinal and transverse reinforcement, are given in Tables 3-1 and 3-2.

The design live load used to determine the amount of flexural and shear reinforcement is the standard HL-93 loading in the AASHTO LRFD Specifications. HL-93 is comprised of a design truck or design tandem plus a lane load. In all cases, the controlling load was the combination of the design truck and lane load. Details of the truck are shown in Figure 3-2, where the spacing between the two rear axles must be varied to achieve the maximum force effect. As for the design lane load, the 2007 AASHTO LRFD Bridge Design Specifications Article 3.6.1.2.4

Table 3-1. Geometrical properties for girder cross-sections used in current study

Girder Cross-Section	L_{girder} (ft)		A_{girder} (in^2)	I_{girder} (in^4)	$cg_{girder\ bottom}$ (in)
	design	as-built			
AASHTO Type II	61	41	369	50979	15.83
Virginia PCBT-45	86	58	746.7	207300	22.23

Table 3-2. Material properties of reinforcing steel used for designing test girders in current study.

Reinforcement	Diameter (in)	Area (in^2)	f_y (ksi)	f_{pu} (ksi)	E_s (ksi)
shear stirrups	0.5	0.4	60	—	29000
prestressing strands	0.5	0.153	—	270	28500

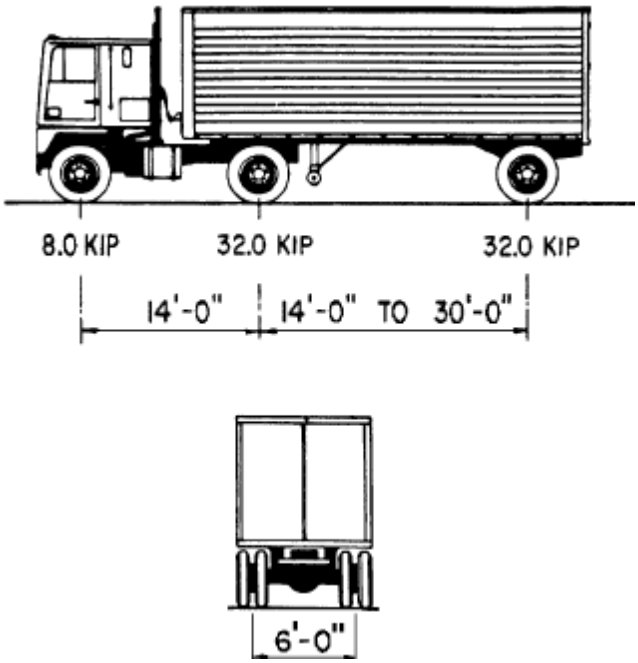

Figure 3-2. Design truck details, from 2007 AASHTO LRFD Specifications, Figure 3.6.1.2.2-1.

dictates that this load shall be 0.64 klf in the longitudinal direction and be applied over a 10-ft width. Multiple presence factors were also considered.

Recall from Section 1.3 that the reinforcement in all of the girders in this study was initially designed for the longest length possible for the given cross-sections and the loading discussed above. The two straight prestressing strands along the top of the Type II girders in Figure 3-1 were fully prestressed. This tensioning was necessary for maintaining the stresses in the top and bottom flanges of the test girders within acceptable limits at release. In addition to the top strands being fully tensioned, the Type II beams had two No. 4 reinforcing bars at the same level as the top prestressing strands, extending 6.75 ft from midspan. Likewise, the PCBT-45 girders had two No. 5 reinforcing bars in the top flange that extended 9.5 ft from midspan. Without the additional bonded mild reinforcement, the concrete tensile stress at the top of the girder would have exceeded the limits stipulated in Table 5.9.4.1.2-1 of the 2007 AASHTO LRFD Bridge Design Specifications. Separately, the four courtesy strands in Figure 3-1(b) were stressed to 1 kip to aid in assembling the vertical and horizontal shear reinforcement in the PCBT-45 girders.

Figure 3-1 and Figure 3-3 also show mild steel installed in the end regions of the girders. This steel is required under Article 5.8.3.5 of the 2007 AASHTO LRFD Bridge Design Specifications to provide sufficient resistance to the tensile forces near the ends of the girder. The amount of this additional longitudinal steel varied amongst the different beams. Details of this reinforcement, along with all other construction details, can be found in the drawings in Appendix A.

As for the vertical reinforcement, stirrup spacing varied amongst the different beams, as shown in Figure 3-3. The two "Min" girders were designed with a minimum amount of shear reinforcement, as limited by Articles 5.8.2.5 and 5.8.2.7 of the 2007 AASHTO LRFD Bridge Design Specifications. AASHTO establishes this minimum in two ways, one of which is to set the maximum stirrup spacing, which is either 12 in. or 24 in. depending on whether or not the shear stress is greater than or equal to 1 ksi if f'_c is 8 ksi or 1.25 ksi for 10 ksi compressive strength. According to Eq. (83) in Chapter 2, the stress resulting from the design loads was greater than 1 ksi in the regions that were going to be tested in beam T2.8.Min. Therefore, the maximum allowable stirrup spacing was 12 in., according to Eq. (82). On the other hand, the design leading to beam BT.10.Min calculated the shear stress would be less than 1.25 ksi, thus allowing the maximum stirrup spacing to be 24 in.

The second manner in which AASHTO specifies a minimum amount of transverse reinforcement is to have a lower bound area of steel. Rearranging this area in Eq. (80) into the form of the shear reinforcing index, $\rho_v f_{yv}$, gives

$$\rho_v f_{yv} = \frac{A_v f_{yv}}{b_v s} \geq 0.0316\sqrt{f'_c\ (\text{ksi})} \qquad \textbf{(133)}$$

Thus, 8 ksi design concrete compressive strength, the minimum reinforcing index is 0.089 ksi. If f'_c is 10 ksi, then that minimum is 0.100 ksi. However, with a 12-in. maximum spacing of No. 4 stirrups, the calculated reinforcing index came out to be 0.333 ksi for beam T2.8.Min. For beam BT.10.Min, the value was 0.143 ksi. Of course, the original girder design could have used No. 3 stirrup instead of the No. 4 size. However, the philosophy behind the design was to create a beam that would reasonably be constructed in an actual bridge. When taking optimization of

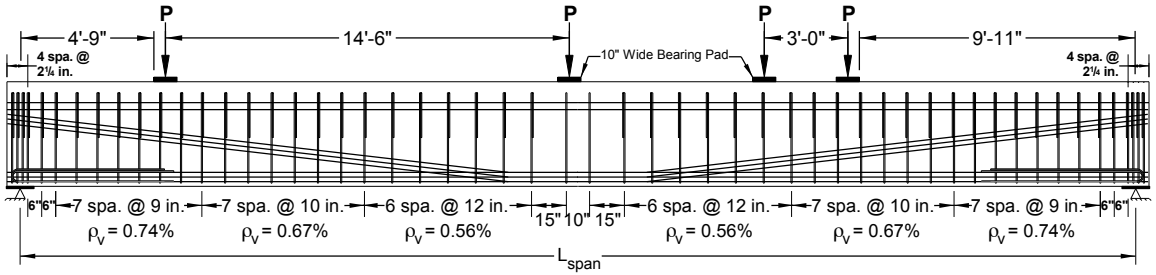

T2.8.Typ

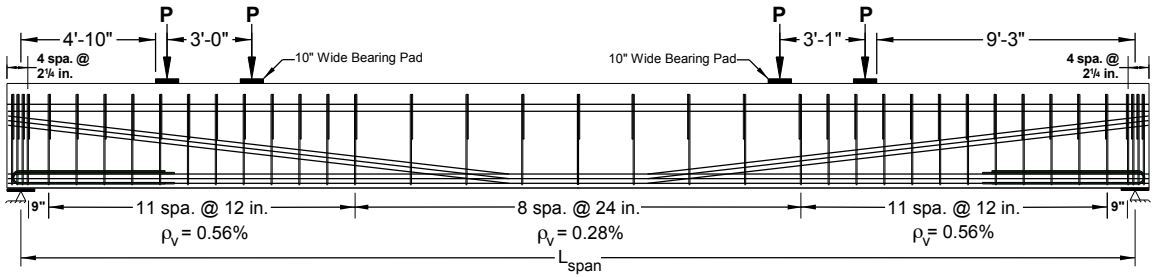

T2.8.Min

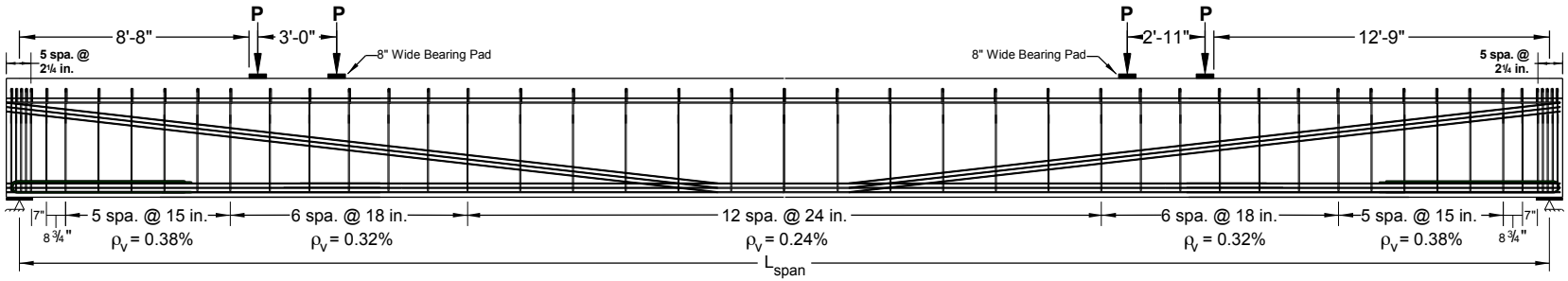

BT.8N.Typ

Figure 3-3. Elevation view of test girders showing stirrup spacing, harped prestress tendons, and concentrated load locations.

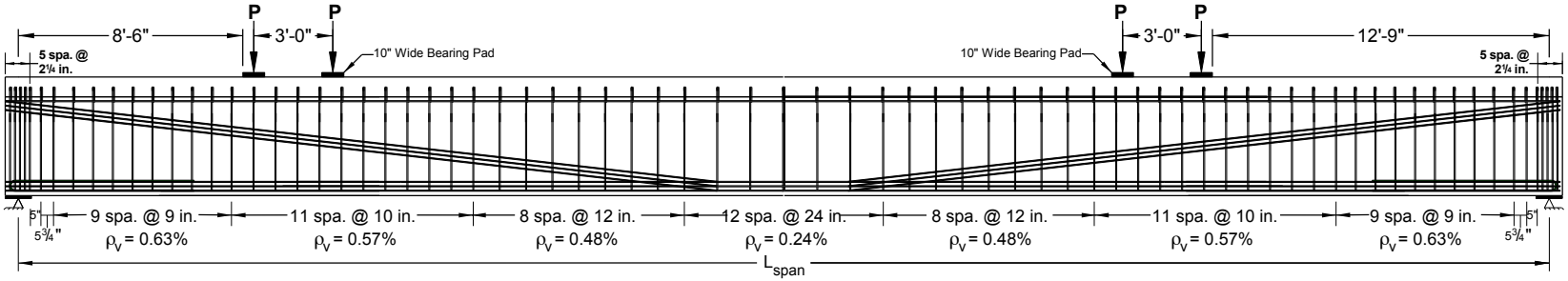

BT.8.Typ

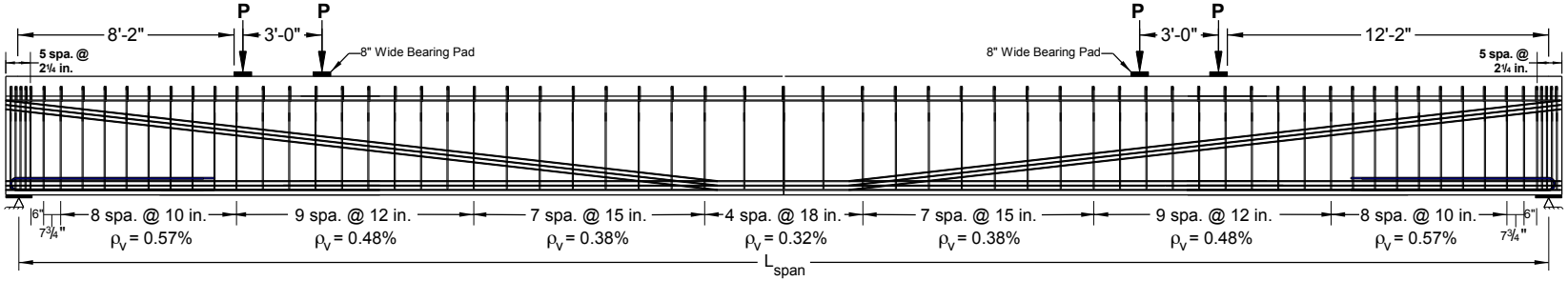

BT.10.Typ

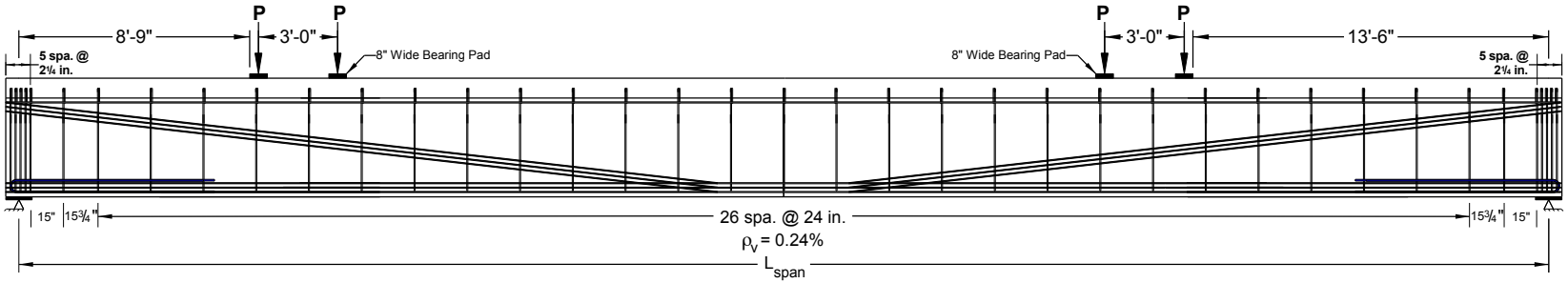

BT.10.Min

Figure 3-3 (cont.). Elevation view of test girders showing stirrup spacing, harped prestress tendons, and concentrated load locations.

size and spacing, in some cases, the No. 3 double-legged stirrup was slightly more efficient in terms of amount of material used. However, when taking into account the labor involved with installing the steel, the No. 4 double-legged stirrup was more economical for all of the girder designs. Thus, the design contained the larger diameter vertical reinforcement. Admittedly, had a No. 3 bar been used, the shear reinforcing index would have been reduced to minimum levels for beam BT.10.Min. The same would be true for beam T2.8.Min, but only if one of each two-legged stirrup had been removed from the plans.

On the other hand, the stirrup spacings in the remaining "Typ" beams were designed according to Articles 5.8.3.3 and 5.8.3.4.2 of the 2007 AASHTO LRFD Bridge Design Specifications, using additional design assumptions given in Table 3-3. In this table, the unit weight of concrete, γ_c, includes 5 pcf that was assumed to be the weight of steel reinforcement uniformly distributed throughout the concrete. Also note that the tensile splitting strength of the concrete

Table 3-3. Additional parameters used for the design of full-scale girders

Beam ID	T2.8.Typ	BT.8.Typ	BT.8N.Typ	BT.10.Typ
γ_c (kcf)	0.125	0.125	0.150	0.125
f'_c (ksi)	8	8	8	10
f'_{ci} (ksi)	6	6	6	7.5
number of beams	6			
S (ft)	8			
$f'_{c\ deck}$ (ksi)	4			
$\gamma_{c\ deck}$ (kcf)	0.125			
t_{deck} (in)	8			
$t_{struct\ deck}$ (in)	7.5			
t_{haunch} (in)	2			
$\gamma_{wearing\ surface}$ (kcf)	0.140			
$t_{wearing\ surface}$ (in)	3			
$b_{barrier}$ (in)	15			
$w_{barrier}$ (klf)	0.320			
b_{bridge} (ft)	42.5			
$b_{bearing}$ (in)	6			
H (%)	70			
harping location from beam end (ft)	20.33	28.67	28.67	28.67
volume-surface area ratio	3.37	3.40	3.40	3.40
composite volume-surface area ratio	3.79	4.33	4.33	4.33

was assumed to be unspecified in all of the designs. Although not listed in Table 3-3, the two "Min" beams were designed with the same parameters as their counterparts containing typical amounts of reinforcement. Note that some of the parameters in Table 3-3 are defined as:

$b_{barrier}$ = width of the guard rails at the sides of the deck

b_{bridge} = width of the bridge, from edge of deck to edge of deck

f'_{ci} = specified compressive strength at release of the prestressing strands

$f'_{c\ deck}$ = 28-day compressive strength of the deck concrete

H = annual average ambient mean relative humidity

S = center-to-center girder spacing

t_{deck} = design thickness of the deck, used for calculating dead load on the girder

$t_{struct\ deck}$ = deck thickness used for determining the structural capacity of the composite section

t_{haunch} = maximum thickness of the haunch between the girder and the deck

$t_{wearing\ surface}$ = thickness of the wearing surface

$w_{barrier}$ = linear weight of the guard rails at the sides of the deck

$\gamma_{c\ deck}$ = unit weight of the deck concrete

$\gamma_{wearing\ surface}$ = unit weight of the wearing surface

Additional vertical mild steel reinforcement was needed for interface shear transfer between the girder and composite deck, as called for by Article 5.8.4 of the 2007 AASHTO LRFD Bridge Design Specifications. Where necessary, this additional interface shear reinforcement was placed adjacent to the stirrups, as indicated in the construction drawings in Appendix A.

As mentioned in Section 1.3, the design span for each girder was the longest span possible for the given cross-sectional geometry. However, to reduce the girder cost as well as the testing footprint in the laboratory, most of the original design between the two harping points for the prestressing tendons was deleted from the fabrication plans for the test beams. All other aspects of the original design remained the same, with the exception being the angle of inclination of the harped strands. To keep the tendons at the original angle of inclination, the harping points would have been at or near midspan. However, the precast contractor did not have the hardware sufficient for resisting the vertical forces from the harped tendons if the harping point was

located at midspan. Thus, the harping points were located 2.5 ft away from midspan without extending the length of the test specimens. As a result, the angle of inclination of these harped strands was a little bit steeper than the true "full-scale" design, but the judgment was that such a change was inconsequential.

3.1.2.2 Deck Design

The testing program included an 8-in. thick composite slab for each girder. These sand-lightweight concrete decks were designed according to traditional design methods in Article 9.7.3 of the 2007 AASHTO LRFD Bridge Design Specifications. As indicated in Table 3-3, the designs assumed that the girders were spaced at 8 ft and the compressive strength of the deck concrete was 4 ksi. Figure 3-4 displays the details for the deck reinforcing for both beam cross-sections used in this study. All of the deck reinforcement was Grade 60 uncoated reinforcement and was optimized for material economy. The only difference between the decks cast on the AASHTO Type II and PCBT-45 girders is the top mat of steel oriented transversely to the beam length. Because the top flange of the Type II girder is narrower than the PCBT-45, the negative moment reinforcing needed to be on a slightly smaller spacing for the AASHTO Type II girder.

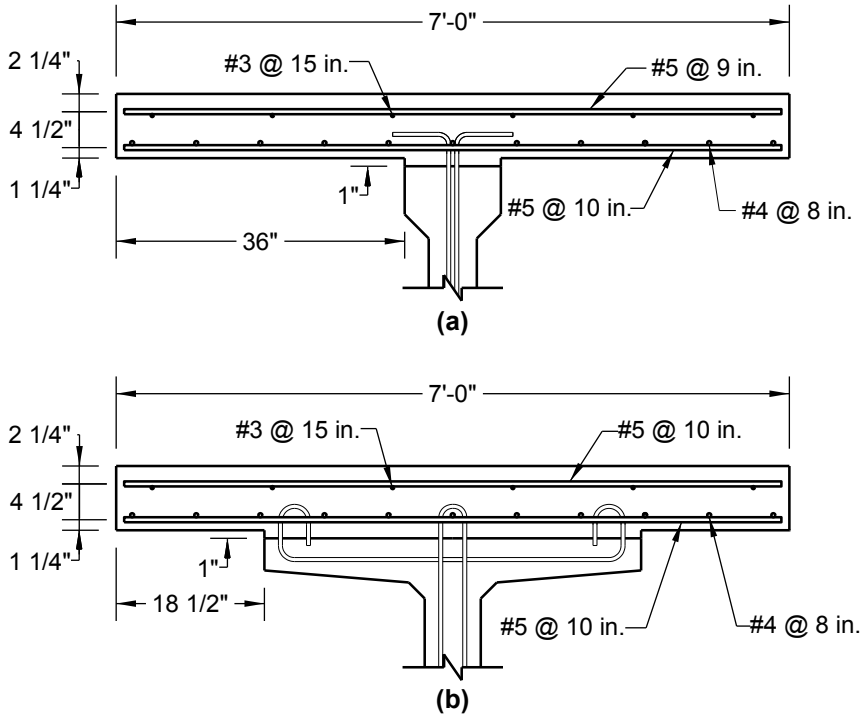

Figure 3-4. Deck reinforcement details for the (a) Type II girders and (b) PCBT-45 girders.

As indicated in Figure 3-4, the as-built dimensions of the deck and haunch differ from those assumed in both the girder and deck design. The reason for the 7-ft deck width, versus the 8 ft assumed from the girder spacing, is the limitations of the testing facility. The strong floor in the laboratory consisted of reaction floor beams that were spaced 8 ft on-center. Taking into account the flange width of the columns of the load frame resulted in limiting decks to a 7-ft width. As for the haunch, the assumed thickness was 2 in., while the actual haunch was 1 in. Haunch thickness is more of a construction issue to account for camber or upward deflection in the beam, which is due to eccentricity in the prestressing strands. In the case of the test specimens, the thicker haunch was not necessary because the camber was not as pronounced. The conclusion was that these differences in geometry would not adversely affect the test results, although the as-built dimensions were used in calculating the theoretical live load that would cause failure.

3.1.3 Construction

3.1.3.1 Girder Construction

Six precast, prestressed beams were produced by Bayshore Concrete Products in Chesapeake, VA over the course of three casting cycles during July and August of 2009. However, a second beam to replace the original BT.8N.Typ beam was cast in May of 2010 because the concrete in the original beam did not reach its 28-day design strength.

3.1.3.1.1 Stirrup Installation

Each casting consisted of two beams constructed on a single prestressing bed, with the exception of the lone normal weight replacement beam. Prior to the morning of concrete placement, crews installed the longitudinal and transverse reinforcement, all of which was galvanized per standard VDOT practice. On the day of casting, crews from Virginia Tech (VT) and the Virginia Center for Transportation Innovation and Research (VCTIR, formerly known as the Virginia Transportation Research Council) delivered additional stirrups fitted with electrical resistance strain gauges, as discussed in Section 3.2.7. Once the steel crew had tied all of the vertical steel into place, the prestressing tendons were tensioned to the standard jacking stress limit of $0.75f_{pu}$, or 202.5 ksi. The exception, of course, was the four courtesy strands in the PCBT-45 girders, mentioned in Section 3.1.2.1.

After strand tensioning, the VT/VCTIR crews uncoiled the lead wires attached to each strain gauge and tied these wires along the length of the given stirrup up to the level of the top row of prestressing strands. From this location, each wire then ran along the tendons out toward the nearest end of the girder, with the VT/VCTIR crews tying the wires to the tendons using plastic zip ties to mitigate the damage to the wires during concrete placement. There was approximately 25 ft of wire remaining at the end of the formwork; this wire was re-coiled and allowed to hang over the formwork bulkhead during concrete placement. In addition to the electrical resistance strain gauges, the research crew also installed three vibrating wire strain gauges, as discussed in Section 3.2.6. The lead wires from these gauges were installed in a similar fashion as the electrical resistance gauges. Once the gauge installation was complete, the precasting crew set the oil-coated side forms into place.

3.1.3.1.2 Special Lifting Devices

With the side forms in place, the precasting crew constructed special block-outs near the ends of the top flanges of the formwork for the PCBT-45 girders. These block-outs, seen in Figure 3-5, consisted of PVC tubing that allowed for passage of threaded rods through concrete in the top flange. These rods were part of a special lifting device for the PCBT-45 beams. Common practice among precasters is to bundle a few, relatively short segments of prestressing strands together and then bend the middle of the bundle at about a 30^{o} angle. Precasting crews then insert the legs of the bundle deep into the formwork prior to concrete placement, with the bent

(a) (b)

Figure 3-5. PVC tubing used for block-outs for threaded rods in special lifting device for PCBT-45 beams in this study, (a) during and (b) after concrete placement.

portion projecting above the top of the beam. After the concrete has cured, cranes use these "hooks" to lift the girder. The concern for this project was that this traditional construction technique would provide additional shear resistance in the region being tested. To avoid this beneficial effect, the construction crew used the aforementioned threaded rods to install a special lifting system first documented by Dymond (*153*) and shown in Figure 3-6. The only modification to Dymond's devices are the ½-in. plate washers welded to the top pieces of tube steel oriented in the beam's longitudinal direction. These plate washers reinforced the tube steel, which had deformed during prior use due to the load being transferred by the nuts on the threaded rods.

The same concern regarding unintended shear resistance from the standard lifting hooks in the PCBT-45 girders existed for the AASHTO Type II beams. However, because the AASHTO Type II beams were lighter but did not have the wide flanges as the PCBT-45 sections, a reinforcing bar hook was designed according to Article 5.11.2 of the 2007 AASHTO LRFD Bridge Design Specifications and Appendix D.5 of the ACI 318-08 code. The hook design was a No. 5 Grade 60 reinforcing bar, with the bend pattern shown in Figure 3-7. The only difference between the hooks used for T2.8.Typ and T2.8.Min was the depth of embedment, where the stirrup spacing for T2.8.Min allowed for a deeper hook without interfering with the region where major diagonal tension cracking was expected to occur, as seen in Figure 3-8. Note that the hooks extended into and through the deck in case the girders needed to be lifted after the deck had been placed. The maximum loads on all of the lifting devices were assumed according to

(a) **(b)**

Figure 3-6. (a) Top and (b) Bottom of special lifting device used for PCBT-45 beams in this study.

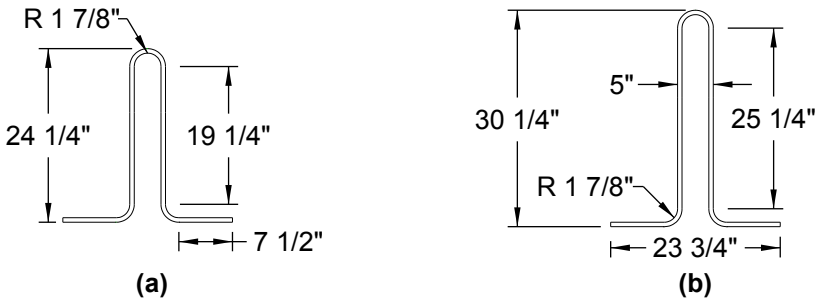

Figure 3-7. Bend details for special lifting hook for test girders (a) T2.8.Typ and (b) T2.8.Min.

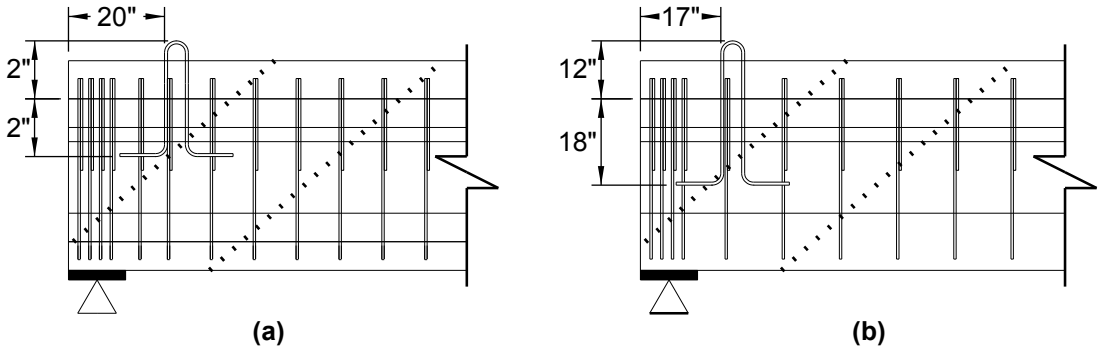

Figure 3-8. Location of special lifting hooks for test girders (a) T2.8.Typ and (b) T2.8.Min. Note that the dotted lines indicate region of anticipated web-shear failure.

Occupational Safety and Health Administration (OSHA) regulations, which state that "lifting inserts which are embedded or otherwise attached to precast concrete members … shall be capable of supporting at least four times the maximum intended load applied or transmitted to them" (*154*).

3.1.3.1.3 Girder Concrete Placement

Concrete placement began once the lifting devices had been set. Collaborating with the precaster, the researchers from VCTIR developed the mix designs for all of the lightweight girders, shown in Table 3-4. The precast company used its standard in-house mix design for the normal weight beam, BT.8N.Typ. The lightweight coarse aggregate in the lightweight concrete girders was ½-in. rotary kiln expanded slate from the Carolina Stalite Company in Salisbury, NC. The normal weight coarse aggregate was No. 67 stone, while the sand was natural sand. Having had prior experience that was less than ideal when switching back and forth between

Table 3-4. Concrete mix design for the test girders. Note: LWC is sand-lightweight concrete and NWC is normal weight concrete.

Material	8 ksi LWC	8 ksi NWC	10 ksi LWC
Type II cement (lb)	480	—	495
Type III cement (lb)	—	720	—
Slag (lb)	320	—	315
Fly ash (lb)	—	180	90
coarse aggregate (lb)	914	1683	876
fine aggregate (lb)	1349	1035	1256
Water (gal)	29.05	33	31.92
Air entrainment (oz)	2.4	8	3.6
Retarder (oz)	—	27	—
Water reducer (oz)	40	—	—
High range water reducer (oz)	24	50	54
w/c ratio	0.3	0.3	0.3
Slump (in.)	5 - 7	0 - 8	5 - 7
Air content (%)	4 - 6	3 - 7	4 - 6

normal weight and lightweight concrete production, the precaster opted to subcontract the lightweight concrete production to a local ready-mix company, Capital Concrete in Norfolk, VA.

Upon arrival, both the precaster and the VCTIR team sampled the concrete for slump, air content and unit weight, as seen in Table 3-5. Note that the unit weights listed in the table are the actual concrete densities and do not include the standard 5 pcf assumed in design for the unit weight of reinforcement steel. However, there were some issues with the concrete during several of the production runs. For the two AASHTO Type II girders, the concrete arrived in two ready-mix trucks. Unfortunately, the first sample was slightly heavier than desired for lightweight concrete, but more importantly, the air content was below the limits set by VDOT. After several attempts to rectify the problem, the concrete no longer had a stable consistency. Thus, the first truck load was rejected. Likewise, the second batch was rejected. Fortunately, the quality in the subsequent two trucks was satisfactory. However, the research team only made sample specimens from one of these two batches.

For the second casting cycle, the concrete for beam BT.8.Typ again arrived in two ready-mix vehicles, but with 1 gal/yd^3 of water withheld from the concrete. At this point, the concrete had

Table 3-5. Fresh concrete properties for the test girders. Note: ends of girders that were predominately made from the same batch of concrete are grouped together.

Test ID	Fresh Concrete Properties	
	Property	Result
T2.8.Typ.1 T2.8.Typ.2 T2.8.Min.1 T2.8.Min.2	Air (%)	4.75
	Slump (in.)	9.5
	Unit Weight (pcf)	116.5
BT.8.Typ.1 BT.8.Typ.2	Air (%)	4.75
	Slump (in.)	—
	Unit Weight (pcf)	120.8
BT.8N.Typ.1	Air (%)	4
	Slump (in.)	8
	Unit Weight (pcf)	145
BT.8N.Typ.2	Air (%)	5
	Slump (in.)	7.75
	Unit Weight (pcf)	145

Test ID	Fresh Concrete Properties	
	Property	Result
BT.10.Typ.1	Air (%)	5
	Slump (in.)	10.75
	Unit Weight (pcf)	119.6
BT.10.Typ.2 BT.10.Min.1	Air (%)	4
	Slump (in.)	—
	Unit Weight (pcf)	124
BT.10.Min.2	Air (%)	3.5
	Slump (in.)	—
	Unit Weight (pcf)	125.6

acceptable slump, air, and unit weight measurements. Therefore, the precast crews began placing this batch into the formwork. However, the concrete soon began to lose its slump. To regain workability, the precaster added the initially withheld water to the concrete remaining in the mixing truck. The same was done for the second ready-mix vehicle, with acceptable results. The one remaining difficulty during casting for the BT.8.Typ girder was that the amount of concrete delivered to the precast plant was about 0.3 yd^3 short of completing the job. The reason for the shortage is unknown, but the time in between finishing the second truck and the arrival of the third batch was about an hour. Only the unit weight of this last batch was measured. Nevertheless, the research team obtained a small number of samples for material testing.

For the third casting cycle, that is beams BT.10.Typ and BT.10.Min, the first two trucks were rejected because both the air content and slump were too high. After these rejections, there were no other issues with the concrete mixes, nor were there any complications with the normal weight replacement beam.

As the concrete was being placed, the precasting crew consolidated the concrete using vibrators that ran along the side forms as well as hand-held vibrators that were inserted into the concrete from the top. Meanwhile, the research crew made samples that would later be used to test the following material properties:

- compressive strength
- tensile splitting strength
- modulus of elasticity
- modulus of rupture
- creep and shrinkage
- permeability
- absorption
- freeze-thaw resistance
- bulk diffusion

Only the results for the first four material tests are reported in this study.

3.1.3.1.4 Girder Concrete Curing and Strand Release

Once the precasting crew finished placing concrete in the formwork, the research team placed all of the material specimens on exterior ledges of the formwork so that the samples could be steam-cured alongside the beams. Steam-curing occurred overnight according to the precaster's standard operating procedures. The design release strength was 75% of the 28-day design compressive strength, according to typical VDOT practice. However, there were some cases where the concrete did not reach this strength by the next morning. In these cases, the concrete was allowed more time to steam-cure, while additional calculations showed that the prestressing strands could be released at a lower strength threshold without exceeding the service stress limits in the concrete.

After shutting down the steam, the precast crews removed the formwork from the beams. The tensioned strands were released using acetylene torches, following the precaster's standard protocol. Afterwards, the transport crew moved each beam to a storage location within the precasting yard, where the beams remained until needed for transport to the laboratory testing facility in Blacksburg, VA. These beams were stored for a period of one month to nine months.

3.1.3.2 Deck Construction

3.1.3.2.1 Deck Formwork

Upon arrival at the Thomas M. Murray Structural Engineering Laboratory at Virginia Tech, the girders were placed on supports and the formwork for the cast-in-place deck was installed. Additional details for the formwork are shown in Figure 3-9.

3.1.3.2.2 Deck Concrete Placement

The deck mix design appears in Table 3-6. Upon arrival, the VT/VCTIR teams tested the concrete for slump, air content and unit weight, with the results shown in Table 3-7. Note that the unit weights listed in the table are the actual concrete densities and do not include the standard 5 pcf assumed in design for the unit weight of reinforcement steel. Also note that beams T2.8.Typ and T2.8.Min have the same fresh concrete properties for both ends of the respective beams because only one batch of concrete was needed for these shorter beams.

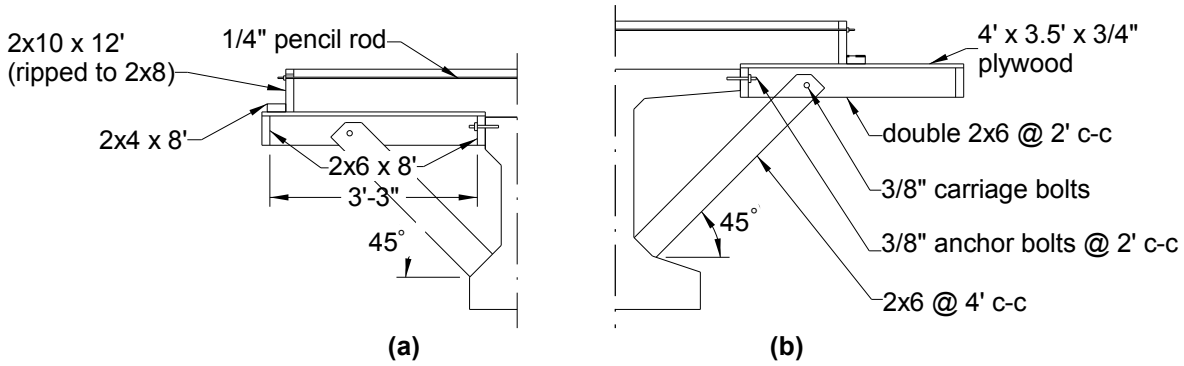

Figure 3-9. Deck formwork details for (a) AASHTO Type II and (b) PCBT-45 girders.

Table 3-6. Concrete mix designs for composite decks.

Material	Quantity
Type II cement (lb)	535
Fly ash (lb)	150
coarse aggregate (lb)	875
fine aggregate (lb)	1305
Water (gal)	36.5
Air entrainment (oz)	as needed
w/c ratio	0.44
Slump (in.)	5 - 7
Air content (%)	4 - 6

Table 3-7. Fresh properties for the deck concrete.

Test ID	Property		
	Air (%)	Slump (in)	Unit Weight (pcf)
T2.8.Typ.1	—	6.5	118.4
T2.8.Typ.2	—	6.5	118.4
T2.8.Min.1	4.5	7.5	120
T2.8.Min.2	4.5	7.5	120
BT.8.Typ.1	3.5	5	123.4
BT.8.Typ.2	3.5	7.5	130.8
BT.8N.Typ.1	2.75	7.5	122
BT.8N.Typ.2	2.5	7.5	122
BT.10.Typ.1	2.5	6	121.6
BT.10.Typ.2	2.25	6.5	124
BT.10.Min.1	3.25	7.5	121.6
BT.10.Min.2	3.25	6.5	122.8

Furthermore, the researchers did not measure the air content of the concrete for the T2.8.Typ deck because the roll-o-meter needed for taking this measurement in lightweight concrete was not available at the time.

The unit weight for the BT.8.Typ.2 deck was nearly 131 pcf, which was much higher than desired for lightweight concrete. For some reason, the batching operation at the ready-mix facility resulted in the first truck for beam BT.8.Typ containing normal weight coarse, even though the batch ticket stated that the concrete contained lightweight aggregate. The second truck had a blend of normal weight and lightweight aggregate, resulting in a unit weight of 130.8 pcf. The last truck contained lightweight aggregate with a unit weight of 123.4 pcf. Unfortunately, the construction crews placed approximately 1 yd^3, or about 9 linear feet of the deck, of the normal weight concrete into the formwork before discovering the unit weight issue. This heavier concrete was too difficult to remove because of the top mat of reinforcing steel, so the researchers decided to leave the concrete in place. Because this end of the girder was the second end being tested, that is the first concentrated load was located about 13 ft from the end of the beam, the researchers concluded that the normal weight concrete would not seriously influence the test results for shear strength. However, the calculations for dead load used in the analysis of the results did take the heavier concrete into account.

While the VCTIR crew made similar material specimens as done for the girder concrete, the VT crews transferred the concrete from the ready-mix truck to the beam using a crane bucket and then consolidated the concrete using handheld vibrators as well as a vibrating screed. After finishing the surface and allowing the concrete to reach a setting point, the team placed wet burlap and plastic over the concrete, allowing the deck to moist-cure for seven days. However, the construction crew removed the side forms after a single day and removed the remaining formwork after a compressive strength check on the concrete at three days.

3.2 Instrumentation

While the deck was curing, the research team installed external instrumentation for each test. This external instrumentation consisted of:

- strain gauge rosettes on the girder web at the critical section
- LVDT rosettes on the girder web at the critical section
- LVDTs at end of the strands
- wire potentiometers at the supports and intermediate points
- load cells

In addition to this external instrumentation, there were a number of gauges inside of the concrete, namely:

- vibrating wire strain gauges
- electrical resistance strain gauges.

3.2.1 Strain Gauge Rosette

The strain gauge rosette was designed to determine the principal stresses in the girder web within the shear span. This rosette consisted of three electrical resistance gauges designed for concrete and manufactured by Vishay Precision Group, Micro-Measurements Division. These gauges had a 3-in. gauge length and were arranged in a -45^o, 0^o, 45^o pattern with the gauges centered over each other, as seen in Figure 3-10(a). The center of the rosette itself was located at the critical section along the length of the beam and then 0.5d_v vertically, per calculations following Article 5.8.2.9 and 5.8.3.2 of the 2007 AASHTO LRFD Bridge Design Specifications.

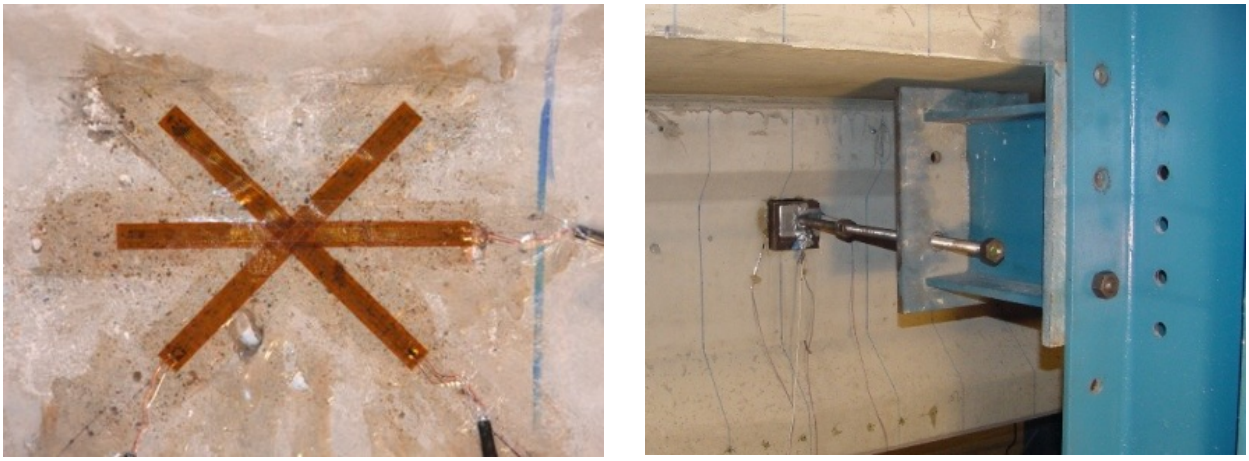

(a) (b)

Figure 3-10. (a) Strain gauge rosette and (b) clamping device used to cure strain gauge adhesive.

Per the manufacturer's instructions, the researchers applied a primer layer of adhesive to fill any voids in the concrete and provide a smooth, continuous surface to adhere the gauges to. Furthermore, the manufacture indicated that the adhesive bonding the gauges to the surface needed to cure for six hours under a clamping pressure of 5 – 20 psi. To maintain this pressure on a vertical surface, a threaded rod applied a force against a bearing plate placed over the gauges. The bearing plate did have a layer of neoprene rubber to cushion the strain gauges. A nut on the threaded rod and tightened against a horizontal stub column was able to hold that force. See Figure 3-10(b) for a picture of the threaded rod / stub column. Furthermore, there was a 10-kip load cell in between the threaded rod and the bearing plate that measured the force on the plate.

Preliminary analysis of the data from the AASHTO Type II beams showed that the strain gauge rosettes did not provide accurate data when compared to other instrumentation. Also, the calculated crack angle found by using the strain rosette results did not appear to match actual results. One possible reason was the fact that all three gauges were affixed simultaneously as opposed to allowing the adhesive for each gauge to cure before applying the subsequent gauge. The reason for bonding all three gauges at once was both a matter of material and time, where the pot life was on the order of minutes while the curing time was on the order of hours. However, following this method raised the possibility that the bond at the location where the gauges overlapped each other was not satisfactory, leading to inaccurate measurements. Given

the amount of time and inaccuracy in using this particular set-up, the research team opted to forego the strain gauge rosette after the fourth test, T2.8.Min.2 and instead use a rosette discussed below.

3.2.2 LVDT Rosette

A rosette comprised three linear variable differential transformers (LVDTs), shown in Figure 3-11, served the same purpose as the strain gauge rosette. In the case of the AASHTO Type II beams, only one LVDT rosette was used in each test, while there were two LVDT rosettes for each test of the PCBT-45 cross-section, one on each side of the girder web.

The LVDTs had a gauge length of about 0.2 in. Because predicting exactly where cracks would form was virtually impossible, the LVDTs were attached to the ends of polyvinyl chloride (PVC) tube extensions that helped to average displacements over a distance much greater than the gauge length. The tubing set at $\pm 45^{o}$ was as long as practical so that the LVDT, tubing, and base supporting the tubing would fit on the girder web. On the other hand, the extension for the horizontal LVDT was slightly longer in order to reduce the error that propagates in the calculations for the angle of rotation of principal stresses. The LVDTs made contact with reusable metal targets, while a pipe clamp tightened a slit cut at the end of the PVC tubing holding the base of the LVDT. The other end of the tubing was clamped by a wooden block, which in turn was screwed to a flat, wooden base that was glued to the concrete. At the

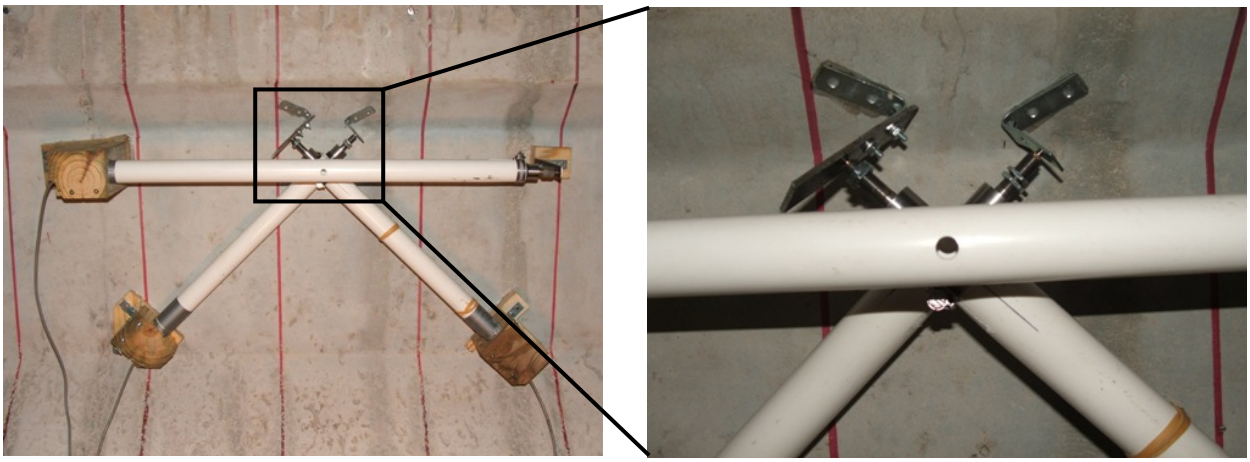

Figure 3-11. LVDT rosette

completion of each test, this wooden base would be discarded while the wood block clamping the PVC tubing could be reused.

The LVDT rosette was arranged in the same 45^{o} pattern as the strain gauge rosette; however, due to the space limitations and the long PVC extensions, this pattern looked more like a "K" on its side instead of the "asterisk" pattern of the strain gauge rosette. Nevertheless, the intersection of the three LVDTs was at the same location as the center of the strain gauge rosette. To orient the entire rosette, the first LVDT, assembled with the wood base, wood block, and tube extension, was approximately oriented at a horizontal level, with a hole in the tubing indicating that the device was centered at the critical location. The wood base was then removed from the assembly and adhered to the concrete with 5-min epoxy. Once the epoxy had hardened, the wood block, tubing, and LVDT assembly was screwed to the wood base and adjusted so that the tube was horizontal. The two remaining LVDT devices were attached in a similar fashion and at the proper angle.

Each LVDT was calibrated individually by connecting the instrument to a System 5000 data acquisition system manufactured by the Micro-Measurements division of Vishay Precision Group, and then forming a best-fit function between the voltage readings on the computer and known measurements from a dial caliper. The LVDTs had a sensitivity of ±0.002 in.

One limitation to using this instrumentation is that the LVDTs had a displacement range that was less than the displacements being measured during testing. Therefore, the devices would frequently go off-scale prior to an actual shear failure. However, enough data was collected to discern the change in the angle of rotation of the principal strains and stresses during most of the testing.

3.2.3 LVDTs at the End of the Strands

In addition to the strain rosettes, there were also LVDTs for measuring strand slip at the ends of the beams. Slip in the prestressing strand indicates a bond failure and is typically the result of applying a load at a distance from the end of the beam that is shorter than the development length of the strand. In this study, slip failure was defined as the strand being pulled into the girder by a

distance greater than 0.02 in. The mechanism used to attach the LVDT to the strand is the same as that used by Dymond (*153*), and can be seen in Figure 3-12. Each test had four LVDTs measuring slip on the bottom row of prestressing strands, two on the extreme exterior strands and two on the extreme interior strands. These LVDTs were calibrated in the same manner as the LVDTs in Section 3.2.2.

3.2.4 Wire Potentiometers at Supports and Intermediate Points

Each test had four wire potentiometers underneath the beam. Two devices were located as close to the abutments as possible. A third potentiometer was directly underneath the concentrated load nearest the end of the beam being tested. The fourth instrument was located at the calculated point of maximum deflection, which was determined assuming an uncracked section. The calculated maximum deflection generally occurred in the vicinity of maximum moment, that is, the second load point. The primary reason for measuring deflection during these tests was to ensure that each girder did not reach flexural capacity prior to test completion. If the potentiometers were to register a large increase in deflection for a relatively small increase in load, then those measurements would indicate that the girder was approaching flexural failure. The two potentiometers at the supports helped to zero out any vertical displacement occurring at the supports. While hooked up to the data acquisition system, each potentiometer was calibrated using a height gauge and finding a best-fit solution to the calibration data. The sensitivity was ±0.005 in.

Figure 3-12. LVDT attached to end of prestressing strand for measuring slip during testing.

3.2.5 Load Cells

As will be discussed in Section 3.3.3, force was applied to each girder in two locations through the use of two hydraulic actuators. Load cells were positioned in between the actuators and the crossbeams in the load frames to monitor the forces from these actuators. One load cell had a 300-kip capacity while the second had a 500-kip capacity. Although coming close, the actuators did not exceed 300 kip. Prior to each test, both load cells were calibrated using a Forney compression chamber, where a best-fit equation was calculated between the voltage readings from the data acquisition system and the readings from the compression machine. The 300-kip load cell had an accuracy of ±1.0 kip, while the 500-kip load cell had an accuracy of ±1.5 kip.

3.2.6 Vibrating Wire Gauges on Prestressing Tendons at Midspan

As mentioned in Section 3.1.3.1.1 , the VT/VCTIR teams installed a number of internal strain gauges prior to the precast crew placing concrete for the girders. Three of these gauges were Geokon Model VCE-4200 vibrating wire strain gauges (VWGs) with a 6-in. gauge length. The researchers installed two of the gauges at the level of the bottom row of prestressing tendons, one each going parallel between the second and third outermost strands on either side of the beam. The third VWG was located at the top level of the strands at mid-width of the flange. See Figure 3-13. All of the VWGs were placed at midspan and held in place away from the strands using zip ties. Data from these gauges was periodically recorded using a Campbell Scientific CR23X datalogger, and helped to measure prestress losses prior to testing and stresses in the

(a) (b)

Figure 3-13. Vibrating wire strain gauges installed at the (a) bottom and (b) top row of prestressing tendons.

strands during testing. These instruments had a nominal range of 3000 με and were calibrated by Geokon to within 0.1% of full scale.

3.2.7 Electrical Resistance Strain Gauges on the Stirrups

The final type of instrumentation used for this project was the electrical resistance strain gauge on the transverse reinforcement. Manufactured by the Micro-Measurements division of Vishay Precision Group, these gauges had a ¼-in. gauge length and were installed and protected according to the manufacturer's instructions. Because the location of cracks in the concrete were not known prior to testing, an ideal instrumentation plan would have had a grid of gauges placed on as tight a spacing as possible on as many stirrups as possible. However, doing so would require approximately 100 gauges in a given beam, which was not feasible. Therefore, the gauges were placed at select locations where cracking was most likely to occur.

Figure 3-14 shows the location of these gauges for each test. Each group of strain gauges on a given stirrup was centered on a straight line connecting the edges of the bearing plates from the first load and the support. The dotted lines in Figure 3-14 indicate an average maximum bound of diagonal cracking observed in the literature from previous full-scale tests. Another way to reduce the number of strain gauges was to only instrument one leg of the double-legged stirrups. Of course, doing so eliminated any redundancy should a gauge fail, but the issue of time was the overriding factor. Following this methodology, there were about 30 gauges installed in each beam, with the second end of the beam, that is, the end with the longer shear span, containing the majority of these gauges because there were more stirrups available for instrumention. Even with the reduced number of gauges, and with the help of a several other researchers, the time to complete the gauge installation for two beams was about 10 days. All strain gauges were shunt calibrated using the data acquisition system just prior to the start of testing. These gauges had a resolution of 10 με.

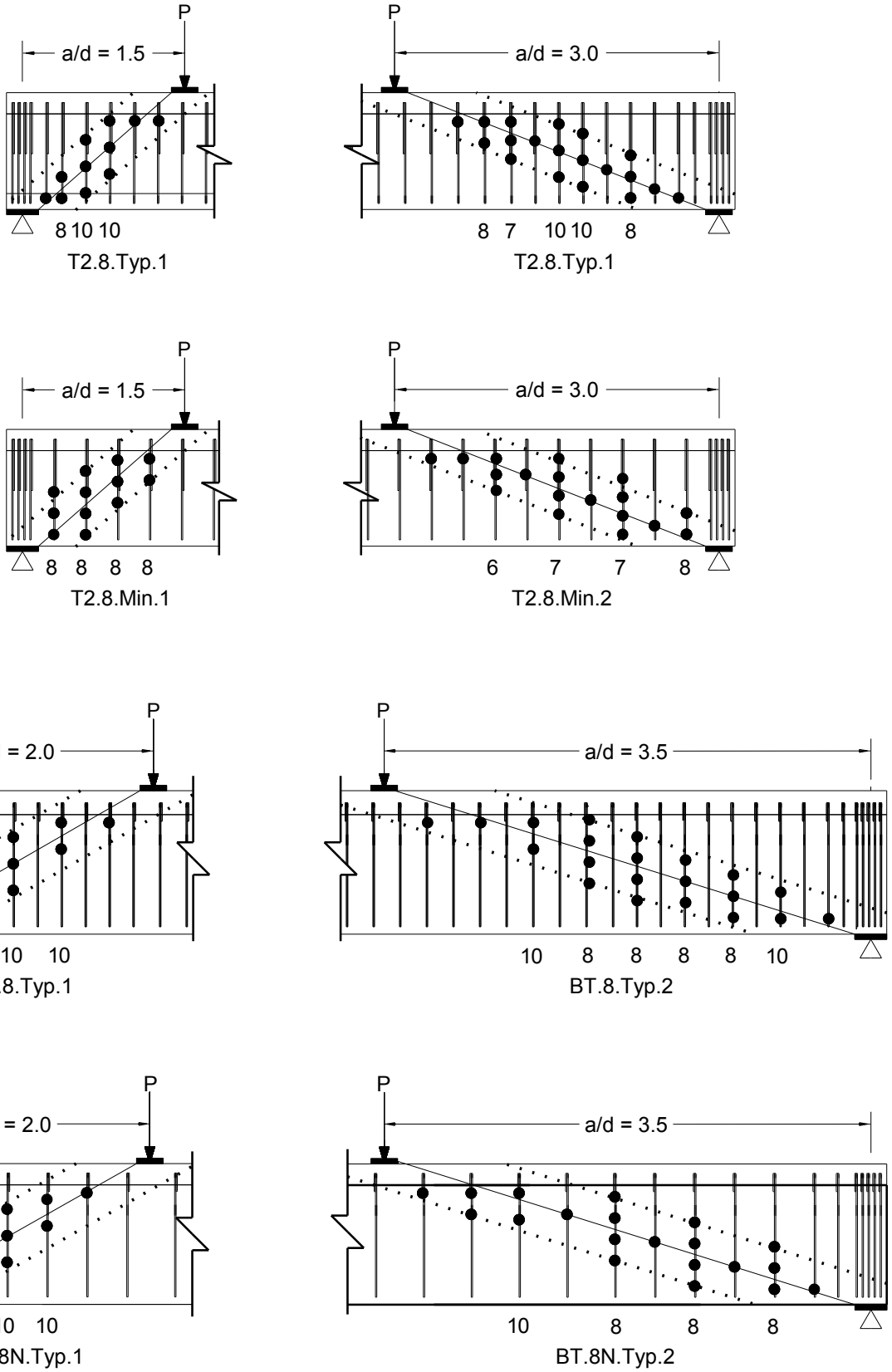

Figure 3-14. Strain gauge locations for each beam indicated by the heavy dot (●). Note that the numbers beneath individual stirrups give the vertical distance between gauges, in inches.

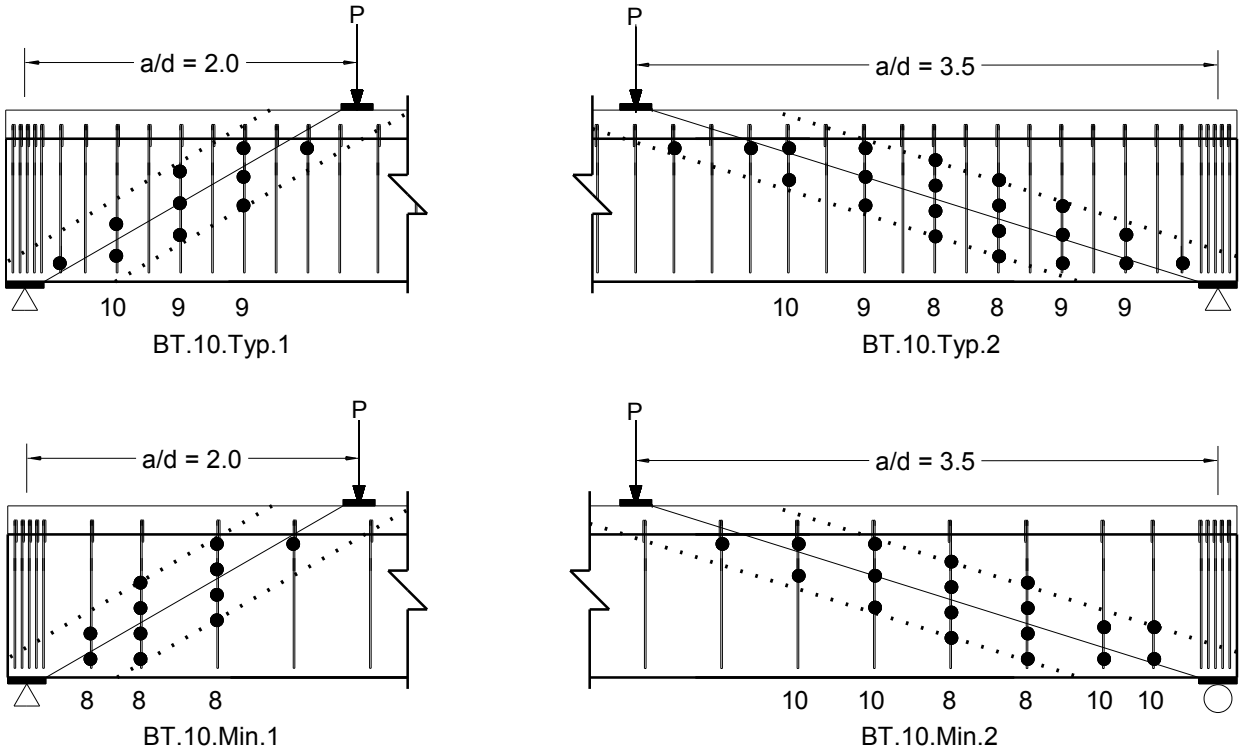

Figure 3-14 (cont.). Strain gauge locations for each test indicated by the heavy dot (●). Note that the numbers below individual stirrups give the vertical distance between gauges, in inches.

3.3 Testing Procedure

3.3.1 Supports

All of the girders were simply-supported by a pin and roller set on top of steel I-beam abutments. There were two pairs of abutments for two different tests set up on the laboratory floor so that one beam could be prepared for testing while the deck concrete for a second beam was curing. One set of abutments consisted of W14x90 I-beams, while the other was a non-standard section but had dimensions that were close to a W21x101. All of the abutment beams had several stiffeners on both sides of the web and were bolted to the strong floor. The pin and roller bearings were the same design documented by Dymond (*153*) and shown in Figure 3-15. In all cases, the pin was located at the end of the girder that was being tested in order to minimize longitudinal movement of the actuators during the experiment. In between the girder and the supports were 1-in. thick by 7-in. wide bearing plates centered 6 in. from the beam end.

(a) (b)

Figure 3-15. (a) Pin and (b) roller bearings.

3.3.2 Load Frames

The two frames used to apply load to the girders satisfied design specifications in the American Institute of Steel Construction manual (*155*). Figure 3-3 in Section 3.1.2.1 shows the location of these two frames relative to the supports. Note that these actual frame locations deviate from the planned shear spans indicated in Figure 3-14 for two reasons. The first reason is relatively minor in that the bolt holes used to connect the frame to the strong floor were spaced at 6 in., thus limiting where the load frames could go. The second reason pertains to changing the original shear span-to-depth ratio for the second test of the PCBT-45 girders from 3.5 to 3.0 or less due to the shear strength results from the AASHTO Type II beams and the first tests of the PCBT-45 girders being higher than anticipated. Those results indicated that potential for reaching flexural capacity prior to producing a shear failure in the PCBT-45 girders with the larger a/d ratios was fairly high. Because the objective of this study was to find the shear capacity of lightweight concrete beams, a new iteration of calculations taking the stronger shear strengths into account suggested that the shear spans needed to be shorter than planned in Table 1-1 in Section 1.3 to achieve that objective.

Also note that the spacing between the two frames for test T2.8.Typ.1 was 14 ft, while the remaining tests had the loads 3 ft apart. The reason for the 14-ft spacing was an attempt to simulate the loading from the rear axles of an AASHTO HL-93 truck. However, the load pattern for test T2.8.Typ.1 created a large moment, resulting in considerable flexural cracking that was

nearing the test region for the second experiment on that girder. Thus, the loading was terminated without a distinct shear failure, and the research crew prepared for the second test. Test T2.8.Typ.2 also started out with the two loads being 14 ft apart, but there was clear evidence that a flexural hinge was forming. Thus, the researchers unloaded the girder and placed the second load frame adjacent to the first frame, that is, the frame nearest the end of the girder being tested. The resulting load spacing was 3 ft.

For the second test on each beam, the experimental team needed to do four things:

- move the load frames into their new positions,
- move the abutment at the first end of the beam,
- switch the locations of the pin and roller supports,
- set up the external instrumentation at the second end of the beam.

The reason for moving the abutment at the first end of the beam was because of the concern that substantial damage had occurred in the concrete and steel reinforcement at this end such that there might not be sufficient shear strength for the second test. Because the amount of shear force in the beam dropped dramatically at the location of the concentrated load closest to the first end of the beam, the structural integrity should have been relatively intact beyond this location. Therefore, the experimental team moved the abutment to the original location of the first load frame, leaving the beam overhanging the support by about 5 ft and 9 ft for the AASHTO Type II and PCBT-45 girders, respectively. To move this abutment, the researchers used a hydraulic actuator underneath the girder to raise the girder off of the support, and then used an overhead crane to move the abutment inward. During this process, the researchers also switched the pin and roller supports. The time to prepare the second test took from a few days to a week after the first.

3.3.3 Actuators and Bearing Pads

Two 400-kip capacity hydraulic actuators applied load to the girders, where the load was distributed through either a squat spreader beam with stiffeners or a series of stacked plates that formed a 45^{o} pyramid. Underneath the bearing steel, there was a bearing pad that was either a 2-in. thick, steel-reinforced neoprene pad measuring 10 in. by 24 in., or a ¾-in. non-reinforced

neoprene pad that was 8 in. wide and several feet long. The reinforced bearing pad was used in the first five load tests because its dimensions somewhat resembled the tire contact area specified in Article 3.6.1.2.5 of the 2007 AASHTO LRFD Bridge Design Specifications. However, during the sixth test, BT.8.Typ.2, one researcher observed a sudden shift in the actuator nearest the beam end. This shift was apparently due to shearing along a horizontal plane of the bearing pad. Therefore, subsequent tests made use of the ¾-in pad even though the size of the contact area with the concrete was smaller than that dictated by AASHTO.

3.3.4 Additional Safety Measures

There was a dramatic accident during test T2.8.Min.2. While the exact chain of events is not clear, there are three possible initiators. The first is that the bearing pads between the actuators and the concrete shifted, as observed in test BT.8.Typ.2 and discussed above. The second possibility is that the actuators started tilting at a significant angle relative to their initially plumb position. Thirdly, the small spreader beam used to transfer the load from the actuator in the first load frame to the bearing plate had yielded. Regardless of the start to the chain of events, the result is that the pivot plate used to allow frictionless rotation of the actuator dislodged from its housing and shot outward from the load frame. The gap left by the pivot plate caused the girder to jump a few inches in the vertical direction. Additionally, the load cell sitting on top of the actuator fell onto the beam and then to the floor. Quite fortunately, there were no injuries. Obviously, the test was terminated at this point; there was no definitive shear failure.

Subsequent to this accident, the research team installed shields on the outside faces of the load frames to prevent any objects from flying outside of those frames, as seen in Figure 3-16(a). Also, layers of solid steel plates, shown in Figure 3-16(b), replaced the short, stiffened spreader beams for transferring the load from the actuator to the concrete deck. As an additional precaution, the researchers took better care in centering the two load cells on top of the actuators. During loading, a set of two levels, oriented parallel to the actuators and on orthogonal axes, helped to monitor the angle of the actuators.

If an actuator began to tilt too much, as was the case for both tests on beam BT.8.Typ, the researchers deployed a third actuator located at midspan to hold the deflection in the girder while

(a) (b)

Figure 3-16. (a) Blast shield deployed during loading and (b) solid plates used to transfer the load to the deck.

unloading the two primary actuators. Although this secondary load frame did not maintain all of the deflection that was present prior to unloading, the research team was able to reset the primary actuators and then reload those cylinders back to the same force reached prior to the actuators tilting. The experimental team did see some flexural cracking, although whether or not these cracks occurred before or after the actuator adjustments is not certain. Using the ¾-in., unreinforced neoprene bearing pad in conjunction with taking extra care in aligning the load cells with the actuators ameliorated much of the tilt in the actuators and eliminated the need to adjust the actuators in all subsequent tests.

One final measure of safety was two short, stout steel sections placed under the beam. Should the girder have a sudden catastrophic collapse in the middle of the span, these sections would prevent the beam from crashing all the way to the floor. Fortunately, no such collapse occurred.

3.3.5 Live Load Testing

With the test setup complete, live load testing was ready to commence. All of the external instrumentation as well as the internal electrical resistance gauges were zeroed and calibrated prior to the start of data collection. With the exception of the VWGs, the instruments were hooked up to the System 5000 data acquisition system, which was set to record at 5 Hz. The VWGs remained hooked up to the Campbell Scientific datalogger, which had a minimum 1-min. record interval.

With the two load actuators under manual control, the research team gradually applied force to the beam up to arbitrary levels. These load increments were 20 kip initially, but decreased as each test neared capacity. Up to an arbitrary point during loading and while the situation was deemed safe, the experimental team marked the progress of crack growth in the concrete, indicating the load in the actuators at end of the new growth. In between load increases, the researchers verified that the roller support and the actuators were still in a safe position. Each test lasted one to two hours.

Upon determining that the beam could not take any additional load, the researchers terminated the test. Because the experimental team ceased outlining the cracks in the concrete when safety became a concern during the test, a fraction of the maximum load remained on the beam to assist in highlighting any additional crack growth. Once the crack mapping was finished, the researchers measured the angle of the shear cracks relative to the horizontal axis as well as the horizontal distance between the cracks. The angle measurement was somewhat arbitrary in that the cracks had local deviations along a given line, and the general direction of a given crack was not necessarily straight. Thus, the experimental team used their judgment to draw an average straight line along the crack, and measured the angle of that line. Lastly, the researchers documented the beam and its cracks with photographs.

3.4 Materials Testing

In conjunction with the structural testing, there were a number of experiments on the materials in the girders. These tests were conducted in collaboration with personnel from VCTIR. Table 3-8 lists the American Society for Testing and Materials International (ASTM) designations for these tests. Except for flexural strength, the concrete material testing generally occurred at 1, 7, and 28

Table 3-8. Material tests and the corresponding ASTM designations.

Test	ASTM Standard
Compressive strength	C 39 – 05
Static modulus of elasticity	C 469 – 02
Splitting tensile strength	C 496 – 04
Flexural strength (using third-point loading)	C 78 – 08
Yield strength of steel reinforcement	A370 – 09a
Elastic modulus of steel reinforcement	A370 – 09a

days from the time of casting, as well as on the day of the test. The flexural strength was tested at 28 days from the time of casting.

3.5 Summary of the Experimental Program

A series of six prestressed, lightweight concrete girders with composite concrete decks were tested for this study. There were two tests per beam, with each test containing a unique set of parameters. Different instrumentations provided data that helps to answer some of the uncertainties behind designing for shear in lightweight concrete girders. Recall that Figure 2-6 in Section 2.5 exhibited a number of gaps in the available database of full-scale tests of lightweight composite concrete girders when considering several different parameters. The aim of the experimental program herein is to provide the data needed to fill in some of those gaps, as exhibited by the shaded regions in Figure 3-17.

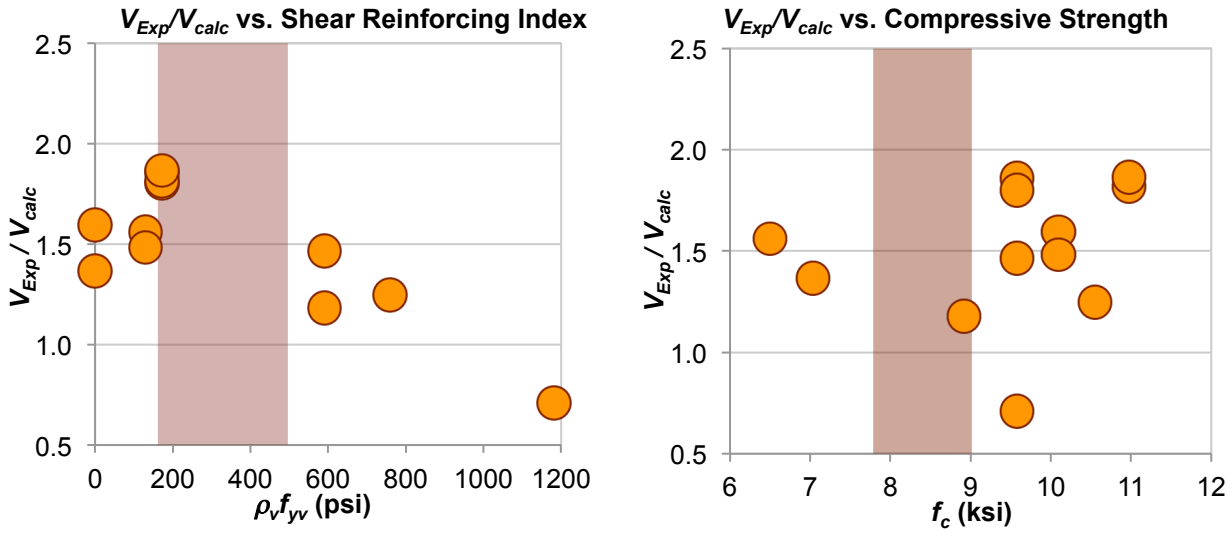

Figure 3-17. Objective data set (shaded regions) from this study versus existing database of full-scale lightweight concrete girders (circular points) for various design parameters.

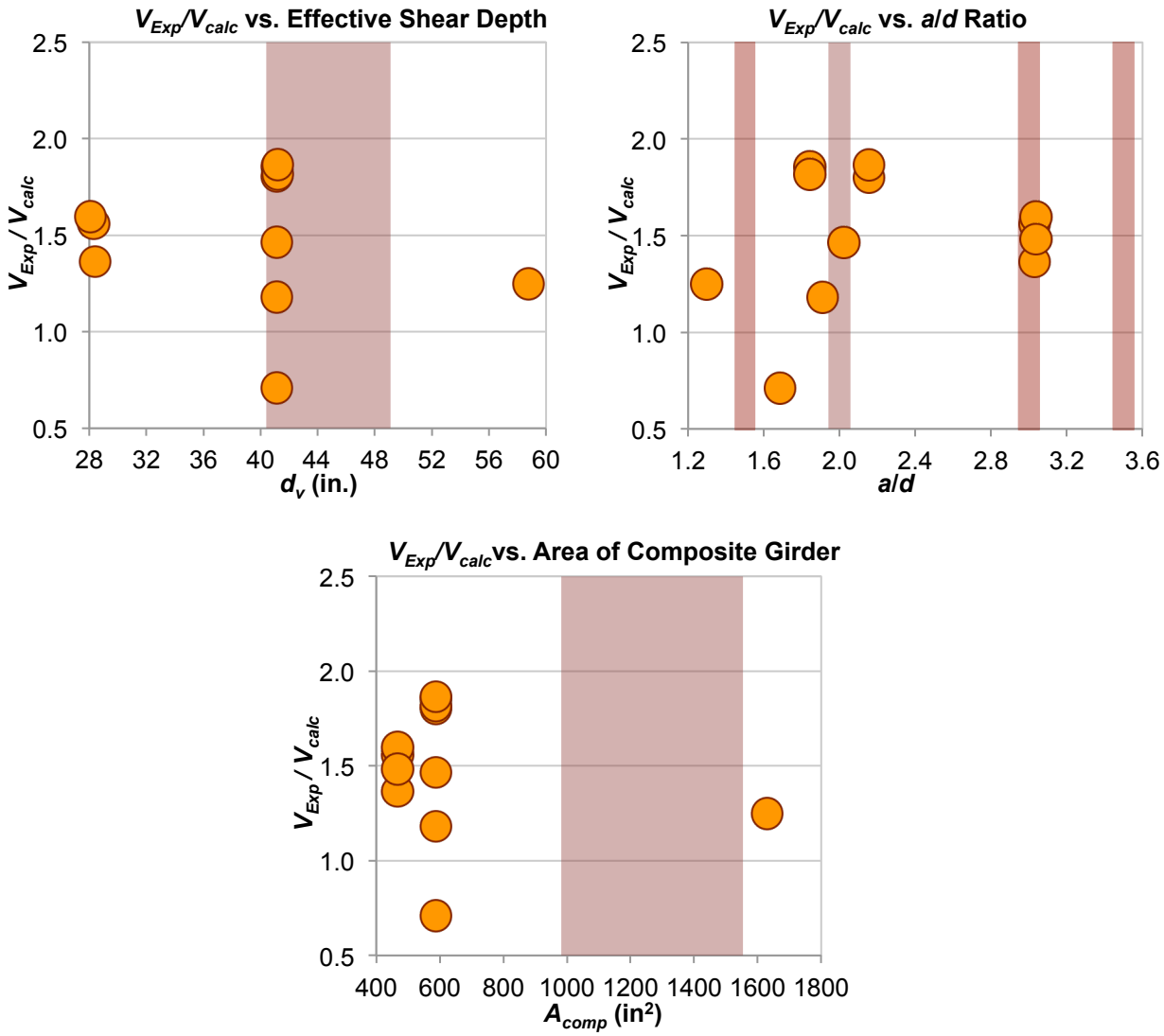

Figure 3-17 (cont). Objective data set (shaded regions) from this study versus existing database of full-scale lightweight concrete girders (circular points) for various design parameters.

Chapter 4

Experimental Results and Analysis

4.1 Material Testing

As discussed in Section 3.4, researchers from VCTIR tested the concrete in each girder for compressive strength, elastic modulus, splitting tensile strength, and modulus of rupture. The results from these tests are shown in Table 4-1. Note that the tests were generally performed at 7, 28, and 56 days from the time of casting as well as on the day of the beam experiment. The exception is the modulus of rupture, which was only measured at 28 days. Note that the numbers in parentheses in the "Testing" column of Table 4-1 indicate the age of the concrete at the time of girder testing and are not related to the rupture modulus.

Like the concrete in the girders, the deck concrete was also tested for compressive strength, elastic modulus, splitting tensile strength, and modulus of rupture. The results from these tests are listed in Table 4-2. Note that for each of the AASHTO Type II beams, only one batch of concrete was required for the entire deck. There were only enough samples taken for beam T2.8.Typ to conduct the material tests at the time of testing of both ends of the girder.

Table 4-3 shows the average results for yield strength and elastic modulus of both the mild reinforcement and the prestressing strands. The results for the mild steel in all of the lightweight girders are the same because this reinforcement was made in the same heat, so a single group of three sample specimens was assumed to represent the rebar in all five lightweight beams. On the other hand, the mild steel used in the normal weight beam was from a different production run and hence had different average properties based on two sample specimens. Note in Table 4-3 that the average modulus of elasticity of the mild steel in the lightweight beams was quite low

Table 4-1. Hardened concrete properties for the test girders. Note: ends of girders that were predominately made from the same batch of concrete are grouped together.

Test ID	Property (ksi)	Days Since Casting				
		Release	7	28	56	Testing
T2.8.Typ.1 T2.8.Typ.2 T2.8.Min.1 T2.8.Min.2	f_c	6.09	7.69	8.15	8.60	8.89
	E_c	3580	3660	3560	3670	3605
	f_t	—	0.660	0.675	0.635	0.690
	f_r	—	—	0.460	—	(116)
BT.8.Typ.1 BT.8.Typ.2	f_c	6.33	7.79	8.10	8.26	9.08
	E_c	3790	3890	3750	3880	3590
	f_t	—	0.690	0.690	0.695	0.705
	f_r	—	—	0.450	—	(211)
BT.8N.Typ.1	f_c	6.18	8.15	9.08	9.11	8.86
	E_c	4670	4790	4890	4880	4820
	f_t	—	0.725	0.740	0.785	0.815
	f_r	—	—	1.005	—	(94)
BT.8N.Typ.2	f_c	—	—	8.14	—	8.57
	E_c	—	—	4680	—	4590
	f_t	—	—	0.725	—	0.735
	f_r	—	—	—	—	(129)
BT.10.Typ.1	f_c	6.12	7.81	7.85	7.85	8.89
	E_c	4230	4270	3910	3820	3910
	f_t	0.620	0.635	0.625	0.655	0.610
	f_r	—	—	0.390	—	(289)
BT.10.Typ.2 BT.10.Min.1	f_c	—	—	8.44	9.15	9.73
	E_c	—	—	3910	4030	4060
	f_t	—	—	0.675	0.620	—
	f_r	—	—	—	—	(260)
BT.10.Min.2	f_c	8.94	—	9.35	9.38	10.32
	E_c	—	—	4140	4070	4140
	f_t	—	—	0.720	0.820	0.765
	f_r	—	—	—	—	(212)

Table 4-2. Hardened concrete properties for the composite decks.

Test ID	Property (ksi)	Days Since Casting			
		1	7	28	Testing
T2.8.Typ.1	f_c	—	—	—	5.83
	E_c	—	—	—	3566
	f_t	—	—	—	0.540
	f_r	—	—	—	(62)
T2.8.Typ.2	f_c	—	—	—	6.09
	E_c	—	—	—	3210
	f_t	—	—	—	0.560
	f_r	—	—	—	(100)
T2.8.Min.1 T2.8.Min.2	f_c	1.72	3.49	4.70	5.36
	E_c	1980	2690	3080	3240
	f_t	0.280	0.440	0.495	0.530
	f_r	—	—	0.640	(67)
BT.8.Typ.1	f_c	3.22	3.86	5.01	5.58
	E_c	3440	2940	3470	3600
	f_t	—	0.460	0.560	—
	f_r	—	—	—	(46)
BT.8.Typ.2	f_c	2.06	4.27	5.88	6.69
	E_c	2640	3410	4060	4050
	f_t	—	0.440	0.605	0.650
	f_r	—	—	0.780	(54)
BT.8N.Typ.1	f_c	—	3.51	4.70	4.89
	E_c	—	2640	2950	2940
	f_t	—	—	0.470	0.520
	f_r	—	—	—	(42)
BT.8N.Typ.2	f_c	2.61	3.50	4.44	4.99
	E_c	2640	2630	3050	3110
	f_t	—	0.430	0.495	0.550
	f_r	—	—	0.760	(77)
BT.10.Typ.1	f_c	1.66	3.48	—	4.13
	E_c	2300	2835	—	3160
	f_t	—	0.490	—	0.440
	f_r	—	—	0.795	(23)
BT.10.Typ.2	f_c	—	4.03	—	4.93
	E_c	—	2970	—	3270
	f_t	—	—	—	0.500
	f_r	—	—	—	(29)

Table 4-2 (cont.). Hardened concrete properties for the composite decks.

Test ID	Property (ksi)	Days Since Casting			
		1	7	28	Testing
BT.10.Min.1	f_c	—	3.20	4.58	5.17
	E_c	—	2500	3060	3200
	f_t	—	—	0.520	0.475
	f_r	—	—	—	(49)
BT.10.Min.2	f_c	1.40	3.90	5.27	5.86
	E_c	1870	2720	3226	3410
	f_t	—	—	0.530	0.520
	f_r	—	—	0.620	(55)

Table 4-3. Average properties of sample steel reinforcement specimens.

Production Run	f_y (ksi)	E_s (ksi)	f_{py} (ksi)	E_p (ksi)
T2.8	67.3	26500	266	31800
BT.8	67.3	26500	250	29700
BT.8N	69.8	29100	265	31700
BT.10	67.3	26500	265	31000

with a standard deviation of 1510 ksi. This result is probably due to the error in the extensometer used to measure strain during testing. Regardless, the resulting error in the calculated elastic modulus using the measured strain has a relatively minor impact on the shear analysis. Beams that were cast in the same production cycle were assumed to have the same material properties for the prestressing reinforcement. The average values listed for the prestressing strands in Table 4-3 are based on three sample specimens, with the exception of the yield stress for the two lightweight beams designed for 10 ksi compressive strength concrete. In that case, two of the three strands failed at the grips prior to reaching yield. There were no tests on the mild steel used in the decks.

4.2 Shear Performance

As discussed in Section 1.3, there were a total of twelve shear tests in this project. All comparisons between experimental capacity and predicted performance have been made using as many known quantities as possible. These values include geometry measurements, fresh unit

weight of concrete given in Table 3.5, hardened concrete properties listed in Tables 4-1 and 4-2, steel material properties in Table 4-3, and structural properties listed in Table 4-4. Note that the prestressing losses incorporated in f_{pe} in Table 4-4 were primarily calculated using the modulus of elasticity in Table 4-3 and the difference between the VWG strain measurements just prior to the first load test on a given beam and just prior to strand release on the prestressing bed. Because the change in stress due to relaxation of the strands could not be measured using the VWGs, the values given in the table include relaxation losses calculated using Eq. 5.9.5.4.2c-1 of the 2010 AASHTO LRFD Bridge Design Specifications, reproduced below:

$$\Delta f_{pR1} = \frac{f_{pt}}{K_L}\left(\frac{f_{pt}}{f_{py}} - 0.55\right)$$

where

Δf_{pR1} = prestress loss due to relaxation of prestressing strands between time of transfer and deck placement

f_{pt} = stress in prestressing steel immediately after transfer

K_L = factor accounting for the type of prestressing steel, taken as 30 for low relaxation strands unless more accurate manufacturer's data is available

Mistakenly, twice the value of Δf_{pR1} was included in the total prestress losses to account for additional relaxation between the time of deck placement and final time, as suggested by Article

Table 4-4. Effective prestress and span lengths for girder tests.

Test ID	f_{pe} (ksi)	L_{span} (ft)
T2.8.Typ.1	165.0	40.0
T2.8.Typ.2	165.0	35.1
T2.8.Min.1	162.6	40.0
T2.8.Min.2	162.6	34.8
BT.8.Typ.1	175.1	58.0
BT.8.Typ.2	175.1	49.5
BT.8N.Typ.1	167.8	57.9
BT.8N.Typ.2	167.8	49.0
BT.10.Typ.1	173.3	57.9
BT.10.Typ.2	173.3	49.4
BT.10.Min.1	179.1	58.0
BT.10.Min.2	179.1	49.5

5.9.4.3c of the 2010 AASHTO LRFD Bridge Design Specifications. However, this additional loss should have been omitted since most of the tests on the composite girders were typically conducted within a few weeks of deck placement. Nevertheless, including the additional relaxation loss has a negligible effect on the overall shear strength results. With that said, the f_{pe} results do assume that the jacking stress including anchorage set and friction loss was 75% of f_{pu}, or 202.5 ksi. Furthermore, the calculations assume that there was no change in stress in the strands during the steam curing operation. Lastly, because the second test on each beam occurred shortly after the first test, and because the VWGs were typically damaged during the first test, f_{pe} in Table 4-4 for the second test on each beam was assumed to be the same as the first test.

As discussed in Section 3.3.1, the bearing length was 6 in. from the ends of the beam. The exception was the end of the beam farthest from the loads during the second test, where the support was located approximately 5 or 9 ft from the end of the AASHTO Type II and PCBT-45 girders, respectively. The reason for setting this support further in from the end of the beam was to avoid placing load on the portion of the beam severely damaged during the first test on the beam.

4.2.1 Overall Shear Capacity

Table 4-5 lists the experimental shear strength, V_{Exp}, along with the type of failure occurring during each test. Broadly speaking, the girders performed exceptionally well compared to the expected shear strengths, regardless of the shear design procedure. Therefore, other failure modes did dominate in some tests prior to achieving a true shear failure; most notably, shear bond failure of the strands at the end of the beams. In the case of test T2.8.Min.2, the operational failure discussed in Section 3.3.4 resulted in no failure mode being obtained. In all cases where a shear failure did not dominate, there were signs of concrete powdering or light flaking in the web, indicating that the girder was nearing its shear capacity. Regardless, the experimental shear strength values listed in Table 4-5 are the maximum shear forces observed during testing.

As mentioned in Section 1.3, each beam was designed for both flexure and shear per the 2007 AASHTO LRFD Bridge Design Specifications. So, Table 4-5 also gives the predicted shear

Table 4-5. Failure modes and experimental versus predicted shear strengths for the twelve large-scale girder tests.

Test ID	Failure Mode(s)	V_{exp} (kip)	Appendix B5				General Procedure				Simplified Procedure			
			$V_{n\,A.B5}$ (kip)	$V_{n\,A.B5}$ No λ_v (kip)	$^{Exp}/_{A.B5}$	$^{Exp}/_{A.B5}$ No λ_v	$V_{n.Gen}$ (kip)	$V_{n.Gen}$ No λ_v (kip)	$^{Exp}/_{Gen}$	$^{Exp}/_{Gen}$ No λ_v	$V_{n.Sim}$ (kip)	$V_{n.Sim}$ No λ_v (kip)	$^{Exp}/_{Sim}$	$^{Exp}/_{Sim}$ No λ_v
T2.8.Typ.1	Flexural / Bond	361	217	222	1.66	1.63	204	207	1.77	1.74	333	339	1.08	1.07
T2.8.Typ.2	Flexural	294	196	199	1.49	1.47	185	188	1.59	1.57	305	311	0.96	0.94
T2.8.Min.1	Web Shear / Bond	382	189	194	2.02	1.97	178	182	2.15	2.10	278	284	1.38	1.35
T2.8.Min.2	——	308	182	186	1.69	1.66	170	173	1.81	1.78	271	277	1.14	1.11
BT.8.Typ.1	Web Shear / Bond	500	306	312	1.63	1.60	289	293	1.73	1.70	373	373	1.34	1.34
BT.8.Typ.2	Flexural	408	269	284	1.52	1.43	269	273	1.52	1.49	339	335	1.20	1.22
BT.8N.Typ.1	Web Shear / Bond	431	259	259	1.66	1.66	248	248	1.74	1.74	317	317	1.36	1.36
BT.8N.Typ.2	Web Shear / Bond	382	241	241	1.58	1.58	239	239	1.60	1.60	290	290	1.32	1.32
BT.10.Typ.1	Web Shear / Bond	518	285	291	1.82	1.78	277	283	1.87	1.83	339	348	1.53	1.49
BT.10.Typ.2	Web Shear / Flex. / Bond	428	268	273	1.60	1.57	260	265	1.65	1.62	328	334	1.30	1.28
BT.10.Min.1	Web Shear / Bond	475	224	232	2.12	2.05	224	233	2.12	2.04	241	244	1.97	1.95
BT.10.Min.2	Web Shear	371	226	232	1.64	1.60	226	235	1.64	1.58	236	240	1.57	1.54
Average $^{Exp}/_{Calc}$ ratio for Lightweight Concrete					**1.72**	**1.68**			**1.78**	**1.75**			**1.35**	**1.33**
Average $^{Exp}/_{Calc}$ ratio for Normal Weight Concrete					**1.62**	**1.62**			**1.67**	**1.67**			**1.34**	**1.34**
Average $^{Exp}/_{Calc}$ ratio for all tests					**1.70**	**1.67**			**1.76**	**1.73**			**1.35**	**1.33**

strength according to the three shear design methods considered in this investigation, where *A.B5, Gen,* and *Sim* signify the shear strengths calculated using the *Appendix B5* method from Appendix B5.2, the *General Procedure* from Article 5.8.3.4.2, or the *Simplified Procedure* from Article 5.8.3.4.3, respectively, of the 2010 AASHTO LRFD Bridge Design Specifications. The columns denoted *Exp*/*A.B5*, *Exp*/*Gen*, and *Exp*/*Sim* in this table give the ratios of the experimental results versus the results predicted by the three AASHTO design methods.

Note that the basic steps for calculating the shear strength of an existing girder using *Appendix B5* and the *General Procedure* parallel the process originally outlined by Kulicki et al. (*156*). The computer programs along with the major inputs and outputs that arrive at the calculated shear strengths using all three shear design procedures are detailed in Appendix C. Also note that all of the calculations assume that all load factors are equal to 1.00, because the dead and live loads were assumed to be known through measurements and instrumentation. Likewise, ϕ_v has been set at 1.00 in these analyses. However, the calculated shear strengths in the three aforementioned columns do include the lightweight modification factor where appropriate. Note that V_{calc} is the nominal shear strength calculated according to a given shear design method.

Recall from Section 2.2.6 that for traditional design of shear stirrups, the engineer divides the beam into segments of ten equal lengths and calculates the spacing and or size of the stirrups within each segment based on the largest shear within that segment. In performing the analysis for this research, the calculations involved dividing the *shear span* into ten equal lengths; thus, there are ten calculated values of shear resistance. The segment with the lowest shear resistance is considered the weakest link, making the shear resistance of that segment within the shear span the calculated shear strength of the beam listed in Table 4-5.

The ratio of experimental versus calculated strength range from 1.49 to 2.12, 1.52 to 2.12, and 0.96 to 1.97 when using the *Appendix B5*, *General Procedure*, and *Simplified Procedure*, respectively. With the average experimental strength ranging from 35% (*Simplified Procedure*) to 76% (*General Procedure*) greater than what was calculated in all of the tests that were conducted in this investigation, AASHTO is evidently fairly conservative in calculating the shear strength. The given percentages compare to the work by Hawkins et al. (*59*), Kahn et al. (*16*),

and Dymond et al. (*24*). Although testing normal weight concrete, Hawkins et al. found that prestressed concrete had average experimental-to-calculated ratios of 1.23 and 1.25 for $V_{n\,LRFD}$ and $V_{n\,CSA}$, respectively. In this case, $V_{n\,LRFD}$ is $V_{n\,A.B5}$ using *Appendix B5* in the 2010 AASHTO LRFD Bridge Design Specifications, while $V_{n\,CSA}$ is the nominal shear strength calculated according to the Canadian design code, CSA A23.3-04 (*76*), and is akin to $V_{n\,Gen}$ using the *General Procedure*. On the other hand, Hawkins et al. determined that the ratio using $V_{n\,Sim}$ was much higher at 1.54. Kahn et al. found that the ratio $V_{Exp} / V_{n\,LRFD}$ ranged from 1.13 to 3.11, where $V_{n\,LRFD}$ is akin to $V_{n\,A.B5}$ in this investigation. For $V_{Exp} / V_{n\,Std}$, the range was 1.21 to 1.86, where $V_{n\,Std}$ is theoretically only slightly different from $V_{n\,Sim}$. For the one beam with results in the Dymond et al. investigation, $V_{Exp} / V_{n\,Sim}$ was 1.38 while $V_{Exp} / V_{n\,A.B5}$ was 1.46.

The fact that the *Simplified Procedure* is the least conservative, yet most accurate, predictor of shear strength is somewhat surprising given that one might think that the easier method tends to be more conservative, along with the fact that AASHTO uses a lower-bound estimate for the concrete tensile strength when calculating V_{cw}. In the case of this study, V_{cw} is the controlling factor for the concrete contribution to the shear strength using the *Simplified Procedure*. However, as shown by Eq. 37 in Section 2.2.4.4, the lower the cracking angle, the higher the predicted steel contribution to the shear capacity. As will be discussed in Sections 4.4.1.3 and 0, the predicted angle of shear cracking, θ, tends to be lower for the *Simplified Procedure* relative to the other two methods. Therefore, the *Simplified Procedure* tends to have a larger calculated contribution from the vertical steel and less conservative overall shear strength prediction.

On the other hand, the *General Procedure* is marginally more conservative than *Appendix B5*, with the difference between the average experimental-to-theoretical ratios of the two methods being about 5 percent. Then again, the *General Procedure* makes somewhat more conservative assumptions in simplifying the calculations. Nevertheless, both methods typically require about thirteen or fourteen iterations to converge in the strength analysis. However, the *Appendix B5* process involves multiple sub-iterations within each main iteration before the calculations for β and θ converge.

What is not apparent in Table 4-5 is that the calculations predicted that roughly half of the failures would occur within the section that was at or near the load closest to the abutment in the four-point load test. Specifically, calculations using *Appendix B5* indicated that failure would occur at the load point in 50% of the tests, while the results from the *General Procedure* and *Simplified Procedure* were at 42% and 58%, respectively. Yet, all of the experimental girders that failed in shear exhibited signs of failure at or near the critical section, as evidenced by concrete powdering or crushing as well as the cracks being the widest in this region. Furthermore, the stirrup strain data discussed in Section 4.2.3.1 and detailed in Appendix B show that the maximum strains within the stirrups near the critical section typically reached yield strains at lower live loads than did the stirrups that were closer to the first load actuator, which indicates that the region near the critical section was failing first. For a perspective on which girders were predicted to fail at the critical section, compare Table 4-5 with Table 4-6, which details the theoretical shear strengths calculated at the critical section.

4.2.2 Effects of Various Parameters on Shear Capacity

As mentioned in Section 2.5, two of the main goals for this research are to fill in some of the gaps in the available data regarding shear strength of beams constructed with sand-lightweight concrete and to compare test results with various design parameters. These parameters include concrete compressive strength, effective shear depth, shear span-to-effective depth ratio, shear reinforcing index, and area of composite cross-section. Figures 4-1 through 4-3 show these comparisons, where the shear strength results are in the form of ratios of the experimental shear strengths divided by the predicted shear strengths from *Appendix B5*, the *General Procedure*, and the *Simplified Procedure*, respectively, as listed in Table 4-5. Note that the calculated values for V_n in Figures 4-1 through 4-3 do include the modification factor for lightweight concrete.

Note that the data from the current study has been superimposed onto the results from previous research on large-scale, prestressed, lightweight concrete girders in Figures 4-1 through 4-3. The data from the previous research has been presented earlier in a similar format in Figure 2-6 and the results are detailed in Table 4-7. The calculated shear strength values in this table have been determined using the geometry and material characteristics provided in the researchers' reporting. The girders in the previous set of research had concrete compressive strengths ranging

Table 4-6. Experimental shear strength versus the failure load predicted at the critical section.
NB: LWC = lightweight concrete, NWC = normal weight concrete

Test ID	V_{Exp} (kip)	Appendix B5				General Procedure				Simplified Procedure			
		$V_{n\ A.B5\ Crit}$ (kip)	$V_{n\ A.B5\ Crit}$ No λ_v (kip)	$^{Exp}/_{A.B5\ Crit}$	$^{Exp}/_{A.B5\ Crit}$ No λ_v	$V_{n\ Gen\ Crit}$ (kip)	$V_{n\ Crit\ Gen}$ No λ_v (kip)	$^{Exp}/_{Gen\ Crit}$	$^{Exp}/_{Gen\ Crit}$ No λ_v	$V_{n\ Sim\ Crit}$ (kip)	$V_{n\ Crit\ Sim}$ No λ_v (kip)	$^{Exp}/_{Sim\ Crit}$	$^{Exp}/_{Sim\ Crit}$ No λ_v
T2.8.Typ.1	361	213	217	1.70	1.66	204	207	1.77	1.74	340	346	1.06	1.04
T2.8.Typ.2	294	213	217	1.37	1.34	185	188	1.58	1.55	305	311	0.96	0.94
T2.8.Min.1	382	185	189	2.07	2.02	178	182	2.15	2.10	283	289	1.35	1.32
T2.8.Min.2	308	186	191	1.65	1.61	173	176	1.78	1.75	273	279	1.13	1.10
BT.8.Typ.1	500	306	312	1.63	1.60	295	301	1.69	1.66	378	373	1.32	1.34
BT.8.Typ.2	408	315	322	1.29	1.27	296	301	1.38	1.35	358	352	1.14	1.15
BT.8N.Typ.1	431	259	259	1.66	1.66	248	248	1.74	1.74	317	317	1.36	1.36
BT.8N.Typ.2	382	258	258	1.48	1.48	248	248	1.54	1.54	301	301	1.27	1.27
BT.10.Typ.1	518	298	306	1.74	1.69	283	290	1.83	1.79	368	361	1.41	1.43
BT.10.Typ.2	428	303	310	1.41	1.38	279	284	1.53	1.51	341	346	1.26	1.24
BT.10.Min.1	475	224	232	2.12	2.05	224	233	2.12	2.04	241	244	1.97	1.95
BT.10.Min.2	371	226	234	1.64	1.59	226	235	1.64	1.58	236	240	1.57	1.54
Average $^{Exp}/_{Calc}$ ratio for LWC				**1.66**	**1.62**			**1.75**	**1.71**			**1.32**	**1.31**
Average $^{Exp}/_{Calc}$ ratio for NWC				**1.57**	**1.57**			**1.64**	**1.64**			**1.31**	**1.31**
Average $^{Exp}/_{Calc}$ ratio for all tests				**1.65**	**1.61**			**1.73**	**1.70**			**1.32**	**1.31**

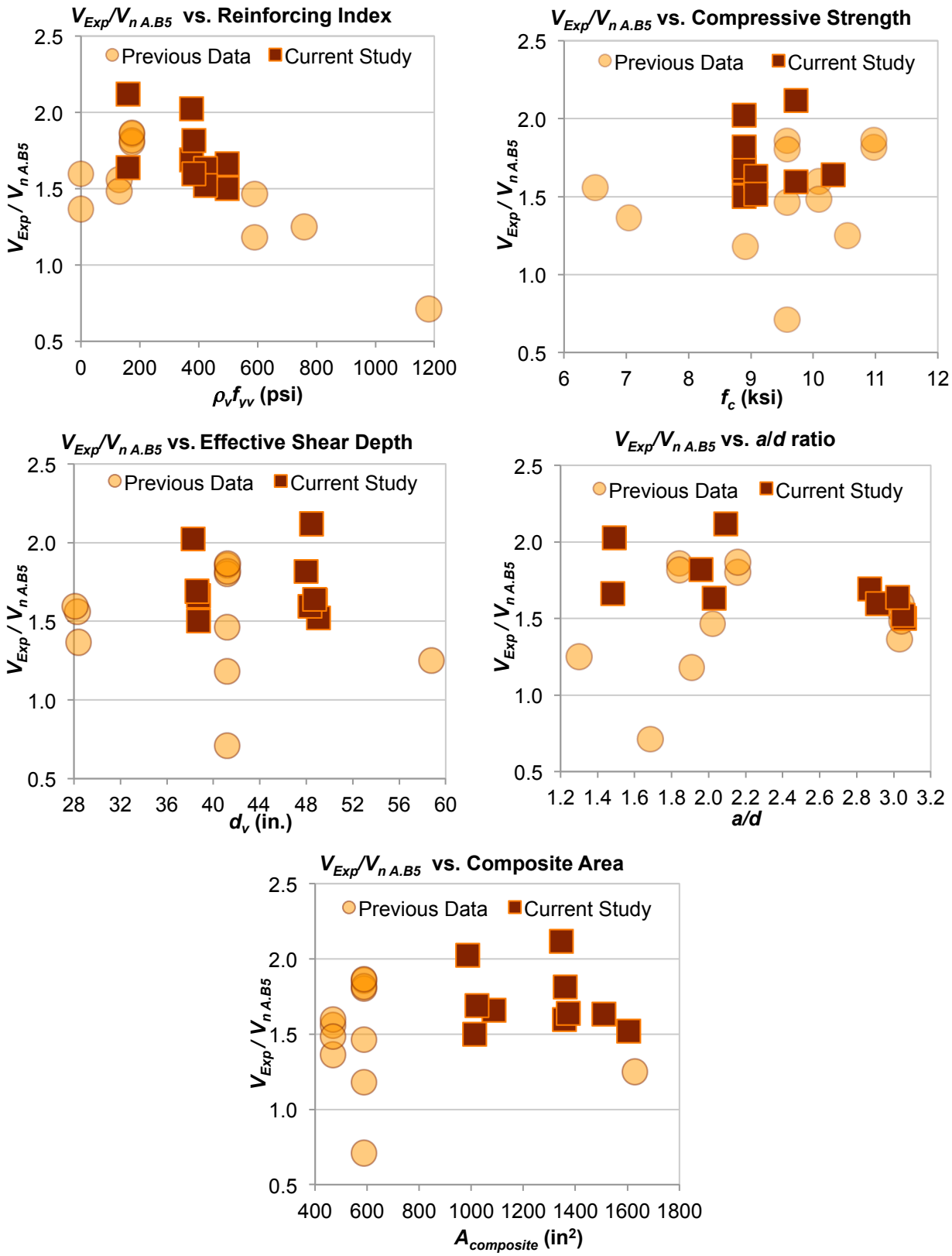

Figure 4-1. Effects of various design parameters on the ratio of the experimental-to-calculated values using *Appendix B5* with λ_v.

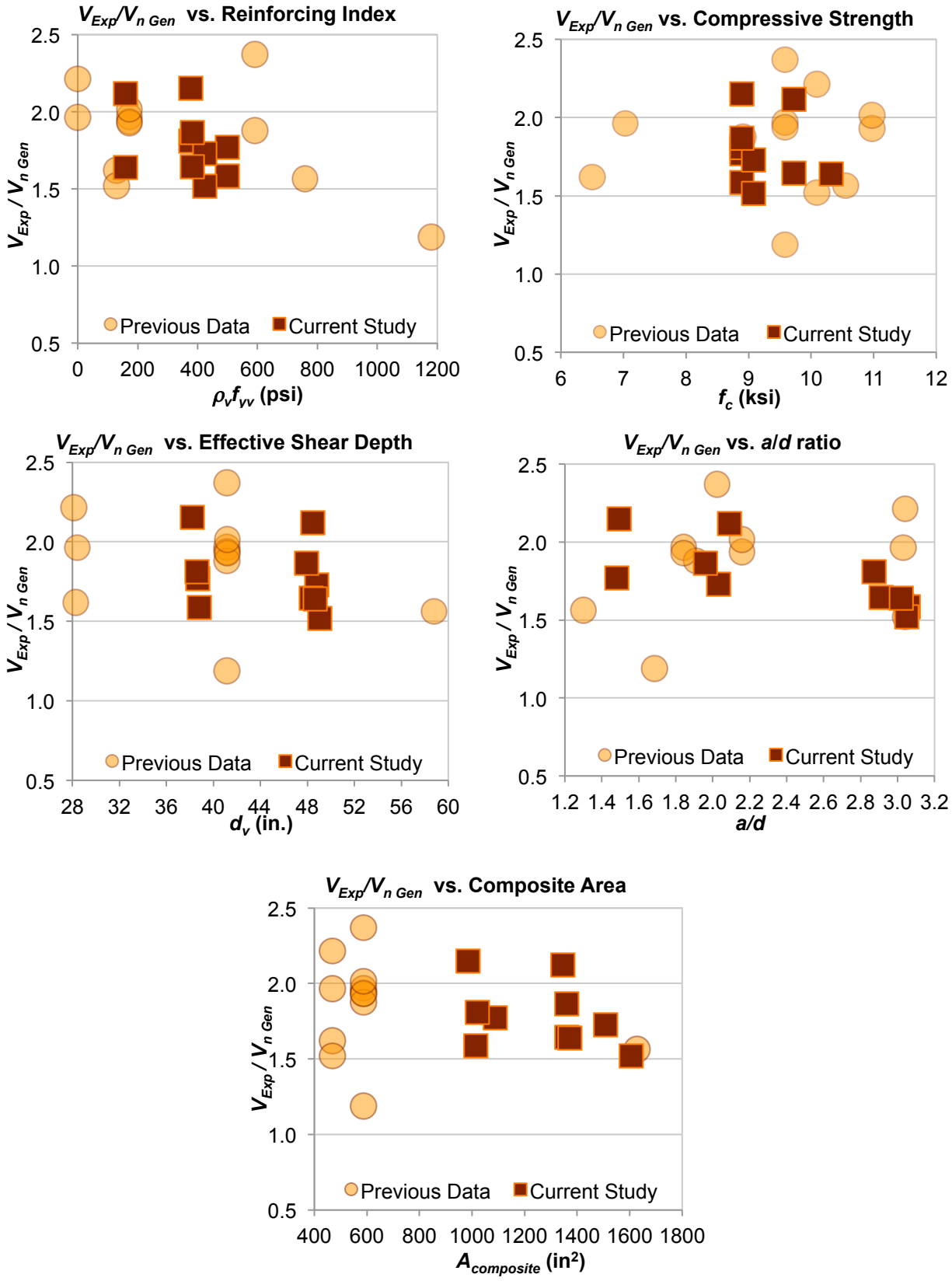

Figure 4-2. Effects of various design parameters on the ratio of the experimental-to-calculated values using the *General Procedure* with λ_v.

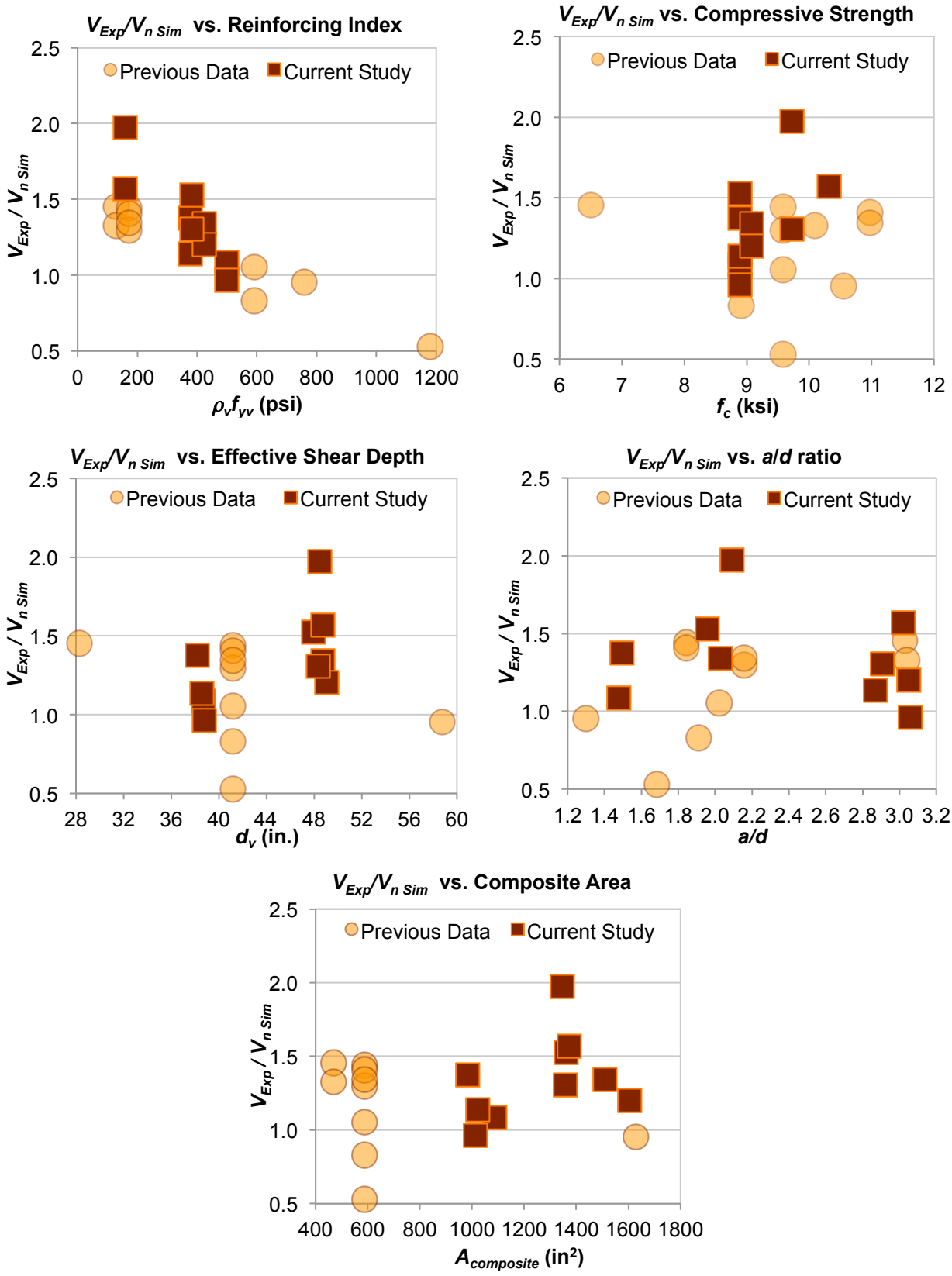

Figure 4-3. Effects of various design parameters on the ratio of the experimental-to-calculated values using the *Simplified Procedure* with λ_v.

from 6.5 ksi to 11.0 ksi. The cross-sectional area ranged from 468 in^2 to 1629 in^2 while the shear span-to-effective depth ratio, *a*/*d*, ranged from 1.3 to 3.0. Some girders had no shear reinforcement, while others had minimal ($\rho_v \approx 0.003$) and typical ($\rho_v \approx 0.019$) shear reinforcement ratios, resulting in reinforcing indices ranging from 0 psi to 1180 psi. Only the one test by Dymond et al. contained harped tendons. On a separate note, Table 4-7 shows that the shear capacity of specimen G1B-East by Kahn et al. was dramatically lower than what was anticipated. One possible reason for this outlier is that the beam experienced shear bond failure. Therefore, the beam did not reach its full potential prior to test termination.

Generally speaking, the results from current study agree with the previous research, with the range of the experimental-to-calculated values of the current research being slightly narrower and some of the strength ratios from the earlier work being lower. Not surprisingly, the results using *Appendix B5* and the *General Procedure* are quite similar in terms of the effects of the different parameters. Unfortunately, there is still a gap in the data for concrete compressive strength because the girders in this research that were designed for f'_c to be 8 ksi proved to have strengths that were closer to 9 ksi. Furthermore, there still is not very much data for *a*/*d* in between 2.2 and 2.8.

Looking more specifically at one of the parameters that could influence the relative accuracy of the predicted strengths, there is a trend in all three of the design models where the experimental strength decreases relative to the expected strength as the amount of vertical reinforcement increases. Paczkowski and Nowak reached a similar conclusion for lightweight reinforced concrete members, as discussed in Section 2.4.3.2. This observation is particularly true for the *Simplified Procedure*. In fact, in most of the test specimens where the shear reinforcing index, $\rho_v f_{yv}$, is greater than 498 psi, the ratio of the experimental-to-predicted shear strengths using the *Simplified Procedure* is less than 1.0. This fact suggests that there should be some sort of limit on the predicted concrete girder strength based on $\rho_v f_{yv}$ when designing with the *Simplified Procedure*. Note that the graph comparing $V_{Exp} / V_{n\,Sim}$ in Figure 4-3 does not show data points for tests PC6N and PC10N because Article 5.8.3.4.3 of the 2010 AASHTO LRFD Bridge Design Specifications does not apply to those beams containing less than the minimum amount of shear reinforcement specified in Article 5.8.2.5.

Table 4-7. Comparison of experimental shear strength versus calculated shear capacity from previous research on large-scale, lightweight concrete girders

Researcher	Specimen ID	V_{Exp} (kip)	Appendix B5				General Procedure				Simplified Procedure			
			$V_{n\ A.B5}$ (kip)	$V_{n\ A.B5}$ No λ_v (kip)	$^{Exp}/_{A.B5}$	$^{Exp}/_{A.B5}$ No λ_v	$V_{n.Gen}$ (kip)	$V_{n.Gen}$ No λ_v (kip)	$^{Exp}/_{Gen}$	$^{Exp}/_{Gen}$ No λ_v	$V_{n.Sim}$ (kip)	$V_{n.Sim}$ No λ_v (kip)	$^{Exp}/_{Sim}$	$^{Exp}/_{Sim}$ No λ_v
Malone	PC6N	80	50	59	1.61	1.37	41	47	1.96	1.70				
Malone	PC6S	117	72	75	1.63	1.56	72	75	1.62	1.56	80	83	1.45	1.41
Malone	PC10N	105	59	65	1.76	1.60	47	54	2.21	1.92				
Malone	PC10S	120	77	81	1.56	1.48	79	83	1.52	1.45	90	93	1.33	1.29
Kahn et al.	G1A-East	363	240	248	1.51	1.46	153	155	2.37	2.35	344	335	1.05	1.08
Kahn et al.	G1A-Center	258	135	139	1.92	1.86	131	134	1.97	1.92	179	186	1.44	1.39
Kahn et al.	G1B-East	312	432	440	0.72	0.71	263	266	1.19	1.17	592	574	0.53	0.54
Kahn et al.	G1B-Center	234	125	130	1.87	1.80	121	124	1.94	1.89	181	187	1.30	1.25
Kahn et al.	G1C-East	289	238	245	1.22	1.18	154	156	1.88	1.86	349	338	0.83	0.86
Kahn et al.	G2A-Center	256	136	141	1.88	1.82	133	136	1.93	1.88	182	188	1.41	1.36
Kahn et al.	G2B-Center	246	127	132	1.93	1.87	122	125	2.02	1.96	183	191	1.34	1.29
Dymond et al.	web-shear	658	514	527	1.28	1.25	421	425	1.56	1.55	690	670	0.95	0.98
Average $^{Exp}/_{Calc}$ ratio					**1.57**	**1.54**			**1.90**	**1.82**			**1.79**	**1.72**

The AASHTO LRFD Bridge Design Specifications do limit the shear strength of concrete girders. However, Eq. 5.8.3.3-2 of the 2010 AASHTO LRFD Bridge Design Specifications, which is Eq. (65) in Chapter 2 of this work, is intended to ensure that the transverse steel yields prior to the concrete crushing in the girder web. Although the information from the previous research does not indicate if such was the case, the stirrups in test T2.8.Typ.2 of the current investigation had certainly started to yield prior to web crushing. Therefore, the experiment satisfied the goal of Eq. (65). Yet, the ratio of actual-to-predicted failure was 0.96 for T2.8.Typ.2 when considering the *Simplified Procedure*. Granted, test T2.8.Typ.2 did experience a flexural failure. However, Section 4.2.1 discusses the powdering and flaking that was evident at termination of the experiment indicating that the girder was near its shear capacity. Thus, AASHTO may need to decrease its maximum limit for shear strength in girders constructed with sand-lightweight concrete, at least when designing according to the *Simplified Procedure*. Again, perhaps that limit should be based on the reinforcing index.

Like the shear reinforcing index, data from the previous research on prestressed, lightweight concrete indicates that the compressive strength of concrete does have an inverse influence on the performance of the strength prediction when using the *Simplified Procedure*. However, the results from the current study show an opposite trend. Similarly, V_{Exp}/V_{calc} determined for *Appendix B5* and the *General Procedure* shows a slightly increasing trend as f_c increases from 6 ksi to 11 ksi. Recall in Section 2.3.2.7.1 that Kawaguchi et al. came to a different conclusion when comparing experimental results of super lightweight concrete versus the JSCE code. In that case, the researchers observed a decrease in the experimental-to-predicted ratio as the compressive strength increased. On the other hand, the current investigation is in line with Paczkowski and Nowak's findings from Section 2.4.3.2, where the level of conservatism in the design calculation increased as the concrete compressive strength increased, regardless of the type of concrete. Elzanaty et al. reached a similar conclusion for normal weight concrete. Paczkowski and Nowak did go on to say that the rate of increase for lightweight concrete was higher than that of normal weight concrete. However, there were not enough tests with normal weight concrete in the current study to assess that conclusion.

In the 2010 AASHTO LRFD Bridge Design Specifications, all three of the shear design methods incorporate another parameter into the equation, the effective shear depth. Interestingly, Walraven (*106*) agreed with this philosophy, but Ivey and Buth (*99*) found that d_v had little if any effect on the shear resistance of a beam. The test versus calculated ratios using the *General Procedure* from both the current investigation and past research on full-scale lightweight concrete girders seem to agree with Ivey and Buth's theory. However, the results using *Appendix B5* contradicts the theory. On the one hand, the prior research indicates that the shear performance of prestressed, lightweight girders declines relative to the *Appendix B5* predictions when the effective shear depth is greater than 40 in. Yet, the current investigation shows that beams with d_v measuring about 48 in. actually had equal or more conservative predictions than other beams with a smaller d_v of 28 in. Similarly, calculations using the *Simplified Procedure* are contradictory, where the earlier test results indicate that the predictions become less conservative as d_v increases, while this investigation finds that the calculations become more conservative for prestressed girders constructed with lightweight concrete. Thus, compared to the other two shear design models, the *General Procedure* does a somewhat better job at incorporating d_v and consistently predicting the shear strength across the range of effective shear depths varying from 28 in. to 52 in.

Another comparison parameter involving the effective shear depth is the shear span-to-effective depth ratio. While the results from previous work show that all three design models are less conservative for smaller values of a/d, the lightweight beams in this research exhibit a trend that goes slightly in the opposite direction. Some beams in the current investigation that have some of the highest experimental-to-calculated ratios also have values for a/d that are less than 2.0. On the other hand, the lightweight results from the present research prove to be slightly less conservative when testing at shear span-to-effective depth ratio around 3.0. In fact, the one case where the strength ratio is less than 1.0, that is T2.8.Typ.2 with the *Simplified Procedure*, has an a/d value of 3.1. Recall from Section 2.3.2.4 that Ahmad et al. had a similar result, where the shear strength of a lightweight reinforced concrete beam of similar a/d was less than predicted by the ACI 318-89 code, which is somewhat similar to the *Simplified Procedure*. Elzanaty et al. found that the same was true for normal weight beams, as mentioned in Section 2.2.4.2.

When comparing the cross-section of a composite section, most of the areas of the beams in the previous research were less than 600 in^2, with the exception of the one test by Dymond et al. (*24*), where the composite cross-sectional area was 1629 in^2. Given that the prior work was heavily biased toward a smaller area, making any firm observations based on those results alone can be difficult. However, the composite areas in this project are between those two values, ranging from 985 in^2 to 1305 in^2. Combining the results from the current testing with the previous experiments shows that the cross-sectional area does not have much of an impact on the relationship between experimental shear strengths of beams constructed with lightweight concrete and the predicted strengths using any of the three AASHTO design methods under consideration. This observation is logical given that none of the three models include the composite cross-sectional area in their formulations for shear strength. However, the area of concrete on the flexural tension side of the cross-section, designated as A_c in the 2010 AASHTO LRFD Bridge Design Specifications, does appear in both the *General Procedure* and *Appendix B5* of the code. Nevertheless, comparing A_c with the actual versus calculated strength ratios yields results that are similar to comparisons using the total composite area.

4.2.3 Steel and Concrete Contributions to Shear Capacity

As discussed in Section 2.2, there are many factors that have a role in the shear strength of concrete members. Eq. (64) in Section 2.2.5.2 condenses these factors into three major resistance components: the strength provided by the transverse reinforcement, V_s; the resistance in the concrete, V_c, and the strength from the vertical component of the draped or harped prestressing strands, V_p.

4.2.3.1 Forces in the Steel

4.2.3.1.1 Strains in the Stirrups

Section 3.2.7 describes the strain gauges that were placed on the vertical reinforcement prior to concrete placement. These gauges were quite fragile; some were damaged during stirrup transport to the construction site or during concrete placement. Others simply malfunctioned after the concrete had finished steam curing. Approximately 20% of the gauges installed on the stirrups were not registering measurements at the time of testing. As noted in Section 3.2.7, there was no redundancy in the instrumentation for the transverse stirrups.

Figure 4-4(a) shows a sample plot of stirrup strains versus the applied live shear force during test T2.8.Typ.1. Graphs of the strain data as well as sketched web-shear crack locations for the remaining tests are in Appendix B. Figure 4-4(b) shows the locations of each gauge for this particular test. The nomenclature of each strain gauge in the (a) portion of the figure is as follows. The first number in the identifier is the stirrup number counted from the end of the beam being tested. This same number corresponds to the number indicated along the bottom of the beam in the (b) figure. The second number in the gauge identifier is the gauge number on a given stirrup, counted from the bottom of the stirrup. This number is also indicated along the given stirrup in the (b) figure. So, for example, gauge 7.2 in test T2.8.Typ.1 is the second gauge from the bottom of the seventh stirrup from the end of the beam. The (b) portion of the figure also indicates whether the gauge yielded during testing, and if so, whether or not yielding developed as concrete cracking occurred at the gauge location. Of course, if the gauge was not working properly, then that gauge does not appear in the (a) figure. In the case of gauge 7.2 of test T2.8.Typ.1, this gauge yielded upon first cracking at that location.

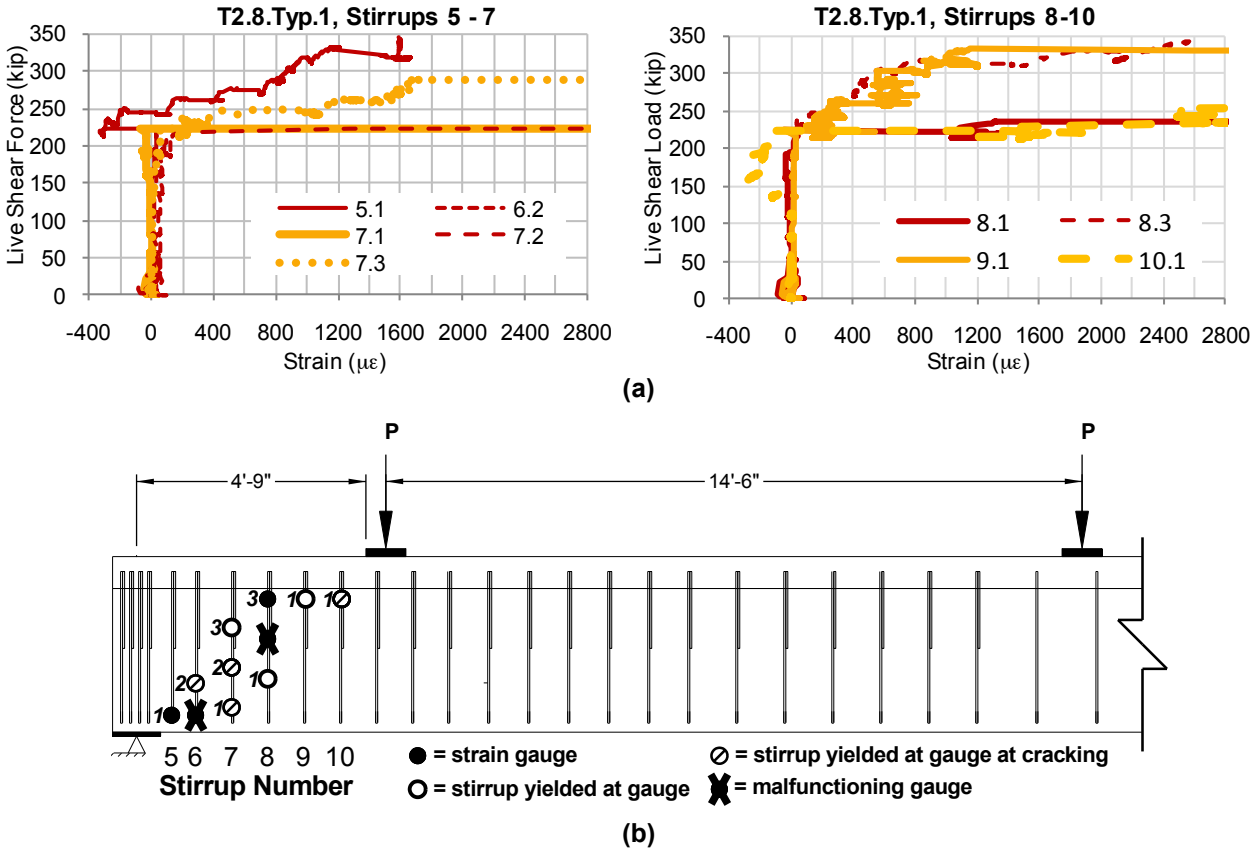

Figure 4-4. (a) Strain gauge measurements and (b) strain gauge locations for Test T2.8.Typ.1.

4.2.3.1.2 Forces in the Stirrups

The boundary crack is an important feature in determining the steel contribution to the shear capacity. Hawkins and Kuchma defined this crack as the widest crack or the crack nearest where the largest strains at failure have been observed. If there are multiple cracks of similar width, then the selected crack is the crack whose midpoint is closest to the critical section location, which is defined as the maximum of the effective shear depth, d_v, or $0.5d_v\cot\theta$ measured from the inside face of the support (*61*).

In six of the twelve tests, at least 50% of the stirrups that intersected the boundary crack yielded when the first web-shear cracks appeared. BT.8.Typ.1 is the only test that didn't have a single stirrup that yielded at first cracking, while BT.10.Min.2 is the lone girder to have all of its stirrups that crossed the boundary crack yield at first cracking. By the end of testing, the majority of the vertical reinforcement along the boundary crack had yielded in all of the girders; all of the stirrups in all of the tests with 10 ksi concrete compressive strength had reached the yield point. The same is true for tests T2.8.Min.1 and BT.8.Typ.2. See Table 4-8 and Appendix B for more detail.

There is a considerable amount of estimation in the values given in Table 4-8 because at best there were only a few strain gauges located at the boundary crack, and there were a number of stirrups that didn't have any instrumentation at all. This fact led to a fair amount of

Table 4-8. Status of stirrups crossing the boundary crack at or soon after the formation of the first web-shear crack, and at the final loading.

Test ID	Number of Stirrups	Number Yielded @ 1st Crack	Number Yielded @ Final Load	% Yielded @ 1st Crack	% Yielded @ Final Load
T2.8.Typ.1	6	3	5	50%	83%
T2.8.Typ.2	10	1	7	10%	70%
T2.8.Min.1	4	3	4	75%	100%
T2.8.Min.2	6	4	5	67%	83%
BT.8.Typ.1	10	0	7	0%	70%
BT.8.Typ.2	8	3	8	38%	100%
BT.8N.Typ.1	6	1	4	17%	67%
BT.8N.Typ.2	7	2	6	29%	86%
BT.10.Typ.1	6	3	6	50%	100%
BT.10.Typ.2	7	5	7	71%	100%
BT.10.Min.1	4	1	4	25%	100%
BT.10.Min.2	4	4	4	100%	100%

interpolation. An additional complicating issue is the exact location of the stirrups wasn't known; the as-built structure might not have had the stirrup spacing as presented in the construction drawings in Appendix A. Although the research team employed a pachometer to locate the vertical stirrups within the concrete, there is still some error in those findings.

Nevertheless, the process for determining the force in the transverse reinforcement throughout each experiment is the same as that described by Hawkins and Kuchma (*61*). The first step is to establish the boundary crack as described earlier. Having established the boundary crack, the strains in the stirrups crossing that crack are recorded from the strain gauge data that was continuously collected throughout the experiment. As discussed in Section 3.2.7, the layout of the strain gauges was designed to capture the strain in the stirrups at the cracks while minimizing the number of gauges that needed to be installed. For any given stirrup, if there was a gauge located on both sides of the crack, then the strain gauge with the highest reading is the recorded strain in the stirrup. If the crack crossed a stirrup where the gauges were only on one side of the crack, the strain in the gauge nearest the crack is the recorded strain in the stirrup. If a particular stirrup was not instrumented with any gauges but had gauged stirrups on either side, then the strain is linearly interpolated from the strains that have been determined for the two neighboring stirrups. If there was a stirrup without strain gauges that did not have a neighboring instrumented stirrup on both sides, then the strain in that stirrup is simply taken as the strain in the gauged stirrup that was closest to the stirrup in question.

Along with the strains in the stirrups, the yield stress, the modulus of elasticity, and the nominal area of the reinforcement are necessary to calculate the forces in those stirrups. Again, the yield stress and modulus of elasticity have been obtained from sample testing, and are given in Table 4-3. If the strain is greater than the yield strain, then the force in the reinforcement is limited to the yield force. Lastly, the total contribution of the transverse steel, V_s, to the overall shear capacity is a summation of all of the forces in the stirrups crossing the boundary crack.

4.2.3.1.3 Vertical Force Component in the Prestressing Tendons

For ease of presentation, V_s in Figure 4-5 has actually been coupled with the vertical component of the force in the prestressing tendons, V_p. The calculation for V_p is given by Eq. (66) in Section 2.2.5.2, but also takes the development length into account. Table 4-4 lists the values for f_{pe},

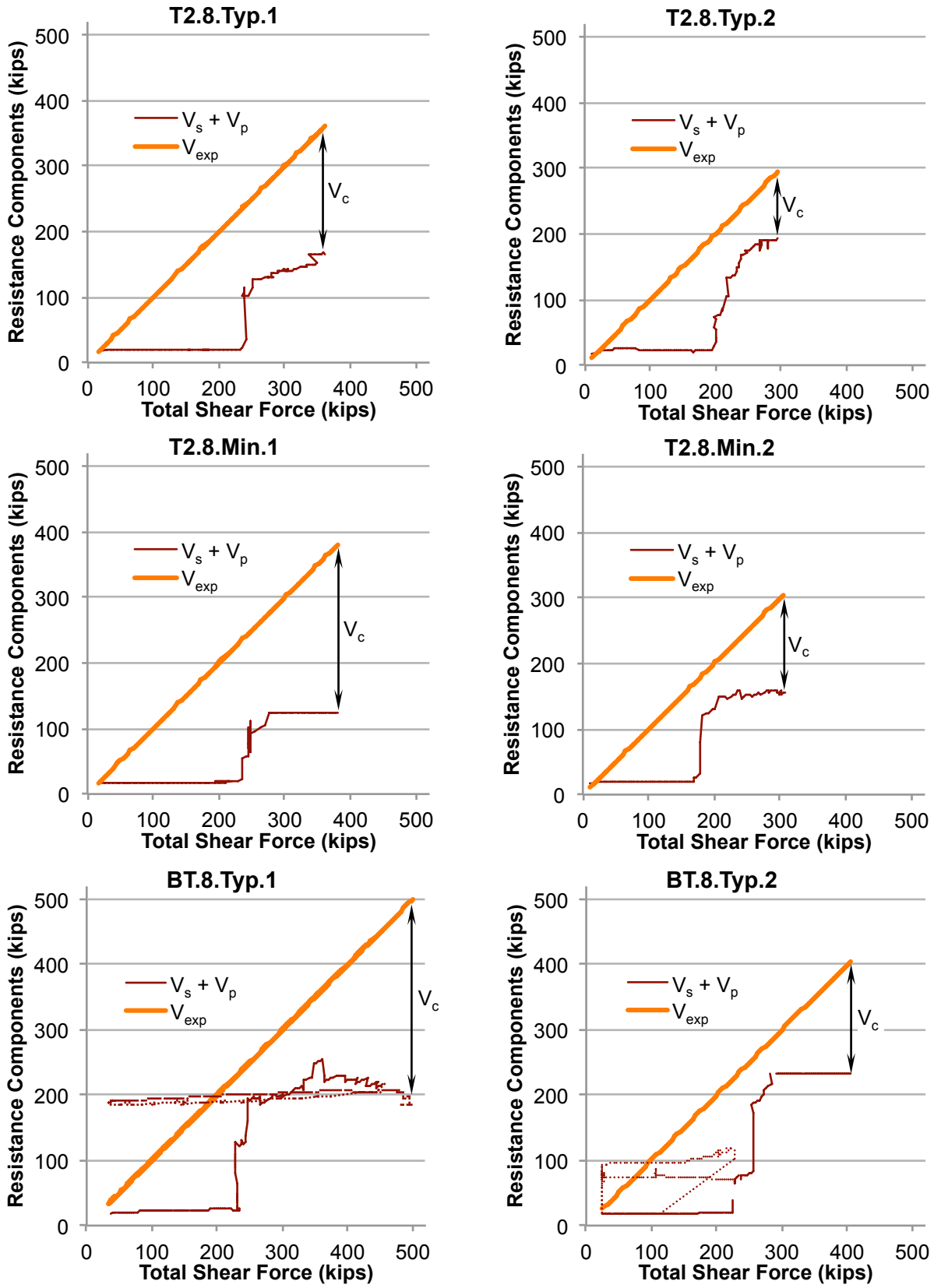

Figure 4-5. Forces in the steel and concrete components versus the total shear force in the individual girder tests.

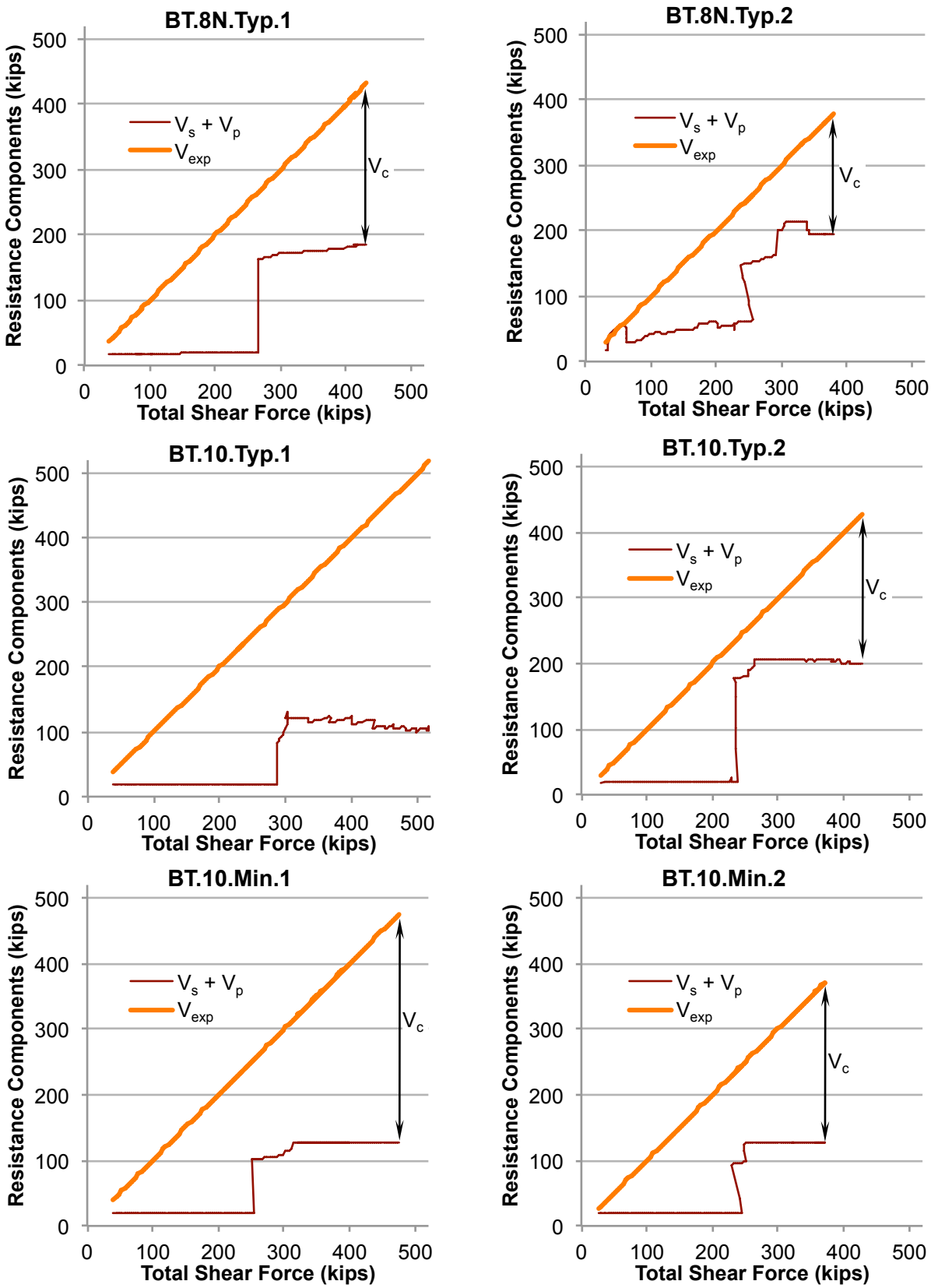

Figure 4-5 (cont.) Forces in the steel and concrete components versus the total shear force in the individual girder tests.

while the angle of the harped strands was 6.60° and 6.47° for the AASHTO Type II and PCBT-45 beams, respectively. The calculated values for V_p appear in Table 4-9. Note that for tests BT.8.Typ.1 and BT.8.Typ.2, the dotted portion of the graph $V_s + V_p$ indicates the unloading and reloading during the tests due to the load actuators beginning to tilt in an unsafe manner, as discussed in Section 3.3.4.

4.2.3.2 Forces in the Concrete

Ideally, V_c would be found through measurements or data collection during an experiment. However, such a task is not practical. Therefore, the concrete contributions for the tests in this study have been found analytically by subtracting the resistance in the steel components from the overall shear force in the girder. This overall shear force in the girder includes the self-weight of the girder as well as the dead load due to the deck. For ease in computation, the shear due to dead load in this analysis is the value at one-half the shear span. Thus, in Figure 4-5, V_c is simply the difference between V_{Exp} and $V_s + V_p$ at any given instant during loading.

4.2.3.3 Discussion of the Steel and Concrete Contributions to Shear Capacity

4.2.3.3.1 General Observations

Looking at Figure 4-5, an overwhelming majority of the tests started with the concrete carrying nearly all of the shear force in girder, followed by a brief moment where much of that force is transferred to the stirrups, as evidenced by the sudden and relatively large jump in the graph of $V_s + V_p$. Following this instantaneous increase, the force in the stirrups typically levels off or only increases a small amount. This behavior is indicative of the concrete withstanding the

Table 4-9. Calculated values for V_p that are combined with V_s in Figure 4-5.

Test ID	V_p
T2.8.Typ.1	17.4
T2.8.Typ.2	17.4
T2.8.Min.1	17.2
T2.8.Min.2	17.2
BT.8.Typ.1	18.1
BT.8.Typ.2	18.1
BT.8N.Typ.1	17.4
BT.8N.Typ.2	17.4
BT.10.Typ.1	17.9
BT.10.Typ.2	17.9
BT.10.Min.1	18.5
BT.10.Min.2	18.5

entire load until reaching the tensile strength of the concrete, and then being able to take on additional load through aggregate interlock after the stirrups begin to yield.

The two aberrations from the above general observation are tests T2.8.Typ.2 and BT.8N.Typ.2. Test T2.8.Typ.2 shows an increase in the force in the stirrups once that force starts to transfer to the stirrups, but that increase is a steady rise instead of the surge seen in the other tests. On the other hand, the stirrups in test BT.8N.Typ.2 appear to slowly increase in force from the beginning of the experiment, followed by two relatively moderate, yet quick, boosts in resistance before leveling off and decreasing near the end of the experiment. The reasons for these anomalies are not entirely clear, but the data for test T2.8.Typ.2 indicate that Stirrup 6 did not yield during the procedure (see Figure B-2 in the Appendix). As for test BT.8N.Typ.2, there may have been a problem with the instrumentation during this operation. The data suggests that early on in the testing, there was more resistance being provided by the stirrups and harped tendons than there was load being applied to the structure. The reason is that the lone working gauge on Stirrup 10 was registering high strains even though there was only a relatively small amount of load present at the time. The amount of strain recorded in this gauge did drop to a more reasonable level as the testing progressed, but perhaps this gauge was not functioning properly beyond a certain point during testing.

Overall, the average ratio of shear resisted by the concrete at the time cracks started to form in the web, $V_{cw\,Exp}$, versus the ultimate failure load, V_{Exp}, is 53%, with a coefficient of variation of 10%. Individual test results are in Table 4-10. While $V_{cw\,Exp}$ is larger in the first test, that is, the end with the shorter shear span, in any given beam, the relative ratio of $V_{cw\,Exp}/V_{Exp}$ had mixed results. In half of the beams, this ratio proved to be larger or the same in the second test compared to the first test. Regardless, $V_{cw\,Exp}$ for all of the tests far exceeded the service loads for shear in the original design beams. Note that the AASHTO Type II beams with a 60-ft span length have a service load of 115 kips, while the service load for the 85-ft PCBT-45 girders is 155 kips.

As an additional comparison, consider the ratio of $V_{cw\,Exp}$ versus $V_{cw\,calc}$ listed in Table 4-11 and shown in Figure 4-7. In this case, $V_{cw\,calc}$ was simply V_{cw} calculated according to the *Simplified*

Table 4-10. Comparison of forces in the resistance components

Test ID	V_{Exp} (kip)	$V_{cw\ Exp}$ (kip)	$V_{c\ Exp}$ (kip)	$V_{s\ Exp}$ (kip)	$\frac{V_{cw\ Exp}}{V_{Exp}}$	$\frac{V_{c\ Exp}}{V_{Exp}}$	$\frac{V_{c\ Exp}}{V_{cw\ Exp}}$	% Increase in V_s after $V_{cw\ Exp}$
T2.8.Typ.1	361	212	196	148	59%	54%	92%	49%
T2.8.Typ.2	294	173	100	177	59%	34%	58%	44%
T2.8.Min.1	382	214	257	108	56%	67%	120%	11%
T2.8.Min.2	308	146	152	139	47%	49%	105%	33%
BT.8.Typ.1	500	214	314	168	43%	63%	147%	31%
BT.8.Typ.2	408	207	175	215	51%	43%	84%	26%
BT.8N.Typ.1	431	243	247	168	56%	57%	102%	15%
BT.8N.Typ.2	382	192	189	177	50%	49%	98%	46%
BT.10.Typ.1	519	270	390	111	52%	75%	144%	59%
BT.10.Typ.2	429	218	227	183	51%	53%	104%	35%
BT.10.Min.1	476	237	350	108	50%	73%	147%	25%
BT.10.Min.2	372	225	246	108	61%	66%	109%	35%
Overall Average					**53%**	**57%**	**109%**	**34%**
Overall Coefficient of Variation					**10%**	**22%**	**25%**	**41%**
Lightweight Average					**53%**	**58%**	**111%**	**35%**
Lightweight Coefficient of Variation					**10%**	**22%**	**25%**	**36%**
Normal weight Average					**53%**	**53%**	**100%**	**30%**
Normal weight Coefficient of Variation					**6%**	**7%**	**2%**	**52%**

Table 4-11. Comparison of $V_{cw\ Exp}$ versus $V_{cw\ calc}$.

Test ID	$V_{cw\ Exp}$ (kip)	$V_{cw\ calc}$ (kip)		$\frac{V_{cw\ Exp}}{V_{cw\ calc}}$	
		with λ_v	no λ_v	with λ_v	no λ_v
T2.8.Typ.1	212	131	137	1.62	1.55
T2.8.Typ.2	173	129	134	1.35	1.29
T2.8.Min.1	214	128	134	1.66	1.59
T2.8.Min.2	146	126	132	1.16	1.11
BT.8.Typ.1	214	143	141	1.50	1.52
BT.8.Typ.2	207	127	136	1.63	1.52
BT.8N.Typ.1	243		157		1.55
BT.8N.Typ.2	192		164		1.18
BT.10.Typ.1	270	150	158	1.80	1.70
BT.10.Typ.2	218	145	154	1.51	1.42
BT.10.Min.1	237	144	153	1.65	1.55
BT.10.Min.2	225	142	152	1.58	1.48
			Average	1.55	1.47
			CoV	0.12	0.11

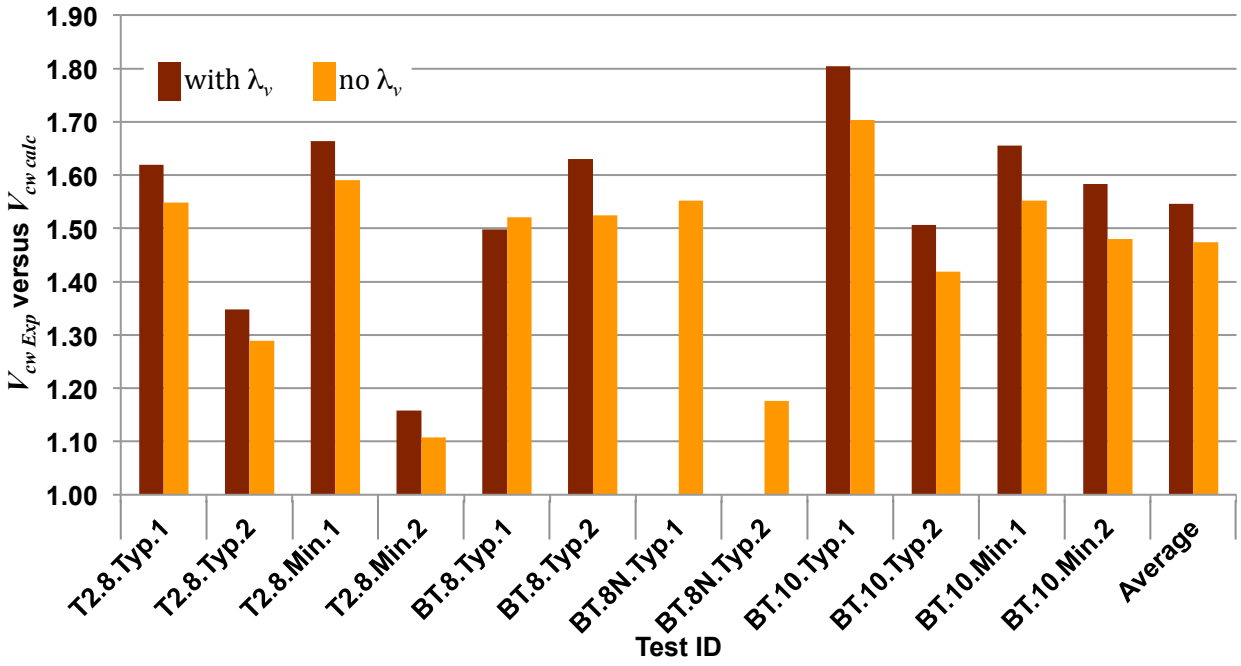

Figure 4-6. Ratio of $V_{cw\ Exp}$ versus $V_{cw\ calc}$.

Procedure. Of course, there are no results including λ_v for the two normal weight tests. Note that the statistics listed at the bottom of Table 4-11 only pertain to the lightweight tests. With that said, the average experimental shear cracking load in the web was about 1.5 times the value of V_{cw}, regardless of whether or not the modification factor for lightweight concrete was included in the calculations. Generally speaking, the first test on each of the beams had a greater ratio of $V_{cw\ Exp}/V_{cw\ calc}$ than the second test with the longer shear span, where the average difference between the ratios of the two tests was about 22%. The exception to this general observation is Beam BT.8.Typ, where test BT.8.Typ.1 had a ratio that was about 8% *lower* than the ratio for test BT.8.Typ.2 when λ_v was included in $V_{cw\ calc}$. If excluding the lightweight modifier, the ratios for the two tests were the same. Nevertheless, the *Simplified Procedure* appears to do a better job of estimating the web-shear cracking load as the shear span increases.

Table 4-10 also details the concrete contribution at the final loading. At ultimate, the concrete provided nearly half if not most of the shear resistance in a majority of the tests. The exceptions are tests T2.8.Typ.2 and BT.8.Typ.2, where the ratio of $V_{c\ Exp}$ versus V_{Exp} is 34% and 43%, respectively. The same two beams experienced the lowest ratios of $V_{c\ Exp}/V_{cw\ Exp}$ of all of the

experiments, with the results being 58% and 84% for T2.8.Typ.2 and BT.8.Typ.2, respectively. Note that the *Simplified Procedure* dictates that V_c shall be limited to V_{cw}, assuming that web-

shear cracking controls. However, the actual resistance in the concrete at failure is typically larger, with an average ratio of shear resistance provided by the concrete at failure versus at the time of first cracking being 1.09 with a coefficient of variation of 0.25. Therefore, $V_{c\,Exp}$ in some cases can be as much as 47% greater than $V_{cw\,Exp}$, although the larger differences in this study only occurred in the shorter shear spans. Of course, Table 4-10 indicates that $V_{c\,Exp}$ is larger in the beam tested with the shorter shear span compared to the second test with the longer shear span on the same beam.

The converse is true for V_s, with the exception of beam BT.10.Min, where both tests in that beam have the same amount of shear force resisted by the stirrups. The average percentage increase in the force in the stirrups after concrete cracking is 34%, but the coefficient of variation for this percentage change is 41%. This result indicates that, despite some stirrups yielding at first cracking, there was still a substantial amount of additional shear resistance remaining in the stirrups. See Table 4-10 for more details. Note that V_s in that table does not include V_p; therefore, $V_c + V_s$ do not sum up to V_{Exp} in this table.

Now consider Table 4-12, which lists the concrete and steel contributions to the overall shear capacity as anticipated by the three different design models in the 2010 AASHTO LRFD Bridge

Table 4-12. Predicted Component Contributions to the Overall Shear Capacity.

Test ID	Appendix B5				General Method				Simplified Method			
	V_c (kip)		V_s (kip)		V_c (kip)		V_s (kip)		V_c (kip)		V_s (kip)	
	λ_v	no λ_v	λ_v	no λ_v	λ_v	no λ_v	λ_v	no λ_v	λ_v	no λ_v	λ_v	no λ_v
T2.8.Typ.1	41	47	159	157	33	38	154	152	131	137	202	202
T2.8.Typ.2	40	46	139	136	33	38	135	133	129	134	177	177
T2.8.Min.1	43	50	128	126	38	44	122	121	128	134	149	149
T2.8.Min.2	42	48	124	119	37	42	116	114	126	132	145	145
BT.8.Typ.1	69	79	219	214	60	67	211	208	143	141	231	232
BT.8.Typ.2	64	74	197	192	64	71	187	184	127	136	213	199
BT.8N.Typ.1		84		158		89		142		157		161
BT.8N.Typ.2		85		139		103		119		164		126
BT.10.Typ.1	71	82	196	191	86	94	174	171	150	158	190	190
BT.10.Typ.2	71	81	180	174	79	87	163	160	145	154	183	180
BT.10.Min.1	89	101	116	112	112	122	94	93	144	153	97	91
BT.10.Min.2	92	103	116	111	113	124	94	92	142	152	94	88

Design Specifications. Clearly, *Appendix B5* and the *General Procedure* suggest that the overwhelming majority of the load-carrying capacity is in the vertical reinforcement instead of the concrete. In most cases, the *Simplified Procedure* also predicts that the largest portion of the shear strength is in the steel. In those cases, however, the concrete contribution is much greater compared to the other two design methods. In fact, the calculations for test BT.8N.Typ.2 and both experiments on beam BT.10.Min predicted that the concrete would resist more of the shear force than the steel reinforcement.

For further analysis Tables 4-13 and 4-14 give the ratio of the experimental results versus the calculated predictions for the concrete and steel contributions, respectively. Figures 4-7 and 4-8 display these ratios in graphical format. Note that the tables and figures provide both cases of including and excluding the modification factor for sand-lightweight concrete. Again, there are no results including λ_v for the two normal weight tests. When the ratio is greater than unity, then the experimental contribution to shear strength is greater than what was expected. The converse is true for ratios that are less than unity.

From Table 4-13, one can clearly see that both *Appendix B5* and the *General Procedure* drastically underpredicted the experimental V_c. While the average ratio for *Appendix B5* assuming no lightweight modifier is 3.29 (with a coefficient of variation of 0.31), the analysis for

Table 4-13. Ratio of $V_{c\,Exp}$ at ultimate versus $V_{c\,calc}$. Given statistics are for lightweight concrete only.

Test ID	$V_{c\,Exp}$ (kip)	Appendix B5		General Method		Simplified Method	
		with λ_v	no λ_v	with λ_v	no λ_v	with λ_v	no λ_v
T2.8.Typ.1	196	4.82	4.13	5.96	5.18	1.49	1.43
T2.8.Typ.2	100	2.52	2.17	3.00	2.64	0.78	0.74
T2.8.Min.1	257	5.93	5.10	6.71	5.87	2.00	1.91
T2.8.Min.2	152	3.66	3.17	4.13	3.66	1.21	1.16
BT.8.Typ.1	314	4.57	3.96	5.27	4.66	2.20	2.23
BT.8.Typ.2	175	2.73	2.37	2.75	2.45	1.38	1.29
BT.8N.Typ.1	247		2.94		2.79		1.58
BT.8N.Typ.2	189		2.23		1.83		1.15
BT.10.Typ.1	390	5.45	4.74	4.55	4.14	2.60	2.46
BT.10.Typ.2	227	3.22	2.81	2.89	2.62	1.57	1.48
BT.10.Min.1	350	3.91	3.45	3.13	2.86	2.44	2.28
BT.10.Min.2	246	2.68	2.39	2.17	1.98	1.73	1.62
Average		**3.95**	**3.29**	**4.05**	**3.39**	**1.74**	**1.61**
CoV		**0.31**	**0.31**	**0.38**	**0.39**	**0.33**	**0.34**

Table 4-14. Ratio of $V_{s\,Exp}$ at ultimate versus $V_{s\,calc}$. Given statistics are for lightweight concrete only.

Test ID	$V_{s\,Exp}$ (kip)	Appendix B5		General Method		Simplified Method	
		with λ_v	no λ_v	with λ_v	no λ_v	with λ_v	no λ_v
T2.8.Typ.1	148	0.93	0.94	0.96	0.97	0.73	0.73
T2.8.Typ.2	177	1.27	1.30	1.31	1.33	1.00	1.00
T2.8.Min.1	108	0.84	0.85	0.88	0.89	0.72	0.72
T2.8.Min.2	139	1.12	1.17	1.20	1.22	0.96	0.96
BT.8.Typ.1	168	0.76	0.78	0.79	0.81	0.73	0.72
BT.8.Typ.2	215	1.09	1.12	1.15	1.17	1.01	1.08
BT.8N.Typ.1	168		1.06		1.18		1.04
BT.8N.Typ.2	177		1.27		1.49		1.40
BT.10.Typ.1	111	0.57	0.58	0.64	0.65	0.59	0.59
BT.10.Typ.2	183	1.02	1.05	1.12	1.14	1.00	1.02
BT.10.Min.1	108	0.93	0.96	1.15	1.16	1.11	1.19
BT.10.Min.2	108	0.93	0.97	1.14	1.16	1.14	1.22
Average		**0.95**	**1.01**	**1.04**	**1.10**	**0.90**	**0.97**
CoV		**0.21**	**0.20**	**0.20**	**0.19**	**0.21**	**0.22**

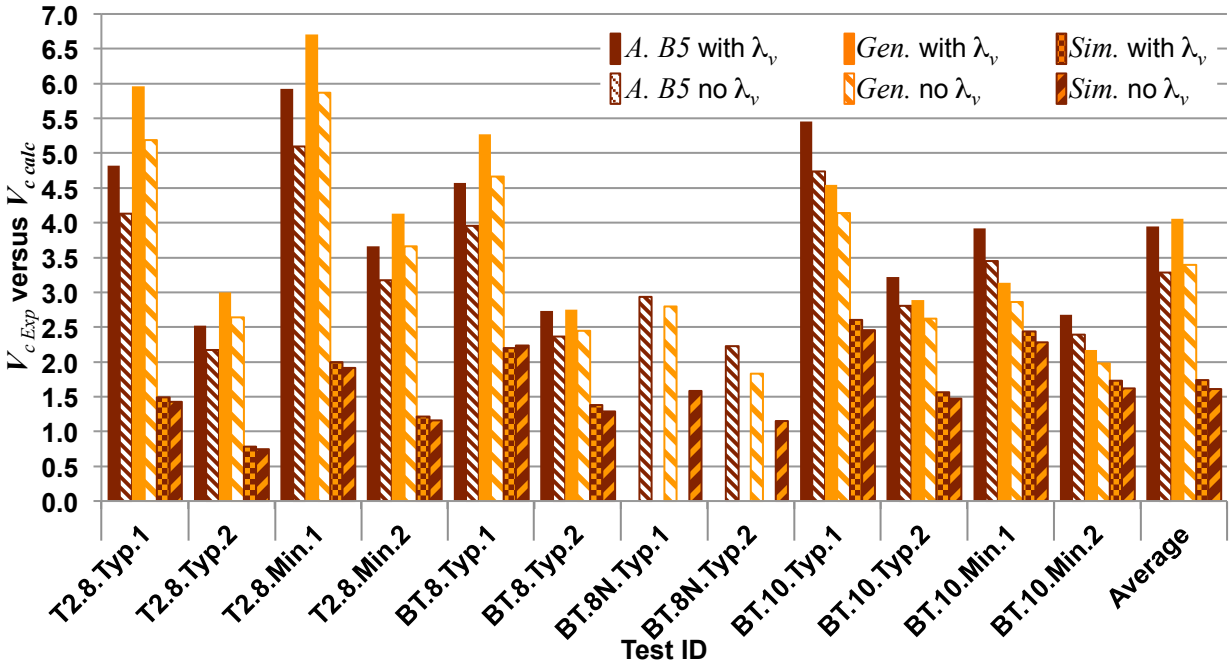

Figure 4-7. Ratio of $V_{c\,Exp}$ at ultimate versus $V_{c\,calc}$.

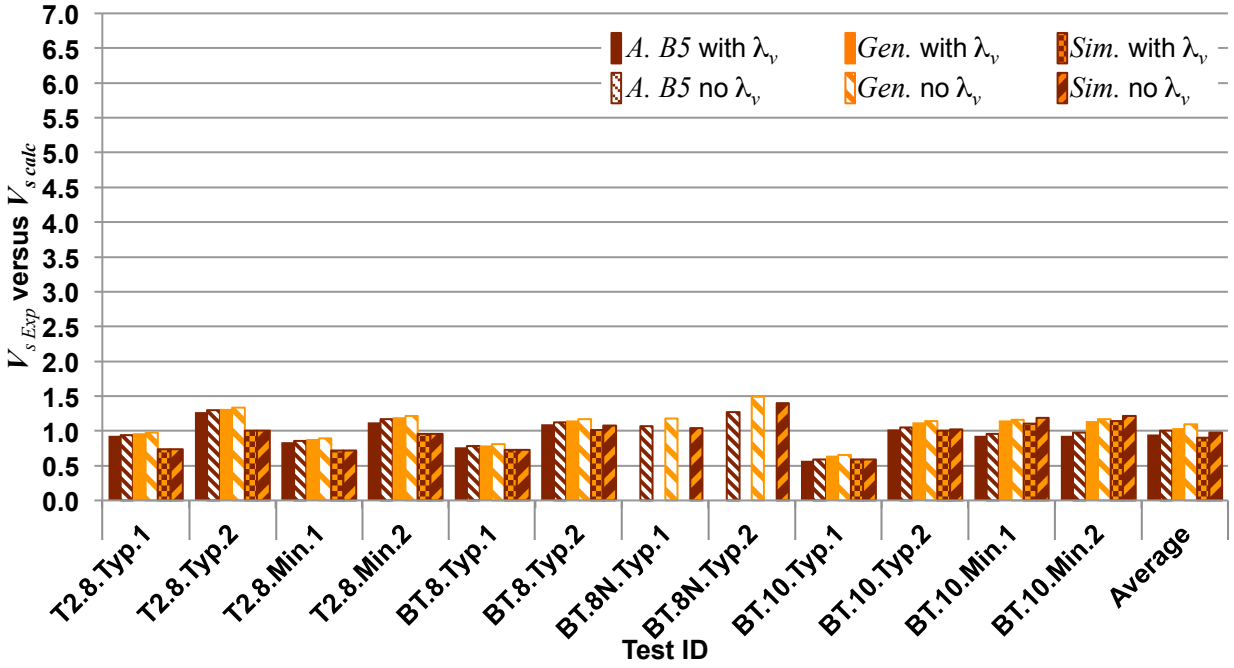

Figure 4-8. Ratio of $V_{s\,Exp}$ at ultimate versus $V_{s\,calc}$.

T2.8.Min.1 predicted a value for V_c that was about 20% of the experimental result. The closest prediction for *Appendix B5* occurs with test T2.8.Typ.2, where the $V_{c\,Exp}/V_{c\,A.B5}$ ratio is 2.17. The average result and accompanying coefficient of variation for the *General Procedure* are slightly larger than that for *Appendix B5*. On the other hand, predictions using the *Simplified Procedure* are much closer to the test results, with the average ratio of $V_{c\,Exp}/V_{c\,Sim}$ being 1.61 and the coefficient of variation equaling 0.34. Again, these results assume that λ_v is ignored in the calculations. However, there is one case where the *Simplified Procedure* overpredicted the concrete contribution to the shear strength; $V_{c\,Exp}$ for test T2.8.Typ.2 was only about 75% of the theoretical value.

In contrast to V_c, the code-calculated values for V_s are much closer to what has been observed during experimentation. The *General Procedure* has the highest average ratio of experimental-to-calculated contribution from the stirrups. That average is 1.10 and the coefficient of variation is 0.19 assuming that the modification factor for sand-lightweight concrete is not used in the calculations. In the case of the *Appendix B5*, the average ratio of $V_{s\,Exp}/V_{s\,A.B5}$ is 1.01 when assuming no λ_v; the coefficient of variation is 0.20. The ratio is actually less than unity if λ_v is

included in the *Appendix B5* analysis. Regardless of whether or not the lightweight modification factor is taken into account, the *Simplified Procedure* overpredicts the strength provided by the vertical reinforcement. The $V_{s\,Exp}/V_{s\,Sim}$ ratio is 0.90 and 0.97 when including and excluding λ_v, respectively. The results for *Appendix B5* and the *Simplified Procedure* are quite a bit different from the conclusions that Malone (*123*) drew from his research. In that study, *Appendix B5* overpredicted the experimental shear strength from the steel by 30%. On the other hand, Malone's calculations using ACI 318-95, which is somewhat similar to AASHTO's *Simplified Procedure*, indicated that the steel contribution would be 37% less than what was actually provided. The ability of any one method to accurately estimate the shear strength provided by the steel reinforcement appears to be connected to that model's success in predicting the angle of inclination of diagonal compression, θ, as will be explained in Sections 4.4.1.3 and 0.

One other interesting note is that the ratio of the experimental-versus-predicted concrete contribution tended to be larger for the shorter of the two span lengths tested in any given beam. For example, the average $V_{c\,Exp}/V_{c\,calc}$ ratio for the *General Procedure* is 4.25 when considering the first test (shorter shear span) on each beam, while the average ratio is only 2.53 for the second test (longer shear span). Thus, the code calculations predict shear strength more accurately as a/d increases, although there is still room for improvement in the models. The converse is true for the steel contribution, where the average $V_{s\,Exp}/V_{s\,Scalc}$ ratio is larger for the longer shear span tested in each beam. However, the difference between the two tests is not nearly as dramatic as is the observation of the concrete strength. In the case of the *General Procedure*, the average ratio is 0.94 for the first test versus 1.25 for the second test.

4.2.3.3.2 Beams with Minimum Reinforcement

As discussed in Section 2.2.7.3, design codes include guidelines for minimum levels of reinforcement in order to control diagonal cracking, ensure that there is some reserve shear strength should the diagonal cracking load be exceeded, provide some degree of ductility against sudden shear failures, and to allow the stirrups to yield prior to the concrete crushing. Assuming the yield stress in the vertical reinforcement is 60 ksi, the minimum reinforcing index is 0.089 ksi for 8 ksi design concrete compressive strength and 0.100 ksi if f'_c is 10 ksi, as discussed in Section 3.1.2.

Section 3.1.2.1 details the design process that led to the decision to use No. 4 double-legged stirrups for shear reinforcement. Unfortunately, with No. 4 stirrups spaced at the maximum 12 in. that had an actual yield strength of 67.3 ksi, the reinforcing index for beam T2.8.Min equates to 0.377 ksi. For beam BT.10.Min, Table 4-15 shows a range of indices. The reason for this range is that the combination of girder length and stirrup spacing were such that an additional stirrup was required near the ends of the beam; otherwise the space between two stirrups near the ends would have been too wide to satisfy the maximum spacing requirement. As it turns out, a sizeable portion of the boundary crack in both tests of this girder crossed the end region with the tighter stirrup spacing. Thus, Table 4-15 includes the higher end of the shear reinforcing index for the tests on BT.10.Min.

From Table 4-15, one can see that the reinforcing index in beam T2.8.Min was about 76% of what was in beam T2.8.Typ. Surprisingly, however, Table 4-10 shows that both tests of beam T2.8.Min outperformed the experiments on beam T2.8.Typ in terms of total shear capacity. Perhaps one reason is that the concrete material properties for all four tests on the Type II girders are assumed to be the same. However, specimens were only taken from one of the two batches used to construct the two beams. The actual material properties for the four tests on the Type II cross-section may have been different. Also, the loading in test T2.8.Typ.1 was different from test T2.8.Min.1 in that the two concentrated loads were 14 ft apart as opposed to 3 ft apart. Furthermore, this wider load spacing may have resulted in undetected damage at the other end of the beam for test T2.8.Typ.2. This damage could affect comparisons with test T2.8.Min.2.

Table 4-15. Shear reinforcement indices for the twelve experiments in this study.

Test ID	ρ_v (%)	f_y (ksi)	$\rho_v f_y$ (ksi)
T2.8.Typ.1	0.74	67.3	0.498
T2.8.Typ.2	0.74	67.3	0.498
T2.8.Min.1	0.56	67.3	0.377
T2.8.Min.2	0.56	67.3	0.377
BT.8.Typ.1	0.63	67.3	0.424
BT.8.Typ.2	0.63	67.3	0.424
BT.8N.Typ.1	0.38	69.8	0.265
BT.8N.Typ.2	0.38	69.8	0.265
BT.10.Typ.1	0.57	67.3	0.384
BT.10.Typ.2	0.57	67.3	0.384
BT.10.Min.1	0.24 - 0.38	67.3	0.160 - 0.256
BT.10.Min.2	0.24 - 0.38	67.3	0.160 - 0.256

Looking back at Table 4-10, the Type II beam with minimum reinforcement showed an increase in the amount of shear carried by the concrete at ultimate compared to when cracks first appeared in the web. On the other hand, that force decreased in the Type II beam with typical reinforcement. Having more vertical reinforcement, the "typical" beam naturally had a greater increase in force in the steel compared to that of the "minimum" beam. Delving deeper, T2.8.Min.1 had essentially the same web-shear cracking strength as its counterpart. However, for a/d that was virtually twice as large, $V_{cw\ Exp}$ was 18% lower in T2.8.Min.2 than in test T2.8.Typ.2. Yet, the shear force resisted by the concrete at the end of test T2.8.Min.2 was more than 50% greater than that of T2.8.Typ.2. Of course, the force resisted by the steel in T2.8.Typ.2 was greater than its companion with minimum reinforcement. That difference was 27%, or about the same difference as in the amount of reinforcement used.

As noted before, the PCBT-45 beams with 10-ksi compressive strength concrete had a larger difference in the amount of vertical reinforcement between the "typical" and "minimum" beams compared to the Type II beams with 8-ksi compressive strength concrete. This difference certainly impacted the results, where the "typical" beams had higher overall shear capacities compared to their "minimum" counterparts. However, test BT.10.Typ.1 was only 9% stronger than BT.10.Min.1, while test BT.10.Typ.2 was 15% stronger than BT.10.Min.2. These results are somewhat surprising considering the fact that the BT.10.Typ tests had a shear reinforcing index that was 50% to 140% larger than that of the minimum tests. Part of the explanation could be that the concrete compression specimens for the minimally reinforced beam had higher strengths than those for beam BT.10.Typ. Furthermore, the concrete tensile strength in test BT.10.Min.2 was greater than test BT.10.Typ.2, although the tensile strengths for tests BT.10.Min.1 and BT.10.Typ.1 were about the same.

Despite having similar concrete tensile strengths, $V_{cw\ Exp}$ was 14% lower in experiment BT.10.Min.1 compared to its "typical" counterpart. On the other hand, the web-cracking load was 3% greater for BT.10.Min.2 relative to BT.10.Typ.2. Both of the "typical" and "minimum" beams with a/d of about 2.0 had the same percentage increase in concrete resistance at ultimate relative to $V_{cw\ Exp}$, which was about 45%. However, similar comparisons with the larger a/d of about 3.0 showed increases that were less than 10%. $V_{c\ Exp}$ for experiment BT.10.Typ.1 was 11%

greater than that of BT.10.Min.1, while $V_{c\,Exp}$ for test BT.10.Typ.2 was about 8% less than the force resisted by the concrete in test BT.10.Min.2.

At the termination of loading, tests BT.10.Typ.1 and BT.10.Min.1 had virtually the same amount of force carried by the vertical reinforcement, although BT.10.Typ.1 experienced a greater increase in that force from the moment of first cracking in the web. Comparing experiments BT.10.Typ.2 versus BT.10.Min.2, the two tests had a 35% increase in V_s at ultimate versus the time of formation of web-shear cracks, although the amount of force in the stirrups for test BT.10.Typ.2 was 70% greater than that of test BT.10.Min.2. One item that is interesting to note is that the two tests on beam BT.10.Min had the same amount of force carried by the transverse reinforcement at ultimate, even though one test had a longer shear span than the other. The reason is due to the location of the boundary cracks that formed in the two tests, where the cracks crossed the same number of stirrups; all of those stirrups had yielded.

For all four of the tests involving minimum reinforcement, the average percentage rise in force in the stirrups after the initial sudden increase at web-shear cracking was 26% with a coefficient of variation of 42%. However, test T2.8.Min.1 only had an 11% increase in force carried by the stirrups. Despite the steel not being able to pick up a larger percentage of force, Table 4-5 shows that the experimental-to-theoretical ratio for this experiment was greater than 2.0 when considering the calculations using *Appendix B5* or the *General Procedure*. Test BT.10.Min.1 had similar results. While not as conservative, tests T2.8.Min.2 and BT.10.Min.2 still far exceeded the predicted strengths with ratios around 1.6. Consistent with the other tests in this investigation, the *Simplified Procedure* produced less conservative estimates for the beams with minimum reinforcement.

Looking back at Table 4-5, the minimally reinforced beams have higher experimental-to-calculated strength ratios relative to the other beams in this investigation having "typical" reinforcement. As a comparison, the average ratio for "minimum" beams ranges from 1.51 to 1.92 amongst the three calculation methods analyzed, while the average for the "typical" beams varies from 1.33 to 1.71. The additional strength beyond V_{cw} and V_s in these tests likely came from aggregate interlock, shear in the uncracked concrete in the compression zone, dowel action in the longitudinal reinforcement, or perhaps even the arching action suggested by Kani (*32*).

Nevertheless, the fact that so many of the stirrups intersecting the boundary cracks in these minimally reinforced girders had yielded at $V_{cw\,Exp}$ gives rise to the concern that there's potential for a beam to fail in a brittle fashion should the load cause cracking in the web. This concern is especially true considering that all of the stirrups crossing the boundary crack in test BT.10.Min.2 had yielded. Unfortunately, making a definitive conclusion regarding the sufficiency of the minimum requirements for shear reinforcement for girders constructed with sand-lightweight concrete is not appropriate at this time because the actual amount of steel supplied in this investigation is substantially larger than what is dictated in the 2010 AASHTO LRFD Bridge Design Specifications.

4.2.3.3.3 Comparison of Lightweight versus Normal Weight Concrete Tests

When comparing the lone normal weight beam with its lightweight counterpart, recall that beams BT.8N.Typ and BT.8.Typ had the same cross section, design concrete strength, flexural reinforcement, and similar *a*/*d* ratios. Furthermore, both beams contained "typical" amounts of vertical reinforcement according to the 2010 AASHTO LRFD Bridge Design Specifications. However, because AASHTO penalizes lightweight concrete, the stirrup spacing in the lightweight girder was 9 in. in the testing region versus 15 in. for the normal weight girder. With these notes in mind, Table 4-10 shows that just prior to the formation of web-shear cracks, the first test with normal weight concrete had about 12% more shear carried by the concrete than the respective lightweight beam. However, for the second set of tests, $V_{cw\,Exp}$ in test BT.8N.Typ.2 was actually 7% lower than BT.8.Typ.2.

This result contradicts the earliest lightweight research coming out of the University of Texas, as discussed in Section 2.3.1.1. The authors for those reports concluded that normal weight concrete had greater diagonal tension strength and the difference between the two types of concrete grew as *a/d* increased. On the other hand, values of $V_{cw\,Exp}$ obtained in this study agree with the subsequent work by Hanson, as reviewed in Section 2.3.1.2. Hanson found that lightweight concrete beams had similar diagonal tension cracking loads as those beams using conventional aggregate and having similar concrete compressive strength. Although the beams in this study had shear stirrups while those from Hanson's work did not, research by Moody et

al. (*37*) and Elzanaty et al. (*36*) showed that vertical reinforcement did not affect the diagonal cracking load.

The results for the current study are in light of the fact that the splitting tensile strength of the lightweight concrete at the time of testing was between 4% and 16% lower than that of the normal weight concrete, according to the hardened concrete properties in Table 4-1. Thus, the conclusion is even when lightweight concrete has a lower tensile splitting strength, this characteristic does not necessarily translate into reduced web-shear cracking strength. Of course, this conclusion is only based on head-to-head comparisons of two sets of girders with composite decks.

By the same token, the concrete contribution to the shear resistance at the failure load, $V_{c\,Exp}$, is 26% greater in the first test of the lightweight girder BT.8.Typ, but is actually 8% lower in the second test when compared to the normal weight beam, BT.8N.Typ. Relative to the load at first web-shear cracking, test BT.8.Typ.1 had a much larger concrete contribution at ultimate compared to its normal weight companion. However, comparison of the second test for each beam shows that the ratio $V_{c\,Exp}/V_{cw\,Exp}$ for BT.8.Typ.2 is smaller than BT.8N.Typ.2. The average ratio of $V_{c\,Exp}/V_{Exp}$ for the two tests on beam BT.8.Typ is 53%, with a coefficient of variation of 19%. For girder BT.8N.Typ, the average ratio is also 53%, but the coefficient of variation is only 7%. Meanwhile, the total load supported during the lightweight beam tests averaged about 11% larger than the experiments on the normal weight girders.

Also note that the shear reinforcing index, $\rho_v f_{yv}$, in the lightweight beam was 60% greater than its normal weight companion, as seen in Table 4-15. With the higher stirrup density, one might think that the total force in the transverse steel at ultimate capacity, $V_{s\,Exp}$, would be greater in the lightweight beam than the normal weight beam. This thinking is correct when comparing tests BT.8.Typ.2 with BT.8N.Typ.2, where $V_{s\,Exp}$ is 22% greater in the lightweight girder. On the other hand, tests BT.8.Typ.1 and BT.8N.Typ.1 actually have the same amount of shear force being resisted by the stirrups at the failure load. After the first web-shear cracks had formed, the percentage increase in the amount of shear force resisted by the vertical reinforcement in test BT.8.Typ.1 is about twice the increase seen in BT.8N.Typ.1, 31% versus 15%. The second

experiments on each beam have the opposite result, where test BT.8.Typ.2 has about half the percentage increase in V_s as does test BT.8N.Typ.2, 26% compared to 46%.

The above information contradicts the findings by Hamadi and Regan in their work on reinforced concrete, discussed in Section 2.3.2.1. The authors had determined that both V_c and V_s were lower in the lightweight concrete beams compared to the normal weight beams. Keep in mind that the reinforcing index was greater in the lightweight girders from the current study. So, the fact that the lightweight beams had a larger force in the steel can be expected. Nevertheless, V_c for the lightweight sections was about the same as or greater than the normal weight members.

One other interesting item to note is that Watanabe et al. concluded that the shear force carried by the lightweight concrete decreased after cracking had occurred, and that the stirrups compensated the loss in concrete resistance. On the other hand, the researchers observed that the normal weight concrete did not decrease its load carrying capability after cracking. However, the graphs in Figure 4-5 generally disagree with Watanabe et al. regarding lightweight concrete. Indeed, there are some cases where the value of $V_{c\,Exp}$ decreases as the loading increases beyond $V_{cw\,Exp}$, but such is also the case for the normal weight test BT.8N.Typ.2. The reason could simply be that the cracks in the concrete progress after the initial web-shear cracking and the vertical reinforcement picks up the additional load. Over the course of the entire test though, V_c tends to increase as the testing continues to the ultimate load.

Making any firm statements based on two sets of data containing only two tests in each set is not realistic. However, based on the information presented above, the conclusion is that there are no distinct structural differences between lightweight and normal weight concrete when it comes to shear strength of prestressed concrete girders.

4.3 Lightweight Modification Factor, λ_v

As discussed in Section 2.3.4, design codes typically penalize lightweight concrete for its reduced splitting tensile strength by multiplying $\sqrt{f'_c}$ by a lightweight modification factor, defined in this project as λ_v. In comparison, beams BT.8.Typ and BT.8N.Typ in Table 4-5 have

fairly similar ratios of experimental versus calculated shear capacities using *Appendix B5* (1.63 versus 1.66 when $a/d \approx 2.0$ and 1.52 versus 1.58 when $a/d \approx 3.0$, for the lightweight and normal weight beams, respectively). Both the *General Procedure* and the *Simplified Procedure* have similar comparisons for $a/d \approx 2.0$, although the disparity between the two concrete densities is somewhat greater when $a/d \approx 3.0$. Thus, if the same level of safety is desired in lightweight girders as seen in normal weight beams, then the λ_v factors used in lightweight design may be necessary. Again, however, this conclusion is based on a comparison of two pairs of tests.

On the other hand, Table 4-5 also has three columns, designated $\frac{V_{n\,A.B5}}{\text{No }\lambda_v}$, $\frac{V_{n\,Gen}}{\text{No }\lambda_v}$, and $\frac{V_{n\,Sim}}{\text{No }\lambda_v}$ for the respective shear design methods *Appendix B5*, *General Procedure*, and *Simplified Procedure*. The calculated values that appear in these columns disregard the modifier for sand-lightweight concrete that is required by Article 5.8.2.2 of the 2010 AASHTO LRFD Bridge Design Specifications. In other words, the coefficient in front of the term $\sqrt{f'_c}$ has been set equal to 1.0 instead of the standard value of 0.85 for sand-lightweight concrete for all instances where $\sqrt{f'_c}$ appears in Articles 5.8.2 and 5.8.3. Similar columns without the λ_v factor also appear in Table 4-7 for tests on large-scale prestressed lightweight concrete that have been performed in the past.

For ease in comparison, the theoretical shear strengths for all of the large-scale, prestressed lightweight concrete tests in Tables 4-5 and 4-7 have been reorganized into Table 4-16, showing the calculated shear strengths including and excluding the modifier for lightweight concrete. One can see that the difference between the calculations for the nominal shear capacity using the modifier for sand-lightweight concrete and those calculations using no modifier is relatively small. If using *Appendix B5*, the average difference is 4%, while the average difference when using the *General Procedure* and the *Simplified Procedure* is about 3% and 1%, respectively. What is interesting is that the two experiments within this data set that did not have any shear reinforcement, tests PC6N and PC10N by Malone, are the two largest outliers in terms of the difference between retaining λ_v versus not doing so. If one were to remove these two outliers, then the average percent difference and corresponding standard deviation would be 3.0% and 1.2% for *Appendix B5*, respectively. The results for the *General Procedure* would be 2.2% and 1.1%, respectively. There would be no change for the *Simplified Procedure* because tests PC6N

Table 4-16. Comparison between using the standard sand-lightweight modification factor and disregarding that factor.

Author	Test ID	Appendix B5			General Procedure			Simplified Procedure		
		$V_{n\,A.B5}$ (kip)	$V_{n\,A.B5}$ No λ_v (kip)	% Diff.	$V_{n.Gen}$ (kip)	$V_{n.Gen}$ No λ_v (kip)	% Diff.	$V_{n.Sim}$ (kip)	$V_{n.Sim}$ No λ_v (kip)	% Diff.
Current Study	T2.8.Typ.1	217	222	2.0	204	207	1.7	333	339	1.8
	T2.8.Typ.2	196	199	1.7	185	188	1.3	305	311	1.9
	T2.8.Min.1	189	194	2.6	178	182	2.3	278	284	2.1
	T2.8.Min.2	182	186	1.9	170	173	1.6	271	277	2.1
	BT.8.Typ.1	306	312	1.7	289	293	1.5	373	373	-0.2
	BT.8.Typ.2	269	284	5.7	269	273	1.7	339	335	-1.4
	BT.10.Typ.1	285	291	1.9	277	283	1.9	339	348	2.6
	BT.10.Typ.2	268	273	1.9	260	265	1.9	328	334	1.9
	BT.10.Min.1	224	232	3.5	224	233	4.0	241	244	1.3
	BT.10.Min.2	226	232	2.6	226	235	4.0	236	240	1.6
Malone	PC6N	50	59	17.6	41	47	15.5			
Malone	PC6S	72	75	4.2	72	75	3.7	80	83	2.7
Malone	PC10N	59	65	10.4	47	54	15.4			
Malone	PC10S	77	81	5.5	79	83	4.6	90	93	3.2
Kahn et al.	G1A-East	240	248	3.1	153	155	1.0	344	335	-2.8
Kahn et al.	G1A-Center	135	139	3.2	131	134	2.5	179	186	3.8
Kahn et al.	G1B-East	432	440	1.8	263	266	1.2	592	574	-2.9
Kahn et al.	G1B-Center	125	130	3.5	121	124	2.5	181	187	3.8
Kahn et al.	G1C-East	238	245	3.0	154	156	1.0	349	338	-3.1
Kahn et al.	G2A-Center	136	141	3.3	133	136	2.5	182	188	3.5
Kahn et al.	G2B-Center	127	132	3.7	122	125	2.6	183	191	3.9
Dymond et al.	web-shear	514	527	2.5	421	425	0.9	690	670	-2.9
			Average	**4.0**			**3.4**			**1.2**
			Standard deviation	**3.6**			**4.0**			**2.5**

and PC10N were not included in the original analysis because those beams did not meet the minimum reinforcement requirement.

One other interesting observation regarding Table 4-16 is that 30% of the beams being analyzed using the *Simplified Procedure* actually had a *greater* predicted shear capacity when using the sand-lightweight concrete modifier versus not doing so. The reason for the increase lies behind Eq. 5.8.3.4.3-4 of the 2010 AASHTO LRFD Bridge Design Specifications, or Eq. (39) in Section 2.2.4.4 reproduced below:

$$\cot\theta = 1.0 + 3\left(\frac{f_{pc}}{\sqrt{f'_c}}\right) \leq 1.8 \qquad (39)$$

Note that Eq. (39) applies if and only if $V_{ci} \geq V_{cw}$, which is the case for all of the tests in the current study as well as the twelve large-scale tests from previous research. However, as discussed in Section 2.3.4.2, Article 5.8.2.2 of the code dictates that the term $\sqrt{f'_c}$ in that equation shall be substituted by $4.7f_{ct} \leq \sqrt{f'_c}$ when the splitting tensile strength is specified or $0.85\sqrt{f'_c}$ when the splitting tensile strength of sand-lightweight concrete is not specified. Because the calculations in this analysis assumed that the splitting tensile strength was not specified, the denominator in Eq. (39) becomes $0.85\sqrt{f'_c}$, thus making the value for cotθ larger for sand-lightweight concrete compared to normal weight concrete. The cotθ term figures into AASHTO's Eq. 5.8.3.3-4, or Eq. 37 from Section 2.2.4.4:

$$V_s = \frac{A_v f_{yv} d_v (\cot\theta + \cot\alpha)\sin\alpha}{s} \qquad (37)$$

Because cotθ is larger when the lightweight concrete modifier is included, the resulting V_s will be larger as well. Although V_c decreases when including λ_v, V_s is large relative to V_c for the subset of tests in question. Therefore, the increase in V_s overcompensates for the decrease in the calculated value of V_c, resulting in a larger theoretical shear capacity when the λ_v "penalty" for lightweight concrete is included.

For the eight lightweight tests where $V_{n\,Sim}$ is less than $V_{n\,Sim}$ No λ_v in the current study, cotθ would have been larger in the latter; however, cotθ is limited in both calculations by the maximum value of 1.8 in Eq. (39). Thus, V_s remains the same while V_c is lower for $V_{n\,Sim}$, resulting in a lower calculated shear capacity. The same is true for past experiments G1A-Center, G1B-Center, and G2A-Center by Kahn et al. For tests PC6S and PC10S by Malone, cotθ does not exceed 1.8, and is larger for the $V_{n\,Sim}$ calculation that includes the λ_v factor compared to excluding λ_v. However, V_c in these cases is larger than V_s, so the relative increase in V_s is not able to compensate for the relative decrease in V_c, resulting in $V_{n\,Sim}$ being lower when the modifier for sand-lightweight concrete is included versus excluded. The same is true

for test G2B-Center by Kahn et al., with the exception that cotθ is limited to 1.8 when including the λ_v factor versus 1.79 when the lightweight modifier is not considered.

As mentioned in Section 2.3.3.5, Dymond et al. also found that the modification for sand-lightweight concrete had a relatively minor impact on the calculated overall shear strength. Coupling the results discussed above with the conclusion at the end of Section 4.2.3.3.3 , one can conclude that modifying the shear strength of sand-lightweight concrete girders is unnecessary. This conclusion is regardless of whether or not V_n is less than or greater than V_n No λ_v, or if V_c is large relative to V_s. Also, this conclusion is in line with findings regarding the material properties characterization analysis in *NCHRP Report 733* (NB: a final copy of the report was not yet available at the time of publication of this work). In that study, the authors concluded that the tensile strength and modulus of rupture of lightweight concrete could be calculated in the same manner as normal weight concrete. Furthermore, the inherent amount of conservatism in the AASHTO LRFD calculations should give further assurance in abandoning the modifier for sand-lightweight concrete.

4.4 θ and β

4.4.1 Angle of Inclination of Diagonal Compressive Stresses, θ

As implied in Section 4.3 above, the *Simplified Procedure* indirectly calculates the angle of inclination of diagonal compressive stresses by determining the value of cotθ in Eq. (39). Likewise, the *Appendix B5* and *General Procedure* have methods for estimating θ. According to the 2010 AASHTO LRFD Bridge Design Specifications, this angle can be calculated using Tables B5.2-1 or B5.2-2 in *Appendix B5* or Eq. 5.8.3.4.2-3 in the *General Procedure*, as discussed in Sections 2.2.5.2 and 2.2.5.3, respectively. These theoretical angles serve as a comparison to the angle of rotation to the principal stresses obtained from strain rosettes discussed in Sections Sections 3.2.1 and 3.2.2.

4.4.1.1 Calculation of the Angle of Rotation of Principal Stresses

The experiments in this investigation included collecting strain and displacement data using instruments arranged in a -45°, 0°, 45° pattern with the intersection of the gauges located

longitudinally at the critical section and then $0.5d_v$ vertically. The centers of these rectangular rosettes generally were above the critical crack in each test. However, longitudinally, the rosettes were in the vicinity of the major cracking, and cracking that did occur at the location of the rosette had more or less the same angle as the critical crack.

For the strain gauge rosettes, that data was used directly in calculating the angle of rotation to the principal strains, and hence, the principal stresses. For the LVDTs, the displacement data first needed to be converted into strain. To do so, the original gauge length was assumed to be the distance between the face of the wooden base holding the extension tubing for the LVDT and the face of the wooden base supporting the target that the LVDT was touching. While this measurement may not be the correct assumption, adding an additional inch in both directions to measure the distance from center-to-center of the wooden bases did not affect the overall angle of rotation to the principal stresses. The gauge length was then divided into the displacement measured by the LVDT to obtain the average engineering strain over the length of the LVDT and extension tubing. This process was repeated for the other two LVDTs in the rosette.

With the three strains from the rosette measurements, one can begin the process of calculating the angle of rotation to the principal stresses using the relationship:

$$M = l^2\varepsilon_{xx} + m^2\varepsilon_{yy} + n^2\varepsilon_{zz} + 2lm\varepsilon_{xy} + 2ln\varepsilon_{xz} + 2mn\varepsilon_{yz} \quad \textbf{(134)}$$

where M, also known as the total Green strain, is the measure of the strain of a line in a given body. The direction cosines of that line are l, m, and n, while ε_{ab} is the strain in the ab–plane. One can set up a system of equations using Eq. (134) such that

$$\begin{aligned}
M_0 &= \varepsilon_0 = (l_0)^2\varepsilon_{xx} + (m_0)^2\varepsilon_{yy} + (n_0)^2\varepsilon_{zz} + 2l_0m_0\varepsilon_{xy} + 2l_0n_0\varepsilon_{xz} + 2m_0n_0\varepsilon_{yz} \\
M_{45} &= \varepsilon_{45} = (l_{45})^2\varepsilon_{xx} + (m_{45})^2\varepsilon_{yy} + (n_{45})^2\varepsilon_{zz} + 2l_{45}m_{45}\varepsilon_{xy} + 2l_{45}n_{45}\varepsilon_{xz} + 2m_{45}n_{45}\varepsilon_{yz} \quad \textbf{(135)} \\
M_{-45} &= \varepsilon_{-45} = (l_{-45})^2\varepsilon_{xx} + (m_{-45})^2\varepsilon_{yy} + (n_{-45})^2\varepsilon_{zz} + 2l_{-45}m_{-45}\varepsilon_{xy} + 2l_{-45}n_{-45}\varepsilon_{xz} + 2m_{-45}n_{-45}\varepsilon_{yz}
\end{aligned}$$

where the subscripts 0 and ±45 represent the three axes of the rosette. Note that the face of the concrete is assumed to be a free surface; therefore, $\varepsilon_{zz} = \varepsilon_{xz} = \varepsilon_{yz} = 0$. Also, the direction cosines

of the LVDT that is oriented at 0° are (1, 0, 0) while the direction cosines for the LVDTs oriented at $\pm 45^{\circ}$ are $\left(\frac{\sqrt{2}}{2}, \pm\frac{\sqrt{2}}{2}, 0\right)$, respectively. Therefore, Eq. (135) becomes

$$\begin{aligned} \varepsilon_0 &= \varepsilon_{xx} \\ \varepsilon_{45} &= \frac{1}{2}\varepsilon_{xx} + \frac{1}{2}\varepsilon_{yy} + \varepsilon_{xy} \\ \varepsilon_{-45} &= \frac{1}{2}\varepsilon_{xx} + \frac{1}{2}\varepsilon_{yy} - \varepsilon_{xy} \end{aligned} \qquad \text{(136)}$$

Solving the above system of equations for the strain components ε_{xx}, ε_{yy}, and ε_{xy} yields

$$\begin{aligned} \varepsilon_{xx} &= \varepsilon_0 \\ \varepsilon_{yy} &= -\varepsilon_0 + \varepsilon_{45} + \varepsilon_{-45} \\ \varepsilon_{xy} &= \frac{1}{2}\varepsilon_{45} - \frac{1}{2}\varepsilon_{-45} \end{aligned} \qquad \text{(137)}$$

Before going further, the strain in the *xx*-direction needs to account for the strain at the location of the center of the rosette due to prestressing and dead loads that were present in the girder prior to the rosette installation. To do so, consider a form of the classic equation for elastic flexural stresses in uncracked prestressed concrete beams:

$$\sigma = -\frac{P_e}{A_g} + \frac{P_e e y}{I_g} - \frac{M_{self} y}{I_g} - \frac{M_{deck} y}{I_g} \qquad \text{(138)}$$

where

P_e = effective prestressing force, or $A_{ps} f_{pe}$

e = eccentricity of the centroid of the strands from the centroid of the girder, taken as positive when the strand centroid is below the girder centroid

y = distance from the girder centroid to the point in question along the height of the beam, taken as positive when that point is above the girder centroid; in this case, the point in question is located $\frac{1}{2} d_v$ below the centroid of the compression force near the top of the composite section

I_g = moment of inertia of the girder by itself, neglecting the reinforcement

M_{self} = dead load moment at the point in question along the longitudinal axis of the girder due to the self weight of the beam

M_{deck} = dead load moment at the point in question along the longitudinal axis of the girder due to the weight of the deck on the non-composite girder

where the values for f_{pe} in this exercise are the same values given in Table 4-4. The stress calculated using Eq. (138) is divided by the modulus of elasticity of the concrete to get the longitudinal strain due to prestressing and dead loads at the location of the center of the rosette, where tensile strains are taken as positive. That strain is then added to ε_{xx} calculated in Eq. (137). Note that this procedure assumes that any creep or shrinkage strains that have occurred from the time of detensioning have a negligible effect on the angle of rotation to the principle stresses.

Having determined the strain components, one can use Mohr's circle to find the angle of rotation to the principal strains, calculated as

$$\theta_{prin} = \frac{1}{2}\operatorname{atan}\left(\frac{\varepsilon_{xy}}{\frac{\varepsilon_{xx} - \varepsilon_{yy}}{2}}\right) \qquad \textbf{(139)}$$

where θ_{prin} is in radians but can be converted into degrees. As mentioned in Section 3.2.2, the sensitivity of the LVDTs was ±0.002 in. However, when used as a group in the rosette, the errors in the LVDT measurements propagate along with the errors in the angle of the arms of the rosette and the original length of each arm, which have been assumed to be 1° and $^{1}/_{32}$ of an inch, respectively. These errors are used to determine the overall error in the angle of rotation of the principal stresses, e_θ, using the equation

$$e_\theta = \sqrt{\sum_{\alpha=A,B,\ldots}\left[\frac{\partial}{\partial\alpha} f(A,B,\ldots)\right]^2 e_\alpha{}^2} \qquad \textbf{(140)}$$

where $f(A,B,\ldots)$ in this case is the function for θ_{prin} in Eq. (139), where A, B, … are the variables in that equation and e_α are the uncertainties in those variables. The resulting error in the calculated angle of rotation of the principal stresses is about ±2°, although in some cases, that error has been determined to be about ±5° when the loading reached $V_{cw\,Exp}$.

4.4.1.2 Results for Angle of Rotation of Principal Stresses, θ_{prin}

The graphs in Figure 4-9 show this calculated value of the angle rotation as the loading progressed during each test. θ_{SG} indicates the calculated principal strain (or stress) orientation using data collected from strain gauges, which were only placed on the AASHTO Type II beams, as discussed in Section 3.2.1. Likewise, θ_{LVDT} indicates the data from the LVDT rosette has been used to calculate the angle. As mentioned in Section 3.2.2, two LVDT rosettes were mounted on the PCBT girders. Thus, the labels θ_E and θ_W represent the calculated angle to the principal strains using LVDT rosettes on the East and West face of the web, respectively. In many cases, the graphs for θ_{LVDT} terminate prior to test completion due to one of the LVDTs extending beyond its operating range and going off-scale, rendering θ_{LVDT} indeterminable beyond that point. Also note that θ_{LVDT} does not appear on the graph for T2.8.Typ.2 because one of the instruments in the LVDT rosette was not working properly during testing. Lastly, the dotted portions of the graphs for both tests on beam BT.8.Typ indicate the portion of the testing where the beams were unloaded and then reloaded, as mentioned in Section 3.3.4.

For the most part, the angle of rotation started out just above 0° and then curved upward with a slightly decreasing slope up to the point of cracking in the web. At V_{cw}, the angle tended to have a substantial drop in conjunction with the large increase in the force in the reinforcement that has been superimposed on the graphs in Figure 4-9. Post cracking, the change in this angle tended to either level off or be relatively small. However, this last observation certainly was not the case for all of the experiments.

Using the results from Figure 4-9, the angle of rotation to the principal stresses, θ_{prin}, just prior to cracking in the web and immediately after that cracking, as well as the last known angle are given in Table 4-17. The last known angle is the last θ_{prin} that could be calculated prior to one of

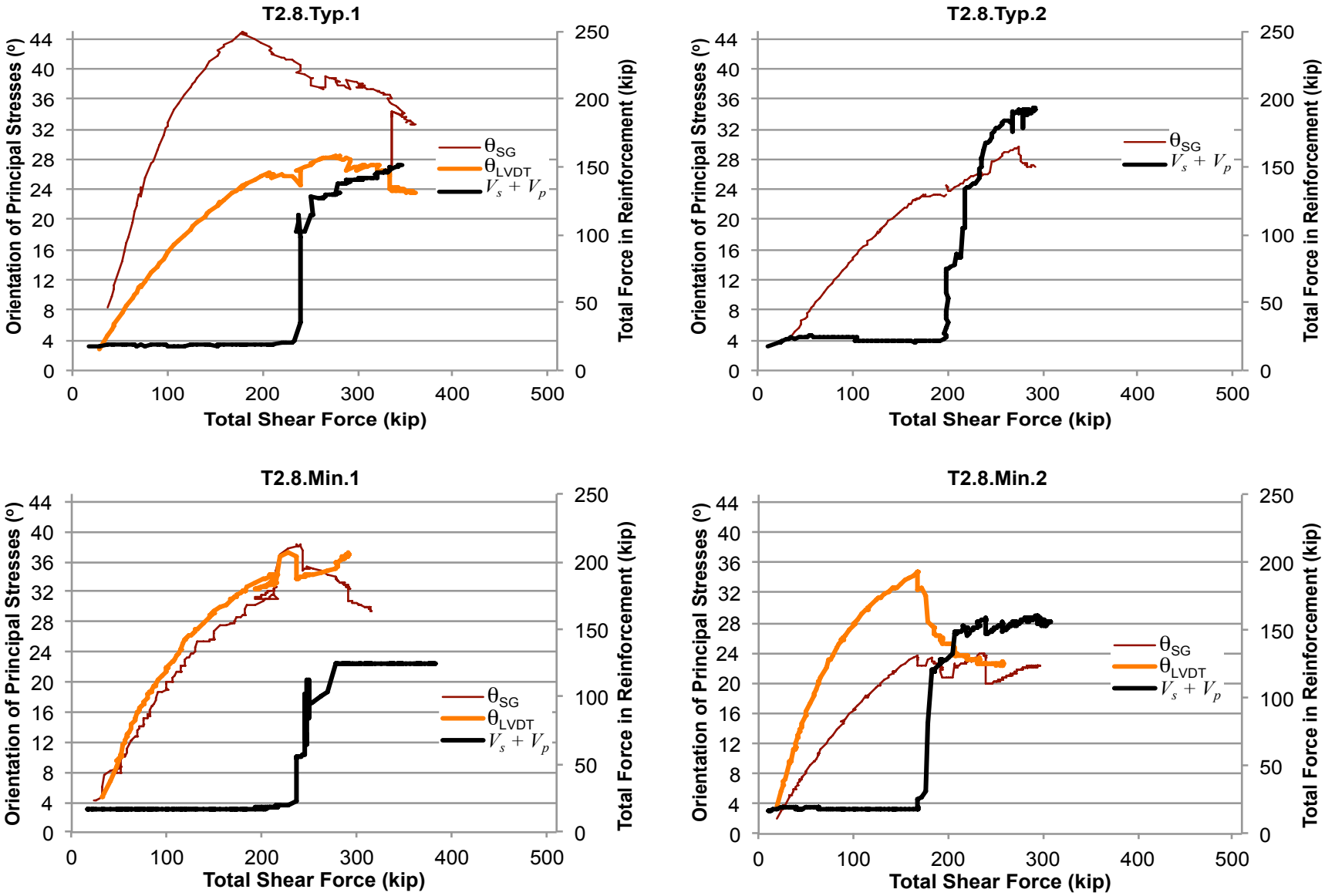

Figure 4-9. Orientation of the principal stresses (or strains) versus the total shear force in the beam. Note that the figure also shows the force resisted by the steel reinforcement as well.

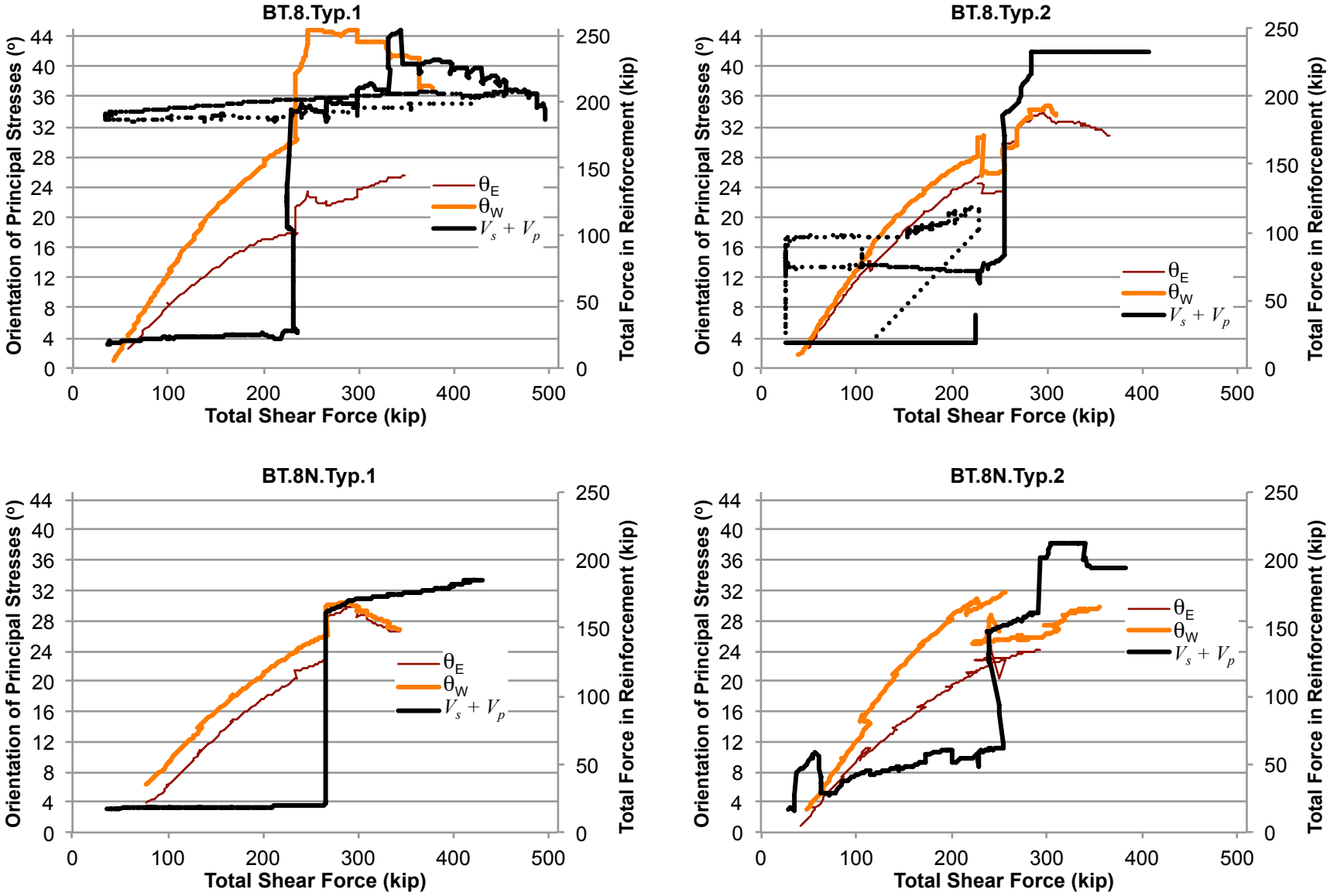

Figure 4-9 (cont.). Orientation of the principal stresses (or strains) versus the total shear force in the beam. Note that the figure also shows the force resisted by the steel reinforcement as well.

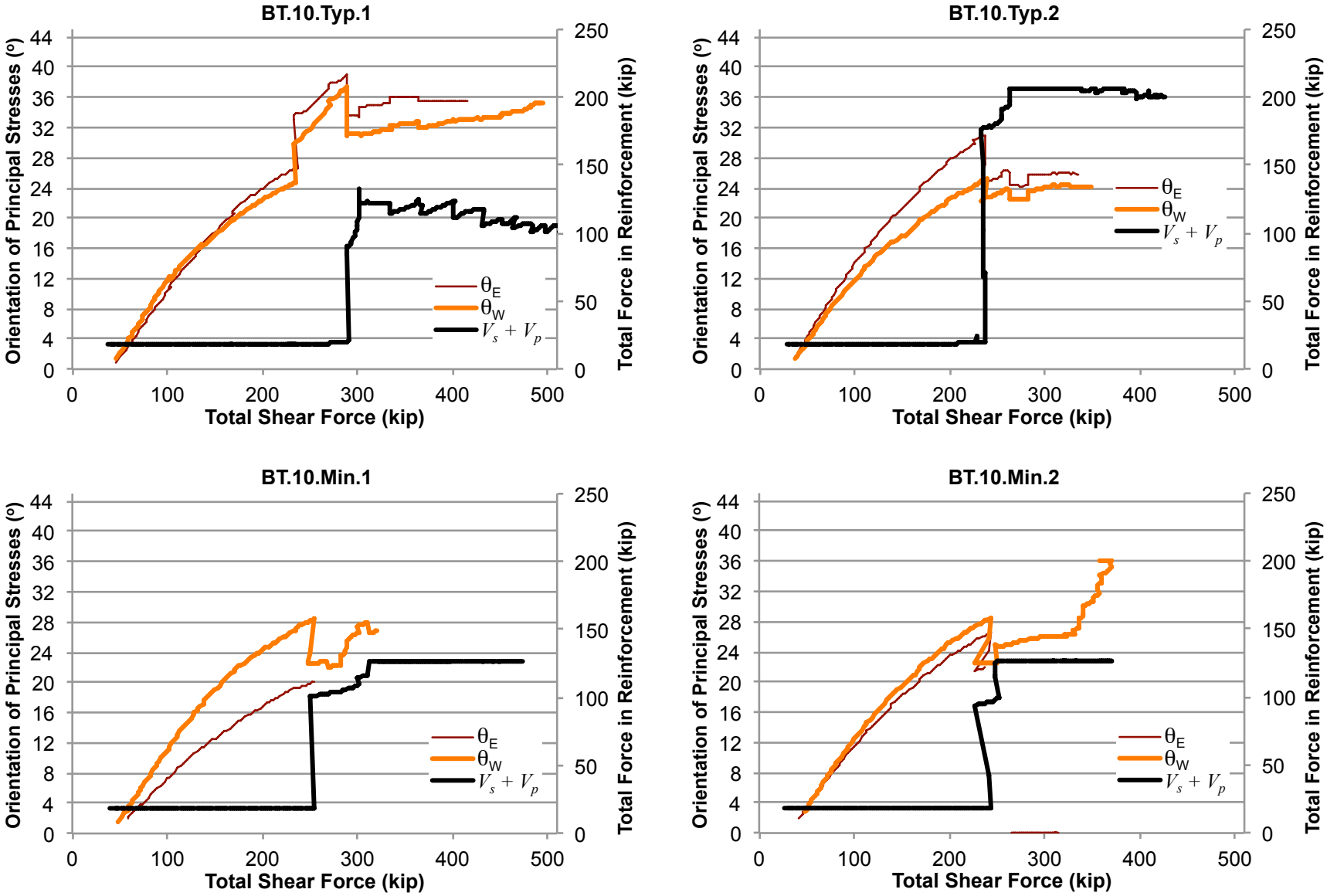

Figure 4-9 (cont.). Orientation of the principal stresses (or strains) versus the total shear force in the beam. Note that the figure also shows the force resisted by the steel reinforcement as well.

the instruments within the rosette going off-scale or at test termination. The "Average" column in Table 4-17 is simply the average between the values given for θ_E and θ_W. For the tests on the AASHTO Type II beams, results for θ_{SG} are listed under the column labeled "θ_E." However, these values are not included in the column labeled "Average" because there was some uncertainty as to whether or not the strain gauges were providing reliable data, as discussed in Section 3.2.1. For experiment BT.10.Min.1, no values are listed for the "post-V_{cw}" and "last" sub-columns of column θ_E because one of the LVDTs in that rosette went off-scale about the time of web-shear cracking during the experiment.

Note that the "post-V_{cw}" and "last" for θ_{prin} described above are provided more for informational purposes. On the other hand, the analysis given below will focus on θ_{prin} "pre-V_{cw}." The reason is that the angle of rotation to the principal strains is calculated using Eqs. (134) through (137), which are based on strains. The relationship between strain and stress is based on the elastic modulus. Certainly, concrete is no longer elastic post cracking. Therefore, $\theta_{prin\ pre\text{-}V_{cw}}$ is the more valid calculation.

Interestingly, analysis of the average $\theta_{prin\ pre\text{-}V_{cw}}$ for beam BT.8.Typ and its normal weight companion indicates that the lightweight beam had a slightly lower angle of rotation to the principal stresses given that the tests were conducted at similar shear spans. However, given the

Table 4-17. Angle of rotation to the principal stresses, calculated using data from strain rosettes. (*) denotes results determined from strain gauge rosettes, but are not included in the averages.

Test ID	θ_{prin} (°)								
	θ_E			θ_W			Average		
	pre-V_{cw}	post-V_{cw}	last	pre-V_{cw}	post-V_{cw}	last	pre-V_{cw}	post-V_{cw}	last
T2.8.Typ.1	41*	40*	33*	25	27	24	25	27	24
T2.8.Typ.2	23*	24*	27*						
T2.8.Min.1	35*	38*	31*	37	34	37	37	34	37
T2.8.Min.2	23*	22*	22*	35	32	23	35	32	23
BT.8.Typ.1	18	18	26	30	30	37	24	24	32
BT.8.Typ.2	24	23	31	30	26	34	27	25	33
BT.8N.Typ.1	23	29	26	26	30	27	25	30	27
BT.8N.Typ.2	23	25	24	32	29	30	28	27	27
BT.10.Typ.1	39	34	35	37	31	35	38	33	35
BT.10.Typ.2	31	24	26	25	22	24	28	23	25
BT.10.Min.1	20			29	23	27	25	23	27
BT.10.Min.2	27	22	22	29	22	36	28	22	29
Average	**27**	**27**	**28**	**30**	**28**	**30**	**29**	**27**	**29**

±2° uncertainty in the calculations for the angle, any differences are unclear for the pre-V_{cw} scenario. Thus, this result agrees with the findings in in Section 2.3.2.5 , where Walraven and Al-Zubi concluded that there was no difference in the rotation to the principal stresses for the two different types of concrete. But again, the comparison in this investigation is only based on two sets of experiments.

4.4.1.3 Comparison of θ_{prin} with θ_{calc}

The average values for all of the tests given at the bottom of Table 4-17 serve no quantitative purpose other than as a tool of comparison with the averages given in Table 4-18, which presents the calculated results for θ using the tables and equations provided in the 2010 AASHTO LRFD Bridge Design Specifications. Table 4-18 shows the calculated results both including and excluding the modification factor for sand-lightweight concrete. Note that the averages listed at the bottom of Table 4-18 do not include the angles for the normal weight beams for the purposes of assessing the effect of λ_v on θ. Regardless of whether or not λ_v is taken into account, θ_{calc} using the *Simplified Procedure* is consistently lower than the angle of diagonal compression stresses calculated using the other two shear design methods. This observation conforms with the results in Table 4-5, where smaller predicted angle of diagonal compression results in a larger contribution from the shear reinforcement, which in turn leads to a higher predicted ultimate shear strength.

Table 4-18. The angle of diagonal compressive stresses calculated using the three AASHTO shear design methods.

Test ID	θ_{calc} with λ_v (°)			θ_{calc} no λ_v (°)		
	A. B5	*Gen*	*Sim*	*A. B5*	*Gen*	*Sim*
T2.8.Typ.1	35.1	37.0	29.1	36.6	37.3	29.1
T2.8.Typ.2	35.3	36.1	29.1	35.9	35.9	29.1
T2.8.Min.1	33.8	35.1	29.1	34.2	35.4	29.1
T2.8.Min.2	33.6	34.8	29.1	34.3	35.3	29.1
BT.8.Typ.1	30.3	34.8	29.1	30.9	35.2	30.0
BT.8.Typ.2	32.2	33.5	30.2	32.8	34.0	31.8
BT.8N.Typ.1				29.8	32.4	29.3
BT.8N.Typ.2				26.9	30.7	29.1
BT.10.Typ.1	28.3	31.2	29.1	28.9	31.8	29.1
BT.10.Typ.2	30.3	31.9	29.1	29.5	32.4	29.1
BT.10.Min.1	25.1	30.0	29.1	25.9	30.5	29.1
BT.10.Min.2	25.3	30.1	29.1	24.9	30.6	29.1
Average	**30.9**	**33.5**	**29.2**	**31.4**	**33.8**	**29.5**

Compared to calculations that retain λ_v, the calculated angle of diagonal compression that doesn't include the lightweight modifier is typically about half of a degree larger when using *Appendix B5* or the *General Procedure*. The larger angles would ordinarily translate into lower calculated shear capacities because a steeper angle would potentially decrease the number of vertical stirrups that would intersect a shear crack. Yet, as evidenced in Table 4-5, the theoretical shear strengths were *greater* without λ_v. The reason is due to $V_{c\ no\ \lambda_v}$ being greater than $V_{c\ \lambda_v}$, as is explained in Section 4.4.3. Table 4-12 shows that the increase in the concrete contribution is greater than the decrease in the steel contribution when considering the lightweight modifier versus having no modifier at all. Thus, the overall calculated shear capacity is greater when λ_v is not included in the calculations. In contrast, there generally is no difference between using λ_v and not doing when calculating θ the *Simplified Procedure* because both sets of calculations are limited by the maximum value of $\cot\theta$, or minimum value of θ. The exceptions are for the two tests on beam BT.8.Typ, where θ_{Sim} is 0.9º and 1.6º greater when excluding the lightweight modifier in predictions for tests BT.8.Typ.1 and BT.8.Typ.2, respectively. Despite the equality in θ_{Sim}, $V_{n\ Sim}$ No λ_v was slightly greater than $V_{n\ Sim}$ in 75% of the tests from this current investigation. Again, the reason is that $V_{c\ Sim\ no\ \lambda_v}$ is greater than $V_{c\ Sim\ \lambda_v}$ due to the λ_v factor.

For comparison of the results in Tables 4-17 and 4-18, consider Figure 4-10. Note that a separate θ_{calc} is given for the three different shear design models, which do not include the modification factor for sand-lightweight concrete. Also note that $\theta_{prin\ post\text{-}V_{cw}}$ is omitted from Figure 4-10 to avoid too much confusion in the figure. Again, this value is not considered a valid result and has only been provided for informational purposes. $\theta_{prin\ pre\text{-}V_{cw}}$ fell outside of the range of θ_{calc} values provided by the three different design methods in 75% of the tests. In those cases, $\theta_{prin\ pre\text{-}V_{cw}}$ was typically lower than the theoretical angles. The one extreme exception is the principal angle of rotation for test BT.10.Typ.1, which is dramatically larger than the calculated angles. The graph of test BT.10.Typ.1 in Figure 4-9 shows that there was a large jump in the rotation angle when the force carried by the concrete was about 215 kips. Delving deeper into the data, the LVDTs in the 0˚ orientation and the LVDTs oriented across the direction of shear cracking (as opposed to the third rosette LVDT oriented along the direction of

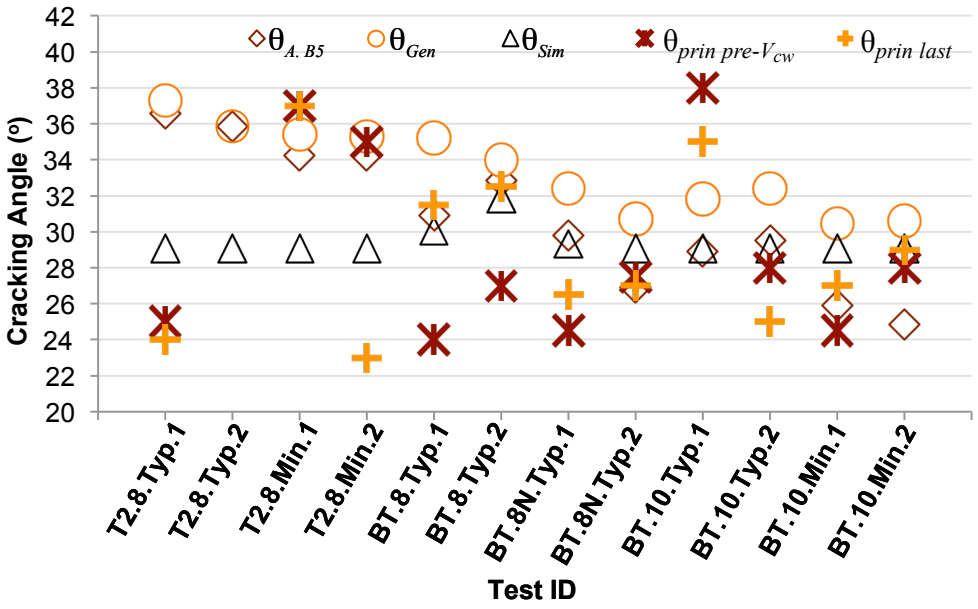

Figure 4-10. Comparison of θ_{calc} versus θ_{prin}.

the compression strut) on both sides of the web showed sizable increases in tension at the aforementioned level of loading. Such an increase may have been indicative of cracking in the web, even though V_{cw} was about 270 kips, as indicated by the sudden increase in the force carried by the stirrups. At V_{cw}, the angle of rotation to the principal stresses dropped. Attributing the increase in the angle of rotation to error in the instrumentation is not the most plausible option because the sudden change occurred simultaneously on both sides of the girder. However, as discussed in Section 4.4.2.1, the absolute difference between the median crack angle and $\theta_{prin\ pre\text{-}V_{cw}}$ in test BT.10.Typ.1 is one of the largest of all of the tests. Furthermore, Table 4-5 shows that the ratio of the experimental versus theoretical shear strengths is also one of the largest of the twelve experiments in this study. If the angle of inclination to the true principal stresses were so large, then the experimental shear strength would generally be lower than predicted. So, test BT.10.Typ.1 in Figure 4-10 does not agree with the results given in Table 4-5. Unfortunately, the reason for larger angle of rotation to the principal stresses in the figure is unknown.

As a point of comparison, $\theta_{prin\ last}$ had a marginally better success rate of being within the range of calculated angles. However, this rate is still less than 50% for all of the tests. The two θ_{prin}

angles given in Figure 4-10 were fairly evenly divided in terms of the number of times one was greater than the other or if they had relatively similar values.

Nevertheless, the effect of assuming a different angle of diagonal compression stress other than that calculated using the AASHTO code can be assessed. Table 4-19 shows the results for the theoretical shear strength using $\theta_{prin\ pre\text{-}V_{cw}}$ and $\theta_{prin\ last}$. Note that *Appendix B5* and *General Procedure* tend to be iterative in nature, and thus, the value of θ can change within each iteration. Therefore, the new set of calculations for θ_{prin} has been performed by adjusting the value of θ in a given iteration by the difference between θ_{calc} and θ_{prin}, taking the sign of that difference into account. The modified θ values were then used in the programs described in Appendix C. Also, note again there are no comparisons for test T2.8.Typ.2 due to the data from the strain gage rosette being excluded in the analysis and the LVDT rosette for this test malfunctioned during testing.

Looking at the overall averages, Table 4-19 suggests that assuming the angle of diagonal compression calculated from experimental measurements has a relatively small effect on the theoretical shear capacity when compared to θ_{calc} as determined from the 2010 AASHTO LRFD Bridge Design Specifications. However, a deeper examination of the results for the individual

Table 4-19. Calculated shear capacity when assuming θ to be $\theta_{prin\ last}$ or $\theta_{prin\ V_{cw}}$.

Test ID	$\theta_{prin\ pre\text{-}V_{cw}}$						$\theta_{prin\ last}$					
	$V_{n\ \theta_{prin\ V_{cw}}}$			%Δ from $V_{n\ calc}$			$V_{n\ \theta_{prin\ last}}$			%Δ from $V_{n\ calc}$		
	A. B5	***Gen***	***Sim***	***A. B5***	***Gen***	***Sim***	***A. B5***	***Gen***	***Sim***	***A. B5***	***Gen***	***Sim***
T2.8.Typ.1	207	196	266	-0.07	-0.06	-0.21	242	223	310	0.09	0.07	-0.09
T2.8.Typ.2												
T2.8.Min.1	186	177	245	-0.04	-0.02	-0.14	186	177	245	-0.04	-0.02	-0.14
T2.8.Min.2	182	173	247	-0.02	0.00	-0.11	230	200	322	0.24	0.16	0.16
BT.8.Typ.1	341	337	326	0.09	0.15	-0.12	307	304	356	-0.01	0.04	-0.05
BT.8.Typ.2	305	296	422	0.07	0.08	0.26	283	276	362	0.00	0.01	0.08
BT.8N.Typ.1	279	273	354	0.08	0.10	0.12	270	265	333	0.04	0.07	0.05
BT.8N.Typ.2	239	244	296	-0.01	0.02	0.02	241	246	301	0.00	0.03	0.04
BT.10.Typ.1	264	267	294	-0.09	-0.05	-0.16	271	276	309	-0.07	-0.02	-0.11
BT.10.Typ.2	278	276	343	0.02	0.04	0.03	288	286	369	0.05	0.08	0.10
BT.10.Min.1	236	246	261	0.02	0.06	0.07	228	240	252	-0.02	0.03	0.03
BT.10.Min.2	225	238	244	-0.03	0.01	0.02	223	237	241	-0.04	0.01	0.00
Average				**0.00**	**0.03**	**-0.02**				**0.02**	**0.04**	**0.01**

tests reveals that there can be some fairly large swings in the predicted shear strength depending on which value of θ is used. For example, the predicted shear capacity would increase by 26% in test BT.8.Typ.2 if $\theta_{prin\ pre\text{-}V_{cw}}$ were used in the *Simplified Procedure*. Likewise, test T2.8.Min.1 would have increased by 24% if $\theta_{prin\ last}$ were to be used in *Appendix B5*. In the opposite direction, the theoretical shear strength of T2.8.Typ.1 with $\theta_{prin\ pre\text{-}V_{cw}}$ and T2.8.Min.1 with $\theta_{prin\ last}$ would have been 21% and 14% lower, respectively, for the *Simplified Procedure*. The conclusion here is that the angle of inclination of diagonal compressive stresses can certainly impact the predicted shear strength of a prestressed girder. Therefore, θ should not be disregarded in a general formulation for V_n, as recommended by Laskar et al. (*85*). Developing better methods that forecast θ could improve the accuracy of those shear strength predictions.

4.4.2 Angle of Inclination of Diagonal Concrete Cracking in the Web

4.4.2.1 Comparison between θ_{crack} and θ_{prin}

As reported in Section 2.2.5.2, Hawkins and Kuchma stated that the angle of diagonal compressive stress is not necessarily the same as the angle of diagonal cracking. However, Hawkins and Kuchma as well as Vecchio and Collins assumed the two to be the same. To investigate this assumption, the measured cracking angles from the twelve tests in this study are given in Table 4-20 and shown in Figure 4-11 along side the average values for $\theta_{prin\ pre\text{-}V_{cw}}$ and $\theta_{prin\ last}$ originally listed in Table 4-17. Note that both the table and figure show a range of measured crack angles because these measurements were somewhat subjective and there were multiple cracks that could be considered as the boundary crack on either side of a given girder web. The column labeled $\theta_{crack\ med}$ in Table 4-20 is the median value within the given range of measured crack angles. Also note that all measured crack angles are relative to the horizontal.

Because each test consisted of two concentrated loads, the measured crack angles approximately paralleled the line from the load closest to the support to the edge of the support bearing. The results are in line with the results in Section 2.3.1.5, where Salandra and Ahmad observed that the angle of critical cracking decreased as *a/d* increased. However, unlike the observation regarding θ_{prin} in Section 4.4.1.2, the lightweight beam BT.8.Typ had larger cracking angles compared to its normal weight counterpart, BT.8N.Typ. This observation is in spite of the fact

Table 4-20. Comparison between θ_{crack} and θ_{prin}.

Test ID	θ_{crack} (°)	$\theta_{crack\ med}$ (°)	$\theta_{prin\ avg}$ (°)			$\lvert\theta_{prin\ avg} - \theta_{crack\ med}\rvert$		
			pre-V_{cw}	post-V_{cw}	last	pre-V_{cw}	post-V_{cw}	last
T2.8.Typ.1	26 – 35	31.5	25	27	24	6.5	4.5	7.5
T2.8.Typ.2	24 – 32	28.5						
T2.8.Min.1	28 – 37	33	37	34	37	4	1	4
T2.8.Min.2	30 – 35	30	35	32	23	5	2	7
BT.8.Typ.1	30 – 45	35	24	24	32	11	11	3.5
BT.8.Typ.2	25 – 30	30	27	25	33	3	5.5	2.5
BT.8N.Typ.1	26 – 37	31.5	25	30	27	7	2	5
BT.8N.Typ.2	24 – 27	24.5	28	27	27	3	2.5	2.5
BT.10.Typ.1	27 – 32	30	38	33	35	8	2.5	5
BT.10.Typ.2	21 – 28	25	28	23	25	3	2	0
BT.10.Min.1	30	30	25	23	27	5.5	7	3
BT.10.Min.2	26 – 31	30	28	22	29	2	8	1
					Average	**5.3**	**4.4**	**3.7**
					Standard deviation	**2.7**	**3.2**	**2.3**

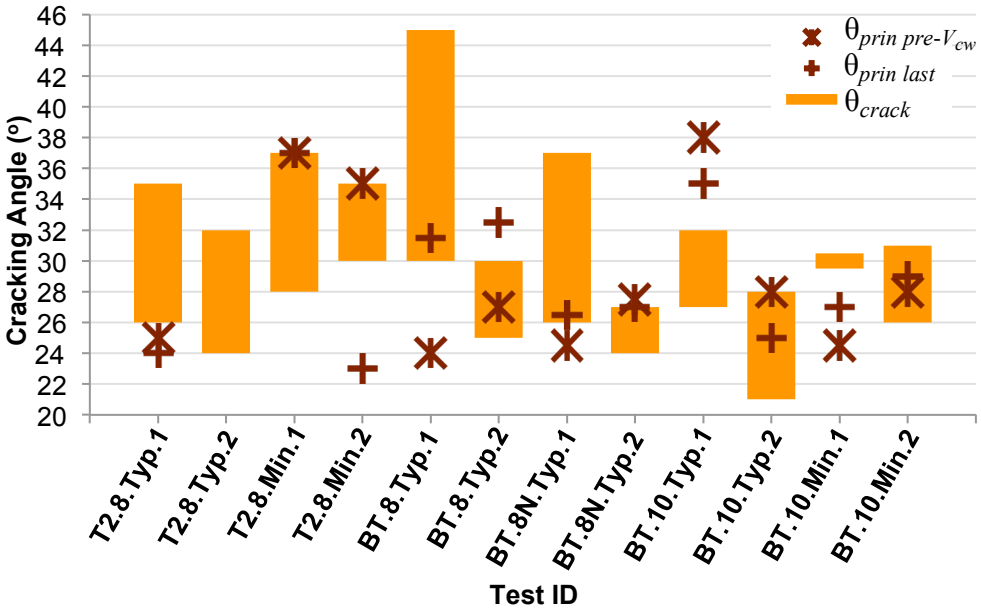

Figure 4-11. Comparison of θ_{crack} versus θ_{prin}.

the companion tests had similar *a*/*d* ratios. Then again, the early University of Texas research on shear in lightweight concrete beams was inconclusive regarding the cracking angle compared to normal weight beams without vertical reinforcement (refer to Section 2.3.1.1).

Regarding the comparison between the measured cracking angle and the calculated angle of rotation to the principal compressive stress using the rosette measurements, the results are mixed. $\theta_{prin\ pre\text{-}V_{cw}}$ fell within the range of measured angles in just over 40% of the tests. Those results for $\theta_{prin\ pre\text{-}V_{cw}}$ that fell outside of the measured crack range were evenly split between being above and below the measured range. $\theta_{prin\ last}$ was only marginally better, falling within the range of measured crack angles 50% of the time. These observations contradict the work of other researchers who suggested that the angle of diagonal compression is smaller than the angle of diagonal cracking due the shear stress being transferred across the cracks.

The average absolute difference between $\theta_{prin\ pre\text{-}V_{cw}}$ and the median θ_{crack} is 5.3º with a standard deviation of 2.7º. For $\theta_{prin\ last}$, that average difference with θ_{crack} is smaller at 3.7º with a standard deviation of 2.3º. Again, these results are stated in light of the aforementioned uncertainty present in the angle of rotation to the principal compressive stresses. Nevertheless, the results appear to agree with Hawkins and Kuchma's statement that this angle is not necessarily the same as the angle of the actual shear crack in the beam.

4.4.2.2 Comparison between θ_{crack} and θ_{calc}

With that said, one can also consider the effect of assuming that θ is the measured angle of the shear cracks observed during testing. Figure 4-12 shows that the AASHTO code incorrectly calculated the angle of the crack leading to failure about half of the time, regardless of which shear calculation procedure was used and regardless of whether or not the lightweight modifier was included in the calculations. Of the calculations that missed their mark, there was a mix of those that overpredicted the cracking angle and those that underpredicted. Section 2.3.3.2 notes that Malone also found that there was no apparent pattern as to whether the experimental result was less than or greater than the predicted angle using the tabular procedure in *Appendix B5*. On the other hand, Dymond et al. determined that the experimental cracking angle was 20% greater than the predicted angle in the lone test reported in Section 2.3.3.5, while Hawkins and Kuchma concluded that the predicted angle of web-shear cracking in normal weight concrete beams was typically smaller than the observed angle (see Section 2.2.5.2).

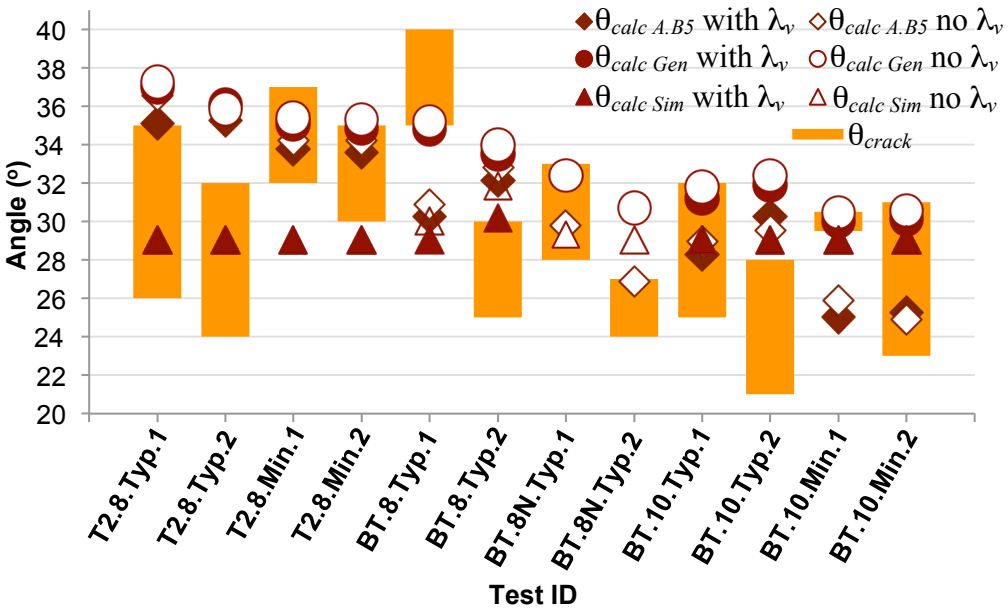

Figure 4-12. Comparison of experimental cracking angle and code-calculated angle of diagonal compressive stresses.

For this study, *Appendix B5* predicted smaller cracking angles than the *General Procedure*. This fact gives partial explanation as to why $V_{n\ Gen}$ is more conservative than $V_{n\ A.B5}$, as noted in Section 4.2.1. The difference between these two methods is typically only one or two degrees, although the largest difference is about five degrees in test BT.10.Min.1. The slightly larger angle determined with the *General Procedure* results in a smaller steel contribution to the shear capacity, which in turn could give a more conservative calculation of the shear strength in the girder. Meanwhile, the *Simplified Procedure* tends to predict the smallest angle of inclination. That angle is typically 29.1°, which relates to the limiting value of 1.8 in Eq. (39).

When assuming no lightweight modifier, the resulting calculations give a cracking angle that generally is greater than those calculations that do include the modifier; however, the difference is relatively minor (ranging from 0.2 degrees to 1.3 degrees). This observation augments the conclusion in Section 4.3 regarding the unnecessary modifier for sand-lightweight concrete. Note that Figure 4-12 only shows data points without λ_v for tests BT.8N.Typ.1 and BT.8N.Type.2, because beam BT.8N.Typ was constructed with normal weight concrete.

Consider Table 4-21, which is an exercise in examining the effect on the theoretical shear capacity when assuming the median angle of the actual cracks in a beam instead of θ_{calc} using

Table 4-21. Calculated shear capacity when assuming θ to be the median θ_{crack} observed from experimentation.

Test ID	$\theta_{crack\ med}$ (°)	$V_{n\ \theta_{crack\ med}}$			%Δ from $V_{n\ calc}$		
		A. B5	*Gen*	*Sim*	*A. B5*	*Gen*	*Sim*
T2.8.Typ.1	31.5	244	228	320	0.10	0.10	-0.05
T2.8.Typ.2	28.5	236	205	316	0.18	0.09	0.01
T2.8.Min.1	33	197	188	262	0.02	0.04	-0.08
T2.8.Min.2	30	193	183	272	0.04	0.06	-0.02
BT.8.Typ.1	35	297	294	333	-0.05	0.00	-0.11
BT.8.Typ.2	30	293	285	350	0.03	0.04	0.04
BT.8N.Typ.1	31.5	253	254	310	-0.02	0.02	-0.02
BT.8N.Typ.2	24.5	245	251	318	0.02	0.05	0.10
BT.10.Typ.1	30	287	287	341	-0.01	0.02	-0.02
BT.10.Typ.2	25	288	286	369	0.05	0.08	0.10
BT.10.Min.1	30	225	234	241	-0.03	0.00	-0.01
BT.10.Min.2	30	221	236	237	-0.05	0.00	-0.01
				Average	**0.02**	**0.04**	**-0.01**

any of the three shear design methods in the 2010 AASHTO LRFD Bridge Design Specifications. Like θ_{prin} in Table 4-19, the average V_n does not change dramatically when assuming θ_{crack}. The largest average effect is in the *General Procedure*, with a 4% increase in the V_n. Again, however, there were some fairly substantial differences amongst the various experiments. For example, test T2.8.Typ.2 would have an 18% greater predicted shear capacity if the experimental cracking angle were used in the strength calculations following the methods in *Appendix B5*. Likewise, both tests BT.8N.Typ.2 and BT.10.Typ.2 see a 10% increase when using the *Simplified Procedure*. Going in the other direction, the *Simplified Procedure* results in an 8% and 11% decrease for the predicted strength of respective tests T2.8.Min.1 and BT.8.Typ.1 when using $\theta_{crack\ med}$ instead of $\theta_{calc\ Sim}$.

Yet, the fact that all three prediction methods for determining θ only fell within the experimental range of angles half of the time brings into question the need for such an iterative and rigorous design procedure for finding the cracking angle that leads to shear failure. However, using a less iterative procedure supported by the *General Procedure* would mean a slightly more conservative shear strength prediction in a case where the results from *Appendix B5* already tend to be excessively cautious. On the other hand, one could certainly employ the simpler formulation implied in the *Simplified Procedure* and Eq. (39). However, the implications

would be that the lower cracking angle will result in larger predicted values for V_s, which impacts the ratio of experimental versus predicted shear capacity, thus reducing the professional factor, and thus require a lower strength reduction factor, as discussed in Section 4.5.

4.4.3 Results for β

As mentioned in Section 2.2.5.2, the term β in Eq. (61) is the parameter linking the longitudinal strain in the concrete to the concrete shear capacity, which is dictated by the amount of tension that can transmit across the diagonal cracks. The 2010 AASHTO LRFD Bridge Design Specifications provide two different methods for calculating β, either using the equations in the *General Procedure* under Article 5.8.3.4.2 or using the tables in *Appendix B5*. The resulting values of those calculations for the twelve tests in this investigation are listed in Table 4-22 and displayed in Figure 4-13.

Note that β is given for two sets of calculations, where one set, β_{λ_v}, includes the modification factor for sand-lightweight concrete, while the other, $\beta_{\text{no }\lambda_v}$, does not. Considering *Appendix B5*, there is a relatively small difference between β_{λ_v} and $\beta_{\text{no }\lambda_v}$, with the average ratio of β_{λ_v} versus $\beta_{\text{no }\lambda_v}$ being 1.02. When using the *General Procedure*, the ratio is a little bit larger, with the average ratio being 1.05. However, the ratio $\beta_{\lambda_v} / \beta_{\text{no }\lambda_v}$ for both design methods is marginally

Table 4-22. Comparison of β calculated with *Appendix B5* and the *General Procedure*.

Test ID	β_{λ_v}		$\beta_{\text{no }\lambda_v}$		$\frac{\beta_{\lambda_v}}{\beta_{\text{no }\lambda_v}}$		$\frac{\beta_{A.\,B5}}{\beta_{Gen}}$		$\frac{V_{n\text{ no }\lambda_v}}{V_{n\,\lambda_v}}$		$\frac{V_{n\,A.\,B5}}{V_{n\,Gen}}$	
	A. B5	*Gen*	*A. B5*	*Gen*	*A. B5*	*Gen*	with λ_v	no λ_v	*A. B5*	*Gen*	with λ_v	no λ_v
T2.8.Typ.1	2.26	1.77	2.24	1.73	1.01	1.02	1.28	1.29	1.02	1.02	1.06	1.07
T2.8.Typ.2	2.27	1.90	2.23	1.84	1.02	1.03	1.19	1.21	1.02	1.02	1.06	1.06
T2.8.Min.1	2.36	2.09	2.33	2.02	1.01	1.03	1.13	1.15	1.02	1.02	1.06	1.07
T2.8.Min.2	2.37	2.13	2.33	2.04	1.02	1.04	1.11	1.14	1.02	1.02	1.07	1.08
BT.8.Typ.1	2.55	2.14	2.50	2.06	1.02	1.04	1.19	1.21	1.02	1.02	1.06	1.06
BT.8.Typ.2	2.45	2.44	2.41	2.32	1.02	1.05	1.00	1.04	1.02	1.01	1.04	1.04
BT.8N.Typ.1			2.64	2.77				0.95	1.00	1.00	1.04	1.04
BT.8N.Typ.2			2.87	3.51				0.82	1.00	1.00	1.01	1.01
BT.10.Typ.1	2.71	3.26	2.66	3.04	1.02	1.07	0.83	0.88	1.02	1.02	1.03	1.03
BT.10.Typ.2	2.66	2.96	2.59	2.77	1.03	1.07	0.90	0.94	1.02	1.02	1.03	1.03
BT.10.Min.1	3.14	3.93	3.03	3.65	1.04	1.08	0.80	0.83	1.04	1.04	1.00	1.00
BT.10.Min.2	3.33	3.86	3.17	3.59	1.05	1.08	0.86	0.88	1.03	1.04	1.00	0.99
				Average	**1.02**	**1.05**	**1.03**	**1.03**	**1.02**	**1.02**	**1.04**	**1.04**

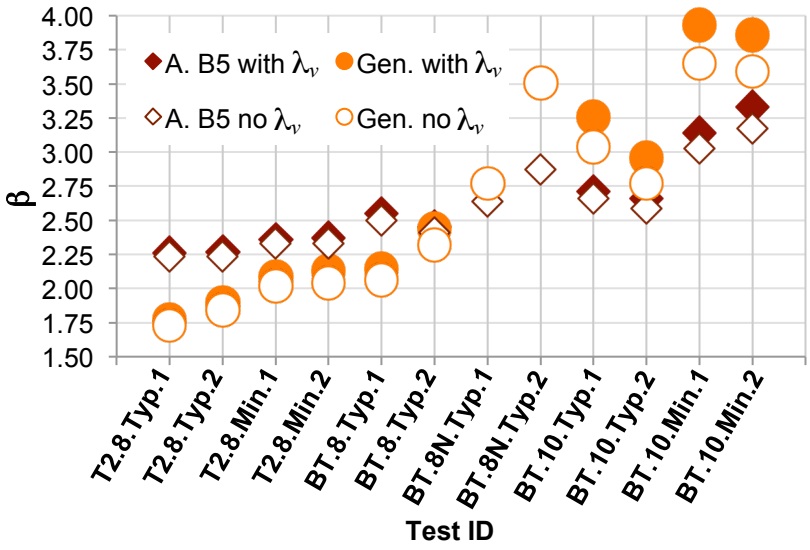

Figure 4-13. β factor used for calculating the shear capacity of concrete, as determined from *Appendix B5* and the *General Procedure*.

higher for 10 ksi concrete compared to 8 ksi concrete. Interestingly, the calculated β with the lightweight modifier is larger than β without the modifier because the calculation process with λ_v predicts a lower shear stress at ultimate, v_u, and a lower longitudinal strain, ε_x (for *Appendix B5*) or ε_s (for the *General Procedure*). These lower values result in a larger β-factor, suggesting that lightweight concrete has greater ability to transmit tension across the shear cracks. However, there is little evidence supporting such a material quality. Furthermore, this result is incongruous with the lower predicted concrete contribution to the shear capacity for lightweight concrete, where V_c in Eq. (62) is reduced by λ_v. Even though β_{λ_v} is larger than $\beta_{\text{no }\lambda_v}$, recall that Table 4-12 shows that $V_{c\,\lambda_v}$ is less than $V_{c\,\text{no }\lambda_v}$ for *Appendix B5* and the *General Procedure*. The reason is that when β_{λ_v} is multiplied by the lightweight modifier, the result is less than $\beta_{\text{no }\lambda_v}$.

Both Table 4-22 and Figure 4-13 show that *Appendix B5* generally gives larger β factors for the 8-ksi lightweight beams, but lower values for the 8-ksi normal weight beam and the 10-ksi lightweight beams when compared to the *General Procedure*. This observation is regardless of whether or not λ_v is taken into consideration. So, while the average ratio $\beta_{A.B5}/\beta_{Gen}$ is about 1.03, the largest ratio is 1.29 for test T2.8.Typ.1, and the lowest ratio is 0.83 for test BT.10.Min.1, assuming no λ_v. Therefore, *Appendix B5* tends to be slightly less conservative when calculating V_c for the lightweight 8-ksi beams while slightly more conservative for the remaining girders.

Note that the differences in β for *Appendix B5* and the *General Procedure* are slightly different compared to the differences in V_c for the two methods. The reason is that the calculation process results in the controlling value of V_n occurring at different distances away from the support. Therefore, the value of d_v may vary. So, the ratio of $V_{c\,A.B5}/V_{c\,Gen}$ can be affected by both the differences in β and d_v. Nevertheless, $V_{c\,A.B5}/V_{c\,Gen}$ is about the same as that of $\beta_{A.\,B5}/\beta_{Gen}$. Given that the concrete contribution to shear capacity tends to be the smaller of the two components in the overall shear strength, the differences discussed above have a subtler effect on the total shear strength. The right-hand column of Table 4-22 says as much. For example, the ratio of $V_{n\,A.B5}$ versus $V_{n\,Gen}$ for test T2.8.Typ.1 is 1.07 instead of the value of 1.29 mentioned above.

4.5 Strength Reduction Factor for Shear, ϕ_v

4.5.1 Professional Factor for Lightweight Concrete

As discussed in Section 2.3.4.2, AASHTO dictates that the strength reduction factor for shear, ϕ_v, is 0.90 for normal weight concrete and 0.70 for lightweight concrete. These values stem from the seminal *NCHRP Report 368* written by Nowak. Subsequently, Paczkowski and Nowak suggested that ϕ_v for lightweight concrete be increased to 0.80. However, as discussed in Section 2.4.3.2, the researchers based that recommendation in part on their findings on the professional factor calculated from 13 beam tests. Recall from Section 2.4.1 that the professional factor is the average ratio of the experimental behavior to the strength predicted by a given model, where that prediction uses known material properties and member geometries. While Paczkowski and Nowak predicted the strengths using what is currently *Appendix B5* in the 2010 AASHTO LRFD Bridge Design Specifications, there are a number of shortcomings in calculating the professional factor based on the data set used in their analysis:

- none of the beams had prestressed reinforcement,
- only eight beams used sand as the fine aggregate,
- only 1 beam had compressive strength that exceeded 8 ksi,
- none of the beams had composite area of concrete greater than 279 in^2,
- all of the shear span-to-effective depth ratios were 2.2 or greater.

Considering the one beam in the above data set that did exceed 8 ksi compressive strength, that beam had a shear strength that was very similar to its normal weight comparative beam (V_{Exp} =

89.1 kips for the 10.5 ksi lightweight girder versus V_{Exp} = 89.3 kips for the 10.9 ksi normal weight girder). Like the results from the current investigation, there does appear to be a trend in the data set described above indicating that smaller composite areas and larger shear span-to-effective depth ratios resulted in less conservative ratios of V_{Exp} versus V_{calc}.

While the information that Paczkowski and Nowak examined can be helpful, a more prudent endeavor might be to develop a professional factor based on another data set that is more representative of lightweight girders used in actual bridges, including concrete girders that are prestressed, use sand as the fine aggregate, have compressive strengths that are 8 ksi or greater, have deeper sections, and have larger cross-sectional areas. For this reason, the 10 lightweight beam experiments in this study have been combined with the results from the 12 prestressed, sand-lightweight beam tests listed in Table 4-7. Recall from Table 4-7 that three of the beams from the Kahn et al. study were dominated by strand-slip bond failure; of those three, two had fairly low experimental strength versus calculated strength ratios. The statistics for some of the parameters of this combined prestressed data set are given in Table 4-23.

By the same token, one can expand the data set to include all available data on shear tests of lightweight beams, regardless of any other parameters. The literature review revealed an additional 282 experiments on the shear strength of lightweight concrete beams containing mild longitudinal reinforcement. Of these, only 160 had sufficient data available to analyze their theoretical shear capacities using the 2010 AASHTO LRFD Bridge Design Specifications. However, of those 160 tests, four experiments by Salandra and Ahmad (*101*) were excluded due to their extremely low a/d ratios of 0.52, effectively rendering the sections as deep beam structures. An additional four results from Ahmad, Xie, and Yu (*119*) were rejected due to the

Table 4-23. Statistics of basic parameters in the dataset used for determining the professional factor of full-scale, lightweight concrete prestressed beams tested in shear.

Statistic	Parameter			
	f_c (ksi)	d_v (in)	A_c (in^2)	a/d
Average	9.36	41.15	921.79	2.32
Standard deviation	1.07	8.00	421.95	0.62
Coefficient of variation	0.11	0.19	0.46	0.27
	207			

excessively large experimental-to-theoretical ratios that varied from 2.5 to 3.4; these large ratios may skew the analysis for ϕ_v too far in the unconservative direction. There were three other experiments by Kahn et al. (*16*) where the failures were strand-slip bond failures; however, these results remained in the data set as the beams were apparently approaching their shear capacities. Of the 152 reinforced concrete beams accepted for analysis, 43 had vertical reinforcement, although only 39 satisfied the minimum shear reinforcement requirement according to the 2010 AASHTO LRFD Bridge Design Specifications. Of the 113 beams that did not meet the minimum reinforcement guidelines, the theoretical shear capacities of 104 beams could be calculated according to Article 5.8.3.4.1 of the the AASHTO code, which assumes that β and θ for nonprestressed members are 2.0 and 45°, respectively. However, this method is not included in this analysis because the article only pertains to reinforced concrete and not prestressed girders typically found in highway bridges. The statistics for some of the parameters of the nonprestressed data set are given in Table 4-24.

In developing the professional factor, the predicted shear strength incorporated as many known material and geometric properties as possible into the calculations using the 2010 edition of the AASHTO LRFD Bridge Design Specifications. As noted in Section 4.2.1, the inputs and results for these calculations are detailed in Appendix C. Calculations using *Appendix B5*, the *General Procedure*, and the *Simplified Procedure* have been performed separately. Note that the calculations did not include the lightweight modification factor, for reasons discussed in Section 4.2.3.3.3 . Naturally, the experimental shear capacities were gleaned from the literature. Results of the experimental-versus-theoretical shear strength ratios are detailed in Appendix E, but Table 4-25 gives a summary of the resulting professional factor for the three shear models in this analysis. Note that this table provides professional factors for all lightweight beams combined as

Table 4-24. Statistics of basic parameters in the dataset used for determining the professional factor of lightweight reinforced concrete beams tested in shear.

Statistic	Parameter			
	f_c (ksi)	d_v (in)	A_c (in^2)	a/d
Average	5.55	10.66	92.71	2.81
Standard deviation	2.50	6.47	104.4	1.00
Coefficient of variation	0.45	0.61	1.13	0.36

Table 4-25. Professional factors and corresponding statistics developed for various categories of lightweight concrete beams. NB: parenthesis indicate the number of tests in each category.

Beam Type	*Appendix B5*			*General Procedure*			*Simplified Procedure*		
	λ_P	σ_P	CoV_P	λ_P	σ_P	CoV_P	λ_P	σ_P	CoV_P
All beams (174)	1.28	0.47	0.37	1.23	0.44	0.36	1.06	0.37	0.35
All RC beams (152)	1.23	0.48	0.39	1.16	0.41	0.35	0.97	0.38	0.40
RC beams without stirrups (109)	1.34	0.48	0.36	1.21	0.44	0.36			
RC beams with stirrups (43)	0.97	0.37	0.38	1.04	0.31	0.30	0.97	0.38	0.40
All PS beams (22)	***1.58***	0.29	***0.19***	***1.76***	0.26	***0.15***	***1.24***	0.29	***0.24***
Current study (10)	1.68	0.20	0.12	1.75	0.20	0.12	1.33	0.29	0.21

well as non-prestressed (*RC*) and prestressed (*PS*) beams separately; the number of test results used to calculate λ_P are given in parentheses within each beam type. Also note that only beams containing the minimum amount of shear reinforcement have been included in the analysis using the *Simplified Procedure*. Lastly, σ_P is the standard deviation corresponding with the professional factor.

Looking at Table 4-25, all three design models prove to be less conservative when predicting the shear strength of reinforced concrete beams versus prestressed concrete girders. In fact, both *Appendix B5* and the *Simplified Procedure* overestimate the shear strengths of reinforced concrete beams that have vertical reinforcement, with the average ratio of the experimental versus theoretical shear strength being 0.97. This observation is in line with results by Paczkowski and Nowak in Section 2.4.3.2, who found that more than a third of the lightweight reinforced concrete tests in their analysis had experimental strengths that were less than what was predicted.

Furthermore, there is wide variation in the reinforced beams, with the coefficient of variation ranging from 35% using the *General Procedure* to 40% using the *Simplified Procedure*. The prestressed girders have relatively lower variability, with the coefficient of variation ranging from 15% to 24%. What is interesting is that while the more complex prestressed structures have the largest professional factor, the reinforced concrete beams without reinforcement have higher professional factors than those beams with stirrups when considering *Appendix B5* or the *General Procedure*. Regardless, the highlighted professional factors developed from 22 tests of

large-scale, prestressed lightweight concrete girders and the accompanying coefficients of variation in Table 4-25 are used in the following section to analyze the reliability of, and develop the strength reduction factors for, bridge design using each of the three shear strength models being considered. The reason for using the larger professional factor for prestressed beams instead of the smaller factor for all beams is that the focus of this analysis is for ordinary prestressed girders found in highway bridges.

4.5.2 Reliability Analysis of Girder Design

4.5.2.1 Statistical Parameters for Reliability Analysis

4.5.2.1.1 Load Components and Parameters

As indicated in Section 2.4.1, there are two main pieces of the puzzle when determining the level of safety in bridge design: the demand or load component and the resistance or strength component. In discussing the demand side of the equation, Nowak indicated that the major load components used for the reliability analysis in his 1999 study were developed using statistical data and other observations. Nowak treated all of these load components as normal random variables having their own bias factors and coefficients of variation. D_1 was the dead load of factory-made components, while D_2 was the dead load of cast-in place members. D_3 was the dead load of the asphalt wearing surface, which was based on statistical data collected by the Ontario Ministry of Transportation in 1984. For live loads, L was the AASHTO Standard Specifications live load model consisting of three cases: an HS20 truck similar to the HL90 truck in the current specifications, a lane load of 0.64 klf superimposed with a concentrated load of 26 kips for shear, and the military loading with two axles weighing 24 kips and spaced 4 ft apart. The truck and military loading did not include the 0.64 klf lane load. I was the dynamic load allowance that was applied to the live load and was calculated as:

$$I = \frac{50}{L + 125} \qquad (141)$$

where L was defined as the distance from the point under consideration to the far reaction, in feet. Eq. (141) only applied to shear due to a truck in a simple span; generally, L tended to be the overall span length.

The statistics for the live load were based on data gathered in 1976 and 1991. The maximum load of a given truck was extrapolated from the available data since the original data set only contained 10,000 trucks, which was a relatively small sample size considering the number of heavily loaded vehicles that crossed a bridge over 75 years. 75 years was the assumed design life of a given bridge, and the maximum 75-year combination of live load and dynamic load was modeled using the statistical parameters derived from simulations.

Now, Nowak formulated Q, the maximum value for the effect due to all load components, as

$$Q = E(D_1 + D_2 + D_3 + L + I) \quad \textbf{(142)}$$

where E was the factor indicating the uncertainty in the load analysis. $\mu_E = 1.0$ and $CoV_E = 0.04$ for simple spans. The mean Q, μ_Q, was simply the sum of the averages of the load components given in Eq. (142). However, the *total* load effect is due to the aforementioned components as well as other environmental factors, such as wind and earthquake loads. Yet, the probability that all of these factors take their maximum values simultaneously is small. Furthermore, the effect of the sum of the loads is not necessarily equal to the sum of the effect of the individual loads, particularly when considering non-linear behavior of a bridge. Therefore, Nowak treated Q as a normal random variable and required rigorous numerical simulations to calculate the statistical parameters for Q (*136*).

Note that with the exception of the dead loads, the other load components are time-dependent. Additionally, the aforementioned load components and live load models are slightly different from what is defined in the 2010 AASHTO LRFD Bridge Design Specifications. Under LRFD, D_1 and D_2 have been combined into DC, the dead load of all structural components and nonstructural attachments. D_3 is now DW, and L is now LL. However, LL is one of only two models: a truck load similar to the HS20 model, and a tandem loading spaced at 4 ft with each wheel load being 25 kips. Both of these two cases include the superimposed 0.64 klf lane load. Lastly, I is now designated as IM, and has a constant value of 1.33 regardless of span length. Unlike the AASHTO Standard Specifications, the dynamic load allowance is applied to the static truck and tandem loads, but not the lane load.

In the *NCHRP Report 368*, Nowak presented tables containing the values for the load components as well as the statistical parameters for the total load effect, μ_Q and σ_Q. Note that σ_Q is the standard deviation of Q. Presumably, these tables were developed for structures constructed with normal weight concrete. Therefore, the reliability analysis for this current study adopts two important assumptions. First, the live loads on a bridge will be the same regardless of whether or not the bridge is constructed with normal weight or lightweight concrete. This first assumption may not be entirely accurate for the longest spans by virtue of the fact that lightweight concrete enables longer spans relative to normal weight concrete. Thus, the live loads effects would be different. Nevertheless, the second assumption is that the dead load due to the structural concrete for a given span length is lower in bridges constructed with lightweight concrete compared to normal weight concrete.

Therefore, the mean total load effect listed in *NCHRP Report 368*, μ_Q, needs to be reduced for use in the reliability analysis of lightweight concrete. Because dead load is not time-dependent, the dead load component of Q can be replaced by the dead load of the lightweight structure, which can be calculated as the original dead load in Nowak's analysis multiplied by the ratio of the density of lightweight concrete versus that of normal weight concrete. Note that both densities include the nominal 5 pcf that is traditionally assumed for steel reinforcement in the concrete. For the purposes of this study, the density of sand-lightweight concrete is assumed to be the average value for the 22 full-scale lightweight girders given in Tables 4-5 and 4-7, which is 124.1 pcf. Therefore, the average total load affect used in the reliability analysis for this study, $\mu_{Q\,lwc}$, is calculated as

$$\begin{aligned} \mu_{Q\,lwc} &= \mu_Q - DC_{NCHRP} + DC_{lwc} \\ &= \mu_Q - DC_{NCHRP} + \frac{124.1 \text{ pcf}}{150 \text{ pcf}} DC_{NCHRP} \\ \mu_{Q\,lwc} &= \mu_Q - 0.17 DC_{NCHRP} \end{aligned} \quad \textbf{(143)}$$

where DC_{NCHRP} is $D_1 + D_2$, which have been taken from Table E-8 of *NCHRP Report 368* for reinforced concrete beams and Table E-9 for prestressed concrete beams. Note that the assumption that D_2 can be reduced by the fraction of the lightweight density relative to the

normal weight density may not be entirely accurate as it is possible that some of the secondary structural elements such as the parapets and the diaphragms may not be constructed with lightweight concrete. Furthermore, the weight of ancillary items such as lighting structures and utility conduits will not change with the change in concrete material. However, the above measure of applying a reduced DC_{NCHRP} should be reasonable given that these auxiliary items would not likely have a large impact on the overall load on the structure. Regardless, Paczkowski and Nowak indicated that the dead load components carry the same bias factors and coefficients of variation regardless of the concrete density (*138*). The results for Eq. (143) are shown in Table 4-26.

The standard deviation for the total load effect, σ_Q, is another parameter that needs to be determined for reliability analysis. The calculation for the standard deviation of the total load effect including sand-lightweight concrete, $\sigma_{Q\ lwc}$, uses the results in Table 4-26, but requires additional steps. To begin, Nowak presented the coefficients of variation for dead load components in Table 1 of *NCHRP Report 368*, as reproduced in Table 4-27. Again, the assumption here is that these coefficients remain the same regardless of what type of concrete is used. According to Nowak, the coefficient of variation for the uncertainty in the load analysis, *E,* is for a simple span bridge, while the value for the live load including impact and live load analysis factor, *LP+I*, is for most spans in two-lane bridges.

Table 4-26. Modified dead load and mean total load effect for bridges with prestressed sand-lightweight concrete.

L_{span} (ft)		*NCHRP Report 368*					Modified LWC values		
	LL_{truck} (kip)	D_1 (kip)	D_2 (kip)	D_3 (kip)	LL_{truck} (kip)	μ_Q (kip)	$D_{1\ lwc}$ (kip)	$D_{2\ lwc}$ (kip)	$\mu_{Q\ lwc}$ (kip)
30	39	6	14	3	39	82	5	12	79
60	47	17	28	6	47	131	14	23	123
90	49	37	41	10	49	185	31	34	172
120	51	63	55	13	51	237	52	46	217
200	66	113	92	22	66	357	93	76	322

Table 4-27. Coefficients of variation for various load components, as suggested by Nowak

Load Component	*CoV*
Factory-made member, D_1	0.08
Cast-in-place member, D_2	0.10
Asphalt wearing surface, D_3	0.25
Live load with impact and analysis factor, $LP+I$	0.18
Uncertainty in load analysis, E	0.04

With the information in Tables 4-26 and 4-27, one can calculate the standard deviation of the individual load components using Eq. (107) in Section 2.4.2.2, seen below:

$$CoV_X = \frac{\sigma_X}{\mu_X} \quad \textbf{(107)}$$

For σ_{LP+I}, Nowak indicated that μ_{LP+I} is equal the live load multiplied by the dynamic load allowance along with the live load analysis factor, *P*. However, the author stated that *P* is equal to 1.0. Once the standard deviations of the components have been obtained, the combined standard deviation for all of the load components including sand-lightweight concrete, $\left(\sigma_{D_1+D_2+D_3+L+I}\right)_{lwc}$, can be calculated as:

$$\left(\sigma_{D_1+D_2+D_3+L+I}\right)_{lwc} = \sqrt{\sigma_{D_1\,lwc}{}^2 + \sigma_{D_2\,lwc}{}^2 + \sigma_{D_3}{}^2 + \sigma_{LP+I}{}^2} \quad \textbf{(144)}$$

Next, the combined coefficient of variation that includes the dead load of sand-lightweight concrete, $\left(CoV_{D_1+D_2+D_3+L+I}\right)_{lwc}$, is calculated as

$$\left(CoV_{D_1+D_2+D_3+L+I}\right)_{lwc} = \frac{\left(\sigma_{D_1+D_2+D_3+L+I}\right)_{lwc}}{\left(\mu_{D_1+D_2+D_3+L+I}\right)_{lwc}} \quad \textbf{(145)}$$

where $\left(\mu_{D_1+D_2+D_3+L+I}\right)_{lwc}$ is simply $\mu_{Q\,lwc}$. Meanwhile, the coefficient of variation for *Q* with sand-lightweight concrete, $CoV_{Q\,lwc}$, is computed as

$$CoV_{Q\,lwc} = \sqrt{CoV_E^2 + CoV_{D_1+D_2+D_3+L+I_{lwc}}{}^2} \quad \textbf{(146)}$$

Finally, one solves for $\sigma_{Q\,lwc}$ by inserting the result from Eq. (146) along with $\mu_{Q\,lwc}$ into Eq. (107). The results of these basic steps for finding the standard deviation of the loads including sand-lightweight concrete are displayed in Table 4-28.

Table 4-28. Standard deviations of the total load component, accounting for sand-lightweight concrete.

L_{span} (ft)	$\sigma_{D1\ lwc}$ (kip)	$\sigma_{D2\ lwc}$ (kip)	σ_{D3} (kip)	σ_{LP+I} (kip)	$(\sigma_{D1+D2+D3+L+I})_{lwc}$ (kip)	$(CoV_{D1+D2+D3+L+I})_{lwc}$	$CoV_{Q\ lwc}$	$\sigma_{Q\ lwc}$ (kip)
30	0	1	1	9	9	0.12	0.12	10
60	1	2	2	11	11	0.09	0.10	12
90	2	3	3	11	12	0.07	0.08	14
120	4	5	3	11	13	0.06	0.07	16
200	7	8	6	14	18	0.06	0.07	22

4.5.2.1.2 Resistance Parameters

The aforementioned mean values and coefficients of variation for the loads are separate from those statistical parameters used on the resistance side of the equation. As discussed in Section 2.4.2.1, the statistical parameters for resistance, λ_R and CoV_R, depend on the professional or modeling factor, fabrication factor, and material factor. The professional factor has already been discussed in Section 4.5.1. As for the fabrication parameters, this study assumes that the variabilities in fabrication issues are the same regardless of the density of the concrete being placed into the structure.

For the material factor, Nowak and Rakoczy indicated that lightweight concrete has mechanical properties that are similar to those of normal weight concrete, and in some cases even better (*151*). With specific reference to compressive strength, the authors noted that lightweight concrete had a slightly higher bias factor and a similar coefficient of variation compared to normal weight concrete. The reseachers provided Eq. (131) for estimating λ_M for lightweight concrete. However, a linear best-fit to their compressive strength data for lightweight concrete, shown in Table 4-29, gives a slightly different equation for the material bias factor:

$$\lambda_{M\ lwc} = -0.059 f_c' + 1.546 \qquad (147)$$

Note that the data in Table 4-29 only includes compression tests on standard 6 in. x 12 in. cylinders, where as the authors provided additional data for 4 in. x 8 in. specimens. Nowak and Rakoczy apparently kept this additional data separate from the "standard" cylinders because there was a concern that size could influence the comparisons versus the tests on normal weight

Table 4-29. Bias and coefficients of variation for the material factor for resistance, gleaned from data provided by Paczkowski and Nowak.

f'_c (ksi)	LWC		NWC	
	λ_M	CoV_M	λ_M	CoV_M
3.0	1.430	0.160	1.333	0.145
3.5	1.296	0.122	1.237	0.122
4.0	1.338	0.123	1.213	0.155
4.5	1.328	0.117	1.189	0.159
5.0	1.110	0.076	1.230	0.122
6.0			1.167	0.079
6.3	1.180	0.110		
6.8	1.190	0.120		
7.1	1.140	0.100		

concrete, which were conducted using the larger specimens. If the information from the smaller test samples were included, then $\lambda_{M\,lwc}$ would be nearly 10% larger. Thus, excluding the 4 in. x 8 in. sample tests from the material bias factor calculation is a slightly more conservative approach.

Regarding the normal weight data provided in Table 4-29, Nowak and Rakoczy indicated that information had been gathered from the earlier work of Nowak and Szerszen (*157*). However, the data in the two sources do not match, where λ_M from Nowak and Szerszen is greater than that of Nowak and Rakoczy, particularly for normal weight concretes with compressive strengths greater than 6 ksi. Even though using the Nowak and Rakoczy data requires extrapolation for concretes with 8 ksi and 10 ksi compressive strength, that data is used in the current reliability analysis because the Nowak and Rakoczy data set contains a greater number of samples. The normal weight data in Table 4-29 suggest that the material bias factor for normal weight concrete, $\lambda_{M\,nwc}$, can be approximated by the linear best fit equation

$$\lambda_{M\,nwc} = -0.043 f'_c + 1.413 \qquad (148)$$

According to Eq. (148), $\lambda_{M\,nwc}$ would be 1.07 and 0.99 for compressive strengths of 8 ksi and 10 ksi, respectively, with the average of these two values resulting in $\lambda_{FM\,nwc}$ being 1.03.

Taking similar steps for sand-lightweight concrete using Eq. (147) yields a value of 1.02 for $\lambda_{M\,lwc}$ for higher strength concretes. Now, recall from Table 2-7 in Section 2.4.3.1 that Nowak

reported that the combined material and fabrication factor for reinforced normal weight concrete containing shear reinforcement, λ_{FM}, was 1.13. Interestingly, multiplying that value by the ratio of $\lambda_{M\,lwc}$ versus $\lambda_{M\,nwc}$ yields 1.12 for a revised value of $\lambda_{FM\,lwc}$ for higher-strength, reinforced sand-lightweight concrete containing shear reinforcement. The 1.12 result is the same value that Paczkowski and Nowak used in their analysis for ϕ_v for bridges constructed with sand-lightweight concrete. Therefore, for this study, $\lambda_{FM\ lwc}$ for shear in prestressed concrete structures will be the same ratio of $\lambda_{M\ lwc}$ versus $\lambda_{M\ nwc}$ multiplied by $\lambda_{FM\ ps}$, which is the combined material and fabrication bias factor for the prestressed beams listed in Table 2-7. In other words, $\lambda_{FM\,lwc}$ for this study is 1.06.

On the other hand, Nowak and Rakoczy concluded that the coefficient of variation associated with the material factor should be the same for both lightweight and normal weight concrete, especially for concretes with higher compressive strengths. Therefore, this investigation shall retain the original CoV_{FM} value of 0.10 for prestressed members, as reported in Table 3 of *NCHRP Report 368*. This value is also the same value that Paczkowski and Nowak used in their analysis. The reason for focusing on the higher levels of compressive strength is that the beams in the current study had design strengths that were in the higher range.

4.5.2.1.3 Minimum Required Nominal Resistance

As discussed in Section 4.5.2.1.1 , the dead load component that is a part of the total load effect, Q, needed to be revised due to the differences in density between lightweight and normal weight concrete. This reduction in the dead load component also affects the minimum required nominal resistance, R_n. However, a more consequential change to R_n stems from load factors that have evolved over time. Under the 1989 AASHTO Standard Specifications for Highway Bridges, the required shear strength is one of two cases:

$$R_n \geq D + L + I \text{ (ASD)} \qquad \textbf{(149)}$$

$$R_n \geq \frac{1.3D + 2.17(L+I)}{\phi_v} \text{ (LFD)} \qquad \textbf{(150)}$$

For the 2010 AASHTO LRFD Bridge Design Specifications, the required shear strength using the Strength I load case is expressed by Eq. (132) in Section 2.4.3.2:

$$R_n = \frac{1.25DC + 1.5DW + 1.75(LL + IM)}{\phi_v} \qquad \textbf{(132)}$$

Note that Eq. (132) is slightly different from Eq. (98) in Section 2.4.2, where the earlier factor for live load was 1.70, which is what Nowak indicated was used in the original calibration of the LRFD code.

Nowak did not provide specific details as to how he achieved the minimum required resistance for both the Standard Specifications, R_{HS20}, and that proposed by Nowak, R_{LRFD}, as presented in Tables E-8 and E-9 of the *NCHRP Report 368*. Unfortunately, computations using the older versions of load components have failed to duplicate the results in the report. Attempts to match the values provided by the author considered different scenarios such as including/excluding the resistance factor, using different resistance factors, using the dynamic load allowances from Standard Specifications versus the LRFD Specifications, applying different load cases, and subtracting out the lane load from the dynamic load effect. The effect from the lane load was calculated as

$$LL_{lane} = \frac{0.64\text{klf} \cdot L_{span}}{2}$$

As best as can be discerned, the results for R_{HS20} in Table E-9 of the *NCHRP Report 368* for prestressed beams used the load factors in Eq. (150), but did not include the resistance factor, ϕ_v, since this alternative calculation made a perfect match with the values for girders spaced on 8-ft centers in Table E-9. Using the full version of Eq. (150) calculates values that are 10% greater than the published values while Eq. (149) calculates even lower values. This alternate scenario of excluding ϕ_v assumes that the HS20 load truck is the controlling live load and does not include the 0.64 klf lane load. A similar analysis examined R_{HS20} for the reinforced concrete data in the report. While the alternative of including the LFD load factors without the resistance factor did not match the given results, that scenario proved to give the best results, being between

0% and 4% of published values. Note that this analysis only considered beams that had a center-to-center spacing of 8 ft because Nowak indicated that girder spacing did not affect the results and the beams in the current study were designed for an 8-ft spacing.

Similar to the above query into R_{HS20}, there was an effort to achieve the same results for R_{LRFD} as presented in *NCHRP Report 368*. In the 1999 study, Nowak had indicated that the same load components used in calculating R_{HS20} were used to determine R_{LRFD}. While not explicitly given in the Table F-10 of the report, the values for R_{LRFD} for the shear capacity of simple span, prestressed concrete girders spaced at 8 ft are listed in terms of r, or the ratio of R_{LRFD} / R_{HS20}. Those ratios range from 1.06 to 1.26 when the assumed live load factor is 1.7 and $\phi_v = 0.90$. While inserting the load components from Table E-9 of the report along with $\phi_v = 0.90$ into Eq. (98) do not result in the same implicit values for R_{LRFD}, this scenario provides the closest match for prestressed girders, ranging from 0% to 8% greater than R_{LRFD}. Note that in this case, the lane load was included, but was not multiplied by *IM*. Similar calculations for the reinforced concrete beams indicate that the same scenario also gives the best results, although the required shear strengths in this analysis are about 3% to 4% *less than* what Nowak had calculated.

The reason for going through the above exercise is that the minimum required shear strength plays a role in the reliability analysis, as will be evidenced in Section 4.5.2.2. Because the exact method of determining either R_{HS20} or R_{LRFD} could not be deduced, the minimum required shear capacity for this study is the value of R_{LRFD} used in *NCRHP Report 368*, with the exception of the difference in dead load due to the difference in concrete unit weight. Therefore, the minimum required resistance to shear forces in a sand-lightweight concrete beam, R_{lwc}, is calculated as

$$\begin{aligned} R_{lwc} &= R_{NCHRP} - \frac{1.25}{\phi_v}(DC_{NCHRP} - DC_{lwc}) \\ &= R_{NCHRP} - \frac{1.25}{0.90}\left(DC_{NCHRP} - \frac{124.1\text{pcf}}{150\text{pcf}}DC_{NCHRP}\right) \\ R_{lwc} &= R_{NCHRP} - 0.24DC_{NCHRP} \end{aligned} \quad \textbf{(151)}$$

Note that 1.25 and ϕ_v = 0.90 are the respective load and resistance factors used in calculating R_{NCHRP} and must be accounted for when modifying the required minimum shear strength using sand-lightweight concrete. Also note that the live load factor that is implicit in Eq. (151) is different from the 1.75 factor in the 2010 AASHTO LRFD Bridge Design Specifications, which is what Paczkowski and Nowak used in their analysis for lightweight concrete. The reason for using the lower load factor is to establish a better head-to-head comparison to the original reliability indices in *NCHRP Report 368* for normal weight concrete. If using the greater live load factor, then the reliability index would be higher compared to when considering the 1.70 factor.

4.5.2.2 Method for Reliability Analysis

Having gathered all of the requisite information to perform a reliability analysis, one can follow the basic outline of the Rackwitz-Fiessler procedure, as discussed in Section 2.4.2.3. For the purposes of this study, a program was written using Mathcad to develop the resistance factors and corresponding reliability indices for different scenarios, incorporating the three design methodologies being investigated and various span lengths. The main program is shown in Figure E-1 of Appendix E, but there is also a subroutine given in Figure E-2 that is at the heart of the Rackwitz-Fiessler method. The steps for obtaining ϕ_v and β are given below by way of an example using *Appendix B5* to design a hypothetical prestressed sand-lightweight concrete bridge spanning 90 ft with girders spaced at 8 ft.

1. Enter the required inputs from the summaries in Tables 4-30 and 4-31. Note that $\mu_{Q\,lwc}$ and $\sigma_{Q\,lwc}$ are taken from Tables 4-26 and 4-28, while R_{HS20} is taken from *NCHRP Report 368*, Table F-10. The value *r* also comes from Table F-10, but is for the scenario where the live load factor is 1.7 and ϕ_v = 0.90 because these were the parameters that Nowak recommended in the report. Again, DC_{NCHRP} is $D_1 + D_2$, which have been taken from Table E-9 of *NCHRP Report 368*. The values for $\lambda_{FM\,lwc}$ and $CoV_{FM\,lwc}$ have been discussed in Section 4.5.2.1.2 , while the values for λ_P and CoV_P using the three different shear design methods under consideration come from Table 4-25 in Section 4.5.1. Lastly, the resistance factors for shear given in Table 4-31 were selected to provide a range of reliability indices. The program listed in Figure E-1 calculates β using the given

Table 4-30. Load parameters required for calculating reliability index of prestressed sand-lightweight beams.

L_{span} (ft)	$\mu_{Q\ lwc}$ (kip)	$\sigma_{Q\ lwc}$ (kip)	R_{HS20} (kip)	r	DC_{NCHRP} (kip)
30	79	10	140	1.06	20
60	123	12	196	1.16	45
90	172	14	246	1.22	78
120	217	16	303	1.26	118
200	322	22	460	1.22	205

Table 4-31. Resistance parameters required for calculating the reliability indices of prestressed sand-lightweight beams.

Design Method	$\lambda_{FM\ lwc}$	$CoV_{FM\ lwc}$	λ_P (kip)	CoV_P (kip)	ϕ_v
Appendix B5	1.12	0.10	1.58	0.19	0.90
General Procedure	1.12	0.10	1.76	0.15	0.90
Simplified Procecure	1.12	0.10	1.24	0.24	0.75

ϕ_v as well two other resistance factors that are in increments of 0.05 greater than ϕ_v listed in Table 4-31.

Therefore, the inputs needed for this example are:

L_{span} = 90 ft
$\mu_{Q.lwc}$ = 172 kip
$\sigma_{Q.lwc}$ = 14 kip
R_{HS20} = 246 kip
r = 1.22
DC_{NCHRP} = 78 kip
$\lambda_{FM.lwc}$ = 1.12
$CoV_{FM.lwc}$ = 0.10
λ_P = 1.58
CoV_P = 0.19
ϕ_v = 0.90

2. Calculate R_{NCHRP}.

$R_{NCHRP} = R_{HS20} \bullet r$
R_{NCHRP} = 246 kip•1.22
R_{NCHRP} = 300.12 kip

3. Calculate the modified minimum required resistance assuming sand-lightweight concrete, R_{lwc}.

$$R_{lwc} = R_{NCHRP} - 0.24DC_{NCHRP}$$
$$R_{lwc} = 300.12 \text{ kip} - 0.24 \bullet 78 \text{ kip}$$
$$R_{lwc} = 281.4 \text{ kip}$$

4. Calculate R_u by multiplying R_{lwc} by the resistance factor used in the 1999 study, that is, 0.90.

$$R_u = 0.90R_{lwc}$$
$$R_u = 0.90 \bullet 281.4 \text{ kip}$$
$$R_u = 253.26 \text{ kip}$$

5. Calculate a new theoretical nominal resistance R_n using the ϕ_v selected for the given shear design method, in this case, *Appendix B5*.

$$R_n = \frac{R_u}{\phi_v}$$
$$R_n = \frac{253.26 \text{ kip}}{0.90}$$
$$R_n = 281.4 \text{ kip}$$

6. Establish λ_R and CoV_R using the given parameters for the combined fabrication and materials factor and the professional factor.

$$\lambda_R = \lambda_{FM.lwc} \bullet \lambda_P$$
$$\lambda_R = 1.12 \bullet 1.58$$
$$\lambda_R = 1.77$$

$$CoV_R = \sqrt{CoV_{FM.lwc}^2 + CoV_P^2}$$
$$CoV_R = \sqrt{0.10^2 + 0.19^2}$$
$$CoV_R = 0.21$$

7. Go into the reliability subroutine, shown in Figure E-2. Calculate the mean resistance effect, μ_R as $\lambda_R R_n$. However, because the resistance is considered a lognormal variable,

one needs to convert both μ_R and σ_R into logarithmic form using Eqs. (106) and (105) from Section 2.4.2.2, respectively.

$$\mu_R = \lambda_R \bullet R_n$$
$$\mu_R = 1.77 \bullet 2.81.4 \text{ kip}$$
$$\mu_R = 497.97 \text{ kip}$$

$$\sigma_{\ln.R} = \sqrt{\ln\left(1 + CoV_R^{\,2}\right)}$$
$$\sigma_{\ln.R} = \sqrt{\ln\left(1 + 0.21^2\right)}$$
$$\sigma_{\ln.R} = 0.21$$

$$\mu_{\ln R} = \left(\ln\left(\frac{\mu_R}{\text{kip}}\right) - 0.5\sigma_{\ln.R}^{\,2}\right)\text{kip}$$
$$\mu_{\ln R} = \left(\ln\left(\frac{497.97 \text{ kip}}{\text{kip}}\right) - 0.5 \bullet 0.21^2\right)\text{kip}$$
$$\mu_{\ln R} = 6.19 \text{ kip}$$

8. For the first iteration, assume that r^* is at the midpoint between μ_R and μ_Q and let $q^* = r^*$. Be sure to use the normal form of μ_R, and not $\mu_{\ln R}$ for the first iteration. For the purposes of avoiding future iterations in this example, a specific value for r^* has been selected.

$$r^* = 192.88 \text{ kip}$$
$$q^* = r^*$$

9. Find equivalent mean and standard deviation for both the resistance and the load. Because R is assumed to be lognormal, σ_R^e and μ_R^e can be calculated using forms of Eqs. (126) and (127), respectively and reproduced below.

$$\sigma_R^e = r^* \sigma_{\ln R} \qquad \textbf{(126)}$$

$$\mu_R^e = r^*\left[1 - \ln\left(r^*\right) + \mu_{\ln R}\right] \qquad \textbf{(127)}$$

Because Q is assumed to be a normal variable, σ_Q^e and μ_Q^e are simply σ_Q and μ_Q, respectively.

$\sigma_{R.equiv} = r^* \bullet \sigma_{ln.R}$

$\sigma_{R.equiv} = 192.88\ kip \bullet 0.21$

$\sigma_{R.equiv} = 40.95\ kip$

$$\mu_{R.equiv} = r^* \bullet \left(1 - \ln\left(\frac{r^*}{kip}\right) + \frac{\mu_{lnR}}{kip}\right)$$

$$\mu_{R.equiv} = 192.88\ kip \bullet \left(1 - \ln\left(\frac{192.88\ kip}{kip}\right) + \frac{6.19\ kip}{kip}\right)$$

$\mu_{R.equiv} = 371.47\ kip$

$\sigma_{Q.lwc.equiv} = \sigma_{Q.lwc}$

$\mu_{Q.lwc.equiv} = \mu_{Q.lwc}$

10. Calculate the vector of reduced variables, $\{z^*\}$, where respective vector elements z_1^* and z_2^* are found for *R* and *Q* using Eq. (118) shown below.

$$z_i^* = \frac{x_i^* - \mu_{X_i}^e}{\sigma_{X_i}^e} \qquad \textbf{(118)}$$

$$z^*_1 = \frac{r^* - \mu_{R.lwc.equiv}}{\sigma_{R.lwc.equiv}}$$

$$z^*_1 = \frac{192.88\ kip - 371.47\ kip}{40.95\ kip}$$

$z^*_1 = -4.36$

$$z^*_2 = \frac{q^* - \mu_{Q.lwc.equiv}}{\sigma_{Q.lwc.equiv}}$$

$$z^*_2 = \frac{192.88\ kip - 172\ kip}{14\ kip}$$

$z^*_2 = 1.49$

11. Calculate the vector {G} using Eqs. (119) and (120), shown below.

$$\frac{\partial g}{\partial Z_i} = \frac{\partial g}{\partial X_i}\frac{\partial X_i}{\partial Z_i} = \frac{\partial g}{\partial X_i}\sigma_{X_i} \qquad \textbf{(119)}$$

$$\{G\} = \begin{Bmatrix} G_1 \\ G_2 \\ \vdots \\ G_n \end{Bmatrix} \text{ where } G_i = -\left.\frac{\partial g}{\partial Z_i}\right|_{\text{evaluated at the design point}} \quad \textbf{(120)}$$

As discussed in Section 2.4.2.3, the term σ_{X_i} must take on its equivalent form, $\sigma^{e}_{X_i}$, if the variable is lognormally distributed. Also note that in the case of this example, the limit state function $g = R - Q$ consists of first order terms, therefore,

$G_1 = -\sigma_{R.equiv}$
$G_1 = -40.95 \text{ kip}$

$G_2 = -(-1)\sigma_{Q.lwc}$
$G_2 = 14 \text{ kip}$

In vector form,

$$G = \begin{pmatrix} -40.95 \\ 14 \end{pmatrix} \text{kip}$$

12. Calculate the reliability index using Eq. (121), shown below.

$$\beta = \frac{\{G\}^T\{z^*\}}{\sqrt{\{G\}^T[\rho]\{G\}}} \quad \textbf{(121)}$$

Note that the variables R and Q are assumed to be uncorrelated; therefore, correlation matrix, $[\rho]$, becomes the identity matrix. Thus,

$$\beta = \frac{G^T \bullet z^*}{\sqrt{G^T \bullet \rho \bullet G}}$$

$$\beta = \frac{(-40.95 \quad 14)\text{kip} \bullet \begin{pmatrix} -4.36 \\ 1.49 \end{pmatrix}}{\sqrt{(-40.95 \quad 14)\text{kip} \bullet \begin{pmatrix} 1 & 0 \\ 0 & 1 \end{pmatrix} \bullet \begin{pmatrix} -40.95 \\ 14 \end{pmatrix} \text{kip}}}$$

$\beta = 4.61$

13. At this point, check to see if β is the same value as the previous iteration. If yes, then the iterations have converged on the calculated value for β. If not, then continue on to Step 14.

14. Calculate the α_n sensitivity factors using Eq. (123), given below

$$\{\alpha\} = \frac{[\rho]\{G\}}{\sqrt{\{G\}^T[\rho]\{G\}}} \qquad \textbf{(123)}$$

$$\alpha = \frac{\rho \cdot G}{\sqrt{G^T \cdot \rho \cdot G}}$$

$$\alpha = \frac{\begin{pmatrix}1 & 0\\ 0 & 1\end{pmatrix} \cdot \begin{pmatrix}-40.95\\ 14\end{pmatrix} \text{kip}}{\sqrt{(-40.95 \quad 14)\text{kip} \cdot \begin{pmatrix}1 & 0\\ 0 & 1\end{pmatrix} \cdot \begin{pmatrix}-40.95\\ 14\end{pmatrix} \text{kip}}}$$

$$\alpha = \begin{pmatrix}-0.95\\ 0.32\end{pmatrix}$$

15. Calculate new values for $n - 1$ reduced variables for a new design point by inserting the recently found α and β into Eq. (123) below.

$$z_i^* = \alpha_i \beta \qquad \textbf{(123)}$$

In the case of this example, where the limit state function only has two variables, only one reduced variable needs to be calculated.

$z^*_1 = \beta \cdot \alpha_1$

$z^*_1 = 4.61 \cdot (-0.95)$

$z^*_1 = -4.36$

16. Calculate the $n - 1$ variables, x_i^*, using the result from Step 14 in Eq. (118). In the case of this example, the reduced variable found above is associated with the resistance, r^*. Therefore,

$r^* = z^*_1 \cdot \sigma_{R.equiv} + \mu_{R.equiv}$

$r^* = -4.36 \cdot 40.95 \text{ kip} + 371.47 \text{ kip}$

$r^* = 192.88 \text{ kip}$

17. Use the result from Step 16 in Step 8 and reiterate the remaining steps until the values for β and $\{x_i^*\}$ converge.

18. Repeat Steps 1 through 17 for the other potential resistance factors and the other shear design models. The programs in Figure E-1 perform this function for three different values of ϕ_v for the three different shear design methodologies in this investigation. The results for 90-ft prestressed beams spaced at 8 ft, using the professional factors found from analysis of full-scale prestressed sand-lightweight concrete girders with all three of the shear design methods are:

$$\text{Reliability}_{90} = \begin{pmatrix} \phi_{A.B5} & R_{n\,A.B5}\ (\text{kip}) & \beta_{A.B5} & \phi_{Gen} & R_{n\,Gen}\ (\text{kip}) & \beta_{Gen} & \phi_{Sim} & R_{n\,Sim}\ (\text{kip}) & \beta_{Sim} \\ 0.90 & 281.4 & 4.61 & 0.90 & 281.40 & 5.96 & 0.70 & 361.80 & 3.89 \\ 0.95 & 266.59 & 4.37 & 0.95 & 266.59 & 5.68 & 0.75 & 337.68 & 3.63 \\ 1.00 & 253.26 & 4.14 & 1.00 & 253.26 & 5.41 & 0.80 & 316.58 & 3.39 \end{pmatrix}$$

4.5.2.3 Results from the Reliability Analysis

The reliability indices that result from following the above 18 steps and using the professional factor developed from 22 large-scale, prestressed lightweight concrete girders are shown in Table 4-32 and Figure 4-14. The table applies to prestressed sand-lightweight concrete beams that use the parameters that have been developed specifically for those beams, as shown in Tables 4-30 and 4-31. Also note that Table 4-32 also lists the β values given in Table F-10 of *NCRHP Report 368*; again the reliability indices from the report assume that $\gamma_{LL} = 1.70$ and $\phi_v = 0.90$.

Now, the reliability index depends in part on the particular resistance factor that is used. Therefore, Table 4-32 shows the results for three different levels of ϕ_v for each span length. For a given span length, the lowest value of ϕ_v for a given shear design model with the corresponding level of reliability that exceeds the target reliability index of 3.5 has been boldfaced. Amongst the various span lengths within a given shear model, the lowest overall boldfaced resistance factor with the lowest reliability index has been highlighted as a means of comparison of the relative degree of safety amongst the three shear design models. Note that in the case of the

Table 4-32. Results from reliability analysis for prestressed sand-lightweight concrete girders.

L_{span} (ft)	*Appendix B5*			*General*			*Simplified*			NCHRP β
	ϕ	R_n (kip)	β	ϕ	R_n (kip)	β	ϕ	R_n (kip)	β	
30	0.90	144	4.77	0.90	144	6.04	0.75	172	3.83	4.04
	0.95	136	4.54	0.95	136	5.77	***0.80***	162	***3.60***	
	1.00	129	***4.33***	***1.00***	129	***5.52***	0.85	152	3.38	
60	0.90	217	4.83	0.90	217	6.18	0.75	260	3.84	3.96
	0.95	205	4.60	0.95	205	5.90	***0.80***	244	***3.60***	
	1.00	195	***4.37***	***1.00***	195	***5.64***	0.85	229	3.38	
90	0.90	281	4.61	0.90	281	5.96	0.70	362	3.89	3.72
	0.95	267	4.37	0.95	267	5.68	***0.75***	338	***3.63***	
	1.00	253	***4.14***	***1.00***	253	***5.41***	0.80	317	3.39	
120	0.90	353	4.63	0.90	353	6.01	0.70	454	3.90	3.75
	0.95	335	4.39	0.95	335	5.72	***0.75***	424	***3.64***	
	1.00	318	***4.16***	***1.00***	318	***5.45***	0.80	398	3.39	
200	0.90	512	4.56	0.90	512	5.93	0.70	658	3.83	3.70
	0.95	485	4.31	0.95	485	5.64	***0.75***	614	***3.56***	
	1.00	461	***4.08***	***1.00***	461	***5.37***	0.80	576	3.32	

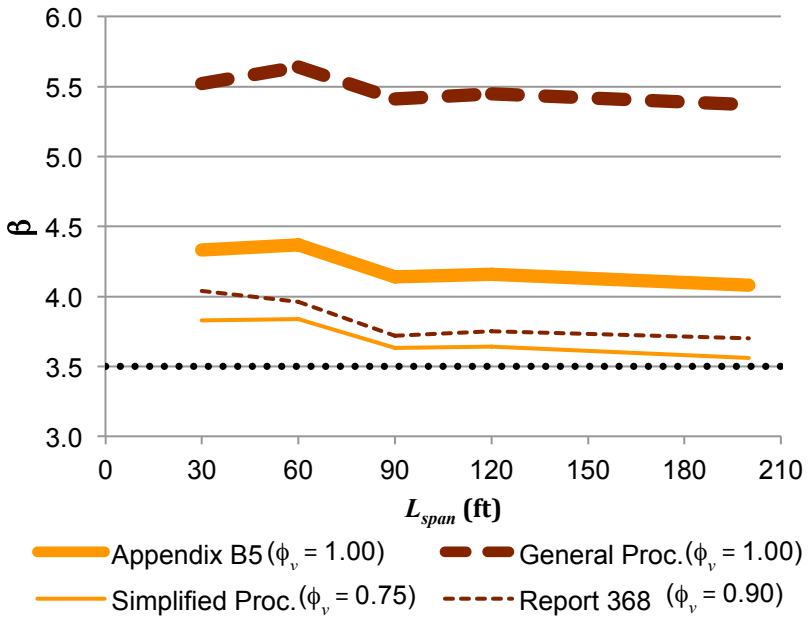

Figure 4-14. Reliability indices for a range of span lengths using the three shear design models under consideration in this study.

Simplified Procedure, some span lengths could have been designed with a strength reduction factor of 0.80. However, other spans needed the slightly lower value of 0.75 in order for β to exceed 3.5.

The lower value of ϕ_v is what is used for the *Simplified Procedure* in Figure 4-14, which graphs the reliability indices as a function of span length given the indicated value of ϕ_v. The graph also presents the results from *NCHRP Report 368* for comparison. Note the dotted line β = 3.5, which is the target reliability index according to the report. Looking at the figure, one can immediately see that the level of safety when using a resistance factor of 1.00 far exceeds the minimum level that was deemed acceptable in *NCHRP Report 368*, provided that the engineer is following *Appendix B5* or the *General Procedure*. If using the *Simplified Procedure*, however, then the designer would need to use a strength reduction factor of 0.75 to meet the reliability standards. Again, all of these results assume that the live load factor is 1.70, which is less than the current factor of 1.75. Increasing γ_{LL} would increase the value of β, thus giving the design a greater degree of safety if using the current design standards.

This study is not the first to recommend that a strength reduction factor of 1.00 be used in shear design. As indicated in Section 2.3.2.3, Clarke (*105*) suggested that ϕ_v could be removed from the calculations, particularly in the case of lightweight reinforced concrete beams containing stirrups. Granted, these beams were relatively small, and the test results were compared to the predictions from the 1985 version of the British design code BS 8110. Furthermore, Ahmad et al. (*106*) followed up Clarke's research with additional testing and concluded that ϕ_v for BS 8110 should be 0.85. Nevertheless, past research has recognized the potential for shear design provisions to be exceedingly conservative.

Certainly, maintaining a single value for ϕ_v across the three shear design methods would help to instill some semblance of simplicity in what is already a rather complicated calculation. If one were to adopt a unified reduction factor, then that value would have to be 0.75, because any ϕ_v greater than 0.75 would generate designs using the *Simplified Procedure* with a degree of safety that is less than desired. However, Table 4-32 clearly shows that the strength reduction factors resulting from calculations using *Appendix B5* and the *General Procedure* are greatly different

from that of the *Simplified Procedure*. Using the unified ϕ_v value for either of these two methods would dramatically penalize the calculated strength of a given bridge design. Therefore, if the design models are going to remain in their present form, the conclusion is that there should be two values for ϕ_v. If the engineer chooses to follow the *Simplified Procedure*, then the strength reduction factor for shear design of prestressed, sand-lightweight concrete girders should be 0.75. If instead, the designer follows the more laborious methods in *Appendix B5* or the *General Procedure*, then that strength reduction factor should be 1.00. One method with its corresponding ϕ_v factor is not inherently advantageous over another, as suggested by Table 4-33. In some of the designs both from this current study as well as past research on prestressed, lightweight concrete girders, the predicted shear strength using the methods in *Appendix B5* or the *General Procedure* combined with a ϕ_v factor of 1.00 would turn out to be greater than that predicted by the *Simplified Procedure* and its strength reduction factor of 0.75. In other cases, the opposite is true.

Figures 4-15 and 4-16 show the factored shear strengths using *Appendix B5* and the *General Procedure*, respectively, relative to the factored shear strength using the *Simplified Procedure*. These figures compare the ratios with the same parameters discussed in Section 4.2.2, that is, reinforcing index, concrete compressive strength, effective shear depth, shear span-to-effective shear depth ratio, and cross-sectional area. Note that the factored strengths use the recommended resistance factors for the given design procedures as discussed above and ignore the modification factor for lightweight concrete. Looking at Figures 4-15 and 4-16, the one case where there is a clear trend is the graph of $\phi_{Gen}V_{n.Gen}/\phi_{Sim}V_{n.Sim}$ versus the reinforcing index, which shows an inverse relationship. If the reinforcing index was greater than 425 psi, then the *Simplified Procedure* generated a larger shear strength when using the recommended resistance factors. While the examined parameters do not exhibit a strong overall influence on the ratio of $\phi_{A.B5}V_{n.A.B5}$ versus $\phi_{Sim}V_{n.Sim}$, the lower limits for a couple of the parameters within this analsysis do show some interesting results. If a beam had no shear reinforcement, then the factored shear strength was much higher when following *Appendix B5* compared to the *Simplified Procedure*. The same is true when the effective shear depth was about 28 in. and the cross-sectional area was about 470 in^2.

Table 4-33. Factored nominal shear strengths using the recommended ϕ_v factors for the respective AASHTO design methods.

Researcher	Test ID	V_{Exp} (kip)	$V_{n\,A.B5}$ No λ_v (kip)	$V_{n.Gen}$ No λ_v (kip)	$V_{n.Sim}$ No λ_v (kip)	$\phi_{A.B5}V_{n\,A.B5}$ No λ_v (kip)	$\phi_{Gen}V_{n.Gen}$ No λ_v (kip)	$\phi_{Sim}V_{n.Sim}$ No λ_v (kip)	$\frac{\phi_{A.B5}V_{n\,A.B5}}{\phi_{Sim}V_{n\,Sim}}$	$\frac{\phi_{Gen}V_{n\,Gen}}{\phi_{Sim}V_{n\,Sim}}$
Current Study	T2.8.Typ.1	361	222	207	339	222	207	254	0.87	0.82
	T2.8.Typ.2	292	199	188	311	199	188	233	0.85	0.80
	T2.8.Min.1	382	194	182	284	194	182	213	0.91	0.85
	T2.8.Min.2	308	186	173	277	186	173	208	0.89	0.83
	BT.8.Typ.1	500	312	293	373	312	293	279	1.12	1.05
	BT.8.Typ.2	407	284	273	335	284	273	251	1.13	1.09
	BT.10.Typ.1	518	291	283	348	291	283	261	1.11	1.08
	BT.10.Typ.2	428	273	265	334	273	265	251	1.09	1.06
	BT.10.Min.1	475	232	233	244	232	233	183	1.27	1.27
	BT.10.Min.2	371	232	235	240	232	235	180	1.29	1.30
Malone	PC6N	80	59	47	49	59	47	37	1.61	1.28
	PC6S	117	75	75	83	75	75	62	1.20	1.20
	PC10N	105	65	54	60	65	54	45	1.44	1.20
	PC10S	120	81	83	93	81	83	70	1.16	1.19
Kahn et al.	G1A-East	363	248	155	335	248	155	251	0.99	0.62
	G1A-Center	258	139	134	186	139	134	140	1.00	0.96
	G1B-East	312	440	266	574	440	266	431	1.02	0.62
	G1B-Center	234	130	124	187	130	124	140	0.93	0.88
	G1C-East	289	245	156	338	245	156	254	0.97	0.62
	G2A-Center	256	141	136	188	141	136	141	1.00	0.96
	G2B-Center	246	132	125	191	132	125	143	0.92	0.87
Dymond et al.	web-shear	658	527	425	670	527	425	503	1.05	0.85

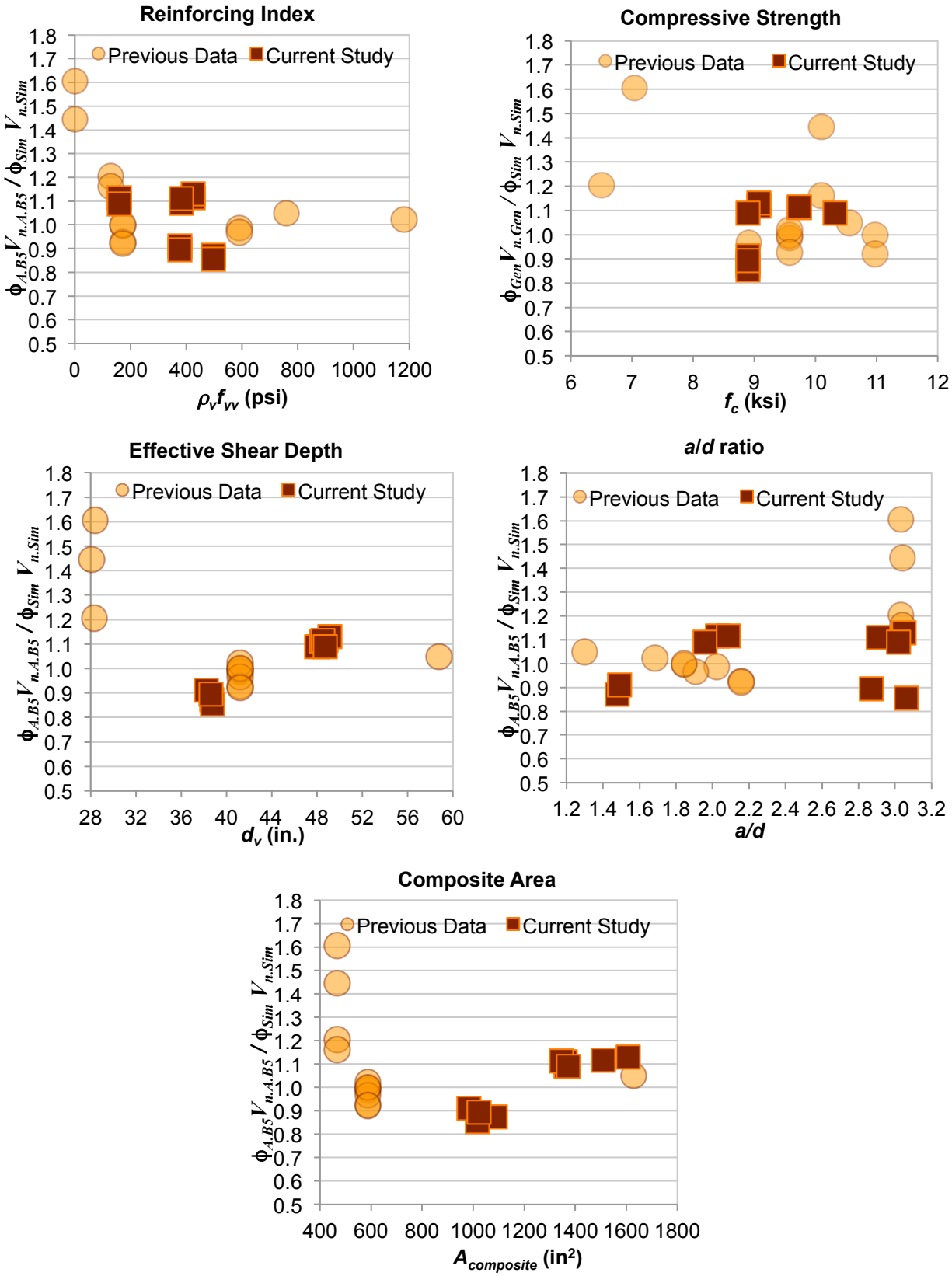

Figure 4-15. Ratio of $\phi V_{n.A.B5}$ versus $\phi V_{n.Sim}$ as a function of various parameters, using the recommended resistance factors for each procedure and assuming no λ_v.

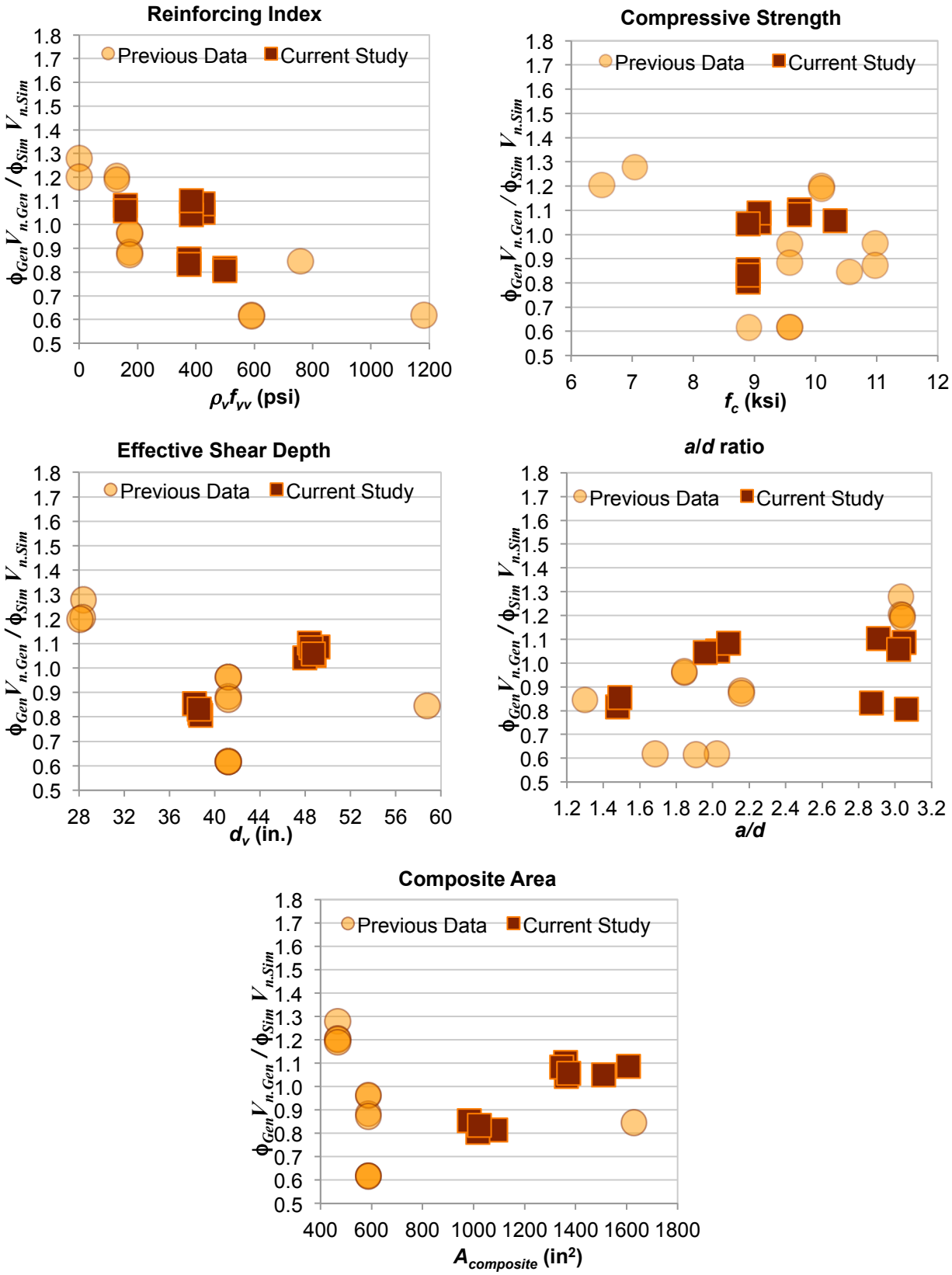

Figure 4-16. Ratio of $\phi V_{n.Gen}$ versus $\phi V_{n.Sim}$ as a function of various parameters, using the recommended resistance factors for each procedure and assuming no λ_v.

As a way of comparison, a second investigation carried out a similar exercise using λ_P and CoV_P developed from 174 lightweight concrete beam tests, without regard to the level of prestressing or amount of shear reinforcement (see Table 4-25). The results of applying this alternative professional factor to the reliability analysis of prestressed lightweight girders are in Table 4-34. In order to achieve the target reliability index, the controlling ϕ_v value using the alternate λ_P would be 0.50 for *Appendix B5* and the *General Procedure*, while that value would need to be 0.45 for the *Simplified Procedure*. Such a strength reduction factor is entirely impractical. Even Paczkowski and Nowak did not go that low in recommending the resistance factor for lightweight concrete. Instead, the authors suggested that ϕ_v should be 0.80 even though the researchers used the larger live load factor of 1.75, as discussed in Section 2.4.3.2. Again, however, the authors' recommendation for ϕ_v was largely affected by the professional factor that Paczkowski and Nowak had determined through their own analysis, which is dramatically lower than the value obtained in this study.

Table 4-34. Results from reliability analysis for prestressed sand-lightweight concrete girders using professional factor determined from all lightweight concrete beam tests

L_{span} (ft)	*Appendix B5*			*General*			*Simplified*			NCHRP β
	ϕ	R_n (kip)	β	ϕ	R_n (kip)	β	ϕ	R_n (kip)	β	
30	0.50	258	3.8	0.50	258	3.79	0.40	323	4.08	4.04
	0.55	235	***3.55***	***0.55***	235	***3.54***	***0.45***	287	***3.76***	
	0.60	215	3.33	0.60	215	3.31	0.50	258	3.48	
60	0.50	390	3.78	0.50	390	3.77	0.40	487	4.07	3.96
	0.55	354	***3.53***	***0.55***	354	***3.52***	***0.45***	433	***3.75***	
	0.60	325	3.31	0.60	325	3.28	0.50	390	3.46	
90	0.45	563	3.9	0.45	563	3.89	0.40	633	3.91	3.72
	0.50	507	***3.62***	***0.50***	507	***3.61***	***0.45***	563	***3.58***	
	0.55	460	3.37	0.55	460	3.35	0.50	507	3.29	
120	0.45	707	3.91	0.45	707	3.9	0.40	795	3.91	3.75
	0.50	636	***3.63***	***0.50***	636	***3.61***	***0.45***	707	***3.58***	
	0.55	578	3.37	0.55	578	3.35	0.50	63	3.29	
200	0.45	1024	3.85	0.45	1024	3.84	0.40	1152	3.86	3.70
	0.50	922	***3.57***	***0.50***	922	***3.55***	***0.45***	1024	***3.53***	
	0.55	838	3.32	0.55	838	3.29	0.50	922	3.23	

However, using ϕ_v = 1.00 for sand-lightweight concrete versus the 0.90 value that Nowak recommended for normal weight concrete in *NCHRP Report 368* does not necessarily mean that designing with sand-lightweight concrete is by any means "safer" than ordinary concrete. Instead, there is the great potential that shear design of concrete beams in general is inherently conservative. The principle reason is that the original professional factors used in calibrating the strength reduction factors in 1999 were based on tests that do not accurately reflect the true nature of today's concrete bridges, that is those bridges with prestressed girders containing relatively high strength concrete and having relatively large composite cross-sectional areas. Perhaps re-analysis of the professional factor considering similar beams in the current study but constructed with normal weight concrete would yield different results. That analysis, however, should be the focus of another study.

Chapter 5

Conclusions and Recommendations

5.1 Conclusions

5.1.1 Summary

This study consisted of a series of twelve shear tests on six full-scale, prestressed girders with composite sand-lightweight concrete decks. All of the beams were simply-supported and subjected to two concentrated loads. Five of the six beams were constructed with sand-lightweight concrete, while the sixth girder contained normal weight concrete to provide two comparisons with its lightweight counterpart. All of the girders were designed for both shear and flexure according to the procedures of the 2007 AASHTO LRFD Bridge Design Specifications. Aside from unit weight, other variables included compressive strength, effective shear depth, shear span-to-effective shear depth ratio, shear reinforcing index, and composite cross-sectional area.

The purpose of these twelve tests was to instill greater confidence in the shear strength of prestressed, sand-lightweight concrete bridge girders. This objective has been achieved by comparing experimental results with the predicted strength calculations using the three shear design procedures found in the AASHTO bridge design code. Additionally, the reliability of those predicted strengths have been calculated using the results of this study as well as past shear tests on large-scale, sand-lightweight concrete beams.

Overall, the lightweight girders performed exceptionally well relative to their predicted shear strengths according to the 2010 AASHTO LRFD Bridge Design Specifications. Comparisons between similar designs for lightweight versus normal weight concrete indicate that the two concrete types have similar levels of performance. Furthermore, calculations show that

including the modification factor for sand-lightweight concrete has only a marginal effect on the predicted shear strength, and thus, is unnecessary. Analysis of the ten lightweight concrete shear test in this investigation along with the other twelve results involving large-scale lightweight concrete beams that have been conducted in the past show that the strength reduction factor dictated by the 2010 AASHTO LRFD Bridge Design Specifications is too conservative for the shear strength of prestressed, sand-lightweight concrete girders. Additional detailed conclusions appear below.

5.1.2 Overall Shear Strength

- All beams exceeded their expected shear capacities calculated using *Appendix B5* and the *General Procedure*. The same is true for the *Simplified Procedure* with the exception of one test.

- The *Simplified Procedure* is the least conservative predictor of shear strength. The *General Procedure* is marginally more conservative than *Appendix B5*, with the difference between the average experimental-to-theoretical ratios of these two methods being less than 4 percent. The averages and corresponding coefficients of variation for the twelve load tests from this study are given in Table 5-1 below. Had the load and resistance factors dictated by the 2010 AASHTO LRFD Bridge Design Specifications been included in the analysis, then the predicted shear strengths would have been lower, thus making the ratios of V_{Exp}/V_{calc} even larger.

Table 5-1. Summary statistics for experimental-to-predicted ratios for shear strength.

Shear Design Method	with λ_v		no λ_v	
	Average	CoV	Average	CoV
Appendix B5	1.70	0.11	1.67	0.11
General Procedure	1.76	0.11	1.73	0.11
Simplified Procedure	1.35	0.20	1.33	0.19

- All of the experimental girders that failed in shear exhibited signs of failure at or near the critical section even though the calculations predicted that roughly half of the failures would occur at or near the load closest to the abutment in the four-point load test.

- Consistent with the other tests in this investigation, the *Simplified Procedure* produced less conservative estimates for the beams with minimum reinforcement. Nevertheless, the minimally reinforced beams had higher experimental-to-calculated strength ratios compared to their counterparts having "typical" reinforcement. For the four tests containing minimum reinforcement, the average percentage rise in force in the stirrups after the initial sudden increase at web-shear cracking was 26% with a coefficient of variation of 42%. However, so many of the stirrups intersecting the boundary cracks in these minimally reinforced girders yielded upon first web cracking, thus giving rise to the concern that there's potential for a beam to fail in a brittle fashion should the load exceed the web-cracking strength. Unfortunately, making a definitive conclusion regarding the sufficiency of the minimum requirements for shear reinforcement for girders constructed with sand-lightweight concrete is not appropriate at this time because the actual amount of steel supplied in this investigation is substantially larger than what is dictated in the 2010 AASHTO LRFD Bridge Design Specifications.

5.1.3 Parametric Effects on Shear Strength

- The experimental strength decreases relative to the expected strength as the amount of vertical reinforcement increases. This observation is particularly true for the *Simplified Procedure*.

- V_{Exp}/V_{calc} tends to increase as the compressive strength of concrete increases. However, there is still a gap in the available database of full-scale, prestressed lightweight concrete girders with compressive strengths between 7 ksi and 9 ksi because the girders in this study designed for 8 ksi compressive strength had much higher strengths.

- The results from this study contradict previous research where the calculated strengths for beams tested at a shear span-to-effective depth ratio less than 2.0 are more conservative than those tests where a/d is around 3.0.

- The *General Procedure* does a somewhat decent job at incorporating d_v and consistently predicting the shear strength across the range of effective shear depths varying from 28 in.

to 52 in. Analyses of past and current results using the other two AASHTO shear design methods yield contradictory and inconclusive results regarding the effective shear depth.

- The cross-sectional area does not have much of an impact on the relationship between experimental shear strengths of beams constructed with sand-lightweight concrete and the predicted strengths using any of the three AASHTO design methods.

5.1.4 Component Contribution to the Shear Capacity

- The average ratio of shear resisted by the concrete at the time cracks appeared in the web versus the ultimate failure load was 53% with a coefficient of variation of 10%. V_{cw} was larger for a shorter shear span compared to a longer shear span. However, in any given beam, the relative ratio of V_{cw}/V_{Exp} had mixed results, where this ratio proved to be larger for the shorter shear span in only half of the girders that were tested. Regardless, V_{cw} for all of the tests far exceeded the service loads for shear in the original design beams.

- Over the course of the entire test, V_c tended to increase as the testing continued to the ultimate load. At ultimate, the concrete provided nearly half if not most of the shear resistance in a majority of the tests, where V_c virtually doubled if not more so from the time of first web-shear cracking to test termination. However, all three shear design methods tended to under predict the concrete contribution to shear resistance. For example, the average ratio of $V_{c\,Exp}/V_{c\,calc}$ for *Appendix B5* was 3.29 with a coefficient of variation of 0.31, when disregarding the modification factor for sand-lightweight concrete in the calculations. Both $V_{c\,Exp}$ and the ratio $V_{c\,Exp}/V_{c\,calc}$ tended to be larger for shorter span lengths compared to longer span lengths.

- The results were mixed for both $V_{c\,Exp}$ and V_{cw} when comparing similar beams with different amounts of reinforcement.

- The average percentage increase in the force in the stirrups after concrete cracking was 34%, although the coefficient of variation for this percentage change was 41%. This result

indicates that, despite some stirrups yielding at first cracking, there was still a substantial amount of additional shear resistance remaining in the stirrups.

- The code-calculated values for V_s matched fairly closely with what has been determined from experimentation, although the *Simplified Procedure* over-predicted the strength provided by the vertical reinforcement, with the average ratio of $V_{s\,Exp}$ versus $V_{s\,Sim}$ being 0.97 when excluding the sand-lightweight concrete modifier. The average $V_{s\,Exp}/V_{s\,calc}$ ratio was larger for the longer shear span tested in each beam.

5.1.5 Lightweight Modification Factor

- There are no distinct structural differences between girders constructed with sand-lightweight and normal weight concrete when it comes to shear strength. Specifically, the results were mixed when considering V_{cw}, $V_{c\,Exp}$, the ratio $V_{c\,Exp}/V_{cw}$, and the percentage increase in the amount of shear force resisted by the vertical reinforcement after web-shear cracking. In terms of the ratio $V_{c\,Exp}/V_{Exp}$, the two tests on the lightweight girder had the same average result as its normal weight counterpart, although the coefficient of variation was higher for the lightweight tests. Even when the lightweight concrete has a lower tensile splitting strength, this characteristic does not necessarily translate into reduced web-shear cracking strength. Of course, this conclusion is only based on head-to-head comparisons of two sets of tests of girders with composite decks, so making any firm statements regarding this issue is not realistic.

- Although the shear reinforcing index in the lightweight beam was 60% greater than its normal weight companion, the total force in the transverse steel at ultimate capacity was the same when comparing the first tests of each girder. For the second tests on each girder, $V_{s\,Exp}$ was only 22% greater in the lightweight girder.

- The angle of rotation to the principal stress just prior to web cracking was slightly lower in the lightweight girder compared to its normal weight companion beam. However, the median crack angle measured on the web proved to be larger in the lightweight girder, regardless of the shear span length.

- Looking at the overall shear capacity, the ratio of experimental versus calculated shear strengths were marginally lower for the lightweight girders compared to the normal weight beams. However, the effect of using a modification factor for sand-lightweight concrete in the calculations for shear strength is virtually irrelevant. In fact, using the modification factor for sand-lightweight concrete can lead to *greater* predicted shear capacity. Furthermore, the inherent amount of conservatism in the AASHTO LRFD calculations should give further assurance in abandoning the modifier for sand-lightweight concrete.

- When excluding the sand-lightweight modifier, the calculated angle of inclination of diagonal stresses is greater than those calculations that do include the modifier; however, the difference is relatively minor, ranging from 0.2 degrees to 1.3 degrees.

- Conversely, the β-factor relating to the shear capacity of concrete is slightly smaller when the sand-lightweight modifier is not considered in the strength calculations compared to when the modifier is included. This observation suggests that lightweight concrete has greater ability to transmit tension across the shear cracks, even though there has been no evidence to support such a claim. Of course, the modification to $\sqrt{f'_c}$ using λ_v counteracts the larger β when calculating V_c.

5.1.6 Angle of Inclination of Diagonal Concrete Cracking in the Web

- The predicted cracking angle of inclination of diagonal compression tends to be about the same as or below the angle of cracking and the angle of rotation to the principal stresses that have been found experimentally. The *Simplified Procedure* calculates an angle that is consistently lower than the other two shear design methods, resulting in a larger theoretical contribution from the shear reinforcement, which in turn leads to a higher predicted ultimate shear strength and the least conservative shear strength prediction.

- There can be fairly large swings in the predicted shear strength when using the angle of diagonal compression determined from experimental measurements instead of the theoretical angle determined from the 2010 AASHTO LRFD Bridge Design Specifications. Thus, the impact of θ should not be disregarded in a general formulation for V_n.

- The results are mixed regarding the comparison between the measured cracking angle and the angle of rotation to the principal compressive stress. $\theta_{prin\ pre\text{-}V_{cw}}$ fell within the range of the actual crack angles only one-fourth of the time. In the remaining cases, $\theta_{prin\ pre\text{-}V_{cw}}$ was typically lower than the theoretical angle. $\theta_{prin\ last}$ only had a marginally better success rate of being within the range of calculated angles.

- The AASHTO code incorrectly calculated the angle of the crack leading to failure about half of the time regardless of which shear design procedure was used to estimate the angle. Of the calculations that missed their mark, there was a mix of those that over predicted the cracking angle and those that under-predicted.

5.1.7 β-factor for Shear Capacity of Concrete

- The ratio $\beta_{\lambda_v} / \beta_{\text{no}\,\lambda_v}$ for both *Appendix B5* and the *General Procedure* is marginally higher for 10 ksi concrete compared to 8 ksi concrete.

- With that said, β for lightweight concrete beams with 8 ksi design strength is quite a bit larger when calculated using the tabular process in *Appendix B5* compared to the equation from the *General Procedure*. On the other hand, *Appendix B5* results in a β that is considerably smaller than the *General Procedure* for normal weight beams and the lightweight concrete girders with 10 ksi design strength. Therefore, *Appendix B5* tends to be slightly less conservative when calculating V_c for the lightweight 8-ksi beams while slightly more conservative for the remaining girders compared to the *General Procedure*.

5.1.8 Strength Reduction Factor for Shear

- Based on a data set of 22 shear tests of large-scale prestressed, sand-lightweight concrete girders, the professional factors using *Appendix B5*, the *General Procedure* and the *Simplified Procedure* are 1.58, 1.76 and 1.24, respectively. The corresponding coefficients of variations are 0.19, 0.15 and 0.24, respectively.

- Based on a couple of assumptions and some modifications to the input provided in *NCHRP Report* 368, the reliability index of prestressed, sand-lightweight structures exceeds the target reliability index of 3.5 even when the resistance factor is set equal to 1.00 for shear strength calculations involving *Appendix B5* or the *General Procedure*. On the other hand, the reliability results for the *Simplified Procedure* suggest that ϕ_v should be set at 0.75, which is still an increase from 0.70 in the 2010 AASHTO LRFD Bridge Design Specifications. Note that this conclusion only applies to prestressed, sand-lightweight concrete girders. If the analysis were to include professional factors calculated from past test results on reinforced lightweight concrete beams, then the resistance factor would need to be impractically low in order to achieve the target reliability index.

- Using a unified ϕ_v value that would be adequate for all three of the shear design methods in the 2010 AASHTO LRFD Bridge Design Specifications would dramatically penalize the calculated strength of a given bridge design when following *Appendix B5* or the *General Procedure*. On the other hand, designing with one method and its corresponding ϕ_v factor is not inherently advantageous over another. In some cases, the predicted shear strength using the methods in *Appendix B5* or the *General Procedure* combined with a ϕ_v factor of 1.00 would turn out to be greater than that predicted by the *Simplified Procedure* and its strength reduction factor of 0.75. In other cases, the opposite is true.

5.2 Recommendations

Based on the conclusions reached in Section 5.1, below are the following recommendations regarding the 2010 AASHTO LRFD Bridge Design Specifications:

1. Eliminate the modification factor for prestressed, sand-lightweight concrete girders.

2. Employ a multiple strength-reduction approach to the shear design of prestressed, sand-lightweight concrete girders. Engineers calculating shear strengths using *Appendix B5* or the *General Procedure* can use $\phi_v = 1.00$, while those calculations following the *Simplified Procedure* should include a value of $\phi_v = 0.75$. While such a specification will make the

design process slightly more complicated, this approach will also allow for more efficient bridge designs while maintaining a satisfactory level of safety.

3. The *General Procedure* in Article 5.8.3.4.2 of the 2010 AASHTO LRFD Bridge Design Specifications is an acceptable alternative to the process in *Appendix B5*. In terms of strength analysis, however, the equations for calculating β and θ in the *General Procedure* only offer a small degree of simplification over the original MCFT procedures that are in *Appendix B5* and tend to be slightly more conservative.

4. AASHTO should consider limiting the predicted strength of sand-lightweight concrete girders when designing with the *Simplified Procedure*. This limit should be based on the shear reinforcement index.

5.3 Recommendations for Future Research

- Despite the intention of filling in the gaps in available data considering various parameters that could affect the ratio of experimental versus theoretical shear strengths, there still is not a lot of data for concrete compressive strengths ranging from 8 ksi to 9 ksi or for shear span-to-effective shear depth ratios ranging from 2.2 to 2.8. Additional testing on full-scale prestressed, sand-lightweight concrete girders encompassing these parameters may be prudent for confirming the trends observed in this study.

- As suggested in Section 4.2.1, none of the beams in this study experienced a flexure-shear failure mode. Additional testing on full-scale prestressed, sand-lightweight concrete girders should be designed to result in flexure-shear failures to assess the effectiveness of the AASHTO LRFD Bridge Design Specifications in predicting this type of failure.

- Another goal in this study that was not achieved was to examine the performance of prestressed, sand-lightweight concrete girders with a minimum amount of shear reinforcement. While this study did follow the AASHTO code regarding this issue, the decision to use No. 4 bar to mimic what would have been used in an actual design resulted in the maximum rebar spacing being the controlling specification instead of the minimum

area of steel. Additional testing should be done with the minimum area of vertical reinforcement to assess the effectiveness of the AASHTO provisions regarding this issue for prestressed, sand-lightweight concrete girders.

- Additional testing can be performed on both normal weight and lightweight concrete beams to confirm the conclusion that there should be some sort of limit placed on the shear reinforcing index to ensure that the actual beam strength is greater than or equal to the predicted shear strength, particularly when using the *Simplified Procedure* in the AASHTO LRFD Bridge Design Specifications.

- Tests of full-scale, prestressed normal weight concrete girders should be considered to see if the shear reinforcing index has an inverse relationship with the ratio of experimental versus calculated shear strength when using the *Simplified Procedure*, and if so, what the limit on that index should be.

- Future full-scale testing should be conducted on full-scale prestressed, lightweight concrete girders versus normal weight girders with the same cross-sections and the same stirrup spacing to provide a greater number of head-to-head comparisons. These results may affirm the conclusion that the shear strength of sand-lightweight concrete does not deserve to be penalized.

- Using the data on full-scale, prestressed sand-lightweight concrete girders collected in this study, other shear design methodologies can be analyzed for their accuracy and compared to the performance of the three procedures endorsed by AASHTO.

- Experimental resolution of the concrete component of shear strength in beams remains elusive. If more efficient methods of measuring the force in concrete develop in the future, such as photogrammetry on the surface of the structure or extensive instrumentation within the concrete web, then perhaps researchers could obtain more accurate means of calculating this quantity.

- Additional analytical work can be done for determining the angle of inclination of diagonal compressive stresses. An improved angle calculation could result in more accurate prediction of shear strength. Of course, improving the strength prediction may result in the need for adjusting the strength reduction factor in order to maintain the desired reliability index.

- Given the conclusions regarding the reliability analysis of the shear strength of full-scale prestressed, sand-lightweight concrete girders, analysis should be conducted on existing data of full-scale prestressed normal weight concrete girders to determine if the professional factors, and hence the strength reduction factors, can be increased while satisfying the established target reliability index of 3.5. The beams in this analysis should be reflective of those girders constructed in actual bridges, including concrete compressive strength, beam depth, amount of prestress force, cross-sectional shape and area, and loading configuration.

References

1. FHWA. Deficient Bridges by State and Highway System. 2010. http://www.fhwa.dot.gov/bridge/nbi/defbr10.cfm. Accessed June 16, 2011.
2. Shoup, L., N. Donohue and M. Lang. *The Fix We're In For: The State of Our Nation's Bridges*. Transportation for America, Washington, D.C., 2011.
3. Chandra, S. and L. Berntsson. *Lightweight Aggregate Concrete: Science, Technology, and Applications*. William Andrew Publishing, Norwich, N.Y., 2002.
4. Expanded Shale, Clay and Slate Institute. *Lightweight Concrete - History, Application, Economics*. Salt Lake City, Utah, 1971.
5. ACI Committee 613. Recommended Practice for Selecting Proportions for Structural Lightweight Concrete. *Journal Proceedings of the American Concrete Institute*, Vol. 55, No. 9, 1958, pp. 305-314.
6. Shideler, J. J. *Bulletin D40: Manufacture and Use of Lightweight Aggregates for Structural Concrete*. Portland Cement Association, 1961, pp. 3-14.
7. ACI Committee 213. *ACI 213R-87: Guide for Structural Lighweight Aggregate Concrete*. American Concrete Institute, Farmington Hills, MI, 1987.
8. ACI Committee 213. *ACI 213R-03: Guide for Structural Lighweight-Aggregate Concrete*. American Concrete Institute, Farmington Hills, MI, 2003.
9. Castrodale, R. W. Lightweight Concrete for Accelerated Bridge Construction. Presented at the 2011 Annual Virginia Concrete Conference, Richmond, Va., Mar. 3-4, 2011.
10. U. S. Energy Information Administration. Weekly Retail Gasoline & Diesel Prices. http://www.eia.gov/dnav/pet/hist/LeafHandler.ashx?n=pet&s=emd_epd2d_pte_nus_dpg&f=w. Accessed Feb. 23, 2011.
11. Bardhan-Roy, B. K. Design Considerations for Presressed Lightweight Aggregate Concrete. *Proc.*, *the 2nd International Congress on Lightweight Concrete*, London, England, 1980.
12. AASHTO. *AASHTO LRFD Bridge Design Specifications*, 4th ed. American Association of State Highway and Transportation Officials, Washington, D.C., 2007.
13. AASHTO. *AASHTO LRFD Bridge Design Specifications*, 4th ed. American Association of State Highway and Transportation Officials, Washington, D.C., 2008.

1. FHWA. Deficient Bridges by State and Highway System. 2010. http://www.fhwa.dot.gov/bridge/nbi/defbr10.cfm. Accessed June 16, 2011.
2. Shoup, L., N. Donohue and M. Lang. *The Fix We're In For: The State of Our Nation's Bridges*. Transportation for America, Washington, D.C., 2011.

3. Chandra, S. and L. Berntsson. *Lightweight Aggregate Concrete: Science, Technology, and Applications*. William Andrew Publishing, Norwich, N.Y., 2002.
4. Expanded Shale, Clay and Slate Institute. *Lightweight Concrete - History, Application, Economics*. Salt Lake City, Utah, 1971.
5. ACI Committee 613. Recommended Practice for Selecting Proportions for Structural Lightweight Concrete. *Journal Proceedings of the American Concrete Institute*, Vol. 55, No. 9, 1958, pp. 305-314.
6. Shideler, J. J. *Bulletin D40: Manufacture and Use of Lightweight Aggregates for Structural Concrete*. Portland Cement Association, 1961, pp. 3-14.
7. ACI Committee 213. *ACI 213R-87: Guide for Structural Lighweight Aggregate Concrete*. American Concrete Institute, Farmington Hills, MI, 1987.
8. ACI Committee 213. *ACI 213R-03: Guide for Structural Lighweight-Aggregate Concrete*. American Concrete Institute, Farmington Hills, MI, 2003.
9. Castrodale, R. W. Lightweight Concrete for Accelerated Bridge Construction. Presented at the 2011 Annual Virginia Concrete Conference, Richmond, Va., Mar. 3-4, 2011.
10. U.S. Energy Information Administration. Weekly Retail Gasoline & Diesel Prices. http://www.eia.gov/dnav/pet/hist/LeafHandler.ashx?n=pet&s=emd_epd2d_pte_nus_dpg&f=w. Accessed Feb. 23, 2011.
11. Bardhan-Roy, B. K. Design Considerations for Presressed Lightweight Aggregate Concrete. *Proc.*, *the 2nd International Congress on Lightweight Concrete*, London, Engl, 1980.
12. AASHTO. *AASHTO LRFD Bridge Design Specifications*, 4th ed. American Association of State Highway and Transportation Officials, Washington, D.C., 2007.
13. AASHTO. *AASHTO LRFD Bridge Design Specifications*, 4th ed. American Association of State Highway and Transportation Officials, Washington, D.C., 2008.
14. Spratt, B. H. *The Structural Use of Lightweight Aggregate Concrete*. Cement and Concrete Assoc., 1974.
15. Zhou, F. P., R. V. Balendran and A. P. Jeary. Size Effect on Flexural, Splitting Tensile, and Torsional Strengths of High-Strength Concrete. *Cement and Concrete Research*, Vol. 28, No. 12, 1998, pp. 1725 - 1736.
16. Kahn, L. F., K. E. Kurtis, J. S. Lai, K. F. Meyer, M. Lopez and B. Buchberg. *Lightweight Concrete for High Strength / High Performance Precast Prestressed Bridge Girders.* Report 04-1. Georgia Institute of Technology, 2004.
17. Ozyildirim, C. and J. Gomez. *First Bridge Substructure with Lightweight High-Performance Concrete Beams and Deck in Virginia.* Report No. FHWA/VTRC 06-R12. Virginia Transportation Research Council, 2005.
18. Hanson, J. A. Shear Strength of Lightweight Reinforced Concrete Beams. *ACI Journal*, Vol. 30, No. 3, 1958, pp. 387-403.

19. Ramirez, J. A., J. Olek and B. J. Malone. Shear Strength of Lightweight Reinforced Concrete Beams. *Proc.*, *High-Performance Structural Lightweight Concrete*, Phoenix, AZ, 2004.

20. American Society for Testing and Materials. *Annual Book of ASTM Standards, Section Four: Construction, Volume 04.02: Concrete and Aggregates*. ASTM International, West Conshohocken, PA, 2009.

21. Slate, F. O., A. H. Nilson and S. Martinez. Mechanical Properties of High-Strength Lightweight Concrete. *Journal of the American Concrete Institute*, Vol. 83, No. 4, 1986, pp. 606-613.

22. Stiffey, E. *Lightweight Concrete Modulus of Elasticity*. B.S. thesis. United States Military Academy, West Point, New York, 2005.

23. Cook, J. E. 10,000 psi Concrete. *Concrete International*, Vol. 11, No. 10, 1989, pp. 67-75.

24. Dymond, B. Z., C. L. Roberts-Wollmann and T. E. Cousins. *Shear Strength of a PCBT-53 Girder Fabricated with Lightweight Self-Consolidating Concrete.* Report FHWA/VTRC 09-CR11. 2009.

25. Precast Prestressed Concrete Institute. *PCI Design Handbook*, 5th ed. PCI, Chicago, Ill., 1995.

26. Short, A. and W. Kinniburgh. *Lightweight Concrete*. John Wiley & Sons, New York, 1963.

27. Holm, T. A., T. W. Bremmer and J. B. Newman. Lightweight Aggregate Concrete Subject to Severe Weathering. *Concrete International*, Vol. 6, No. 6, 1984, pp. 49-54.

28. Holm, T. A. *Performance of Structural Lightweight Concrete in a Marine Environment*. American Concrete Institute, Farmington Hills, Mich., 1980.

29. Talbot, A. N. *Tests of Reinforced Concrete Beams: Resistance to Web Stresses. Series of 1907 and 1908*. University of Illinois, 1909.

30. Clark, A. P. Diagonal Tension in Reinforced Concrete Beams. *American Concrete Institute Journal*, Vol. 23, No. 2, 1951, pp. 145-156.

31. Kuchma, D. A. and E. C. Bentz. Shear Capacity and Design Strength of Reinforced and Prestressed Members Cast with High Performance Concrete. *Proc.*, *PCI/FHWA/FIB International Symposium on High Performance Concrete*, Orlando, FL, 2000.

32. Kani, G. N. J. Riddle of Shear Failure and Its Solution. *American Concrete Institute -- Journal*, Vol. 61, No. 4, 1964, pp. 441-467.

33. Walraven, J. C. Fundamental Analysis of Aggregate Interlock. *Journal of the Structural Division*, Vol. 107, No. 11, 1981, pp.

34. Ma, Z., M. Saleh and M. K. Tadros. Shear Design of Stemmed Bridge Members - How Complex Should It Be? *PCI Journal*, Vol. 42, No. 5, 1997, pp. 88-93.

35. Elzanaty, A. H., A. H. Nilson and F. O. Slate. Shear Capacity of Prestressed Concrete Beams Using High-Strength Concrete. *Journal of the American Concrete Institute*, Vol. 83, No. 3, 1986, pp. 359-368.

36. Elzanaty, A. H., A. H. Nilson and F. O. Slate. Shear Capacity of Reinforced Concrete Beams Using High-Strength Concrete. *Journal of the American Concrete Institute*, Vol. 83, No. 2, 1986, pp. 290-296.

37. Moody, K. G., I. M. Viest, R. C. Elstner and E. Hognestad. Shear Strength of Reinforced Concrete Beams, Part 1 - Tests of Simple Beams. *American Concrete Institute -- Journal*, Vol. 26, No. 4, 1954, pp. 317-332.

38. Shioya, T., Iguro, M., Nojiri, Y., Akiyama, H., and Okada, T. Shear Strength of Large Reinforced Concrete Beams In *Fracture Mechanics: Application to Concrete, ACI SP-118* ed.), American Concrete Institute, Detroit, 1990, pp. 259-280.

39. Bentz, E. C., F. J. Vecchio and M. P. Collins. Simplified Modified Compression Field Theory for Calculating Shear Strength of Reinforced Concrete Elements. *ACI Structural Journal*, Vol. 103, No. 4, 2005, pp. 614-624.

40. Kani, G. N. J. Basic Facts Concerning Shear Failure. *ACI Journal, Proceedings*, Vol. 63, No. 6, 1966, pp. 675-692.

41. Ma, Z. and M. K. Tadros. Simplified Method for Shear Design Based on AASHTO Load and Resistance Factor Design Specifications. *Transportation Research Record*, Vol. No. 1688, 1999, pp. 10-20.

42. ACI Committee 318. *Building Code Requirements for Reinforced Concrete (ACI 318-56)*, American Concrete Institute, Detroit, Mich., 1956.

43. AASHTO. *Standard Specifications for Highway Bridges*, 6th ed. Association of General Offices, Washington, D. C., 1953.

44. ACI Committee 318. *Building Code Requirements for Structural Concrete (ACI 318-11) and Commentary*, American Concrete Institute, Farmington Hills, Mich., 2011.

45. AASHTO. *AASHTO LRFD Bridge Design Specifications*, 5th ed. American Association of State Highway and Transportation Officials, Washington, D.C., 2010.

46. Ritter, W. Die Bauweise Hennebique (The Hennebique System of Construction). *Schweizerische Bauzeitung*, Vol. No. 1899, pp. 59-61.

47. Mörsch, E. *Concrete-Steel Construction*. McGraw-Hill Book Co., New York, 1909, (English translation of 3rd ed. of *Der Eisenbetonbau*, 1st ed., 1902).

48. Collins, M. P. and D. Mitchell. *Prestressed Concrete Structures*. Prentice Hall, Inc., Englewood Cliffs, N.J., 1991.

49. Withey, M. O. *Tests on Plain and Reinforced Concrete: Series of 1907*. Madison, Wisconsin, 1908.

50. Withey, M. O. *Tests of Plain and Reinforced Concrete: Series of 1906*. Madison, Wisconsin, 1907.

51. Kani, G. N. J. How Safe Are Our Large Reinforced Concrete Beams. *American Concrete Institute Journal*, Vol. 64, No. 3, 1967, pp. 128-141.

52. Bažant, Z. P. and M. T. Kazemi. Size Effect on Diagonal Shear Failure of Beams without Stirrups. *ACI Structural Journal*, Vol. 88, No. 3, 1991, pp. 268-276.

53. Bažant, Z. P., Q. Yu, W. Gerstle, J. Hanson and J. W. Ju. Justification of ACI 446 Code Provisions for Shear Design of Reinforced Concrete Beams. *ACI Structural Journal*, Vol. 104, No. 5, 2007, pp. 601-610.

54. Hegger, J., A. Sherif and S. Gortz. Investigation of Pre- and Postcracking Shear Behavior of Prestressed Concrete Beams Using Innovative Measuring Techniques. *ACI Structural Journal*, Vol. 101, No. 2, 2004, pp. 183-192.

55. ASCE-ACI Committee 445 on Shear and Torsion. Recent Approaches to Shear Design of Structural Concrete. *Journal of Structural Engineering*, Vol. 124, No. 12, 1998, pp. 1375-1417.

56. ACI Committee 318. *Building Code Requirements for Reinforced Concrete (ACI 318-63)*, American Concrete Institute, Detroit, Mich., 1963.

57. ACI Committee 318. *Building Code Requirements for Reinforced Concrete (ACI 318-71)*. American Concrete Institute, Detroit, Mich., 1971.

58. AASHTO. *Standard Specifications for Highway Bridges*, 11th ed. American Association of State Highway and Transportation Officials, Washington, D.C., 1973.

59. Hawkins, N. M., D. A. Kuchma, R. F. Mast, M. L. Marsh and K.-H. Reineck. *NCHRP Report 549: Simplified Shear Design of Structural Concrete Members*. Transportation Research Board of the National Academies, Washington, D.C., 2005.

60. ACI Committee 318. *Commentary on Building Code Requirements for Reinforced Concrete (ACI 318-63)*. American Concrete Institute, Detroit, Mich., 1965.

61. Hawkins, N. M. and D. A. Kuchma. *NCHRP Report 579: Application of LRFD Bridge Design Specifications to High-Strength Structural Concrete: Shear Provisions*. Transportation Research Board of the National Academies, Washington, D.C., 2007.

62. Carino, N. J. and H. S. Lew. Re-examination of the Relation between Splitting Tensile and Compressive Strength of Normal Weight Concrete. *ACI Journal, Proceedings*, Vol. 79, No. 3, 1982, pp. 214-219.

63. AASHTO. *Standard Specifications for Highway Bridges*, 13th ed. American Association of State Highway and Transportation Officials, Washington, D.C., 1983.

64. Tozser, O. and R. E. Loov. Shear Design of Prestressed Beams Using Shear Friction. *Proc.*, *Canadian Society for Civil Engineering - 1999 Annual Conference*, Regina Saskatchewan, Canada, 1, 1999.

65. Mitchell, D. and M. P. Collins. Diagonal Compression Field Theory - A Rational Model for Structural Concrete in Pure Torsion. *ACI Journal*, Vol. 71, No. 8, 1974, pp. 396-408.

66. Collins, M. P. Towards a Rational Theory for RC Members in Shear. *Proceedings, ASCE*, Vol. 104, No. 4, 1978, pp. 649-666.

67. Collins, M. P. and D. Mitchell. Shear and Torsion Design of Prestressed and Non-Prestressed Concrete Beams. *Journal of the Prestressed Concrete Institute*, Vol. 25, No. 5, 1980, pp. 32-100.

68. Collins, M. P. and D. Mitchell. A Rational Approach to Shear Design - The 1984 Canadian Code Provisions. *ACI Structural Journal*, Vol. 83, No. 6, 1986, pp. 925-933.

69. Vecchio, F. J. and M. P. Collins. *The Response of Reinforced Concrete to In-Plane Shear and Normal Stresses*. Report No. 82-03. University of Toronto, Department of Civil Engineering, 1982.

70. Vecchio, F. J. and M. P. Collins. The Modified Compression-Field Theory for Reinforced Concrete Elements Subjected to Shear. *ACI Journal, Proceedings*, Vol. 83, No. 2, 1986, pp. 219-231.

71. Vecchio, F. J. and M. P. Collins. Predicting the Response of Reinforced Concrete Beams Subjected to Shear Using Modified Compression Field Theory. *ACI Structural Journal*, Vol. 85, No. 3, 1988, pp. 258-268.

72. Collins, M. P., D. Mitchell, P. Adebar and F. J. Vecchio. A General Shear Design Method. *ACI Structural Journal*, Vol. 93, No. 1, 1996, pp. 36-45.

73. Kupfer, H. *Bulletin d'Information No. 40: Erweiterung der Morsch schen Fachwerkanalogie mit Hilfe des Prinzips vom Minimum der Formanderungsarbeit (Generalization of Morsch's Truss Analogy Using the Principle of Minimum Strain Energy)*. Comite Euro-International du Beton, 1964, pp. 44-57.

74. Shahawy, M. A. and B. deV Batchelor. Shear Behavior of Full-Scale Prestressed Concrete Girders: Comparison between AASHTO Specifications and LRFD Code. *PCI Journal*, Vol. 41, No. 3, 1996, pp. 48-62.

75. Ma, Z., M. K. Tadros and M. Baishya. Shear Behavior of Pretensioned High-Strength Concrete Bridge I-Girders. *ACI Structural Journal*, Vol. 97, No. 1, 2000, pp. 185-192.

76. CSA Committee A23.3. *Design of Concrete Structures (CSA A23.3-04)*, Canadian Standards Association, Rexdale, Ontario, Can., 2004.

77. Hsu, T. T. C. Is The 'Staggering Concept' of Shear Design Safe? *ACI Journal*, Vol. 79, No. 6, 1982, pp. 435-443.

78. Ramirez, J. A. Shear Strength of Lightweight Concrete Beams with Stirrups Near Code Minimum. In *Art and Science of Structural Concrete Design - a Symposium Honoring Richard W. Furlong* (S. A. Mirza, ed.), 2003, pp. 119-134.

79. Johnson, M. K. and J. A. Ramirez. Minimum Shear Reinforcement in Beams with Higher Strength Concrete. *ACI Structural Journal (American Concrete Institute)*, Vol. 86, No. 4, 1989, pp. 376-382.

80. Roller, J. J. and H. G. Russell. Shear Strength of High-Strength Concrete Beams with Web Reinforcement. *ACI Structural Journal (American Concrete Institute)*, Vol. 87, No. 2, 1990, pp. 191-198.

81. ACI Committee 318. *Building Code Requirements for Structural Concrete (ACI 318-89) and Commentary (ACI 318R-89)*. American Concrete Institute, Farmington Hills, Mich., 1989.

82. ACI Committee 318. *Building Code Requirements for Structural Concrete (ACI 318-02) and Commentary (ACI 318R-02)*, American Concrete Institute, Farmington Hills, Mich., 2002.

83. Angelakos, D., Bentz, E. C., and Collins, M.P. The Effect of Concrete Strength and Minimum Stirrups on the Shear Strength of Large Members. *ACI Structural Journal*, Vol. 98, No. 3, 2001, pp. 291-300.

84. Collins, M. P., and Kuchma, D.A. How Safe Are Our Large, Lightly Reinforced Concrete Beams, Slabs, and Footings? *ACI Structural Journal*, Vol. 96, No. 4, 1999, pp. 482-490.

85. Laskar, A., T. T. C. Hsu, and Y. L. Mo. Shear Strengths of Prestressed Concrete Beams Part 1: Experiments and Shear Design Equations. *ACI Structural Journal*, Vol. 107, No. 3, 2010, pp. 330-339.

86. Laskar, A., T. T. C. Hsu, and Y. L. Mo. Shear Strengths of Prestressed Concrete Beams Part 2: Comparisons with ACI and AASHTO Provisions. *ACI Structural Journal*, Vol. 107, No. 3, 2010, pp. 340-345.

87. ACI Committee 318. *Building Code Requirements for Structural Concrete (ACI 318-08) and Commentary*, American Concrete Institute, Farmington Hills, Mich., 2008.

88. AASHTO. *Standard Specifications for Highway Bridges*, 10th ed. American Association of State Highway and Transportation Officials, Washington, D.C., 1969.

89. AASHTO. *Standard Specifications for Highway Bridges*, 12th ed. American Association of State Highway and Transportation Officials, Washington, D.C., 1977.

90. AASHTO. *Standard Specifications for Highway Bridges*, 17th ed. American Association of State and Highway Transportation Officials, Washington, D.C., 2002.

91. AASHTO. *AASHTO LRFD Bridge Design Specifications*, 1st ed. American Association of State Highway and Transportation Officials, Washington, D.C., 1994.

92. Godbold, S. D. *Diagonal Tension in Rectangular Lightweight Aggregate Beams with Varying Steel Percentages*. M.S. thesis. University of Texas, 1957.

93. Maltepe, H. *Effect of Varying Shear Span on the Diagonal Tension Strength of Lightweight Aggregate Concrete Beams without Web Reinforcement*. M.S. thesis. University of Texas, 1957.

94. Aguirre, R. G. *Effects of Varying Shear Span on the Diagonal Tension Strength of Lightweight Aggregate Concrete Beams*. M.S. thesis. University of Texas, 1959.

95. Eldridge, W. F. *The Relationship between Diagonal Tension and Compressive Strength of Lightweight Aggregate Concrete Beams*. M.S. thesis. University of Texas, 1958.

96. Guzman, G. J. *Diagonal Tension Strength of Lightweight Aggregate Beams with Varying Shear Span*. M.S. thesis. University of Texas, 1958.

97. Thompson, E. G. *Shrinkage Effect on the Diagonal Tension Strength of Lightweight Aggregate Concrete Beams*. M.S. thesis. University of Texas, 1959.

98. Hanson, J. A. Tensile Strength and Diagonal Tension Resistance of Structural Lightweight Concrete. *Journal of the American Concrete Institute, Proceedings*, Vol. 58, No. 1961, pp. 1-37.

99. Ivey, D. L. and E. Buth. Shear Capacity of Lightweight Concrete Beams. *American Concrete Institute Journal*, Vol. 64, No. 10, 1967, pp. 634-643.

100. Taylor, R. and R. S. Brewer. Effect of Type of Aggregate on Diagonal Cracking of Reinforced Concrete Beams. *Magazine of Concrete Research*, Vol. 15, No. 44, 1963, pp. 87-92.

101. Salandra, M. A. and S. H. Ahmad. Shear Capacity of Reinforced Lightweight High-strength Concrete Beams. *ACI Structural Journal (American Concrete Institute)*, Vol. 86, No. 6, 1989, pp. 697-704.

102. ACI Committee 318. *Building Code Requirements for Reinforced Concrete (ACI 318-83)*. American Concrete Institute, Detroit, Mich., 1983.

103. Evans, R. H. and A. V. Dongre. Suitability of Lightweight Aggregate (Aglite) for Structural Concrete. *Magazine of Concrete Research*, Vol. 15, No. 44, 1963, pp. 93-100.

104. Jindal, B. K. Behaviour of Reinforced Lightweight Concrete Beams in Flexure and Shear. *Indian Concrete Journal*, Vol. 40, No. 1, 1966, pp. 26-33.

105. Nishibayashi, S., K. Kobayashi and Y. Yoshioka. Fundamental Studies on Flexural and Shearing Properties of Concrete Beams with Artificial Lightweight Aggregate. *Transactions of the Japan Society of Civil Engineers*, Vol. No. 155, 1968, pp. 53-63.

106. Walraven, J. C. *The Influence of Depth on the Shear Strength of Lightweight Concrete Beams without Shear Reinforcement.* Report 5-78-4. Delft University Press, 1978.

107. Swamy, R. N. and A. K. Bandyopadhyay. Shear Behaviour of Structural Lightweight Concrete T-Beams without Web Refinforcement. *Proceedings of the Institution of Civil Engineers (London). Part 1 - Design & Construction*, Vol. 67, No. 2, 1979, pp. 341-354.

108. Hanson, J. A. Strength of Structural Lightweight Concrete under Combined Stress. *Journal of the PCA Research and Development Laboratories*, Vol. 5, No. 1, 1963, pp. 39-46.

109. Swamy, R. N. and G. H. Lambert. Shear Strength of Lightweight Concrete T-Beams without Web Reinforcement. *Structural Engineer, Part B: R&D Quarterly*, Vol. 61B, No. 4, 1983, pp. 69-78.

110. Hoff, A., K. Hoiseth and T. A. Haverstad. Testing of High Strength Lightweight Aggregate Concrete Elements. *Nordic Concrete Research*, Vol. No. 3, 1984, pp. 63-91.

111. Hoff, G. C. Part 3 - Structural Parameters. In *SP-136: High Strength Lightweight Aggregate Concrete for Arctic Applications* ed.), American Concrete Institute, Farmington Hills, Mich., 1993, pp. 175-246.

112. Murayama, Y. and A. Iwabuchi. Flexural and Shear Strength of Reinforced High-Strength Lightweight Concrete Beams. *Proc.*, *the Annual Japanese Concrete Institute Meeting*, 8, 1986.

113. ASCE-ACI Committee 426. The Shear Strength of Reinforced Concrete Members. *Journal of the Structural Division*, Vol. 99, No. 6, 1973, pp. 1091-1187.

114. Funahashi, M., N. Hara, H. Yokota and J. Niwa. Shear Capacity of Reinforced Concrete Beams Using Super Lightweight Concrete. *Transactions of the Japan Concrete Institute*, Vol. 23, No. 2001, pp. 377-384.

115. Hamadi, Y. D. and P. E. Regan. Behaviour of Normal and Lightweight Aggregate Beams with Shear Cracks. *The Structural Engineer*, Vol. 58B, No. 4, 1980, pp. 71-79.

116. Kirmair, H. R. Shear Carrying Behaivor of Lightweight Concrete Beams as Compared to Nomral Weight Concrete Beams. Presented at the Concrete International Conference, London, England, 1980.

117. British Standards Institution. *Structural Use of Concrete, Part 2: Code of Practice for Special Circumstances*, BS 8110. British Standards Institution, London, 1985.

118. Clarke, J. L. Shear Strength of Lightweight Aggregate Concrete Beams: Design to BS 8110. *Magazine of Concrete Research*, Vol. 39, No. 141, 1987, pp. 205-213.

119. Ahmad, S. H., Y. Xie and T. Yu. Shear Strength of Reinforced Lightweight Concrete Beams of Normal and High Strength Concrete. *Magazine of Concrete Research*, Vol. 46, No. 166, 1994, pp. 57-66.

120. Walraven, J. C. and N. Al-Zubi. Shear Capacity of Lightweight Concrete Beams with Shear Reinforcement. *Proc.*, *International Symposium on Structural Lightweight Aggregate Concrete*, Sandefjord, Norway, 1995.

121. AASHTO. *AASHTO LRFD Bridge Design Specifications*, 2nd ed. American Association of State Highway and Transportation Officials, Washington, D.C., 1998.

122. Bhide, S. B. and M. P. Collins. Influence of Axial Tension on the Shear Capacity of Reinforced Concrete Members. *ACI Structural Journal*, Vol. 86, No. 5, 1989, pp. 570-581.

123. Malone, B. J. *Shear Strength of Reinforced and Prestressed Concrete Beams With Lightweight Aggregate Concrete*. Ph.D. dissertation. Purdue University, West Lafayette, IN, 1999.

124. Kawaguchi, T., J. Niwa, J.-H. Moon and S. Maehori. Shear Capacity of Normal Strength Super Lightweight RC Beams. *Transactions of the Japan Concrete Institute*, Vol. 22, No. 2000, pp. 385-392.

125. Kobayashi, K., Y. Matsuzaki, H. Fukuyama and S. Hakuto. Performance Evaluation of RC Elements with Ultra Lightweight Concrete. In *Composite and Hybrid Structures, Vols. 1 and 2* (Y. Xiao and S. A. Mahin, ed.), 2000, pp. 977-984.

126. Architectural Institute of Japan. *Design Guidelines for Earthquake Resistant Reinforced Concrete Buildings Based on Ultimate Strength Concept*, Architectural Institute of Japan, 1990.

127. Brettle, H. J. Structural Aspects of Prestressed Lightweight Aggregate Concrete. *Constructional Review*, Vol. 35, No. 5, 1962, pp. 31-40.

128. ACI Committee 318. *Building Code Requirements for Structural Concrete (ACI 318-99) and Commentary (ACI 318R-99)*. American Concrete Institute, Farmington Hills, Mich., 1999.

129. AASHTO. *Standard Specifications for Highway Bridges*, 16th ed. American Association of State Highway and Transportation Officials, Washington, D. C., 1996.

130. Watanabe, H., H. Kawano, M. Suzuki and S. Sato. Shear Strength of PC Beams with High Strength Lightweight Aggregate Concrete. *Concrete Library International*, Vol. 43, No. 2004, pp. 41-54.

131. AASHTO. *AASHTO LRFD Bridge Design Specifications*, 3rd ed. American Association of State Highway and Transportation Officials, Washington, D.C., 2006.

132. Kupfer, H. B. and K. H. Gerstle. Behavior of Concrete under Biaxial Stress. *American Society of Civil Engineers Journal of the Engineering Mechanics Division*, Vol. 99, No. 4, 1973, pp. 853-866.

133. Mor, A. Steel-Concrete Bond in High-strength Lightweight Concrete. *ACI Materials Journal (American Concrete Institute)*, Vol. 89, No. 1, 1992, pp. 76-82.

134. Meyer, K. F., L. F. Kahn, K. E. Kurtis and J. S. Lai. *Transfer and Development Length of High Strength Lightweight Concrete Precast Prestressed Bridge Girders.* Report 2004.

135. Mitchell, D. W. and H. Marzouk. Bond Characteristics of High-strength Lightweight Concrete. *ACI Structural Journal*, Vol. 104, No. 1, 2007, pp. 22-29.

136. Nowak, A. S. *NCHRP Report 368: Calibration of LRFD Bridge Design Code.* Transportation Research Board, Washington, D.C., 1999.

137. Nowak, A. S. and K. R. Collins. *Reliability of Structures*. McGraw-Hill, Boston, 2000.

138. Paczkowski, P. and A. S. Nowak. Reliability Models for Shear in Lightweight Reinforced Concrete Bridges. Presented at the 2010 Concrete Bridge Conference: Achieving Safe, Smart & Sustainable Bridges, Phoenix, AZ, February 24-26, 2010.

139. Yamani, A. S. *Reliability Evaluation of Shear Strength in Highway Girder Bridges*. Ph.D. dissertation. The University of Michigan, Ann Arbor, MI, 1992.

140. Ellingwood, B., J. G. MacGregor, T. V. Galambros and C. A. Cornell. Probability Based Load Criteria: Load Factors and Load Combinations. *Journal of the Structural Division*, Vol. 108, No. 5, 1982, pp. 978-997.

141. Ellingwood, B., T. V. Galambos, J. G. MacGregor and C. A. Cornell. *Development of a Probability Based Load Criterion for American National Standard A58: Building Code Requirements for Minimum Design Loads in Buildings and Other Structures. National Bureau of Standards, U. S. Department of Commerce,* 1980.

142. Siriaksorn, A. *Serviceability and Reliability Analysis of Partially Prestressed Concrete Beams*. Ph.D. dissertation. University of Illinois at Chicago, Chicago, 1980.

143. Melchers, R. E. *Structural Reliability Analysis and Prediction*. John Wiley & Sons, Chichester, England, 1999.

144. Mirza, S. A. and J. G. MacGregor. Statistical Study of Shear Strength of Reinforced Concrete Slender Beams. *ACI Journal*, Vol. 76, No. 11, 1979, pp. 1159-1177.

145. ACI Committee 318. *Building Code Requirements for Reinforced Concrete (ACI 318-77)*, American Concrete Institute, Detroit, Mich., 1977.

146. Kani, M. *An Experimental Investigation of Reinforced and Prestressed Beams in Shear*. M.A.Sc. thesis. University of Toronto, Toronto, CA, 1977.

147. Arbesman, B. *The Effect of Stirrup Cover and Amount of Reinforcement on Shear Capacity of Reinforced Concrete Beams*. thesis. University of Toronto, Toronto, CA, 1975.

148. Sadler, C. *Investigating Shear Design Criteria for Prestressed Concrete Girders*. M.A.Sc. thesis. University of Toronto, Toronto, CA, 1978.

149. Morawski, J. D. *The Effect of Load History on the Shear Behaviour of Reinforced Concrete Members with Non-Yielding Longitudinal Steel*. M.A.Sc. thesis. University of Toronto, Toronto, CA, 1980.

150. Nawy, E. G. and P. T. Haung. Crack and Deflection Control of Pretensioned Prestressed Beams. *PCI Journal*, Vol. 22, No. 3, 1977, pp. 30-43.

151. Nowak, A. S. and A. M. Rakoczy. Statistical Parameters for Compressive Strength of Lightweight Concrete. Presented at the 2010 Concrete Bridge Conference: Achieving Safe, Smart & Sustainable Bridges, Phoenix, AZ, February 24-26, 2010.

152. Ramirez, J. A., J. Olek, E. Rolle and B. Malone. *Performance of Bridge Decks and Griders with Lightweight-Aggregate Concrete.* Report FHWA/IN/JTRP - 98/17. 2000.

153. Dymond, B. Z. *Shear Strength of a PCBT-53 Girder Fabricated with Lightweight, Self-Consolidating Concrete*. M.S. thesis. Virginia Polytechnic Institue and State University, Blacksburg, VA, 2007.

154. Occupational Safety and Health Administration. *Safety and Health Regulations for Construction - Concrete and Masonry Construction: Requirements for Precast Concrete*, 1926.704 (c). U.S. Department of Labor, Washington, D.C., 2010.

155. American Institute of Steel Construction. *Steel Construction Manual*, 13th ed. American Institute of Steel Construction, Chicago, Ill., 2005.

156. Kulicki, J. M., S. R. Eshenaur and A. L. Thomas. Reader Comments on *Shear Behavior of Full-Scale Prestressed Concrete Girders: Comparison Between AASHTO Specifications and LRFD Code by M. A. Shahawy and B. deV Batchelor* (PCI Journal, V. 41, No. 3, May-June 1996, pp. 48-62). *PCI Journal*, Vol. 42, No. 3, 1997, pp. 72-93.

157. Nowak, A. S. and M. M. Szerszen. Calibration of design Code for Buildings (ACI 318): Part 1 - Statistical Models for Resistance. *ACI Structural Journal*, Vol. 100, No. 3, 2003, pp. 377-382.

Appendix A

Construction Plans of Test Girders

PRELIMINARY PLAN DRAWINGS FOR

NATIONAL COOPERATIVE HIGHWAY RESEARCH PROGRAM
PROJECT 18-15

HIGH-STRENGTH/HIGH PERFORMANCE LIGHTWEIGHT

VirginiaTech *Invent the Future*

VTRC Virginia Transportation Research Council

VDOT Virginia Department of Transportation

GIRDER PRODUCTION MATRIX						
BEAM ID	Section	Length (ft)	No. of Strands	Concrete Weight (pcf)	f_c' (ksi)	Casting Stage
1	Type II	41	24	120	8	1
2	Type II	41	24	120	8	
3	PCBT-45	59	34	145	8	2
4	PCBT-45	59	34	120	8	
5	PCBT-45	59	34	120	10	3
6	PCBT-45	59	34	120	10	

Notes to Bidders:

1) The girders in the following plans are for a research project; all potential contractors shall attend a mandatory pre-bid meeting (meeting time and location to be announced).
2) First set of beams shall be ready for delivery by June 1, 2009
3) The preferred order of casting stages is indicated in the Girder Production Matrix table on this sheet. Casting stages should be at least two weeks apart.
4) Winning bidder shall give one week notice prior to the date of beam casting.
5) Virginia Tech will require one extra day prior to concrete placement for each casting in order to install instrumentation on the steel reinforcement.
6) Virginia Tech will also require one-half day per beam after form removal and prior to strand detensioning to install instrumentation on the concrete surfaces.
7) Because Virginia Tech will be testing one beam at a time, Contractors will need to provide storage for beams six months to one year prior to being shipped to Virginia Tech.
8) Virginia Tech will provide all shipping and disposal arrangements for the concrete beams.
9) Mix designs for all concrete used in this project will be provided by Virginia Tech.
10) Lightweight aggregate used in this project shall be Carolina Stalite rotary kiln expanded slate lightweight aggregate, or an approved equivalent.
11) Bids shall allow for an additional 4 ft^3 of fresh concrete per beam used to make sample specimens for quality control testing at Virginia Tech.
12) All beams in this project shall be steam cured.
13) Any additional inquiries regarding these notes may be directed to Tommy Cousins (tcousins@vt.edu, 540-231-6753) or Carin Roberts-Wollmann (wollmann@vt.edu, 540-231-2052) of Virginia Tech.

VIRGINIA TECH			
LIGHTWEIGHT CONCRETE LARGE-SCALE TEST BEAMS			
Scale:1/2"=1'-0"	Rev. 3	Date: 4/15/09	Sheet: No.1 of 7

Figure A-1. Cover sheet for construction plans

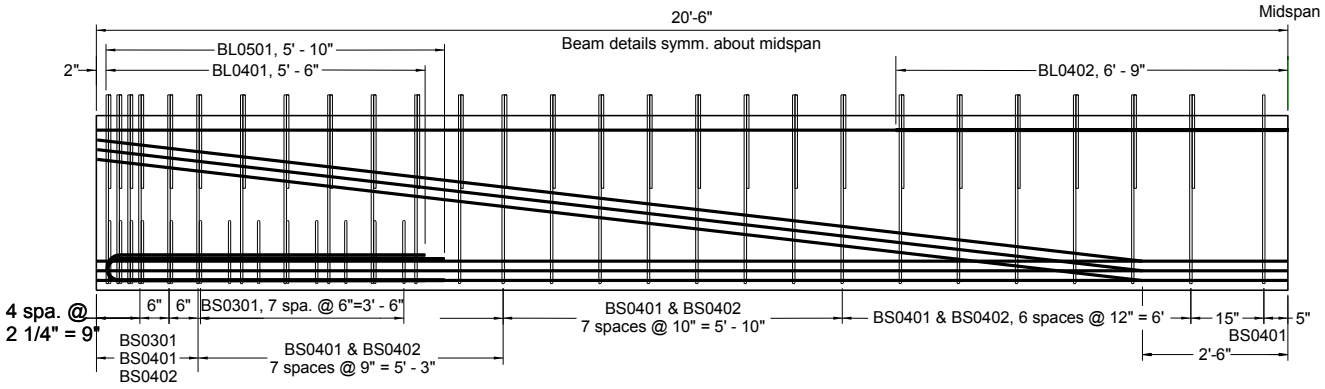

Part Elevation of Beam

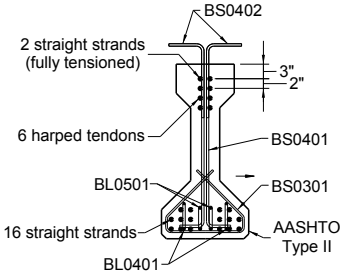

End View

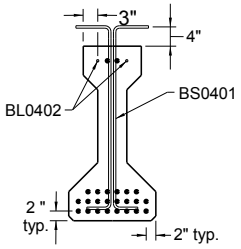

Midspan View

Notes:

1) Concrete strength at release = 6000psi

2) Concrete 28 day strength = 8000 psi

3) Concrete unit weight = 120 pcf

4) Concrete is a lightweight mix design

5) All strands are 0.5" diameter, Grade 270

6) All strands are stressed to 75% GUTS = 31 kips per strand

7) Beam is a standard AASHTO Type II shape

8) Surface of top flange shall be intentionally roughened to an amplitude of 1/4"

REINFORCING STEEL SCHEDULE

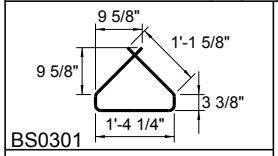

BS0301

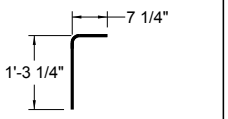

BS0402

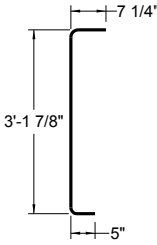

BS0401

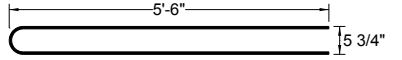

BL0401

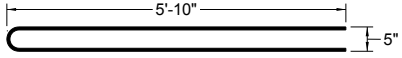

BL0501

Mark	Size	Pin Ø	Length	Wt./bar lbs.	Quantity	Weight lbs.
BS0301	#3	1.5"	4' - 0 1/4"	1.51	26	39.3
BS0401	#4	2"	3' - 11 1/2"	2.64	53	139.9
BS0402	#4	2"	1' - 9 1/2"	1.20	50	60.0
BL0401	#4	4 3/4"	11' - 2 1/2"	7.49	2	15.0
BL0402	#4	-	13' - 6"	5.08	2	10.1
BL0501	#5	3 3/4"	11' - 9 7/8"	12.33	2	24.7
					Total Weight	289.0

Dimensions in bending diagram are out-to-out of the bars.

Reinforcing bars shown on the above schedule are for beams shown in this sheet only.

Reinforcing bars BS0401 and BS0402 shall be galvanized. All other reinforcing bars shall be epoxy coated.

At the contractors option and at no additional cost, bar BS0403 may be fabricated as a two-piece bar with a minimum 1' - 8" overlap

VIRGINIA TECH

LIGHTWEIGHT PRESTRESSED BEAM
AASHTO TYPE II
TYPICAL SHEAR REINFORCEMENT

Scale: 1/2"=1'-0"	Rev. 2	Date: 04/05/09	Sheet No.: 2 of 7

Figure A-2. Plans for Bam T2.8.Typ

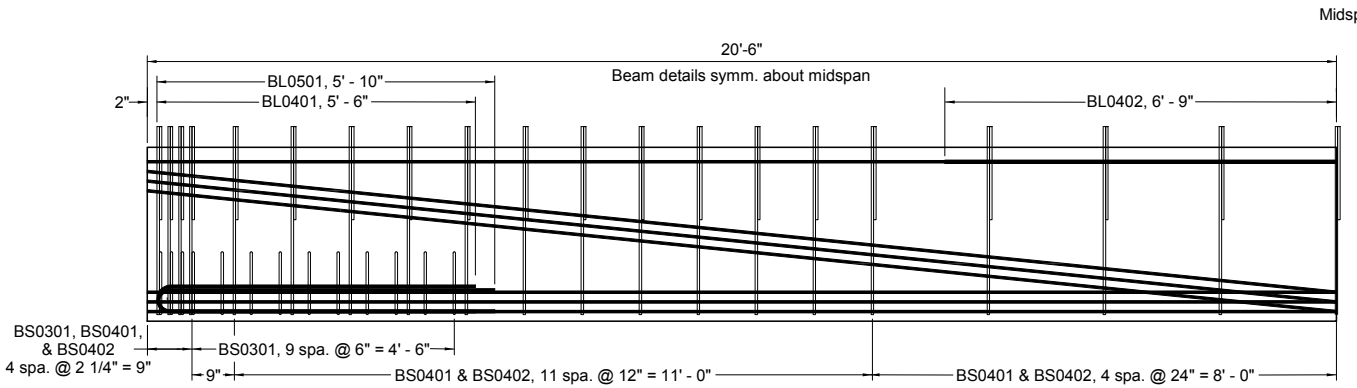

Part Elevation of Beam

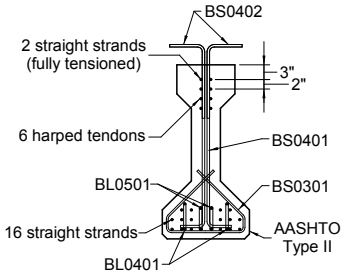

End View

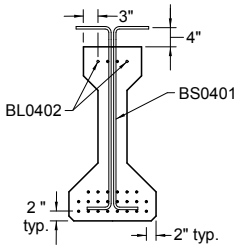

Midspan View

Notes:

1) Concrete strength at release = 6000psi
2) Concrete 28 day strength = 8000 psi
3) Concrete unit weight = 120 pcf
4) Concrete is a lightweight mix design
5) All strands are 0.5" diameter, Grade 270
6) All strands are stressed to 75% GUTS = 31 kips per strand
7) Beam is a standard AASHTO Type II shape
8) Surface of top flange shall be intentionally roughened to an amplitude of 1/4"

REINFORCING STEEL SCHEDULE

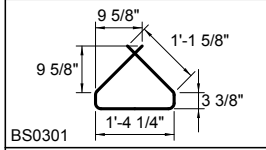

BS0301

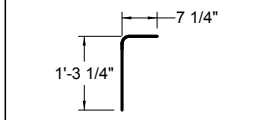

BS0402

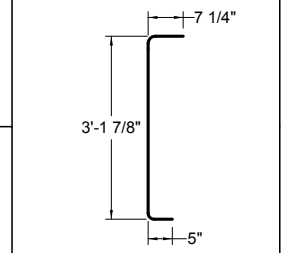

BS0401

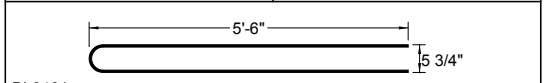

BL0401

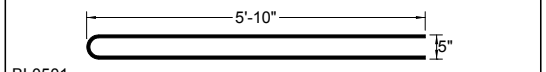

BL0501

Mark	Size	Pin Ø	Length	Wt./bar lbs.	Quantity	Weight lbs
BS0301	#3	1.5"	4' - 0 1/4"	1.51	26	39.3
BS0401	#4	2"	3' - 11 1/2"	2.64	39	103.0
BS0402	#4	2"	1' - 9 1/2"	1.20	39	46.8
BL0401	#4	4 3/4"	11' - 2 1/2"	7.49	2	15.0
BL0402	#4	-	13' - 6"	5.08	2	10.1
BL0501	#5	3 3/4"	11' - 9 7/8"	12.33	2	24.7
				Total Weight		238.9

Dimensions in bending diagram are out-to-out of the bars.

Reinforcing bars shown on the above schedule are for beams shown in this sheet only.

Reinforcing bars BS0401 and BS0402 shall be galvanized. All other reinforcing bars shall be epoxy coated.

At the contractors option and at no additional cost, bar BS0403 may be fabricated as a two-piece bar with a minimum 1' - 8" overlap

VIRGINIA TECH

LIGHTWEIGHT PRESTRESSED BEAM
AASHTO TYPE II
MINIMUM SHEAR REINFORCEMENT

Scale: 1/2"=1'-0"	Rev. 2	Date: 04/05/09	Sheet No.: 3 of 7

Figure A-3. Plans for Beam T2.8.Min.

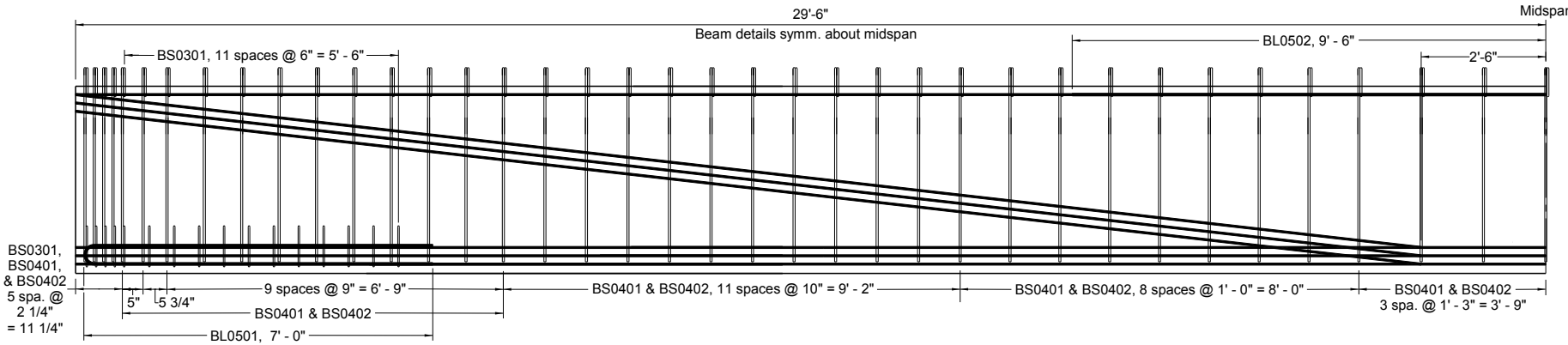

Partial Elevation

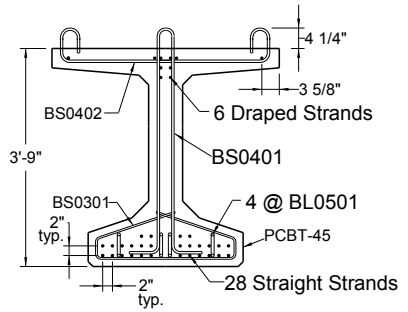

End View

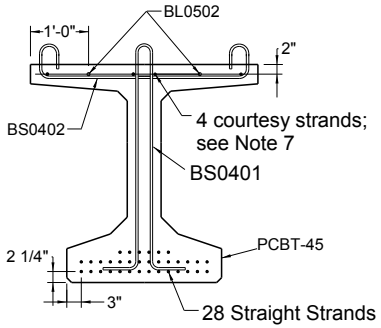

Center Line View

REINFORCING STEEL SCHEDULE

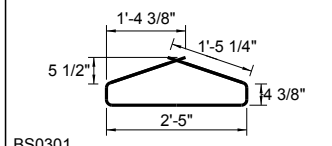

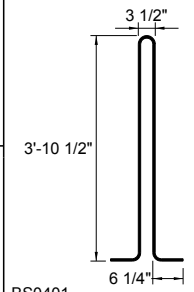

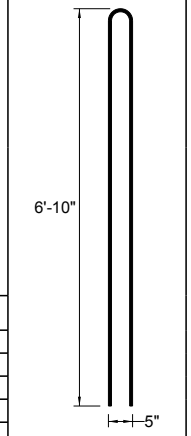

Mark	Size	Pin Ø	Length	Wt./bar lbs	Qty.	Weight lbs
BS0301	#3	2"	5' - 11 1/2"	2.24	32	71.7
BS0401	#4	2 1/2"	8' - 8 1/2"	5.82	75	436.5
BS0402	#4	3"	5' - 8 1/4"	3.80	75	284.9
BL0501	#5	3 3/4"	13' - 9 7/8"	14.42	8	115.3
BL0502	#5	-	19' - 0"	19.8	2	39.6
				Total Weight		948.0

Notes:

1) Concrete strength at release = 6000psi
2) Concrete 28 day strength = 8000 psi
3) Concrete unit weight = 120 pcf
4) Concrete is lightweight mix design
5) All strands are 0.5" diameter, Grade 270
6) Bottom and draped strands are stressed to 75% GUTS = 31 kips per strand
7) 4 - 1/2 Ø strands stressed to 1000 lbs
8) Beam is standard PCBT-45 shape
9) Surface of top flange shall be intentionally roughened to an amplitude of 1/4"

Dimensions in bending diagram are out-to-out of the bars.

Reinforcing bars shown on the above schedule are for beams shown in this sheet only.

Reinforcing bars BS0401 and BS0402 shall be galvanized. All other reinforcing bars shall be epoxy coated.

VIRGINIA TECH

8-KSI LIGHTWEIGHT PRESTRESSED BEAM
VIRGINIA PCBT-45

Scale: 1/2"=1'-0" | Rev. 2 | Date: 04/05/09 | Sheet No.: 5 of 7

Figure A-4. Plans for Beam BT.8.Typ.

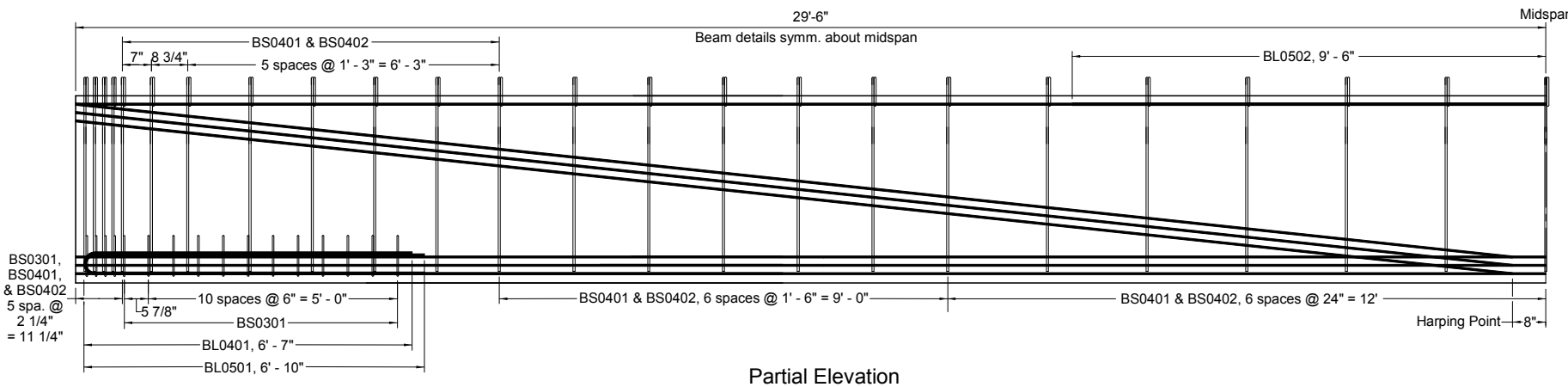

Partial Elevation

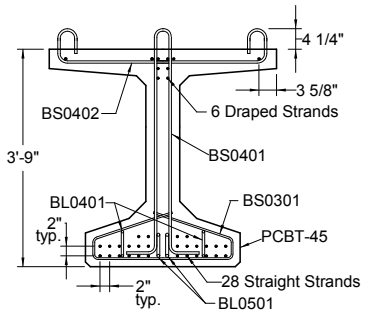

End View

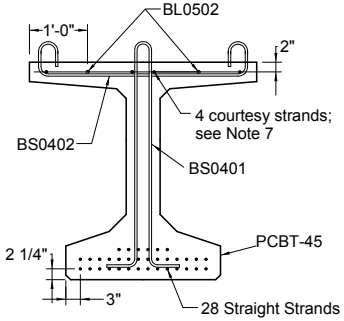

Center Line View

Notes:

1) Concrete strength at release = 6000psi
2) Concrete 28 day strength = 8000 psi
3) Concrete unit weight = 145 pcf
4) Concrete is normal weight mix design
5) All strands are 0.5" diameter, Grade 270
6) Bottom and draped strands are stressed to 75% GUTS = 31 kips per strand
7) 4 - 1/2 Ø strands stressed to 1000 lbs
8) Beam is standard PCBT-45 shape
9) Surface of top flange shall be intentionally roughened to an amplitude of 1/4"

REINFORCING STEEL SCHEDULE

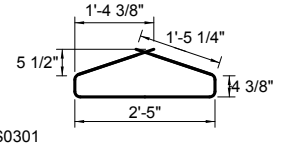

BS0301

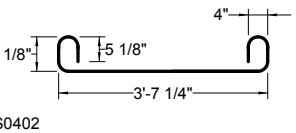

BS0402

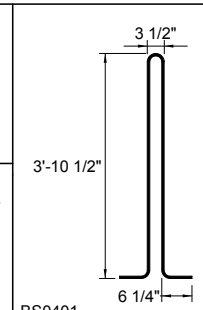

BS0401

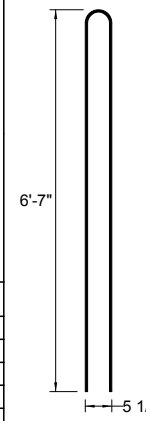

BL0401

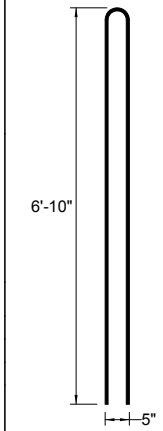

BL0501

Mark	Size	Pin Ø	Length	Wt./bar lbs	Qty.	Weight lbs
BS0301	#3	2"	5' - 11 1/2"	2.24	32	71.7
BS0401	#4	2 1/2"	8' - 8 1/2"	5.82	47	273.4
BS0402	#4	3"	5' - 8 1/4"	3.80	47	178.6
BL0401	#4	4 1/2"	13' - 4 3/8"	8.93	4	35.7
BL0501	#5	3 3/4"	13' - 9 7/8"	14.42	4	57.7
BL0502	#5	-	19' - 0"	19.8	2	39.6
				Total Weight		656.7

Dimensions in bending diagram are out-to-out of the bars.

Reinforcing bars shown on the above schedule are for beams shown in this sheet only.

Reinforcing bars BS0401 and BS0402 shall be galvanized. All other reinforcing bars shall be epoxy coated.

VIRGINIA TECH

NORMAL WEIGHT PRESTRESSED BEAM
VIRGINIA PCBT-45

Scale: 1/2"=1'-0" | Rev. 2 | Date: 04/05/09 | Sheet No.: 4 of 7

Figure A-5. Plans for Beam BT.8N.Typ.

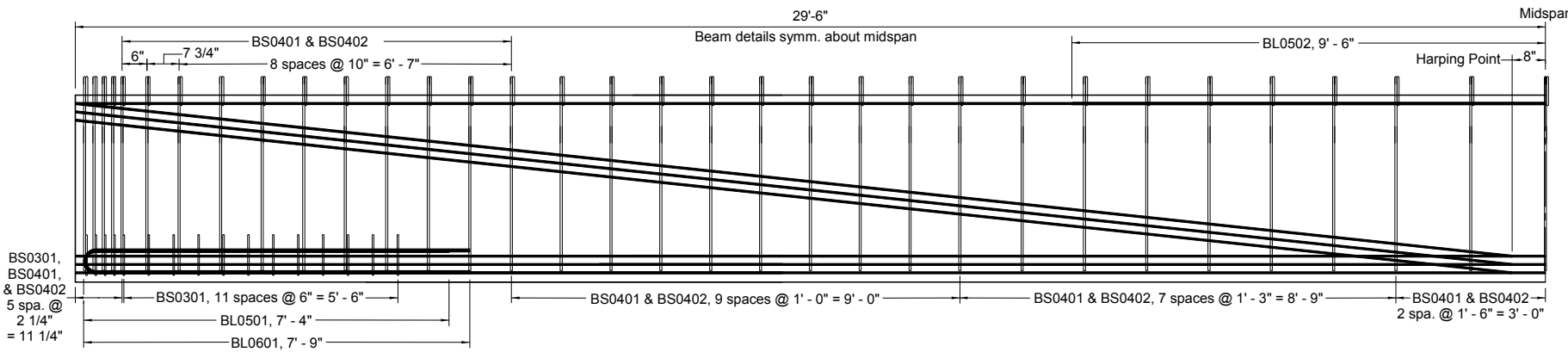

Partial Elevation

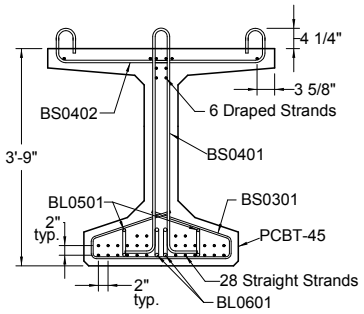

End View

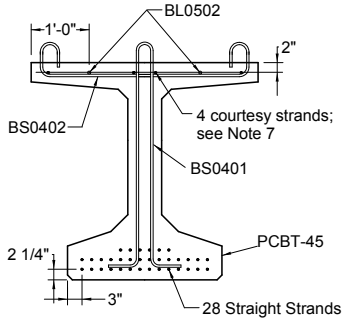

Center Line View

REINFORCING STEEL SCHEDULE

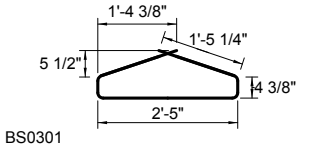

BS0301

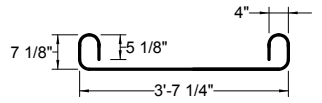

BS0402

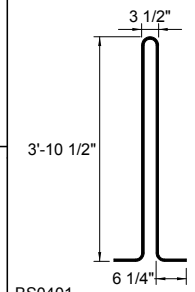

BS0401

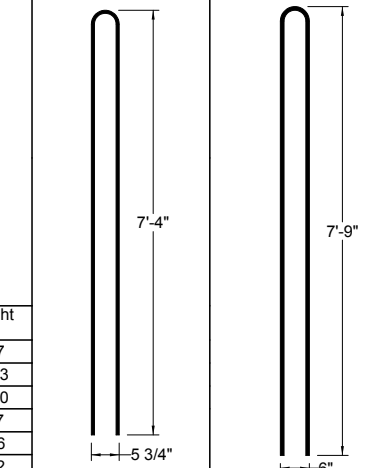

BL0501

BL0601

Mark	Size	Pin Ø	Length	Wt./bar lbs	Qty.	Weight lbs
BS0301	#3	2"	5' - 11 1/2"	2.24	32	71.7
BS0401	#4	2 1/2"	8' - 8 1/2"	5.82	65	378.3
BS0402	#4	3"	5' - 8 1/4"	3.80	65	247.0
BL0501	#5	4 1/2"	14' - 10 1/4"	9.92	4	39.7
BL0502	#5	-	19' - 0"	19.8	2	39.6
BL0601	#6	4 1/2"	15' - 8 1/4"	13.05	4	94.2
				Total Weight		870.5

Notes:

1) Concrete strength at release = 7500psi
2) Concrete 28 day strength = 10000 psi
3) Concrete unit weight = 120 pcf
4) Concrete is lightweight mix design
5) All strands are 0.5" diameter, Grade 270
6) Bottom and draped strands are stressed to 75% GUTS = 31 kips per strand
7) 4 - 1/2 Ø strands stressed to 1000 lbs
8) Beam is standard PCBT-45 shape
9) Surface of top flange shall be intentionally roughened to an amplitude of 1/4"

Dimensions in bending diagram are out-to-out of the bars.

Reinforcing bars shown on the above schedule are for beams shown in this sheet only.

Reinforcing bars BS0401 and BS0402 shall be galvanized. All other reinforcing bars shall be epoxy coated.

VIRGINIA TECH

10-KSI LIGHTWEIGHT PRESTRESSED BEAM
VIRGINIA PCBT-45
TYPICAL SHEAR REINFORCEMENT

Scale: 1/2"=1'-0"	Rev. 3	Date: 04/15/09	Sheet No.: 6 of 7

Figure A-6. Plans for Beam BT.10.Typ.

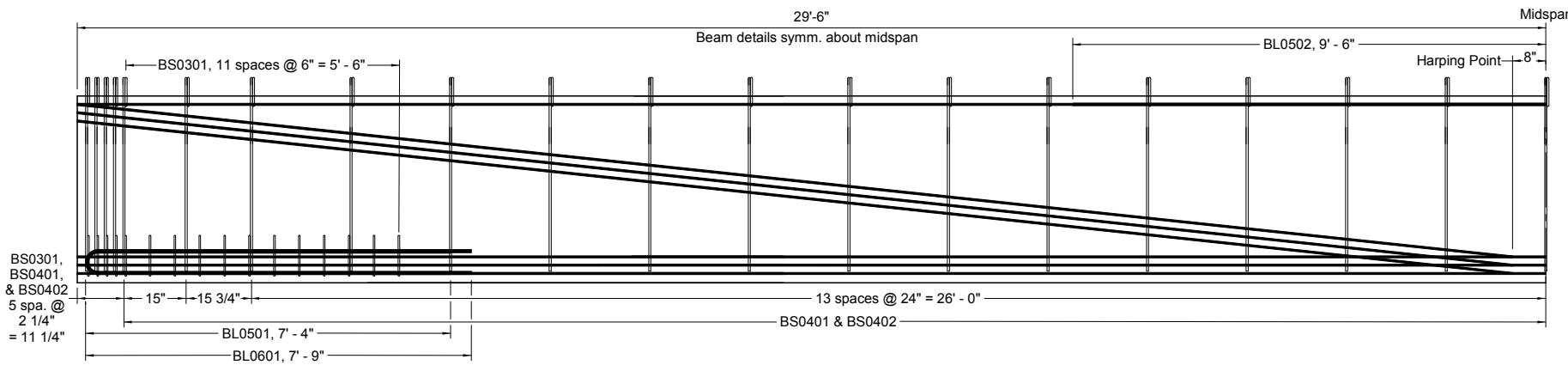

Partial Elevation

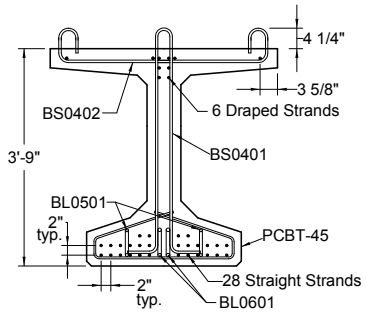

End View

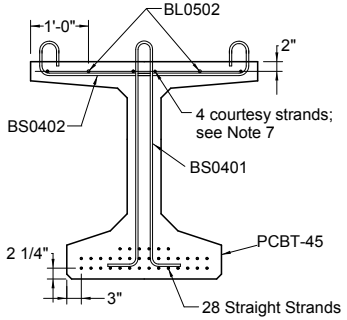

Center Line View

REINFORCING STEEL SCHEDULE

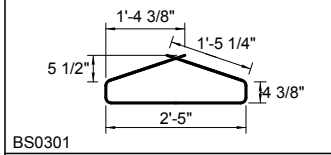

BS0301

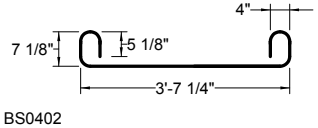

BS0402

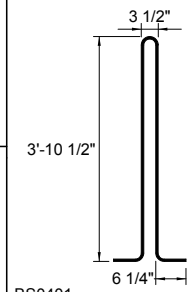

BS0401

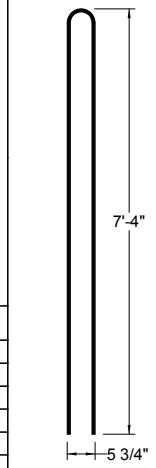

BL0501

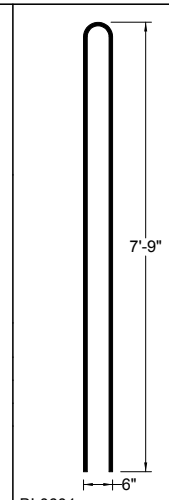

BL0601

Mark	Size	Pin Ø	Length	Wt./bar lbs	Qty.	Weight lbs
BS0301	#3	2"	5' - 11 1/2"	2.24	32	71.7
BS0401	#4	2 1/2"	8' - 8 1/2"	5.82	39	227.0
BS0402	#4	3"	5' - 8 1/4"	3.80	39	148.2
BL0501	#5	4 1/2"	14' - 10 1/4"	9.92	4	39.7
BL0502	#5	-	19' - 0"	19.8	2	39.6
BL0601	#6	4 1/2"	15' - 8 1/4"	13.05	4	94.2
				Total Weight		620.4

Notes:

1) Concrete strength at release = 7500psi
2) Concrete 28 day strength = 10000 psi
3) Concrete unit weight = 120 pcf
4) Concrete is lightweight mix design
5) All strands are 0.5" diameter, Grade 270
6) Bottom and draped strands are stressed to 75% GUTS = 31 kips per strand
7) 4 - 1/2 Ø strands stressed to 1000 lbs
8) Beam is standard PCBT-45 shape
9) Surface of top flange shall be intentionally roughened to an amplitude of 1/4"

Dimensions in bending diagram are out-to-out of the bars.

Reinforcing bars shown on the above schedule are for beams shown in this sheet only.

Reinforcing bars BS0401 and BS0402 shall be galvanized. All other reinforcing bars shall be epoxy coated.

VIRGINIA TECH

10-KSI LIGHTWEIGHT PRESTRESSED BEAM
VIRGINIA PCBT-45
MINIMUM SHEAR REINFORCEMENT

Scale: 1/2"=1'-0" | Rev. 3 | Date: 04/15/09 | Sheet No.: 7 of 7

Figure A-7. Plans for Beam BT.10.Min.

Appendix B

Stirrup Strains and Concrete Web Cracking

Figures B-1 through B-12 show the graphs of the strain in the stirrups versus the applied live shear force for individual tests, along with the locations of each gauge and web-shear cracks that were discernible in the concrete. The nomenclature of each strain gauge in the (a) portion of the figure is as follows. The first number in the identifier is the stirrup number counted from the end of the beam being tested. This same number corresponds to the number indicated along the bottom of the beam in the (b) figure. The second number in the gauge identifier is the gauge number on a given stirrup, counted from the bottom of the stirrup. This number is also indicated along the given stirrup in the (b) figure. So, for example, Figure B-1 shows that gauge 7.2 in test T2.8.Typ.1 is the second gauge from the bottom of the seventh stirrup from the end of the beam. The (b) portion of the figure also indicates whether the gauge yielded during testing, and if so, whether or not yielding developed as concrete cracking occurred at the gauge location. Of course, if the gauge was not working properly, then that gauge does not appear in the (a) figure. In the case of gauge 7.2 of test T2.8.Typ.1, Figure B-1 indicates that this gauge yielded upon first cracking at that location. The cracks sketched in the (c) portion of each figure only show the most severe cracks that formed within the web and extended to the top flange-web junction down to the pin support. Note that separate cracks were sketched for both sides of the girder web. These cracks were used to determine the boundary crack for each test, as discussed in Section 4.2.3.1.2.

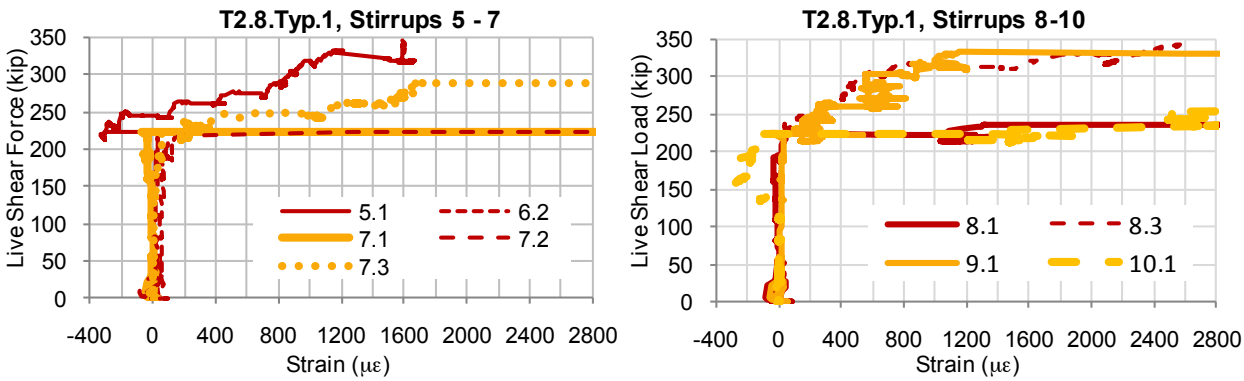

(a)

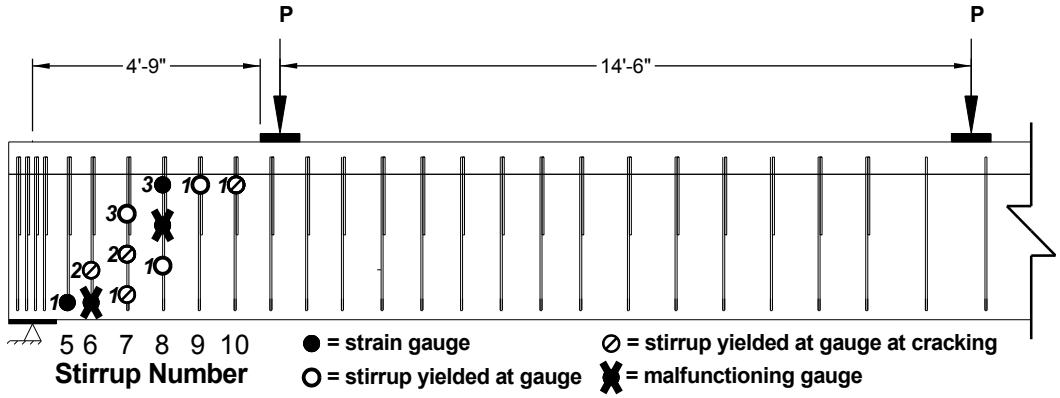

(b)

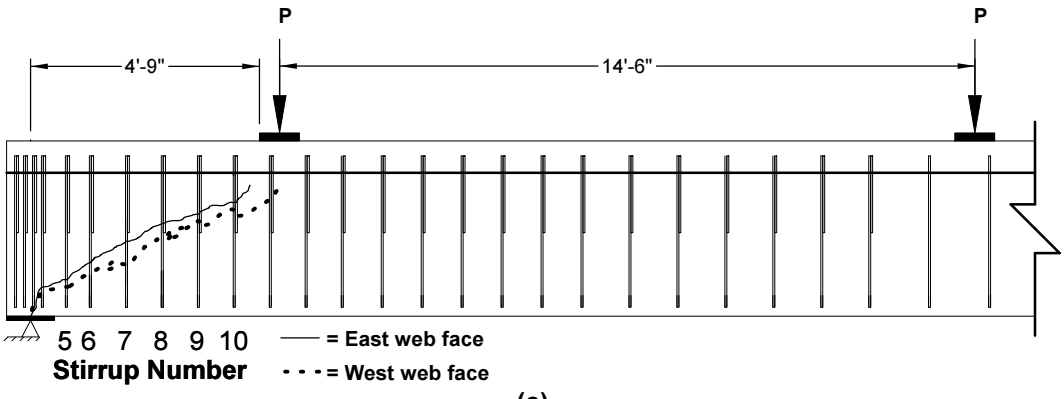

(c)

Figure B-1. (a) Strain gauge measurements, (b) strain gauge locations, and (c) primary web-shear cracks for Test T2.8.Typ.1.

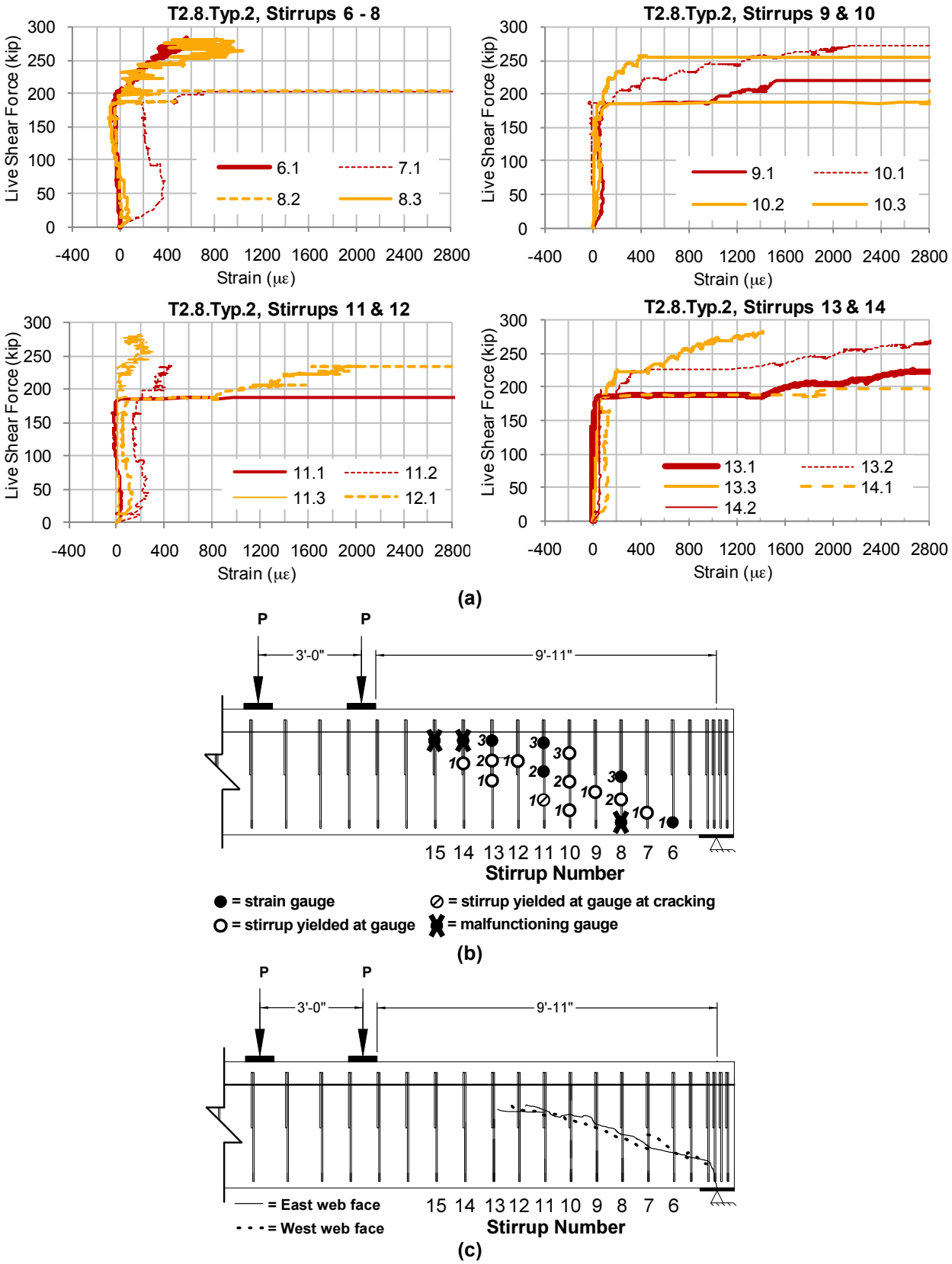

Figure B-2. (a) Strain gauge measurements, (b) strain gauge locations, and (c) primary web-shear cracks for Test T2.8.Typ.2.

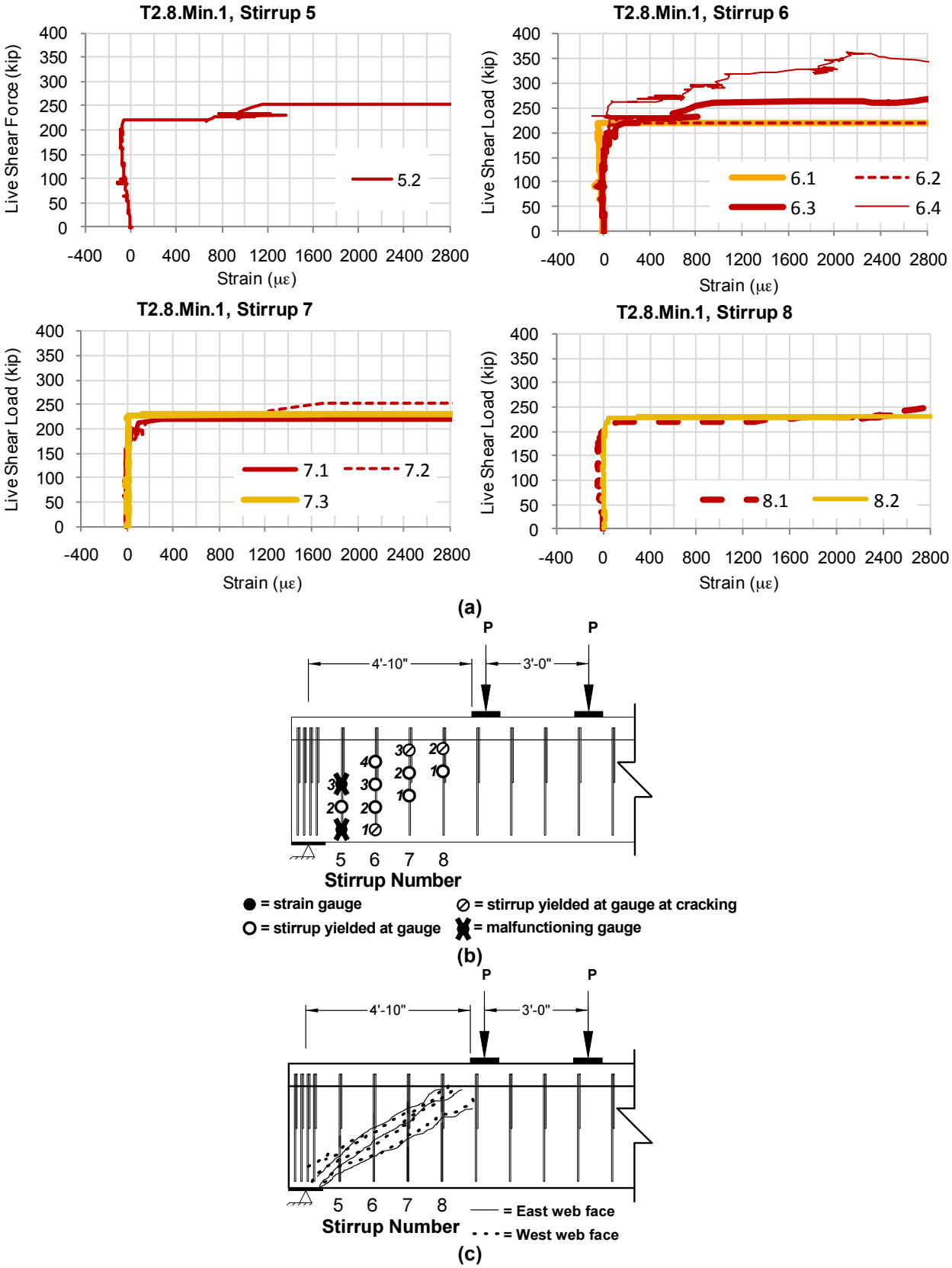

Figure B-3. (a) Strain gauge measurements, (b) strain gauge locations, and (c) primary web-shear cracks for Test T2.8.Min.1.

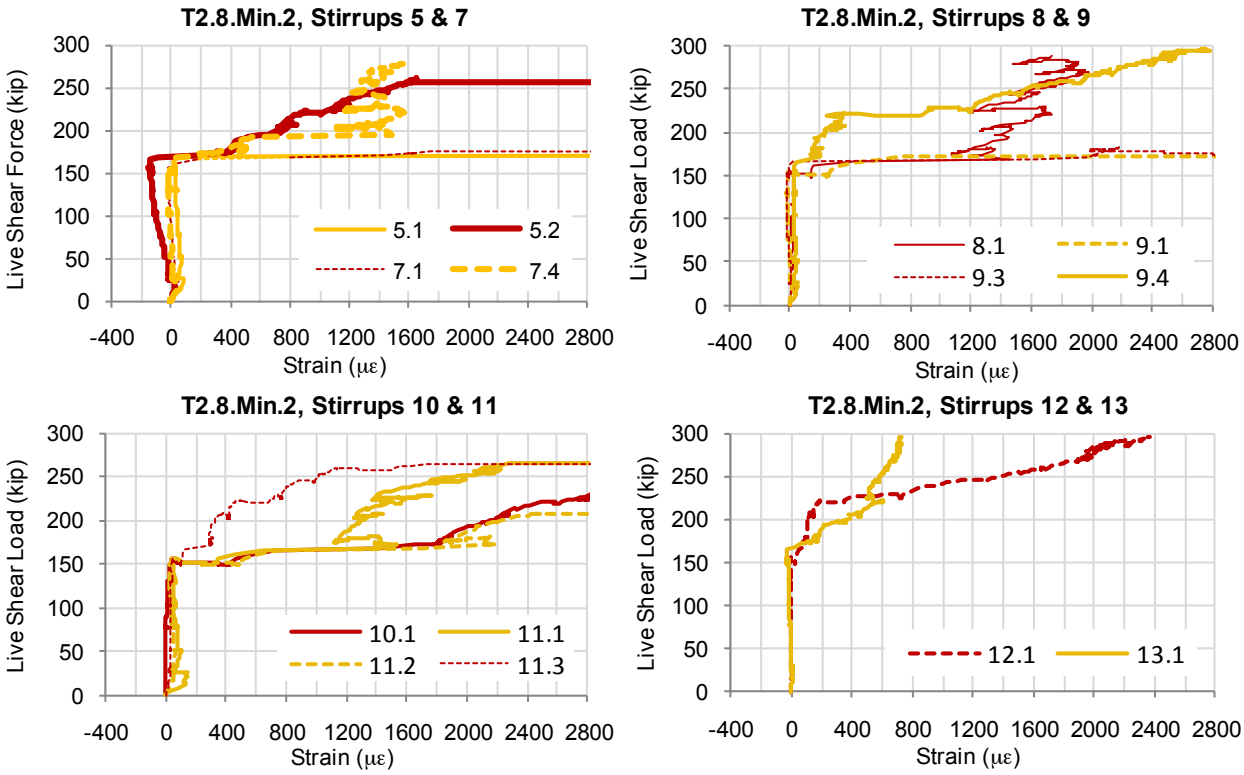

(a)

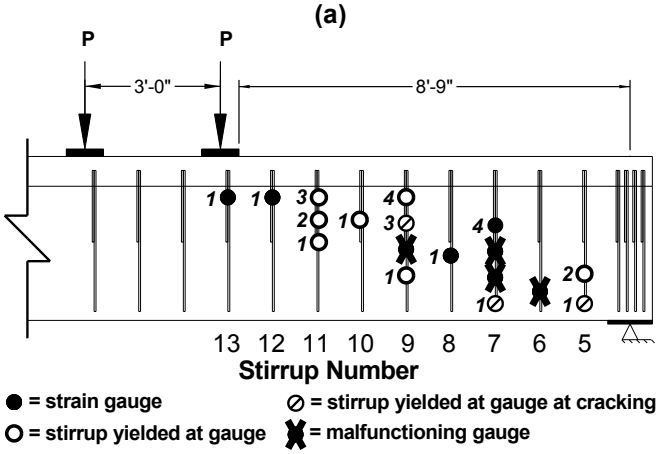

(b)

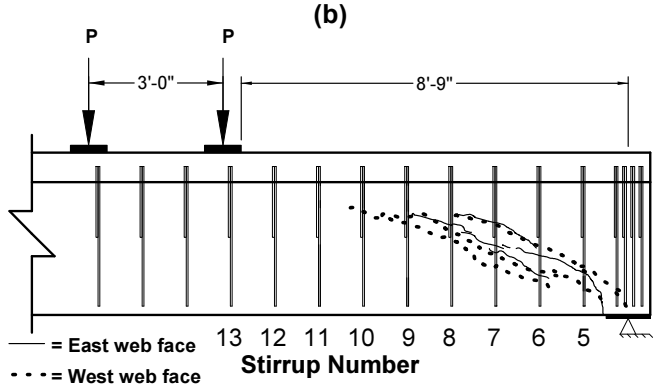

(c)

Figure B-4. (a) Strain gauge measurements, (b) strain gauge locations, and (c) primary web-shear cracks for Test T2.8.Min.2.

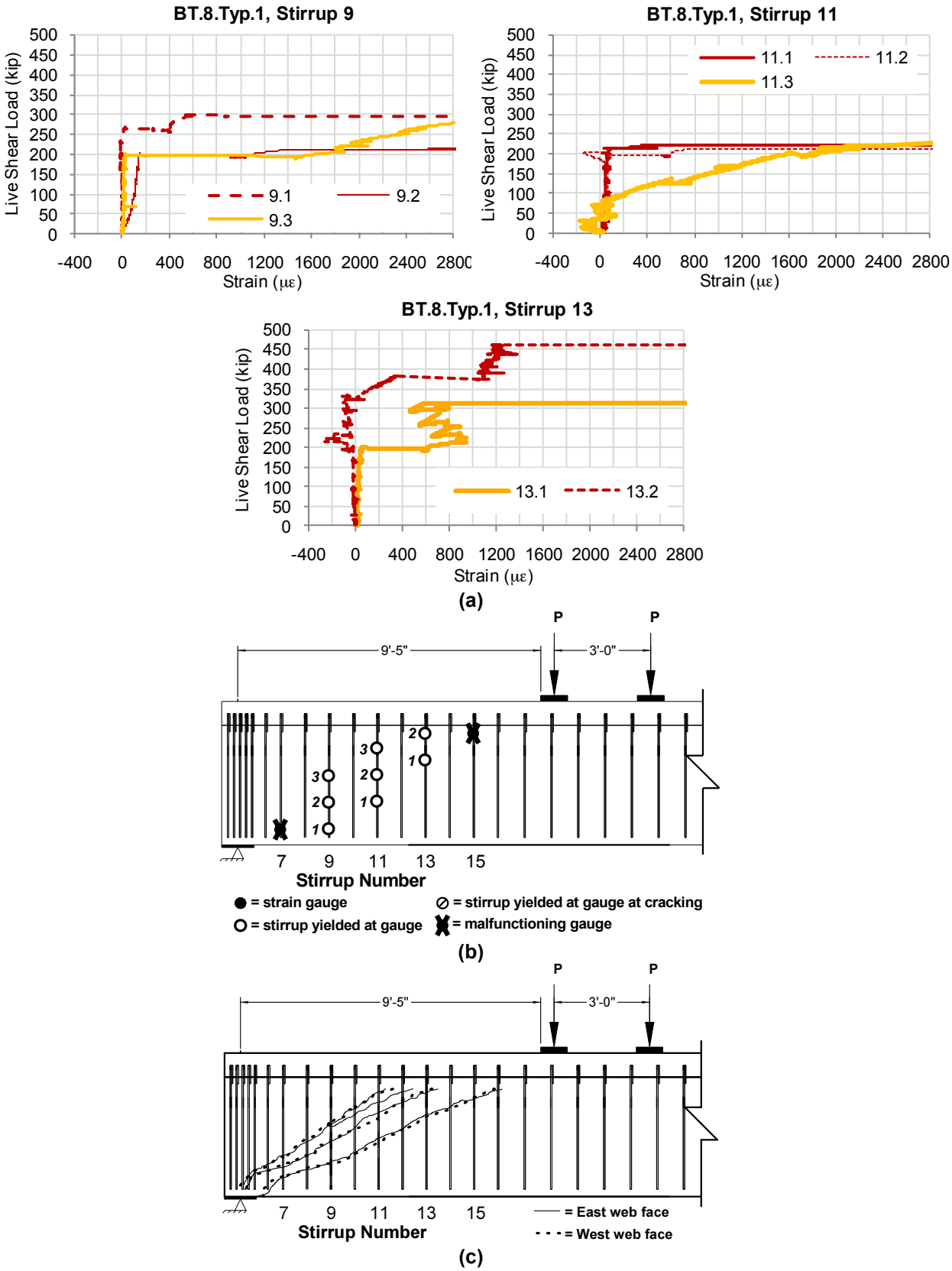

Figure B-5. (a) Strain gauge measurements, (b) strain gauge locations, and (c) primary web-shear cracks for Test BT.8.Typ.1.

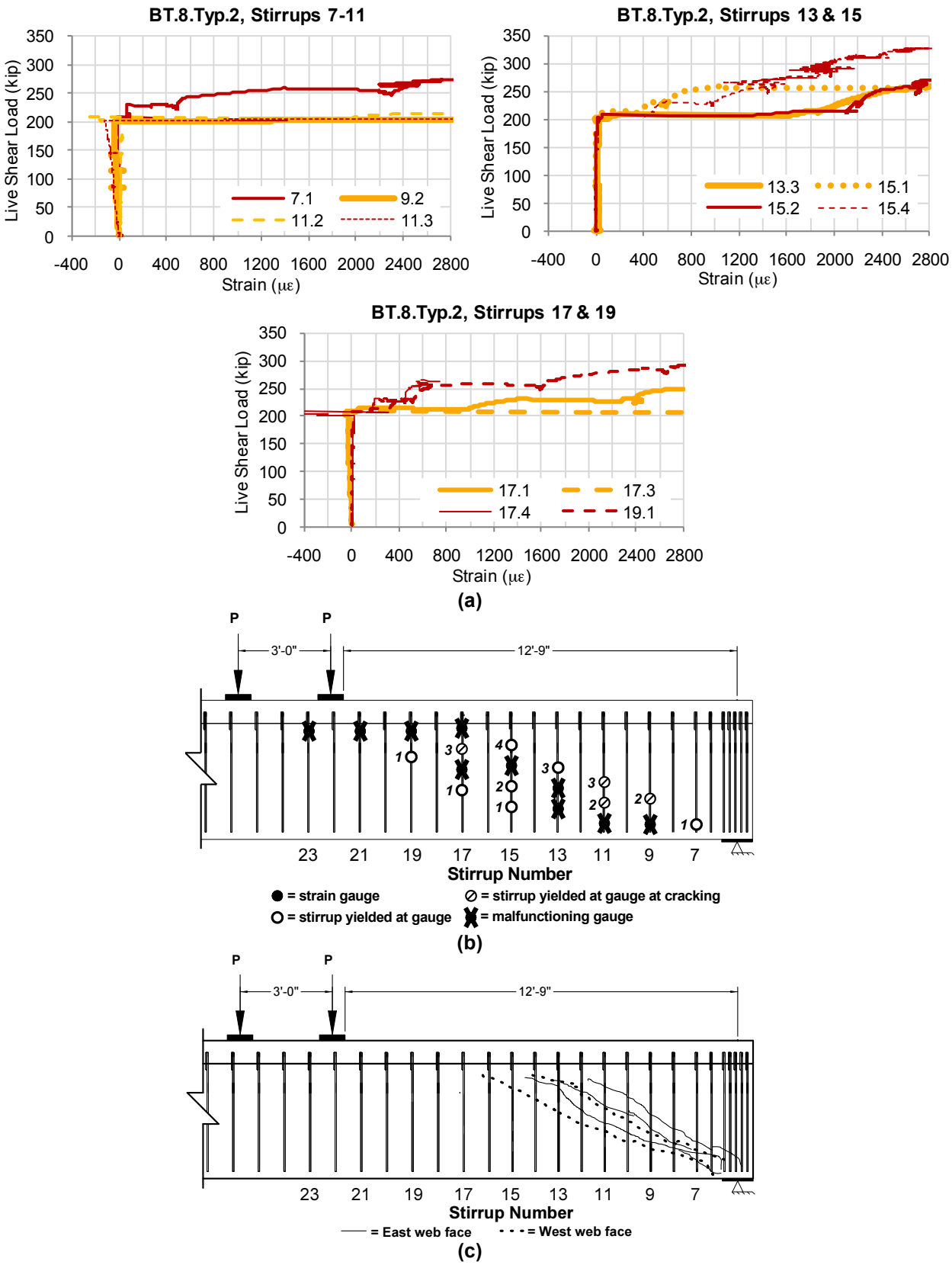

Figure B-6. (a) Strain gauge measurements, (b) strain gauge locations, and (c) primary web-shear cracks for Test BT.8.Typ.2.

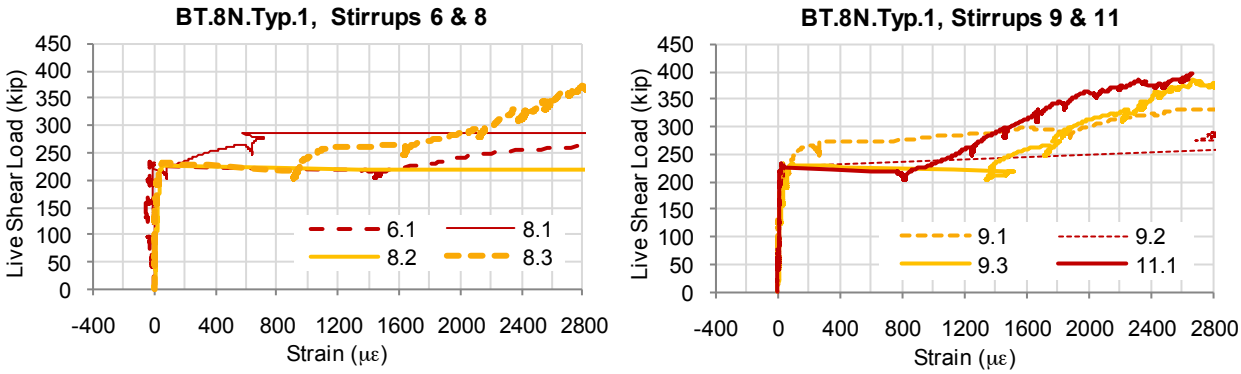

(a)

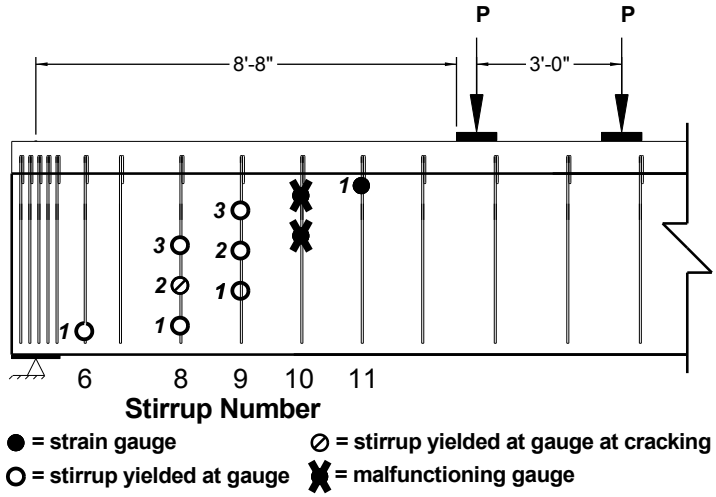

(b)

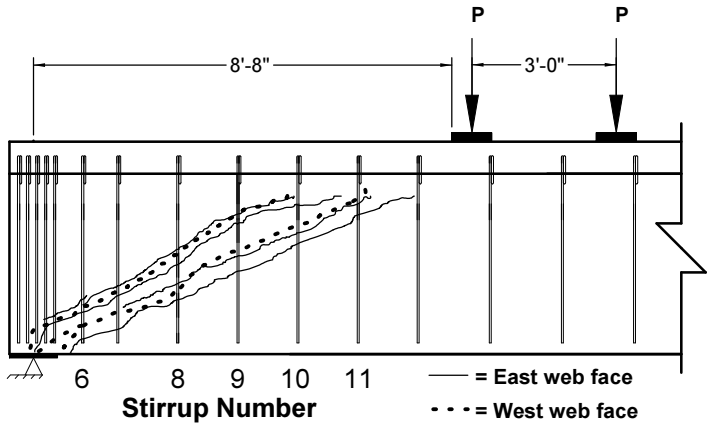

(c)

Figure B-7. (a) Strain gauge measurements, (b) strain gauge locations, and primary web-shear cracks for Test BT.8N.Typ.1.

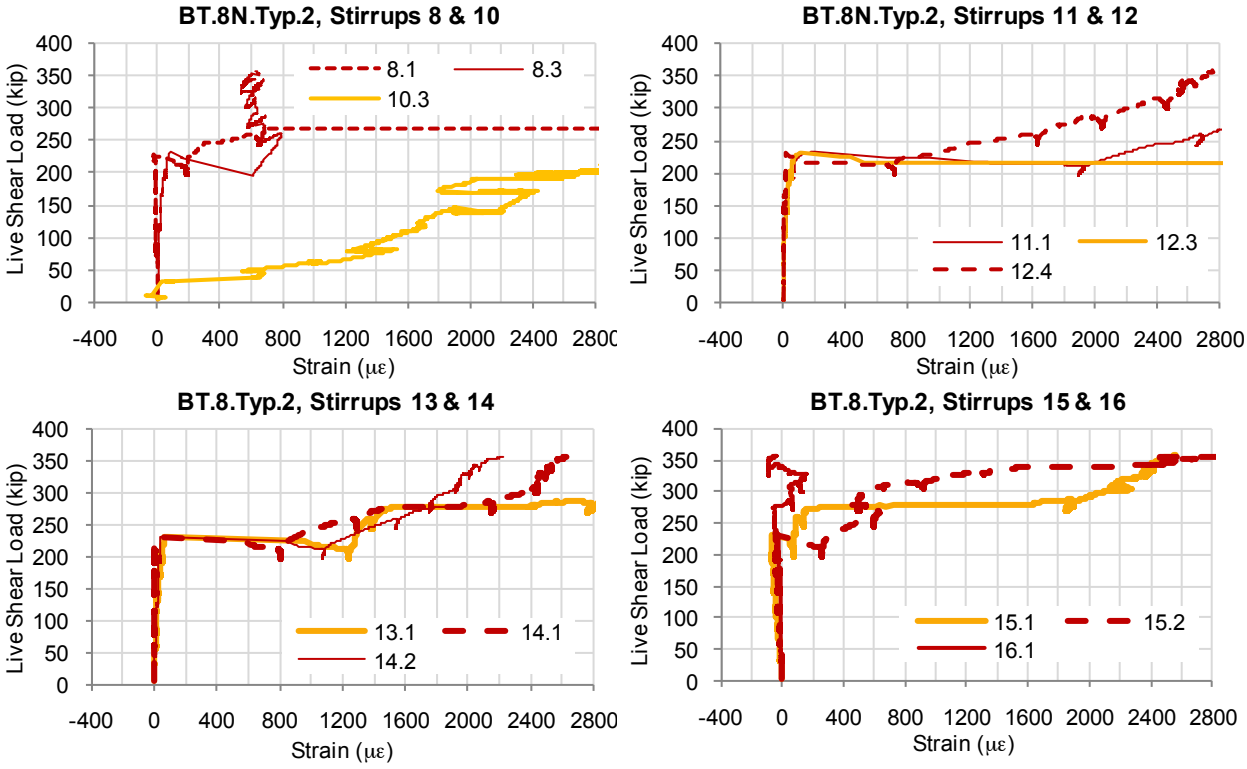

(a)

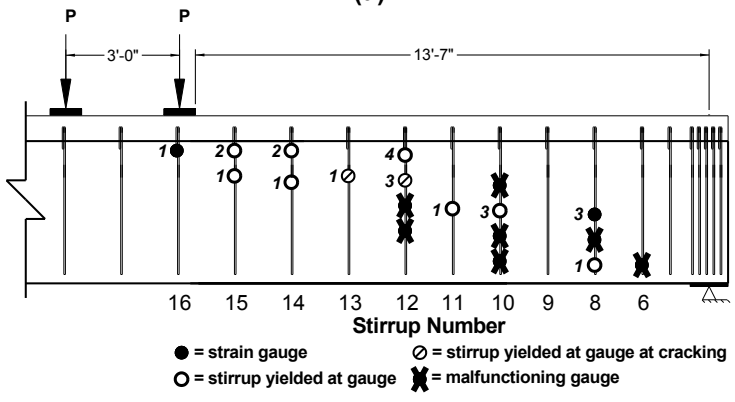

(b)

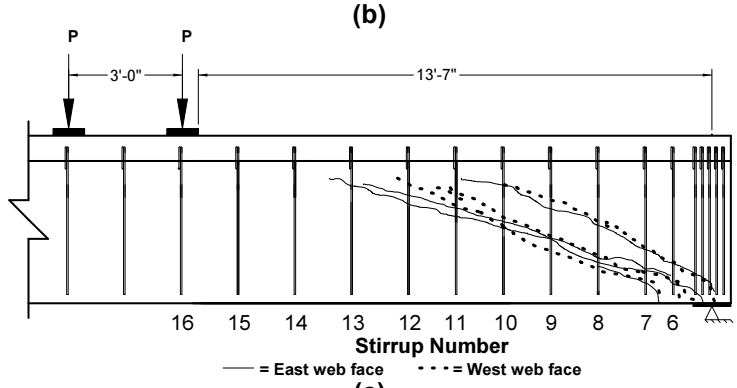

(c)

Figure B-8. (a) Strain gauge measurements, (b) strain gauge locations, and primary web-shear cracks for Test BT.8N.Typ.2.

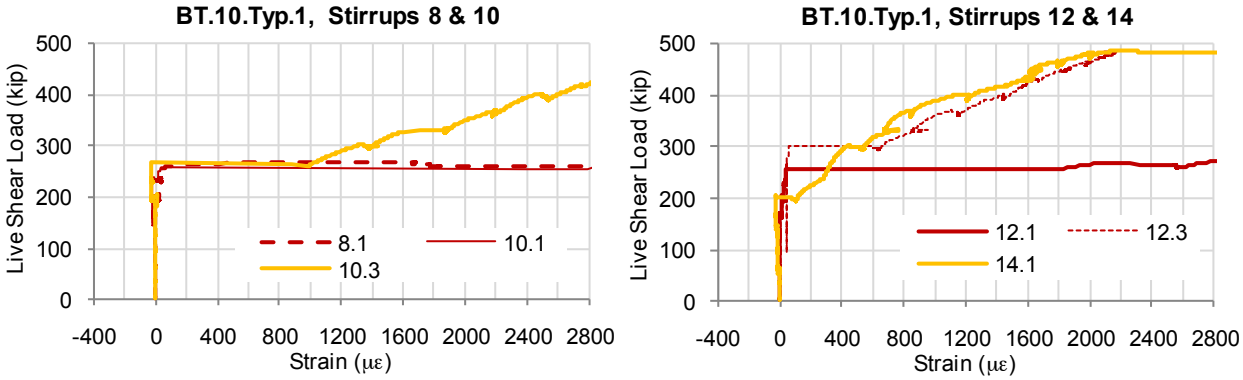

(a)

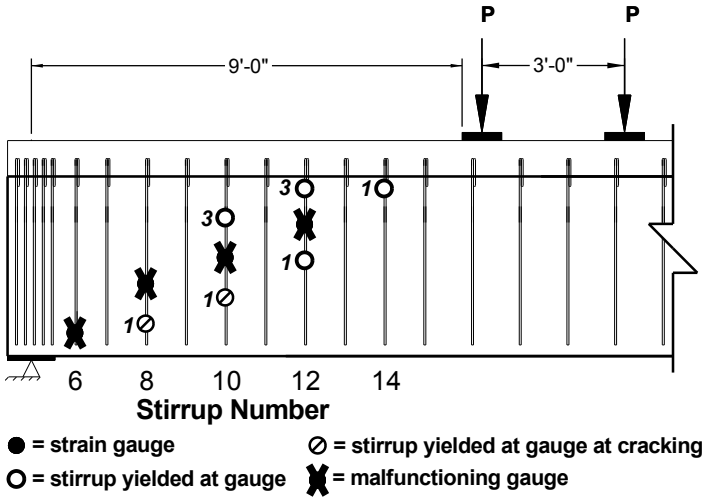

(b)

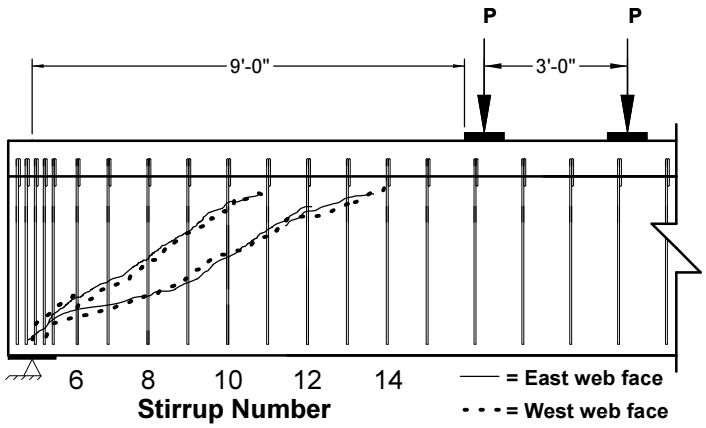

(c)

Figure B-9. (a) Strain gauge measurements, (b) strain gauge locations, and (c) primary web-shear cracks for Test BT.10.Typ.1.

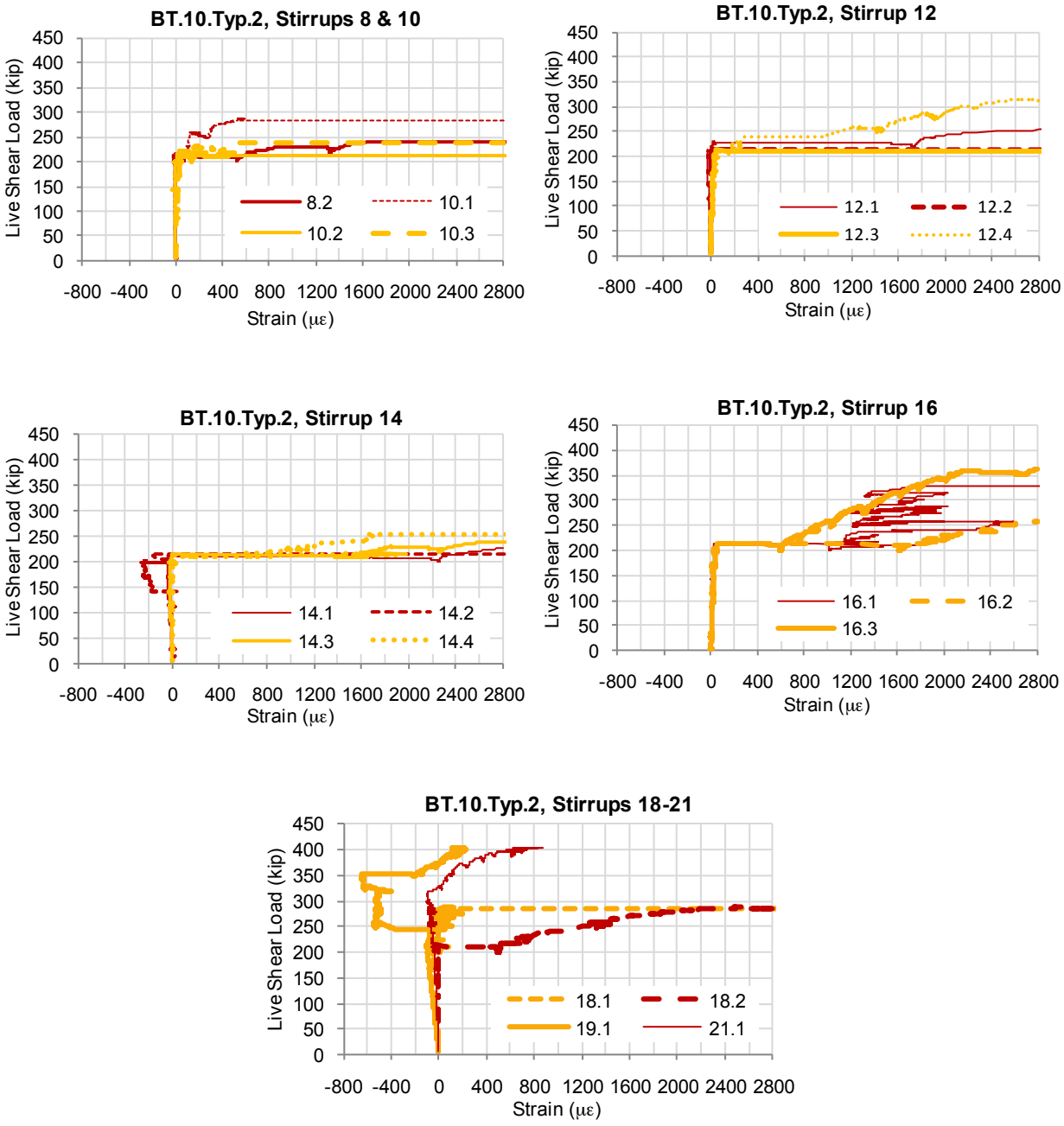

(a)

Figure B-10. (a) Strain gauge measurements, (b) strain gauge locations, and (c) primary web-shear cracks for Test BT.10.Typ.2.

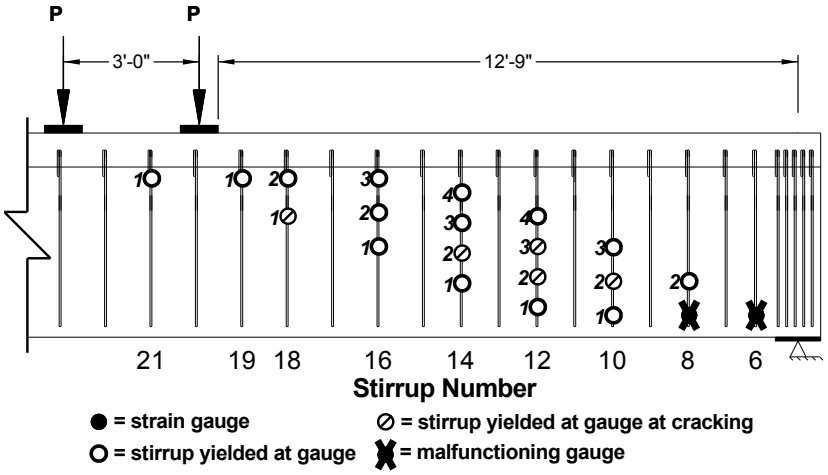

(b)

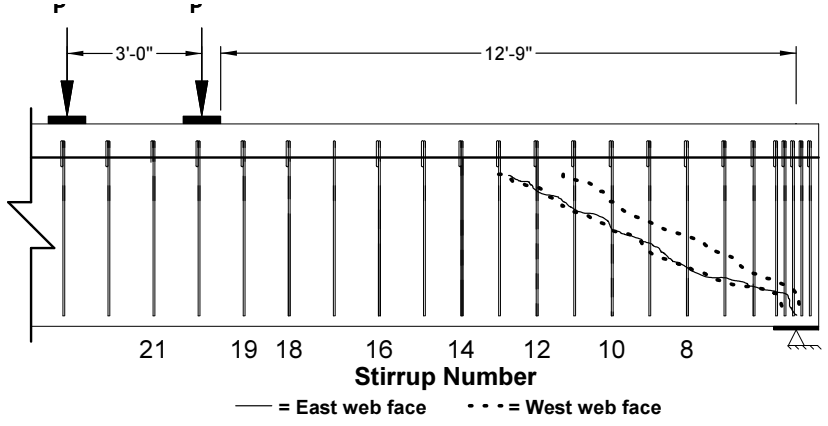

(c)

Figure B-10 (cont.). (a) Strain gauge measurements, (b) strain gauge locations, and (c) primary web-shear cracks for Test BT.10.Typ.2.

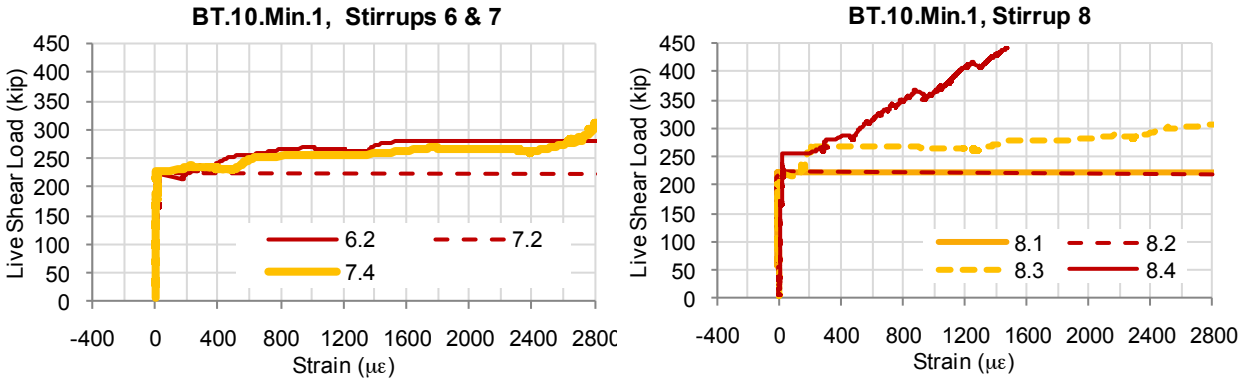

(a)

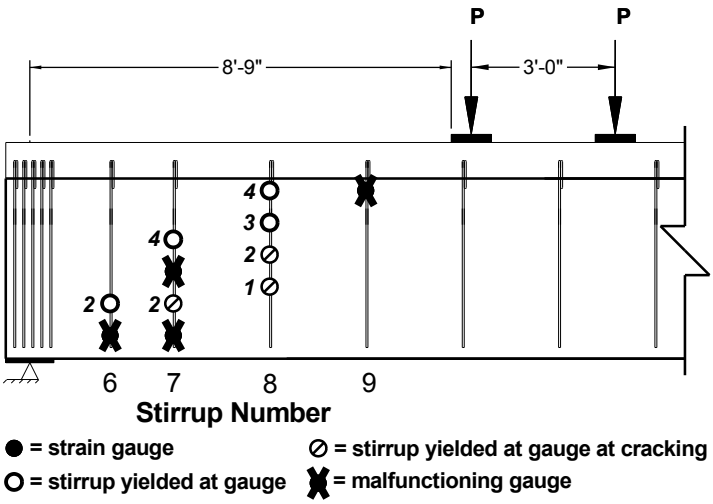

(b)

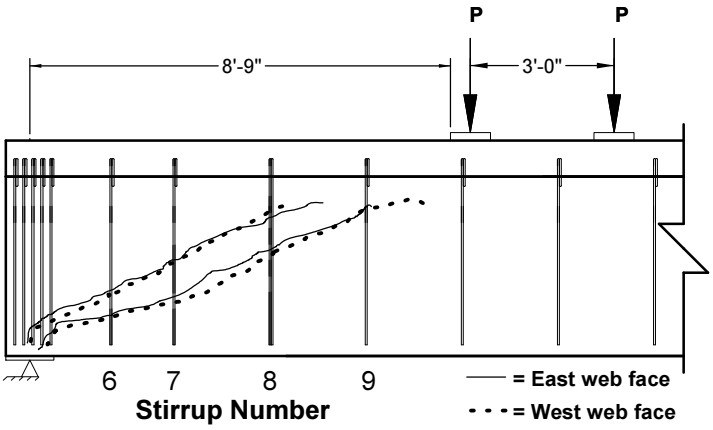

(c)

Figure B-11. (a) Strain gauge measurements, (b) strain gauge locations, and (c) primary web-shear cracks for Test BT.10.Min.1.

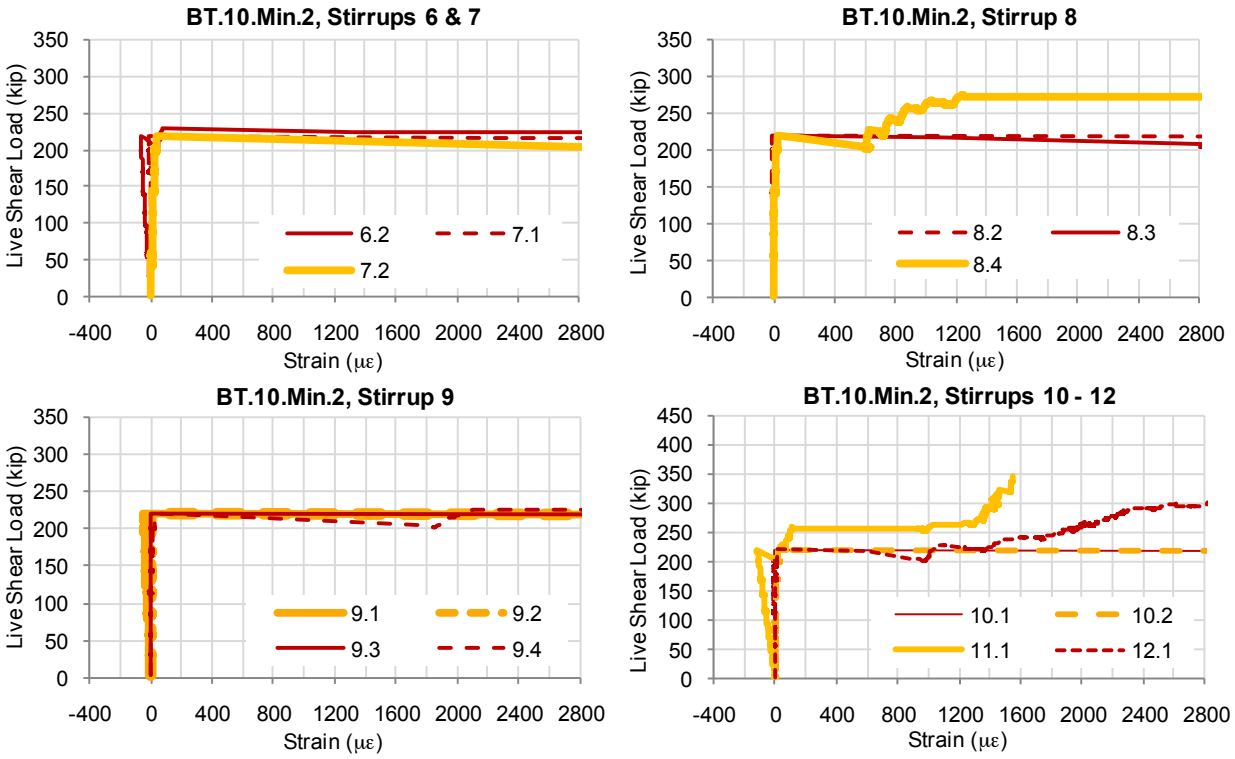

(a)

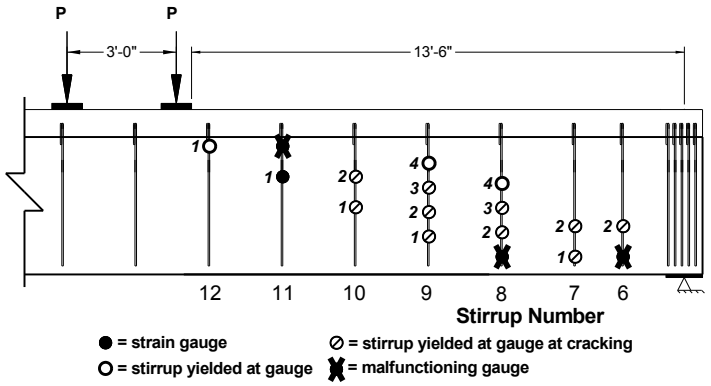

(b)

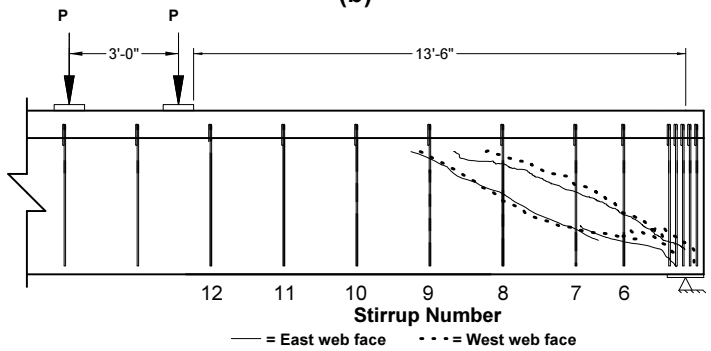

(c)

Figure B-12. (a) Strain gauge measurements, (b) strain gauge locations, and (c) primary web-shear cracks for Test BT.10.Min.2.

Appendix C
Example Shear Calculations

C.1 Computer Programs

Due to the iterative nature of shear design following the General Procedure in Article 5.8.3.4.2 of the AASHTO LRFD Bridge Specifications, computer programs have been developed in order to help speed up the calculation process. All programs were created using Mathcad software, v. 14.0, copyrighted by Parametric Technology Corporation. Although similar in procedure, calculations using Appendix B5 of the 2010 AASHTO LRFD Bridge Design Specifications and those conforming to the General Procedure in Article 5.8.3.4.2 utilize two different programs. The main program for *Appendix B5* appears in Figure C-1, with the supplemental subroutines shown in Figure C-2. There is an additional program that can interpolate the tabularized values for β and θ found in Appendix B5 of the 2010 AASHTO LRFD Bridge Design Specifications. However, this program is not presented here due to the size of the program rendering the program impractical to display. The main program for the *General Procedure* is in Figure C-5, with any additional subroutines that do not appear in Figure C-2 being in Figure C-4. Although not nearly as iterative in nature, a third program has been developed for calculating the shear strength following the Simplified Procedure for Prestressed and Nonprestressed Sections in Article 5.8.4.3.3 of the AASHTO LRFD Bridge Specifications. That program is given in Figure C-5.

```
calc = | ShearStrengthCheckFinal ← "NG"
       | iterations ← 0
       | iterations_θ.tot ← 0
       | for i ∈ 1.. rows(P_assume)
       |   θ_i ← 28
       | while ShearStrengthCheckFinal = "NG"
       |   iterations ← iterations + 1
       |   for i ∈ 1.. 1
       |     x_dist ← x_θ(x_critical.assume)_1
       |     if rows(x_dist) ≠ rows(P_assume)
       |       for i ∈ 1.. rows(x_dist)                    if rows(x_dist) < rows(P_assume)
       |         P_assume.old_i ← P_assume_i
       |         θ_old_i ← θ_i
       |       for i ∈ 1.. rows(x_dist) − rows(P_assume)    if rows(x_dist) > rows(P_assume)
       |         P_assume.old ← P_assume
       |         P_assume.old_(i+rows(P_assume)) ← P_assume_rows(P_assume)
       |         θ_old ← θ
       |         θ_old_(i+rows(P_assume)) ← θ_rows(P_assume)
       |       P_assume ← P_assume.old
       |       θ ← θ_old
       |     LiveLoad ← Load_Live(x_dist, P_assume, ShearSpan, LoadSpacing, L_span)
       |     DeadLoad ← Dead_Load(x_dist, L_span, x_bearing, x_bearing.roller, ShearSpan, w_beam, DC_1, DC_2, DW, P_diaphragm)
       |     V_assume ← ⌈1.00·(DeadLoad⟨5⟩ + DeadLoad⟨7⟩) + 1.00·DeadLoad⟨9⟩ + 1.00·LiveLoad⟨3⟩⌉·kip
       |     M_assume1 ← ⌈1.00·(DeadLoad⟨6⟩ + DeadLoad⟨8⟩) + 1.00·DeadLoad⟨10⟩ + 1.00·LiveLoad⟨4⟩⌉·kip·ft
       |     V_p ← V_p.(x_dist)
       |     cg_harp ← cg_harp.(x_dist)
       |     f_c'c ← | f_c'deck   if f_c'deck > 0
       |             | f_c'       otherwise
       |     β_1 ← β_1.(f_c'c)
       |   for i ∈ 1.. rows(x_dist)
       |     cg_ps_i ← (Num_straight·cg_straight + Num_harp·cg_harp_i) / Num_strand
       |     d_p_i ← h_c − cg_ps_i
       |   c ← c_calc(x_dist, A_ps, f_pu, A_s.bot, A_s.top, f_y, f_c'c, β_1, b_eff, b_v, h_flange, k, d_p)
```

Figure C-1. Program for calculating the design shear strength following *Appendix B5*.

$c \leftarrow c_{calc}(x_{dist}, A_{ps}, f_{pu}, A_{s.bot}, A_{s.top}, f_y, f_{c'c}, \beta_1, b_{eff}, b_v, h_{flange}, k, d_p)$

for $i \in 1..\text{rows}(x_{dist})$

$f_{ps.max_i} \leftarrow f_{pu} \cdot \left(1 - k \cdot \frac{c_i}{d_{p_i}}\right)$

$l_{d.ps_i} \leftarrow \kappa \cdot \left(f_{ps.max_i} - \frac{2}{3} \cdot f_{pe}\right) \varphi$

$f_{ps} \leftarrow f_{ps.}(x_{dist}, l_{d.ps}, f_{ps.max})$

$\varepsilon_{s.yield} \leftarrow \frac{f_y}{E_s}$

$Num_{strand.bot} \leftarrow Num_{strand.bot.}(x_{dist}, cg_{harp})$

$cg_{ps.bot} \leftarrow cg_{ps.bot.}(x_{dist}, cg_{straight}, cg_{harp}, h_c, Num_{straight})$

for $i \in 1..\text{rows}(x_{dist})$

$d_{p.bot_i} \leftarrow h_c - cg_{ps.bot_i}$

$d_{s.bot_i} \leftarrow h_c - cg_{s.bot_i}$

$A_{ps.bot_i} \leftarrow Num_{strand.bot_i} A_{strand}$

$d_{e_i} \leftarrow \frac{A_{ps.bot_i} \cdot f_{ps_i} \cdot d_{p.bot_i} + A_{s.bot_i} \cdot f_y \cdot d_{s.bot_i}}{A_{ps.bot_i} \cdot f_{ps_i} + A_{s.bot_i} \cdot f_y}$

$\varepsilon_{s_i} \leftarrow \frac{0.003}{c_i} \cdot (d_{e_i} - c_i)$

return $\left("\text{Tension steel does not yield at x.dist (inches)"} \quad \frac{x_{dist_i}}{in}\right)$ if $\varepsilon_{s_i} < \varepsilon_{s.yield}$

$a_i \leftarrow \beta_1 \cdot c_i$

$d_{v_i} \leftarrow \max\left(d_{e_i} - \frac{a_i}{2}, 0.9 d_{e_i}, 0.72 h_c\right)$

$M_{assume_i} \leftarrow \max\left(M_{assume1_i}, \left|V_{assume_i} - V_{p_i}\right| \cdot d_{v_i}\right)$

$v_u \leftarrow v_{u.}(x_{dist}, V_{assume}, V_p, d_v, MinReinforcingCheck)$

$l_{d.mild} \leftarrow l_{d.mild.}(d_{long.rebar}, f_{c'}, f_y, IsTopBarEffectApplicable, IsLongSteelEpoxyCoated, LongSteelCover, LongSteelCl$

for $i \in 1..\text{rows}(x_{dist})$

$RedFactor_{\varepsilon x.ps_i} \leftarrow \begin{cases} \frac{x_{dist_i} + x_{bearing}}{l_{d.ps_i}} & \text{if } x_{dist_i} + x_{bearing} < l_{d.ps_i} \\ 1 & \text{if } x_{dist_i} + x_{bearing} \geq l_{d.ps_i} \end{cases}$

$A_{ps.bot.\varepsilon x_i} \leftarrow Num_{strand.bot_i} \cdot A_{strand} \cdot RedFactor_{\varepsilon x.ps_i}$

Figure C-1 (cont.) Program for calculating the design shear strength following *Appendix B5*.

$$A_{ps.bot.\,\varepsilon x_i} \leftarrow Num_{strand.bot_i} \cdot A_{strand} \cdot RedFactor_{\varepsilon x.ps_i}$$

$$RedFactor_{\varepsilon x.s_i} \leftarrow \begin{cases} \dfrac{x_{dist_i} + x_{bearing}}{l_{d.mild}} & \text{if } x_{dist_i} + x_{bearing} < l_{d.mild} \\ 1 & \text{if } x_{dist_i} + x_{bearing} \geq l_{d.mild} \end{cases}$$

$$A_{s.bot.\,\varepsilon x_i} \leftarrow A_{s.bot_i} \cdot RedFactor_{\varepsilon x.s_i}$$

$$\theta\beta \leftarrow \theta_{iterate}\left(x_{dist}, A_{ps.bot.\,\varepsilon x}, A_{s.bot.\,\varepsilon x}, f_{ps}, c, d_p, M_{assume}, d_v, V_{assume}, V_p, \theta, cg_{harp}, v_u, MinReinforcingCheck,\right.$$

$$\theta \leftarrow \theta\beta_1$$

$$\beta \leftarrow \theta\beta_2$$

$$iterations_{\theta.tot} \leftarrow iterations_{\theta.tot} + \theta\beta_3 \quad \text{if } \theta\beta method = \text{"General"}$$

$$V_r \leftarrow V_{r.}\left(x_{dist}, \beta, d_v, \theta, s_{v.design}, V_p\right)$$

for $i \in 1..\,rows\left(x_{dist}\right)$

$$ShearStrengthCheck_i \leftarrow \text{"OK"} \quad \text{if } V_{r_i} - V_{assume_i} \leq 0.1kip \wedge V_{r_i} - V_{assume_i} \geq 0kip$$

$$\text{if } V_{r_i} - V_{assume_i} > 0.1kip \vee V_{r_i} - V_{assume_i} < 0kip$$

$$ShearStrengthCheck_i \leftarrow \text{"NG!!!"}$$

$$ShearStrengthSum \leftarrow ShearStrengthSum + 1$$

$$V_{assume_i} \leftarrow \frac{1}{2}\left(V_{r_i} + V_{assume_i}\right) - 0.01kip$$

$$P_{assume_i} \leftarrow \begin{cases} \dfrac{\left[V_{assume_i} - \left\lceil 1.00\left\lceil \left(DeadLoad^{\langle 5 \rangle}\right)_i + \left(DeadLoad^{\langle 7 \rangle}\right)_i \right\rceil + 1.00 \cdot \left(DeadLoad^{\langle 9 \rangle}\right)_i \right\rceil \cdot kip\right] \cdot L_{span}}{\left\lceil 2\left(L_{span} - ShearSpan\right) - LoadSpacing \right\rceil} & \text{if } x_{c} \\ \dfrac{\left[V_{assume_i} - \left\lceil 1.00\left\lceil \left(DeadLoad^{\langle 5 \rangle}\right)_i + \left(DeadLoad^{\langle 7 \rangle}\right)_i \right\rceil + 1.00 \cdot \left(DeadLoad^{\langle 9 \rangle}\right)_i \right\rceil \cdot kip\right] \cdot L_{span}}{L_{span} - 2ShearSpan - LoadSpacing} & \text{if } Sl \\ \dfrac{\left[V_{assume_i} - \left\lceil 1.00\left\lceil \left(DeadLoad^{\langle 5 \rangle}\right)_i + \left(DeadLoad^{\langle 7 \rangle}\right)_i \right\rceil + 1.00 \cdot \left(DeadLoad^{\langle 9 \rangle}\right)_i \right\rceil \cdot kip\right] \cdot L_{span}}{2ShearSpan + LoadSpacing} & \text{if } x_{c} \end{cases}$$

$$vect\_elemnt_{x.critical} \leftarrow \frac{x\_\theta\left(x_{critical.assume}\right)2}{in}$$

for $i \in 1..\,1$

$$ShearStrengthCheckFinal \leftarrow \text{"OK"} \quad \text{if } ShearStrengthSum = 0 \vee iterations > 500$$

$$\text{if } rows\left(vect\_elemnt_{x.critical}\right) > 1$$

$$d_{v.critical} \leftarrow d_v\left(vect\_elemnt_{x.critical_1}\right)$$

$$\theta_{critical} \leftarrow \theta\left(vect\_elemnt_{x.critical_1}\right)$$

$$\text{if } rows\left(vect\_elemnt_{x.critical}\right) \leq 1$$

$$d_{v.critical} \leftarrow d_v\left(vect\_elemnt_{x.critical}\right)$$

$$\theta_{critical} \leftarrow \theta\left(vect\_elemnt_{x.critical}\right)$$

Figure C-1 (cont.) Program for calculating the design shear strength following *Appendix B5*.

```
        θcritical ← θ(vect_elemnt_x.critical)
    xcritical.assume ← max(d_v.critical, (1/2)·d_v.critical·cot(θcritical·π/180))
(V_n.critical  x_critical) ← (0  0)
for i ∈ 1.. rows(vect_elemnt_x.critical)          if rows(vect_elemnt_x.critical) > 1
    V_n.critical_i ← V_r(vect_elemnt_x.critical_i)
    x_critical_i ← x_dist(vect_elemnt_x.critical_i)
if rows(vect_elemnt_x.critical) ≤ 1
    V_n.critical ← V_r_vect_elemnt_x.critical
    x_critical ← x_dist_vect_elemnt_x.critical
for i ∈ 1.. rows(x_dist)
    θβcalc_i ← "Simple"  if θβmethod = "Simple" ∧ (N_u = 0 ∧ MinReinforcingCheck_i = "OK" ∨ h_c < 16in)
    θβcalc_i ← "General"  if θβmethod = "General"
    "error"  otherwise
(V_r/kip  P_assume/kip  θ  β  x_dist/in  x_critical/in  V_n.critical/kip  iterations  iterations_θ.tot  θβcalc  MinReinforcingCheck  ε_s)
```

Figure C-1 (cont.) Mathcad program used to calculate the design shear strength following *Appendix B5*.

$$\kappa = \frac{in^2}{kip} \cdot \begin{cases} 1.6 & \text{if } h \geq 24in \\ 1.0 & \text{if } h < 24in \\ \text{"error"} & \text{otherwise} \end{cases}$$

$$f_{r.V} = \begin{cases} 0.20 \cdot \sqrt{\frac{f_c'}{ksi}} ksi & \text{if FineAggType} = \text{"sand"} \\ \left(0.17 \cdot \sqrt{\frac{f_c'}{ksi}} ksi\right) & \text{if FineAggType} = \text{"lightweight"} \\ \text{"error"} & \text{otherwise} \end{cases}$$

$$cg_{harp.}(x_{dist}) = \begin{cases} cg_{harp} \leftarrow 0 \\ \text{for } i \in 1..\text{rows}(x_{dist}) \\ \quad cg_{harp_i} \leftarrow \left[cg_{harp.end} - \left(x_{dist_i} + x_{bearing}\right)\tan\left(\Psi_{harp}\right)\right] & \text{if } x_{dist_i} \leq HarpDist \\ \quad cg_{harp_i} \leftarrow cg_{harp.ms} & \text{if } x_{dist_i} > HarpDist \\ \quad cg_{harp_i} \leftarrow \text{"error"} & \text{otherwise} \\ cg_{harp} \end{cases}$$

$$A_{rebar}(r, RebarSize) = \begin{cases} \text{for } i \in 1..r \\ \quad A_{rebar_i} \leftarrow 0.0438 & \text{if } RebarSize_i = 1.9 \\ \quad A_{rebar_i} \leftarrow 0.0491 & \text{if } RebarSize_i = 2 \\ \quad A_{rebar_i} \leftarrow 0.078 & \text{if } RebarSize_i = 2.5 \\ \quad A_{rebar_i} \leftarrow 0.11 & \text{if } RebarSize_i = 3 \\ \quad A_{rebar_i} \leftarrow 0.20 & \text{if } RebarSize_i = 4 \\ \quad A_{rebar_i} \leftarrow 0.31 & \text{if } RebarSize_i = 5 \\ \quad A_{rebar_i} \leftarrow 0.44 & \text{if } RebarSize_i = 6 \\ \quad A_{rebar_i} \leftarrow 0.60 & \text{if } RebarSize_i = 7 \\ \quad A_{rebar_i} \leftarrow 0.79 & \text{if } RebarSize_i = 8 \\ \quad A_{rebar_i} \leftarrow 1.00 & \text{if } RebarSize_i = 9 \\ \quad A_{rebar_i} \leftarrow 1.27 & \text{if } RebarSize_i = 10 \\ \quad A_{rebar_i} \leftarrow 1.56 & \text{if } RebarSize_i = 11 \\ \quad A_{rebar_i} \leftarrow 0 & \text{if } RebarSize_i = 0 \\ A_{rebar} \end{cases} \cdot in^2$$

Figure C-2. Subroutines used in the main calculation program given in Figure C-1.

$$\alpha_v = \begin{cases} 1 \text{ if ConcreteType} = \text{"NWC"} \vee \text{ConcreteType} = \text{"LWC"} \wedge \text{Value\_}f_{ct} = \text{"specified"} \wedge 4.7 \cdot f_{ct} \geq \sqrt{f_{c'} \cdot \text{ksi}} \\ \dfrac{4.7 \cdot f_{ct}}{\sqrt{f_{c'} \cdot \text{ksi}}} \text{ if ConcreteType} = \text{"LWC"} \wedge \text{Value\_}f_{ct} = \text{"specified"} \wedge 4.7 \cdot f_{ct} \leq \sqrt{f_{c'} \cdot \text{ksi}} \\ 0.85 \text{ if ConcreteType} = \text{"LWC"} \wedge \text{Value\_}f_{ct} = \text{"not specified"} \wedge \text{FineAggType} = \text{"sand"} \\ 0.75 \text{ if ConcreteType} = \text{"LWC"} \wedge \text{Value\_}f_{ct} = \text{"not specified"} \wedge \text{FineAggType} = \text{"lightweight"} \\ \text{"error"} \quad \text{otherwise} \end{cases}$$

$$\text{MinReinforcingCheck}_r = \begin{cases} \text{"OK"} \quad \text{if } 0.0316 \alpha_v \cdot \sqrt{f_{c'} \cdot (\text{ksi})} \cdot \dfrac{b_v \cdot s_{v.\text{design}_r}}{f_{yv}} \leq A_{v_r} \\ \text{"NG!!!"} \quad \text{if } 0.0316 \alpha_v \cdot \sqrt{f_{c'} \cdot (\text{ksi})} \cdot \dfrac{b_v \cdot s_{v.\text{design}_r}}{f_{yv}} > A_{v_r} \\ \text{"error"} \quad \text{otherwise} \end{cases}$$

$$\beta_1\left(f_{c'\text{deck}}\right) = \begin{cases} 0.85 \text{ if } f_{c'\text{deck}} \leq 4\text{ksi} \\ \max\left[0.85 - 0.05 \cdot \left(\dfrac{f_{c'\text{deck}}}{\text{ksi}} - 4.0\right), 0.65\right] \text{ if } f_{c'\text{deck}} > 4\text{ksi} \end{cases}$$

$$x\_\theta\left(x_{\text{critical.assume}}\right) = \begin{cases} \left(x \; x_1 \; m \; o\right) \leftarrow (0 \; 0 \; 1 \; 0) \\ x \leftarrow 0 \\ x_1 \leftarrow 0 \\ m \leftarrow 1 \\ \text{for } i \in 1..12 \\ \quad \begin{cases} \text{if } 0.1\text{ShearSpan} \cdot (i-1) < x_{\text{critical.assume}} \wedge x_{\text{critical.assume}} \leq 0.1\text{ShearSpan} \cdot (i) \\ \quad \begin{cases} x_{i+1} \leftarrow x_{\text{critical.assume}} \\ n \leftarrow i + 1 \end{cases} \\ \text{if } 0.1\text{ShearSpan} \cdot (i-1) < \text{ShearSpan} - x_{\text{critical.assume}} \wedge \text{ShearSpan} - x_{\text{critical.assume}} \leq 0.1\text{ShearSpan} \\ \quad \begin{cases} x_{i+2} \leftarrow \text{ShearSpan} - x_{\text{critical.assume}} \\ o \leftarrow i + 2 \end{cases} \end{cases} \\ \text{for } i \in 2..13 \\ \quad \begin{cases} m \leftarrow 2 \text{ if } i = n \\ m \leftarrow 3 \text{ if } i = o \\ (\text{break}) \text{ if } i = 13 \wedge x_{\text{critical.assume}} > \dfrac{1}{2}\text{ShearSpan} \\ x_i \leftarrow 0.1\text{ShearSpan} \cdot (i - m) \text{ otherwise} \end{cases} \\ X_1 \leftarrow x \\ X_2 \leftarrow \begin{cases} \binom{n}{o} \text{in if } o > 0 \\ (n \cdot \text{in}) \text{ if } o = 0 \\ \text{"error"} \quad \text{otherwise} \end{cases} \\ X \end{cases}$$

Figure C-2 (cont.) Subroutines used in the main calculation program given in Figure C-1.

$$
\begin{aligned}
&\text{LoadLive}(x_{dist}) = \\
&\quad x_{dist} \leftarrow \frac{x_{dist}}{ft} \\
&\quad V_{assume} \leftarrow \frac{V_{assume}}{kip} \\
&\quad ShearSpan \leftarrow \frac{ShearSpan}{ft} \\
&\quad LoadSpacing \leftarrow \frac{LoadSpacing}{ft} \\
&\quad L_{span} \leftarrow \frac{L_{span}}{ft} \\
&\quad \text{for } i \in 1..\text{rows}(x_{dist}) \\
&\qquad x\%_i \leftarrow \frac{x_{dist_i}}{ShearSpan} \\
&\qquad \text{if } x_{dist_i} \le ShearSpan + 10^{-12} \\
&\qquad\quad V_{LL_i} \leftarrow \frac{V_{assume_i}}{L_{span}} \cdot \left\lceil 2\left(L_{span} - ShearSpan\right) - LoadSpacing \right\rceil \\
&\qquad\quad M_{LL_i} \leftarrow \frac{V_{assume_i}}{L_{span}} \cdot \left\lceil 2\left(L_{span} - ShearSpan\right) - LoadSpacing \right\rceil \cdot x_{dist_i} \\
&\qquad \text{if } ShearSpan + 10^{-12} < x_{dist_i} \wedge x_{dist_i} \le ShearSpan + LoadSpacing \\
&\qquad\quad V_{LL_i} \leftarrow \frac{V_{assume_i}}{L_{span}} \left(L_{span} - 2ShearSpan - LoadSpacing\right) \\
&\qquad\quad M_{LL_i} \leftarrow \frac{V_{assume_i}}{L_{span}} \cdot \left\lceil 2\left(L_{span} - ShearSpan\right) - LoadSpacing \right\rceil \cdot x_{dist_i} - V_{assume_i} \cdot \left(x_{dist_i} - ShearSpan\right) \\
&\qquad \text{if } x_{dist_i} > ShearSpan + LoadSpacing \\
&\qquad\quad V_{LL_i} \leftarrow -\frac{V_{assume_i}}{L_{span}} \cdot (2ShearSpan + LoadSpacing) \\
&\qquad\quad M_{LL_i} \leftarrow \frac{V_{assume_i}}{L_{span}} \cdot (2ShearSpan + LoadSpacing) \cdot \left(L_{span} - x_{dist_i}\right) \\
&\quad ans \leftarrow \text{augment}\left(x_{dist}, x\%, V_{LL}, M_{LL}\right) \\
&\quad ans
\end{aligned}
$$

Figure C-2 (cont.) Subroutines used in the main calculation program given in Figure C-1.

$$\text{Dead}_{\text{Load}}(x_{\text{dist}}) =$$

$$x_{\text{dist}} \leftarrow \frac{x_{\text{dist}}}{\text{ft}}$$

$$L_{\text{span}} \leftarrow \frac{L_{\text{span}}}{\text{ft}}$$

$$x_{\text{bearing}} \leftarrow \frac{x_{\text{bearing}}}{\text{ft}}$$

$$x_{\text{bearing.roller}} \leftarrow \frac{x_{\text{bearing.roller}}}{\text{ft}}$$

$$\text{ShearSpan} \leftarrow \frac{\text{ShearSpan}}{\text{ft}}$$

$$w_{\text{beam}} \leftarrow \frac{w_{\text{beam}}}{\text{klf}}$$

$$DC_1 \leftarrow \frac{DC_1}{\text{klf}}$$

$$DC_2 \leftarrow \frac{DC_2}{\text{klf}}$$

$$DW \leftarrow \frac{DW}{\text{klf}}$$

$$P_{\text{diaphragm}} \leftarrow \frac{P_{\text{diaphragm}}}{\text{kip}}$$

for $i \in 1..\text{rows}(x_{\text{dist}})$

$$x\%_i \leftarrow \frac{x_{\text{dist}_i}}{\text{ShearSpan}}$$

$$V_{\text{beam}_i} \leftarrow \frac{w_{\text{beam}}}{2L_{\text{span}}} \cdot \left(x_{\text{bearing}} + L_{\text{span}} + x_{\text{bearing.roller}}\right)^2 - \frac{w_{\text{beam}} \cdot x_{\text{bearing.roller}}}{L_{\text{span}}} \left(x_{\text{bearing}} + L_{\text{span}} + x_{\text{bearing.roller}}\right) - w_{\text{beam}} \cdot \left(x_{\text{dist}_i} + x_{\text{bearing}}\right)$$

$$M_{\text{beam}_i} \leftarrow \left[\left(\frac{w_{\text{beam}}}{2L_{\text{span}}}\right)\left(x_{\text{bearing}} + L_{\text{span}} + x_{\text{bearing.roller}}\right)^2 - \frac{w_{\text{beam}} \cdot x_{\text{bearing.roller}}}{L_{\text{span}}}\left(x_{\text{bearing}} + L_{\text{span}} + x_{\text{bearing.roller}}\right)\right] \cdot x_{\text{dist}_i} - \frac{1}{2} w_{\text{beam}} \cdot \left(x_{\text{dist}_i} + x_{\text{bea}}\right.$$

$$V_{\text{diaphragm}_i} \leftarrow P_{\text{diaphragm}} \quad \text{if } x_{\text{dist}_i} < \frac{L_{\text{span}}}{3}$$

Figure C-2 (cont.) Subroutines used in the main calculation program given in Figure C-1.

$$V_{diaphragm_i} \leftarrow P_{diaphragm} \quad \text{if } x_{dist_i} < \frac{L_{span}}{3}$$

$$V_{diaphragm_i} \leftarrow 0 \quad \text{otherwise}$$

$$M_{diaphragm_i} \leftarrow P_{diaphragm} \cdot x_{dist_i} \quad \text{if } x_{dist_i} < \frac{L_{span}}{3}$$

$$M_{diaphragm_i} \leftarrow P_{diaphragm} \cdot \frac{L_{span}}{3} \quad \text{otherwise}$$

$$V_{DC1_i} \leftarrow \frac{DC_1}{2L_{span}} \cdot \left(x_{bearing} + L_{span} + x_{bearing.roller}\right)^2 - \frac{DC_1 \cdot x_{bearing.roller}}{L_{span}} \left(x_{bearing} + L_{span} + x_{bearing.roller}\right) - DC_1 \cdot \left(x_{dist_i} + x_{bearing}\right) + V_{diaphragm_i}$$

$$M_{DC1_i} \leftarrow \left[\left(\frac{DC_1}{2L_{span}}\right)\left(x_{bearing} + L_{span} + x_{bearing.roller}\right)^2 - \frac{DC_1 \cdot x_{bearing.roller}}{L_{span}}\left(x_{bearing} + L_{span} + x_{bearing.roller}\right)\right] \cdot x_{dist_i} - \frac{1}{2} DC_1 \cdot \left(x_{dist_i} + x_{bearing}\right)^2 + M_{diaphragm_i}$$

$$V_{DC2_i} \leftarrow \frac{DC_2}{2L_{span}} \cdot \left(x_{bearing} + L_{span} + x_{bearing.roller}\right)^2 - \frac{DC_2 \cdot x_{bearing.roller}}{L_{span}} \left(x_{bearing} + L_{span} + x_{bearing.roller}\right) - DC_2 \cdot \left(x_{dist_i} + x_{bearing}\right)$$

$$M_{DC2_i} \leftarrow \left[\left(\frac{DC_2}{2L_{span}}\right)\left(x_{bearing} + L_{span} + x_{bearing.roller}\right)^2 - \frac{DC_2 \cdot x_{bearing.roller}}{L_{span}}\left(x_{bearing} + L_{span} + x_{bearing.roller}\right)\right] \cdot x_{dist_i} - \frac{1}{2} DC_2 \cdot \left(x_{dist_i} + x_{bearing}\right)^2$$

$$V_{DW_i} \leftarrow \frac{DW}{2L_{span}} \cdot \left(x_{bearing} + L_{span} + x_{bearing.roller}\right)^2 - \frac{DW \cdot x_{bearing.roller}}{L_{span}} \left(x_{bearing} + L_{span} + x_{bearing.roller}\right) - DW \cdot \left(x_{dist_i} + x_{bearing}\right)$$

$$M_{DW_i} \leftarrow \left[\left(\frac{DW}{2L_{span}}\right)\left(x_{bearing} + L_{span} + x_{bearing.roller}\right)^2 - \frac{DW \cdot x_{bearing.roller}}{L_{span}}\left(x_{bearing} + L_{span} + x_{bearing.roller}\right)\right] \cdot x_{dist_i} - \frac{1}{2} DW \cdot \left(x_{dist_i} + x_{bearing}\right)^2$$

$$ans \leftarrow augment\left(x_{dist}, x\%, V_{beam}, M_{beam}, V_{DC1}, M_{DC1}, V_{DC2}, M_{DC2}, V_{DW}, M_{DW}\right)$$

$$ans$$

Figure C-2 (cont.) Subroutines used in the main calculation program given in Figure C-1.

$$V_{p.}(x_{dist}) = \left|\begin{array}{l} V_p \leftarrow 0 \\ \text{for } i \in 1..\text{rows}(x_{dist}) \\ \quad \left|\begin{array}{l} V_{p_i} \leftarrow \dfrac{f_{pe}\cdot\left(x_{dist_i} + x_{bearing}\right)}{l_t}\cdot Num_{harp}\cdot A_{strand}\cdot\sin\left(\Psi_{harp}\right) \text{ if } x_{dist_i} + x_{bearing} \le l_t \wedge x_{dist_i} \le L_{span}\cdot HarpDistRatio \\ V_{p_i} \leftarrow f_{pe}\cdot Num_{harp}\cdot A_{strand}\cdot\sin\left(\Psi_{harp}\right) \text{ if } x_{dist_i} + x_{bearing} > l_t \wedge x_{dist_i} \le L_{span}\cdot HarpDistRatio \\ V_{p_i} \leftarrow 0 \text{ if } x_{dist_i} > L_{span}\cdot HarpDistRatio \\ \text{"error"} \quad \text{otherwise} \end{array}\right. \\ V_p \end{array}\right.$$

$$f_{ps.}(x_{dist}, l_d, f_{ps.max}) = \left|\begin{array}{l} f_{ps} \leftarrow 0 \\ \text{for } i \in 1..\text{rows}(x_{dist}) \\ \quad \left|\begin{array}{l} f_{ps_i} \leftarrow \dfrac{f_{pe}\cdot\left(x_{dist_i} + x_{bearing}\right)}{l_t} \text{ if } x_{dist_i} + x_{bearing} \le l_t \\ f_{ps_i} \leftarrow f_{pe} + \dfrac{x_{dist_i} + x_{bearing} - l_t}{l_{d_i} - l_t}\cdot\left(f_{ps.max_i} - f_{pe}\right) \text{ if } x_{dist_i} + x_{bearing} > l_t \wedge x_{dist_i} + x_{bearing} < l_{d_i} \\ f_{ps_i} \leftarrow f_{ps.max_i} \text{ if } x_{dist_i} + x_{bearing} \ge l_{d_i} \\ f_{ps_i} \leftarrow \text{"error"} \quad \text{otherwise} \end{array}\right. \\ f_{ps} \end{array}\right.$$

$$c_{calc}(x_{dist}) = \left|\begin{array}{l} \text{for } i \in 1..\text{rows}(x_{dist}) \\ \quad \left|\begin{array}{l} d_{p_i} \leftarrow 10^6\cdot in \text{ if } d_{p_i} = 0 \\ c_i \leftarrow \dfrac{A_{ps}\cdot f_{pu} + A_{s.bot_i}\cdot f_y - A_{s.top}\cdot f_y}{0.85\cdot f_{c'c}\cdot\beta_1\cdot b_{eff} + k\cdot A_{ps}\cdot\dfrac{f_{pu}}{d_{p_i}}} \\ c_i \leftarrow \dfrac{A_{ps}\cdot f_{pu} + A_{s.bot_i}\cdot f_y - A_{s.top}\cdot f_y - 0.85\cdot f_{c'c}\cdot\left(b_{eff} - b_v\right)\cdot h_{flange}}{0.85\cdot f_{c'c}\cdot\beta_1\cdot b_v + k\cdot A_{ps}\cdot\dfrac{f_{pu}}{d_{p_i}}} \text{ if } c_i > h_{flange} \end{array}\right. \\ c \end{array}\right.$$

Figure C-2 (cont.) Subroutines used in the main calculation program given in Figure C-1

$l_{d.mild}(d_{long.rebar}) =$

$A_{long.rebar} \leftarrow A_{rebar}(\text{rows}(d_{long.rebar}), d_{long.rebar})$

for $i \in 1..\text{rows}(d_{long.rebar})$

$l_{db_i} \leftarrow \max\left(\frac{1.25 A_{long.rebar_i} \cdot f_y}{\sqrt{f_c' \cdot \text{ksi}}\,\text{in}}, 0.4 \frac{d_{long.rebar_i}}{8} \cdot \frac{f_y}{\text{ksi}}\,\text{in}\right)$

$\kappa 1_i \leftarrow$
- 1.0 if IsTopBarEffectApplicable = "No"
- 1.4 if IsTopBarEffectApplicable = "Yes"
- "error" otherwise

$\kappa 2_i \leftarrow$
- 1.0 if IsLongSteelEpoxyCoated = "No"
- 1.5 if IsLongSteelEpoxyCoated = "Yes" $\wedge$ $\left(\text{LongSteelCover} < 3 \frac{d_{long.rebar_i}}{8} \cdot \text{in} \vee \text{LongSteelClearSpacing} < 6 \frac{d_{long.rebar_i}}{8} \cdot \text{in}\right)$
- 1.2 if IsLongSteelEpoxyCoated = "Yes" $\wedge$ $\text{LongSteelCover} \geq 3 \frac{d_{long.rebar_i}}{8} \cdot \text{in} \wedge \text{LongSteelClearSpacing} \geq 6. \frac{d_{long.rebar_i}}{8} \cdot \text{in}$
- "error" otherwise

$\kappa 12_i \leftarrow \min(\kappa 1 \cdot \kappa 2, 1.7)$

$f_{ct} \leftarrow 10^6 \text{ksi}$ if $f_{ct} = 0 \wedge \text{Value\_}f_{ct} = \text{"not specified"}$

$\kappa 3_i \leftarrow$
- 1 if ConcreteType = "NWC"
- $\max\left(0.22 \frac{\sqrt{f_c' \cdot \text{ksi}}}{f_{ct}}, 1.0\right)$ if ConcreteType = "LWC" $\wedge$ $\text{Value\_}f_{ct}$ = "specified"
- 1.3 if ConcreteType = "LWC" $\wedge$ $\text{Value\_}f_{ct}$ = "not specified" $\wedge$ FineAggType = "lightweight"
- 1.2 if ConcreteType = "LWC" $\wedge$ $\text{Value\_}f_{ct}$ = "not specified" $\wedge$ FineAggType = "sand"
- "error" otherwise

$\kappa 123_i \leftarrow \kappa 12_i \cdot \kappa 3_i$

$l_{d.mild_i} \leftarrow l_{db_i} \cdot \kappa 123_i$

$l_{d.mild_l}$

Figure C-2 (cont.) Subroutines used in the main calculation program given in Figure C-1.

$$\text{Num}_{\text{strand.bot.}}\left(x_{\text{dist}}, cg_{\text{harp}}\right) = \left|\begin{array}{l} \text{Num}_{\text{strand.bot}} \leftarrow 0 \\ \text{for } i \in 1..\text{rows}\left(x_{\text{dist}}\right) \\ \quad \left|\begin{array}{l} \text{Num}_{\text{strand.bot}_i} \leftarrow \left(\text{Num}_{\text{strand}} - \text{Num}_{\text{harp}}\right) \text{ if } cg_{\text{harp}_i} - 2\text{in} \geq \frac{1}{2}h_c \\ \text{Num}_{\text{strand.bot}_i} \leftarrow \left(\text{Num}_{\text{strand}} - \text{Num}_{\text{harp}} + 2\right) \text{ if } cg_{\text{harp}_i} - 2\text{in} < \frac{1}{2}h_c \wedge cg_{\text{harp}_i} \geq \frac{1}{2}h_c \\ \text{Num}_{\text{strand.bot}_i} \leftarrow \text{Num}_{\text{strand}} - \text{Num}_{\text{harp}} + 4 \text{ if } cg_{\text{harp}_i} < \frac{1}{2}h_c \wedge cg_{\text{harp}_i} + 2\text{in} \geq \frac{1}{2}h_c \\ \text{Num}_{\text{strand.bot}_i} \leftarrow \text{Num}_{\text{strand}} \text{ if } cg_{\text{harp}_i} + 2\text{in} < \frac{1}{2}h_c \\ \text{Num}_{\text{strand.bot}_i} \leftarrow \text{"error"} \text{ otherwise} \end{array}\right. \\ \text{Num}_{\text{strand.bot}} \end{array}\right.$$

$$\varepsilon_x\left(x_{\text{dist}}\right) = \left|\begin{array}{l} \left(\varepsilon_{x1}\ \varepsilon_{x2}\ \varepsilon_{x3}\ \varepsilon_x\right) \leftarrow (0\ 0\ 0\ 0) \\ \theta \leftarrow \theta \cdot \frac{\pi}{180} \\ \text{for } i \in 1..\text{rows}\left(x_{\text{dist}}\right) \\ \quad \left|\begin{array}{l} \varepsilon_{x1_i} \leftarrow \dfrac{\frac{\left|M_{\text{assume}_i}\right|}{d_{v_i}} + 0.5 \cdot N_u + 0.5 \cdot \left|V_{\text{assume}_i} - V_{p_i}\right| \cot\left(\theta_i\right) - A_{\text{ps.bot.}\varepsilon x_i} \cdot f_{po}}{2 \cdot \left(E_s \cdot A_{\text{s.bot.}\varepsilon x_i} + E_p \cdot A_{\text{ps.bot.}\varepsilon x_i}\right)} \\ \varepsilon_{x2_i} \leftarrow \dfrac{\frac{\left|M_{\text{assume}_i}\right|}{d_{v_i}} + 0.5 \cdot N_u + 0.5 \cdot \left|V_{\text{assume}_i} - V_{p_i}\right| \cot\left(\theta_i\right) - A_{\text{ps.bot.}\varepsilon x_i} \cdot f_{po}}{E_s \cdot A_{\text{s.bot.}\varepsilon x_i} + E_p \cdot A_{\text{ps.bot.}\varepsilon x_i}} \\ \varepsilon_{x3_i} \leftarrow \dfrac{\frac{\left|M_{\text{assume}_i}\right|}{d_{v_i}} + 0.5 \cdot N_u + 0.5 \cdot \left|V_{\text{assume}_i} - V_{p_i}\right| \cot\left(\theta_i\right) - A_{\text{ps.bot.}\varepsilon x_i} \cdot f_{po}}{2 \cdot \left(E_{\text{beam}} \cdot A_{ct} + E_s \cdot A_{\text{s.bot.}\varepsilon x_i} + E_p \cdot A_{\text{ps.bot.}\varepsilon x_i}\right)} \\ \varepsilon_{x_i} \leftarrow \left|\begin{array}{l} \varepsilon_{x1_i} \text{ if } \text{MinReinforcingCheck}_i = \text{"OK"} \wedge \varepsilon_{x1_i} \geq 0 \\ \varepsilon_{x2_i} \text{ if } \text{MinReinforcingCheck}_i = \text{"NG!!!"} \wedge \varepsilon_{x2_i} \geq 0 \\ \varepsilon_{x3_i} \text{ if } \varepsilon_{x1_i} < 0 \vee \varepsilon_{x2_i} < 0 \end{array}\right. \end{array}\right. \\ \varepsilon_x \end{array}\right.$$

Figure C-2 (cont.) Subroutines used in the main calculation program given in Figure C-1.

$$cg_{ps.bot.}\left(x_{dist}, cg_{straight}, cg_{harp}, h_c, Num_{straight}\right) = \left| \begin{array}{l} \text{for } i \in 1..\text{rows}\left(x_{dist}\right) \\ \quad \left| \begin{array}{l} cg_{ps.bot_i} \leftarrow cg_{straight} \quad \text{if } cg_{harp_i} - 2\text{in} \geq \frac{1}{2}h_c \\ cg_{ps.bot_i} \leftarrow \frac{Num_{straight} \cdot cg_{straight} + 2 \cdot \left(cg_{harp_i} - 2\text{in}\right)}{Num_{straight} + 2} \quad \text{if } cg_{harp_i} - 2\text{in} < \frac{1}{2}h_c \wedge cg_{harp_i} \geq \frac{1}{2}h_c \\ cg_{ps.bot_i} \leftarrow \frac{Num_{straight} \cdot cg_{straight} + 2 \cdot \left(cg_{harp_i} - 2\text{in} + cg_{harp_i}\right)}{Num_{straight} + 4} \quad \text{if } cg_{harp_i} < \frac{1}{2}h_c \wedge cg_{harp_i} + 2\text{in} \geq \frac{1}{2}h_c \\ cg_{ps.bot_i} \leftarrow \frac{Num_{straight} \cdot cg_{straight} + 6 \cdot cg_{harp_i}}{Num_{straight} + 6} \quad \text{if } cg_{harp_i} + 2\text{in} < \frac{1}{2}h_c \end{array} \right. \\ cg_{ps.bot} \end{array} \right.$$

$$v_{u.}\left(x_{dist}, V_{assume}, V_p, d_v, MinReinforcingCheck\right) = \left| \begin{array}{l} \left(v_1 \;\; s_x \;\; s_{xe} \;\; v\right) \leftarrow (0 \;\; 0 \;\; 0 \;\; 0) \\ \text{for } i \in 1..\text{rows}\left(x_{dist}\right) \\ \quad \left| \begin{array}{l} v1_i \leftarrow \frac{\left|V_{assume_i} - \phi_v \cdot V_{p_i}\right|}{\phi_v \cdot b_v \cdot d_{v_i}} \\ s_{x_i} \leftarrow d_{v_i} \\ s_{xe_i} \leftarrow \min\left(s_{x_i} \cdot \frac{1.38\text{in}}{a_g + 0.63\text{in}}, 80\text{in}\right) \\ v_i \leftarrow \left| \begin{array}{l} \frac{v1_i}{f_{c'}} \quad \text{if } MinReinforcingCheck_i = \text{"OK"} \\ \frac{s_{xe_i}}{\text{in}} \quad \text{if } MinReinforcingCheck_i = \text{"NG!!!"} \end{array} \right. \end{array} \right. \\ v \end{array} \right.$$

Figure C-2 (cont.) Subroutines used in the main calculation program given in Figure C-1.

$$\theta\beta\left(x_{dist}, cg_{harp}, \varepsilon_x, v_u, MinReinforcingCheck\right) = \left|\begin{array}{l}
\left(\theta_L \;\; \theta_R \;\; \theta_r \;\; \beta_L \;\; \beta_R \;\; \beta\right) \leftarrow (0 \;\; 0 \;\; 0 \;\; 0 \;\; 0 \;\; 0) \\
u \leftarrow \text{rows}\left(x_{dist}\right) \\
Num_{strand.bot} \leftarrow Num_{strand.bot.}\left(x_{dist}, cg_{harp}\right) \\
\text{for } i \in 1..1 \\
\quad v_{u1.} \leftarrow v_{u1}\left(v_u, \varepsilon_x, u, MinReinforcingCheck\right) \\
\quad v_{u2.} \leftarrow v_{u2}\left(v_u, \varepsilon_x, u, MinReinforcingCheck\right) \\
\quad \varepsilon_{xL.} \leftarrow \varepsilon_{xL}\left(v_u, \varepsilon_x, u, MinReinforcingCheck\right) \\
\quad \varepsilon_{xR.} \leftarrow \varepsilon_{xR}\left(v_u, \varepsilon_x, u, MinReinforcingCheck\right) \\
\text{for } i \in 1..1 \\
\quad MinOK1\theta_{1L.} \leftarrow MinOK1\theta_{1L}\left(v_{u1.}, \varepsilon_{xL.}, u, MinReinforcingCheck\right) \\
\quad MinOK2\theta_{1L.} \leftarrow MinOK2\theta_{1L}\left(v_{u1.}, \varepsilon_{xL.}, u, MinReinforcingCheck\right) \\
\quad MinNG1\theta_{1L.} \leftarrow MinNG1\theta_{1L}\left(v_{u1.}, \varepsilon_{xL.}, u, MinReinforcingCheck\right) \\
\quad MinNG2\theta_{1L.} \leftarrow MinNG2\theta_{1L}\left(v_{u1.}, \varepsilon_{xL.}, u, MinReinforcingCheck\right) \\
\text{for } i \in 1..1 \\
\quad MinOK1\theta_{1R.} \leftarrow MinOK1\theta_{1R}\left(v_{u1.}, \varepsilon_{xR.}, u, MinReinforcingCheck\right) \\
\quad MinOK2\theta_{1R.} \leftarrow MinOK2\theta_{1R}\left(v_{u1.}, \varepsilon_{xR.}, u, MinReinforcingCheck\right) \\
\quad MinNG1\theta_{1R.} \leftarrow MinNG1\theta_{1R}\left(v_{u1.}, \varepsilon_{xR.}, u, MinReinforcingCheck\right) \\
\quad MinNG2\theta_{1R.} \leftarrow MinNG2\theta_{1R}\left(v_{u1.}, \varepsilon_{xR.}, u, MinReinforcingCheck\right) \\
\text{for } i \in 1..1 \\
\quad MinOK1\beta_{1L.} \leftarrow MinOK1\beta_{1L}\left(v_{u1.}, \varepsilon_{xL.}, u, MinReinforcingCheck\right) \\
\quad MinOK2\beta_{1L.} \leftarrow MinOK2\beta_{1L}\left(v_{u1.}, \varepsilon_{xL.}, u, MinReinforcingCheck\right) \\
\quad MinNG1\beta_{1L.} \leftarrow MinNG1\beta_{1L}\left(v_{u1.}, \varepsilon_{xL.}, u, MinReinforcingCheck\right) \\
\quad MinNG2\beta_{1L.} \leftarrow MinNG2\beta_{1L}\left(v_{u1.}, \varepsilon_{xL.}, u, MinReinforcingCheck\right) \\
\text{for } i \in 1..1 \\
\quad MinOK1\beta_{1R.} \leftarrow MinOK1\beta_{1R}\left(v_{u1.}, \varepsilon_{xR.}, u, MinReinforcingCheck\right) \\
\quad MinOK2\beta_{1R.} \leftarrow MinOK2\beta_{1R}\left(v_{u1.}, \varepsilon_{xR.}, u, MinReinforcingCheck\right) \\
\quad MinNG1\beta_{1R.} \leftarrow MinNG1\beta_{1R}\left(v_{u1.}, \varepsilon_{xR.}, u, MinReinforcingCheck\right) \\
\quad MinNG2\beta_{1R.} \leftarrow MinNG2\beta_{1R}\left(v_{u1.}, \varepsilon_{xR.}, u, MinReinforcingCheck\right) \\
\text{for } i \in 1..1 \\
\quad MinOK1\theta_{2L.} \leftarrow MinOK1\theta_{2L}\left(v_{u2.}, \varepsilon_{xL.}, u, MinReinforcingCheck\right) \\
\quad MinOK2\theta_{2L.} \leftarrow MinOK2\theta_{2L}\left(v_{u2.}, \varepsilon_{xL.}, u, MinReinforcingCheck\right) \\
\quad MinNG1\theta_{2L.} \leftarrow MinNG1\theta_{2L}\left(v_{u2.}, \varepsilon_{xL.}, u, MinReinforcingCheck\right) \\
\quad MinNG2\theta_{2L.} \leftarrow MinNG2\theta_{2L}\left(v_{u2.}, \varepsilon_{xL.}, u, MinReinforcingCheck\right) \\
\text{for } i \in 1..1
\end{array}\right.$$

Figure C-2 (cont.) Subroutines used in the main calculation program given in Figure C-1.

for $i \in 1..1$

$MinOK1\theta_{2R_{\cdot}} \leftarrow MinOK1\theta_{2R}(v_{u2_{\cdot}}, \varepsilon_{xR_{\cdot}}, u, MinReinforcingCheck)$

$MinOK2\theta_{2R_{\cdot}} \leftarrow MinOK2\theta_{2R}(v_{u2_{\cdot}}, \varepsilon_{xR_{\cdot}}, u, MinReinforcingCheck)$

$MinNG1\theta_{2R_{\cdot}} \leftarrow MinNG1\theta_{2R}(v_{u2_{\cdot}}, \varepsilon_{xR_{\cdot}}, u, MinReinforcingCheck)$

$MinNG2\theta_{2R_{\cdot}} \leftarrow MinNG2\theta_{2R}(v_{u2_{\cdot}}, \varepsilon_{xR_{\cdot}}, u, MinReinforcingCheck)$

for $i \in 1..1$

$MinOK1\beta_{2L_{\cdot}} \leftarrow MinOK1\beta_{2L}(v_{u2_{\cdot}}, \varepsilon_{xL_{\cdot}}, u, MinReinforcingCheck)$

$MinOK2\beta_{2L_{\cdot}} \leftarrow MinOK2\beta_{2L}(v_{u2_{\cdot}}, \varepsilon_{xL_{\cdot}}, u, MinReinforcingCheck)$

$MinNG1\beta_{2L_{\cdot}} \leftarrow MinNG1\beta_{2L}(v_{u2_{\cdot}}, \varepsilon_{xL_{\cdot}}, u, MinReinforcingCheck)$

$MinNG2\beta_{2L_{\cdot}} \leftarrow MinNG2\beta_{2L}(v_{u2_{\cdot}}, \varepsilon_{xL_{\cdot}}, u, MinReinforcingCheck)$

for $i \in 1..1$

$MinOK1\beta_{2R_{\cdot}} \leftarrow MinOK1\beta_{2R}(v_{u2_{\cdot}}, \varepsilon_{xR_{\cdot}}, u, MinReinforcingCheck)$

$MinOK2\beta_{2R_{\cdot}} \leftarrow MinOK2\beta_{2R}(v_{u2_{\cdot}}, \varepsilon_{xR_{\cdot}}, u, MinReinforcingCheck)$

$MinNG1\beta_{2R_{\cdot}} \leftarrow MinNG1\beta_{2R}(v_{u2_{\cdot}}, \varepsilon_{xR_{\cdot}}, u, MinReinforcingCheck)$

$MinNG2\beta_{2R_{\cdot}} \leftarrow MinNG2\beta_{2R}(v_{u2_{\cdot}}, \varepsilon_{xR_{\cdot}}, u, MinReinforcingCheck)$

for $i \in 1..1$

$\theta_{1L} \leftarrow MinOK1\theta_{1L_{\cdot}} + MinOK2\theta_{1L_{\cdot}} + MinNG1\theta_{1L_{\cdot}} + MinNG2\theta_{1L_{\cdot}}$

$\theta_{1R} \leftarrow MinOK1\theta_{1R_{\cdot}} + MinOK2\theta_{1R_{\cdot}} + MinNG1\theta_{1R_{\cdot}} + MinNG2\theta_{1R_{\cdot}}$

$\beta_{1L} \leftarrow MinOK1\beta_{1L_{\cdot}} + MinOK2\beta_{1L_{\cdot}} + MinNG1\beta_{1L_{\cdot}} + MinNG2\beta_{1L_{\cdot}}$

$\beta_{1R} \leftarrow MinOK1\beta_{1R_{\cdot}} + MinOK2\beta_{1R_{\cdot}} + MinNG1\beta_{1R_{\cdot}} + MinNG2\beta_{1R_{\cdot}}$

$\theta_{2L} \leftarrow MinOK1\theta_{2L_{\cdot}} + MinOK2\theta_{2L_{\cdot}} + MinNG1\theta_{2L_{\cdot}} + MinNG2\theta_{2L_{\cdot}}$

$\theta_{2R} \leftarrow MinOK1\theta_{2R_{\cdot}} + MinOK2\theta_{2R_{\cdot}} + MinNG1\theta_{2R_{\cdot}} + MinNG2\theta_{2R_{\cdot}}$

$\beta_{2L} \leftarrow MinOK1\beta_{2L_{\cdot}} + MinOK2\beta_{2L_{\cdot}} + MinNG1\beta_{2L_{\cdot}} + MinNG2\beta_{2L_{\cdot}}$

$\beta_{2R} \leftarrow MinOK1\beta_{2R_{\cdot}} + MinOK2\beta_{2R_{\cdot}} + MinNG1\beta_{2R_{\cdot}} + MinNG2\beta_{2R_{\cdot}}$

for $i \in 1..rows(x_{dist})$

$$\theta_{L_i} \leftarrow \begin{cases} \theta_{2L_i} & \text{if } v_{u2_{\cdot i}} - v_{u1_{\cdot i}} = 0 \\ \left[\left(\theta_{1L_i} - \theta_{2L_i}\right) \cdot \dfrac{\left(v_{u2_{\cdot i}} - v_{u_i}\right)}{v_{u2_{\cdot i}} - v_{u1_{\cdot i}}} + \theta_{2L_i}\right] & \text{otherwise} \end{cases}$$

$$\theta_{R_i} \leftarrow \begin{cases} \theta_{2R_i} & \text{if } v_{u2_{\cdot i}} - v_{u1_{\cdot i}} = 0 \\ \left(\theta_{1R_i} - \theta_{2R_i}\right) \cdot \dfrac{\left(v_{u2_{\cdot i}} - v_{u_i}\right)}{v_{u2_{\cdot i}} - v_{u1_{\cdot i}}} + \theta_{2R_i} & \text{otherwise} \end{cases}$$

$$\theta_{r_i} \leftarrow \begin{cases} \theta_{R_i} & \text{if } \varepsilon_{xR_i} - \varepsilon_{xL_i} = 0 \\ \left(\theta_{L_i} - \theta_{R_i}\right) \cdot \dfrac{\left(\varepsilon_{xR_i} - \varepsilon_{x_i}\right)}{\varepsilon_{xR_i} - \varepsilon_{xL_i}} + \theta_{R_i} & \text{otherwise} \end{cases}$$

Figure C-2 (cont.) Subroutines used in the main calculation program given in Figure C-1.

$$\left|\begin{array}{l}
\left|\begin{array}{l}
\left|\begin{array}{l}
\left(\theta_{L_i} - \theta_{R_i}\right)\cdot\dfrac{\left(\varepsilon_{xR_i} - \varepsilon_{x_i}\right)}{\varepsilon_{xR_i} - \varepsilon_{xL_i}} + \theta_{R_i} \quad \text{otherwise}
\end{array}\right. \\
\beta_{L_i} \leftarrow \left|\begin{array}{l}
\beta_{2L_i} \quad \text{if } v_{u2_i} - v_{u1_i} = 0 \\
\left(\beta_{1L_i} - \beta_{2L_i}\right)\cdot\dfrac{\left(v_{u2_i} - v_{u_i}\right)}{v_{u2_i} - v_{u1_i}} + \beta_{2L_i} \quad \text{otherwise}
\end{array}\right. \\
\beta_{R_i} \leftarrow \left|\begin{array}{l}
\beta_{2R_i} \quad \text{if } v_{u2_i} - v_{u1_i} = 0 \\
\left(\beta_{1R_i} - \beta_{2R_i}\right)\cdot\dfrac{\left(v_{u2_i} - v_{u_i}\right)}{v_{u2_i} - v_{u1_i}} + \beta_{2R_i} \quad \text{otherwise}
\end{array}\right. \\
\beta_i \leftarrow \left|\begin{array}{l}
\beta_{R_i} \quad \text{if } \varepsilon_{xR_i} - \varepsilon_{xL_i} = 0 \\
\left(\beta_{L_i} - \beta_{R_i}\right)\cdot\dfrac{\left(\varepsilon_{xR_i} - \varepsilon_{x_i}\right)}{\varepsilon_{xR_i} - \varepsilon_{xL_i}} + \beta_{R_i} \quad \text{otherwise}
\end{array}\right.
\end{array}\right. \\
\begin{pmatrix} \theta_r \\ \beta \end{pmatrix}
\end{array}\right.$$

$$V_r\left(x_{dist}, \beta, d_v, \theta, s_{v.design}, V_p\right) = \left|\begin{array}{l}
\left(V_c \;\; V_s \;\; V_n \;\; V_r\right) \leftarrow (0 \;\; 0 \;\; 0 \;\; 0) \\
\theta \leftarrow \theta\cdot\dfrac{\pi}{180} \\
\text{for } i \in 1..\text{rows}\left(x_{dist}\right) \\
\quad \left|\begin{array}{l}
V_{c_i} \leftarrow 0.0316\beta_i\cdot\alpha_v\sqrt{f_{c'}\cdot ksi}\cdot b_v\cdot d_{v_i} \\
V_{s_i} \leftarrow \dfrac{A_{v_i}\cdot f_{yv}\cdot d_{v_i}\cdot\left(\cot\left(\theta_i\right) + \cot(\alpha)\right)\cdot\sin(\alpha)}{s_{v.design_i}}
\end{array}\right. \\
V_{n1} \leftarrow V_c + V_s + V_p \\
V_{n2} \leftarrow 0.25\cdot f_{c'}\cdot b_v\cdot d_v + V_p \\
\text{for } i \in 1..\text{rows}\left(x_{dist}\right) \\
\quad V_{n_i} \leftarrow \min\left(V_{n1_i}, V_{n2_i}\right) \\
V_r \leftarrow \phi_v\cdot V_n \\
V_r
\end{array}\right.$$

Figure C-2 (cont.) Subroutines used in the main calculation program given in Figure C-1.

$$\theta_{iterate}(x_{dist}) = \left|\begin{array}{l}
\text{for } i \in 1..\text{rows}(x_{dist}) \text{ if } \theta\beta\text{method} = \text{"Simple"} \wedge \left(N_u = 0 \wedge \text{MinReinforcingCheck}_1 = \text{"OK"} \vee h_c < 16\text{in}\right) \\
\quad \left|\begin{array}{l} \theta_{r_i} \leftarrow 45 \\ \beta_i \leftarrow 2 \end{array}\right. \\
\text{otherwise} \\
\quad \left|\begin{array}{l}
\text{AngleCheck} \leftarrow \text{"NG"} \\
\text{iterations}_\theta \leftarrow 0 \\
\text{Num}_{strand.bot} \leftarrow \text{Num}_{strand.bot.}(x_{dist}, cg_{harp}) \\
\text{while AngleCheck} = \text{"NG"} \\
\quad \left|\begin{array}{l}
\text{iterations}_\theta \leftarrow \text{iterations}_\theta + 1 \\
\text{iterations}_{\theta.tot} \leftarrow \text{iterations}_{\theta.tot} + 1 \\
\theta_{sum} \leftarrow 0 \\
\varepsilon_x \leftarrow \left|\begin{array}{l}
(\varepsilon_{x1}\ \varepsilon_{x2}\ \varepsilon_{x3}\ \varepsilon_x) \leftarrow (0\ 0\ 0\ 0) \\
\theta \leftarrow \theta \cdot \frac{\pi}{180} \\
\text{for } i \in 1..\text{rows}(x_{dist}) \\
\quad \left|\begin{array}{l}
\varepsilon x1_i \leftarrow \dfrac{\frac{\left|M_{assume_i}\right|}{d_{v_i}} + 0.5 \cdot N_u + 0.5 \cdot \left|V_{assume_i} - V_{p_i}\right| \cot(\theta_i) - A_{ps.bot.\varepsilon x_i} \cdot f_{po}}{2 \cdot \left(E_s \cdot A_{s.bot.\varepsilon x_i} + E_p \cdot A_{ps.bot.\varepsilon x_i}\right)} \\
\varepsilon x2_i \leftarrow \dfrac{\frac{\left|M_{assume_i}\right|}{d_{v_i}} + 0.5 \cdot N_u + 0.5 \cdot \left|V_{assume_i} - V_{p_i}\right| \cot(\theta_i) - A_{ps.bot.\varepsilon x_i} \cdot f_{po}}{E_s \cdot A_{s.bot.\varepsilon x_i} + E_p \cdot A_{ps.bot.\varepsilon x_i}} \\
\varepsilon x3_i \leftarrow \dfrac{\frac{\left|M_{assume_i}\right|}{d_{v_i}} + 0.5 \cdot N_u + 0.5 \cdot \left|V_{assume_i} - V_{p_i}\right| \cot(\theta_i) - A_{ps.bot.\varepsilon x_i} \cdot f_{po}}{2 \cdot \left(E_{beam} \cdot A_{ct} + E_s \cdot A_{s.bot.\varepsilon x_i} + E_p \cdot A_{ps.bot.\varepsilon x_i}\right)} \\
\varepsilon x_i \leftarrow \left|\begin{array}{l}
\varepsilon x1_i \text{ if } \text{MinReinforcingCheck}_i = \text{"OK"} \wedge \varepsilon x1_i \geq 0 \\
\varepsilon x2_i \text{ if } \text{MinReinforcingCheck}_i = \text{"NG!!!"} \wedge \varepsilon x2_i \geq 0 \\
\varepsilon x3_i \text{ if } \varepsilon x1_i < 0 \vee \varepsilon x2_i < 0
\end{array}\right.
\end{array}\right. \\
\varepsilon_x
\end{array}\right. \\
\theta_r \leftarrow \theta\beta(x_{dist}, cg_{harp}, \varepsilon_x, v_u, \text{MinReinforcingCheck})_1 \\
\beta \leftarrow \theta\beta(x_{dist}, cg_{harp}, \varepsilon_x, v_u, \text{MinReinforcingCheck})_2 \\
\theta \leftarrow \theta \cdot \frac{180}{\pi} \\
\text{for } i \in 1..\text{rows}(x_{dist})
\end{array}\right.
\end{array}\right.$$

Figure C-2 (cont.) Subroutines used in the main calculation program given in Figure C-1.

```
for i ∈ 1.. rows(x_dist)
    if |θ_r_i − θ_i| > .0005
        θ_sum ← θ_sum + 1
        θ_i ← (1/2)(θ_r_i + θ_i)
AngleCheck ← "OK" if θ_sum = 0 ∨ iterations_θ = 50
(θ_r
 β
 iterations_θ
 ε_x)
```

Figure C-2 (cont.) Subroutines used in the main calculation program given in Figure C-1.

```
calc = ShearStrengthCheckFinal ← "NG"
iterations ← 0
iterations_θ.tot ← 0
i ← 1.. rows(P_assume)
while ShearStrengthCheckFinal = "NG"
    (ShearStrengthSum d_v P_assume.old LiveLoad DeadLoad V_assume M_assume1 V_p cg_harp cg_ps d_p d_p.bot c
    iterations ← iterations + 1
    for i ∈ 1.. 1
        x_dist ← x_θ(x_critical.assume)1
        if rows(x_dist) ≠ rows(P_assume)
            for i ∈ 1.. rows(x_dist)        if rows(x_dist) < rows(P_assume)
                P_assume.old_i ← P_assume_i
            for i ∈ 1.. rows(x_dist) − rows(P_assume)        if rows(x_dist) > rows(P_assume)
                P_assume.old ← P_assume
                P_assume.old_(i+rows(P_assume)) ← P_assume_rows(P_assume)
            P_assume ← P_assume.old
        return ("error" "error" rows(x_dist) rows(P_assume) "error" "error" "error" iterations) if rows(x_dist) ≠ rows
        LiveLoad ← Live_Load(x_dist, P_assume, ShearSpan, LoadSpacing, L_span)
        DeadLoad ← Dead_Load(x_dist, L_span, x_bearing, x_bearing.roller, ShearSpan, w_beam, DC_1, DC_2, DW, P_diaphragm)
        V_assume ← ⌈1.00(DeadLoad⟨5⟩ + DeadLoad⟨7⟩) + 1.00·DeadLoad⟨9⟩ + 1.00LiveLoad⟨3⟩⌉·kip
        M_assume1 ← ⌈1.00·(DeadLoad⟨6⟩ + DeadLoad⟨8⟩) + 1.00DeadLoad⟨10⟩ + 1.00LiveLoad⟨4⟩⌉·kip·ft
        V_p ← V_p.(x_dist)
        cg_harp ← cg_harp.(x_dist)
        f_c'c ← f_c'deck if f_c'deck > 0
                f_c' otherwise
        β_1 ← β_1.(f_c'c)
```

Figure C-3. Program for calculating the design shear strength following the *General Procedure*.

$$\beta_1 \leftarrow \beta_1.\left(f_{c'c}\right)$$

for $i \in 1..\text{rows}\left(x_{dist}\right)$

$$cg_{ps_i} \leftarrow \frac{Num_{straight} \cdot cg_{straight} + Num_{harp} \cdot cg_{harp_i}}{Num_{strand}}$$

$$d_{p_i} \leftarrow h_c - cg_{ps_i}$$

$$c \leftarrow c_{calc}\left(x_{dist}, A_{ps}, f_{pu}, A_{s.bot}, A_{s.top}, f_y, f_{c'c}, \beta_1, b_{eff}, b_v, h_{flange}, k, d_p\right)$$

for $i \in 1..\text{rows}\left(x_{dist}\right)$

$$f_{ps.max_i} \leftarrow f_{pu} \cdot \left(1 - k \cdot \frac{c_i}{d_{p_i}}\right)$$

$$l_{d.ps_i} \leftarrow \kappa \cdot \left(f_{ps.max_i} - \frac{2}{3} \cdot f_{pe}\right) \varphi$$

$$f_{ps} \leftarrow f_{ps.}\left(x_{dist}, l_{d.ps}, f_{ps.max}\right)$$

$$\varepsilon_{s.yield} \leftarrow \frac{f_y}{E_s}$$

$$Num_{strand.bot} \leftarrow Num_{strand.bot.}\left(x_{dist}, cg_{harp}\right)$$

$$cg_{ps.bot} \leftarrow cg_{ps.bot.}\left(x_{dist}, cg_{straight.bot}, cg_{harp}, h_c, Num_{straight.bot}\right)$$

for $i \in 1..\text{rows}\left(x_{dist}\right)$

return ("error" "error" "need additional inputs for each constant variable" iterations rows(x_{dist}) rows(A_s) "er

$$d_{p.bot_i} \leftarrow h_c - cg_{ps.bot_i}$$

$$d_{s.bot_i} \leftarrow h_c - cg_{s.bot_i}$$

$$A_{ps.bot_i} \leftarrow Num_{strand.bot_i} A_{strand}$$

$$d_{e_i} \leftarrow \frac{A_{ps.bot_i} \cdot f_{ps_i} \cdot d_{p.bot_i} + A_{s.bot_i} \cdot f_y \cdot d_{s.bot_i}}{A_{ps.bot_i} \cdot f_{ps_i} + A_{s.bot_i} \cdot f_y}$$

$$\varepsilon_{s.ten_i} \leftarrow \frac{0.003}{c_i} \cdot \left(d_{e_i} - c_i\right)$$

return $\left("\text{Tension steel does not yield at x.dist (inches)}" \quad \frac{x_{dist_i}}{in}\right)$ if $\varepsilon_{s.ten_i} < \varepsilon_{s.yield}$

$$a_i \leftarrow \beta_1 \cdot c_i$$

$$d_{v_i} \leftarrow \max\left(d_{e_i} - \frac{a_i}{2}, 0.9 d_{e_i}, 0.72 h_c\right)$$

$$M_{assume_i} \leftarrow \max\left(M_{assume1_i}, \left|V_{assume_i} - V_{p_i}\right| \cdot d_{v_i}\right)$$

$$l_{d.mild} \leftarrow l_{d.mild}\left(d_{long.rebar}, f_{c'}, f_y, IsTopBarEffectApplicable, IsLongSteelEpoxyCoated, LongSteelCover, LongSteelCl$$

for $i \in 1..\text{rows}\left(x_{dist}\right)$

Figure C-3 (cont.) Program for calculating the design shear strength following the *General Procedure*.

for $i \in 1..\text{rows}(x_{dist})$

$\text{RedFactor}_{\varepsilon s.ps_i} \leftarrow \begin{cases} \dfrac{x_{dist_i} + x_{bearing}}{l_{d.ps_i}} & \text{if } x_{dist_i} + x_{bearing} < l_{d.ps_i} \\ 1 & \text{if } x_{dist_i} + x_{bearing} \geq l_{d.ps_i} \end{cases}$

$A_{ps.bot.\varepsilon s_i} \leftarrow \text{Num}_{strand.bot_i} \cdot A_{strand} \cdot \text{RedFactor}_{\varepsilon s.ps_i}$

$\text{RedFactor}_{\varepsilon s.s_i} \leftarrow \begin{cases} \dfrac{x_{dist_i} + x_{bearing}}{l_{d.mild}} & \text{if } x_{dist_i} + x_{bearing} < l_{d.mild} \\ 1 & \text{if } x_{dist_i} + x_{bearing} \geq l_{d.mild} \end{cases}$

$A_{s.bot.\varepsilon s_i} \leftarrow A_{s.bot_i} \cdot \text{RedFactor}_{\varepsilon s.s_i}$

$\text{vect\_elemnt}_{x.critical} \leftarrow \dfrac{x\_\theta(x_{critical.assume})2}{\text{in}}$

$\varepsilon_s \leftarrow$ for $i \in 1..\text{rows}(x_{dist})$

$\varepsilon s1_i \leftarrow \min\left(\dfrac{\dfrac{\left|M_{assume_i}\right|}{d_{v_i}} + 0.5N_u + \left|V_{assume_i} - V_{p_i}\right| - A_{ps.bot.\varepsilon s_i} \cdot f_{po}}{E_s \cdot A_{s.bot.\varepsilon s_i} + E_p \cdot A_{ps.bot.\varepsilon s_i}}, 0.006\right)$

$\varepsilon s2_i \leftarrow \max\left[\dfrac{\left(\dfrac{\left|M_{assume_i}\right|}{d_{v_i}} + 0.5N_u + \left|V_{assume_i} - V_{p_i}\right| - A_{ps.bot.\varepsilon s_i} \cdot f_{po}\right)}{E_{beam} \cdot A_{ct} + E_s \cdot A_{s.bot.\varepsilon s_i} + E_p \cdot A_{ps.bot.\varepsilon s_i}}, -0.0004\right]$

for $i \in 1..\text{rows}(x_{dist})$

$\varepsilon_{s_i} \leftarrow \varepsilon s1_i$ if $\varepsilon s1_i \geq 0$

$\varepsilon_{s_i} \leftarrow \varepsilon s2_i$ if $\varepsilon s1_i < 0$

$\varepsilon_{s_i} \leftarrow 2 \cdot \varepsilon s1_i$ if $\varepsilon s1_i \geq 0 \wedge \dfrac{N_u}{A_c} \geq f_{r.V}$

for $i \in 1..\text{vect\_elemnt}_{x.critical_1}$ if $\text{rows}(\text{vect\_elemnt}_{x.critical}) > 1$

$\varepsilon_{s_i} \leftarrow \varepsilon_{s(\text{vect\_elemnt}_{x.critical_1})}$ if $x_{dist_i} \leq d_{v_i}$

for $i \in 1..\text{vect\_elemnt}_{x.critical}$ if $\text{rows}(\text{vect\_elemnt}_{x.critical}) \leq 1$

$\varepsilon_{s_i} \leftarrow \varepsilon_{s(\text{vect\_elemnt}_{x.critical})}$ if $x_{dist_i} \leq d_{v_i}$

ε_s

$\beta \leftarrow \beta(x_{dist}, d_v, \varepsilon_s)$

$\theta \leftarrow \theta(x_{dist}, \varepsilon_s)$

$V_c \leftarrow V_r.(x_{dist}, \beta, d_v, \theta, s_{v.design}, V_p)_1$

$V_s \leftarrow V_r.(x_{dist}, \beta, d_v, \theta, s_{v.design}, V_p)_2$

Figure C-3 (cont.) Program for calculating the design shear strength following the *General Procedure*.

$V_s \leftarrow V_{r.}(x_{dist}, \beta, d_v, \theta, s_{v.design}, V_p)_2$

$V_{n1} \leftarrow V_{r.}(x_{dist}, \beta, d_v, \theta, s_{v.design}, V_p)_3$

$V_{n2} \leftarrow V_{r.}(x_{dist}, \beta, d_v, \theta, s_{v.design}, V_p)_4$

$V_r \leftarrow V_{r.}(x_{dist}, \beta, d_v, \theta, s_{v.design}, V_p)_5$

for $i \in 1..\text{rows}(x_{dist})$

$\text{ShearStrengthCheck}_i \leftarrow \text{"OK"} \quad \text{if } V_{r_i} - V_{\text{assume}_i} \le 0.1\text{kip} \wedge V_{r_i} - V_{\text{assume}_i} \ge 0\text{kip}$

if $V_{r_i} - V_{\text{assume}_i} > 0.1\text{kip} \vee V_{r_i} - V_{\text{assume}_i} < 0\text{kip}$

$\text{ShearStrengthCheck}_i \leftarrow \text{"NG!!!"}$

$\text{ShearStrengthSum} \leftarrow \text{ShearStrengthSum} + 1$

$V_{\text{assume}_i} \leftarrow \frac{1}{2}\left(V_{r_i} + V_{\text{assume}_i}\right) - 0.01\text{kip}$

$$P_{\text{assume}_i} \leftarrow \begin{cases} \dfrac{\left[V_{\text{assume}_i} - \left\lceil 1.00\left\lceil \left(\text{DeadLoad}^{\langle 5 \rangle}\right)_i + \left(\text{DeadLoad}^{\langle 7 \rangle}\right)_i \right\rceil + 1.00\cdot\left(\text{DeadLoad}^{\langle 9 \rangle}\right)_i \right\rceil \cdot \text{kip}\right] \cdot L_{span}}{\left\lceil 2\left(L_{span} - \text{ShearSpan}\right) - \text{LoadSpacing} \right\rceil} & \text{if } x_{dis} \\ \dfrac{\left[V_{\text{assume}_i} - \left\lceil 1.00\left\lceil \left(\text{DeadLoad}^{\langle 5 \rangle}\right)_i + \left(\text{DeadLoad}^{\langle 7 \rangle}\right)_i \right\rceil + 1.00\cdot\left(\text{DeadLoad}^{\langle 9 \rangle}\right)_i \right\rceil \cdot \text{kip}\right] \cdot L_{span}}{L_{span} - 2\text{ShearSpan} - \text{LoadSpacing}} & \text{if She} \\ \dfrac{\left[V_{\text{assume}_i} - \left\lceil 1.00\left\lceil \left(\text{DeadLoad}^{\langle 5 \rangle}\right)_i + \left(\text{DeadLoad}^{\langle 7 \rangle}\right)_i \right\rceil + 1.00\cdot\left(\text{DeadLoad}^{\langle 9 \rangle}\right)_i \right\rceil \cdot \text{kip}\right] \cdot L_{span}}{2\text{ShearSpan} + \text{LoadSpacing}} & \text{if } x_{dis} \end{cases}$$

$\text{vect\_elemnt}_{x.\text{critical}} \leftarrow \dfrac{x\_\theta\left(x_{\text{critical.assume}}\right)2}{\text{in}}$

for $i \in 1..1$

$\text{ShearStrengthCheckFinal} \leftarrow \text{"OK"} \quad \text{if } \text{ShearStrengthSum} = 0 \vee \text{iterations} > 500$

if $\text{rows}\left(\text{vect\_elemnt}_{x.\text{critical}}\right) > 1$

$d_{v.\text{critical}} \leftarrow d_v\left(\text{vect\_elemnt}_{x.\text{critical}_1}\right)$

$\theta_{\text{critical}} \leftarrow \theta\left(\text{vect\_elemnt}_{x.\text{critical}_1}\right)$

if $\text{rows}\left(\text{vect\_elemnt}_{x.\text{critical}}\right) \le 1$

$d_{v.\text{critical}} \leftarrow d_v\left(\text{vect\_elemnt}_{x.\text{critical}}\right)$

$\theta_{\text{critical}} \leftarrow \theta\left(\text{vect\_elemnt}_{x.\text{critical}}\right)$

$x_{\text{critical.assume}} \leftarrow \max\left(d_{v.\text{critical}}, \frac{1}{2}\cdot d_{v.\text{critical}}\cdot\cot\left(\theta_{\text{critical}}\cdot\frac{\pi}{180}\right)\right)$

$\left(V_{n.\text{critical}} \quad x_{\text{critical}}\right) \leftarrow (0 \quad 0)$

for $i \in 1..\text{rows}\left(\text{vect\_elemnt}_{x.\text{critical}}\right) \quad \text{if } \text{rows}\left(\text{vect\_elemnt}_{x.\text{critical}}\right) > 1$

$V_{n.\text{critical}_i} \leftarrow V_r\left(\text{vect\_elemnt}_{x.\text{critical}_i}\right)$

Figure C-3 (cont.) Program for calculating the design shear strength following the *General Procedure*.

$$
\begin{array}{l}
\left|\begin{array}{l}
V_{n.critical_i} \leftarrow V_{r}\left(vect\_elemnt_{x.critical_i}\right) \\
x_{critical_i} \leftarrow x_{dist}\left(vect\_elemnt_{x.critical_i}\right)
\end{array}\right. \\
\text{if } rows\left(vect\_elemnt_{x.critical}\right) \le 1 \\
\left|\begin{array}{l}
V_{n.critical} \leftarrow V_{r_{vect\_elemnt_{x.critical}}} \\
x_{critical} \leftarrow x_{dist_{vect\_elemnt_{x.critical}}}
\end{array}\right. \\
\left(\begin{array}{cccccccccccc}
\frac{V_r}{kip} & \frac{P_{assume}}{kip} & \theta & \beta & \frac{x_{dist}}{in} & \frac{x_{critical}}{in} & \frac{V_{n.critical}}{kip} & iterations & iterations_{\theta.tot} & MinReinforcingCheck & \varepsilon_s & LiveLoad^{\langle 3 \rangle} \quad Liv
\end{array}\right)
\end{array}
$$

Figure C-3 (cont.) Program for calculating the design shear strength following the *General Procedure*.

$$
\varepsilon_{s.}\left(x_{dist}, f_{ps}, c, d_p, d_v, V_p\right) = \left|\begin{array}{l}
\text{for } i \in 1..rows\left(x_{dist}\right) \\
\left|\begin{array}{l}
\varepsilon s1_i \leftarrow \min\left(\dfrac{\left|\dfrac{\left|M_{assume_i}\right|}{d_{v_i}} + 0.5N_u + \left|V_{assume_i} - V_{p_i}\right| - A_{ps.bot.\varepsilon s_i} \cdot f_{po}}{E_s \cdot A_{s.bot.\varepsilon s_i} + E_p \cdot A_{ps.bot.\varepsilon s_i}}, 0.006\right) \\
\varepsilon s2_i \leftarrow \max\left[\dfrac{\left(\dfrac{\left|M_{assume_i}\right|}{d_{v_i}} + 0.5N_u + \left|V_{assume_i} - V_{p_i}\right| - A_{ps.bot.\varepsilon s_i} \cdot f_{po}\right)}{E_{beam} \cdot A_{ct} + E_s \cdot A_{s.bot.\varepsilon s_i} + E_p \cdot A_{ps.bot.\varepsilon s_i}}, -0.0004\right]
\end{array}\right. \\
\text{for } i \in 1..rows\left(x_{dist}\right) \\
\left|\begin{array}{l}
\varepsilon_{s_i} \leftarrow \varepsilon s1_i \quad \text{if } \varepsilon s1_i \ge 0 \\
\varepsilon_{s_i} \leftarrow \varepsilon s2_i \quad \text{if } \varepsilon s1_i < 0 \\
\varepsilon_{s_i} \leftarrow 2 \cdot \varepsilon s1_i \quad \text{if } \varepsilon s1_i \ge 0 \wedge \dfrac{N_u}{A_c} \ge f_{r.V}
\end{array}\right. \\
\text{for } i \in 1..vect\_elemnt_{x.critical_l} \qquad \text{if } rows\left(vect\_elemnt_{x.critical}\right) > 1 \\
\quad \varepsilon_{s_i} \leftarrow \varepsilon_s\left(vect\_elemnt_{x.critical_l}\right) \quad \text{if } x_{dist_i} \le d_{v_i} \\
\text{for } i \in 1..vect\_elemnt_{x.critical} \qquad \text{if } rows\left(vect\_elemnt_{x.critical}\right) \le 1 \\
\quad \varepsilon_{s_i} \leftarrow \varepsilon_s\left(vect\_elemnt_{x.critical}\right) \quad \text{if } x_{dist_i} \le d_{v_i} \\
\varepsilon_s
\end{array}\right.
$$

$$
\theta\left(x_{dist}, \varepsilon_s\right) = \left|\begin{array}{l}
\text{for } i \in 1..rows\left(x_{dist}\right) \\
\quad \theta_i \leftarrow \left(29 + 3500 \cdot \varepsilon_{s_i}\right) \\
\theta
\end{array}\right.
$$

Figure C-4. Additional subroutines for the main calculation program given in Figure C-3.

```
β(x_dist, d_v, ε_s) = | for i ∈ 1.. rows(x_dist)
                      |   β_min.reinfo_i ← 4.8 / (1 + 750ε_s_i)
                      |   s_x_i ← d_v_i
                      |   s_xe_i ← min( max( 12in, s_x_i · 1.38in / (a_g + 0.63in) ), 80in )
                      |   β_no.min.reinfo_i ← (4.8 / (1 + 750ε_s_i)) · (51in / (39in + s_xe_i))
                      |   β_i ← β_min.reinfo_i  if MinReinforcingCheck_i = "OK"
                      |   β_i ← β_no.min.reinfo_i  if MinReinforcingCheck_i = "NG!!!"
                      |   β_i ← "error"  otherwise
                      | β
```

Figure C-4 (cont.) Additional subroutines for the main calculation program given in Figure C-3.

```
calc = | ShearStrengthCheckFinal ← "NG"
       | iterations ← 0
       | while iterations < 1
       |   iterations ← iterations + 1
       |   for i ∈ 1.. 1
       |     x_dist ← x_θ(x_critical.assume)_1
       |     if rows(x_dist) ≠ rows(P_assume)
       |       for i ∈ 1.. rows(x_dist)          if rows(x_dist) < rows(P_assume)
       |         P_assume.old_i ← P_assume_i
       |       for i ∈ 1.. rows(x_dist) − rows(P_assume)          if rows(x_dist) > rows(P_assume)
       |         P_assume.old ← P_assume
       |         P_assume.old_(i+rows(P_assume)) ← P_assume_rows(P_assume)
       |       P_assume ← P_assume.old
       |     LiveLoad ← Load_Live(x_dist, P_assume, ShearSpan, LoadSpacing, L_span)
       |     DeadLoad ← Dead_Load(x_dist, L_span, x_bearing, x_bearing.roller, ShearSpan, w_beam, DC_1, DC_2, DW, P_diaphragm)
       |     (LiveLoad^⟨4⟩)_1 ← 10^5  if (LiveLoad^⟨4⟩)_1 = 0
       |     V_assume ← ⌈1.00(DeadLoad^⟨5⟩ + DeadLoad^⟨7⟩) + 1.00·DeadLoad^⟨9⟩ + 1.00LiveLoad^⟨3⟩⌉·kip
       |     M_assume ← ⌈1.00·(DeadLoad^⟨6⟩ + DeadLoad^⟨8⟩) + 1.00DeadLoad^⟨10⟩ + 1.00LiveLoad^⟨4⟩⌉·kip·ft
       |     M_DC1 ← DeadLoad^⟨6⟩·kip·ft
       |     V_d ← (DeadLoad^⟨5⟩ + DeadLoad^⟨7⟩ + DeadLoad^⟨9⟩)·kip
```

Figure C-5. Program for calculating the design shear strength following the *Simplified Procedure*.

$V_d \leftarrow \left(DeadLoad^{\langle 5 \rangle} + DeadLoad^{\langle 7 \rangle} + DeadLoad^{\langle 9 \rangle}\right) \cdot kip$

$V_i \leftarrow V_{assume} - V_d$

$M_{max} \leftarrow M_{assume} - \left(DeadLoad^{\langle 6 \rangle} + DeadLoad^{\langle 8 \rangle} + DeadLoad^{\langle 10 \rangle}\right) \cdot kip \cdot ft$

$V_p \leftarrow V_{p.}(x_{dist})$

$cg_{harp} \leftarrow cg_{harp.}(x_{dist})$

$f_{c'c} \leftarrow \begin{cases} f_{c'deck} & \text{if } f_{c'deck} > 0 \\ f_{c'} & \text{otherwise} \end{cases}$

$\beta_1 \leftarrow \beta_{1.}(f_{c'c})$

$\varepsilon_{s.yield} \leftarrow \frac{f_y}{E_s}$

$Num_{strand.bot} \leftarrow Num_{strand.bot.}(x_{dist}, cg_{harp})$

$cg_{ps.bot} \leftarrow cg_{ps.bot.}(x_{dist}, cg_{straight.bot}, cg_{harp}, h_c, Num_{straight.bot})$

for $i \in 1.. rows(x_{dist})$

$cg_{ps_i} \leftarrow \frac{Num_{straight} \cdot cg_{straight} + Num_{harp} \cdot cg_{harp_i}}{Num_{strand}}$

$d_{p_i} \leftarrow h_c - cg_{ps_i}$

$c_i \leftarrow \begin{cases} d_{p_i} \leftarrow 10^6 \cdot in & \text{if } d_{p_i} = 0 \\ c_i \leftarrow \dfrac{A_{ps} \cdot f_{pu} + A_{s.bot_i} \cdot f_y - A_{s.top} \cdot f_y}{0.85 \cdot f_{c'c} \cdot \beta_1 \cdot b_{eff} + k \cdot A_{ps} \cdot \dfrac{f_{pu}}{d_{p_i}}} & \\ c_i \leftarrow \dfrac{A_{ps} \cdot f_{pu} + A_{s.bot_i} \cdot f_y - A_{s.top} \cdot f_y - 0.85 \cdot f_{c'c} \cdot (b_{eff} - b_v) \cdot h_{flange}}{0.85 \cdot f_{c'c} \cdot \beta_1 \cdot b_v + k \cdot A_{ps} \cdot \dfrac{f_{pu}}{d_{p_i}}} & \text{if } c_i > h_{flange} \end{cases}$

$f_{ps.max_i} \leftarrow f_{pu} \cdot \left(1 - k \cdot \frac{c_i}{d_{p_i}}\right)$

$l_{d.ps_i} \leftarrow \kappa \cdot \left(f_{ps.max_i} - \frac{2}{3} \cdot f_{pe}\right) \varphi$

$f_{ps} \leftarrow f_{ps.}(x_{dist}, l_{d.ps}, f_{ps.max})$

for $i \in 1.. rows(x_{dist})$

$A_{ps.bot_i} \leftarrow Num_{strand.bot_i} \cdot A_{strand}$

$d_{p.bot_i} \leftarrow h_c - cg_{ps.bot_i}$

$d_{s.bot_i} \leftarrow h_c - cg_{s.bot_i}$

Figure C-5 (cont.) Program for calculating the design shear strength following the *Simplified Procedure*.

$$d_{s.bot_i} \leftarrow h_c - cg_{s.bot_i}$$

$$d_{e_i} \leftarrow \frac{A_{ps.bot_i} \cdot f_{ps_i} \cdot d_{p.bot_i} + A_{s.bot_i} \cdot f_y \cdot d_{s.bot_i}}{A_{ps.bot_i} \cdot f_{ps_i} + A_{s.bot_i} \cdot f_y}$$

$$\varepsilon_{s_i} \leftarrow \frac{0.003}{c_i} \cdot \left(d_{e_i} - c_i\right)$$

return $\left("\text{Tension steel does not yield at x.dist}" \quad \frac{x_{dist_i}}{in}\right)$ if $\varepsilon_{s_i} < \varepsilon_{s.yield}$

$$a_i \leftarrow \beta_1 \cdot c_i$$

$$d_{v_i} \leftarrow \max\left(d_{e_i} - \frac{a_i}{2}, 0.9 d_{e_i}, 0.72 h_c\right)$$

$$f_{r.V} \leftarrow \begin{cases} 0.20 \cdot \sqrt{\frac{f_c'}{ksi}}\, ksi & \text{if FineAggType = "sand"} \\ \left(0.17 \cdot \sqrt{\frac{f_c'}{ksi}}\, ksi\right) & \text{if FineAggType = "lightweight"} \\ \text{"error"} & \text{otherwise} \end{cases}$$

$$e_{strand} \leftarrow y_b - cg_{ps}$$

$$l_t \leftarrow 60 \cdot \varphi$$

for $i \in 1..\text{rows}(x_{dist})$

$$P_{f.cpe_i} \leftarrow \begin{cases} f_{pe} \cdot A_{strand} \cdot Num_{strand} \cdot \frac{x_{dist_i} + x_{bearing}}{l_t} & \text{if } x_{dist_i} + x_{bearing} < l_t \\ f_{pe} \cdot A_{strand} \cdot Num_{strand} & \text{if } x_{dist_i} + x_{bearing} \geq l_t \\ \text{"error"} & \text{otherwise} \end{cases}$$

$$f_{cpe_i} \leftarrow \frac{P_{f.cpe_i}}{A_{beam}} + \frac{P_{f.cpe_i} \cdot e_{strand_i}}{S_b}$$

$$M_{cre_i} \leftarrow S_{bc} \cdot \left[f_{r.V} + f_{cpe_i} - \frac{\left(DeadLoad\langle 6\rangle \cdot kip \cdot ft\right)_i}{S_b}\right]$$

$$V_{ci_i} \leftarrow \max\left(0.02 \alpha_v \cdot \sqrt{\frac{f_c'}{ksi}} \cdot ksi \cdot b_v \cdot d_{v_i} + V_{d_i} + \frac{V_{i_i} \cdot M_{cre_i}}{M_{max_i}}, 0.06 \cdot \alpha_v \sqrt{\frac{f_c'}{ksi}} \cdot ksi \cdot b_v \cdot d_{v_i}\right)$$

$$P_{f.pc_i} \leftarrow f_{ps_i} \cdot A_{strand} \cdot Num_{strand}$$

$$f_{pc_i} \leftarrow \begin{cases} \frac{P_{f.pc_i}}{A_{beam}} + \frac{P_{f.pc_i} \cdot e_{strand_i} \cdot \left(y_b - y_{bc}\right)}{I_{beam}} - \frac{M_{DC1_i} \cdot \left(y_b - y_{bc}\right)}{I_{beam}} & \text{if } y_{bc} \leq h_{top.flange} \\ \frac{P_{f.pc_i}}{A_{beam}} + \frac{P_{f.pc_i} \cdot e_{strand_i} \cdot \left(y_b - h_{top.flange}\right)}{I_{beam}} - \frac{M_{DC1_i} \cdot \left(y_b - h_{top.flange}\right)}{I_{beam}} & \text{if } y_{bc} > h_{top.flange} \end{cases}$$

$$V_{cw_i} \leftarrow \left(0.06 \cdot \alpha_v \cdot \sqrt{\frac{f_c'}{ksi}} \cdot ksi + 0.30 \cdot f_{pc_i}\right) \cdot b_v \cdot d_{v_i} + V_{p_i}$$

Figure C-5 (cont.) Program for calculating the design shear strength following the *Simplified Procedure.*

$$V_{cw_i} \leftarrow \left(0.06 \cdot \alpha_v \cdot \sqrt{\frac{f_{c'}}{ksi}} \cdot ksi + 0.30 \cdot f_{pc_i}\right) \cdot b_v \cdot d_{v_i} + V_{p_i}$$

$$V_{c_i} \leftarrow \min\left(V_{ci_i}, V_{cw_i}\right)$$

$$\cot\theta_i \leftarrow \begin{cases} 1 & \text{if } V_{ci_i} < V_{cw_i} \\ \min\left(1 + 3 \cdot \dfrac{f_{pc_i}}{\alpha_v \cdot \sqrt{f_{c'}} \cdot ksi^{0.5}}, 1.8\right) & \text{if } V_{ci_i} \geq V_{cw_i} \end{cases}$$

$$V_{s_i} \leftarrow \frac{A_{v_i} \cdot f_{yv} \cdot d_{v_i} \cdot \left(\cot\theta_i + \cot(\alpha)\right) \cdot \sin(\alpha)}{s_{v.design_i}}$$

$$V_{n1} \leftarrow V_c + V_s$$

$$V_{n2} \leftarrow 0.25 \cdot f_{c'} \cdot b_v \cdot d_v + V_p$$

for $i \in 1..\text{rows}(x_{dist})$

$$V_{r_i} \leftarrow \phi_v \cdot \min\left(V_{n1_i}, V_{n2_i}\right)$$

$$ShearStrengthCheck_i \leftarrow \text{"OK"} \quad \text{if } V_{r_i} - V_{assume_i} \leq 0.1kip \wedge V_{r_i} - V_{assume_i} \geq 0kip$$

if $V_{r_i} - V_{assume_i} > 0.1kip \vee V_{r_i} - V_{assume_i} < 0kip$

$$ShearStrengthCheck_i \leftarrow \text{"NG!!!"}$$

$$ShearStrengthSum \leftarrow ShearStrengthSum + 1$$

$$V_{assume_i} \leftarrow \frac{1}{2}\left(V_{r_i} + V_{assume_i}\right) - 0.01kip$$

$$P_{assume.r_i} \leftarrow P_{assume_i}$$

$$P_{assume_i} \leftarrow \begin{cases} \dfrac{\left[V_{assume_i} - \left\lceil 1.00\left\lceil \left(DeadLoad^{\langle 5 \rangle}\right)_i + \left(DeadLoad^{\langle 7 \rangle}\right)_i \right\rceil + 1.00 \cdot \left(DeadLoad^{\langle 9 \rangle}\right)_i \right\rceil \cdot kip\right] \cdot L_{span}}{\left\lceil 2\left(L_{span} - ShearSpan\right) - LoadSpacing \right\rceil} & \text{if } x_{dist_i} \leq ShearSpan \\ \dfrac{\left[V_{assume_i} - \left\lceil 1.00\left\lceil \left(DeadLoad^{\langle 5 \rangle}\right)_i + \left(DeadLoad^{\langle 7 \rangle}\right)_i \right\rceil + 1.00 \cdot \left(DeadLoad^{\langle 9 \rangle}\right)_i \right\rceil \cdot kip\right] \cdot L_{span}}{L_{span} - 2ShearSpan - LoadSpacing} & \text{if } ShearSpan + 10^{-1} \\ \dfrac{\left[V_{assume_i} - \left\lceil 1.00\left\lceil \left(DeadLoad^{\langle 5 \rangle}\right)_i + \left(DeadLoad^{\langle 7 \rangle}\right)_i \right\rceil + 1.00 \cdot \left(DeadLoad^{\langle 9 \rangle}\right)_i \right\rceil \cdot kip\right] \cdot L_{span}}{2ShearSpan + LoadSpacing} & \text{if } x_{dist_i} > ShearSpan \end{cases}$$

$$vect\_elemnt_{x.critical} \leftarrow \frac{x\_\theta\left(x_{critical.assume}\right)2}{in}$$

for $i \in 1..1$

$$ShearStrengthCheckFinal \leftarrow \text{"OK"} \quad \text{if } ShearStrengthSum = 0 \vee iterations > 500$$

$$d_{v.critical} \leftarrow d_{v\left(vect\_elemnt_{x.critical_1}\right)} \quad \text{if } \text{rows}\left(vect\_elemnt_{x.critical}\right) > 1$$

$$d_{v.critical} \leftarrow d_{vvect\_elemnt_{x.critical}} \quad \text{if } \text{rows}\left(vect\_elemnt_{x.critical}\right) \leq 1$$

$$x_{critical.assume} \leftarrow \max\left[d_{v.critical}, \frac{1}{2} \cdot d_{v.critical} \cdot \cot\theta_{\left(vect\_elemnt_{x.critical_1}\right)}\right] \quad \text{if } \text{rows}\left(vect\_elemnt_{x.critical}\right) > 1$$

Figure C-5 (cont.) Program for calculating the design shear strength following the *Simplified Procedure*.

$$x_{critical.assume} \leftarrow \max\left[d_{v.critical}, \frac{1}{2}\cdot d_{v.critical}\cdot\cot\theta_{\left(vect\_elemnt_{x.critical_1}\right)}\right] \quad \text{if } rows\left(vect\_elemnt_{x.critical}\right) > 1$$

$$x_{critical.assume} \leftarrow \max\left(d_{v.critical}, \frac{1}{2}\cdot d_{v.critical}\cdot\cot\theta_{vect\_elemnt_{x.critical}}\right) \quad \text{if } rows\left(vect\_elemnt_{x.critical}\right) \leq 1$$

$$\left(V_{n.critical} \;\; x_{critical}\right) \leftarrow (0 \;\; 0)$$

for $i \in 1..rows\left(vect\_elemnt_{x.critical}\right)$ if $rows\left(vect\_elemnt_{x.critical}\right) > 1$

$$V_{n.critical_i} \leftarrow V_{r_{\left(vect\_elemnt_{x.critical_i}\right)}}$$

$$x_{critical_i} \leftarrow x_{dist_{\left(vect\_elemnt_{x.critical_i}\right)}}$$

otherwise

$$V_{n.critical} \leftarrow V_{r_{vect\_elemnt_{x.critical}}}$$

$$x_{critical} \leftarrow x_{dist_{vect\_elemnt_{x.critical}}}$$

Figure C-5 (cont.) Program for calculating the design shear strength following the *Simplified Procedure*.

C.2 Example Calculations

C.2.1 Example Following Appendix B5

The following calculations are for a simply-supported, Type II prestressed girder with a cast-in-place composite deck, containing a typical amount of shear reinforcement found in such a girder spanning 60 ft. As discussed in Section 3.1.2.1, for the actual beam in this example, a portion of the girder was removed from the original 60-ft design such that that girder was shortened by some distance between the harping points. The drawing details for this example beam, T2.8.Typ, is shown in Figure A-2. The parameters that are necessary to perform the calculations are given the section below.

C.2.1.1 Inputs

ConcreteType = "NWC"
FineAggType = "sand"

Programming mechanism used for setting the lightweight concrete modifier. In this example, the assumption is that the lightweight concrete should not have a modifier; hence the concrete is assumed to be normal weight.

$\gamma_c = 121.5\,pcf$

$f_{c'} = 8865\,psi$

$f_{ci'} = 6090\,psi$

$f_{c'deck} = 5829\,psi$

$\gamma_{c.deck} = 123.4\,pcf$

$E_{beam} = 3605\,ksi$

$E_{beam.i} = 3585\,ksi$

$E_{slab} = 3566\,ksi$

$Value\_f_{ct} = \text{"not specified"}$ the splitting tensile strength was assumed to be unspecified

$h = 36\,in$ height of the beam

$A_{beam} = 369\,in^2$

$I_{beam} = 50979\,in^4$

$L_{beam} = 41\,ft$

$b_v = 6\,in$ web width

$y_b = 15.83\,in$ distance from bottom of beam to beam centroid

$y_t = 20.17\,in$ distance from top of beam to beam centroid

$S = 7\,ft$ girder spacing, which in this case, is the width of the deck

$t_{haunch} = 1\,in$ thickness of the haunch

$t_{struct} = 8.5\,in$ structural depth of the deck

$A_{ct} = 243\,in^2$ area of concrete in the flexural tension zone, as defined in A. 5.8.3.4.2

$h_{flange} = 8.5\,in$ distance from the extreme compression flange to the web-flange intersection

$Num_{strand} = 24$

$Num_{straight} = 18$ number of unharped tendons

$Num_{straight.bot} = 16$ number of unharped tendons near the bottom of the beam

$Num_{harp} = 6$ number of harped tendons

$cg_{straight} = 7in$ centroid of the unharped tendons

$cg_{harp.end} = 29in$ centroid of the harped tendons at the end of the beam

$cg_{harp.ms} = 4in$ centroid of the harped tendons at the harping location

$cg_{straight.bot} = 3.75in$ centroid of the unharped tendons near the bottom of the beam

$A_{strand} = 0.153\,in^2$

$\varphi = 0.5\,in$ strand diameter

$f_{pu} = 270\,ksi$

$f_{pe} = 164.96\,ksi$

$E_p = 28500\,ksi$

$HarpDist = 17.5ft$ distance from the support to the harping location

$f_y = 67.3\,ksi$

$f_{yv} = 67.3\,ksi$ yield strength of the stirrups

$E_s = 29000\,ksi$

$RebarSize = 4$ stirrup size

$A_v = 0.4\,in^2$ area of a double-legged stirrup

$\alpha = \frac{\pi}{2}$ angle of the stirrups relative to the longitudinal axis of the beam

$A_{s.top} = 0in^2$ area of the mild steel reinforcement at the top of the girder

$d_{top} = 9.5\,in$ distance from the extreme compression fiber to the steel in the top of the girder

$cg_s = 4.4\,in$ distance from the girder bottom to the centroid of the mild steel

$cg_{s.bot} = 4.4\,in$ distance from the bottom of the girder to the centroid of the mild steel used for tension reinforcement

$d_{long.rebar} = 5$ size of the longitudinal mild reinforcement

$IsLongSteelEpoxyCoated = "No"$

$LongSteelClearSpacing = 3.38\,in$

$LongSteelCover = 1.75\,in$

$IsTopBarEffectApplicable = "No"$

$s_{vs.design} = (2.5\ \ 6\ \ 6\ \ 9\ \ 9\ \ 9\ \ 9\ \ 9\ \ 9\ \ 9\ \ 9\ \ 9)^T\,in$ stirrup spacing, listed at distinct points along the shear span; see calculation for variable x_{dist} below

$A_{s.bot} = (2.04\ \ 2.04\ \ 2.04\ \ 2.04\ \ 2.04\ \ 2.04\ \ 2.04\ \ 2.04\ \ 2.04\ \ 2.04\ \ 2.04\ \ 2.04)^T\,in^2$

area of mild reinforcing steel in the bottom of the beam, listed at distinct points along the shear span; see explanation for variable x_{dist} below.

$A_{long.rebar} = 0.31in^2$ area of the mild steel in the longitudinal direction

$A_{diaphragm} = 0\,in^2$

$t_{wear} = 0\,in$

$\gamma_{wear} = 0\,pcf$

$b_{barrier} = 0\,in$

$w_{barrier} = 0\,klf$

$b_{bridge} = 0\,in$

additional parameters for dead load that were all set to equal zero since the beam being tested was a stand-alone structure with a cast-in-place composite deck

$ShearSpan = 57.34in$

$LoadSpacing = 174.19\,in$

$x_{bearing} = 6\,in$ distance from the end of the beam to the center of bearing of the pin support

$x_{bearing.roller} = 6\,in$ distance from the end of the beam to the center of bearing of the roller support

$x_{critical.assume} = 38.69\,in$ assumed distance from the support to the critical section

$N_u = 0$ axial force, assumed to be equal to zero

$\phi_v = 1.00$ resistance factor for shear, assumed to be equal to zero for analysis purposes

$\theta\beta method = \text{"General"}$ programming mechanism used to calculate the shear strength following A. 5.8.3.4.1 (if applicable) or A. 5.8.3.4.2

$P_{assume} = (369.68 \;\; 196.22 \;\; 199.24 \;\; 148.17 \;\; 150.98 \;\; 151.77 \;\; 146.7 \;\; 147.75 \;\; 147.81 \;\; 148.07 \;\; 148.01 \;\; 148.65)\,kip$

Note that individual values for P_{assume} are listed at distinct locations along the shear span (see the calculations for x_{dist} below. Each value is the assumed load applied by each of the actuators, whose locations are specified by the parameters *ShearSpan* and *LoadSpacing*, that would result in a shear failure at the corresponding section indicated in x_{dist}. Ordinarily, the calculation would start with an arbitrary value for all of the section locations, say 150 kips or 250 kips. However, for the purposes of this example, the given P_{assume} values are used to mitigate the number of iterations necessary to reach convergence.

Subsequent calculations will require knowing the location of the sections for which the shear strength is being calculated. Those locations are defined by the term x_{dist}, given in this example in terms of the distance from the support closest to the point loads:

$$x_{dist} = (0 \;\; 5.73 \;\; 11.47 \;\; 17.2 \;\; 22.93 \;\; 28.67 \;\; 34.4 \;\; 36.5 \;\; 40.14 \;\; 45.87 \;\; 51.6 \;\; 57.34)\,in$$

where each location is a tenth point along the length of the shear span, with the exception of the critical section, which in this case, is assumed to be 36.5 in.

C.2.1.2 Basic Geometry Calculations

$$h_c = h + t_{haunch} + t_{struct}$$

$$h_c = 36in + 1in + 8.5in$$

$$h_c = 45.5\,in$$

$$L_{span} = L_{beam} - \left(x_{bearing} + x_{bearing.roller}\right)$$

$$L_{span} = 41ft - (6in + 6in)$$

$$L_{span} = 40\,ft$$

$$A_{ps} = Num_{strand} \cdot A_{strand}$$

$$A_{ps} = 24 \cdot 0.153in^2$$

$$A_{ps} = 3.67\,in^2$$

$$A_{ps.bot} = Num_{strand.bot} \cdot A_{strand}$$

Area of unharped prestessing tendons along the bottom of the girder.

$$A_{ps.bot} = 16 \cdot 0.153in^2$$

$$A_{ps.bot} = 2.45\,in^2$$

$$b_{eff} = S = 7\,ft$$

$$\Psi_{harp} = atan\left(\frac{cg_{harp.end} - cg_{harp.ms}}{HarpDist + x_{bearing}}\right)$$

Angle of the harped tendon, relative to the longitudinal axis of the beam

$$\Psi_{harp} = atan\left(\frac{29in - 4in}{17.5ft + 6in}\right)$$

$$\Psi_{harp} = 0.12$$

$$d_s = h_c - cg_s$$

depth from the top of the composite section to the centroid of the mild steel reinforcement at the bottom of the beam.

$$d_s = 45.5in - 4.4in$$

$$d_s = 41.1\,in$$

$$cg_{harp_i} = cg_{harp.end} - \left(x_{dist_i} + x_{bearing}\right)\cdot\tan\left(\Psi_{harp}\right)$$ centroid of the harped tedons

$$cg_{harp_2} = 29\text{in} - (5.73\text{in} + 6\text{in})\tan(0.12)$$

$$cg_{harp_2} = 27.64\,\text{in}$$

$$cg_{harp}^{T} = (28.31 \quad 27.64 \quad 26.98 \quad 26.31 \quad 25.65 \quad 24.99 \quad 24.32 \quad 24.08 \quad 23.66 \quad 23 \quad 22.33 \quad 21.67)\,\text{in}$$

Note that the centroid of the harped tendons changes along the length of the shear span. Thus, the example above and all other example calculations that are dependent on the location of the section give a detailed calculation at a specific location, x_{dist} = 5.73 in., which is the second location given in the parameter x_{dist}. The results for all sections are then given at the end of each specific calculation.

C.2.1.3 Basic Material Calculations

$$f_{po} = 0.70 f_{pu}$$

$$f_{po} = 0.70\cdot 270\text{ksi}$$

$$f_{po} = 189\,\text{ksi}$$

$$\kappa = \frac{\text{in}^2}{\text{kip}}\cdot \begin{cases} 1.6 & \text{if } h \geq 24\text{in} \\ 1.0 & \text{if } h < 24\text{in} \\ \text{"error"} & \text{otherwise} \end{cases}$$

$$\kappa = 1.6\,\frac{\text{in}^2}{\text{kip}}$$

$$f_{r.V} = \begin{cases} 0.20\cdot\sqrt{\frac{f_{c'}}{\text{ksi}}}\,\text{ksi} & \text{if FineAggType} = \text{"sand"} \\ \left(0.17\cdot\sqrt{\frac{f_{c'}}{\text{ksi}}}\,\text{ksi}\right) & \text{if FineAggType} = \text{"lightweight"} \\ \text{"error"} & \text{otherwise} \end{cases}$$ modululs of rupture for shear calculations

$$f_{r.V} = 0.20\cdot\sqrt{8.87\text{ksi}}$$

$$f_{r.V} = 595.48\,\text{psi}$$

$$\beta_1(f_{c'deck}) = \begin{cases} 0.85 & \text{if } f_{c'deck} \le 4ksi \\ \max\left[0.85 - 0.05\cdot\left(\frac{f_{c'deck}}{ksi} - 4.0\right), 0.65\right] & \text{if } f_{c'deck} > 4ksi \end{cases}$$

$$\beta_1(5.83ksi) = \max[0.85 - 0.05\cdot(5.83 - 4.0), 0.65]$$

$$\beta_1 = 0.76$$

$$\alpha_v = 1 \quad \text{if ConcreteType} = \text{"NWC"}$$

As discussed earlier, although the concrete in this beam was actually lightweight concrete, the assumption was that the lightweight modifier was not necessary. Hence, this example assumes that lightweight concrete behaves similarly to normal weight concrete.

C.2.1.4 Load Effects

C.2.1.4.1 Live Loads

For a simply-supported beam subjected to two point loads, the shear at any point along the beam within the shear span, V_{LL}, can be calculated as

$$V_{LL_i} = \frac{P_{assume_i}}{L_{span}}\cdot\left[2\left(L_{span} - ShearSpan\right) - LoadSpacing\right]$$

$$V_{LL_2} = \frac{196.22kip}{40ft}\cdot[2\cdot(40ft - 57.34in) - 14.52ft]$$

$$V_{LL.2} = 274.4kip$$

$$V_{LL}^{T} = (516.9 \quad 274.4 \quad 278.6 \quad 207.2 \quad 211.1 \quad 212.2 \quad 205.1 \quad 206.6 \quad 206.7 \quad 207 \quad 206.9 \quad 207.8)\,kip$$

The moment at the same locations, M_{LL}, can be calculated as

$$M_{LL_i} = \frac{P_{assume_i}}{L_{span}}\cdot\left[2\left(L_{span} - ShearSpan\right) - LoadSpacing\right]\cdot x_{dist_i}$$

$$M_{LL_2} = \frac{196.22kip}{40ft}\cdot[2(40ft - 57.34in) - 14.52ft]\,5.73in$$

$$M_{LL_2} = 131.1ft\cdot kip$$

$$M_{LL}^{T} = (0 \quad 131.1 \quad 266.2 \quad 297 \quad 403.5 \quad 507 \quad 588.1 \quad 666.5 \quad 691.2 \quad 791.4 \quad 889.9 \quad 993.1)\,ft\cdot kip$$

C.2.1.4.2 Dead Loads

The uniformly distributed forces due to the weight of the beam, the haunch and the deck are calculated as:

$$w_{beam} = \gamma_c \cdot A_{beam}$$
$$w_{beam} = 121.5pcf \cdot 369in^2$$
$$w_{beam} = 311.34\,plf$$

$$w_{deck} = t_s \cdot S \cdot \gamma_{c.deck}$$
$$w_{deck} = 8.5in \cdot 7ft \cdot 123.4pcf$$
$$w_{deck} = 611.86\,plf$$

$$w_{haunch} = t_{haunch} \cdot b_f \cdot \gamma_{c.deck}$$
$$w_{haunch} = 1in \cdot 12in \cdot 123.4pcf$$
$$w_{haunch} = 10.28\,plf$$

$$DC_1 = w_{beam} + w_{deck} + w_{haunch}$$
$$DC_1 = 311.34plf + 611.86plf + 10.28plf$$
$$DC_1 = 933.49\,plf$$

where DC_1 is the dead load of the composite structure. There were no other dead loads present. These results can be used to calculate the shear and moment due to composite dead loads, V_{DC1} and M_{DC1}, respectively, as:

$$V_{DC1_i} = \frac{DC_1}{2L_{span}} \cdot \left(x_{bearing} + L_{span} + x_{bearing.roller}\right)^2 - \frac{DC_1 \cdot x_{bearing.roller}}{L_{span}} \left(x_{bearing} + L_{span} + x_{bearing.roller}\right)$$
$$-DC_1 \cdot \left(x_{dist_i} + x_{bearing}\right) + V_{diaphragm_i}$$

$$V_{DC1_2} = \frac{933.49plf}{2 \cdot 40ft} \cdot (6in + 40ft + 6in)^2 - \frac{933.49plf \cdot 6in}{40ft} \cdot (6in + 40ft + 6in) - 933.49plf \cdot (6in + 6in) + 0$$

$$V_{DC1_2} = 18.22kip$$

$$V_{DC1}^T = (18.67 \quad 18.22 \quad 17.78 \quad 17.33 \quad 16.89 \quad 16.44 \quad 15.99 \quad 15.83 \quad 15.55 \quad 15.1 \quad 14.66 \quad 14.21)\ kip$$

$$M_{DC1_i} \leftarrow \left[\left(\frac{DC_1}{2L_{span}}\right)\left(x_{bearing} + L_{span} + x_{bearing.roller}\right)^2 - \frac{DC_1 \cdot x_{bearing.roller}}{L_{span}}\left(x_{bearing} + L_{span} + x_{bearing.roller}\right)\right] \cdot x_{dist_i}$$
$$-\frac{1}{2} DC_1 \cdot \left(x_{dist_i} + x_{bearing}\right)^2 + M_{diaphragm_i}$$

$$M_{DC1_2} = \left[\left(\frac{933.49plf}{2 \cdot 40ft}\right) \cdot (6in + 40ft + 6in)^2 - \frac{933.49plf \cdot 6in}{40ft}(6in + 40ft + 6in)\right] \cdot 5.37in - \frac{1}{2} 933.49plf \cdot (6in + 6in)^2 + 0$$

$$M_{DC1_2} = 8.7ft \cdot kip$$

$$M_{DC1}^T = (-0.12 \quad 8.7 \quad 17.3 \quad 25.69 \quad 33.86 \quad 41.82 \quad 49.57 \quad 52.35 \quad 57.11 \quad 64.43 \quad 71.54 \quad 78.43)\ ft \cdot kip$$

C.2.1.4.3 Total Load Effects

Given the assumed live loads, the total assumed shear and moment in the girder, V_{assume} and $M_{assume1}$ are the sum of the live and dead loads given in Sections C.2.1.4.1 and C.2.1.4.2 above, such that:

$$V_{assume} = V_{LL} + V_{DC1}$$

$$V_{assume_2} = 274.35kip + 18.22kip$$

$$V_{assume_2} = 292.6kip$$

$$V_{assume}^T = (535.6 \quad 292.6 \quad 296.4 \quad 224.5 \quad 228 \quad 228.6 \quad 221.1 \quad 222.3 \quad 222.2 \quad 222.1 \quad 221.6 \quad 222.1)\ kip$$

$$M_{assume1} = M_{LL} + M_{DC1}$$

$$M_{assume1_2} = 131.09\,ft\cdot kip + 8.7\,ft\cdot kip$$

$$M_{assume1_2} = 139.8\,ft\cdot kip$$

$$M_{assume1}^{T} = (-0.1 \;\; 139.8 \;\; 283.5 \;\; 322.6 \;\; 437.3 \;\; 548.8 \;\; 637.6 \;\; 721.8 \;\; 748.3 \;\; 855.8 \;\; 961.5 \;\; 1071.5)\,ft\cdot kip$$

C.2.1.5 Calculate the Shear Resistance

C.2.1.5.1 Determine β and θ

C.2.1.5.1.1 Calculate the Effective Shear Depth of the Beam, d_v

C.2.1.5.1.1.1 Calculate the Depth of the Compression Block, c

Assuming that the depth of the compression block is less than the thickness of the deck, and thus the compressive strength of the concrete, $f_{c'c}$, is that of the deck concrete, $f_{c'deck}$, then

$$cg_{ps_i} = \frac{Num_{straight}\cdot cg_{straight} + Num_{harp}\cdot cg_{harp_i}}{Num_{strand}}$$

$$cg_{ps_2} = \frac{18\cdot 7in + 6\cdot 27.64in}{24}$$

$$cg_{ps_2} = 12.16\,in$$

$$cg_{ps}^{T} = (12.33 \;\; 12.16 \;\; 11.99 \;\; 11.83 \;\; 11.66 \;\; 11.5 \;\; 11.33 \;\; 11.27 \;\; 11.16 \;\; 11 \;\; 10.83 \;\; 10.67)\,in$$

$$d_{p_i} = h_c - cg_{ps_i}$$

$$d_{p_2} = 45.5in - 12.16in$$

$$d_{p_2} = 33.34\,in$$

$$d_p^{T} = (33.17 \;\; 33.34 \;\; 33.51 \;\; 33.67 \;\; 33.84 \;\; 34 \;\; 34.17 \;\; 34.23 \;\; 34.34 \;\; 34.5 \;\; 34.67 \;\; 34.83)\,in$$

$$c_i = \frac{A_{ps} \cdot f_{pu} + A_{s.bot_i} \cdot f_y - A_{s.top} \cdot f_y}{0.85 \cdot f_{c'c} \cdot \beta_1 \cdot b_{eff} + k \cdot A_{ps} \cdot \frac{f_{pu}}{d_{p_i}}}$$

$$c_2 = \frac{3.67in^2 \cdot 270ksi + 2.04in^2 \cdot 67.3ksi - 0}{0.85 \cdot 5.83ksi \cdot 0.76 \cdot 7ft + 0.28 \cdot 3.67in^2 \cdot \frac{270ksi}{33.34in}}$$

$$c_2 = 3.48\,in$$

$$c^T = (3.48 \;\; 3.48 \;\; 3.48 \;\; 3.48 \;\; 3.48 \;\; 3.49 \;\; 3.49 \;\; 3.49 \;\; 3.49 \;\; 3.49 \;\; 3.49 \;\; 3.49)\,in$$

$$a = \beta_1 \cdot c$$

$$a_2 = 0.76 \cdot 3.48in$$

$$a_2 = 2.64\,in$$

$$a^T = (2.64 \;\; 2.64 \;\; 2.64 \;\; 2.64 \;\; 2.64 \;\; 2.64 \;\; 2.64 \;\; 2.64 \;\; 2.64 \;\; 2.64 \;\; 2.64 \;\; 2.65)\,in$$

C.2.1.5.1.1.2 Calculate the Stress in the Prestressing Strands, f_{ps}

Let $f_{ps.max}$ be the stress in the steel according to Eq. 5.7.3.1.1-1 in the AASHTO LRFD Bridge Specifications, and $l_{d.ps}$ be the development length of the prestress. Then,

$$f_{ps_i} = \begin{cases} \frac{f_{pe} \cdot \left(x_{dist_i} + x_{bearing}\right)}{l_t} & \text{if } x_{dist_i} + x_{bearing} \le l_t \\ f_{pe} + \frac{x_{dist_i} + x_{bearing} - l_t}{l_{d.ps_i} - l_t} \cdot \left(f_{ps.max_i} - f_{pe}\right) & \text{if } x_{dist_i} + x_{bearing} > l_t \wedge x_{dist_i} + x_{bearing} < l_{d.ps_i} \\ f_{ps.max_i} & \text{if } x_{dist_i} + x_{bearing} \ge l_{d.ps_i} \end{cases}$$

$$f_{ps_2} = \frac{164.96ksi \cdot (5.73in + 6in)}{30in} \quad \text{if } 5.73in + 6in \le 30in$$

$$f_{ps_2} = 64.5\,ksi$$

$$f_{ps}^T = (32.99 \;\; 64.5 \;\; 96.06 \;\; 127.57 \;\; 159.08 \;\; 169.91 \;\; 175.98 \;\; 178.21 \;\; 182.06 \;\; 188.14 \;\; 194.21 \;\; 200.3)\,ksi$$

C.2.1.5.1.1.3 Find the Effective Depth, d_e

The centroid of the prestressing steel in the flexural tension region of the beam is calculated as:

$$cg_{ps.bot_i} = \begin{cases} cg_{straight.bot} & \text{if } cg_{harp_i} - 2in \geq \frac{1}{2}h_c \\ \frac{Num_{straight.bot} \cdot cg_{straight.bot} + 2 \cdot \left(cg_{harp_i} - 2in\right)}{Num_{straight.bot} + 2} & \text{if } cg_{harp_i} - 2in < \frac{1}{2}h_c \wedge cg_{harp_i} \geq \frac{1}{2}h_c \\ \frac{Num_{straight.bot} \cdot cg_{straight.bot} + 2 \cdot \left(cg_{harp_i} - 2in + cg_{harp_i}\right)}{Num_{straight.bot} + 4} & \text{if } cg_{harp_i} < \frac{1}{2}h_c \wedge cg_{harp_i} + 2in \geq \frac{1}{2}h_c \\ \frac{Num_{straight.bot} \cdot cg_{straight.bot} + 6 \cdot cg_{harp_i}}{Num_{straight.bot} + 6} & \text{if } cg_{harp_i} + 2in < \frac{1}{2}h_c \end{cases}$$

$$cg_{ps.bot_2} = cg_{strand.bot} \quad \text{if } cg_{harp_2} - 2in \geq \frac{1}{2}h_c$$

$$cg_{ps.bot_2} = 3.75in \quad \text{if } 27.64in - 2in \geq \frac{1}{2}45.5in$$

$$cg_{ps.bot_2} = 3.75in \quad \text{if } 25.64in \geq 22.75in$$

$$cg_{ps.bot_2} = 3.75\,in$$

$$cg_{ps.bot}^{T} = (3.75 \;\; 3.75 \;\; 3.75 \;\; 3.75 \;\; 3.75 \;\; 3.75 \;\; 5.81 \;\; 5.79 \;\; 5.74 \;\; 5.67 \;\; 7.27 \;\; 7.13)\,in$$

Therefore, $d_{p.bot}$ and $d_{s.bot}$, the depths from the top of the composite section to the centroid of the prestressing steel and mild steel, respectively, that are on the flexural tension side of the beam, are calculated as:

$$d_{p.bot} = h_c - cg_{ps.bot}$$

$$d_{p.bot_2} = 45.5in - 3.75in$$

$$d_{p.bot_2} = 41.75\,in$$

$$d_{p.bot}^{T} = (41.75 \;\; 41.75 \;\; 41.75 \;\; 41.75 \;\; 41.75 \;\; 41.75 \;\; 39.69 \;\; 39.71 \;\; 39.76 \;\; 39.83 \;\; 38.23 \;\; 38.37)\,in$$

$$d_{s.bot} = h_c - cg_{s.bot}$$

$$d_{s.bot_2} = 45.5in - 4.4in$$

$$d_{s.bot_2} = 41.1\,in$$

$$d_{s.bot}^{T} = (41.1 \;\; 41.1 \;\; 41.1 \;\; 41.1 \;\; 41.1 \;\; 41.1 \;\; 41.1 \;\; 41.1 \;\; 41.1 \;\; 41.1 \;\; 41.1 \;\; 41.1)\,in$$

In order to calculate the area of strand in the flexural tension side of the beam, the number of strands is determined as:

$$Num_{strand.bot_i} = \begin{cases} Num_{strand} - Num_{harp} - Num_{strand.top} & \text{if } cg_{harp_i} - 2in \geq \frac{1}{2}h_c \\ Num_{strand} - Num_{harp} - Num_{strand.top} + 2 & \text{if } cg_{harp_i} - 2in < \frac{1}{2}h_c \wedge cg_{harp_i} \geq \frac{1}{2}h_c \\ Num_{strand} - Num_{harp} - Num_{strand.top} + 4 & \text{if } cg_{harp_i} < \frac{1}{2}h_c \wedge cg_{harp_i} + 2in \geq \frac{1}{2}h_c \\ Num_{strand} - Num_{strand.top} & \text{if } cg_{harp_i} + 2in < \frac{1}{2}h_c \end{cases}$$

$$Num_{strand.bot_2} = Num_{strand} - Num_{harp} - Num_{strand.top} \quad \text{if } cg_{harp_2} - 2in \geq \frac{1}{2}h_c$$

$$Num_{strand.bot_2} = 24 - 6 - 2 \quad \text{if } 27.64in \geq \frac{1}{2}45.5in$$

$$Num_{strand.bot_2} = 16 \quad \text{if } 27.64in \geq 22.75in$$

$$Num_{strand.bot_2} = 16$$

$$Num_{strand.bot}^{T} = (16 \;\; 16 \;\; 16 \;\; 16 \;\; 16 \;\; 16 \;\; 18 \;\; 18 \;\; 18 \;\; 18 \;\; 20 \;\; 20)$$

Consequently, the area of strand in the flexural tension side of the beam is:

$$A_{ps.bot_i} = Num_{strand.bot_i} \cdot A_{strand}$$

$$A_{ps.bot_2} = Num_{strand.bot_2} \cdot A_{strand}$$

$$A_{ps.bot_2} = 16 \cdot 0.153in^2$$

$$A_{ps.bot_2} = 2.45\,in^2$$

$$A_{ps.bot}^{T} = (2.45 \;\; 2.45 \;\; 2.45 \;\; 2.45 \;\; 2.45 \;\; 2.45 \;\; 2.75 \;\; 2.75 \;\; 2.75 \;\; 2.75 \;\; 3.06 \;\; 3.06)\,in^2$$

Using the information above, the effective depth, d_e, is calculated as:

$$d_{e_i} = \frac{A_{ps.bot_i} \cdot f_{ps_i} \cdot d_{p.bot_i} + A_{s.bot_i} \cdot f_y \cdot d_{s.bot_i}}{A_{ps.bot_i} \cdot f_{ps_i} + A_{s.bot_i} \cdot f_y}$$

$$d_{e_2} = \frac{A_{ps.bot_2} \cdot f_{ps_2} \cdot d_{p.bot_2} + A_{s.bot_2} \cdot f_y \cdot d_{s.bot_2}}{A_{ps.bot_2} \cdot f_{ps_2} + A_{s.bot_2} \cdot f_y}$$

$$d_{e_2} = \frac{2.45\text{in}^2 \cdot 64.5\text{ksi} \cdot 41.75\text{in} + 2.04\text{in}^2 \cdot 67.3\text{ksi} \cdot 41.1\text{in}}{2.45\text{in}^2 \cdot 64.5\text{ksi} + 2.04\text{in}^2 \cdot 67.3\text{ksi}}$$

$$d_{e_2} = 41.45\,\text{in}$$

$$d_e^T = (41.34 \quad 41.45 \quad 41.51 \quad 41.55 \quad 41.58 \quad 41.59 \quad 40 \quad 40.02 \quad 40.05 \quad 40.1 \quad 38.77 \quad 38.87)\,\text{in}$$

Ensure that the mild steel in the flexural tension side yields:

$$\varepsilon_{s.yield} = \frac{f_y}{E_s}$$

$$\varepsilon_{s.yield} = \frac{67.3\text{ksi}}{29000\text{ksi}}$$

$$\varepsilon_{s.yield} = 0.002$$

$$\varepsilon_{s_i} = \frac{0.003}{c_i} \cdot \left(d_{e_i} - c_i\right)$$

$$\varepsilon_{s_2} = \frac{0.003}{c_2} \cdot \left(d_{e_2} - c_2\right)$$

$$\varepsilon_{s_2} = \frac{0.003}{3.48\text{in}} \cdot (41.45\text{in} - 3.48\text{in})$$

$$\varepsilon_{s_2} = 0.033$$

$$\varepsilon_s^T = (0.03 \quad 0.03 \quad 0.03 \quad 0.03 \quad 0.03 \quad 0.03 \quad 0.03 \quad 0.03 \quad 0.03 \quad 0.03 \quad 0.03 \quad 0.03)$$

Since the strain in the steel is greater than the yield strain, all assumptions used in calculating the depth of the compression block, *c*, are validated.

C.2.1.5.1.1.4 Find the effective shear depth, d_v

$$d_{v_i} = \max\left(d_{e_i} - \frac{a_i}{2}, 0.9\,d_{e_i}, 0.72h_c\right)$$

$$d_{v_2} = \max\left(d_{e_2} - \frac{a_2}{2}, 0.9\,d_{e_2}, 0.72h_c\right)$$

$$d_{v_2} = \max\left(41.45\text{in} - \frac{2.64\text{in}}{2}, 0.9 \cdot 41.45\text{in}, 0.72 \cdot 45.5\text{in}\right)$$

$$d_{v_2} = \max(40.13\text{in}, 37.31\text{in}, 32.76\text{in})$$

$$d_{v_2} = 40.13\,\text{in}$$

$$d_v^T = (40.02 \quad 40.13 \quad 40.19 \quad 40.23 \quad 40.26 \quad 40.27 \quad 38.68 \quad 38.69 \quad 38.73 \quad 38.78 \quad 37.45 \quad 37.54)\,\text{in}$$

C.2.1.5.1.2 Find the Factored Moment, M_{assume}

According to Article 5.8.3.4.2 of the AASHTO LRFD Bridge Specifications, the factored moment used in determining β and θ should not exceed

$$|M_u| \geq |V_u - V_p| d_v \qquad \text{(C - 1)}$$

where V_p is calculated as:

$$V_{p_i} = \begin{cases} \frac{f_{pe} \cdot \left(x_{dist_i} + x_{bearing}\right)}{l_t} \cdot Num_{harp} \cdot A_{strand} \cdot \sin\left(\Psi_{harp}\right) & \text{if } x_{dist_i} + x_{bearing} \le l_t \wedge x_{dist_i} \le HarpDist \\ f_{pe} \cdot Num_{harp} \cdot A_{strand} \cdot \sin\left(\Psi_{harp}\right) & \text{if } x_{dist_i} + x_{bearing} > l_t \wedge x_{dist_i} \le HarpDist \\ 0 & \text{if } x_{dist_i} > L_{span} \cdot HarpDistRatio \end{cases}$$

$$V_{p_2} = \frac{f_{pe} \cdot \left(x_{dist_2} + x_{bearing}\right)}{l_t} \cdot Num_{harp} \cdot A_{strand} \cdot \sin\left(\Psi_{harp}\right) \quad \text{if } x_{dist_2} + x_{bearing} \le l_t \wedge x_{dist_2} \le HarpDist$$

$$V_{p_2} = \frac{164.96ksi \cdot (5.73in + 6in)}{30in} \cdot 6 \cdot 0.153in^2 \cdot \sin(0.1152) \quad \text{if } 5.73in + 6in \le 30in \wedge 5.73in \le 17.5ft$$

$$V_{p_2} = 6.81kip \quad \text{if } 11.73in \le 30in \wedge 5.73in \le 17.5ft$$

$$V_{p_2} = 6.81kip$$

$$V_p^T = (3.48 \quad 6.81 \quad 10.14 \quad 13.46 \quad 16.79 \quad 17.41 \quad 17.41 \quad 17.41 \quad 17.41 \quad 17.41 \quad 17.41 \quad 17.41)\,kip$$

Therefore, the assumed moment in the girder at the time of failure, M_{assume}, is the maximum of $M_{assume1}$ found in Section C.2.1.4.3 and Eq. (C - 1):

$$M_{assume_i} = \max\left(M_{assume1_i}, \left|V_{assume_i} - V_{p_i}\right| \cdot d_{v_i}\right)$$

$$M_{assume_2} = \max\left(M_{assume1_2}, \left|V_{assume_2} - V_{p_2}\right| \cdot d_{v_2}\right)$$

$$M_{assume_2} = \max(139.79ft \cdot kip, \left|292.58kip - 6.81kip\right| \cdot 40.13in)$$

$$M_{assume_2} = \max(139.79ft \cdot kip, 955.66ft \cdot kip)$$

$$M_{assume_2} = 955.59\,ft \cdot kip$$

C.2.1.5.1.3 Find The Average Factored Shear Stress on the Concrete, v_u

C.2.1.5.1.3.1 Check for Minimum Reinforcement Requirements

$$MinReinforcingCheck_i = \begin{cases} \text{"OK"} & \text{if } 0.0316\alpha_v\cdot\sqrt{f_{c'}\cdot(ksi)}\cdot\dfrac{b_v\cdot s_{v.design_i}}{f_{yv}} \le A_{v_i} \\ \text{"NG!!!"} & \text{if } 0.0316\alpha_v\cdot\sqrt{f_{c'}\cdot(ksi)}\cdot\dfrac{b_v\cdot s_{v.design_i}}{f_{yv}} > A_{v_i} \\ \text{"error"} & \text{otherwise} \end{cases}$$

$$MinReinforcingCheck_2 = \text{"OK"} \quad \text{if } 0.0316\alpha_v\cdot\sqrt{f_{c'}\cdot(ksi)}\cdot\frac{b_v\cdot s_{v.design_2}}{f_{yv}} \le A_{v_2}$$

$$MinReinforcingCheck_2 = \text{"OK"} \quad \text{if } 0.0316(1)\cdot\sqrt{8.87ksi}\cdot\frac{6in\cdot 6in}{67.3ksi} \le 0.4in^2$$

$$MinReinforcingCheck_2 = \text{"OK"} \quad \text{if } 0.05in^2 \le 0.4in^2$$

$$MinReinforcingCheck^T = (\text{"OK"} \quad \text{"OK"} \quad \text{"OK"} \quad \text{"OK"} \quad \text{"OK"} \quad \text{"OK"} \quad \text{"OK"} \quad \text{"OK"} \quad \text{"OK"}$$

C.2.1.5.1.3.2 Calculate v_u

$$v_{u_i} = \begin{cases} \dfrac{\dfrac{\left|V_{assume_i} - \phi_v\cdot V_{p_i}\right|}{\phi_v\cdot b_v\cdot d_{v_i}}}{f_{c'}} & \text{if } MinReinforcingCheck_i = \text{"OK"} \\ \dfrac{\min\left(s_{x_i}\cdot\dfrac{1.38in}{a_g + 0.63in}, 80in\right)}{in} & \text{if } MinReinforcingCheck_i = \text{"NG!!!"} \end{cases}$$

$$v_{u_2} = \frac{\frac{\left|V_{assume_2} - \phi_V \cdot V_{p_2}\right|}{\phi_V \cdot b_v \cdot d_{v_2}}}{f_{c'}} \text{ if } MinReinforcingCheck_2 = \text{"OK"}$$

$$v_{u_2} = \frac{\frac{\left|292.58kip - (1.00) \cdot 6.81kip\right|}{(1.00) \cdot 6in \cdot 40.13in}}{8.87ksi} \text{ if } MinReinforcingCheck_2 = \text{"OK"}$$

$$v_{u_2} = 0.134$$

$$v_u^T = (0.25 \quad 0.134 \quad 0.134 \quad 0.099 \quad 0.099 \quad 0.099 \quad 0.099 \quad 0.1 \quad 0.099 \quad 0.099 \quad 0.103 \quad 0.102)$$

C.2.1.5.1.4 Determine the Reduced Area of Steel, $A_{ps.bot.\varepsilon x}$ and $A_{s.bot.\varepsilon x}$

According the Article 5.8.3.4.2, if the full development length has not been reached at a given section, then the area of steel must be reduced proportionately to the ratio of the length of the steel at that section versus the development length.

C.2.1.5.1.4.1 Calculate the Development Length of the Mild Reinforcement

$$l_{db} = \max\left(\frac{1.25A_{long.rebar} \cdot f_y}{\sqrt{f_{c'} \cdot ksi}\,in}, 0.4\frac{d_{long.rebar}}{8} \cdot \frac{f_y}{ksi}in\right)$$

$$l_{db} = \max\left(\frac{1.25 \cdot 0.31in^2 \cdot 67.3ksi}{\sqrt{8.87ksi^2 \cdot in}}, 0.4 \cdot \frac{5}{8} \cdot \frac{67.3ksi}{ksi}in\right)$$

$$l_{db} = \max(8.76in, 16.82in)$$

$$l_{db} = 16.82\,in$$

$$\kappa_1 = \begin{cases} 1.0 & \text{if } IsTopBarEffectApplicable = \text{"No"} \\ 1.4 & \text{if } IsTopBarEffectApplicable = \text{"Yes"} \\ \text{"error"} & \text{otherwise} \end{cases}$$

$$\kappa_1 = 1.0 \text{ if } IsTopBarEffectApplicable = \text{"No"}$$

$$\kappa_1 = 1$$

$$\kappa_2 = \begin{cases} 1.0 \text{ if } IsLongSteelEpoxyCoated = \text{"No"} \\ 1.5 \text{ if } IsLongSteelEpoxyCoated = \text{"Yes"} \wedge \left(LongSteelCover < 3 \frac{d_{long.rebar}}{8} \cdot in \vee LongSteelClearSpacing < 6 \frac{d_{long.rebar}}{8} \cdot in \right) \\ 1.2 \text{ if } IsLongSteelEpoxyCoated = \text{"Yes"} \wedge LongSteelCover \geq 3 \frac{d_{long.rebar}}{8} \cdot in \wedge LongSteelClearSpacing \geq 6. \frac{d_{long.rebar}}{8} \cdot in \end{cases}$$

$\kappa_2 = 1.0$ if $IsLongSteelEpoxyCoated = \text{"No"}$

$\kappa_2 = 1$

$\kappa_{12} = \min(\kappa_1 \cdot \kappa_2, 1.7)$

$\kappa_{12} = \min(1 \cdot 1, 1.7$

$\kappa_{12} = \min(1, 1.7)$

$\kappa_{12} = 1$

$$\kappa_3 = \begin{cases} 1 \text{ if } ConcreteType = \text{"NWC"} \\ \max\left(0.22 \frac{\sqrt{f_c \cdot ksi}}{f_{ct}}, 1.0 \right) \text{ if } ConcreteType = \text{"LWC"} \wedge Value\_f_{ct} = \text{"specified"} \\ 1.3 \text{ if } ConcreteType = \text{"LWC"} \wedge Value\_f_{ct} = \text{"not specified"} \wedge FineAggType = \text{"lightweight"} \\ 1.2 \text{ if } ConcreteType = \text{"LWC"} \wedge Value\_f_{ct} = \text{"not specified"} \wedge FineAggType = \text{"sand"} \\ \text{"error"} \quad \text{otherwise} \end{cases}$$

$\kappa_3 = 1$ if $ConcreteType = \text{"NWC"}$

$\kappa_3 = 1$

$\kappa_{123} = \kappa_{12} \cdot \kappa_3$

$\kappa_{123} = 1 \cdot 1$

$\kappa_{123} = 1$

$l_{d.mild} = l_{db} \cdot \kappa_{123}$

$l_{d.mild} = 16.82in \cdot 1$

$l_{d.mild} = 16.82\,in$

C.2.1.5.1.4.2 Determine the Area Reduction Factors

$$RedFactor_{\varepsilon x.s_i} = \begin{cases} \dfrac{x_{dist_i} + x_{bearing}}{l_{d.mild}} & \text{if } x_{dist_i} + x_{bearing} < l_{d.mild} \\ 1 & \text{if } x_{dist_i} + x_{bearing} \geq l_{d.mild} \end{cases}$$

$$RedFactor_{\varepsilon x.s_2} = \frac{x_{dist_2} + x_{bearing}}{l_{d.mild}} \quad \text{if } x_{dist_2} + x_{bearing} < l_{d.mild}$$

$$RedFactor_{\varepsilon x.s_2} = \frac{5.73in + 6in}{16.82in} \quad \text{if } 5.73in + 6in < 16.82in$$

$$RedFactor_{\varepsilon x.s_2} = 0.697 \quad \text{if } 11.73in < 16.82in$$

$$RedFactor_{\varepsilon x.s_2} = 0.697$$

$$RedFactor_{\varepsilon x.s}^{T} = (0.357 \;\; 0.697 \;\; 1 \;\; 1 \;\; 1 \;\; 1 \;\; 1 \;\; 1 \;\; 1 \;\; 1 \;\; 1)$$

$$RedFactor_{\varepsilon x.ps_i} = \begin{cases} \dfrac{x_{dist_i} + x_{bearing}}{l_{d.ps_i}} & \text{if } x_{dist_i} + x_{bearing} < l_{d.ps_i} \\ 1 & \text{if } x_{dist_i} + x_{bearing} \geq l_{d.ps_i} \end{cases}$$

$$RedFactor_{\varepsilon x.ps_2} = \frac{x_{dist_2} + x_{bearing}}{l_{d.ps_2}} \quad \text{if } x_{dist_2} + x_{bearing} < l_{d.ps_2}$$

$$RedFactor_{\varepsilon x.ps_2} = \frac{5.73in + 6in}{121.7in} \quad \text{if } 5.73in + 6in < 121.7in$$

$$RedFactor_{\varepsilon x.ps_2} = 0.096$$

$$RedFactor_{\varepsilon x.ps}^{T} = (0.049 \;\; 0.096 \;\; 0.144 \;\; 0.191 \;\; 0.238 \;\; 0.285 \;\; 0.332 \;\; 0.349 \;\; 0.379 \;\; 0.425 \;\; 0.472 \;\; 0.519)$$

C.2.1.5.1.4.3 Calculate the Reduced Area of Steel, $A_{s.bot.\varepsilon x}$ and $A_{ps.bot.\varepsilon x}$

$$A_{s.bot.\varepsilon x_i} = A_{s.bot_i} \cdot RedFactor_{\varepsilon x.s_i}$$

$$A_{s.bot.\varepsilon x_2} = A_{s.bot_2} \cdot RedFactor_{\varepsilon x.s_2}$$

$$A_{s.bot.\varepsilon x_2} = 2.04\text{in}^2 \cdot 0.697$$

$$A_{s.bot.\varepsilon x_2} = 1.42\,\text{in}^2$$

$$A_{s.bot.\varepsilon x}^{T} = (0.73 \;\; 1.42 \;\; 2.04 \;\; 2.04 \;\; 2.04 \;\; 2.04 \;\; 2.04 \;\; 2.04 \;\; 2.04 \;\; 2.04 \;\; 2.04 \;\; 2.04)\,\text{in}^2$$

$$A_{ps.bot.\varepsilon x_i} = \text{Num}_{strand.bot_i} \cdot A_{strand} \cdot \text{RedFactor}_{\varepsilon x.ps_i}$$

$$A_{ps.bot.\varepsilon x_2} = \text{Num}_{strand.bot_2} \cdot A_{strand} \cdot \text{RedFactor}_{\varepsilon x.ps_2}$$

$$A_{ps.bot.\varepsilon x_2} = 16 \cdot 0.153\text{in}^2 \cdot 0.096$$

$$A_{ps.bot.\varepsilon x_2} = 0.24\,\text{in}^2$$

$$A_{ps.bot.\varepsilon x}^{T} = (0.12 \;\; 0.24 \;\; 0.35 \;\; 0.47 \;\; 0.58 \;\; 0.7 \;\; 0.91 \;\; 0.96 \;\; 1.04 \;\; 1.17 \;\; 1.45 \;\; 1.59)\,\text{in}^2$$

C.2.1.5.1.5 Determine β and θ

Even within each iteration for calculating the shear strength of a girder, the process for finding θ itself can be iterative. The reason is because θ, the predicted crack angle relative to the horizontal axis, depends on the longitudinal strain at mid-depth of the beam, ε_x, which in turn, depends on θ, according to Article B5.2. If following the General Procedures in Article 5.8.3.4.2, then this process is not as iterative because the cracking angle was removed from the equation for longitudinal strain as a conservative simplification. If using Appendix B5, one must assume an initial value for the cracking angle and then repeat the calculation until a value for θ converges. In the case of this example, which again, follows the tabularized method in Appendix B5 for finding β and θ, the assumed values for θ (in radians) at specific sections along the length of the shear span are:

$$\theta_{assume} = (0.6231 \;\; 0.6476 \;\; 0.6476 \;\; 0.6402 \;\; 0.6402 \;\; 0.6402 \;\; 0.6382 \;\; 0.6357 \;\; 0.636 \;\; 0.6369 \;\; 0.6198 \;\; 0.62)^{T}$$

Having assumed θ, and knowing all of the other necessary parameters, one can calculate ε_x as:

$$\varepsilon_{x_i} = \left| \begin{array}{l} \varepsilon_{x1_i} \leftarrow \dfrac{\dfrac{\left|M_{assume_i}\right|}{d_{v_i}} + 0.5 \cdot N_u + 0.5 \cdot \left|V_{assume_i} - V_{p_i}\right| \cot\left(\theta_{assume_i}\right) - A_{ps.bot.\varepsilon x_i} \cdot f_{po}}{2 \cdot \left(E_s \cdot A_{s.bot.\varepsilon x_i} + E_p \cdot A_{ps.bot.\varepsilon x_i}\right)} \\ \varepsilon_{x2_i} \leftarrow \dfrac{\dfrac{\left|M_{assume_i}\right|}{d_{v_i}} + 0.5 \cdot N_u + 0.5 \cdot \left|V_{assume_i} - V_{p_i}\right| \cot\left(\theta_{assume_i}\right) - A_{ps.bot.\varepsilon x_i} \cdot f_{po}}{E_s \cdot A_{s.bot.\varepsilon x_i} + E_p \cdot A_{ps.bot.\varepsilon x_i}} \\ \varepsilon_{x3_i} \leftarrow \dfrac{\dfrac{\left|M_{assume_i}\right|}{d_{v_i}} + 0.5 \cdot N_u + 0.5 \cdot \left|V_{assume_i} - V_{p_i}\right| \cot\left(\theta_{assume_i}\right) - A_{ps.bot.\varepsilon x_i} \cdot f_{po}}{2 \cdot \left(E_{beam} \cdot A_{ct} + E_s \cdot A_{s.bot.\varepsilon x_i} + E_p \cdot A_{ps.bot.\varepsilon x_i}\right)} \\ \varepsilon_{x_i} \leftarrow \left| \begin{array}{ll} \varepsilon_{x1_i} & \text{if } MinReinforcingCheck_i = \text{"OK"} \wedge \varepsilon_{x1_i} \geq 0 \\ \varepsilon_{x2_i} & \text{if } MinReinforcingCheck_i = \text{"NG!!!"} \wedge \varepsilon_{x2_i} \geq 0 \\ \varepsilon_{x3_i} & \text{if } \varepsilon_{x1_i} < 0 \vee \varepsilon_{x2_i} < 0 \end{array} \right. \end{array} \right.$$

$$\varepsilon_{x_2} = \frac{\dfrac{\left|M_{assume_2}\right|}{d_{v_2}} + 0.5 \cdot N_u + 0.5 \cdot \left|V_{assume_2} - V_{p_2}\right| \cot\left(\theta_{assume_2}\right) - A_{ps.bot.\varepsilon x_2} \cdot f_{po}}{2 \cdot \left(E_s \cdot A_{s.bot.\varepsilon x_2} + E_p \cdot A_{ps.bot.\varepsilon x_2}\right)} \text{ if } Mi$$

$$\varepsilon_{x_2} = \frac{\dfrac{\left|955.59\text{ft}\cdot\text{kip}\right|}{40.13\text{in}} + 0 + 0.5 \cdot \left|292.58\text{kip} - 6.81\text{kip}\right| \cdot \cot(0.6476) - 0.24\text{in}^2 \cdot 189\text{ksi}}{2 \cdot \left(29000\text{ksi} \cdot 1.42\text{in}^2 + 28500\text{ksi} \cdot 0.24\text{in}^2\right)} \text{ if MinReinforc}$$

$$\varepsilon_{x_2} = 0.00448 \text{ if } MinReinforcingCheck_2 = \text{"OK"} \wedge 0.00448 \geq 0$$

$$\varepsilon_{x_2} = 0.00448$$

$$\varepsilon_x^T = (0.01792 \;\; 0.00448 \;\; 0.00296 \;\; 0.00183 \;\; 0.0016 \;\; 0.0014 \;\; 0.00099 \;\; 0.00105 \;\; 0.00098 \;\; 0.00098 \;\; 0.00089 \;\; 0.00089$$

Using the results for ε_x and for v_u, found in Section C.2.1.5.1.3, one can go to the tables in Appendix B5 of the AASHTO LRFD Bridge Specifications to obtain β and θ. Note that Article B5.2 states that if ε_x is greater than zero, then the initial value for ε_x should not be greater than

0.001 if at least the minimum transverse reinforcement is used or 0.002 if the beam has less than the minimum transverse reinforcement. Hence, in this example, most of the values for ε_x along the length of the shear span were taken as 0.001. As discussed in Section C.1, a separate computer program was developed to facilitate linear interpolation of these values using the ranges given in the aforementioned tables. That program is not discussed here, but is a relatively basic routine. Using the values for ε_x and v_u, the resulting values for β and θ are:

$$\theta^T = (0.6231 \quad 0.6476 \quad 0.6476 \quad 0.6402 \quad 0.6402 \quad 0.6402 \quad 0.6382 \quad 0.6357 \quad 0.6359 \quad 0.637 \quad 0.6198 \quad 0.62)$$

$$\beta^T = (1.5 \quad 2.11 \quad 2.11 \quad 2.18 \quad 2.18 \quad 2.18 \quad 2.19 \quad 2.2 \quad 2.19 \quad 2.19 \quad 2.24 \quad 2.24)$$

Note that the results for θ are quite similar to the assumed cracking angle, θ_{assume}. In terms of degrees, θ is:

$$\theta^T = (35.7 \quad 37.107 \quad 37.107 \quad 36.683 \quad 36.683 \quad 36.683 \quad 36.566 \quad 36.694 \quad 36.438 \quad 36.495 \quad 35.512 \quad 35.523)$$

C.2.1.5.2 Calculate the Concrete Contribution to the Shear Resistance, V_c

$$V_{c_i} = 0.0316 \cdot \beta_i \cdot \alpha_v \sqrt{f_{c'} \cdot \text{ksi}} \cdot b_v \cdot d_{v_i}$$

$$V_{c_2} = 0.0316 \cdot \beta_2 \cdot \alpha_v \sqrt{f_{c'} \cdot \text{ksi}} \cdot b_v \cdot d_{v_2}$$

$$V_{c_2} = 0.0316 \cdot 2.11 \cdot (1) \cdot \sqrt{8.87\text{ksi}^2} \cdot 6\text{in} \cdot 40.13\text{in}$$

$$V_{c_2} = 47.85\,\text{kip}$$

$$V_c^T = (33.89 \quad 47.85 \quad 47.92 \quad 49.57 \quad 49.61 \quad 49.62 \quad 47.78 \quad 47.97 \quad 47.97 \quad 47.98 \quad 47.31 \quad 47.42)\,\text{kip}$$

C.2.1.5.3 Calculate the Steel Contribution to the Shear Resistance, V_s

$$V_{s_i} = \frac{A_{v_i} \cdot f_{yv} \cdot d_{v_i} \cdot \left(\cot\left(\theta_i\right) + \cot(\alpha)\right) \cdot \sin(\alpha)}{s_{v.design_i}}$$

$$V_{s_2} \leftarrow \frac{A_{v_2} \cdot f_{yv} \cdot d_{v_2} \cdot \left(\cot\left(\theta_2\right) + \cot(\alpha)\right) \cdot \sin(\alpha)}{s_{v.design_2}}$$

$$V_{s_2} = \frac{0.4\text{in}^2 \cdot 67.3\text{ksi} \cdot 40.13 \cdot \left(\cot(0.6476) + \cot\left(\frac{\pi}{2}\right)\right) \sin\left(\frac{\pi}{2}\right)}{6\text{in}}$$

$$V_{s_2} = 237.99\,\text{kip}$$

$$V_s^T = (599.7 \quad 238 \quad 238.4 \quad 161.5 \quad 161.7 \quad 161.7 \quad 156 \quad 156.9 \quad 156.9 \quad 156.8 \quad 157 \quad 157.3)\,\text{kip}$$

C.2.1.5.4 Calculate the Nominal Shear Resistance

$$V_{n1} = V_c + V_s + V_p$$

$$V_{n1_2} = V_{c_2} + V_{s_2} + V_{p_2}$$

$$V_{n1_2} = 47.85\text{kip} + 237.99\text{kip} + 6.81\text{kip}$$

$$V_{n1_2} = 292.6\,\text{kip}$$

$$V_{n1}^T = (637.1 \quad 292.6 \quad 296.4 \quad 224.6 \quad 228 \quad 228.7 \quad 221.2 \quad 222.3 \quad 222.3 \quad 222.2 \quad 221.7 \quad 222.1)\,\text{kip}$$

$$V_{n2} = 0.25 \cdot f_{c'} \cdot b_v \cdot d_v + V_p$$

$$V_{n2_2} = 0.25 \cdot f_{c'} \cdot b_v \cdot d_{v_2} + V_{p_2}$$

$$V_{n2_2} = 0.25 \cdot 8.87\text{ksi} \cdot 6\text{in} \cdot 40.13\text{in} + 6.81\text{kip}$$

$$V_{n2_2} = 540.4\,\text{kip}$$

$$V_{n2}^T = (535.6 \quad 540.4 \quad 544.6 \quad 548.4 \quad 552.1 \quad 552.9 \quad 531.7 \quad 532.2 \quad 532.4 \quad 533 \quad 515.4 \quad 516.7)\,\text{kip}$$

$$V_{n_i} = \min\left(V_{n1_i}, V_{n2_i}\right)$$

$$V_{n_2} = \min\left(V_{n1_2}, V_{n2_2}\right)$$

$$V_{n_2} = \min(292.64\text{kip}, 540.39\text{kip})$$

$$V_{n_2} = 292.6\,\text{kip}$$

$$V_n^T = (535.6 \;\; 292.6 \;\; 296.4 \;\; 224.6 \;\; 228 \;\; 228.7 \;\; 221.2 \;\; 222.3 \;\; 222.3 \;\; 222.2 \;\; 221.7 \;\; 222.1)\,\text{kip}$$

C.2.1.6 Reiterate with New Value for P_{assume}

In order to refine the calculations for the nominal shear strength, the engineer might need to assume a different value for the externally applied load to the beam, P_{assume}, based on a revised input for the shear in the beam, V_{assume}. The new V_{assume} can be taken as the midpoint between the original V_{assume} and V_n found in Section C.2.1.5.4 above. In the case of this example,

$$V_{assume.new_i} = \frac{1}{2}\left(V_{n_i} + V_{assume_i}\right)$$

$$V_{assume.new_2} = \frac{1}{2}\left(V_{n_2} + V_{assume_2}\right)$$

$$V_{assume.new_2} = \frac{1}{2}(292.6\text{kip} + 292.58\text{kip})$$

$$V_{assume.new_2} = 292.6\,\text{kip}$$

$$V_{assume.new}^T = (535.6 \;\; 292.6 \;\; 296.4 \;\; 224.5 \;\; 228 \;\; 228.7 \;\; 221.1 \;\; 221.3 \;\; 222.3 \;\; 222.1 \;\; 221.7 \;\; 222.1)\,\text{kip}$$

Therefor, the new assumed load from each of the two actuators located at the distances indicated by the parameters *ShearSpan* and *LoadSpacing* that would result in a shear failure

$$P_{assume.new_i} = \frac{\left(V_{assume.new_i} - V_{DC1_i}\right)\cdot L_{span}}{2\left(L_{span} - ShearSpan\right) - LoadSpacing} \quad \text{if } x_{dist_i} \le ShearSpan$$

$$P_{assume.new_2} = \frac{\left(V_{assume.new_2} - V_{DC1_2}\right)\cdot L_{span}}{2\left(L_{span} - ShearSpan\right) - LoadSpacing} \quad \text{if } x_{dist_2} \le ShearSpan$$

$$P_{assume.new_2} = \frac{(292.6kip - 18.22kip)\cdot 40ft}{2\cdot(40ft - 57.34in) - 14.52ft} \quad \text{if } 5.73in \le 57.34in$$

$$P_{assume.new_2} = 196.2\,kip$$

$$P_{assume.new}^{T} = (369.7 \;\; 196.2 \;\; 199.3 \;\; 148.2 \;\; 151 \;\; 151.8 \;\; 146.7 \;\; 147.8 \;\; 147.8 \;\; 148.1 \;\; 148 \;\; 148.7)\,kip$$

However, note that $P_{assume.new}$ is practically the same as P_{assume} given in Section C.2.1.1. In this case, the calculations for the shear strength have converged, resulting in the shear strengths at the various sections along the shear span, indicated by V_n in Section C.2.1.5.4. The lowest value in V_n is taken as the beam's shear strength, provided that the distance from the support to the corresponding section is not less than the critical section. The critical section, $x_{critical}$, depends on the effective shear depth and the theoretical cracking angle, which in turn, are indirectly dependent on the critical section. Hence, finding $x_{critical}$ is also iterative in nature, and this iteration has been incorporated into the program indicated in Figure C-1. Using $x_{critical.assume}$ = 38.69 in., which is the eighth element in the parameter x_{dist} given in Section C.2.1.1, the shear depth at the critical section, $d_{v.critical}$ is the eighth element in d_v calculated in Section C.2.1.5.1.1.4. Likewise, the corresponding cracking angle at the critical section is the eighth element of θ, given in radians in Section C.2.1.5.1.5 as 0.6357. Thus, $x_{critical}$ can be calculated as:

$$x_{critical} = \max\left(d_{v.critical}, \frac{1}{2} \cdot d_{v.critical} \cdot \cot(\theta_{critical})\right)$$

$$x_{critical} = \max\left(38.69\text{in}, \frac{1}{2} 38.69\text{in} \cdot \cot(0.6357)\right)$$

$$x_{critical} = \max(38.69\text{in}, 26.22\text{in})$$

$$x_{critical} = 38.69\,\text{in}$$

Again, note that the calculated value for $x_{critical}$ is the same as $x_{critical.assume}$, so no further iterations are required. So, for this example, the smallest shear strength given in V_n is 221.1 kip at x_{dist} = 34.40 in. However, since the distance to this section is less than the critical section, the nominal shear strength for the beam should be taken as 222.3 kip, which is rounded to 222 kip.

C.2.2 Example Following the General Procedure

C.2.2.1 Inputs

The same scenario provided in Section C.2.1 is used for example calculations following the General Procedure in Article 5.8.3.4.2 in the 2010 AASHTO LRFD Bridge Design Specifications. Therefore, the same inputs listed in Section C.2.1.1 apply here, with the exception that the values in P_{assume} are different:

$$P_{assume} = (369.7 \quad 189 \quad 192 \quad 138.4 \quad 141.2 \quad 142 \quad 136.8 \quad 137.1 \quad 137.3 \quad 138 \quad 139.2 \quad 140.2)\,\text{kip}$$

C.2.2.2 Basic Geometry Calculations

Again, the results for the *Appendix B5* example from Section C.2.1.2 can be used here for the *General Procedure*.

C.2.2.3 Basic Material Calculations

Likewise, the calculations that appear in Section C.2.1.3 apply here.

C.2.2.4 Load Effects

Because this example uses the same scenario provided in the *Appendix B5* example, whereby the geometry and dead loads are the same, the same calculations provided in Section C.2.1.4 apply in this case. The exceptions are those calculations that are directly affected by the assumed live load given in Section C.2.2.1. See Sections C.2.2.4.1 and C.2.2.4.2 below.

C.2.2.4.1 Live Loads

For a simply-supported beam subjected to two point loads, the shear at any point along the beam within the shear span, V_{LL}, can be calculated as

$$V_{LL_i} = \frac{P_{assume_i}}{L_{span}} \cdot \left[2\left(L_{span} - ShearSpan\right) - LoadSpacing\right]$$

$$V_{LL_2} = \frac{189.01\,kip}{40\,ft} \cdot [2 \cdot (40\,ft - 57.34\,in) - 14.52\,ft]$$

$$V_{LL_2} = 264.27\,kip$$

$$V_{LL}^{T} = (516.88 \;\; 264.27 \;\; 268.51 \;\; 193.47 \;\; 197.41 \;\; 198.51 \;\; 191.22 \;\; 191.74 \;\; 191.99 \;\; 193.01 \;\; 194.65 \;\; 196.02)\,kip$$

The moment at the same locations, M_{LL}, can be calculated as

$$M_{LL_i} = \frac{P_{assume_i}}{L_{span}} \cdot \left[2\left(L_{span} - ShearSpan\right) - LoadSpacing\right] \cdot x_{dist_i}$$

$$M_{LL_2} = \frac{189.022\,kip}{40\,ft} \cdot [2(40\,ft - 57.3\,in) - 14.52\,ft]\,5.734\,in$$

$$M_{LL_2} = 126.27\,ft \cdot kip$$

$$M_{LL}^{T} = (0 \;\; 126.27 \;\; 256.6 \;\; 277.33 \;\; 377.31 \;\; 474.25 \;\; 548.2 \;\; 618.55 \;\; 642.15 \;\; 737.79 \;\; 837.05 \;\; 936.59)\,ft \cdot kip$$

C.2.2.4.2 Total Load Effects

Given the assumed live loads, the total assumed shear and moment in the girder, V_{assume} and $M_{assume1}$ are the sum of the dead and live loads given in Sections C.2.1.4.2 and C.2.2.4.1, respectively. Therefore,

$V_{assume} = V_{LL} + V_{DC1}$

$V_{assume_2} = 264.27\text{kip} + 18.22\text{kip}$

$V_{assume_2} = 282.49\,\text{kip}$

$V_{assume}^{T} = (535.55 \;\; 282.49 \;\; 286.29 \;\; 210.81 \;\; 214.3 \;\; 214.95 \;\; 207.21 \;\; 207.4 \;\; 207.54 \;\; 208.11 \;\; 209.3 \;\; 210.23)\,\text{kip}$

$M_{assume1} = M_{LL} + M_{DC1}$

$M_{assume1_2} = 126.27\text{ft}\cdot\text{kip} + 8.7\text{ft}\cdot\text{kip}$

$M_{assume1_2} = 134.97\,\text{ft}\cdot\text{kip}$

$M_{assume1}^{T} = (-0.12 \;\; 134.97 \;\; 273.89 \;\; 303.02 \;\; 411.17 \;\; 516.07 \;\; 597.77 \;\; 673.8 \;\; 699.25 \;\; 802.21 \;\; 908.58 \;\; 1015.02)\,\text{ft}\cdot\text{kip}$

C.2.2.5 Calculate the Shear Resistance

C.2.2.5.1 Determine β and θ

C.2.2.5.1.1 Calculate the Effective Shear Depth of the Beam, d_v

With the girder geometry being the same in the *General Procedure* as they are under *Appendix B5*, the subset of calculations leading to the determination of β and θ remain the same up to the point of finding the factored moment. Thus, the results given in Section C.2.1.5.1.1 apply to this example.

C.2.2.5.1.2 Find the Factored Moment, M_{assume}

While the vertical component of the prestressing force remains the same regardless of which shear design method is used, the factored assumed moment will change due to the fact that the assumed live load is different. Therefore, M_{assume} is calculated as

$$M_{assume_i} = \max\left(M_{assume1_i}, \left|V_{assume_i} - V_{p_i}\right| \cdot d_{v_i}\right)$$

$$M_{assume_2} = \max\left(M_{assume1_2}, \left|V_{assume_2} - V_{p_2}\right| \cdot d_{v_2}\right)$$

$$M_{assume_2} = \max(134.97\,ft\cdot kip, |282.49\,kip - 6.81\,kip| \cdot 40.13\,in)$$

$$M_{assume_2} = \max(134.97\,ft\cdot kip, 921.86\,ft\cdot kip)$$

$$M_{assume_2} = 921.86\,ft\cdot kip$$

$$M_{assume}^{T} = (1774.43 \;\; 921.86 \;\; 924.85 \;\; 661.59 \;\; 662.62 \;\; 662.85 \;\; 611.73 \;\; 673.80 \;\; 699.25 \;\; 802.21 \;\; 908.58 \;\; 1015.02)\,ft\cdot kip$$

where V_p comes from Section C.2.1.5.1.2.

C.2.2.5.1.3 Determine the Reduced Area of Steel, $A_{ps.bot.\varepsilon s}$ and $A_{s.bot.\varepsilon s}$

Both *Appendix B5* and the *General Procedure* reduce the area of the longitudinal steel used for calculating the longitudinal strain in the concrete. The one small difference is that $A_{s.bot.\varepsilon x}$ and $A_{ps.bot.\varepsilon x}$ for *Appendix B5* are denoted as $A_{s.bot.\varepsilon s}$ and $A_{ps.bot.\varepsilon s}$ respectively, for the *General Procedure*, but retain the same values as before in Section C.2.1.5.1.4.3.

C.2.2.5.1.4 Calculate ε_s

Assuming that the strain is positive, the longitudinal strain in the concrete at the level of the tension reinforcement is calculated as

$$\varepsilon_{s1_i} = \min\left(\frac{\frac{\left|M_{assume_i}\right|}{d_{v_i}} + 0.5N_u + \left|V_{assume_i} - V_{p_i}\right| - A_{ps.bot.\varepsilon s_i} \cdot f_{po}}{E_s \cdot A_{s.bot.\varepsilon s_i} + E_p \cdot A_{ps.bot.\varepsilon s_i}}, 0.006\right)$$

$$\varepsilon_{s1_2} = \min\left[\frac{\frac{\left|921.86\text{kip}\cdot\text{ft}\right|}{40.13\text{in}} + 0.5\cdot(0) + \left|282.49\text{kip} - 6.81\text{kip}\right| - 0.236\text{in}^2\cdot 189\text{ksi}}{29000\text{ksi}\cdot 0.236\text{in}^2 + 28500\text{ksi}\cdot 1.42\text{in}^2}, 0.006\right]$$

$$\varepsilon_{s1_2} = \min(0.0107, 0.006)$$

$$\varepsilon_{s1_2} = 0.006$$

$$\varepsilon_{s1}^{T} = (0.006 \;\; 0.006 \;\; 0.006 \;\; 0.00423 \;\; 0.00376 \;\; 0.00333 \;\; 0.00243 \;\; 0.00236 \;\; 0.00236 \;\; 0.00235 \;\; 0.00209 \;\; 0.00208)$$

However, according to Article 5.8.3.4.2 of the 2010 AASHTO LRFD Bridge Design Specifications, for locations along the length of the beam that are closer than d_v to the support, then ε_s can be taken as the value of ε_s at d_v. Therefore, ε_s is taken as

$$\varepsilon_{s_i} = \varepsilon_{s\left(vect\_elemnt_{x.critical}\right)} \quad \text{if} \quad x_{dist_i} \le d_{v_i}$$

$$\varepsilon_{s_2} = \varepsilon_{s_8} \quad \text{if} \quad x_{dist_2} \le d_{v_2}$$

$$\varepsilon_{s_2} = 0.00236 \quad \text{if} \quad 5.73\text{in} \le 40.13\text{in}$$

$$\varepsilon_{s_2} = 0.00236$$

$$\varepsilon_{s}^{T} = (0.00236 \;\; 0.00236 \;\; 0.00236 \;\; 0.00236 \;\; 0.00236 \;\; 0.00236 \;\; 0.00236 \;\; 0.00236 \;\; 0.00236 \;\; 0.00235 \;\; 0.00209 \;\; 0.00208)$$

C.2.2.5.1.5 Determine β and θ

For beams with at least the minimum amount of required shear reinforcement, β is calculated as

$$\beta_i = \frac{4.8}{1 + 750\,\varepsilon_{s_i}}$$

$$\beta_2 = \frac{4.8}{1 + 750\,\varepsilon_{s_2}}$$

$$\beta_2 = \frac{4.8}{1 + 750 \cdot 0.00236}$$

$$\beta_2 = 1.731$$

$$\beta^T = (1.731 \quad 1.731 \quad 1.731 \quad 1.731 \quad 1.731 \quad 1.731 \quad 1.731 \quad 1.731 \quad 1.733 \quad 1.738 \quad 1.869 \quad 1.877)$$

Regardless of the amount of vertical stirrups, θ is calculated as (in degrees):

$$\theta_i = 29 + 3500 \cdot \varepsilon_{s_i}$$

$$\theta_2 = 29 + 3500\,\varepsilon_{s_2}$$

$$\theta_2 = 29 + 3500 \cdot (0.00236)$$

$$\theta_2 = 37.272$$

$$\theta^T = (37.272 \quad 37.272 \quad 37.272 \quad 37.272 \quad 37.272 \quad 37.272 \quad 37.272 \quad 37.272 \quad 37.262 \quad 37.225 \quad 36.318 \quad 36.268)$$

Converted to radians, θ is:

$$\theta^T = (0.6505 \quad 0.6505 \quad 0.6505 \quad 0.6505 \quad 0.6505 \quad 0.6505 \quad 0.6505 \quad 0.6505 \quad 0.6503 \quad 0.6497 \quad 0.6339 \quad 0.6330)$$

C.2.2.5.2 Calculate the Concrete Contribution to Shear Resistance, V_c

$$V_{c_i} = 0.0316 \cdot \beta_i \cdot \alpha_v \sqrt{f_c' \cdot \text{ksi}} \cdot b_v \cdot d_{v_i}$$

$$V_{c_2} = 0.0316 \cdot \beta_2 \cdot \alpha_v \cdot \sqrt{f_c' \cdot \text{ksi}} b_v \cdot d_{v_2}$$

$$V_{c_2} = 0.0316(1.731) \cdot (1.00) \cdot \sqrt{8.87\text{ksi}^2} \cdot 6\text{in} \cdot 40.13\text{in}$$

$$V_{c_2} = 39.22\,\text{kip}$$

$$V_c^T = (39.11 \quad 39.22 \quad 39.28 \quad 39.32 \quad 39.35 \quad 39.35 \quad 37.8 \quad 37.84 \quad 37.88 \quad 38.04 \quad 39.51 \quad 39.78)\,\text{kip}$$

C.2.2.5.3 Calculate the Steel Contribution to Shear Resistance, V_s

$$V_{s_i} = \frac{A_{v_i} \cdot f_{yv} \cdot d_{v_i} \cdot \left(\cot\left(\theta_i\right) + \cot(\alpha)\right) \cdot \sin(\alpha)}{s_{v.design_i}}$$

$$V_{s_2} = \frac{A_{v_2} \cdot f_{yv} \cdot d_{v_2} \cdot \left(\cot\left(\theta_2\right) + \cot(\alpha)\right) \cdot \sin(\alpha)}{s_{v.design_2}}$$

$$V_{s_2} = \frac{0.40\text{in}^2 \cdot 67.3\text{ksi} \cdot 40.13\text{in} \cdot (\cot(0.6505) + \cot(1.5708)) \cdot \sin(1.5708)}{6\text{in}}$$

$$V_{s_2} = 236.57\,\text{kip}$$

$$V_s^T = (566.25 \quad 236.57 \quad 236.94 \quad 158.12 \quad 158.23 \quad 158.26 \quad 152.01 \quad 152.16 \quad 152.26 \quad 152.67 \quad 152.39 \quad 153.05)\,\text{kip}$$

Note that θ has been converted into radians.

C.2.2.5.4 Calculate the Nominal Shear Resistance

$$V_{n1_i} = V_{c_i} + V_{s_i} + V_{p_i}$$

$$V_{n1_2} = V_{c_2} + V_{s_2} + V_{p_2}$$

$$V_{n1_2} = 39.22\text{kip} + 236.57\text{kip} + 6.81\text{kip}$$

$$V_{n1_2} = 282.59\,\text{kip}$$

$$V_{n1}^T = (608.85 \quad 282.59 \quad 286.35 \quad 210.90 \quad 214.37 \quad 215.03 \quad 207.22 \quad 207.40 \quad 207.55 \quad 208.12 \quad 209.31 \quad 210.24)\,\text{kip}$$

$$V_{n2_i} = 0.25 \cdot f_{c'} \cdot b_v \cdot d_{v_i} + V_{p_i}$$

$$V_{n2_2} = 0.25 \cdot f_{c'} \cdot b_v \cdot d_{v_2} + V_{p_2}$$

$$V_{n2_2} = 0.25 \cdot 8.87\text{ksi} \cdot 6\text{in} \cdot 40.13\text{in} + 6.81\text{kip}$$

$$V_{n2_2} = 540.39\,\text{kip}$$

$$V_{n2}^T = (535.64 \quad 540.39 \quad 544.55 \quad 548.42 \quad 552.14 \quad 552.86 \quad 531.71 \quad 532.20 \quad 532.37 \quad 533.04 \quad 515.39 \quad 516.65)\,\text{kip}$$

$$V_{n_i} = \min\left(V_{n1_i}, V_{n2_i}\right)$$

$$V_{n_2} = \min\left(V_{n1_2}, V_{n2_2}\right)$$

$$V_{n_2} = \min(282.59\,\text{kip}, 540.39\,\text{kip})$$

$$V_{n_2} = 282.59\,\text{kip}$$

$$V_n^T = (535.6 \;\; 282.6 \;\; 286.4 \;\; 210.9 \;\; 214.4 \;\; 215 \;\; 207.2 \;\; 207.4 \;\; 207.6 \;\; 208.1 \;\; 209.3 \;\; 210.2)\,\text{kip}$$

C.2.2.6 Reiterate with New Value for P_{assume}

In order to refine the calculations for the nominal shear strength, the engineer might need to assume a different value for the externally applied load to the beam, P_{assume}, based on a revised input for the shear in the beam, V_{assume}. The new V_{assume} can be taken as the midpoint between the original V_{assume} and V_n found in Section C.2.2.5.4 above. In the case of this example,

$$V_{assume.new_i} = \frac{1}{2}\left(V_{n_i} + V_{assume_i}\right)$$

$$V_{assume.new_2} = \frac{1}{2}\left(V_{n_2} + V_{assume_2}\right)$$

$$V_{assume.new_2} = \frac{1}{2}(282.59\,\text{kip} + 282.49\,\text{kip})$$

$$V_{assume.new_2} = 282.54\,\text{kip}$$

$$V_{assume.new}^T = (535.6 \;\; 282.5 \;\; 286.3 \;\; 210.9 \;\; 214.3 \;\; 215 \;\; 207.2 \;\; 207.4 \;\; 207.5 \;\; 208.1 \;\; 209.3 \;\; 210.2)\,\text{kip}$$

Therefor, the new assumed load from each of the two actuators located at the distances indicated by the parameters *ShearSpan* and *LoadSpacing* that would result in a shear failure is:

$$P_{assume.new_i} = \frac{\left(V_{assume.new_i} - V_{DC1_i}\right)\cdot L_{span}}{2\left(L_{span} - ShearSpan\right) - LoadSpacing} \quad \text{if } x_{dist_i} \le ShearSpan$$

$$P_{assume.new_2} = \frac{\left(V_{assume.new_2} - V_{DC1_2}\right)\cdot L_{span}}{2\left(L_{span} - ShearSpan\right) - LoadSpacing} \quad \text{if } x_{dist_2} \le ShearSpan$$

$$P_{assume.new_2} = \frac{(282.54\text{kip} - 18.22\text{kip})\cdot 40\text{ft}}{2\cdot(40\text{ft} - 57.34\text{in}) - 14.52\text{ft}} \quad \text{if } 5.73\text{in} \le 57.34\text{in}$$

$$P_{assume.new_2} = 189.0\,\text{kip}$$

$$P_{assume.new}^{T} = (369.7 \;\; 189.0 \;\; 192.1 \;\; 138.4 \;\; 141.2 \;\; 142.0 \;\; 136.8 \;\; 137.1 \;\; 137.3 \;\; 138.0 \;\; 139.2 \;\; 140.2)\,\text{kip}$$

$$P_{assume}^{T} = (369.7 \;\; 189.0 \;\; 192.0 \;\; 138.4 \;\; 141.2 \;\; 142.0 \;\; 136.8 \;\; 137.1 \;\; 137.3 \;\; 138.0 \;\; 139.2 \;\; 140.2)\,\text{kip}$$

However, note that $P_{assume.new}$ is the same as P_{assume} given in Section C.2.2.1. In this case, the calculations for the shear strength have converged, resulting in the shear strengths at the various sections along the shear span, indicated by V_n in Section C.2.2.5.4. The lowest value in V_n is taken as the beam's shear strength, provided that the distance from the support to the corresponding section is not less than the critical section. The critical section, $x_{critical}$, depends on the effective shear depth and the theoretical cracking angle, which in turn, are indirectly dependent on the critical section. Hence, finding $x_{critical}$ is also iterative in nature, and this iteration has been incorporated into the program indicated in Figure C-1. Using $x_{critical.assume}$ = 38.71 in., which is the eighth element in the parameter x_{dist} given in Section C.2.2.1, the shear depth at the critical section, $d_{v.critical}$ is the eighth element in d_v calculated in Section C.2.1.5.1.1.4. Likewise, the corresponding cracking angle at the critical section is the eighth element of θ, given in radians in Section 0 as 0.6505. Thus, $x_{critical}$ can be calculated as:

$$x_{critical} = \max\left(d_{v.critical}, \frac{1}{2}\cdot d_{v.critical}\cdot\cot\left(\theta_{critical}\right)\right)$$

$$x_{critical} = \max\left(38.71\text{in}, \frac{1}{2}38.71\text{in}\cdot\cot(0.6505)\right)$$

$$x_{critical} = \max(38.71\text{in}, 25.43\text{in})$$

$$x_{critical} = 38.71\,\text{in}$$

Again, note that the calculated value for $x_{critical}$ is the same as $x_{critical.assume}$, so no further iterations are required. So, for this example, the smallest shear strength given in V_n is 207.2 kip at x_{dist} =

34.40 in. However, since the distance to this section is less than the critical section, the nominal shear strength for the beam should be taken as 207.4 kip, which is rounded to 207 kip.

C.2.3 Beam Example Following the Simplified Procedure for Prestressed and Nonprestressed Sections

C.2.3.1 Inputs

The same scenario provided in Section C.2.1 is used for example calculations following Article 5.8.3.4.3 in the AASHTO LRFD Bridge Specifications. Therefore, the same inputs listed in Section C.2.1.1 apply here, with the exception that the values in P_{assume} are different:

$$P_{assume1} = (325.48 \quad 229.2 \quad 270.06 \quad 226.13 \quad 238.59 \quad 242.5 \quad 234.72 \quad 236.2 \quad 236.68 \quad 238.51 \quad 231.75 \quad 233.55)\,kip$$

One additional required input is the distance from the bottom of the girder to the intersection of the web and top flange:

$$h_{top.flange} = 30\,in$$

C.2.3.2 Basic Geometry Calculations

Again, the results for the *Appendix B5* example from Section C.2.1.2 can be used here for the *General Procedure*. One additional basic geometry calculation is needed for the section modulus:

$$S_b = \frac{I_{beam}}{y_b}$$

$$S_b = \frac{50979\,in^4}{15.83\,in}$$

$$S_b = 3220.4\,in^3$$

C.2.3.3 Basic Material Calculations

Likewise, the calculations that appear in Section C.2.1.3 apply here.

C.2.3.4 Load Effects

Because this example uses the same scenario provided in the *Appendix B5* example, whereby the geometry and dead loads are the same, the results provided in Section C.2.1.4 apply in this case. The exceptions are those calculations that are directly affected by the assumed live load given in Sections C.2.3.4.1 and below.

C.2.3.4.1 Live Loads

For a simply-supported beam subjected to two point loads, the shear at any point along the beam within the shear span, V_{LL}, can be calculated as

$$V_{LL_i} = \frac{P_{assume_i}}{L_{span}} \cdot \left[2\left(L_{span} - ShearSpan\right) - LoadSpacing\right]$$

$$V_{LL_2} = \frac{229.2kip}{40ft} \cdot [2 \cdot (40ft - 57.34in) - 14.52ft]$$

$$V_{LL.2} = 320.5kip$$

$$V_{LL}^{T} = (455.1 \quad 320.5 \quad 377.6 \quad 316.2 \quad 333.6 \quad 339.1 \quad 328.2 \quad 330.3 \quad 330.9 \quad 333.5 \quad 324 \quad 326.5)\,kip$$

The moment at the same locations, M_{LL}, can be calculated as:

$$M_{LL_i} = \frac{P_{assume_i}}{L_{span}} \cdot \left[2\left(L_{span} - ShearSpan\right) - LoadSpacing\right] \cdot x_{dist_i}$$

$$M_{LL_2} = \frac{229.2kip}{40ft} \cdot [2(40ft - 57.34in) - 14.52ft]\, 5.73in$$

$$M_{LL_2} = 153.ft \cdot kip$$

$$M_{LL}^{T} = (1000000 \quad 153.1 \quad 360.8 \quad 453.2 \quad 637.6 \quad 810 \quad 940.9 \quad 1064.7 \quad 1106.8 \quad 1274.7 \quad 1393.4 \quad 1560.3)\,ft \cdot kip$$

C.2.3.4.2 Total Load Effects

Given the assumed live loads, the total assumed shear and moment in the girder, V_{assume} and M_{assume} are the sum of the dead and live loads given in Sections C.2.1.4.2 and C.2.3.4.1, respectively. Therefore,

$V_{assume} = V_{LL} + V_{DC1}$

$V_{assume_2} = 320.47\text{kip} + 18.22\text{kip}$

$V_{assume_2} = 338.7\text{kip}$

$V_{assume}^{T} = (473.8 \;\; 338.7 \;\; 395.4 \;\; 333.5 \;\; 350.5 \;\; 355.5 \;\; 344.2 \;\; 345.9 \;\; 346.5 \;\; 348.6 \;\; 338.7 \;\; 340.8)\,\text{kip}$

$M_{assume} = M_{LL} + M_{DC1}$

$M_{assume_2} = 153.12\text{ft}\cdot\text{kip} + 8.7\text{ft}\cdot\text{kip}$

$M_{assume_2} = 161.8\cdot\text{ft}\cdot\text{kip}$

$M_{assume}^{T} = (999999.9 \;\; 161.8 \;\; 378.1 \;\; 478.9 \;\; 671.4 \;\; 851.9 \;\; 990.4 \;\; 1120 \;\; 1163.9 \;\; 1339.2 \;\; 1465 \;\; 1638.7)\,\text{ft}\cdot\text{kip}$

Additionally, the maximum shear and moment due to externally applied loads, V_i and M_{max} are:

$V_i = V_{assume} - V_d$

$V_{i_2} = V_{assume_2} - V_{d_2}$

$V_{i_2} = 338.69\text{kip} - 18.22\text{kip}$

$V_{i_2} = 320.47\,\text{kip}$

$V_i^{T} = (455.08 \;\; 320.47 \;\; 377.6 \;\; 316.17 \;\; 333.6 \;\; 339.06 \;\; 328.18 \;\; 330.25 \;\; 330.92 \;\; 333.48 \;\; 324.03 \;\; 326.55)\,\text{kip}$

$M_{max} = M_{assume} - M_d$

$M_{max_2} = M_{assume_2} - M_{d_2}$

$M_{max_2} = 161.82\text{ft}\cdot\text{kip} - 8.7\text{ft}\cdot\text{kip}$

$M_{max_2} = 153.12\,\text{ft}\cdot\text{kip}$

$M_{max}^{T} = (1000000 \;\; 153.12 \;\; 360.84 \;\; 453.21 \;\; 637.58 \;\; 810.03 \;\; 940.86 \;\; 1064.74 \;\; 1106.83 \;\; 1274.73 \;\; 1393.43 \;\; 1560.28)\,\text{ft}\cdot\text{kip}$

where, in the case of this example, the terms V_d and M_d are equivalent to V_{DC1} and M_{DC1}.

C.2.3.5 Calculate the Shear Resistance

C.2.3.5.1 Determine the Concrete Contribution to the Shear Resistance

C.2.3.5.1.1 Calculate V_{ci}

C.2.3.5.1.1.1 Calculate f_{cpe}

The compressive stress in the concrete due to effective prestress forces is calculated using the following steps:

$$P_{f.cpe_i} = \begin{cases} f_{pe} \cdot A_{strand} \cdot Num_{strand} \cdot \dfrac{x_{dist_i} + x_{bearing}}{l_t} & \text{if } x_{dist_i} + x_{bearing} < l_t \\ f_{pe} \cdot A_{strand} \cdot Num_{strand} & \text{if } x_{dist_i} + x_{bearing} \geq l_t \\ \text{"error"} & \text{otherwise} \end{cases}$$

$$P_{f.cpe_2} = f_{pe} \cdot A_{strand} \cdot Num_{strand} \cdot \frac{x_{dist_2} + x_{bearing}}{l_t} \quad \text{if } x_{dist_2} < l_t$$

$$P_{f.cpe_2} = 164.96\text{ksi} \cdot 0.153\text{in}^2 \cdot 24 \cdot \frac{5.73\text{in} + 6\text{in}}{30\text{in}} \quad \text{if } 5.73\text{in} < 30\text{in}$$

$$P_{f.cpe_2} = 236.84\text{kip}$$

$$P_{f.cpe}^{T} = (121.1 \quad 236.8 \quad 352.7 \quad 468.4 \quad 584.1 \quad 605.7 \quad 605.7 \quad 605.7 \quad 605.7 \quad 605.7 \quad 605.7 \quad 605.7)\text{ kip}$$

$$e_{strand_i} = y_b - cg_{ps_i}$$

$$e_{strand_2} = y_b - cg_{ps_2}$$

$$e_{strand_2} = 15.83\text{in} - 12.16\text{in}$$

$$e_{strand_2} = 3.67\,\text{in}$$

$$e_{strand}^{T} = (3.5 \;\; 3.67 \;\; 3.84 \;\; 4 \;\; 4.17 \;\; 4.33 \;\; 4.5 \;\; 4.62 \;\; 4.67 \;\; 4.83 \;\; 5 \;\; 5.16)\,\text{in}$$

$$f_{cpe_i} = \frac{P_{f.cpe_i}}{A_{beam}} + \frac{P_{f.cpe_i} \cdot e_{strand_i}}{S_b}$$

$$f_{cpe_2} = \frac{236.84\text{kip}}{369\text{in}^2} + \frac{236.84\text{kip} \cdot 3.67\text{in}}{3220.4\text{in}^3}$$

$$f_{cpe_2} = 0.91\,\text{ksi}$$

$$f_{cpe}^{T} = (0.46 \;\; 0.91 \;\; 1.38 \;\; 1.85 \;\; 2.34 \;\; 2.46 \;\; 2.49 \;\; 2.51 \;\; 2.52 \;\; 2.55 \;\; 2.58 \;\; 2.61)\,\text{ksi}$$

C.2.3.5.1.1.2 Calculate M_{cre}

Calculations for the moment due to externally applied loads causing that results in cracking, M_{cre}, begins with determining M_{dnc}, the total unfactored dead load moment acting on the noncomposite section. In the case of this example, M_{dnc}, is simply M_{DC1} found in Section C.2.1.4.2. Therefore,

$$M_{cre_i} = S_{bc} \cdot \left(f_{r.V} + f_{cpe_i} - \frac{M_{dnc_i}}{S_b} \right)$$

$$M_{cre_2} = 6510.03\text{in}^3 \cdot \left(0.595\text{ksi} + 0.912\text{ksi} - \frac{8.697\text{ft} \cdot \text{kip}}{3220.4\text{in}^3} \right)$$

$$M_{cre_2} = 800.08\,\text{ft} \cdot \text{kip}$$

$$M_{cre}^{T} = (572.9 \;\; 800.1 \;\; 1034.6 \;\; 1275.6 \;\; 1523.4 \;\; 1571.2 \;\; 1572.5 \;\; 1573.6 \;\; 1574.2 \;\; 1576.3 \;\; 1578.8 \;\; 1581.9)\,\text{ft} \cdot \text{kip}$$

C.2.3.5.1.1.3 Calculate V_{ci}

$$V_{ci_i} = \max\left(0.02\alpha_v\cdot\sqrt{\frac{f_{c'}}{ksi}}\cdot ksi\cdot b_v\cdot d_{v_i} + V_{d_i} + \frac{V_i\cdot M_{cre_i}}{M_{max_i}}, 0.06\cdot\alpha_v\sqrt{\frac{f_{c'}}{ksi}}\cdot ksi\cdot b_v\cdot d_{v_i}\right)$$

$$V_{ci_2} = \max\left(0.02\alpha_v\cdot\sqrt{\frac{f_{c'}}{ksi}}\cdot ksi\cdot b_v\cdot d_{v_2} + V_{d_2} + \frac{V_{i_2}\cdot M_{cre_2}}{M_{max_2}}, 0.06\cdot\alpha_v\sqrt{\frac{f_{c'}}{ksi}}\cdot ksi\cdot b_v\cdot d_{v_2}\right)$$

$$V_{ci_2} = \max\left[0.02(1)\cdot\sqrt{8.87}ksi\cdot 6in\cdot 40.13in + 18.22kip + \frac{320.47kip\cdot 800.08ft\cdot kip}{153.12ft\cdot kip}, 0.06(1)\cdot\sqrt{8.87}ksi\cdot 6in\cdot 40.13in\right]$$

$$V_{ci_2} = \max(1707.08kip, 43.03kip)$$

$$V_{ci_2} = 1707.03\,kip$$

$$V_{ci}^{T} = (42.9 \quad 1707.03 \quad 1114.78 \quad 921.58 \quad 828.36 \quad 688.5 \quad 578.31 \quad 517.27 \quad 500.04 \quad 441.33 \quad 395.19 \quad 358.69)\,kip$$

C.2.3.5.1.2 Calculate V_{cw}

C.2.3.5.1.2.1 Determine the Compressive Stress at the Composite Centroid, f_{pc}

$$P_{f.pc_i} = f_{ps_i}\cdot A_{strand}\cdot Num_{strand}$$

$$P_{f.pc_2} = f_{ps_2}\cdot A_{strand}\cdot Num_{strand}$$

$$P_{f.pc_2} = 64.5ksi\cdot 0.153in^2\cdot 24$$

$$P_{f.pc_2} = 236.84\,kip$$

$$P_{f.pc}^{T} = (121.15 \quad 236.84 \quad 352.74 \quad 468.43 \quad 584.13 \quad 623.9 \quad 646.2 \quad 662.89 \quad 668.54 \quad 690.84 \quad 713.14 \quad 735.49)\,kip$$

$$f_{pc_i} = \begin{cases} \dfrac{P_{f.pc_i}}{A_{beam}} + \dfrac{P_{f.pc_i} \cdot e_{strand_i} \cdot (y_b - y_{bc})}{I_{beam}} - \dfrac{M_{DC1_i} \cdot (y_b - y_{bc})}{I_{beam}} & \text{if } y_{bc} \le h_{top.flange} \\ \dfrac{P_{f.pc_i}}{A_{beam}} + \dfrac{P_{f.pc_i} \cdot e_{strand_i} \cdot (y_b - h_{top.flange})}{I_{beam}} - \dfrac{M_{DC1_i} \cdot (y_b - h_{top.flange})}{I_{beam}} & \text{if } y_{bc} > h_{top.flange} \end{cases}$$

$$f_{pc_2} = \frac{P_{f.pc_2}}{A_{beam}} + \frac{P_{f.pc_2} \cdot e_{strand_2} \cdot (y_b - h_{top.flange})}{I_{beam}} - \frac{M_{DC1_2} \cdot (y_b - h_{top.flange})}{I_{beam}} \quad \text{if } y_{bc} > h_{top.flange}$$

$$f_{pc_2} = \frac{236.84\text{kip}}{369\text{in}^2} + \frac{236.84\text{kip} \cdot 3.67\text{in} \cdot (15.83\text{in} - 30\text{in})}{50979\text{in}^4} - \frac{8.7\text{ft} \cdot \text{kip} \cdot (15.83\text{in} - 30\text{in})}{50979\text{in}^4} \quad \text{if } 32.57\text{in} > 30\text{in}$$

$$f_{pc_2} = 0.43\text{ksi} \quad \text{if } 32.57\text{in} > 30\text{in}$$

$$f_{pc_2} = 0.43\,\text{ksi}$$

$$f_{pc}^{T} = (0.21 \;\; 0.43 \;\; 0.64 \;\; 0.83 \;\; 1.02 \;\; 1.08 \;\; 1.11 \;\; 1.13 \;\; 1.14 \;\; 1.16 \;\; 1.18 \;\; 1.2)\,\text{ksi}$$

C.2.3.5.1.2.2Determine V_{cw}

$$V_{cw_i} = \left(0.06 \cdot \alpha_v \cdot \sqrt{\frac{f_{c'}}{\text{ksi}}} \cdot \text{ksi} + 0.30 \cdot f_{pc_i}\right) \cdot b_v \cdot d_{v_i} + V_{p_i}$$

$$V_{cw_2} = \left(0.06 \cdot \alpha_v \cdot \sqrt{\frac{f_{c'}}{\text{ksi}}} \cdot \text{ksi} + 0.30 \cdot f_{pc_2}\right) \cdot b_v \cdot d_{v_2} + V_{p_2}$$

$$V_{cw_2} = \left[0.06 \cdot (1) \cdot \sqrt{8.87}\text{ksi} + 0.30 \cdot 0.429\text{ksi}\right] \cdot 6\text{in} \cdot 40.13\text{in} + 6.81\text{kip}$$

$$V_{cw_2} = 80.82\,\text{kip}$$

$$V_{cw}^{T} = (61.5 \;\; 80.8 \;\; 99.3 \;\; 117 \;\; 133.8 \;\; 138.8 \;\; 136 \;\; 137.6 \;\; 138.1 \;\; 139.9 \;\; 137.1 \;\; 138.7)\,\text{kip}$$

C.2.3.5.1.3 Calculate V_c

$$V_{c_i} = \min\left(V_{ci_i}, V_{cw_i}\right)$$

$$V_{c_2} = \min\left(V_{ci_2}, V_{cw_2}\right)$$

$$V_{c_2} = \min(1707.03\text{kip}, 80.82\text{kip})$$

$$V_{c_2} = 80.82\,\text{kip}$$

$$V_{c}^{T} = (42.9 \;\; 80.82 \;\; 99.34 \;\; 116.99 \;\; 133.81 \;\; 138.77 \;\; 136.04 \;\; 137.57 \;\; 138.06 \;\; 139.9 \;\; 137.15 \;\; 138.7)\,\text{kip}$$

C.2.3.5.2 Calculate the Steel Contribution to the Shear Resistance

C.2.3.5.2.1 Determine cotθ

$$\cot\theta_i = \begin{cases} 1 & \text{if } V_{ci_i} < V_{cw_i} \\ \min\left(1 + 3\cdot\frac{f_{pc_i}}{\alpha_v\cdot\sqrt{f_{c'}\cdot ksi}}, 1.8\right) & \text{if } V_{ci_i} \geq V_{cw_i} \end{cases}$$

$$\cot\theta_2 = \min\left(1 + 3\cdot\frac{f_{pc_2}}{\alpha_v\cdot\sqrt{f_{c'}\cdot ksi}}, 1.8\right) \quad \text{if } 1707.03kip \geq 80.82kip$$

$$\cot\theta_2 = \min\left[1 + 3\cdot\frac{0.429ksi}{(1)\cdot\sqrt{8.87\cdot ksi}}, 1.8\right] \quad \text{if } 1707.03kip \geq 80.82kip$$

$$\cot\theta_2 = \min(1.43, 1.8) \quad \text{if } 1707.03kip \geq 80.82kip$$

$$\cot\theta_2 = 1.433$$

$$\cot\theta^T = (1.00 \;\; 1.43 \;\; 1.64 \;\; 1.80 \;\; 1.80 \;\; 1.80 \;\; 1.80 \;\; 1.80 \;\; 1.80 \;\; 1.80 \;\; 1.80 \;\; 1.80)$$

C.2.3.5.2.2 Find V_s

$$V_{s_i} = \frac{A_{v_i}\cdot f_{yv}\cdot d_{v_i}\cdot\left(\cot\theta_i + \cot(\alpha)\right)\cdot\sin(\alpha)}{s_{v.design_i}}$$

$$V_{s_2} = \frac{A_{v_2}\cdot f_{yv}\cdot d_{v_2}\cdot\left(\cot\theta_2 + \cot(\alpha)\right)\cdot\sin(\alpha)}{s_{v.design_2}}$$

$$V_{s_2} = \frac{0.4in^2\cdot 67.3ksi\cdot 40.13in\cdot\left(1.433 + \cot\left(\frac{\pi}{2}\right)\cdot\sin\left(\frac{\pi}{2}\right)\right)}{6in}$$

$$V_{s_2} = 257.91\,kip$$

$$V_s^T = (430.9 \;\; 257.9 \;\; 296.2 \;\; 216.6 \;\; 216.8 \;\; 216.8 \;\; 208.2 \;\; 208.4 \;\; 208.5 \;\; 208.8 \;\; 201.6 \;\; 202.1)\,kip$$

C.2.3.5.3 Determine the Nominal Shear Resistance

$$V_{n1} = V_c + V_s$$

$$V_{n1_2} = V_{c_2} + V_{s_2}$$

$$V_{n1_2} = 80.82\text{kip} + 257.91\text{kip} + 6.81\text{kip}$$

$$V_{n1_2} = 338.7\,\text{kip}$$

$$V_{n1}^{T} = (473.8 \;\; 338.7 \;\; 395.5 \;\; 333.6 \;\; 350.6 \;\; 355.6 \;\; 344.3 \;\; 346 \;\; 346.6 \;\; 348.7 \;\; 338.8 \;\; 340.8)\,\text{kip}$$

Note that for V_{n1}, V_p is taken as zero. Since V_{n2} is the same as what was calculated in Section C.2.1.5.4, the nominal shear resistance is calculated as:

$$V_{n_i} = \min\left(V_{n1_i}, V_{n2_i}\right)$$

$$V_{n_2} = \min\left(V_{n1_2}, V_{n2_2}\right)$$

$$V_{n_2} = \min(338.7\text{kip}, 540.4\text{kip})$$

$$V_{n_2} = 338.7\,\text{kip}$$

$$V_n^{T} = (473.8 \;\; 338.7 \;\; 395.5 \;\; 333.6 \;\; 350.6 \;\; 355.6 \;\; 344.3 \;\; 346 \;\; 346.6 \;\; 348.7 \;\; 338.8 \;\; 340.8)\,\text{kip}$$

Although not nearly as iterative as *Appendix B5* or the *General Procedure* for finding the shear strength, the Simplified approach may require one or two refinements of $P_{asssume}$ before the results for V_n converge. If necessary, the same process as outlined in Section C.2.1.6 can be done to refine the values for P_{assume}. However, in the case of this example, such refinement is not necessary because the assumed live loads leading to shear failure were correctly chosen.

The critical section in this example is determined in a similar fashion as for the *General Procedure*, with the exception that the term $cot\theta$ may be different, in which case, $x_{critical}$ is calculated as:

$$x_{critical} = \max\left(d_{v.critical}, \frac{1}{2} \cdot d_{v.critical} \cdot \cot\theta_{critical}\right)$$

$$x_{critical} = \max\left(38.69\text{in}, \frac{1}{2} 38.69\text{in} \cdot 1.8\right)$$

$$x_{critical} = \max(38.69\text{in}, 34.82\text{in})$$

$$x_{critical} = 38.69\,\text{in}$$

where as in the previous example, the assumed critical section was at 38.69 in from the support. This distance corresponded to the eighth element in the parameter *cot*θ, whose value is 1.8. Note that although the parameter *cot*θ may be different than that used in the earlier example, the critical section is the same since $d_{v.critical}$ was the controlling parameter.

In any event, the corresponding shear strength at the critical section is the eighth element of V_n above, which is 346.0 kip. However, the calculated shear strength at the section located 51.6 in. from the support was 338.8 kip. Since this location is further from the support than the critical section, the corresponding value is taken as the predicted shear strength, or 339 kip after rounding to the nearest kip.

C.3 Inputs and Detailed Results for Shear Calculations

C.3.1 Using Appendix B5

C.3.1.1 Beam T2.8.Typ.1

C.3.1.1.1 Inputs

γ_c (pcf)	121.5
f_c' (psi)	8865
f_{ci}' (psi)	6090
$f_{c.deck}$ (psi)	5829
$\gamma_{c.deck}$ (pcf)	123.4
E_{beam} (ksi)	3605
$E_{beam.i}$ (ksi)	3585
E_{slab} (ksi)	3566
h (in)	36
A_{beam} (in^2)	369
I_{beam} (in^4)	50979
L_{beam} (ft)	41
b_v (in)	6
y_b (in)	15.83
y_t (in)	20.17
S (ft)	7
t_{haunch} (in)	1

t_{struct} (in)	8.5
A_{ct} (in^2)	243
h_{flange} (in)	8.5
Num_{strand}	24
$Num_{straight}$	18
$Num_{straight.bot}$	16
Num_{harp}	6
$cg_{straight}$ (in)	7.00
$cg_{harp.end}$ (in)	29
$cg_{harp.ms}$ (in)	4
$cg_{straight.bot}$ (in)	3.75
A_{strand} (in^2)	0.153
φ (in)	0.5
f_{pu} (ksi)	270
f_{pe} (ksi)	164.96
E_p (ksi)	28500
$HarpDist$ (ft)	17.5

f_y (ksi)	67.3
f_{yv} (ksi)	67.3
E_s (ksi)	29000
α	1.57
$A_{s.top}$ (in^2)	0
d_{top} (in)	9.5
$d_{long.rebar}$	5
$IsLongSteelEpoxyCoated$	No
$LongSteelClearSpacing$ (in)	3.38
$LongSteelCover$ (in)	1.75
$IsTopBarEffectApplicable$	No
$A_{long.rebar}$ (in2)	0.31
$ShearSpan$ (in)	57.34
$x_{bearing}$ (in)	6
$x_{bearing.roller}$ (in)	6
$x_{critical.assume}$ (in)	34.12

x_{dist} (in)	A_{ct} (in^2)	$cg_{s.bot}$ (in)	cg_s (in)	$s_{v.design}$ (in)	A_v (in^2)	P_{assume} (kip)	θ_{assume} (rad)
0	2.04	4.4	4.4	2.5	0.4	150	0.62
5.73	2.04	4.4	4.4	6	0.4	150	0.65
11.47	2.04	4.4	4.4	6	0.4	150	0.6500
17.20	2.04	4.4	4.4	9	0.4	150	0.64
22.93	2.04	4.4	4.4	9	0.4	150	0.64
28.67	2.04	4.4	4.4	9	0.4	150	0.64
34.40	2.04	4.4	4.4	9	0.4	150	0.64
38.71	2.04	4.4	4.4	9	0.4	150	0.64
40.14	2.04	4.4	4.4	9	0.4	150	0.64
45.87	2.04	4.4	4.4	9	0.4	150	0.6400
51.60	2.04	4.4	4.4	9	0.4	150	0.62
57.34	2.04	4.4	4.4	9	0.4	150	0.62

C.3.1.1.2 Basic Geometry and Material Calculations

x_{dist} (in)	d_s (in)	$A_{ps.bot}$ (in^2)	cg_{harp} (in)
0.00	41.10	2.45	28.31
5.73	41.10	2.45	27.64
11.47	41.10	2.45	26.98
17.20	41.10	2.45	26.31
22.94	41.10	2.45	25.65
28.67	41.10	2.45	24.99
34.40	41.10	2.75	24.32
38.71	41.10	2.75	23.82
40.14	41.10	2.75	23.66
45.87	41.10	2.75	23.00
51.60	41.10	3.06	22.33
57.34	41.10	3.06	21.67

h_c (in)	L_{span} (ft)	A_{ps} (in^2)	Ψ_{harp} (rad)	f_{po} (ksi)	$f_{r.V}$ (psi)	β_1
45.5	40	3.672	0.1152	189	595.5	0.7585

C.3.1.1.3 Load Effect Calculations

x_{dist} (in)	V_{LL} (kip)	M_{LL} (ft-kip)	V_{DC1} (kip)	M_{DC1} (ft-kip)	V_{assume} (kip)	$M_{assume1}$ (ft-kip)	M_{assume} (ft-kip)	V_p (kip)
0.0	516.9	0.0	18.7	-0.1	535.5	-0.1	1774.4	3.5
5.7	274.3	131.1	18.2	8.7	292.6	139.8	955.5	6.8
11.5	278.5	266.2	17.8	17.3	296.3	283.5	958.5	10.1
17.2	207.2	297.1	17.3	25.7	224.6	322.7	707.7	13.5
22.9	211.1	403.4	16.9	33.9	228.0	437.3	708.4	16.8
28.7	212.2	506.9	16.4	41.8	228.6	548.8	708.8	17.4
34.4	205.1	588.1	16.0	49.6	221.1	637.7	656.6	17.4
38.7	206.6	666.6	15.7	55.3	222.3	721.8	721.8	17.4
40.1	206.7	691.3	15.5	57.1	222.2	748.4	748.4	17.4
45.9	207.0	791.4	15.1	64.4	222.1	855.9	855.9	17.4
51.6	207.0	890.2	14.7	71.5	221.7	961.7	961.7	17.4
57.3	207.9	993.3	14.2	78.4	222.1	1071.7	1071.7	17.4

C.3.1.1.4 Calculations for β and θ

x_{dist} (in)	cg_{ps} (in)	d_p (in)	c (in)	a (in)	$f_{ps.max}$ (ksi)	$l_{d.ps}$ (in)	f_{ps} (ksi)	$cg_{ps.bot}$ (in)	$d_{p.bot}$ (in)	$d_{s.bot}$ (in)	$Num_{strand.bot}$	$RedFactor_{\varepsilon x.s}$	$RedFactor_{\varepsilon x.ps}$
0.00	12.33	33.17	3.48	2.64	262.1	121.67	32.99	3.75	41.75	41.10	16.00	0.36	0.05
5.73	12.16	33.34	3.48	2.64	262.1	121.70	64.52	3.75	41.75	41.10	16.00	0.70	0.10
11.47	11.99	33.51	3.48	2.64	262.1	121.73	96.05	3.75	41.75	41.10	16.00	1.00	0.14
17.20	11.83	33.67	3.48	2.64	262.2	121.76	127.58	3.75	41.75	41.10	16.00	1.00	0.19
22.94	11.66	33.84	3.48	2.64	262.2	121.79	159.10	3.75	41.75	41.10	16.00	1.00	0.24
28.67	11.50	34.00	3.49	2.64	262.3	121.82	169.91	3.75	41.75	41.10	16.00	1.00	0.28
34.40	11.33	34.17	3.49	2.64	262.3	121.85	175.98	5.81	39.69	41.10	18.00	1.00	0.33
38.71	11.21	34.29	3.49	2.64	262.3	121.87	180.55	5.76	39.74	41.10	18.00	1.00	0.37
40.14	11.17	34.34	3.49	2.64	262.3	121.88	182.06	5.74	39.76	41.10	18.00	1.00	0.38
45.87	11.00	34.50	3.49	2.64	262.4	121.91	188.14	5.67	39.83	41.10	18.00	1.00	0.43
51.60	10.83	34.67	3.49	2.65	262.4	121.94	194.21	7.27	38.23	41.10	20.00	1.00	0.47
57.34	10.67	34.83	3.49	2.65	262.4	121.97	200.29	7.13	38.37	41.10	20.00	1.00	0.52

x_{dist} (in)	$A_{ps.bot}$ (in^2)	d_e (in)	ε_s	d_v (in)	v_u	$A_{s.bot.\varepsilon x}$ (in^2)	$A_{ps.bot.\varepsilon x}$ (in^2)	ε_x	θ (rad)	β	$MinReinfCheck$
0.00	2.45	41.34	0.03	40.02	0.250	0.73	0.12	0.0179	0.6231	1.50	OK
5.73	2.45	41.45	0.03	40.13	0.134	1.42	0.24	0.0045	0.6476	2.11	OK
11.47	2.45	41.51	0.03	40.19	0.134	2.04	0.35	0.0030	0.6476	2.11	OK
17.20	2.45	41.55	0.03	40.23	0.099	2.04	0.47	0.0018	0.6403	2.18	OK
22.94	2.45	41.58	0.03	40.26	0.099	2.04	0.58	0.0016	0.6402	2.18	OK
28.67	2.45	41.59	0.03	40.27	0.099	2.04	0.70	0.0014	0.6402	2.18	OK
34.40	2.75	40.00	0.03	38.68	0.099	2.04	0.91	0.0010	0.6382	2.19	OK
38.71	2.75	40.04	0.03	38.71	0.100	2.04	1.01	0.0010	0.6358	2.19	OK
40.14	2.75	40.05	0.03	38.73	0.099	2.04	1.04	0.0010	0.6360	2.19	OK
45.87	2.75	40.10	0.03	38.78	0.099	2.04	1.17	0.0010	0.6370	2.19	OK
51.60	3.06	38.77	0.03	37.45	0.103	2.04	1.45	0.0009	0.6199	2.24	OK
57.34	3.06	38.87	0.03	37.54	0.103	2.04	1.59	0.0009	0.6201	2.24	OK

C.3.1.1.5 Final Results for Shear Strength

x_{dist} (in)	V_c (kip)	V_s (kip)	V_{n1} (kip)	V_{n2} (kip)	V_n (kip)
0.00	33.9	599.7	637.1	535.6	535.6
5.73	47.8	238.0	292.6	540.4	292.6
11.47	47.9	238.4	296.4	544.6	296.4
17.20	49.6	161.5	224.6	548.4	224.6
22.94	49.6	161.7	228.1	552.1	228.1
28.67	49.6	161.7	228.7	552.9	228.7
34.40	47.8	156.0	221.1	531.7	221.1
38.71	48.0	156.9	222.3	532.2	222.3
40.14	48.0	156.9	222.3	532.4	222.3
45.87	48.0	156.8	222.2	533.0	222.2
51.60	47.3	157.0	221.7	515.4	221.7
57.34	47.4	157.3	222.1	516.6	222.1

C.3.1.2 Beam T2.8.Typ.2

C.3.1.2.1 Inputs

γ_c (pcf)	121.5
f_c' (psi)	8890
f_{ci}' (psi)	6090
$f_{c.deck}$ (psi)	6088
$\gamma_{c.deck}$ (pcf)	123.4
E_{beam} (ksi)	3605
$E_{beam.i}$ (ksi)	3585
E_{slab} (ksi)	3210
h (in)	36
A_{beam} (in^2)	369
I_{beam} (in^4)	50979
L_{beam} (ft)	41
b_v (in)	6
y_b (in)	15.83
y_t (in)	20.17
S (ft)	7
t_{haunch} (in)	1

t_{struct} (in)	8.5
A_{ct} (in^2)	243
h_{flange} (in)	8.5
Num_{strand}	24
$Num_{straight}$	18
$Num_{straight.bot}$	16
Num_{harp}	6
$cg_{straight}$ (in)	7.00
$cg_{harp.end}$ (in)	29
$cg_{harp.ms}$ (in)	4
$cg_{straight.bot}$ (in)	3.75
A_{strand} (in^2)	0.153
φ (in)	0.5
f_{pu} (ksi)	270
f_{pe} (ksi)	164.96
E_p (ksi)	28500
$HarpDist$ (ft)	17.5

f_y (ksi)	67.3
f_{yv} (ksi)	67.3
E_s (ksi)	29000
α	1.57
$A_{s.top}$ (in^2)	0
d_{top} (in)	9.5
$d_{long.rebar}$	5
$IsLongSteelEpoxyCoated$	No
$LongSteelClearSpacing$ (in)	3.38
$LongSteelCover$ (in)	1.75
$IsTopBarEffectApplicable$	No
$A_{long.rebar}$ (in2)	0.31
$ShearSpan$ (in)	118.76
$x_{bearing}$ (in)	6
$x_{bearing.roller}$ (in)	64.5
$x_{critical.assume}$ (in)	34.14

x_{dist} (in)	A_{ct} (in^2)	$cg_{s.bot}$ (in)	cg_s (in)	$s_{v.design}$ (in)	A_v (in^2)	P_{assume} (kip)	θ_{assume} (rad)
0	2.04	4.4	4.4	2.5	0.4	150	0.62
11.88	2.04	4.4	4.4	6	0.4	150	0.65
23.75	2.04	4.4	4.4	9	0.4	150	0.6400
35.63	2.04	4.4	4.4	9	0.4	150	0.64
38.77	2.04	4.4	4.4	9	0.4	150	0.64
47.50	2.04	4.4	4.4	9	0.4	150	0.64
59.38	2.04	4.4	4.4	9	0.4	150	0.62
71.26	0	0	0	9	0.4	150	0.64
79.99	0	0	0	10	0.4	150	0.63
83.13	0	0	0	10	0.4	150	0.62
95.01	0	0	0	10	0.4	150	0.6200
106.88	0	0	0	10	0.4	150	0.62
118.76	0	0	0	10	0.4	150	0.62

C.3.1.2.2 Basic Geometry and Material Calculations

x_{dist} (in)	d_s (in)	$A_{ps.bot}$ (in^2)	cg_{harp} (in)
0	41.10	2.45	28.31
11.88	41.10	2.45	26.93
23.75	41.10	2.45	25.56
35.63	41.10	2.75	24.18
38.77	41.10	2.75	23.82
47.50	41.10	2.75	22.81
59.38	41.10	3.06	21.43
71.26	45.50	3.37	20.06
79.99	45.50	3.37	19.05
83.13	45.50	3.37	18.68
95.01	45.50	3.37	17.31
106.88	45.50	3.37	15.93
118.76	45.50	3.37	14.56

h_c (in)	L_{span} (ft)	A_{ps} (in^2)	Ψ_{harp} (rad)	f_{po} (ksi)	$f_{r.V}$ (psi)	β_1
45.5	35.125	3.672	0.1152	189	596.3	0.7456

C.3.1.2.3 Load Effect Calculations

x_{dist} (in)	V_{LL} (kip)	M_{LL} (ft-kip)	V_{DC1} (kip)	M_{DC1} (ft-kip)	V_{assume} (kip)	$M_{assume1}$ (ft-kip)	M_{assume} (ft-kip)	V_p (kip)
0.0	521.8	0.0	16.0	-0.1	537.8	-0.1	1784.4	3.5
11.9	282.0	279.1	15.1	15.3	297.1	294.4	961.8	10.4
23.8	214.7	424.9	14.2	29.8	228.8	454.7	710.9	17.3
35.6	209.3	621.5	13.2	43.3	222.6	664.8	664.8	17.4
38.8	209.5	676.9	13.0	46.7	222.5	723.6	723.6	17.4
47.5	210.0	831.3	12.3	56.0	222.3	887.3	887.3	17.4
59.4	211.1	1044.4	11.4	67.7	222.5	1112.1	1112.1	17.4
71.3	196.9	1169.3	10.5	78.5	207.4	1247.8	1247.8	17.4
80.0	189.5	1263.0	9.8	85.9	199.3	1348.8	1348.8	17.4
83.1	190.7	1321.0	9.5	88.4	200.2	1409.4	1409.4	17.4
95.0	195.0	1544.1	8.6	97.4	203.7	1641.5	1641.5	17.4
106.9	199.1	1773.7	7.7	105.5	206.8	1879.2	1879.2	17.4
118.8	201.6	1995.0	6.8	112.7	208.4	2107.7	2107.7	17.4

C.3.1.2.4 Calculations for β and θ

x_{dist} (in)	cg_{ps} (in)	d_p (in)	c (in)	a (in)	$f_{ps.max}$ (ksi)	$l_{d.ps}$ (in)	f_{ps} (ksi)	$cg_{ps.bot}$ (in)	$d_{p.bot}$ (in)	$d_{s.bot}$ (in)	$Num_{strand.bot}$	$RedFactor_{\varepsilon x.s}$	$RedFactor_{\varepsilon x.ps}$
0.00	12.33	33.17	3.40	2.53	262.3	121.83	32.99	3.75	41.75	41.10	16.00	0.36	0.05
11.88	11.98	33.52	3.40	2.53	262.3	121.89	98.29	3.75	41.75	41.10	16.00	1.00	0.15
23.75	11.64	33.86	3.40	2.53	262.4	121.95	163.60	3.75	41.75	41.10	16.00	1.00	0.24
35.63	11.30	34.20	3.40	2.53	262.5	122.01	177.28	5.80	39.70	41.10	18.00	1.00	0.34
38.77	11.20	34.30	3.40	2.53	262.5	122.03	180.62	5.76	39.74	41.10	18.00	1.00	0.37
47.50	10.95	34.55	3.40	2.53	262.6	122.07	189.88	5.65	39.85	41.10	18.00	1.00	0.44
59.38	10.61	34.89	3.40	2.53	262.6	122.13	202.47	7.09	38.41	41.10	20.00	1.00	0.54
71.26	10.26	35.24	2.99	2.23	263.6	122.90	215.13	8.20	37.30	45.50	22.00	1.00	0.63
79.99	10.01	35.49	2.99	2.23	263.6	122.93	224.41	7.92	37.58	45.50	22.00	1.00	0.70
83.13	9.92	35.58	2.99	2.23	263.7	122.94	227.75	7.82	37.68	45.50	22.00	1.00	0.73
95.01	9.58	35.92	2.99	2.23	263.7	122.99	240.37	7.45	38.05	45.50	22.00	1.00	0.82
106.88	9.23	36.27	2.99	2.23	263.8	123.04	252.99	7.07	38.43	45.50	22.00	1.00	0.92
118.76	8.89	36.61	2.99	2.23	263.8	123.08	263.83	6.70	38.80	45.50	22.00	1.00	1.00

x_{dist} (in)	$A_{ps.bot}$ (in^2)	d_e (in)	ε_s	d_v (in)	v_u	$A_{s.bot.\varepsilon x}$ (in^2)	$A_{ps.bot.\varepsilon x}$ (in^2)	ε_x	θ (rad)	β	$MinReinfCheck$
0.00	2.45	41.34	0.03	40.08	0.250	0.73	0.12	0.0180	0.6231	1.50	OK
11.88	2.45	41.51	0.03	40.25	0.134	2.04	0.36	0.0029	0.6476	2.11	OK
23.75	2.45	41.58	0.03	40.32	0.098	2.04	0.60	0.0016	0.6402	2.18	OK
35.63	2.75	40.01	0.03	38.74	0.099	2.04	0.94	0.0010	0.6355	2.20	OK
38.77	2.75	40.04	0.03	38.77	0.099	2.04	1.01	0.0010	0.6361	2.19	OK
47.50	2.75	40.11	0.03	38.85	0.099	2.04	1.21	0.0010	0.6375	2.19	OK
59.38	3.06	38.90	0.03	37.63	0.102	2.04	1.64	0.0009	0.6204	2.24	OK
71.26	3.37	37.30	0.03	36.19	0.098	0.00	2.12	0.0012	0.6402	2.18	OK
79.99	3.37	37.58	0.03	36.46	0.094	0.00	2.35	0.0009	0.6258	2.23	OK
83.13	3.37	37.68	0.03	36.56	0.094	0.00	2.44	0.0009	0.6244	2.24	OK
95.01	3.37	38.05	0.04	36.94	0.095	0.00	2.76	0.0009	0.6199	2.25	OK
106.88	3.37	38.43	0.04	37.31	0.095	0.00	3.09	0.0009	0.6164	2.26	OK
118.76	3.37	38.80	0.04	37.69	0.095	0.00	3.37	0.0009	0.6174	2.26	OK

C.3.1.2.5 Final Results for Shear Strength

x_{dist} (in)	V_c (kip)	V_s (kip)	V_{n1} (kip)	V_{n2} (kip)	V_n (kip)
0.00	34.0	600.5	638.0	537.9	537.9
11.88	48.1	238.7	297.2	547.1	297.2
23.75	49.8	161.9	228.9	554.9	228.9
35.63	48.1	157.1	222.6	534.0	222.6
38.77	48.1	157.0	222.5	534.4	222.5
47.50	48.1	156.9	222.4	535.4	222.4
59.38	47.6	157.5	222.5	519.3	222.5
71.26	44.7	145.3	207.4	500.0	207.4
79.99	46.0	135.8	199.3	503.7	199.3
83.13	46.2	136.6	200.2	505.0	200.2
95.01	47.0	139.3	203.7	510.0	203.7
106.88	47.7	141.8	206.9	515.0	206.9
118.76	48.1	142.9	208.4	520.0	208.4

C.3.1.3 Beam T2.8.Min.1

C.3.1.3.1 Inputs

γ_c (pcf)	121.5
f_c' (psi)	8890
f_{ci}' (psi)	6090
$f_{c.deck}$ (psi)	5360
$\gamma_{c.deck}$ (pcf)	125
E_{beam} (ksi)	3605
$E_{beam.i}$ (ksi)	3585
E_{slab} (ksi)	3240
h (in)	36
A_{beam} (in^2)	369
I_{beam} (in^4)	50979
L_{beam} (ft)	40.9688
b_v (in)	6
y_b (in)	15.83
y_t (in)	20.17
S (ft)	7
t_{haunch} (in)	1.125

t_{struct} (in)	8
A_{ct} (in^2)	243
h_{flange} (in)	8.5
Num_{strand}	24
$Num_{straight}$	18
$Num_{straight.bot}$	16
Num_{harp}	6
$cg_{straight}$ (in)	7.00
$cg_{harp.end}$ (in)	29
$cg_{harp.ms}$ (in)	4
$cg_{straight.bot}$ (in)	3.75
A_{strand} (in^2)	0.153
φ (in)	0.5
f_{pu} (ksi)	270
f_{pe} (ksi)	162.64
E_p (ksi)	28500
$HarpDist$ (ft)	17.5

f_y (ksi)	67.3
f_{yv} (ksi)	67.3
E_s (ksi)	29000
α	1.57
$A_{s.top}$ (in^2)	0
d_{top} (in)	9.5
$d_{long.rebar}$	5
$IsLongSteelEpoxyCoated$	No
$LongSteelClearSpacing$ (in)	3.38
$LongSteelCover$ (in)	1.75
$IsTopBarEffectApplicable$	No
$A_{long.rebar}$ (in2)	0.31
$ShearSpan$ (in)	58.00
$x_{bearing}$ (in)	6
$x_{bearing.roller}$ (in)	6
$x_{critical.assume}$ (in)	34.19

x_{dist} (in)	A_{ct} (in^2)	$cg_{s.bot}$ (in)	cg_s (in)	$s_{v.design}$ (in)	A_v (in^2)	P_{assume} (kip)	θ_{assume} (rad)
0	2.04	4.4	4.4	2.5	0.4	150	0.62
5.80	2.04	4.4	4.4	9	0.4	150	0.64
11.60	2.04	4.4	4.4	12	0.4	150	0.6400
17.40	2.04	4.4	4.4	12	0.4	150	0.64
23.20	2.04	4.4	4.4	12	0.4	150	0.64
29.00	2.04	4.4	4.4	12	0.4	150	0.63
34.80	2.04	4.4	4.4	12	0.4	150	0.6
38.22	2.04	4.4	4.4	12	0.4	150	0.6
40.60	2.04	4.4	4.4	12	0.4	150	0.6
46.40	2.04	4.4	4.4	12	0.4	150	0.6000
52.20	2.04	4.4	4.4	12	0.4	150	0.58
58.00	2.04	4.4	4.4	12	0.4	150	0.58

C.3.1.3.2 Basic Geometry and Material Calculations

x_{dist} (in)	d_s (in)	$A_{ps.bot}$ (in^2)	cg_{harp} (in)
0.00	40.73	2.45	28.31
5.80	40.73	2.45	27.63
11.60	40.73	2.45	26.96
17.40	40.73	2.45	26.29
23.20	40.73	2.45	25.62
29.00	40.73	2.45	24.95
34.80	40.73	2.75	24.28
38.22	40.73	2.75	23.88
40.60	40.73	2.75	23.61
46.40	40.73	2.75	22.94
52.20	40.73	3.06	22.26
58.00	40.73	3.06	21.59

h_c (in)	L_{span} (ft)	A_{ps} (in^2)	Ψ_{harp} (rad)	f_{po} (ksi)	$f_{r.V}$ (psi)	β_1
45.125	39.9688	3.672	0.1152	189	596.3	0.782

C.3.1.3.3 Load Effect Calculations

x_{dist} (in)	V_{LL} (kip)	M_{LL} (ft-kip)	V_{DC1} (kip)	M_{DC1} (ft-kip)	V_{assume} (kip)	$M_{assume1}$ (ft-kip)	M_{assume} (ft-kip)	V_p (kip)
0.0	512.4	0.0	18.1	-0.1	530.5	-0.1	1736.1	3.4
5.8	197.2	95.3	17.7	8.5	214.8	103.8	687.3	6.8
11.6	163.1	157.7	17.2	17.0	180.4	174.7	563.4	10.1
17.4	167.1	242.2	16.8	25.2	183.9	267.4	564.6	13.4
23.2	171.0	330.5	16.4	33.2	187.3	363.7	565.4	16.7
29.0	172.7	417.3	15.9	41.0	188.6	458.3	568.2	17.2
34.8	178.0	516.1	15.5	48.6	193.5	564.7	564.7	17.2
38.2	178.4	568.3	15.2	53.0	193.7	621.3	621.3	17.2
40.6	178.7	604.7	15.0	56.0	193.8	660.7	660.7	17.2
46.4	179.5	693.9	14.6	63.1	194.1	757.0	757.0	17.2
52.2	180.1	783.5	14.2	70.1	194.3	853.6	853.6	17.2
58.0	181.3	876.1	13.7	76.8	195.0	953.0	953.0	17.2

C.3.1.3.4 Calculations for β and θ

x_{dist} (in)	cg_{ps} (in)	d_p (in)	c (in)	a (in)	$f_{ps.max}$ (ksi)	$l_{d.ps}$ (in)	f_{ps} (ksi)	$cg_{ps.bot}$ (in)	$d_{p.bot}$ (in)	$d_{s.bot}$ (in)	$Num_{strand.bot}$	$RedFactor_{\cdot x.s}$	$RedFactor_{\cdot x.ps}$
0.00	12.33	32.80	3.67	2.87	261.5	122.50	32.53	3.75	41.38	40.73	16.00	0.36	0.05
5.80	12.16	32.97	3.67	2.87	261.6	122.53	63.97	3.75	41.38	40.73	16.00	0.70	0.10
11.60	11.99	33.13	3.67	2.87	261.6	122.56	95.41	3.75	41.38	40.73	16.00	1.00	0.14
17.40	11.82	33.30	3.67	2.87	261.7	122.59	126.86	3.75	41.38	40.73	16.00	1.00	0.19
23.20	11.66	33.47	3.67	2.87	261.7	122.63	158.30	3.75	41.38	40.73	16.00	1.00	0.24
29.00	11.49	33.64	3.67	2.87	261.8	122.66	167.99	3.75	41.38	40.73	16.00	1.00	0.29
34.80	11.32	33.81	3.67	2.87	261.8	122.69	174.19	5.81	39.32	40.73	18.00	1.00	0.33
38.22	11.22	33.90	3.67	2.87	261.8	122.71	177.86	5.76	39.36	40.73	18.00	1.00	0.36
40.60	11.15	33.97	3.67	2.87	261.8	122.72	180.40	5.73	39.39	40.73	18.00	1.00	0.38
46.40	10.98	34.14	3.67	2.87	261.9	122.75	186.60	5.66	39.47	40.73	18.00	1.00	0.43
52.20	10.82	34.31	3.67	2.87	261.9	122.79	192.81	7.25	37.87	40.73	20.00	1.00	0.47
58.00	10.65	34.48	3.67	2.87	261.9	122.82	199.02	7.12	38.01	40.73	20.00	1.00	0.52

x_{dist} (in)	$A_{ps.bot}$ (in^2)	d_e (in)	ε_s	d_v (in)	v_u	$A_{s.bot.\cdot x}$ (in^2)	$A_{ps.bot.\cdot x}$ (in^2)	ε_x	θ (rad)	β	*MinReinfCheck*
0.00	2.45	40.96	0.03	39.53	0.250	0.73	0.12	0.0178	0.6231	1.50	OK
5.80	2.45	41.07	0.03	39.64	0.098	1.43	0.24	0.0031	0.6402	2.18	OK
11.60	2.45	41.13	0.03	39.70	0.080	2.04	0.35	0.0016	0.6364	2.22	OK
17.40	2.45	41.18	0.03	39.74	0.080	2.04	0.47	0.0014	0.6364	2.22	OK
23.20	2.45	41.21	0.03	39.77	0.080	2.04	0.58	0.0012	0.6364	2.22	OK
29.00	2.45	41.21	0.03	39.78	0.081	2.04	0.70	0.0010	0.6340	2.23	OK
34.80	2.75	39.63	0.03	38.19	0.087	2.04	0.92	0.0008	0.5973	2.33	OK
38.22	2.75	39.66	0.03	38.22	0.087	2.04	0.99	0.0008	0.5972	2.33	OK
40.60	2.75	39.68	0.03	38.24	0.087	2.04	1.05	0.0008	0.5971	2.33	OK
46.40	2.75	39.73	0.03	38.30	0.087	2.04	1.18	0.0008	0.5969	2.33	OK
52.20	3.06	38.41	0.03	36.97	0.090	2.04	1.45	0.0007	0.5779	2.39	OK
58.00	3.06	38.51	0.03	37.07	0.090	2.04	1.59	0.0007	0.5772	2.39	OK

C.3.1.3.5 Final Results for Shear Strength

x_{dist} (in)	V_c (kip)	V_s (kip)	V_{n1} (kip)	V_{n2} (kip)	V_n (kip)
0.00	33.5	592.4	629.3	530.6	530.6
5.80	48.9	159.2	214.8	535.3	214.8
11.60	49.8	120.5	180.4	539.5	180.4
17.40	49.9	120.6	183.9	543.3	183.9
23.20	49.9	120.7	187.3	547.0	187.3
29.00	50.1	121.4	188.6	547.6	188.6
34.80	50.3	126.0	193.5	526.5	193.5
38.22	50.4	126.1	193.7	526.9	193.7
40.60	50.4	126.2	193.8	527.2	193.8
46.40	50.5	126.4	194.1	527.8	194.1
52.20	50.0	127.2	194.3	510.2	194.3
58.00	50.1	127.7	195.0	511.5	195.0

C.3.1.4 Beam T2.8.Min.2

C.3.1.4.1 Inputs

γ_c (pcf)	121.5
f_c' (psi)	8890
f_{ci}' (psi)	6090
$f_{c.deck}$ (psi)	5360
$\gamma_{c.deck}$ (pcf)	125
E_{beam} (ksi)	3605
$E_{beam.i}$ (ksi)	3580
E_{slab} (ksi)	3240
h (in)	36
A_{beam} (in^2)	369
I_{beam} (in^4)	50979
L_{beam} (ft)	41
b_v (in)	6
y_b (in)	15.83
y_t (in)	20.17
S (ft)	7
t_{haunch} (in)	1

t_{struct} (in)	8.5
A_{ct} (in^2)	243
h_{flange} (in)	8.5
Num_{strand}	24
$Num_{straight}$	18
$Num_{straight.bot}$	16
Num_{harp}	6
$cg_{straight}$ (in)	7.00
$cg_{harp.end}$ (in)	29
$cg_{harp.ms}$ (in)	4
$cg_{straight.bot}$ (in)	3.75
A_{strand} (in^2)	0.153
φ (in)	0.5
f_{pu} (ksi)	270
f_{pe} (ksi)	162.64
E_p (ksi)	28500
$HarpDist$ (ft)	17.5

f_y (ksi)	67.3
f_{yv} (ksi)	67.3
E_s (ksi)	29000
α	1.57
$A_{s.top}$ (in^2)	0
d_{top} (in)	9.5
$d_{long.rebar}$	5
$IsLongSteelEpoxyCoated$	No
$LongSteelClearSpacing$ (in)	3.38
$LongSteelCover$ (in)	1.75
$IsTopBarEffectApplicable$	No
$A_{long.rebar}$ (in2)	0.31
$ShearSpan$ (in)	116.25
$x_{bearing}$ (in)	6
$x_{bearing.roller}$ (in)	69
$x_{critical.assume}$ (in)	34.07

x_{dist} (in)	A_{ct} (in^2)	$cg_{s.bot}$ (in)	cg_s (in)	$s_{v.design}$ (in)	A_v (in^2)	P_{assume} (kip)	θ_{assume} (rad)
0	2.04	4.4	4.4	2.5	0.4	150	0.62
11.63	2.04	4.4	4.4	9	0.4	150	0.64
23.25	2.04	4.4	4.4	12	0.4	150	0.6400
34.88	2.04	4.4	4.4	12	0.4	150	0.6
38.60	2.04	4.4	4.4	12	0.4	150	0.6
46.50	2.04	4.4	4.4	12	0.4	150	0.6
58.13	2.04	4.4	4.4	12	0.4	150	0.58
69.75	0	0	0	12	0.4	150	0.6
77.65	0	0	0	12	0.4	150	0.59
81.38	0	0	0	12	0.4	150	0.59
93.00	0	0	0	12	0.4	150	0.5900
104.63	0	0	0	12	0.4	150	0.58
116.25	0	0	0	12	0.4	150	0.58

C.3.1.4.2 Basic Geometry and Material Calculations

x_{dist} (in)	d_s (in)	$A_{ps.bot}$ (in^2)	cg_{harp} (in)
0.00	41.10	2.45	28.31
11.63	41.10	2.45	26.96
23.25	41.10	2.45	25.61
34.88	41.10	2.75	24.27
38.60	41.10	2.75	23.84
46.50	41.10	2.75	22.92
58.13	41.10	3.06	21.58
69.75	45.50	3.37	20.23
77.65	45.50	3.37	19.32
81.38	45.50	3.37	18.89
93.00	45.50	3.37	17.54
104.63	45.50	3.37	16.20
116.25	45.50	3.37	14.85

h_c (in)	L_{span} (ft)	A_{ps} (in^2)	Ψ_{harp} (rad)	f_{po} (ksi)	$f_{r.V}$ (psi)	β_1
45.5	34.75	3.672	0.1152	189	596.3	0.782

C.3.1.4.3 Load Effect Calculations

x_{dist} (in)	V_{LL} (kip)	M_{LL} (ft-kip)	V_{DC1} (kip)	M_{DC1} (ft-kip)	V_{assume} (kip)	$M_{assume1}$ (ft-kip)	M_{assume} (ft-kip)	V_p (kip)
0.0	519.5	0.0	15.9	-0.1	535.5	-0.1	1769.2	3.4
11.6	205.4	199.0	15.0	14.9	220.4	213.8	702.3	10.1
23.3	174.9	338.8	14.1	29.0	189.0	367.8	576.2	16.7
34.9	181.7	528.1	13.2	42.2	194.9	570.3	571.3	17.2
38.6	182.3	586.4	12.9	46.2	195.2	632.6	632.6	17.2
46.5	183.3	710.4	12.3	54.5	195.6	764.9	764.9	17.2
58.1	185.2	897.3	11.4	65.9	196.6	963.2	963.2	17.2
69.8	172.7	1003.9	10.4	76.5	183.2	1080.4	1080.4	17.2
77.6	175.8	1137.8	9.8	83.2	185.7	1221.0	1221.0	17.2
81.4	177.2	1202.0	9.5	86.2	186.8	1288.1	1288.1	17.2
93.0	181.5	1406.8	8.6	94.9	190.1	1501.8	1501.8	17.2
104.6	185.5	1617.7	7.7	102.9	193.2	1720.6	1720.6	17.2
116.3	189.3	1834.1	6.8	109.9	196.1	1944.0	1944.0	17.2

C.3.1.4.4 Calculations for β and θ

x_{dist} (in)	cg_{ps} (in)	d_p (in)	c (in)	a (in)	$f_{ps.max}$ (ksi)	$l_{d.ps}$ (in)	f_{ps} (ksi)	$cg_{ps.bot}$ (in)	$d_{p.bot}$ (in)	$d_{s.bot}$ (in)	$Num_{strand.bot}$	$RedFactor_{\cdot x.s}$	$RedFactor_{\cdot x.ps}$
0.00	12.33	33.17	3.67	2.87	261.6	122.57	32.53	3.75	41.75	41.10	16.00	0.36	0.05
11.63	11.99	33.51	3.67	2.87	261.7	122.64	95.55	3.75	41.75	41.10	16.00	1.00	0.14
23.25	11.65	33.85	3.67	2.87	261.8	122.70	158.57	3.75	41.75	41.10	16.00	1.00	0.24
34.88	11.32	34.18	3.67	2.87	261.9	122.76	174.27	5.81	39.69	41.10	18.00	1.00	0.33
38.60	11.21	34.29	3.67	2.87	261.9	122.78	178.26	5.76	39.74	41.10	18.00	1.00	0.36
46.50	10.98	34.52	3.67	2.87	262.0	122.82	186.71	5.66	39.84	41.10	18.00	1.00	0.43
58.13	10.64	34.86	3.67	2.87	262.0	122.88	199.16	7.12	38.38	41.10	20.00	1.00	0.52
69.75	10.31	35.19	3.23	2.52	263.1	123.71	211.67	8.25	37.25	45.50	22.00	1.00	0.61
77.65	10.08	35.42	3.23	2.52	263.1	123.75	220.14	8.00	37.50	45.50	22.00	1.00	0.68
81.38	9.97	35.53	3.23	2.52	263.1	123.76	224.13	7.88	37.62	45.50	22.00	1.00	0.71
93.00	9.64	35.86	3.23	2.53	263.2	123.81	236.60	7.51	37.99	45.50	22.00	1.00	0.80
104.63	9.30	36.20	3.23	2.53	263.3	123.86	249.07	7.14	38.36	45.50	22.00	1.00	0.89
116.25	8.96	36.54	3.23	2.53	263.3	123.91	261.54	6.78	38.72	45.50	22.00	1.00	0.99

x_{dist} (in)	$A_{ps.bot}$ (in^2)	d_e (in)	ε_s	d_v (in)	v_u	$A_{s.bot.\cdot x}$ (in^2)	$A_{ps.bot.\cdot x}$ (in^2)	ε_x	θ (rad)	β	$MinReinfCheck$
0.00	2.45	41.34	0.03	39.90	0.250	0.73	0.12	0.0179	0.6231	1.50	OK
11.63	2.45	41.51	0.03	40.07	0.098	2.04	0.35	0.0021	0.6402	2.18	OK
23.25	2.45	41.58	0.03	40.14	0.080	2.04	0.58	0.0012	0.6364	2.22	OK
34.88	2.75	40.01	0.03	38.57	0.086	2.04	0.92	0.0008	0.5982	2.33	OK
38.60	2.75	40.04	0.03	38.60	0.086	2.04	1.00	0.0008	0.5978	2.33	OK
46.50	2.75	40.11	0.03	38.67	0.087	2.04	1.18	0.0008	0.5976	2.33	OK
58.13	3.06	38.88	0.03	37.45	0.090	2.04	1.60	0.0007	0.5779	2.39	OK
69.75	3.37	37.25	0.03	35.99	0.087	0.00	2.06	0.0008	0.5977	2.33	OK
77.65	3.37	37.50	0.03	36.24	0.087	0.00	2.28	0.0008	0.5934	2.34	OK
81.38	3.37	37.62	0.03	36.36	0.088	0.00	2.38	0.0008	0.5917	2.35	OK
93.00	3.37	37.99	0.03	36.73	0.088	0.00	2.69	0.0007	0.5867	2.36	OK
104.63	3.37	38.36	0.03	37.09	0.089	0.00	3.01	0.0007	0.5827	2.38	OK
116.25	3.37	38.72	0.03	37.46	0.090	0.00	3.32	0.0007	0.5793	2.39	OK

C.3.1.4.5 Final Results for Shear Strength

x_{dist} (in)	V_c (kip)	V_s (kip)	V_{n1} (kip)	V_{n2} (kip)	V_n (kip)
0.00	33.8	598.0	635.2	535.6	535.6
11.63	49.5	160.9	220.5	544.5	220.5
23.25	50.4	121.9	189.0	552.1	189.0
34.88	50.8	127.0	194.9	531.5	194.9
38.60	50.8	127.2	195.2	531.9	195.2
46.50	51.0	127.5	195.6	532.8	195.6
58.13	50.6	128.8	196.6	516.5	196.6
69.75	47.4	118.6	183.2	497.1	183.2
77.65	48.0	120.5	185.7	500.5	185.7
81.38	48.3	121.4	186.8	502.0	186.8
93.00	49.1	123.9	190.2	506.9	190.2
104.63	49.8	126.3	193.3	511.8	193.3
116.25	50.5	128.5	196.2	516.7	196.2

C.3.1.5 Beam BT.8N.Typ.1

C.3.1.5.1 Inputs

γ_c (pcf)	150
f_c' (psi)	8860
f_{ci}' (psi)	6183
$f_{c.deck}$ (psi)	4890
$\gamma_{c.deck}$ (pcf)	127
E_{beam} (ksi)	4823
$E_{beam.i}$ (ksi)	4670
E_{slab} (ksi)	2940
h (in)	45
A_{beam} (in^2)	746.7
I_{beam} (in^4)	207300
L_{beam} (ft)	58.875
b_v (in)	7
y_b (in)	22.23
y_t (in)	22.77
S (ft)	7
t_{haunch} (in)	1

t_{struct} (in)	8.5
A_{ct} (in^2)	423.25
h_{flange} (in)	8.5
Num_{strand}	34
$Num_{straight}$	28
$Num_{straight.bot}$	28
Num_{harp}	6
$cg_{straight}$ (in)	3.68
$cg_{harp.end}$ (in)	41
$cg_{harp.ms}$ (in)	4.25
$cg_{straight.bot}$ (in)	3.68
A_{strand} (in^2)	0.153
φ (in)	0.5
f_{pu} (ksi)	270
f_{pe} (ksi)	167.8
E_p (ksi)	28500
$HarpDist$ (ft)	26.5

f_y (ksi)	69.8
f_{yv} (ksi)	69.8
E_s (ksi)	29000
α	1.5708
$A_{s.top}$ (in^2)	0
d_{top} (in)	9.5
$d_{long.rebar}$	5
$IsLongSteelEpoxyCoated$	No
$LongSteelClearSpacing$ (in)	3.75
$LongSteelCover$ (in)	2
$IsTopBarEffectApplicable$	No
$A_{long.rebar}$ (in2)	0.31
$ShearSpan$ (in)	104.39
$x_{bearing}$ (in)	6
$x_{bearing.roller}$ (in)	6
$x_{critical.assume}$ (in)	48.98

x_{dist} (in)	A_{ct} (in^2)	$cg_{s.bot}$ (in)	cg_s (in)	$s_{v.design}$ (in)	A_v (in^2)	P_{assume} (kip)	θ_{assume} (rad)
0	2.04	4.6	4.6	2.5	0.4	250	0.6231
10.44	2.04	4.6	4.6	7	0.4	250	0.6424
20.88	2.04	4.6	4.6	8.75	0.4	250	0.6390
31.32	2.04	4.6	4.6	15	0.4	250	0.5734
41.75	2.04	4.6	4.6	15	0.4	250	0.5344
48.54	2.04	4.6	4.6	15	0.4	250	0.5201
52.19	2.04	4.6	4.6	15	0.4	250	0.5167
55.85	2.04	4.6	4.6	15	0.4	250	0.5136
62.63	2.04	4.6	4.6	15	0.4	250	0.5082
73.07	1.2	4.5	4.5	15	0.4	250	0.5087
83.51	0	0	0	15	0.4	250	0.5130
93.95	0	0	0	15	0.4	250	0.5056
104.39	0	0	0	15	0.4	250	0.4789

C.3.1.5.2 Basic Geometry and Material Calculations

x_{dist} (in)	d_s (in)	$A_{ps.bot}$ (in^2)	cg_{harp} (in)
0.00	49.90	4.28	40.32
10.44	49.90	4.28	39.14
20.88	49.90	4.28	37.95
31.32	49.90	4.28	36.77
41.75	49.90	4.28	35.58
48.54	49.90	4.28	34.81
52.19	49.90	4.28	34.40
55.85	49.90	4.28	33.99
62.63	49.90	4.28	33.22
73.07	50.00	4.28	32.03
83.51	54.50	4.28	30.85
93.95	54.50	4.28	29.66
104.39	54.50	4.59	28.48

h_c (in)	L_{span} (ft)	A_{ps} (in^2)	Ψ_{harp} (rad)	f_{po} (ksi)	$f_{r.V}$ (psi)	β_1
54.5	57.875	5.202	0.1129	189	595.315	0.8055

C.3.1.5.3 Load Effect Calculations

x_{dist} (in)	V_{LL} (kip)	M_{LL} (ft-kip)	V_{DC1} (kip)	M_{DC1} (ft-kip)	V_{assume} (kip)	$M_{assume1}$ (ft-kip)	M_{assume} (ft-kip)	V_p (kip)
0.0	709.0	0.0	41.9	-0.2	751.0	-0.2	3003.4	3.5
10.4	295.9	257.4	40.7	35.7	336.6	293.2	1320.0	9.5
20.9	254.6	442.9	39.4	70.6	294.0	513.5	1125.4	15.6
31.3	196.9	513.9	38.1	104.3	235.1	618.2	880.4	17.4
41.8	215.3	749.3	36.9	136.9	252.2	886.2	949.9	17.4
48.5	223.2	903.0	36.1	157.6	259.3	1060.5	1060.5	17.4
52.2	225.4	980.4	35.6	168.5	261.0	1148.9	1148.9	17.4
55.8	227.5	1058.7	35.2	179.3	262.7	1238.0	1238.0	17.4
62.6	231.0	1205.9	34.4	198.9	265.4	1404.8	1404.8	17.4
73.1	232.8	1417.5	33.1	228.3	265.9	1645.8	1645.8	17.4
83.5	232.8	1619.8	31.8	256.5	264.6	1876.3	1876.3	17.4
93.9	237.8	1861.8	30.6	283.7	268.4	2145.4	2145.4	17.4
104.4	245.0	2131.2	29.3	309.7	274.3	2440.9	2440.9	17.4

C.3.1.5.4 Calculations for β and θ

x_{dist} (in)	cg_{ps} (in)	d_p (in)	c (in)	a (in)	$f_{ps.max}$ (ksi)	$l_{d.ps}$ (in)	f_{ps} (ksi)	$cg_{ps.bot}$ (in)	$d_{p.bot}$ (in)	$d_{s.bot}$ (in)	$Num_{strand.bot}$	$RedFactor_{\cdot x.s}$	$RedFactor_{\cdot x.ps}$
0.00	3.78	44.36	5.33	4.30	260.9	119.24	33.56	3.68	50.82	49.90	28.00	0.34	0.05
10.44	3.78	44.56	5.33	4.30	261.0	119.27	91.95	3.68	50.82	49.90	28.00	0.94	0.14
20.88	3.78	44.77	5.33	4.30	261.0	119.30	150.33	3.68	50.82	49.90	28.00	1.00	0.23
31.32	3.78	44.98	5.33	4.30	261.0	119.33	175.44	3.68	50.82	49.90	28.00	1.00	0.31
41.75	3.78	45.19	5.34	4.30	261.1	119.37	186.33	3.68	50.82	49.90	28.00	1.00	0.40
48.54	3.78	45.33	5.34	4.30	261.1	119.39	193.41	3.68	50.82	49.90	28.00	1.00	0.46
52.19	3.78	45.40	5.34	4.30	261.1	119.40	197.23	3.68	50.82	49.90	28.00	1.00	0.49
55.85	3.78	45.47	5.34	4.30	261.1	119.41	201.05	3.68	50.82	49.90	28.00	1.00	0.52
62.63	3.78	45.61	5.34	4.30	261.2	119.43	208.13	3.68	50.82	49.90	28.00	1.00	0.57
73.07	3.78	45.82	5.14	4.14	261.5	119.73	219.06	3.68	50.82	50.00	28.00	1.00	0.66
83.51	3.78	46.03	4.85	3.90	262.0	120.14	230.02	3.68	50.82	54.50	28.00	1.00	0.75
93.95	3.78	46.24	4.85	3.90	262.1	120.17	240.93	3.68	50.82	54.50	28.00	1.00	0.83
104.39	3.78	46.44	4.85	3.91	262.1	120.19	251.85	5.20	49.30	54.50	30.00	1.00	0.92

x_{dist} (in)	$A_{ps.bot}$ (in^2)	d_e (in)	ε_s	d_v (in)	v_u	$A_{s.bot.\cdot x}$ (in^2)	$A_{ps.bot.\cdot x}$ (in^2)	ε_x	θ (rad)	β	$MinReinfCheck$
0.00	4.28	50.36	0.03	48.22	0.250	0.70	0.22	0.0232	0.6231	1.50	OK
10.44	4.28	50.58	0.03	48.43	0.109	1.92	0.59	0.0030	0.6424	2.16	OK
20.88	4.28	50.65	0.03	48.51	0.093	2.04	0.97	0.0016	0.6390	2.19	OK
31.32	4.28	50.67	0.03	48.53	0.072	2.04	1.34	0.0007	0.5734	2.44	OK
41.75	4.28	50.68	0.03	48.53	0.078	2.04	1.71	0.0005	0.5344	2.57	OK
48.54	4.28	50.69	0.03	48.54	0.080	2.04	1.96	0.0005	0.5201	2.64	OK
52.19	4.28	50.69	0.03	48.54	0.081	2.04	2.09	0.0004	0.5167	2.65	OK
55.85	4.28	50.69	0.03	48.54	0.082	2.04	2.22	0.0004	0.5136	2.66	OK
62.63	4.28	50.69	0.03	48.55	0.082	2.04	2.46	0.0004	0.5082	2.69	OK
73.07	4.28	50.75	0.03	48.69	0.082	1.20	2.83	0.0004	0.5087	2.68	OK
83.51	4.28	50.82	0.03	48.87	0.082	0.00	3.19	0.0004	0.5130	2.67	OK
93.95	4.28	50.82	0.03	48.87	0.083	0.00	3.56	0.0004	0.5056	2.70	OK
104.39	4.59	49.30	0.03	47.35	0.088	0.00	4.22	0.0003	0.4789	2.80	OK

C.3.1.5.5 Final Results for Shear Strength

x_{dist} (in)	V_c (kip)	V_s (kip)	V_{n1} (kip)	V_{n2} (kip)	V_n (kip)
0.00	47.6	749.4	800.5	751.1	751.1
10.44	68.9	258.1	336.6	760.4	336.6
20.88	70.1	208.3	294.0	767.6	294.0
31.32	77.8	139.9	235.1	769.8	235.1
41.75	82.2	152.6	252.2	769.9	252.2
48.54	84.2	157.7	259.3	769.9	259.3
52.19	84.7	159.0	261.1	770.0	261.1
55.85	85.1	160.2	262.7	770.0	262.7
62.63	85.8	162.2	265.4	770.1	265.4
73.07	86.0	162.5	265.9	772.2	265.9
83.51	85.8	161.5	264.6	775.1	264.6
93.95	86.8	164.3	268.4	775.1	268.4
104.39	87.2	169.7	274.4	751.5	274.4

C.3.1.6 Beam BT.8N.Typ.2

C.3.1.6.1 Inputs

γ_c (pcf)	150
f_c' (psi)	8570
f_{ci}' (psi)	6183
$f_{c.deck}$ (psi)	4990
$\gamma_{c.deck}$ (pcf)	127
E_{beam} (ksi)	4950
$E_{beam.i}$ (ksi)	4670
E_{slab} (ksi)	3110
h (in)	45
A_{beam} (in^2)	746.7
I_{beam} (in^4)	207300
L_{beam} (ft)	58.875
b_v (in)	7
y_b (in)	22.23
y_t (in)	22.77
S (ft)	7
t_{haunch} (in)	1

t_{struct} (in)	8.5
A_{ct} (in^2)	423.25
h_{flange} (in)	8.5
Num_{strand}	34
$Num_{straight}$	28
$Num_{straight.bot}$	28
Num_{harp}	6
$cg_{straight}$ (in)	3.68
$cg_{harp.end}$ (in)	41
$cg_{harp.ms}$ (in)	4.25
$cg_{straight.bot}$ (in)	3.68
A_{strand} (in^2)	0.153
φ (in)	0.5
f_{pu} (ksi)	270
f_{pe} (ksi)	167.8
E_p (ksi)	28500
$HarpDist$ (ft)	26.5

f_y (ksi)	69.8
f_{yv} (ksi)	69.8
E_s (ksi)	29000
α	1.57
$A_{s.top}$ (in^2)	0
d_{top} (in)	9.5
$d_{long.rebar}$	5
$IsLongSteelEpoxyCoated$	No
$LongSteelClearSpacing$ (in)	3.75
$LongSteelCover$ (in)	2
$IsTopBarEffectApplicable$	No
$A_{long.rebar}$ (in2)	0.31
$ShearSpan$ (in)	152.62
$x_{bearing}$ (in)	6
$x_{bearing.roller}$ (in)	113
$x_{critical.assume}$ (in)	49.12

x_{dist} (in)	A_{ct} (in^2)	$cg_{s.bot}$ (in)	cg_s (in)	$s_{v.design}$ (in)	A_v (in^2)	P_{assume} (kip)	θ_{assume} (rad)
0	2.04	4.6	4.6	2.5	0.4	250	0.62
15.26	2.04	4.6	4.6	8.75	0.4	250	0.64
30.52	2.04	4.6	4.6	15	0.4	250	0.5800
45.78	2.04	4.6	4.6	15	0.4	250	0.52
48.58	2.04	4.6	4.6	15	0.4	250	0.52
61.05	2.04	4.6	4.6	15	0.4	250	0.51
76.31	2.04	4.6	4.6	15	0.4	250	0.5
91.57	0	0	0	15	0.4	250	0.51
104.04	0	0	0	18	0.4	250	0.45
106.83	0	0	0	18	0.4	250	0.45
122.09	0	0	0	18	0.4	250	0.4400
137.35	0	0	0	18	0.4	250	0.45
152.62	0	0	0	18	0.4	250	0.47

C.3.1.6.2 Basic Geometry and Material Calculations

x_{dist} (in)	d_s (in)	$A_{ps.bot}$ (in^2)	cg_{harp} (in)
0.00	49.90	4.28	40.32
15.26	49.90	4.28	38.59
30.52	49.90	4.28	36.86
45.78	49.90	4.28	35.13
48.58	49.90	4.28	34.81
61.05	49.90	4.28	33.40
76.31	49.90	4.28	31.66
91.57	54.50	4.28	29.93
104.04	54.50	4.59	28.52
106.83	54.50	4.59	28.20
122.09	54.50	4.90	26.47
137.35	54.50	5.20	24.74
152.62	54.50	5.20	23.01

h_c (in)	L_{span} (ft)	A_{ps} (in^2)	Ψ_{harp} (rad)	f_{po} (ksi)	$f_{r.V}$ (psi)	β_1
54.5	48.9583	5.202	0.1129	189	585.5	0.8005

C.3.1.6.3 Load Effect Calculations

x_{dist} (in)	V_{LL} (kip)	M_{LL} (ft-kip)	V_{DC1} (kip)	M_{DC1} (ft-kip)	V_{assume} (kip)	$M_{assume1}$ (ft-kip)	M_{assume} (ft-kip)	V_p (kip)
0.0	693.0	0.0	34.2	-0.2	727.2	-0.2	2910.2	3.5
15.3	256.9	326.7	32.3	42.1	289.2	368.8	1119.5	12.3
30.5	202.5	515.0	30.5	82.0	232.9	597.0	872.5	17.4
45.8	228.4	871.3	28.6	119.6	257.0	990.9	990.9	17.4
48.6	230.1	931.5	28.3	126.2	258.4	1057.7	1057.7	17.4
61.0	237.0	1205.7	26.8	154.9	263.8	1360.6	1360.6	17.4
76.3	244.2	1552.7	24.9	187.8	269.1	1740.5	1740.5	17.4
91.6	243.6	1859.2	23.1	218.3	266.7	2077.5	2077.5	17.4
104.0	239.4	2075.2	21.6	241.5	261.0	2316.7	2316.7	17.4
106.8	240.6	2142.2	21.3	246.5	261.9	2388.8	2388.8	17.4
122.1	241.2	2453.6	19.4	272.4	260.6	2726.0	2726.0	17.4
137.4	234.1	2679.6	17.6	295.9	251.7	2975.5	2975.5	17.4
152.6	225.4	2866.5	15.7	317.1	241.1	3183.6	3183.6	17.4

C.3.1.6.4 Calculations for β and θ

x_{dist} (in)	cg_{ps} (in)	d_p (in)	c (in)	a (in)	$f_{ps.max}$ (ksi)	$l_{d.ps}$ (in)	f_{ps} (ksi)	$cg_{ps.bot}$ (in)	$d_{p.bot}$ (in)	$d_{s.bot}$ (in)	$Num_{strand.bot}$	$RedFactor_{\cdot x.s}$	$RedFactor_{\cdot x.ps}$
0.00	3.78	44.36	5.26	4.21	261.0	119.33	33.56	3.68	50.82	49.90	28.00	0.34	0.05
15.26	3.78	44.66	5.26	4.21	261.1	119.38	118.92	3.68	50.82	49.90	28.00	1.00	0.18
30.52	3.78	44.97	5.26	4.21	261.2	119.43	174.61	3.68	50.82	49.90	28.00	1.00	0.31
45.78	3.78	45.27	5.26	4.21	261.2	119.47	190.54	3.68	50.82	49.90	28.00	1.00	0.43
48.58	3.78	45.33	5.26	4.21	261.2	119.48	193.46	3.68	50.82	49.90	28.00	1.00	0.46
61.05	3.78	45.58	5.26	4.21	261.3	119.52	206.48	3.68	50.82	49.90	28.00	1.00	0.56
76.31	3.78	45.88	5.27	4.22	261.3	119.57	222.42	3.68	50.82	49.90	28.00	1.00	0.69
91.57	3.78	46.19	4.78	3.83	262.2	120.25	238.46	3.68	50.82	54.50	28.00	1.00	0.81
104.04	3.78	46.44	4.78	3.83	262.2	120.28	251.50	5.20	49.30	54.50	30.00	1.00	0.91
106.83	3.78	46.49	4.78	3.83	262.2	120.29	254.43	5.18	49.32	54.50	30.00	1.00	0.94
122.09	3.78	46.80	4.78	3.83	262.3	120.32	262.27	6.40	48.10	54.50	32.00	1.00	1.00
137.35	3.78	47.10	4.78	3.83	262.3	120.36	262.32	7.40	47.10	54.50	34.00	1.00	1.00
152.62	3.78	47.41	4.79	3.83	262.4	120.40	262.37	7.09	47.41	54.50	34.00	1.00	1.00

x_{dist} (in)	$A_{ps.bot}$ (in^2)	d_e (in)	ε_s	d_v (in)	v_u	$A_{s.bot.\cdot x}$ (in^2)	$A_{ps.bot.\cdot x}$ (in^2)	ε_x	θ (rad)	β	$MinReinfCheck$
0.00	4.28	50.36	0.03	48.26	0.250	0.70	0.22	0.0224	0.6231	1.50	OK
15.26	4.28	50.62	0.03	48.51	0.095	2.04	0.76	0.0020	0.6395	2.19	OK
30.52	4.28	50.67	0.03	48.57	0.074	2.04	1.31	0.0007	0.5758	2.43	OK
45.78	4.28	50.68	0.03	48.58	0.082	2.04	1.86	0.0005	0.5220	2.62	OK
48.58	4.28	50.69	0.03	48.58	0.083	2.04	1.96	0.0004	0.5192	2.63	OK
61.05	4.28	50.69	0.03	48.59	0.085	2.04	2.40	0.0004	0.5085	2.68	OK
76.31	4.28	50.70	0.03	48.59	0.086	2.04	2.95	0.0004	0.4982	2.72	OK
91.57	4.28	50.82	0.03	48.91	0.085	0.00	3.48	0.0004	0.5059	2.69	OK
104.04	4.59	49.30	0.03	47.38	0.086	0.00	4.20	0.0002	0.4493	2.97	OK
106.83	4.59	49.32	0.03	47.41	0.086	0.00	4.31	0.0002	0.4477	2.98	OK
122.09	4.90	48.10	0.03	46.18	0.088	0.00	4.90	0.0002	0.4381	3.02	OK
137.35	5.20	47.10	0.03	45.19	0.086	0.00	5.20	0.0002	0.4453	2.99	OK
152.62	5.20	47.41	0.03	45.49	0.082	0.00	5.20	0.0003	0.4694	2.87	OK

C.3.1.6.5 Final Results for Shear Strength

x_{dist} (in)	V_c (kip)	V_s (kip)	V_{n1} (kip)	V_{n2} (kip)	V_n (kip)
0.00	46.9	750.0	800.4	727.2	727.2
15.26	68.8	208.1	289.2	739.9	289.2
30.52	76.3	139.3	232.9	745.8	232.9
45.78	82.4	157.2	257.0	745.9	257.0
48.58	82.8	158.2	258.4	745.9	258.4
61.05	84.2	162.3	263.8	746.0	263.8
76.31	85.5	166.3	269.1	746.2	269.1
91.57	85.1	164.3	266.8	750.9	266.8
104.04	91.2	152.4	261.0	728.0	261.0
106.83	91.5	153.1	261.9	728.3	261.9
122.09	90.3	152.9	260.6	710.0	260.6
137.35	87.5	146.9	251.8	695.1	251.8
152.62	84.7	139.1	241.2	699.7	241.2

C.3.1.7 Beam BT.8.Typ.1

C.3.1.7.1 Inputs

γ_c (pcf)	125.8
f_c' (psi)	9080
f_{ci}' (psi)	6330
$f_{c.deck}$ (psi)	5580
$\gamma_{c.deck}$ (pcf)	128.4
E_{beam} (ksi)	3590
$E_{beam.i}$ (ksi)	3790
E_{slab} (ksi)	3600
h (in)	45
A_{beam} (in^2)	746.7
I_{beam} (in^4)	207300
L_{beam} (ft)	59
b_v (in)	7
y_b (in)	22.23
y_t (in)	22.77
S (ft)	7
t_{haunch} (in)	1

t_{struct} (in)	8.5
A_{ct} (in^2)	423.25
h_{flange} (in)	8.5
Num_{strand}	34
$Num_{straight}$	28
$Num_{straight.bot}$	28
Num_{harp}	6
$cg_{straight}$ (in)	3.68
$cg_{harp.end}$ (in)	41
$cg_{harp.ms}$ (in)	4.25
$cg_{straight.bot}$ (in)	3.68
A_{strand} (in^2)	0.153
φ (in)	0.5
f_{pu} (ksi)	270
f_{pe} (ksi)	175.09
E_p (ksi)	28500
$HarpDist$ (ft)	26.5

f_y (ksi)	67.3
f_{yv} (ksi)	67.3
E_s (ksi)	29000
α	1.57
$A_{s.top}$ (in^2)	0
d_{top} (in)	9.5
$d_{long.rebar}$	5
$IsLongSteelEpoxyCoated$	No
$LongSteelClearSpacing$ (in)	3.75
$LongSteelCover$ (in)	2
$IsTopBarEffectApplicable$	No
$A_{long.rebar}$ (in2)	0.31
$ShearSpan$ (in)	102.10
$x_{bearing}$ (in)	6
$x_{bearing.roller}$ (in)	6
$x_{critical.assume}$ (in)	44.15

x_{dist} (in)	A_{ct} (in^2)	$cg_{s.bot}$ (in)	cg_s (in)	$s_{v.design}$ (in)	A_v (in^2)	P_{assume} (kip)	θ_{assume} (rad)
0	2.48	4.5	4.5	2.5	0.4	250	0.62
10.21	2.48	4.5	4.5	5.75	0.4	250	0.64
20.42	2.48	4.5	4.5	9	0.4	250	0.6400
30.63	2.48	4.5	4.5	9	0.4	250	0.63
40.84	2.48	4.5	4.5	9	0.4	250	0.59
48.77	2.48	4.5	4.5	9	0.4	250	0.58
51.05	2.48	4.5	4.5	9	0.4	250	0.57
53.33	2.48	4.5	4.5	9	0.4	250	0.57
61.26	2.48	4.5	4.5	9	0.4	250	0.57
71.47	2.48	4.5	4.5	9	0.4	250	0.56
81.68	0	0	0	9	0.4	250	0.5900
91.89	0	0	0	9	0.4	250	0.59
102.10	0	0	0	10	0.4	250	0.54

C.3.1.7.2 Basic Geometry and Material Calculations

x_{dist} (in)	d_s (in)	$A_{ps.bot}$ (in^2)	cg_{harp} (in)
0.00	50.00	4.28	40.32
10.21	50.00	4.28	39.16
20.42	50.00	4.28	38.00
30.63	50.00	4.28	36.85
40.84	50.00	4.28	35.69
48.77	50.00	4.28	34.79
51.05	50.00	4.28	34.53
53.33	50.00	4.28	34.27
61.26	50.00	4.28	33.37
71.47	50.00	4.28	32.21
81.68	54.50	4.28	31.05
91.89	54.50	4.28	29.90
102.10	54.50	4.59	28.74

h_c (in)	L_{span} (ft)	A_{ps} (in^2)	Ψ_{harp} (rad)	f_{po} (ksi)	$f_{r.V}$ (psi)	β_1
54.5	58	5.202	0.1129	189	602.7	0.771

C.3.1.7.3 Load Effect Calculations

x_{dist} (in)	V_{LL} (kip)	M_{LL} (ft-kip)	V_{DC1} (kip)	M_{DC1} (ft-kip)	V_{assume} (kip)	$M_{assume1}$ (ft-kip)	M_{assume} (ft-kip)	V_p (kip)
0.0	735.2	0.0	38.6	-0.2	773.8	-0.2	3110.9	3.6
10.2	344.7	293.3	37.5	32.2	382.1	325.4	1510.0	9.8
20.4	248.0	422.1	36.3	63.6	284.4	485.6	1090.1	16.0
30.6	257.1	656.1	35.2	94.0	292.3	750.2	1113.9	18.1
40.8	276.4	940.8	34.1	123.5	310.5	1064.3	1188.2	18.1
48.8	287.3	1167.8	33.2	145.7	320.5	1313.5	1313.5	18.1
51.0	288.4	1226.9	32.9	152.0	321.3	1378.9	1378.9	18.1
53.3	289.4	1286.3	32.7	158.2	322.1	1444.5	1444.5	18.1
61.3	292.8	1494.9	31.8	179.5	324.6	1674.4	1674.4	18.1
71.5	296.8	1767.4	30.7	206.1	327.4	1973.5	1973.5	18.1
81.7	283.0	1926.3	29.5	231.7	312.5	2158.0	2158.0	18.1
91.9	288.0	2205.1	28.4	256.4	316.4	2461.4	2461.4	18.1
102.1	284.3	2418.8	27.3	280.0	311.6	2698.8	2698.8	18.1

C.3.1.7.4 Calculations for β and θ

x_{dist} (in)	cg_{ps} (in)	d_p (in)	c (in)	a (in)	$f_{ps.max}$ (ksi)	$l_{d.ps}$ (in)	f_{ps} (ksi)	$cg_{ps.bot}$ (in)	$d_{p.bot}$ (in)	$d_{s.bot}$ (in)	$Num_{strand.bot}$	$RedFactor_{\cdot x.s}$	$RedFactor_{\cdot x.ps}$
0.00	3.78	44.36	4.97	3.83	261.5	115.84	35.02	3.68	50.82	50.00	28.00	0.36	0.05
10.21	3.78	44.56	4.97	3.83	261.6	115.87	94.61	3.68	50.82	50.00	28.00	0.96	0.14
20.42	3.78	44.76	4.97	3.83	261.6	115.90	154.20	3.68	50.82	50.00	28.00	1.00	0.23
30.63	3.78	44.97	4.97	3.84	261.6	115.93	181.77	3.68	50.82	50.00	28.00	1.00	0.32
40.84	3.78	45.17	4.97	3.84	261.7	115.96	192.05	3.68	50.82	50.00	28.00	1.00	0.40
48.77	3.78	45.33	4.98	3.84	261.7	115.98	200.04	3.68	50.82	50.00	28.00	1.00	0.47
51.05	3.78	45.38	4.98	3.84	261.7	115.99	202.34	3.68	50.82	50.00	28.00	1.00	0.49
53.33	3.78	45.42	4.98	3.84	261.7	115.99	204.64	3.68	50.82	50.00	28.00	1.00	0.51
61.26	3.78	45.58	4.98	3.84	261.7	116.02	212.63	3.68	50.82	50.00	28.00	1.00	0.58
71.47	3.78	45.79	4.98	3.84	261.8	116.04	222.92	3.68	50.82	50.00	28.00	1.00	0.67
81.68	3.78	45.99	4.45	3.43	262.7	116.77	233.32	3.68	50.82	54.50	28.00	1.00	0.75
91.89	3.78	46.19	4.45	3.43	262.7	116.79	243.63	3.68	50.82	54.50	28.00	1.00	0.84
102.10	3.78	46.40	4.45	3.43	262.8	116.82	253.95	5.22	49.28	54.50	30.00	1.00	0.93

x_{dist} (in)	$A_{ps.bot}$ (in^2)	d_e (in)	ε_s	d_v (in)	v_u	$A_{s.bot.\cdot x}$ (in^2)	$A_{ps.bot.\cdot x}$ (in^2)	ε_x	θ (rad)	β	$MinReinfCheck$
0.00	4.28	50.39	0.03	48.47	0.250	0.88	0.22	0.0198	0.6231	1.50	OK
10.21	4.28	50.58	0.03	48.66	0.120	2.39	0.60	0.0029	0.6448	2.14	OK
20.42	4.28	50.66	0.03	48.74	0.087	2.48	0.98	0.0013	0.6377	2.21	OK
30.63	4.28	50.68	0.03	48.76	0.089	2.48	1.35	0.0009	0.6267	2.24	OK
40.84	4.28	50.68	0.03	48.77	0.094	2.48	1.73	0.0008	0.5927	2.33	OK
48.77	4.28	50.69	0.03	48.77	0.098	2.48	2.02	0.0007	0.5753	2.38	OK
51.05	4.28	50.69	0.03	48.77	0.098	2.48	2.11	0.0007	0.5740	2.39	OK
53.33	4.28	50.69	0.03	48.77	0.098	2.48	2.19	0.0007	0.5726	2.39	OK
61.26	4.28	50.69	0.03	48.78	0.099	2.48	2.48	0.0006	0.5684	2.40	OK
71.47	4.28	50.70	0.03	48.78	0.100	2.48	2.86	0.0006	0.5638	2.42	OK
81.68	4.28	50.82	0.03	49.11	0.094	0.00	3.22	0.0008	0.5927	2.33	OK
91.89	4.28	50.82	0.03	49.11	0.096	0.00	3.59	0.0007	0.5860	2.35	OK
102.10	4.59	49.28	0.03	47.57	0.097	0.00	4.25	0.0005	0.5391	2.50	OK

C.3.1.7.5 Final Results for Shear Strength

x_{dist} (in)	V_c (kip)	V_s (kip)	V_{n1} (kip)	V_{n2} (kip)	V_n (kip)
0.00	48.5	726.4	778.5	773.8	773.8
10.21	69.4	303.0	382.1	783.1	382.1
20.42	71.7	196.7	284.4	790.4	284.4
30.63	72.7	201.4	292.3	792.9	292.3
40.84	75.8	216.6	310.5	793.0	310.5
48.77	77.5	224.9	320.5	793.1	320.5
51.05	77.6	225.6	321.3	793.1	321.3
53.33	77.7	226.3	322.1	793.1	322.1
61.26	78.1	228.4	324.6	793.2	324.6
71.47	78.6	230.8	327.4	793.2	327.4
81.68	76.3	218.1	312.6	798.4	312.6
91.89	77.0	221.3	316.4	798.4	316.4
102.10	79.4	214.1	311.6	774.0	311.6

C.3.1.8 Beam BT.8.Typ.2

C.3.1.8.1 Inputs

γ_c (pcf)	125.8
f_c' (psi)	9080
f_{ci}' (psi)	6330
$f_{c.deck}$ (psi)	6690
$\gamma_{c.deck}$ (pcf)	135.8
E_{beam} (ksi)	3590
$E_{beam.i}$ (ksi)	3790
E_{slab} (ksi)	4050
h (in)	45
A_{beam} (in^2)	746.7
I_{beam} (in^4)	207300
L_{beam} (ft)	59
b_v (in)	7
y_b (in)	22.23
y_t (in)	22.77
S (ft)	7
t_{haunch} (in)	1

t_{struct} (in)	8.5
A_{ct} (in^2)	423.25
h_{flange} (in)	8.5
Num_{strand}	34
$Num_{straight}$	28
$Num_{straight.bot}$	28
Num_{harp}	6
$cg_{straight}$ (in)	3.68
$cg_{harp.end}$ (in)	41
$cg_{harp.ms}$ (in)	4.25
$cg_{straight.bot}$ (in)	3.68
A_{strand} (in^2)	0.153
φ (in)	0.5
f_{pu} (ksi)	270
f_{pe} (ksi)	175.09
E_p (ksi)	28500
$HarpDist$ (ft)	26.5

f_y (ksi)	67.3
f_{yv} (ksi)	67.3
E_s (ksi)	29000
α	1.57
$A_{s.top}$ (in^2)	0
d_{top} (in)	9.5
$d_{long.rebar}$	5
$IsLongSteelEpoxyCoated$	No
$LongSteelClearSpacing$ (in)	3.75
$LongSteelCover$ (in)	2
$IsTopBarEffectApplicable$	No
$A_{long.rebar}$ (in2)	0.31
$ShearSpan$ (in)	153.28
$x_{bearing}$ (in)	6
$x_{bearing.roller}$ (in)	108.5
$x_{critical.assume}$ (in)	44.35

x_{dist} (in)	A_{ct} (in^2)	$cg_{s.bot}$ (in)	cg_s (in)	$s_{v.design}$ (in)	A_v (in^2)	P_{assume} (kip)	θ_{assume} (rad)
0	2.48	4.5	4.5	2.5	0.4	250	0.62
15.33	2.48	4.5	4.5	5.75	0.4	250	0.64
30.66	2.48	4.5	4.5	9	0.4	250	0.6200
45.98	2.48	4.5	4.5	9	0.4	250	0.57
49.08	2.48	4.5	4.5	9	0.4	250	0.57
61.31	2.48	4.5	4.5	9	0.4	250	0.56
76.64	0	0	0	9	0.4	250	0.59
91.97	0	0	0	10	0.4	250	0.56
104.19	0	0	0	10	0.4	250	0.53
107.29	0	0	0	10	0.4	250	0.53
122.62	0	0	0	10	0.4	250	0.5300
137.95	0	0	0	10	0.4	250	0.54
153.28	0	0	0	10	0.4	250	0.56

C.3.1.8.2 Basic Geometry and Material Calculations

x_{dist} (in)	d_s (in)	$A_{ps.bot}$ (in^2)	cg_{harp} (in)
0.00	50.00	4.28	40.32
15.33	50.00	4.28	38.58
30.66	50.00	4.28	36.84
45.98	50.00	4.28	35.10
49.08	50.00	4.28	34.75
61.31	50.00	4.28	33.37
76.64	54.50	4.28	31.63
91.97	54.50	4.28	29.89
104.19	54.50	4.59	28.50
107.29	54.50	4.59	28.15
122.62	54.50	4.90	26.41
137.95	54.50	5.20	24.67
153.28	54.50	5.20	22.93

h_c (in)	L_{span} (ft)	A_{ps} (in^2)	Ψ_{harp} (rad)	f_{po} (ksi)	$f_{r.V}$ (psi)	β_1
54.5	49.4583	5.202	0.1129	189	602.7	0.7155

C.3.1.8.3 Load Effect Calculations

x_{dist} (in)	V_{LL} (kip)	M_{LL} (ft-kip)	V_{DC1} (kip)	M_{DC1} (ft-kip)	V_{assume} (kip)	$M_{assume1}$ (ft-kip)	M_{assume} (ft-kip)	V_p (kip)
0.0	743.4	0.0	32.7	-0.2	776.2	-0.2	3140.8	3.6
15.3	347.1	443.3	31.0	40.5	378.1	483.8	1491.8	12.9
30.7	256.9	656.4	29.3	79.0	286.2	735.4	1096.3	18.1
46.0	286.0	1096.1	27.5	115.3	313.5	1211.4	1211.4	18.1
49.1	287.6	1176.4	27.1	122.3	314.8	1298.7	1298.7	18.1
61.3	293.2	1497.8	25.8	149.3	318.9	1647.0	1647.0	18.1
76.6	281.5	1797.7	24.0	181.0	305.5	1978.8	1978.8	18.1
92.0	278.5	2134.3	22.3	210.6	300.7	2344.9	2344.9	18.1
104.2	286.7	2489.5	20.9	232.5	307.6	2722.1	2722.1	18.1
107.3	288.1	2576.4	20.5	237.9	308.6	2814.3	2814.3	18.1
122.6	282.8	2890.2	18.8	263.0	301.6	3153.2	3153.2	18.1
137.9	273.6	3145.2	17.0	285.8	290.6	3431.0	3431.0	18.1
153.3	263.6	3366.5	15.3	306.4	278.8	3672.9	3672.9	18.1

C.3.1.8.4 Calculations for β and θ

x_{dist} (in)	cg_{ps} (in)	d_p (in)	c (in)	a (in)	$f_{ps.max}$ (ksi)	$l_{d.ps}$ (in)	f_{ps} (ksi)	$cg_{ps.bot}$ (in)	$d_{p.bot}$ (in)	$d_{s.bot}$ (in)	$Num_{strand.bot}$	$RedFactor_{\cdot x.s}$	$RedFactor_{\cdot x.ps}$
0.00	3.78	44.36	4.48	3.21	262.4	116.51	35.02	3.68	50.82	50.00	28.00	0.30	0.05
15.33	3.78	44.66	4.48	3.21	262.4	116.55	124.48	3.68	50.82	50.00	28.00	1.00	0.18
30.66	3.78	44.97	4.48	3.21	262.5	116.59	181.81	3.68	50.82	50.00	28.00	1.00	0.31
45.98	3.78	45.28	4.48	3.21	262.5	116.63	197.27	3.68	50.82	50.00	28.00	1.00	0.45
49.08	3.78	45.34	4.48	3.21	262.5	116.64	200.40	3.68	50.82	50.00	28.00	1.00	0.47
61.31	3.78	45.58	4.48	3.21	262.6	116.67	212.75	3.68	50.82	50.00	28.00	1.00	0.58
76.64	3.78	45.89	4.01	2.87	263.4	117.33	228.31	3.68	50.82	54.50	28.00	1.00	0.70
91.97	3.78	46.20	4.01	2.87	263.4	117.37	243.82	3.68	50.82	54.50	28.00	1.00	0.83
104.19	3.78	46.44	4.01	2.87	263.5	117.40	256.19	5.20	49.30	54.50	30.00	1.00	0.94
107.29	3.78	46.50	4.01	2.87	263.5	117.40	259.32	5.18	49.32	54.50	30.00	1.00	0.97
122.62	3.78	46.81	4.01	2.87	263.5	117.44	263.52	6.40	48.10	54.50	32.00	1.00	1.00
137.95	3.78	47.12	4.01	2.87	263.6	117.47	263.56	7.38	47.12	54.50	34.00	1.00	1.00
153.28	3.78	47.42	4.01	2.87	263.6	117.50	263.60	7.08	47.42	54.50	34.00	1.00	1.00

x_{dist} (in)	$A_{ps.bot}$ (in^2)	d_e (in)	ε_s	d_v (in)	v_u	$A_{s.bot.\cdot x}$ (in^2)	$A_{ps.bot.\cdot x}$ (in^2)	ε_x	θ (rad)	β	$MinReinfCheck$
0.00	4.28	50.39	0.03	48.79	0.249	0.74	0.22	0.0229	0.6231	1.50	OK
15.33	4.28	50.63	0.03	49.02	0.117	2.48	0.78	0.0024	0.6441	2.15	OK
30.66	4.28	50.68	0.03	49.07	0.086	2.48	1.35	0.0009	0.6208	2.26	OK
45.98	4.28	50.69	0.03	49.08	0.095	2.48	1.91	0.0007	0.5709	2.40	OK
49.08	4.28	50.69	0.03	49.08	0.095	2.48	2.02	0.0006	0.5689	2.41	OK
61.31	4.28	50.69	0.03	49.09	0.096	2.48	2.47	0.0006	0.5619	2.43	OK
76.64	4.28	50.82	0.04	49.39	0.092	0.00	3.02	0.0007	0.5879	2.35	OK
91.97	4.28	50.82	0.04	49.39	0.090	0.00	3.58	0.0006	0.5565	2.46	OK
104.19	4.59	49.30	0.03	47.87	0.095	0.00	4.31	0.0005	0.5290	2.55	OK
107.29	4.59	49.32	0.03	47.89	0.096	0.00	4.43	0.0005	0.5275	2.55	OK
122.62	4.90	48.10	0.03	46.67	0.096	0.00	4.90	0.0005	0.5269	2.56	OK
137.95	5.20	47.12	0.03	45.68	0.094	0.00	5.20	0.0005	0.5357	2.52	OK
153.28	5.20	47.42	0.03	45.99	0.089	0.00	5.20	0.0006	0.5612	2.45	OK

C.3.1.8.5 Final Results for Shear Strength

x_{dist} (in)	V_c (kip)	V_s (kip)	V_{n1} (kip)	V_{n2} (kip)	V_n (kip)
0.00	41.6	731.1	776.3	778.8	776.3
15.33	59.6	305.6	378.1	791.8	378.1
30.66	62.8	205.3	286.2	797.9	286.2
45.98	66.9	228.6	313.6	798.0	313.6
49.08	67.0	229.6	314.8	798.1	314.8
61.31	67.6	233.2	318.9	798.2	318.9
76.64	65.8	221.6	305.6	802.9	305.6
91.97	68.9	213.7	300.8	802.9	300.8
104.19	69.1	220.4	307.6	778.7	307.6
107.29	69.3	221.3	308.7	779.1	308.7
122.62	67.6	216.0	301.7	759.7	301.7
137.95	65.3	207.2	290.6	744.0	290.6
153.28	63.8	197.0	278.9	748.9	278.9

C.3.1.9 Beam BT.10.Typ.1

C.3.1.9.1 Inputs

γ_c (pcf)	124.6
f_c' (psi)	8890
f_{ci}' (psi)	6120
$f_{c.deck}$ (psi)	4130
$\gamma_{c.deck}$ (pcf)	126.6
E_{beam} (ksi)	3910
$E_{beam.i}$ (ksi)	4230
E_{slab} (ksi)	3160
h (in)	45
A_{beam} (in^2)	746.7
I_{beam} (in^4)	207300
L_{beam} (ft)	58.9375
b_v (in)	7
y_b (in)	22.23
y_t (in)	22.77
S (ft)	7
t_{haunch} (in)	1

t_{struct} (in)	8.5
A_{ct} (in^2)	423.25
h_{flange} (in)	8.5
Num_{strand}	34
$Num_{straight}$	28
$Num_{straight.bot}$	28
Num_{harp}	6
$cg_{straight}$ (in)	3.68
$cg_{harp.end}$ (in)	41
$cg_{harp.ms}$ (in)	4.25
$cg_{straight.bot}$ (in)	3.68
A_{strand} (in^2)	0.153
φ (in)	0.5
f_{pu} (ksi)	270
f_{pe} (ksi)	173.34
E_p (ksi)	28500
$HarpDist$ (ft)	26.5

f_y (ksi)	67.3
f_{yv} (ksi)	67.3
E_s (ksi)	29000
α	1.57
$A_{s.top}$ (in^2)	0
d_{top} (in)	9.5
$d_{long.rebar}$	6
$IsLongSteelEpoxyCoated$	No
$LongSteelClearSpacing$ (in)	1
$LongSteelCover$ (in)	2
$IsTopBarEffectApplicable$	No
$A_{long.rebar}$ (in2)	0.31
$ShearSpan$ (in)	98.39
$x_{bearing}$ (in)	6
$x_{bearing.roller}$ (in)	6
$x_{critical.assume}$ (in)	44.18

x_{dist} (in)	A_{ct} (in^2)	$cg_{s.bot}$ (in)	cg_s (in)	$s_{v.design}$ (in)	A_v (in^2)	P_{assume} (kip)	θ_{assume} (rad)
0	3	4.95	4.95	2.5	0.4	250	0.62
9.84	3	4.95	4.95	7.75	0.4	250	0.64
19.68	3	4.95	4.95	10	0.4	250	0.6300
29.52	3	4.95	4.95	10	0.4	250	0.59
39.36	3	4.95	4.95	10	0.4	250	0.56
47.94	3	4.95	4.95	10	0.4	250	0.54
49.19	3	4.95	4.95	10	0.4	250	0.54
50.44	3	4.95	4.95	10	0.4	250	0.54
59.03	3	4.95	4.95	10	0.4	250	0.54
68.87	3	4.95	4.95	10	0.4	250	0.53
78.71	3	4.95	4.95	10	0.4	250	0.5300
88.55	1.76	5	5	10	0.4	250	0.54
98.39	0	0	0	12	0.4	250	0.49

C.3.1.9.2 Basic Geometry and Material Calculations

x_{dist} (in)	d_s (in)	$A_{ps.bot}$ (in^2)	cg_{harp} (in)
0.00	49.55	4.28	40.32
9.84	49.55	4.28	39.20
19.68	49.55	4.28	38.09
29.52	49.55	4.28	36.97
39.36	49.55	4.28	35.86
47.94	49.55	4.28	34.88
49.19	49.55	4.28	34.74
50.44	49.55	4.28	34.60
59.03	49.55	4.28	33.62
68.87	49.55	4.28	32.51
78.71	49.55	4.28	31.39
88.55	49.50	4.28	30.28
98.39	54.50	4.59	29.16

h_c (in)	L_{span} (ft)	A_{ps} (in^2)	Ψ_{harp} (rad)	f_{po} (ksi)	$f_{r.V}$ (psi)	β_1
54.5	57.9375	5.202	0.1129	189	596.3	0.8435

C.3.1.9.3 Load Effect Calculations

x_{dist} (in)	V_{LL} (kip)	M_{LL} (ft-kip)	V_{DC1} (kip)	M_{DC1} (ft-kip)	V_{assume} (kip)	$M_{assume1}$ (ft-kip)	M_{assume} (ft-kip)	V_p (kip)
0.0	703.7	0.0	38.1	-0.2	741.8	-0.2	2919.7	3.6
9.8	254.2	208.4	37.0	30.6	291.2	239.0	1121.2	9.5
19.7	216.7	355.4	35.9	60.5	252.7	416.0	947.0	15.4
29.5	237.0	582.9	34.9	89.6	271.8	672.5	1014.1	17.9
39.4	254.8	835.6	33.8	117.7	288.6	953.3	1081.1	17.9
47.9	265.6	1061.2	32.8	141.6	298.5	1202.8	1202.8	17.9
49.2	266.2	1091.2	32.7	145.0	298.9	1236.2	1236.2	17.9
50.4	266.8	1121.4	32.6	148.4	299.3	1269.8	1269.8	17.9
59.0	270.4	1330.4	31.6	171.3	302.1	1501.8	1501.8	17.9
68.9	274.5	1575.2	30.6	196.8	305.0	1772.0	1772.0	17.9
78.7	278.1	1824.2	29.5	221.4	307.6	2045.6	2045.6	17.9
88.6	276.3	2038.8	28.4	245.2	304.7	2284.0	2284.0	17.9
98.4	257.9	2114.3	27.3	268.0	285.2	2382.3	2382.3	17.9

C.3.1.9.4 Calculations for β and θ

x_{dist} (in)	cg_{ps} (in)	d_p (in)	c (in)	a (in)	$f_{ps.max}$ (ksi)	$l_{d.ps}$ (in)	f_{ps} (ksi)	$cg_{ps.bot}$ (in)	$d_{p.bot}$ (in)	$d_{s.bot}$ (in)	$Num_{strand.bot}$	$RedFactor_{\cdot x.s}$	$RedFactor_{\cdot x.ps}$
0.00	3.78	44.36	6.24	5.26	259.4	115.05	34.67	3.68	50.82	49.55	28.00	0.25	0.05
9.84	3.78	44.55	6.24	5.26	259.4	115.09	91.52	3.68	50.82	49.55	28.00	0.65	0.14
19.68	3.78	44.75	6.24	5.26	259.5	115.12	148.37	3.68	50.82	49.55	28.00	1.00	0.22
29.52	3.78	44.95	6.24	5.26	259.5	115.16	178.92	3.68	50.82	49.55	28.00	1.00	0.31
39.36	3.78	45.14	6.24	5.26	259.6	115.19	188.88	3.68	50.82	49.55	28.00	1.00	0.39
47.94	3.78	45.32	6.24	5.26	259.6	115.22	197.57	3.68	50.82	49.55	28.00	1.00	0.47
49.19	3.78	45.34	6.24	5.26	259.6	115.23	198.84	3.68	50.82	49.55	28.00	1.00	0.48
50.44	3.78	45.37	6.24	5.26	259.6	115.23	200.10	3.68	50.82	49.55	28.00	1.00	0.49
59.03	3.78	45.54	6.24	5.26	259.6	115.26	208.80	3.68	50.82	49.55	28.00	1.00	0.56
68.87	3.78	45.73	6.24	5.27	259.7	115.30	218.76	3.68	50.82	49.55	28.00	1.00	0.65
78.71	3.78	45.93	6.24	5.27	259.7	115.33	228.73	3.68	50.82	49.55	28.00	1.00	0.73
88.55	3.78	46.13	5.92	4.99	260.3	115.79	238.77	3.68	50.82	49.50	28.00	1.00	0.82
98.39	3.78	46.32	5.46	4.61	261.1	116.42	248.87	5.24	49.26	54.50	30.00	1.00	0.90

x_{dist} (in)	$A_{ps.bot}$ (in^2)	d_e (in)	ε_s	d_v (in)	v_u	$A_{s.bot.\cdot x}$ (in^2)	$A_{ps.bot.\cdot x}$ (in^2)	ε_x	θ (rad)	β	$MinReinfCheck$
0.00	4.28	50.09	0.02	47.46	0.250	0.74	0.22	0.0217	0.6231	1.50	OK
9.84	4.28	50.39	0.02	47.76	0.095	1.96	0.59	0.0024	0.6394	2.19	OK
19.68	4.28	50.51	0.02	47.88	0.080	3.00	0.96	0.0010	0.6291	2.24	OK
29.52	4.28	50.56	0.02	47.93	0.085	3.00	1.32	0.0008	0.5942	2.34	OK
39.36	4.28	50.57	0.02	47.94	0.091	3.00	1.69	0.0006	0.5618	2.44	OK
47.94	4.28	50.58	0.02	47.94	0.094	3.00	2.01	0.0005	0.5439	2.50	OK
49.19	4.28	50.58	0.02	47.95	0.094	3.00	2.05	0.0005	0.5431	2.50	OK
50.44	4.28	50.58	0.02	47.95	0.094	3.00	2.10	0.0005	0.5423	2.50	OK
59.03	4.28	50.59	0.02	47.95	0.095	3.00	2.42	0.0005	0.5376	2.51	OK
68.87	4.28	50.60	0.02	47.96	0.096	3.00	2.78	0.0005	0.5327	2.53	OK
78.71	4.28	50.60	0.02	47.97	0.097	3.00	3.15	0.0005	0.5284	2.55	OK
88.55	4.28	50.68	0.02	48.19	0.096	1.76	3.50	0.0005	0.5354	2.52	OK
98.39	4.59	49.26	0.02	46.95	0.092	0.00	4.12	0.0003	0.4934	2.71	OK

C.3.1.9.5 Final Results for Shear Strength

x_{dist} (in)	V_c (kip)	V_s (kip)	V_{n1} (kip)	V_{n2} (kip)	V_n (kip)
0.00	39.9	711.2	754.7	741.9	741.9
9.84	58.6	223.1	291.2	752.5	291.2
19.68	60.2	177.1	252.7	760.3	252.7
29.52	63.0	191.0	271.9	763.5	271.9
39.36	65.7	205.0	288.6	763.7	288.6
47.94	67.1	213.4	298.5	763.8	298.5
49.19	67.2	213.8	298.9	763.8	298.9
50.44	67.2	214.2	299.3	763.9	299.3
59.03	67.6	216.6	302.1	764.0	302.1
68.87	68.0	219.0	305.0	764.1	305.0
78.71	68.4	221.2	307.6	764.2	307.6
88.55	68.1	218.7	304.7	767.6	304.7
98.39	71.4	195.9	285.2	748.4	285.2

C.3.1.10 Beam BT.10.Typ.2

C.3.1.10.1 Inputs

γ_c (pcf)	129
f_c' (psi)	9730
f_{ci}' (psi)	6123
$f_{c.deck}$ (psi)	4930
$\gamma_{c.deck}$ (pcf)	129
E_{beam} (ksi)	4060
$E_{beam.i}$ (ksi)	4230
E_{slab} (ksi)	3270
h (in)	45
A_{beam} (in^2)	746.7
I_{beam} (in^4)	207300
L_{beam} (ft)	58.9375
b_v (in)	7
y_b (in)	22.23
y_t (in)	22.77
S (ft)	7
t_{haunch} (in)	1

t_{struct} (in)	8.5
A_{ct} (in^2)	423.25
h_{flange} (in)	8.5
Num_{strand}	34
$Num_{straight}$	28
$Num_{straight.bot}$	28
Num_{harp}	6
$cg_{straight}$ (in)	3.68
$cg_{harp.end}$ (in)	41
$cg_{harp.ms}$ (in)	4.25
$cg_{straight.bot}$ (in)	3.68
A_{strand} (in^2)	0.153
φ (in)	0.5
f_{pu} (ksi)	270
f_{pe} (ksi)	173.34
E_p (ksi)	28500
$HarpDist$ (ft)	26.5

f_y (ksi)	67.3
f_{yv} (ksi)	67.3
E_s (ksi)	29000
α	1.57
$A_{s.top}$ (in^2)	0
d_{top} (in)	9.5
$d_{long.rebar}$	6
$IsLongSteelEpoxyCoated$	No
$LongSteelClearSpacing$ (in)	1
$LongSteelCover$ (in)	2
$IsTopBarEffectApplicable$	No
$A_{long.rebar}$ (in2)	0.31
$ShearSpan$ (in)	146.21
$x_{bearing}$ (in)	6
$x_{bearing.roller}$ (in)	107.89
$x_{critical.assume}$ (in)	44.23

x_{dist} (in)	A_{ct} (in^2)	$cg_{s.bot}$ (in)	cg_s (in)	$s_{v.design}$ (in)	A_v (in^2)	P_{assume} (kip)	θ_{assume} (rad)
0	3	4.95	4.95	2.5	0.4	250	0.62
14.62	3	4.95	4.95	7.75	0.4	250	0.64
29.24	3	4.95	4.95	10	0.4	250	0.6000
43.86	3	4.95	4.95	10	0.4	250	0.55
48.36	3	4.95	4.95	10	0.4	250	0.55
58.48	3	4.95	4.95	10	0.4	250	0.54
73.11	3	4.95	4.95	10	0.4	250	0.53
87.73	0	0	0	12	0.4	250	0.53
97.85	0	0	0	12	0.4	250	0.5
102.35	0	0	0	12	0.4	250	0.5
116.97	0	0	0	12	0.4	250	0.4800
131.59	0	0	0	12	0.4	250	0.51
146.21	0	0	0	12	0.4	250	0.52

C.3.1.10.2 Basic Geometry and Material Calculations

x_{dist} (in)	d_s (in)	$A_{ps.bot}$ (in^2)	cg_{harp} (in)
0.00	49.55	4.28	40.32
14.62	49.55	4.28	38.66
29.24	49.55	4.28	37.00
43.86	49.55	4.28	35.34
48.36	49.55	4.28	34.83
58.48	49.55	4.28	33.69
73.11	49.55	4.28	32.03
87.73	54.50	4.28	30.37
97.85	54.50	4.59	29.22
102.35	54.50	4.59	28.71
116.97	54.50	4.90	27.05
131.59	54.50	4.90	25.39
146.21	54.50	5.20	23.74

h_c (in)	L_{span} (ft)	A_{ps} (in^2)	Ψ_{harp} (rad)	f_{po} (ksi)	$f_{r.V}$ (psi)	β_1
54.5	49.447	5.202	0.1129	189	623.9	0.8035

C.3.1.10.3 Load Effect Calculations

x_{dist} (in)	V_{LL} (kip)	M_{LL} (ft-kip)	V_{DC1} (kip)	M_{DC1} (ft-kip)	V_{assume} (kip)	$M_{assume1}$ (ft-kip)	M_{assume} (ft-kip)	V_p (kip)
0.0	733.3	0.0	32.3	-0.2	765.6	-0.2	3040.3	3.6
14.6	270.1	329.1	30.6	38.2	300.7	367.3	1159.6	12.3
29.2	245.9	599.3	29.0	74.5	274.9	673.8	1035.3	17.9
43.9	272.1	994.7	27.4	108.8	299.5	1103.5	1134.6	17.9
48.4	275.8	1111.6	26.8	119.0	302.7	1230.6	1230.6	17.9
58.5	280.2	1365.7	25.7	141.2	305.9	1506.9	1506.9	17.9
73.1	285.8	1741.1	24.1	171.5	309.9	1912.6	1912.6	17.9
87.7	258.9	1892.7	22.4	199.8	281.3	2092.5	2092.5	17.9
97.8	266.6	2174.1	21.3	218.2	287.9	2392.3	2392.3	17.9
102.3	268.8	2292.3	20.8	226.1	289.5	2518.4	2518.4	17.9
117.0	270.7	2639.0	19.1	250.4	289.9	2889.5	2889.5	17.9
131.6	259.2	2842.9	17.5	272.7	276.7	3115.6	3115.6	17.9
146.2	252.2	3073.1	15.8	293.0	268.1	3366.1	3366.1	17.9

C.3.1.10.4 Calculations for β and θ

x_{dist} (in)	cg_{ps} (in)	d_p (in)	c (in)	a (in)	$f_{ps.max}$ (ksi)	$l_{d.ps}$ (in)	f_{ps} (ksi)	$cg_{ps.bot}$ (in)	$d_{p.bot}$ (in)	$d_{s.bot}$ (in)	$Num_{strand.bot}$	$RedFactor_{\cdot x.s}$	$RedFactor_{\cdot x.ps}$
0.00	3.78	44.36	5.51	4.43	260.6	116.04	34.67	3.68	50.82	49.55	28.00	0.25	0.05
14.62	3.78	44.65	5.51	4.43	260.7	116.09	119.15	3.68	50.82	49.55	28.00	0.85	0.18
29.24	3.78	44.94	5.51	4.43	260.7	116.14	178.66	3.68	50.82	49.55	28.00	1.00	0.30
43.86	3.78	45.23	5.51	4.43	260.8	116.18	193.50	3.68	50.82	49.55	28.00	1.00	0.43
48.36	3.78	45.32	5.51	4.43	260.8	116.20	198.06	3.68	50.82	49.55	28.00	1.00	0.47
58.48	3.78	45.53	5.51	4.43	260.8	116.23	208.34	3.68	50.82	49.55	28.00	1.00	0.55
73.11	3.78	45.82	5.51	4.43	260.9	116.28	223.18	3.68	50.82	49.55	28.00	1.00	0.68
87.73	3.78	46.11	4.82	3.87	262.1	117.23	238.18	3.68	50.82	54.50	28.00	1.00	0.80
97.85	3.78	46.31	4.82	3.87	262.1	117.26	248.49	5.25	49.25	54.50	30.00	1.00	0.89
102.35	3.78	46.40	4.82	3.87	262.1	117.27	253.07	5.21	49.29	54.50	30.00	1.00	0.92
116.97	3.78	46.70	4.82	3.87	262.2	117.31	262.19	6.48	48.02	54.50	32.00	1.00	1.00
131.59	3.78	46.99	4.82	3.88	262.2	117.34	262.24	6.27	48.23	54.50	32.00	1.00	1.00
146.21	3.78	47.28	4.82	3.88	262.3	117.38	262.29	7.22	47.28	54.50	34.00	1.00	1.00

x_{dist} (in)	$A_{ps.bot}$ (in^2)	d_e (in)	ε_s	d_v (in)	v_u	$A_{s.bot.\cdot x}$ (in^2)	$A_{ps.bot.\cdot x}$ (in^2)	ε_x	θ (rad)	β	$MinReinfCheck$
0.00	4.28	50.09	0.02	47.88	0.234	0.74	0.22	0.0224	0.6231	1.59	OK
14.62	4.28	50.46	0.02	48.25	0.088	2.55	0.76	0.0018	0.6380	2.20	OK
29.24	4.28	50.56	0.02	48.34	0.078	3.00	1.30	0.0008	0.5990	2.34	OK
43.86	4.28	50.57	0.02	48.36	0.086	3.00	1.84	0.0006	0.5528	2.49	OK
48.36	4.28	50.58	0.02	48.36	0.086	3.00	2.00	0.0006	0.5472	2.51	OK
58.48	4.28	50.59	0.02	48.37	0.087	3.00	2.38	0.0005	0.5416	2.52	OK
73.11	4.28	50.60	0.02	48.39	0.089	3.00	2.91	0.0005	0.5350	2.54	OK
87.73	4.28	50.82	0.03	48.88	0.079	0.00	3.43	0.0005	0.5266	2.61	OK
97.85	4.59	49.25	0.03	47.32	0.084	0.00	4.07	0.0004	0.4995	2.72	OK
102.35	4.59	49.29	0.03	47.35	0.084	0.00	4.24	0.0004	0.4970	2.73	OK
116.97	4.90	48.02	0.03	46.09	0.087	0.00	4.90	0.0003	0.4836	2.78	OK
131.59	4.90	48.23	0.03	46.29	0.082	0.00	4.90	0.0004	0.5092	2.68	OK
146.21	5.20	47.28	0.03	45.34	0.081	0.00	5.20	0.0004	0.5155	2.66	OK

C.3.1.10.5 Final Results for Shear Strength

x_{dist} (in)	V_c (kip)	V_s (kip)	V_{n1} (kip)	V_{n2} (kip)	V_n (kip)
0.00	44.7	717.4	765.7	818.8	765.7
14.62	62.4	226.0	300.8	833.9	300.8
29.24	66.4	190.6	274.9	841.1	274.9
43.86	70.6	211.0	299.5	841.4	299.5
48.36	71.1	213.7	302.7	841.4	302.7
58.48	71.6	216.5	305.9	841.6	305.9
73.11	72.1	219.8	309.9	841.8	309.9
87.73	74.8	188.6	281.3	850.3	281.3
97.85	75.5	194.5	288.0	823.6	288.0
102.35	75.9	195.8	289.6	824.2	289.6
116.97	75.2	196.8	290.0	802.7	290.0
131.59	72.8	186.0	276.8	806.2	276.8
146.21	70.6	179.5	268.1	790.0	268.1

C.3.1.11 Beam BT.10.Min.1

C.3.1.11.1 Inputs

γ_c (pcf)	129
f_c' (psi)	9730
f_{ci}' (psi)	6120
$f_{c.deck}$ (psi)	5170
$\gamma_{c.deck}$ (pcf)	126.6
E_{beam} (ksi)	4060
$E_{beam.i}$ (ksi)	4230
E_{slab} (ksi)	3200
h (in)	45
A_{beam} (in^2)	746.7
I_{beam} (in^4)	207300
L_{beam} (ft)	59
b_v (in)	7
y_b (in)	22.23
y_t (in)	22.77
S (ft)	7
t_{haunch} (in)	1

t_{struct} (in)	8.5
A_{ct} (in^2)	423.25
h_{flange} (in)	8.5
Num_{strand}	34
$Num_{straight}$	28
$Num_{straight.bot}$	28
Num_{harp}	6
$cg_{straight}$ (in)	3.68
$cg_{harp.end}$ (in)	41
$cg_{harp.ms}$ (in)	4.25
$cg_{straight.bot}$ (in)	3.68
A_{strand} (in^2)	0.153
φ (in)	0.5
f_{pu} (ksi)	270
f_{pe} (ksi)	179.11
E_p (ksi)	28500
$HarpDist$ (ft)	26.5

f_y (ksi)	67.3
f_{yv} (ksi)	67.3
E_s (ksi)	29000
α	1.57
$A_{s.top}$ (in^2)	0
d_{top} (in)	9.5
$d_{long.rebar}$	6
$IsLongSteelEpoxyCoated$	No
$LongSteelClearSpacing$ (in)	1
$LongSteelCover$ (in)	2
$IsTopBarEffectApplicable$	No
$A_{long.rebar}$ (in2)	0.31
$ShearSpan$ (in)	105.00
$x_{bearing}$ (in)	6
$x_{bearing.roller}$ (in)	6
$x_{critical.assume}$ (in)	55.66

x_{dist} (in)	A_{ct} (in^2)	$cg_{s.bot}$ (in)	cg_s (in)	$s_{v.design}$ (in)	A_v (in^2)	P_{assume} (kip)	θ_{assume} (rad)
0	3	4.95	4.95	2.5	0.4	250	0.62
10.50	3	4.95	4.95	15	0.4	250	0.64
21.00	3	4.95	4.95	15.75	0.4	250	0.5700
31.50	3	4.95	4.95	15.75	0.4	250	0.53
42.00	3	4.95	4.95	24	0.4	250	0.45
51.85	3	4.95	4.95	24	0.4	250	0.44
52.50	3	4.95	4.95	24	0.4	250	0.44
53.15	3	4.95	4.95	24	0.4	250	0.44
63.00	3	4.95	4.95	24	0.4	250	0.43
73.50	3	4.95	4.95	24	0.4	250	0.42
84.00	0	0	0	24	0.4	250	0.4200
94.50	0	0	0	24	0.4	250	0.41
105.00	0	0	0	24	0.4	250	0.39

C.3.1.11.2 Basic Geometry and Material Calculations

x_{dist} (in)	d_s (in)	$A_{ps.bot}$ (in^2)	cg_{harp} (in)
0.00	49.55	4.28	40.32
10.50	49.55	4.28	39.13
21.00	49.55	4.28	37.94
31.50	49.55	4.28	36.75
42.00	49.55	4.28	35.56
51.85	49.55	4.28	34.44
52.50	49.55	4.28	34.36
53.15	49.55	4.28	34.29
63.00	49.55	4.28	33.17
73.50	49.55	4.28	31.98
84.00	54.50	4.28	30.79
94.50	54.50	4.28	29.60
105.00	54.50	4.59	28.41

h_c (in)	L_{span} (ft)	A_{ps} (in^2)	Ψ_{harp} (rad)	f_{po} (ksi)	$f_{r.V}$ (psi)	β_1
54.5	58	5.202	0.1129	189	623.9	0.7915

C.3.1.11.3 Load Effect Calculations

x_{dist} (in)	V_{LL} (kip)	M_{LL} (ft-kip)	V_{DC1} (kip)	M_{DC1} (ft-kip)	V_{assume} (kip)	$M_{assume1}$ (ft-kip)	M_{assume} (ft-kip)	V_p (kip)
0.0	728.7	0.0	38.8	-0.2	767.5	-0.2	3054.4	3.7
10.5	153.3	134.1	37.6	33.3	190.9	167.4	727.4	10.2
21.0	177.9	311.2	36.5	65.7	214.3	376.9	797.5	16.7
31.5	197.3	517.9	35.3	97.1	232.6	615.0	864.4	18.5
42.0	182.4	638.5	34.1	127.4	216.6	766.0	799.7	18.5
51.8	191.1	825.8	33.0	155.0	224.1	980.8	980.8	18.5
52.5	191.6	838.0	32.9	156.8	224.5	994.8	994.8	18.5
53.1	192.0	850.2	32.9	158.6	224.8	1008.8	1008.8	18.5
63.0	198.0	1039.4	31.8	185.1	229.8	1224.5	1224.5	18.5
73.5	204.2	1250.4	30.6	212.4	234.8	1462.8	1462.8	18.5
84.0	207.1	1450.0	29.4	238.7	236.6	1688.6	1688.6	18.5
94.5	213.1	1678.0	28.3	263.9	241.4	1941.9	1941.9	18.5
105.0	222.8	1949.5	27.1	288.1	249.9	2237.6	2237.6	18.5

C.3.1.11.4 Calculations for β and θ

x_{dist} (in)	cg_{ps} (in)	d_p (in)	c (in)	a (in)	$f_{ps.max}$ (ksi)	$l_{d.ps}$ (in)	f_{ps} (ksi)	$cg_{ps.bot}$ (in)	$d_{p.bot}$ (in)	$d_{s.bot}$ (in)	$Num_{strand.bot}$	$RedFactor_{\cdot x.s}$	$RedFactor_{\cdot x.ps}$
0.00	3.78	44.36	5.34	4.22	260.9	113.20	35.82	3.68	50.82	49.55	28.00	0.25	0.05
10.50	3.78	44.57	5.34	4.22	260.9	113.23	98.51	3.68	50.82	49.55	28.00	0.68	0.15
21.00	3.78	44.78	5.34	4.22	261.0	113.26	161.19	3.68	50.82	49.55	28.00	1.00	0.24
31.50	3.78	44.99	5.34	4.23	261.0	113.30	186.48	3.68	50.82	49.55	28.00	1.00	0.33
42.00	3.78	45.20	5.34	4.23	261.1	113.33	196.81	3.68	50.82	49.55	28.00	1.00	0.42
51.85	3.78	45.39	5.34	4.23	261.1	113.36	206.50	3.68	50.82	49.55	28.00	1.00	0.51
52.50	3.78	45.41	5.34	4.23	261.1	113.36	207.14	3.68	50.82	49.55	28.00	1.00	0.52
53.15	3.78	45.42	5.34	4.23	261.1	113.36	207.78	3.68	50.82	49.55	28.00	1.00	0.52
63.00	3.78	45.62	5.34	4.23	261.1	113.39	217.47	3.68	50.82	49.55	28.00	1.00	0.61
73.50	3.78	45.83	5.34	4.23	261.2	113.43	227.81	3.68	50.82	49.55	28.00	1.00	0.70
84.00	3.78	46.04	4.67	3.70	262.3	114.34	238.31	3.68	50.82	54.50	28.00	1.00	0.79
94.50	3.78	46.25	4.67	3.70	262.4	114.37	248.68	3.68	50.82	54.50	28.00	1.00	0.88
105.00	3.78	46.46	4.67	3.70	262.4	114.39	259.05	5.19	49.31	54.50	30.00	1.00	0.97

x_{dist} (in)	$A_{ps.bot}$ (in^2)	d_e (in)	ε_s	d_v (in)	v_u	$A_{s.bot.\cdot x}$ (in^2)	$A_{ps.bot.\cdot x}$ (in^2)	ε_x	θ (rad)	β	$MinReinfCheck$
0.00	4.28	50.10	0.03	47.99	0.234	0.74	0.23	0.0224	0.6231	1.59	OK
10.50	4.28	50.41	0.03	48.30	0.055	2.04	0.62	0.0012	0.6353	2.23	OK
21.00	4.28	50.53	0.03	48.42	0.060	3.00	1.02	0.0007	0.5726	2.44	OK
31.50	4.28	50.56	0.03	48.45	0.065	3.00	1.42	0.0005	0.5326	2.59	OK
42.00	4.28	50.58	0.03	48.46	0.060	3.00	1.81	0.0002	0.4522	3.03	OK
51.85	4.28	50.59	0.03	48.47	0.062	3.00	2.19	0.0002	0.4373	3.14	OK
52.50	4.28	50.59	0.03	48.47	0.062	3.00	2.21	0.0002	0.4366	3.15	OK
53.15	4.28	50.59	0.03	48.47	0.063	3.00	2.24	0.0002	0.4359	3.15	OK
63.00	4.28	50.60	0.03	48.48	0.064	3.00	2.61	0.0001	0.4266	3.22	OK
73.50	4.28	50.60	0.03	48.49	0.066	3.00	3.00	0.0001	0.4185	3.31	OK
84.00	4.28	50.82	0.03	48.97	0.065	0.00	3.37	0.0001	0.4190	3.30	OK
94.50	4.28	50.82	0.03	48.97	0.067	0.00	3.76	0.0001	0.4119	3.38	OK
105.00	4.59	49.31	0.03	47.46	0.072	0.00	4.45	0.0000	0.3891	3.65	OK

C.3.1.11.5 Final Results for Shear Strength

x_{dist} (in)	V_c (kip)	V_s (kip)	V_{n1} (kip)	V_{n2} (kip)	V_n (kip)
0.00	44.8	719.1	767.6	820.8	767.6
10.50	63.2	117.6	190.9	832.6	190.9
21.00	69.3	128.4	214.3	841.2	214.3
31.50	73.6	140.5	232.6	843.6	232.6
42.00	86.1	111.9	216.6	843.7	216.6
51.85	89.3	116.3	224.2	843.9	224.2
52.50	89.5	116.5	224.5	843.9	224.5
53.15	89.6	116.7	224.9	843.9	224.9
63.00	91.6	119.7	229.8	844.0	229.8
73.50	94.0	122.3	234.8	844.2	234.8
84.00	94.8	123.3	236.6	852.4	236.6
94.50	97.1	125.7	241.4	852.4	241.4
105.00	101.6	129.8	250.0	826.6	250.0

C.3.1.12 Beam BT.10.Min.2

C.3.1.12.1 Inputs

γ_c (pcf)	130.6
f_c' (psi)	10315
f_{ci}' (psi)	8940
$f_{c.deck}$ (psi)	5860
$\gamma_{c.deck}$ (pcf)	127.8
E_{beam} (ksi)	4140
$E_{beam.i}$ (ksi)	4230
E_{slab} (ksi)	3410
h (in)	45
A_{beam} (in^2)	746.7
I_{beam} (in^4)	207300
L_{beam} (ft)	59
b_v (in)	7
y_b (in)	22.23
y_t (in)	22.77
S (ft)	7
t_{haunch} (in)	1

t_{struct} (in)	8.5
A_{ct} (in^2)	423.25
h_{flange} (in)	8.5
Num_{strand}	34
$Num_{straight}$	28
$Num_{straight.bot}$	28
Num_{harp}	6
$cg_{straight}$ (in)	3.68
$cg_{harp.end}$ (in)	41
$cg_{harp.ms}$ (in)	4.25
$cg_{straight.bot}$ (in)	3.68
A_{strand} (in^2)	0.153
φ (in)	0.5
f_{pu} (ksi)	270
f_{pe} (ksi)	179.11
E_p (ksi)	28500
$HarpDist$ (ft)	26.5

f_y (ksi)	67.3
f_{yv} (ksi)	67.3
E_s (ksi)	29000
α	1.57
$A_{s.top}$ (in^2)	0
d_{top} (in)	9.5
$d_{long.rebar}$	6
$IsLongSteelEpoxyCoated$	No
$LongSteelClearSpacing$ (in)	1
$LongSteelCover$ (in)	2
$IsTopBarEffectApplicable$	No
$A_{long.rebar}$ (in2)	0.31
$ShearSpan$ (in)	151.80
$x_{bearing}$ (in)	6
$x_{bearing.roller}$ (in)	108.25
$x_{critical.assume}$ (in)	55.82

x_{dist} (in)	A_{ct} (in^2)	$cg_{s.bot}$ (in)	cg_s (in)	$s_{v.design}$ (in)	A_v (in^2)	P_{assume} (kip)	θ_{assume} (rad)
0	3	4.95	4.95	2.5	0.4	250	0.62
15.18	3	4.95	4.95	15	0.4	250	0.61
30.36	3	4.95	4.95	15.75	0.4	250	0.5400
45.54	3	4.95	4.95	24	0.4	250	0.45
51.63	3	4.95	4.95	24	0.4	250	0.44
60.72	3	4.95	4.95	24	0.4	250	0.43
75.90	3	4.95	4.95	24	0.4	250	0.42
91.08	3	0	0	24	0.4	250	0.41
100.17	3	0	0	24	0.4	250	0.39
106.26	3	0	0	24	0.4	250	0.39
121.44	0	0	0	24	0.4	250	0.3900
136.62	0	0	0	24	0.4	250	0.4
151.80	0	0	0	24	0.4	250	0.42

C.3.1.12.2 Basic Geometry and Material Calculations

x_{dist} (in)	d_s (in)	$A_{ps.bot}$ (in^2)	cg_{harp} (in)
0.00	49.55	4.28	40.32
15.18	49.55	4.28	38.60
30.36	49.55	4.28	36.88
45.54	49.55	4.28	35.15
51.63	49.55	4.28	34.46
60.72	49.55	4.28	33.43
75.90	49.55	4.28	31.71
91.08	54.50	4.28	29.99
100.17	54.50	4.59	28.96
106.26	54.50	4.59	28.27
121.44	54.50	4.90	26.54
136.62	54.50	5.20	24.82
151.80	54.50	5.20	23.10

h_c (in)	L_{span} (ft)	A_{ps} (in^2)	Ψ_{harp} (rad)	f_{po} (ksi)	$f_{r.V}$ (psi)	β_1
54.5	49.4792	5.202	0.1129	189	642.3	0.757

C.3.1.12.3 Load Effect Calculations

x_{dist} (in)	V_{LL} (kip)	M_{LL} (ft-kip)	V_{DC1} (kip)	M_{DC1} (ft-kip)	V_{assume} (kip)	$M_{assume1}$ (ft-kip)	M_{assume} (ft-kip)	V_p (kip)
0.0	740.8	0.0	32.4	-0.2	773.1	-0.2	3092.6	3.7
15.2	173.5	219.5	30.6	39.7	204.1	259.1	773.8	13.1
30.4	203.8	515.7	28.9	77.4	232.8	593.1	869.4	18.5
45.5	195.3	741.0	27.2	112.9	222.5	853.9	853.9	18.5
51.6	199.4	858.0	26.5	126.5	226.0	984.6	984.6	18.5
60.7	205.1	1037.9	25.5	146.2	230.6	1184.2	1184.2	18.5
75.9	213.7	1352.0	23.8	177.4	237.5	1529.4	1529.4	18.5
91.1	224.7	1705.4	22.1	206.4	246.8	1911.8	1911.8	18.5
100.2	232.6	1941.6	21.1	222.8	253.6	2164.3	2164.3	18.5
106.3	235.5	2085.0	20.4	233.3	255.8	2318.3	2318.3	18.5
121.4	227.1	2297.9	18.7	258.0	245.7	2555.9	2555.9	18.5
136.6	220.5	2510.3	17.0	280.5	237.4	2790.8	2790.8	18.5
151.8	211.1	2670.5	15.2	300.9	226.3	2971.4	2971.4	18.5

C.3.1.12.4 Calculations for β and θ

x_{dist} (in)	cg_{ps} (in)	d_p (in)	c (in)	a (in)	$f_{ps.max}$ (ksi)	$l_{d.ps}$ (in)	f_{ps} (ksi)	$cg_{ps.bot}$ (in)	$d_{p.bot}$ (in)	$d_{s.bot}$ (in)	$Num_{strand.bot}$	$RedFactor_{\cdot x.s}$	$RedFactor_{\cdot x.ps}$
0.00	3.78	44.36	4.93	3.73	261.6	113.75	35.82	3.68	50.82	49.55	28.00	0.25	0.05
15.18	3.78	44.66	4.93	3.74	261.6	113.79	126.45	3.68	50.82	49.55	28.00	0.87	0.19
30.36	3.78	44.96	4.94	3.74	261.7	113.84	185.38	3.68	50.82	49.55	28.00	1.00	0.32
45.54	3.78	45.27	4.94	3.74	261.8	113.88	200.33	3.68	50.82	49.55	28.00	1.00	0.45
51.63	3.78	45.39	4.94	3.74	261.8	113.90	206.33	3.68	50.82	49.55	28.00	1.00	0.51
60.72	3.78	45.57	4.94	3.74	261.8	113.92	215.30	3.68	50.82	49.55	28.00	1.00	0.59
75.90	3.78	45.87	4.94	3.74	261.9	113.96	230.26	3.68	50.82	49.55	28.00	1.00	0.72
91.08	3.78	46.18	4.94	3.74	261.9	114.01	245.23	3.68	50.82	54.50	28.00	1.00	0.85
100.17	3.78	46.36	4.94	3.74	261.9	114.03	254.20	5.23	49.27	54.50	30.00	1.00	0.93
106.26	3.78	46.48	4.94	3.74	262.0	114.05	260.21	5.18	49.32	54.50	30.00	1.00	0.98
121.44	3.78	46.79	4.32	3.27	263.0	114.89	263.02	6.41	48.09	54.50	32.00	1.00	1.00
136.62	3.78	47.09	4.32	3.27	263.1	114.93	263.06	7.41	47.09	54.50	34.00	1.00	1.00
151.80	3.78	47.39	4.32	3.27	263.1	114.96	263.11	7.11	47.39	54.50	34.00	1.00	1.00

x_{dist} (in)	$A_{ps.bot}$ (in^2)	d_e (in)	ε_s	d_v (in)	v_u	$A_{s.bot.\cdot x}$ (in^2)	$A_{ps.bot.\cdot x}$ (in^2)	ε_x	θ (rad)	β	$MinReinfCheck$
0.00	4.28	50.10	0.03	48.23	0.221	0.74	0.23	0.0225	0.6242	1.66	OK
15.18	4.28	50.48	0.03	48.61	0.054	2.62	0.80	0.0009	0.6144	2.30	OK
30.36	4.28	50.56	0.03	48.70	0.061	3.00	1.37	0.0005	0.5398	2.56	OK
45.54	4.28	50.58	0.03	48.71	0.058	3.00	1.94	0.0002	0.4476	3.06	OK
51.63	4.28	50.59	0.03	48.72	0.059	3.00	2.17	0.0002	0.4408	3.12	OK
60.72	4.28	50.59	0.03	48.72	0.060	3.00	2.51	0.0001	0.4320	3.18	OK
75.90	4.28	50.61	0.03	48.74	0.062	3.00	3.08	0.0001	0.4202	3.29	OK
91.08	4.28	51.41	0.03	49.55	0.064	3.00	3.65	0.0001	0.4121	3.38	OK
100.17	4.59	50.04	0.03	48.17	0.068	3.00	4.27	0.0000	0.3930	3.60	OK
106.26	4.59	50.07	0.03	48.20	0.068	3.00	4.52	0.0000	0.3901	3.64	OK
121.44	4.90	48.09	0.03	46.45	0.068	0.00	4.90	0.0000	0.3923	3.61	OK
136.62	5.20	47.09	0.03	45.45	0.067	0.00	5.20	0.0000	0.3974	3.55	OK
151.80	5.20	47.39	0.03	45.76	0.063	0.00	5.20	0.0001	0.4167	3.33	OK

C.3.1.12.5 Final Results for Shear Strength

x_{dist} (in)	V_c (kip)	V_s (kip)	V_{n1} (kip)	V_{n2} (kip)	V_n (kip)
0.00	48.5	721.0	773.2	874.3	773.2
15.18	67.4	123.6	204.1	890.5	204.1
30.36	75.3	138.9	232.8	897.5	232.8
45.54	90.1	113.8	222.5	897.8	222.5
51.63	91.6	115.8	226.0	897.9	226.0
60.72	93.6	118.5	230.7	898.1	230.7
75.90	96.7	122.3	237.6	898.3	237.6
91.08	101.1	127.1	246.8	912.9	246.8
100.17	104.8	130.3	253.7	888.1	253.7
106.26	105.9	131.5	255.9	888.5	255.9
121.44	101.3	125.9	245.8	857.1	245.8
136.62	97.5	121.5	237.5	839.0	237.5
151.80	91.9	115.9	226.4	844.5	226.4

C.3.2 Using the General Procedure (Article 5.8.3.4.2)

The same inputs and many of the basic calculations for *Appendix B5* detailed in Section C.3.1 apply to calculating the shear strength when following the *General Procedure*. Additional information and intermediate calculations that are required for the *General Procedure* are provided for each beam test in the subsections on the following pages.

C.3.2.1 Beam T2.8.Typ.1

x_{dist} (in)	P_{assume} (kip)	V_{LL} (kip)	M_{LL} (ft-kip)	V_{assume} (kip)	$M_{assume1}$ (ft-kip)	M_{assume} (ft-kip)	ε_s	θ (rad)	β	V_c (kip)	V_s (kip)	V_{n1} (kip)	V_{n2} (kip)	V_n (kip)
0.00	369.7	516.9	0.0	535.5	-0.1	1774.4	0.0024	0.6505	1.73	39.1	566.2	608.8	535.6	535.6
5.73	189.0	264.3	126.3	282.5	135.0	921.9	0.0024	0.6505	1.73	39.2	236.6	282.6	540.4	282.6
11.47	192.0	268.5	256.6	286.3	273.9	924.9	0.0024	0.6505	1.73	39.3	236.9	286.3	544.6	286.3
17.20	138.4	193.5	277.3	210.8	303.0	661.6	0.0024	0.6505	1.73	39.3	158.1	210.9	548.4	210.9
22.94	141.2	197.4	377.3	214.3	411.2	662.6	0.0024	0.6505	1.73	39.3	158.2	214.4	552.1	214.4
28.67	142.0	198.5	474.2	214.9	516.1	662.9	0.0024	0.6505	1.73	39.4	158.3	215.0	552.9	215.0
34.40	136.8	191.2	548.2	207.2	597.8	611.7	0.0024	0.6505	1.73	37.8	152.0	207.2	531.7	207.2
38.71	137.1	191.7	618.6	207.4	673.8	673.8	0.0024	0.6505	1.73	37.8	152.2	207.4	532.2	207.4
40.14	137.3	192.0	642.1	207.5	699.3	699.3	0.0024	0.6503	1.73	37.9	152.3	207.6	532.4	207.6
45.87	138.0	193.0	737.8	208.1	802.2	802.2	0.0023	0.6497	1.74	38.0	152.7	208.1	533.0	208.1
51.60	139.2	194.6	837.0	209.3	908.6	908.6	0.0021	0.6339	1.87	39.5	152.4	209.3	515.4	209.3
57.34	140.2	196.0	936.6	210.2	1015.0	1015.0	0.0021	0.6330	1.88	39.8	153.1	210.2	516.6	210.2

C.3.2.2 Beam T2.8.Typ.2

x_{dist} (in)	P_{assume} (kip)	V_{LL} (kip)	M_{LL} (ft-kip)	V_{assume} (kip)	$M_{assume1}$ (ft-kip)	M_{assume} (ft-kip)	ε_s	θ (rad)	β	V_c (kip)	V_s (kip)	V_{n1} (kip)	V_{n2} (kip)	V_n (kip)
0.00	386.2	521.8	0.0	537.8	-0.1	1784.4	0.0023	0.6460	1.77	34.0	572.4	609.9	537.9	537.9
11.88	199.0	268.9	266.1	284.0	281.4	917.7	0.0023	0.6460	1.77	34.2	239.5	284.1	547.1	284.1
23.75	146.0	197.2	390.3	211.4	420.1	652.1	0.0023	0.6460	1.77	34.2	160.0	211.5	554.9	211.5
35.63	141.1	190.7	566.2	203.9	609.5	609.5	0.0023	0.6460	1.77	32.9	153.7	204.0	534.0	204.0
38.77	141.5	191.1	617.5	204.1	664.3	664.3	0.0023	0.6460	1.77	32.9	153.8	204.1	534.4	204.1
47.50	142.6	192.7	762.9	205.0	818.9	818.9	0.0023	0.6449	1.78	33.1	154.5	205.0	535.4	205.0
59.38	145.0	195.9	969.3	207.3	1037.0	1037.0	0.0020	0.6279	1.92	34.8	155.1	207.3	519.3	207.3
71.26	131.4	177.6	1054.4	188.0	1132.9	1132.9	0.0024	0.6544	1.70	29.6	141.1	188.1	500.0	188.1
79.99	129.9	175.5	1169.9	185.3	1255.8	1255.8	0.0020	0.6301	1.90	33.3	134.6	185.4	503.7	185.4
83.13	131.0	177.0	1225.9	186.5	1314.3	1314.3	0.0020	0.6285	1.92	33.7	135.4	186.6	505.0	186.6
95.01	134.8	182.1	1441.5	190.7	1538.9	1538.9	0.0019	0.6231	1.97	35.0	138.4	190.8	510.0	190.8
106.88	138.2	186.8	1663.6	194.5	1769.1	1769.1	0.0018	0.6188	2.01	36.1	141.0	194.6	515.0	194.6
118.76	140.4	189.7	1877.0	196.4	1989.7	1989.7	0.0018	0.6185	2.02	36.5	142.6	196.5	520.0	196.5

C.3.2.3 Beam T2.8.Min.1

x_{dist} (in)	P_{assume} (kip)	V_{LL} (kip)	M_{LL} (ft-kip)	V_{assume} (kip)	$M_{assume1}$ (ft-kip)	M_{assume} (ft-kip)	ε_s	θ (rad)	β	V_c (kip)	V_s (kip)	V_{n1} (kip)	V_{n2} (kip)	V_n (kip)
0.00	304.6	512.4	0.0	530.5	-0.1	1736.1	0.0018	0.6178	2.02	45.2	599.0	647.7	530.6	530.6
5.80	119.6	201.2	97.3	218.9	105.8	700.7	0.0018	0.6178	2.02	45.4	166.9	219.0	535.3	219.0
11.60	97.2	163.6	158.1	180.8	175.1	564.9	0.0018	0.6178	2.02	45.4	125.3	180.8	539.5	180.8
17.40	99.6	167.5	242.8	184.2	268.0	565.8	0.0018	0.6178	2.02	45.5	125.5	184.3	543.3	184.3
23.20	101.9	171.3	331.2	187.7	364.5	566.7	0.0018	0.6178	2.02	45.5	125.6	187.8	547.0	187.8
29.00	102.4	172.3	416.3	188.2	457.3	566.9	0.0018	0.6178	2.02	45.5	125.6	188.3	547.6	188.3
34.80	98.7	166.0	481.3	181.5	529.9	529.9	0.0018	0.6178	2.02	43.7	120.6	181.5	526.5	181.5
38.22	98.9	166.4	529.9	181.6	582.9	582.9	0.0018	0.6178	2.02	43.8	120.7	181.6	526.9	181.6
40.60	99.2	166.9	564.6	181.9	620.5	620.5	0.0018	0.6173	2.03	43.9	120.9	181.9	527.2	181.9
46.40	99.9	168.1	650.0	182.7	713.1	713.1	0.0018	0.6161	2.04	44.2	121.3	182.7	527.8	182.7
52.20	101.2	170.3	740.6	184.4	810.7	810.7	0.0016	0.6011	2.22	46.3	121.0	184.4	510.2	184.4
58.00	102.1	171.8	830.1	185.5	907.0	907.0	0.0015	0.5999	2.23	46.8	121.6	185.5	511.5	185.5

C.3.2.4 Beam T2.8.Min.2

x_{dist} (in)	P_{assume} (kip)	V_{LL} (kip)	M_{LL} (ft-kip)	V_{assume} (kip)	$M_{assume1}$ (ft-kip)	M_{assume} (ft-kip)	ε_s	θ (rad)	β	V_c (kip)	V_s (kip)	V_{n1} (kip)	V_{n2} (kip)	V_n (kip)
0.00	383.6	519.5	0.0	535.5	-0.1	1769.2	0.0017	0.6128	2.08	39.9	611.2	654.5	535.6	535.6
11.63	151.8	205.5	199.1	220.5	214.0	702.9	0.0017	0.6128	2.08	40.0	170.5	220.6	544.5	220.6
23.25	126.1	170.8	330.9	184.9	359.8	562.5	0.0017	0.6128	2.08	40.1	128.1	184.9	552.1	184.9
34.88	122.3	165.6	481.2	178.7	523.3	523.3	0.0017	0.6128	2.08	38.5	123.1	178.8	531.5	178.8
38.60	122.6	166.0	534.0	178.9	580.2	580.2	0.0017	0.6128	2.08	38.6	123.2	178.9	531.9	178.9
46.50	123.9	167.8	650.1	180.0	704.6	704.6	0.0017	0.6109	2.10	39.0	123.9	180.1	532.8	180.1
58.13	126.7	171.5	830.8	182.9	896.8	896.8	0.0014	0.5944	2.30	41.4	124.3	182.9	516.5	182.9
69.75	117.8	159.5	927.3	170.0	1003.8	1003.8	0.0017	0.6080	2.13	36.9	116.0	170.1	497.1	170.1
77.65	120.6	163.3	1056.8	173.1	1140.0	1140.0	0.0016	0.6035	2.19	38.1	117.9	173.2	500.5	173.2
81.38	121.8	165.0	1118.8	174.5	1205.0	1205.0	0.0016	0.6017	2.21	38.6	118.8	174.6	502.0	174.6
93.00	125.4	169.9	1316.5	178.5	1411.5	1411.5	0.0015	0.5968	2.27	40.1	121.3	178.5	506.9	178.5
104.63	128.7	174.3	1520.1	182.0	1622.9	1622.9	0.0014	0.5929	2.32	41.4	123.5	182.1	511.8	182.1

C.3.2.5 Beam BT.8N.Typ.1

x_{dist} (in)	P_{assume} (kip)	V_{LL} (kip)	M_{LL} (ft-kip)	V_{assume} (kip)	$M_{assume1}$ (ft-kip)	M_{assume} (ft-kip)	ε_s	θ (rad)	β	V_c (kip)	V_s (kip)	V_{n1} (kip)	V_{n2} (kip)	V_n (kip)
0.00	430.3	709.0	0.0	751.0	-0.2	3003.4	0.0010	0.5657	2.77	88.0	848.0	939.5	751.1	751.1
10.44	219.3	361.4	314.4	402.0	350.1	1584.2	0.0010	0.5657	2.77	88.4	304.2	402.1	760.4	402.1
20.88	187.1	308.3	536.5	347.8	607.0	1342.8	0.0010	0.5657	2.77	88.5	243.8	347.9	767.6	347.9
31.32	127.5	210.0	548.1	248.2	652.4	933.4	0.0010	0.5657	2.77	88.6	142.3	248.2	769.8	248.2
41.75	128.3	211.3	735.3	248.2	872.3	933.7	0.0010	0.5657	2.77	88.6	142.3	248.2	769.9	248.2
48.54	128.8	212.2	858.1	248.2	1015.7	1015.7	0.0010	0.5657	2.77	88.6	142.3	248.2	769.9	248.2
52.19	130.4	214.8	934.4	250.5	1102.9	1102.9	0.0009	0.5633	2.82	90.1	143.0	250.5	770.0	250.5
55.85	131.9	217.4	1011.9	252.6	1191.2	1191.2	0.0009	0.5612	2.86	91.5	143.7	252.6	770.0	252.6
62.63	134.7	221.9	1158.0	256.2	1356.9	1356.9	0.0008	0.5576	2.94	94.0	144.9	256.2	770.1	256.2
73.07	135.9	223.9	1363.2	257.0	1591.5	1591.5	0.0008	0.5576	2.94	94.3	145.3	257.0	772.2	257.0
83.51	135.7	223.6	1556.4	255.5	1812.9	1812.9	0.0009	0.5599	2.89	93.0	145.1	255.5	775.1	255.5
93.95	139.5	229.9	1799.9	260.5	2083.6	2083.6	0.0008	0.5551	3.00	96.5	146.7	260.5	775.1	260.5
104.39	146.3	241.0	2096.6	270.3	2406.3	2406.3	0.0006	0.5398	3.40	105.9	147.1	270.4	751.5	270.4

C.3.2.6 Beam BT.8N.Typ.2

x_{dist} (in)	P_{assume} (kip)	V_{LL} (kip)	M_{LL} (ft-kip)	V_{assume} (kip)	$M_{assume1}$ (ft-kip)	M_{assume} (ft-kip)	ε_s	θ (rad)	β	V_c (kip)	V_s (kip)	V_{n1} (kip)	V_{n2} (kip)	V_n (kip)
0.00	488.0	693.0	0.0	727.1	-0.2	2910.2	0.0010	0.5651	2.79	87.0	850.0	940.5	727.2	727.2
15.26	219.4	311.6	396.2	343.9	438.3	1340.5	0.0010	0.5651	2.79	87.5	244.2	344.0	739.9	344.0
30.52	152.8	217.1	552.1	247.5	634.1	931.6	0.0010	0.5651	2.79	87.6	142.6	247.5	745.8	247.5
45.78	154.2	218.9	835.4	247.6	955.0	955.0	0.0010	0.5651	2.79	87.6	142.6	247.6	745.9	247.6
48.58	154.4	219.3	887.8	247.6	1014.0	1014.0	0.0010	0.5651	2.79	87.6	142.6	247.6	745.9	247.6
61.05	160.5	227.9	1159.6	254.7	1314.4	1314.4	0.0008	0.5577	2.94	92.5	145.0	254.8	746.0	254.8
76.31	166.8	236.9	1506.2	261.8	1694.0	1694.0	0.0007	0.5511	3.09	97.3	147.2	261.8	746.2	261.8
91.57	166.0	235.8	1799.4	258.9	2017.7	2017.7	0.0008	0.5552	2.99	94.8	146.7	259.0	750.9	259.0
104.04	169.2	240.2	2082.9	261.8	2324.4	2324.4	0.0003	0.5263	3.85	118.1	126.5	261.9	728.0	261.9
106.83	170.2	241.7	2152.1	263.0	2398.7	2398.7	0.0003	0.5256	3.87	118.9	126.8	263.1	728.3	263.1
122.09	171.5	243.5	2477.6	262.9	2750.0	2750.0	0.0002	0.5214	4.04	120.9	124.7	263.0	710.0	263.0
137.35	165.5	235.1	2690.8	252.7	2986.8	2986.8	0.0003	0.5248	3.91	114.3	121.1	252.7	695.1	252.7
152.62	157.5	223.7	2844.6	239.4	3161.7	3161.7	0.0005	0.5361	3.51	103.3	118.8	239.5	699.7	239.5

C.3.2.7 BT.8.Typ.1

x_{dist} (in)	P_{assume} (kip)	V_{LL} (kip)	M_{LL} (ft-kip)	V_{assume} (kip)	$M_{assume1}$ (ft-kip)	M_{assume} (ft-kip)	ε_s	θ (rad)	β	V_c (kip)	V_s (kip)	V_{n1} (kip)	V_{n2} (kip)	V_n (kip)
0.00	444.2	735.2	0.0	773.8	-0.2	3110.9	0.0016	0.6028	2.20	70.9	758.4	832.9	773.8	773.8
10.21	226.3	374.5	318.6	411.9	350.8	1630.9	0.0016	0.6028	2.20	71.2	331.0	412.0	783.1	412.0
20.42	158.8	262.7	447.1	299.1	510.7	1149.9	0.0016	0.6028	2.20	71.3	211.8	299.1	790.4	299.1
30.63	160.8	266.2	679.4	301.4	773.4	1150.9	0.0016	0.6028	2.20	71.3	211.9	301.4	792.9	301.4
40.84	161.5	267.3	909.8	301.4	1033.3	1151.2	0.0016	0.6028	2.20	71.4	211.9	301.4	793.0	301.4
48.77	162.1	268.2	1090.1	301.4	1235.8	1235.8	0.0016	0.6028	2.20	71.4	212.0	301.4	793.1	301.4
51.05	162.9	269.7	1147.1	302.6	1299.1	1299.1	0.0016	0.6014	2.21	71.9	212.6	302.6	793.1	302.6
53.33	163.8	271.0	1204.5	303.7	1362.7	1362.7	0.0015	0.6001	2.23	72.4	213.2	303.7	793.1	303.7
61.26	166.5	275.5	1406.6	307.3	1586.1	1586.1	0.0015	0.5961	2.28	74.2	215.1	307.4	793.2	307.4
71.47	169.6	280.7	1671.9	311.4	1878.0	1878.0	0.0014	0.5916	2.34	76.1	217.1	311.4	793.2	311.4
81.68	159.5	263.9	1796.5	293.5	2028.2	2028.2	0.0018	0.6147	2.06	67.3	208.0	293.5	798.4	293.5
91.89	163.4	270.4	2070.9	298.9	2327.3	2327.3	0.0017	0.6081	2.13	69.8	211.0	298.9	798.4	298.9
102.10	164.5	272.3	2316.4	299.5	2596.4	2596.4	0.0011	0.5736	2.63	83.3	198.2	299.6	774.0	299.6

C.3.2.8 BT.8.Typ.2

x_{dist} (in)	P_{assume} (kip)	V_{LL} (kip)	M_{LL} (ft-kip)	V_{assume} (kip)	$M_{assume1}$ (ft-kip)	M_{assume} (ft-kip)	ε_s	θ (rad)	β	V_c (kip)	V_s (kip)	V_{n1} (kip)	V_{n2} (kip)	V_n (kip)
0.00	444.2	735.2	0.0	773.8	-0.2	3110.9	0.0016	0.6028	2.20	70.9	758.4	832.9	773.8	773.8
10.21	226.3	374.5	318.6	411.9	350.8	1630.9	0.0016	0.6028	2.20	71.2	331.0	412.0	783.1	412.0
20.42	158.8	262.7	447.1	299.1	510.7	1149.9	0.0016	0.6028	2.20	71.3	211.8	299.1	790.4	299.1
30.63	160.8	266.2	679.4	301.4	773.4	1150.9	0.0016	0.6028	2.20	71.3	211.9	301.4	792.9	301.4
40.84	161.5	267.3	909.8	301.4	1033.3	1151.2	0.0016	0.6028	2.20	71.4	211.9	301.4	793.0	301.4
48.77	162.1	268.2	1090.1	301.4	1235.8	1235.8	0.0016	0.6028	2.20	71.4	212.0	301.4	793.1	301.4
51.05	162.9	269.7	1147.1	302.6	1299.1	1299.1	0.0016	0.6014	2.21	71.9	212.6	302.6	793.1	302.6
53.33	163.8	271.0	1204.5	303.7	1362.7	1362.7	0.0015	0.6001	2.23	72.4	213.2	303.7	793.1	303.7
61.26	166.5	275.5	1406.6	307.3	1586.1	1586.1	0.0015	0.5961	2.28	74.2	215.1	307.4	793.2	307.4
71.47	169.6	280.7	1671.9	311.4	1878.0	1878.0	0.0014	0.5916	2.34	76.1	217.1	311.4	793.2	311.4
81.68	159.5	263.9	1796.5	293.5	2028.2	2028.2	0.0018	0.6147	2.06	67.3	208.0	293.5	798.4	293.5
91.89	163.4	270.4	2070.9	298.9	2327.3	2327.3	0.0017	0.6081	2.13	69.8	211.0	298.9	798.4	298.9
102.10	164.5	272.3	2316.4	299.5	2596.4	2596.4	0.0011	0.5736	2.63	83.3	198.2	299.6	774.0	299.6

C.3.2.9 BT.10.Typ.1

x_{dist} (in)	P_{assume} (kip)	V_{LL} (kip)	M_{LL} (ft-kip)	V_{assume} (kip)	$M_{assume1}$ (ft-kip)	M_{assume} (ft-kip)	ε_s	θ (rad)	β	V_c (kip)	V_s (kip)	V_{n1} (kip)	V_{n2} (kip)	V_n (kip)
0.00	422.6	703.8	0.0	741.9	-0.2	2919.8	0.0012	0.5791	2.53	67.4	781.5	852.4	741.9	741.9
9.84	176.5	293.8	240.9	330.8	271.5	1279.0	0.0012	0.5791	2.53	67.8	253.7	330.9	752.5	330.9
19.68	146.8	244.5	400.9	280.4	461.4	1057.7	0.0012	0.5791	2.53	68.0	197.1	280.4	760.3	280.4
29.52	149.2	248.4	610.9	283.2	700.5	1059.5	0.0012	0.5791	2.53	68.0	197.3	283.2	763.5	283.2
39.36	149.8	249.5	818.3	283.3	936.0	1060.0	0.0012	0.5791	2.53	68.0	197.3	283.3	763.7	283.3
47.94	150.4	250.5	1000.8	283.3	1142.3	1142.3	0.0012	0.5791	2.53	68.0	197.4	283.3	763.8	283.3
49.19	150.9	251.2	1029.9	283.9	1174.9	1174.9	0.0012	0.5785	2.54	68.3	197.7	283.9	763.8	283.9
50.44	151.3	251.9	1059.1	284.5	1207.5	1207.5	0.0012	0.5778	2.55	68.6	198.0	284.5	763.9	284.5
59.03	154.1	256.6	1262.5	288.3	1433.9	1433.9	0.0011	0.5737	2.62	70.6	199.8	288.3	764.0	288.3
68.87	157.0	261.5	1500.6	292.0	1697.4	1697.4	0.0010	0.5697	2.70	72.5	201.6	292.0	764.1	292.0
78.71	159.6	265.8	1743.3	295.3	1964.8	1964.8	0.0010	0.5663	2.76	74.2	203.1	295.3	764.2	295.3
88.55	158.5	263.9	1947.5	292.3	2192.6	2192.6	0.0011	0.5707	2.68	72.3	202.1	292.4	767.6	292.4
98.39	150.2	250.1	2050.5	277.4	2318.5	2318.5	0.0006	0.5448	3.26	85.7	173.8	277.5	748.4	277.5

C.3.2.10 BT.10.Typ.2

x_{dist} (in)	P_{assume} (kip)	V_{LL} (kip)	M_{LL} (ft-kip)	V_{assume} (kip)	$M_{assume1}$ (ft-kip)	M_{assume} (ft-kip)	ε_s	θ (rad)	β	V_c (kip)	V_s (kip)	V_{n1} (kip)	V_{n2} (kip)	V_n (kip)
0.00	543.7	786.4	0.0	818.7	-0.2	3252.1	0.0012	0.5819	2.49	69.8	783.6	857.1	818.8	818.8
14.62	212.0	306.7	373.7	337.4	411.9	1306.9	0.0012	0.5819	2.49	70.4	254.8	337.5	833.9	337.5
29.24	177.9	257.3	626.9	286.3	701.4	1081.0	0.0012	0.5819	2.49	70.5	197.8	286.3	841.1	286.3
43.86	179.0	259.0	946.7	286.4	1055.5	1081.7	0.0012	0.5819	2.49	70.5	197.9	286.4	841.4	286.4
48.36	179.4	259.5	1046.0	286.4	1165.0	1165.0	0.0012	0.5819	2.49	70.5	197.9	286.4	841.4	286.4
58.48	183.3	265.2	1292.3	290.9	1433.5	1433.5	0.0012	0.5769	2.57	72.9	200.1	290.9	841.6	290.9
73.11	188.2	272.2	1658.3	296.3	1829.8	1829.8	0.0011	0.5713	2.67	75.7	202.6	296.3	841.8	296.3
87.73	170.7	247.0	1805.5	269.4	2005.3	2005.3	0.0010	0.5664	2.76	79.1	172.4	269.4	850.3	269.4
97.85	178.1	257.6	2100.8	278.9	2319.0	2319.0	0.0007	0.5488	3.15	87.4	173.6	279.0	823.6	279.0
102.35	179.8	260.1	2218.8	280.9	2444.9	2444.9	0.0007	0.5471	3.19	88.7	174.4	281.0	824.2	281.0
116.97	182.5	264.0	2573.5	283.1	2824.0	2824.0	0.0005	0.5391	3.42	92.4	172.9	283.2	802.7	283.2
131.59	173.3	250.8	2749.7	268.2	3022.4	3022.4	0.0008	0.5536	3.03	82.3	168.0	268.3	806.2	268.3
146.21	168.7	244.0	2973.3	259.9	3266.4	3266.4	0.0008	0.5569	2.96	78.6	163.4	260.0	790.0	260.0

C.3.2.11 Beam BT.10.Min.1

x_{dist} (in)	P_{assume} (kip)	V_{LL} (kip)	M_{LL} (ft-kip)	V_{assume} (kip)	$M_{assume1}$ (ft-kip)	M_{assume} (ft-kip)	ε_s	θ (rad)	β	V_c (kip)	V_s (kip)	V_{n1} (kip)	V_{n2} (kip)	V_n (kip)
0.00	474.8	781.9	0.0	820.7	-0.2	3267.2	0.0003	0.5243	3.93	110.5	893.6	1007.8	820.8	820.8
10.50	141.8	233.6	204.4	271.2	237.6	1050.4	0.0003	0.5243	3.93	111.2	149.9	271.3	832.6	271.3
21.00	142.5	234.7	410.8	271.2	476.4	1027.0	0.0003	0.5243	3.93	111.5	143.1	271.3	841.2	271.3
31.50	144.5	237.9	624.5	273.2	721.6	1028.3	0.0003	0.5243	3.93	111.5	143.2	273.3	843.6	273.3
42.00	115.4	190.0	664.9	224.1	792.3	830.2	0.0003	0.5243	3.93	111.6	94.0	224.1	843.7	224.1
48.47	115.8	190.7	770.3	224.1	915.9	915.9	0.0003	0.5243	3.93	111.6	94.0	224.1	843.8	224.1
52.50	117.8	194.0	848.7	226.9	1005.4	1005.4	0.0003	0.5222	4.01	114.0	94.5	227.0	843.9	227.0
56.53	119.7	197.1	928.4	229.6	1096.2	1096.2	0.0002	0.5203	4.09	116.2	94.9	229.6	844.0	229.6
63.00	122.5	201.8	1059.4	233.6	1244.5	1244.5	0.0002	0.5177	4.21	119.6	95.5	233.6	844.0	233.6
73.50	126.7	208.7	1278.3	239.3	1490.7	1490.7	0.0001	0.5140	4.38	124.5	96.3	239.3	844.2	239.3
84.00	129.5	213.3	1492.9	242.7	1731.6	1731.6	0.0001	0.5132	4.42	126.8	97.5	242.8	852.4	242.8
94.50	133.5	219.8	1731.2	248.1	1995.0	1995.0	0.0001	0.5101	4.58	131.5	98.2	248.2	852.4	248.2
105.00	135.8	223.6	1956.7	250.7	2244.8	2244.8	0.0000	0.5048	4.88	135.9	96.3	250.8	826.6	250.8

C.3.2.12 Beam BT.10.Min.2

x_{dist} (in)	P_{assume} (kip)	V_{LL} (kip)	M_{LL} (ft-kip)	V_{assume} (kip)	$M_{assume1}$ (ft-kip)	M_{assume} (ft-kip)	ε_s	θ (rad)	β	V_c (kip)	V_s (kip)	V_{n1} (kip)	V_{n2} (kip)	V_n (kip)
0.00	589.5	841.9	0.0	874.3	-0.2	3499.0	0.0003	0.5260	3.86	112.4	894.5	1010.6	874.3	874.3
15.18	172.2	245.8	311.0	276.5	350.7	1067.0	0.0003	0.5260	3.86	113.2	150.3	276.6	890.5	276.6
30.36	172.5	246.3	623.2	275.2	700.5	1041.7	0.0003	0.5260	3.86	113.4	143.4	275.3	897.5	275.3
45.54	139.3	198.9	754.7	226.1	867.6	867.6	0.0003	0.5260	3.86	113.5	94.1	226.1	897.8	226.1
48.71	139.5	199.3	808.9	226.1	928.9	928.9	0.0003	0.5260	3.86	113.5	94.1	226.1	897.9	226.1
60.72	146.0	208.5	1054.9	234.0	1201.1	1201.1	0.0002	0.5204	4.08	120.2	95.4	234.0	898.1	234.0
75.90	153.0	218.5	1381.8	242.3	1559.2	1559.2	0.0001	0.5151	4.32	127.2	96.6	242.3	898.3	242.3
91.08	161.1	230.0	1745.7	252.1	1952.2	1952.2	0.0001	0.5116	4.50	134.7	99.0	252.2	912.9	252.2
103.09	165.7	236.7	2033.1	257.4	2260.9	2260.9	0.0000	0.5053	4.85	141.2	97.7	257.4	888.3	257.4
106.26	166.2	237.4	2102.1	257.8	2335.4	2335.4	0.0000	0.5051	4.86	141.5	97.8	257.8	888.5	257.8
121.44	161.1	230.1	2328.7	248.8	2586.6	2586.6	0.0000	0.5053	4.85	136.1	94.2	248.8	857.1	248.8
136.62	158.0	225.7	2569.5	242.6	2850.0	2850.0	0.0000	0.5059	4.81	132.1	92.0	242.7	839.0	242.7
151.80	150.4	214.7	2716.5	230.0	3017.4	3017.4	0.0001	0.5142	4.37	120.7	90.9	230.1	844.5	230.1

C.3.3 Using the Simplified Procedure (Article 5.8.3.4.3)

Many of the inputs and basic calculations detailed in Section C.3.1 apply to calculating the shear strength when following the *General Procedure*. Differences between the two procedures arise from different assumed live loads and the steps for calculating β and θ. These intermediate results are provided for each beam test in the subsections on the following pages.

C.3.3.1 Beam T2.8.Typ.1

C.3.3.1.1 Additional Input and Basic Calculation

$h_{top.flange}$ (in)	30
S_b (in^3)	3220.4

C.3.3.1.2 Load Effects

x_{dist} (in)	V_{LL} (kip)	M_{LL} (ft-kip)	V_{DC1} (kip)	M_{DC1} (ft-kip)	V_{assume} (kip)	M_{assume} (ft-kip)
0.00	455.1	100000	18.7	-0.1	473.7	100000
5.73	320.5	153.1	18.2	8.7	338.7	161.8
11.47	377.6	360.9	17.8	17.3	395.4	378.2
17.20	316.2	453.2	17.3	25.7	333.5	478.9
22.94	333.6	637.6	16.9	33.9	350.5	671.5
28.67	339.0	810.0	16.4	41.8	355.5	851.8
34.40	328.2	940.9	16.0	49.6	344.2	990.5
38.71	330.3	1065.5	15.7	55.3	345.9	1120.7
40.14	330.9	1106.9	15.5	57.1	346.5	1164.0
45.87	333.5	1274.8	15.1	64.4	348.6	1339.2
51.60	324.0	1393.5	14.7	71.5	338.7	1465.0
57.34	326.6	1560.3	14.2	78.4	340.8	1638.7

C.3.3.1.3 Nominal Shear Strength Calculations

x_{dist} (in)	$P_{f.cpe}$ (kip)	e_{strand} (in)	f_{cpe} (ksi)	M_{cre} (ft-kip)	$P_{f.pc}$ (kip)	f_{pc} (ksi)	$cot\theta$
0.00	121.1	3.50	0.46	572.9	121.1	0.21	1.00
5.73	236.9	3.67	0.91	800.2	236.9	0.43	1.43
11.47	352.7	3.84	1.38	1034.5	352.7	0.64	1.64
17.20	468.5	4.00	1.85	1275.6	468.5	0.83	1.80
22.94	584.2	4.17	2.34	1523.7	584.2	1.02	1.80
28.67	605.7	4.33	2.46	1571.2	623.9	1.08	1.80
34.40	605.7	4.50	2.49	1572.5	646.2	1.11	1.80
38.71	605.7	4.62	2.51	1573.7	663.0	1.13	1.80
40.14	605.7	4.67	2.52	1574.2	668.5	1.14	1.80
45.87	605.7	4.83	2.55	1576.3	690.8	1.16	1.80
51.60	605.7	5.00	2.58	1578.9	713.2	1.18	1.80
57.34	605.7	5.16	2.61	1581.8	735.5	1.20	1.80

C.3.3.1.4 Final Shear Strength Results

x_{dist} (in)	V_{ci} (kip)	V_{cw} (kip)	V_c (kip)	V_s (kip)	V_{n1} (kip)	V_{n2} (kip)	V_n (kip)
0.0	42.9	61.5	42.9	430.9	473.8	535.6	473.8
5.7	1707.4	80.8	80.8	257.9	338.8	540.4	338.8
11.5	1114.7	99.3	99.3	296.1	395.5	544.6	395.5
17.2	922	117.0	117.0	216.6	333.6	548.4	333.6
22.9	828	133.8	133.8	216.8	350.6	552.1	350.6
28.7	689	138.8	138.8	216.8	355.6	552.9	355.6
34.4	578	136.0	136.0	208.2	344.3	531.7	344.3
38.7	517	137.6	137.6	208.4	346.0	532.2	346.0
40.1	500	138.1	138.1	208.5	346.6	532.4	346.6
45.9	441	139.9	139.9	208.8	348.7	533.0	348.7
51.6	395	137.2	137.2	201.6	338.8	515.4	338.8
57.3	359	138.7	138.7	202.1	340.8	516.7	340.8

C.3.3.2 Beam T2.8.Typ.2

C.3.3.2.1 Additional Input and Basic Calculation

$h_{top.flange}$ (in)	30
S_b (in^3)	3220.4

C.3.3.2.2 Load Effects

x_{dist} (in)	V_{LL} (kip)	M_{LL} (ft-kip)	V_{DC1} (kip)	M_{DC1} (ft-kip)	V_{assume} (kip)	M_{assume} (ft-kip)
0.00	458.4	100000	16.0	-0.1	474.5	100000
11.88	382.4	378.5	15.1	15.3	397.5	393.8
23.75	337.9	668.9	14.2	29.8	352.1	698.6
35.63	330.1	980.2	13.2	43.3	343.4	1023.5
38.77	331.5	1070.9	13.0	46.7	344.5	1117.7
47.50	334.9	1325.8	12.3	56.0	347.2	1381.8
59.38	327.6	1621.2	11.4	67.7	339.0	1688.9
71.26	317.5	1885.1	10.5	78.5	327.9	1963.6
79.99	301.3	2008.4	9.8	85.9	311.1	2094.3
83.13	302.4	2094.8	9.5	88.4	311.9	2183.2
95.01	306.0	2422.7	8.6	97.4	314.6	2520.1
106.88	308.8	2750.6	7.7	105.5	316.5	2856.1
118.76	310.5	3072.4	6.8	112.7	317.2	3185.1

C.3.3.2.3 Nominal Shear Strength Calculations

x_{dist} (in)	$P_{f.cpe}$ (kip)	e_{strand} (in)	f_{cpe} (ksi)	M_{cre} (ft-kip)	$P_{f.pc}$ (kip)	f_{pc} (ksi)	$cot\theta$
0.00	121.1	3.50	0.46	567.4	121.1	0.21	1.00
11.88	360.9	3.85	1.41	1046.1	360.9	0.64	1.65
23.75	600.7	4.19	2.41	1554.2	600.7	1.03	1.80
35.63	605.7	4.54	2.49	1572.6	651.0	1.09	1.80
38.77	605.7	4.63	2.51	1574.9	663.2	1.10	1.80
47.50	605.7	4.88	2.56	1582.0	697.2	1.13	1.80
59.38	605.7	5.22	2.62	1593.2	743.5	1.16	1.80
71.26	605.7	5.57	2.69	1606.3	790.0	1.18	1.80
79.99	605.7	5.82	2.74	1617.0	824.0	1.19	1.80
83.13	605.7	5.91	2.75	1621.1	836.3	1.19	1.80
95.01	605.7	6.25	2.82	1637.9	882.6	1.18	1.80
106.88	605.7	6.60	2.88	1656.4	929.0	1.17	1.80
118.76	605.7	6.94	2.95	1676.8	968.8	1.13	1.80

C.3.3.2.4 Final Shear Strength Results

x_{dist} (in)	V_{ci} (kip)	V_{cw} (kip)	V_c (kip)	V_s (kip)	V_{n1} (kip)	V_{n2} (kip)	V_n (kip)
0.0	43.0	61.6	43.0	431.5	474.5	537.9	474.5
11.9	1086.6	100.2	100.2	297.4	397.6	547.1	397.6
23.8	813.8	135.1	135.1	217.1	352.2	554.9	352.2
35.6	556.8	134.9	134.9	208.6	343.5	534.0	343.5
38.8	514	135.8	135.8	208.7	344.6	534.4	344.6
47.5	426	138.2	138.2	209.2	347.3	535.4	347.3
59.4	347	136.5	136.5	202.6	339.1	519.3	339.1
71.3	294	133.2	133.2	194.8	328.0	500.0	328.0
80.0	265	134.5	134.5	176.7	311.2	503.7	311.2
83.1	257	134.8	134.8	177.2	312.0	505.0	312.0
95.0	229	135.7	135.7	179.0	314.7	510.0	314.7
106.9	207	135.8	135.8	180.8	316.6	515.0	316.6
118.8	190	134.7	134.7	182.6	317.3	520.0	317.3

C.3.3.3 Beam T2.8.Min.1

C.3.3.3.1 Additional Input and Basic Calculation

$h_{top.flange}$ (in)	30
S_b (in^3)	3220.4

C.3.3.3.2 Load Effects

x_{dist} (in)	V_{LL} (kip)	M_{LL} (ft-kip)	V_{DC1} (kip)	M_{DC1} (ft-kip)	V_{assume} (kip)	M_{assume} (ft-kip)
0.00	449.9	100000	18.1	-0.1	468.0	100000
5.80	231.3	111.8	17.7	8.5	248.9	120.3
11.60	226.3	218.8	17.2	17.0	243.6	235.7
17.40	258.9	375.3	16.8	25.2	275.7	400.5
23.20	276.0	533.5	16.4	33.2	292.3	566.7
29.00	280.7	678.2	15.9	41.0	296.6	719.2
34.80	272.0	788.7	15.5	48.6	287.5	837.4
38.22	273.6	871.5	15.2	53.0	288.8	924.5
40.60	274.7	929.3	15.0	56.0	289.7	985.2
46.40	277.1	1071.5	14.6	63.1	291.7	1134.7
52.20	269.5	1172.2	14.2	70.1	283.7	1242.3
58.00	271.8	1313.8	13.7	76.8	285.6	1390.7

C.3.3.3.3 Nominal Shear Strength Calculations

x_{dist} (in)	$P_{f.cpe}$ (kip)	e_{strand} (in)	f_{cpe} (ksi)	M_{cre} (ft-kip)	$P_{f.pc}$ (kip)	f_{pc} (ksi)	$cot\theta$
0.00	119.4	3.50	0.45	557.1	119.4	0.21	1.00
5.80	234.9	3.67	0.90	779.0	234.9	0.43	1.43
11.60	350.4	3.84	1.37	1007.8	350.4	0.63	1.64
17.40	465.8	4.01	1.84	1243.3	465.8	0.83	1.80
23.20	581.3	4.18	2.33	1485.7	581.3	1.01	1.80
29.00	597.2	4.34	2.42	1520.6	616.8	1.06	1.80
34.80	597.2	4.51	2.46	1522.1	639.6	1.09	1.80
38.22	597.2	4.61	2.47	1523.2	653.1	1.11	1.80
40.60	597.2	4.68	2.49	1524.1	662.4	1.12	1.80
46.40	597.2	4.85	2.52	1526.4	685.2	1.15	1.80
52.20	597.2	5.01	2.55	1529.2	708.0	1.17	1.80
58.00	597.2	5.18	2.58	1532.3	730.8	1.18	1.80

C.3.3.3.4 Final Shear Strength Results

x_{dist} (in)	V_{ci} (kip)	V_{cw} (kip)	V_c (kip)	V_s (kip)	V_{n1} (kip)	V_{n2} (kip)	V_n (kip)
0.0	42.4	60.6	42.4	425.7	468.1	530.6	468.1
5.8	1643.7	79.6	79.6	169.3	248.9	535.3	248.9
11.6	1074.0	97.9	97.9	145.7	243.6	539.5	243.6
17.4	889	115.3	115.3	160.5	275.7	543.3	275.7
23.2	799	131.8	131.8	160.6	292.4	547.0	292.4
29.0	659	136.0	136.0	160.6	296.7	547.6	296.7
34.8	554	133.4	133.4	154.2	287.6	526.5	287.6
38.2	507	134.6	134.6	154.4	288.9	526.9	288.9
40.6	479	135.4	135.4	154.4	289.8	527.2	289.8
46.4	423	137.2	137.2	154.6	291.8	527.8	291.8
52.2	379	134.4	134.4	149.3	283.8	510.2	283.8
58.0	344	136.0	136.0	149.7	285.7	511.5	285.7

C.3.3.4 T2.8.Min.2

C.3.3.4.1 Additional Input and Basic Calculation

$h_{top.flange}$ (in)	30
S_b (in^3)	3220.4

C.3.3.4.2 Load Effects

x_{dist} (in)	V_{LL} (kip)	M_{LL} (ft-kip)	V_{DC1} (kip)	M_{DC1} (ft-kip)	V_{assume} (kip)	M_{assume} (ft-kip)
0.00	456.5	100000	15.9	-0.1	472.4	100000
11.63	278.5	269.8	15.0	14.9	293.5	284.7
23.25	279.9	542.3	14.1	29.0	294.0	571.3
34.88	275.5	800.6	13.2	42.2	288.7	842.8
38.60	277.0	891.2	12.9	46.2	289.9	937.4
46.50	280.1	1085.5	12.3	54.5	292.4	1140.0
58.13	274.5	1329.6	11.4	65.9	285.8	1395.5
69.75	266.3	1548.0	10.4	76.5	276.8	1624.5
77.65	269.2	1742.1	9.8	83.2	279.0	1825.2
81.38	270.5	1834.1	9.5	86.2	280.0	1920.3
93.00	273.9	2122.5	8.6	94.9	282.5	2217.5
104.63	276.5	2410.8	7.7	102.9	284.2	2513.6
116.25	278.3	2696.4	6.8	109.9	285.1	2806.3

C.3.3.4.3 Nominal Shear Strength Calculations

x_{dist} (in)	$P_{f.cpe}$ (kip)	e_{strand} (in)	f_{cpe} (ksi)	M_{cre} (ft-kip)	$P_{f.pc}$ (kip)	f_{pc} (ksi)	$cot\theta$
0.00	119.4	3.50	0.45	564.4	119.4	0.21	1.00
11.63	350.9	3.84	1.37	1026.4	350.9	0.63	1.63
23.25	582.3	4.18	2.33	1516.2	582.3	1.00	1.80
34.88	597.2	4.51	2.46	1555.4	639.9	1.07	1.80
38.60	597.2	4.62	2.48	1558.0	654.6	1.09	1.80
46.50	597.2	4.85	2.52	1564.2	685.6	1.12	1.80
58.13	597.2	5.19	2.58	1574.8	731.3	1.15	1.80
69.75	597.2	5.52	2.64	1587.2	777.2	1.17	1.80
77.65	597.2	5.75	2.69	1596.6	808.3	1.18	1.80
81.38	597.2	5.86	2.71	1601.3	823.0	1.18	1.80
93.00	597.2	6.20	2.77	1617.3	868.8	1.18	1.80
104.63	597.2	6.53	2.83	1635.0	914.6	1.16	1.80
116.25	597.2	6.87	2.89	1654.4	960.4	1.14	1.80

C.3.3.4.4 Final Shear Strength Results

x_{dist} (in)	V_{ci} (kip)	V_{cw} (kip)	V_c (kip)	V_s (kip)	V_{n1} (kip)	V_{n2} (kip)	V_n (kip)
0.0	42.8	61.1	42.8	429.7	472.5	535.6	472.5
11.6	1088.9	98.3	98.3	195.4	293.6	544.5	293.6
23.3	811.0	132.0	132.0	162.1	294.1	552.1	294.1
34.9	562	133.0	133.0	155.7	288.8	531.5	288.8
38.6	511	134.2	134.2	155.9	290.0	531.9	290.0
46.5	430	136.3	136.3	156.2	292.5	532.8	292.5
58.1	350	134.7	134.7	151.2	285.9	516.5	285.9
69.8	296	131.5	131.5	145.3	276.8	497.1	276.8
77.7	270	132.8	132.8	146.3	279.1	500.5	279.1
81.4	259	133.3	133.3	146.8	280.1	502.0	280.1
93.0	230	134.3	134.3	148.3	282.6	506.9	282.6
104.6	209	134.5	134.5	149.8	284.3	511.8	284.3
116.3	191	134.0	134.0	151.3	285.2	516.7	285.2

C.3.3.5 Beam BT.8.Typ.1

C.3.3.5.1 Additional Input and Basic Calculation

$h_{top.flange}$ (in)	41
S_b (in^3)	9325.24

C.3.3.5.2 Load Effects

x_{dist} (in)	V_{LL} (kip)	M_{LL} (ft-kip)	V_{DC1} (kip)	M_{DC1} (ft-kip)	V_{assume} (kip)	M_{assume} (ft-kip)
0.00	549.2	100000	38.6	-0.2	587.8	100000
10.21	352.7	300.1	37.5	32.2	390.1	332.2
20.42	298.0	507.1	36.3	63.6	334.4	570.7
30.63	321.9	821.6	35.2	94.0	357.1	915.7
40.84	332.0	1129.7	34.1	123.5	366.0	1253.2
48.77	339.4	1379.2	33.2	145.7	372.6	1524.9
51.05	341.4	1452.5	32.9	152.0	374.4	1604.5
53.33	343.5	1526.5	32.7	158.2	376.2	1684.7
61.26	350.4	1788.6	31.8	179.5	382.2	1968.1
71.47	358.7	2136.5	30.7	206.1	389.4	2342.6
81.68	369.1	2512.1	29.5	231.7	398.6	2743.9
91.89	376.3	2881.8	28.4	256.4	404.7	3138.2
102.10	346.1	2944.9	27.3	280.0	373.4	3224.9

C.3.3.5.3 Nominal Shear Strength Calculations

x_{dist} (in)	$P_{f.cpe}$ (kip)	e_{strand} (in)	f_{cpe} (ksi)	M_{cre} (ft-kip)	$P_{f.pc}$ (kip)	f_{pc} (ksi)	$cot\theta$
0.00	182.2	12.09	0.48	1251.8	182.2	0.10	1.00
10.21	492.1	12.29	1.31	2160.4	492.1	0.28	1.28
20.42	802.1	12.49	2.15	3086.1	802.1	0.45	1.45
30.63	910.8	12.70	2.46	3400.5	945.6	0.53	1.53
40.84	910.8	12.90	2.48	3379.8	999.1	0.57	1.56
48.77	910.8	13.06	2.50	3364.6	1040.6	0.59	1.59
51.05	910.8	13.11	2.50	3360.4	1052.6	0.60	1.60
53.33	910.8	13.15	2.50	3356.3	1064.5	0.61	1.61
61.26	910.8	13.31	2.52	3342.5	1106.1	0.63	1.63
71.47	910.8	13.52	2.54	3326.1	1159.6	0.66	1.66
81.68	910.8	13.72	2.56	3311.1	1213.7	0.69	1.69
91.89	910.8	13.93	2.58	3297.5	1267.4	0.71	1.71
102.10	910.8	14.13	2.60	3285.3	1321.0	0.74	1.73

C.3.3.5.4 Final Shear Strength Results

x_{dist} (in)	V_{ci} (kip)	V_{cw} (kip)	V_c (kip)	V_s (kip)	V_{n1} (kip)	V_{n2} (kip)	V_n (kip)
0.0	65.9	74.6	65.9	522.0	587.9	773.8	587.9
10.2	2597.1	99.6	99.6	290.5	390.1	783.1	390.1
20.4	1870.5	123.5	123.5	210.9	334.4	790.4	334.4
30.6	1388	134.2	134.2	222.9	357.1	792.9	357.1
40.8	1048	137.9	137.9	228.2	366.0	793.0	366.0
48.8	882	140.6	140.6	232.0	372.6	793.1	372.6
51.1	843	141.3	141.3	233.1	374.4	793.1	374.4
53.3	808	142.1	142.1	234.1	376.2	793.1	376.2
61.3	707	144.5	144.5	237.6	382.2	793.2	382.2
71.5	610	147.5	147.5	241.9	389.4	793.2	389.4
81.7	537	151.2	151.2	247.4	398.6	798.4	398.6
91.9	480	153.7	153.7	251.0	404.7	798.4	404.7
102.1	433	151.7	151.7	221.7	373.4	774.0	373.4

C.3.3.6 Beam BT.8.Typ.2

C.3.3.6.1 Additional Input and Basic Calculation

$h_{top.flange}$ (in)	41
S_b (in^3)	9325.24

C.3.3.6.2 Load Effects

x_{dist} (in)	V_{LL} (kip)	M_{LL} (ft-kip)	V_{DC1} (kip)	M_{DC1} (ft-kip)	V_{assume} (kip)	M_{assume} (ft-kip)
0.00	554.2	100000	32.8	-0.2	587.0	100000
15.33	382.1	488.0	31.0	40.5	413.1	528.6
30.66	316.2	807.7	29.3	79.0	345.4	886.7
45.98	328.8	1259.8	27.5	115.3	356.3	1375.1
49.08	331.2	1354.5	27.1	122.3	358.3	1476.8
61.31	340.0	1737.2	25.8	149.3	365.8	1886.4
76.64	352.0	2248.2	24.0	181.0	376.0	2429.2
91.97	336.7	2580.4	22.3	210.6	359.0	2791.0
104.19	331.6	2879.3	20.9	232.5	352.5	3111.9
107.29	333.0	2977.6	20.5	237.9	353.5	3215.5
122.62	325.9	3330.1	18.8	263.0	344.6	3593.1
137.95	318.5	3660.9	17.0	285.8	335.5	3946.7
153.28	319.6	4082.5	15.3	306.4	334.9	4388.9

C.3.3.6.3 Nominal Shear Strength Calculations

x_{dist} (in)	$P_{f.cpe}$ (kip)	e_{strand} (in)	f_{cpe} (ksi)	M_{cre} (ft-kip)	$P_{f.pc}$ (kip)	f_{pc} (ksi)	$cot\theta$
0.00	182.2	12.09	0.48	1267.0	182.2	0.09	1.00
15.33	647.5	12.39	1.73	2665.3	647.5	0.33	1.33
30.66	910.8	12.70	2.46	3464.4	945.8	0.48	1.47
45.98	910.8	13.01	2.49	3444.9	1026.2	0.52	1.52
49.08	910.8	13.07	2.50	3441.3	1042.5	0.53	1.52
61.31	910.8	13.31	2.52	3428.7	1106.7	0.56	1.55
76.64	910.8	13.62	2.55	3415.9	1187.7	0.59	1.59
91.97	910.8	13.93	2.58	3406.5	1268.3	0.62	1.61
104.19	910.8	14.17	2.60	3401.4	1332.7	0.63	1.63
107.29	910.8	14.23	2.61	3400.5	1349.0	0.64	1.64
122.62	910.8	14.54	2.64	3397.8	1370.8	0.64	1.63
137.95	910.8	14.85	2.67	3398.5	1371.1	0.63	1.62
153.28	910.8	15.15	2.70	3402.5	1371.3	0.61	1.61

C.3.3.6.4 Final Shear Strength Results

x_{dist} (in)	V_{ci} (kip)	V_{cw} (kip)	V_c (kip)	V_s (kip)	V_{n1} (kip)	V_{n2} (kip)	V_n (kip)
0.0	61.7	74.2	61.7	525.3	587.1	778.8	587.1
15.3	2138.4	108.7	108.7	304.5	413.1	791.8	413.1
30.7	1406.1	129.2	129.2	216.2	345.4	797.9	345.4
46.0	947	133.7	133.7	222.6	356.3	798.0	356.3
49.1	889	134.5	134.5	223.8	358.3	798.1	358.3
61.3	718	137.6	137.6	228.2	365.8	798.2	365.8
76.6	580	141.7	141.7	234.3	376.0	802.9	376.0
92.0	488	144.5	144.5	214.5	359.0	802.9	359.0
104.2	433	142.4	142.4	210.1	352.5	778.7	352.5
107.3	421	142.8	142.8	210.7	353.5	779.1	353.5
122.6	371	139.5	139.5	205.2	344.7	759.7	344.7
138.0	332	135.9	135.9	199.5	335.5	744.0	335.5
153.3	301	135.5	135.5	199.4	334.9	748.9	334.9

C.3.3.7 Beam BT.8N.Typ.1

C.3.3.7.1 Additional Input and Basic Calculation

$h_{top.flange}$ (in)	41
S_b (in^3)	9325.24

C.3.3.7.2 Load Effects

x_{dist} (in)	V_{LL} (kip)	M_{LL} (ft-kip)	V_{DC1} (kip)	M_{DC1} (ft-kip)	V_{assume} (kip)	M_{assume} (ft-kip)
0.00	565.0	100000	41.9	-0.2	606.9	100000
10.44	329.6	286.7	40.7	35.7	370.2	322.4
20.88	343.6	597.8	39.4	70.6	383.0	668.3
31.32	263.7	688.1	38.1	104.3	301.8	792.4
41.76	274.4	954.6	36.9	136.9	311.2	1091.6
48.54	281.1	1137.0	36.1	157.6	317.2	1294.6
52.19	284.7	1238.2	35.6	168.5	320.3	1406.7
55.85	287.4	1337.4	35.2	179.3	322.5	1516.7
62.63	291.2	1519.6	34.4	198.9	325.5	1718.5
73.07	297.7	1812.8	33.1	228.3	330.8	2041.1
83.51	304.4	2118.3	31.8	256.5	336.2	2374.8
93.95	309.7	2424.5	30.6	283.7	340.3	2708.2
104.39	304.6	2649.9	29.3	309.7	333.9	2959.6

C.3.3.7.3 Nominal Shear Strength Calculations

x_{dist} (in)	$P_{f.cpe}$ (kip)	e_{strand} (in)	f_{cpe} (ksi)	M_{cre} (ft-kip)	$P_{f.pc}$ (kip)	f_{pc} (ksi)	$cot\theta$
0.00	174.6	12.09	0.46	1152.6	174.6	0.13	1.00
10.44	478.3	12.29	1.27	1987.8	478.3	0.36	1.36
20.88	782.0	12.50	2.10	2839.4	782.0	0.59	1.59
31.32	872.9	12.71	2.36	3079.3	912.6	0.69	1.70
41.76	872.9	12.92	2.38	3054.7	969.3	0.74	1.75
48.54	872.9	13.06	2.39	3039.7	1006.1	0.77	1.78
52.19	872.9	13.13	2.40	3031.8	1026.0	0.79	1.79
55.85	872.9	13.20	2.41	3024.1	1045.8	0.80	1.80
62.63	872.9	13.34	2.42	3010.4	1082.7	0.83	1.80
73.07	872.9	13.55	2.44	2990.5	1139.5	0.88	1.80
83.51	872.9	13.76	2.46	2972.1	1196.5	0.92	1.80
93.95	872.9	13.97	2.48	2955.3	1253.3	0.96	1.80
104.39	872.9	14.18	2.50	2940.1	1310.1	0.99	1.80

C.3.3.7.4 Final Shear Strength Results

x_{dist} (in)	V_{ci} (kip)	V_{cw} (kip)	V_c (kip)	V_s (kip)	V_{n1} (kip)	V_{n2} (kip)	V_n (kip)
0.00	68.5	76.5	68.5	538.5	607.0	751.1	607.0
10.44	2346.0	106.8	106.8	263.5	370.3	760.4	370.3
20.88	1691.7	136.3	136.3	246.8	383.0	767.6	383.0
31.32	1238	148.5	148.5	153.3	301.8	769.8	301.8
41.75	935	153.5	153.5	157.8	311.3	769.9	311.3
48.54	808	156.6	156.6	160.6	317.2	769.9	317.2
52.19	753	158.3	158.3	162.0	320.3	770.0	320.3
55.85	705	159.9	159.9	162.6	322.6	770.0	322.6
62.63	631	162.9	162.9	162.7	325.5	770.1	325.5
73.07	545	167.7	167.7	163.1	330.8	772.2	330.8
83.51	479	172.5	172.5	163.7	336.3	775.1	336.3
93.95	428	176.6	176.6	163.7	340.3	775.1	340.3
104.39	387	175.3	175.3	158.6	334.0	751.5	334.0

C.3.3.8 Beam BT.8N.Typ.2

C.3.3.8.1 Additional Input and Basic Calculation

$h_{top.flange}$ (in)	41
S_b (in^3)	9325.24

C.3.3.8.2 Load Effects

x_{dist} (in)	V_{LL} (kip)	M_{LL} (ft-kip)	V_{DC1} (kip)	M_{DC1} (ft-kip)	V_{assume} (kip)	M_{assume} (ft-kip)
0.00	565.1	100000	34.2	-0.2	599.3	100000
15.26	312.9	397.9	32.3	42.1	345.2	440.0
30.52	266.6	678.0	30.5	82.0	297.0	760.1
45.79	280.9	1071.7	28.6	119.6	309.5	1191.3
48.58	283.4	1147.4	28.3	126.2	311.7	1273.6
61.05	293.6	1493.7	26.8	154.9	320.4	1648.5
76.31	301.2	1915.2	24.9	187.8	326.1	2102.9
91.57	310.3	2368.0	23.1	218.3	333.4	2586.3
104.04	279.4	2422.5	21.6	241.5	301.0	2664.0
106.83	280.7	2499.2	21.3	246.5	302.0	2745.7
122.09	277.0	2818.8	19.4	272.4	296.5	3091.2
137.35	272.2	3115.9	17.6	295.9	289.8	3411.9
152.62	275.1	3499.0	15.7	317.1	290.9	3816.1

C.3.3.8.3 Nominal Shear Strength Calculations

x_{dist} (in)	$P_{f.cpe}$ (kip)	e_{strand} (in)	f_{cpe} (ksi)	M_{cre} (ft-kip)	$P_{f.pc}$ (kip)	f_{pc} (ksi)	$cot\theta$
0.00	174.6	12.09	0.46	1146.2	174.6	0.12	1.00
15.26	618.6	12.39	1.65	2391.2	618.6	0.46	1.47
30.52	872.9	12.70	2.36	3109.7	908.3	0.67	1.68
45.79	872.9	13.00	2.39	3088.1	991.2	0.73	1.75
48.58	872.9	13.06	2.39	3084.4	1006.4	0.74	1.76
61.05	872.9	13.31	2.42	3069.7	1074.1	0.79	1.80
76.31	872.9	13.61	2.44	3054.6	1157.0	0.85	1.80
91.57	872.9	13.92	2.47	3042.9	1240.5	0.90	1.80
104.04	872.9	14.17	2.50	3035.7	1308.3	0.94	1.80
106.83	872.9	14.22	2.50	3034.4	1323.5	0.94	1.80
122.09	872.9	14.53	2.53	3029.3	1364.3	0.96	1.80
137.35	872.9	14.84	2.56	3027.4	1364.6	0.96	1.80
152.62	872.9	15.14	2.59	3028.9	1364.8	0.95	1.80

C.3.3.8.4 Final Shear Strength Results

x_{dist} (in)	V_{ci} (kip)	V_{cw} (kip)	V_c (kip)	V_s (kip)	V_{n1} (kip)	V_{n2} (kip)	V_n (kip)
0.0	60.4	75.3	60.4	538.9	599.4	727.2	599.4
15.3	1932.4	118.3	118.3	226.9	345.2	739.9	345.2
30.5	1273.0	145.0	145.0	152.1	297.1	745.8	297.1
45.8	858	151.5	151.5	158.0	309.5	745.9	309.5
48.6	810	152.7	152.7	159.1	311.7	745.9	311.7
61.1	650	157.6	157.6	162.8	320.4	746.0	320.4
76.3	525	163.3	163.3	162.8	326.1	746.2	326.1
91.6	442	169.6	169.6	163.9	333.4	750.9	333.4
104.0	391	168.7	168.7	132.3	301.0	728.0	301.0
106.8	382	169.6	169.6	132.4	302.0	728.3	302.0
122.1	336	167.5	167.5	128.9	296.5	710.0	296.5
137.4	301	163.6	163.6	126.2	289.8	695.1	289.8
152.6	273	163.8	163.8	127.0	290.9	699.7	290.9

C.3.3.9 Beam BT.10.Typ.1

C.3.3.9.1 Additional Input and Basic Calculation

$h_{top.flange}$ (in)	41
S_b (in^3)	9325.24

C.3.3.9.2 Load Effects

x_{dist} (in)	V_{LL} (kip)	M_{LL} (ft-kip)	V_{DC1} (kip)	M_{DC1} (ft-kip)	V_{assume} (kip)	M_{assume} (ft-kip)
0.00	537.3	100000	38.1	-0.2	575.4	100000
9.84	280.1	229.6	37.0	30.6	317.1	260.3
19.68	282.4	463.1	35.9	60.5	318.3	523.6
29.52	310.1	762.7	34.9	89.6	344.9	852.2
39.36	320.1	1049.7	33.8	117.7	353.9	1167.4
47.95	328.4	1312.3	32.8	141.6	361.3	1453.8
49.20	329.6	1351.4	32.7	145.0	362.3	1496.4
50.45	330.8	1390.7	32.6	148.4	363.4	1539.1
59.03	338.8	1666.7	31.6	171.3	370.4	1838.0
68.87	347.5	1994.4	30.6	196.8	378.0	2191.2
78.71	355.8	2333.6	29.5	221.4	385.2	2555.0
88.55	364.5	2689.5	28.4	245.2	392.9	2934.6
98.39	320.7	2629.7	27.3	268.0	348.1	2897.7

C.3.3.9.3 Nominal Shear Strength Calculations

x_{dist} (in)	$P_{f.cpe}$ (kip)	e_{strand} (in)	f_{cpe} (ksi)	M_{cre} (ft-kip)	$P_{f.pc}$ (kip)	f_{pc} (ksi)	$cot\theta$
0.00	180.3	12.09	0.48	1210.1	180.3	0.11	1.00
9.84	476.1	12.28	1.27	2056.6	476.1	0.31	1.31
19.68	771.8	12.48	2.07	2918.4	771.8	0.50	1.50
29.52	901.7	12.68	2.43	3290.5	930.8	0.60	1.60
39.36	901.7	12.87	2.45	3271.1	982.6	0.64	1.64
47.95	901.7	13.05	2.47	3255.2	1027.8	0.67	1.67
49.20	901.7	13.07	2.47	3253.0	1034.4	0.67	1.68
50.45	901.7	13.10	2.47	3250.8	1040.9	0.68	1.68
59.03	901.7	13.27	2.49	3236.2	1086.2	0.71	1.71
68.87	901.7	13.46	2.51	3220.6	1138.0	0.74	1.75
78.71	901.7	13.66	2.53	3206.4	1189.8	0.77	1.78
88.55	901.7	13.86	2.55	3193.4	1242.1	0.80	1.80
98.39	901.7	14.06	2.57	3181.7	1294.6	0.83	1.80

C.3.3.9.4 Final Shear Strength Results

x_{dist} (in)	V_{ci} (kip)	V_{cw} (kip)	V_c (kip)	V_s (kip)	V_{n1} (kip)	V_{n2} (kip)	V_n (kip)
0.0	64.4	74.0	64.4	511.0	575.5	741.9	575.5
9.8	2565.2	100.0	100.0	217.1	317.1	752.5	317.1
19.7	1835.7	125.2	125.2	193.2	318.4	760.3	318.4
29.5	1393	138.2	138.2	206.7	344.9	763.5	344.9
39.4	1051	142.1	142.1	211.8	353.9	763.7	353.9
47.9	868	145.3	145.3	216.0	361.3	763.8	361.3
49.2	846	145.8	145.8	216.6	362.4	763.9	362.4
50.4	826	146.3	146.3	217.2	363.4	763.9	363.4
59.0	709	149.3	149.3	221.1	370.4	764.0	370.4
68.9	612	152.7	152.7	225.4	378.1	764.1	378.1
78.7	538	155.8	155.8	229.5	385.2	764.2	385.2
88.6	481	159.4	159.4	233.5	392.9	767.6	392.9
98.4	435	158.5	158.5	189.6	348.1	748.4	348.1

C.3.3.10 Beam BT.10.Typ.2

C.3.3.10.1 Additional Input and Basic Calculation

$h_{top.flange}$ (in)	41
S_b (in^3)	9325.24

C.3.3.10.2 Load Effects

x_{dist} (in)	V_{LL} (kip)	M_{LL} (ft-kip)	V_{DC1} (kip)	M_{DC1} (ft-kip)	V_{assume} (kip)	M_{assume} (ft-kip)
0.00	545.9	100000	32.3	-0.2	578.2	100000
14.62	316.2	385.3	30.6	38.2	346.8	423.4
29.24	315.8	769.6	29.0	74.5	344.8	844.1
43.86	329.2	1203.5	27.4	108.8	356.6	1312.3
48.36	333.2	1342.8	26.8	119.0	360.0	1461.8
58.49	341.7	1665.4	25.7	141.2	367.4	1806.6
73.11	353.2	2152.0	24.1	171.5	377.3	2323.5
87.73	329.4	2408.5	22.4	199.8	351.9	2608.3
97.85	324.8	2648.6	21.3	218.2	346.1	2866.9
102.35	327.6	2794.4	20.8	226.1	348.4	3020.6
116.97	323.7	3155.7	19.1	250.4	342.9	3406.1
131.59	325.3	3567.3	17.5	272.7	342.8	3840.0
146.21	318.5	3880.5	15.8	293.0	334.3	4173.5

C.3.3.10.3 Nominal Shear Strength Calculations

x_{dist} (in)	$P_{f.cpe}$ (kip)	e_{strand} (in)	f_{cpe} (ksi)	M_{cre} (ft-kip)	$P_{f.pc}$ (kip)	f_{pc} (ksi)	$cot\theta$
0.00	180.3	12.09	0.48	1240.7	180.3	0.11	1.00
14.62	619.8	12.38	1.65	2514.0	619.8	0.40	1.38
29.24	901.7	12.67	2.43	3341.5	929.4	0.59	1.57
43.86	901.7	12.96	2.46	3323.6	1006.6	0.64	1.62
48.36	901.7	13.05	2.47	3318.7	1030.3	0.66	1.63
58.49	901.7	13.26	2.49	3308.6	1083.8	0.69	1.66
73.11	901.7	13.55	2.52	3296.5	1161.0	0.73	1.70
87.73	901.7	13.84	2.55	3287.3	1239.0	0.77	1.74
97.85	901.7	14.04	2.57	3282.7	1292.6	0.79	1.76
102.35	901.7	14.13	2.57	3281.0	1316.5	0.81	1.77
116.97	901.7	14.43	2.60	3277.7	1363.9	0.82	1.79
131.59	901.7	14.72	2.63	3277.2	1364.2	0.81	1.78
146.21	901.7	15.01	2.66	3279.7	1364.4	0.80	1.77

C.3.3.10.4 Final Shear Strength Results

x_{dist} (in)	V_{ci} (kip)	V_{cw} (kip)	V_c (kip)	V_s (kip)	V_{n1} (kip)	V_{n2} (kip)	V_n (kip)
0.0	62.7	77.4	62.7	515.5	578.3	818.8	578.3
14.6	2115.0	115.6	115.6	231.3	346.8	833.9	346.8
29.2	1421.4	141.0	141.0	203.8	344.8	841.1	344.8
43.9	958	146.3	146.3	210.3	356.6	841.4	356.6
48.4	871	147.8	147.8	212.2	360.0	841.4	360.0
58.5	726	151.1	151.1	216.3	367.4	841.6	367.4
73.1	586	155.6	155.6	221.8	377.3	841.8	377.3
87.7	493	161.0	161.0	190.9	351.9	850.3	351.9
97.9	445	158.9	158.9	187.2	346.1	823.6	346.1
102.4	426	160.0	160.0	188.4	348.4	824.2	348.4
117.0	376	157.8	157.8	185.1	342.9	802.7	342.9
131.6	337	157.7	157.7	185.1	342.8	806.2	342.8
146.2	305	153.9	153.9	180.4	334.3	790.0	334.3

C.3.3.11 Beam BT.10.Min.1

C.3.3.11.1 Additional Input and Basic Calculation

$h_{top.flange}$ (in)	41
S_b (in^3)	9325.24

C.3.3.11.2 Load Effects

x_{dist} (in)	V_{LL} (kip)	M_{LL} (ft-kip)	V_{DC1} (kip)	M_{DC1} (ft-kip)	V_{assume} (kip)	M_{assume} (ft-kip)
0.00	544.4	100000	38.8	-0.2	583.2	100000
10.50	184.4	161.3	37.6	33.3	222.0	194.6
21.00	225.2	394.2	36.5	65.7	261.7	459.8
31.50	244.5	641.7	35.3	97.1	279.8	738.8
42.00	206.1	721.1	34.1	127.4	240.2	848.6
48.47	210.5	850.0	33.4	145.6	243.8	995.7
52.50	213.1	932.4	32.9	156.8	246.1	1089.2
56.53	215.8	1016.4	32.5	167.8	248.3	1184.1
63.00	219.9	1154.4	31.8	185.1	251.7	1339.5
73.50	226.3	1386.2	30.6	212.4	256.9	1598.6
84.00	234.9	1644.3	29.4	238.7	264.3	1882.9
94.50	240.1	1890.5	28.3	263.9	268.3	2154.4
105.00	236.3	2067.4	27.1	288.1	263.4	2355.5

C.3.3.11.3 Nominal Shear Strength Calculations

x_{dist} (in)	$P_{f.cpe}$ (kip)	e_{strand} (in)	f_{cpe} (ksi)	M_{cre} (ft-kip)	$P_{f.pc}$ (kip)	f_{pc} (ksi)	$cot\theta$
0.00	186.3	12.09	0.49	1255.4	186.3	0.12	1.00
10.50	512.4	12.30	1.36	2187.4	512.4	0.34	1.32
21.00	838.5	12.51	2.25	3137.5	838.5	0.55	1.52
31.50	931.7	12.72	2.52	3396.9	970.1	0.63	1.61
42.00	931.7	12.93	2.54	3376.5	1023.8	0.67	1.65
48.47	931.7	13.06	2.55	3364.7	1056.9	0.70	1.67
52.50	931.7	13.14	2.56	3357.7	1077.6	0.71	1.69
56.53	931.7	13.22	2.57	3350.8	1098.2	0.73	1.70
63.00	931.7	13.35	2.58	3340.3	1131.3	0.75	1.72
73.50	931.7	13.56	2.60	3324.4	1185.1	0.78	1.75
84.00	931.7	13.77	2.62	3310.0	1239.7	0.81	1.78
94.50	931.7	13.98	2.64	3297.0	1293.6	0.84	1.80
105.00	931.7	14.19	2.67	3285.6	1347.6	0.87	1.80

C.3.3.11.4 Final Shear Strength Results

x_{dist} (in)	V_{ci} (kip)	V_{cw} (kip)	V_c (kip)	V_s (kip)	V_{n1} (kip)	V_{n2} (kip)	V_n (kip)
0.0	66.6	78.2	66.6	516.7	583.3	820.8	583.3
10.5	2558.8	107.4	107.4	114.6	222.0	832.6	222.0
21.0	1850.5	135.6	135.6	126.2	261.7	841.2	261.7
31.5	1351	146.5	146.5	133.3	279.8	843.6	279.8
42.0	1020	150.6	150.6	89.6	240.2	843.7	240.2
48.5	888	153.0	153.0	90.8	243.9	843.8	243.9
52.5	822	154.5	154.5	91.6	246.1	843.9	246.1
56.5	765	155.9	155.9	92.3	248.3	844.0	248.3
63.0	689	158.2	158.2	93.5	251.7	844.1	251.7
73.5	595	161.7	161.7	95.3	256.9	844.2	256.9
84.0	524	166.4	166.4	97.9	264.4	852.4	264.4
94.5	468	169.5	169.5	98.9	268.4	852.4	268.4
105.0	423	167.6	167.6	95.8	263.4	826.6	263.4

C.3.3.12 Beam BT.10.Min.2

C.3.3.12.1 Additional Input and Basic Calculation

$h_{top.flange}$ (in)	41
S_b (in^3)	9325.24

C.3.3.12.2 Load Effects

x_{dist} (in)	V_{LL} (kip)	M_{LL} (ft-kip)	V_{DC1} (kip)	M_{DC1} (ft-kip)	V_{assume} (kip)	M_{assume} (ft-kip)
0.00	552.0	100000	32.4	-0.2	584.4	100000
15.18	211.0	266.9	30.6	39.7	241.6	306.6
30.36	246.7	624.1	28.9	77.4	275.6	701.5
45.54	211.6	802.9	27.2	112.9	238.8	915.8
48.71	213.5	866.6	26.9	120.0	240.3	986.6
60.72	220.4	1115.3	25.5	146.2	245.9	1261.5
75.90	228.6	1445.7	23.8	177.4	252.4	1623.1
91.08	240.0	1821.4	22.1	206.4	262.1	2027.8
103.09	238.6	2049.8	20.7	227.9	259.3	2277.7
106.26	240.0	2125.3	20.4	233.3	260.4	2358.6
121.44	232.9	2357.2	18.7	258.0	251.6	2615.2
136.62	228.4	2600.0	17.0	280.5	245.3	2880.6
151.80	230.1	2910.8	15.2	300.9	245.3	3211.7

C.3.3.12.3 Nominal Shear Strength Calculations

x_{dist} (in)	$P_{f.cpe}$ (kip)	e_{strand} (in)	f_{cpe} (ksi)	M_{cre} (ft-kip)	$P_{f.pc}$ (kip)	f_{pc} (ksi)	$cot\theta$
0.00	186.3	12.09	0.49	1282.7	186.3	0.11	1.00
15.18	657.8	12.39	1.76	2654.6	657.8	0.41	1.39
30.36	931.7	12.69	2.52	3460.9	964.3	0.60	1.56
45.54	931.7	13.00	2.55	3443.6	1042.1	0.65	1.61
48.71	931.7	13.06	2.55	3440.4	1058.4	0.66	1.62
60.72	931.7	13.30	2.58	3429.4	1120.0	0.70	1.65
75.90	931.7	13.61	2.61	3418.3	1197.8	0.74	1.69
91.08	931.7	13.91	2.64	3410.4	1275.7	0.78	1.73
103.09	931.7	14.15	2.66	3406.4	1337.3	0.80	1.75
106.26	931.7	14.21	2.67	3405.7	1353.6	0.81	1.76
121.44	931.7	14.52	2.70	3404.0	1368.2	0.81	1.76
136.62	931.7	14.82	2.73	3405.6	1368.5	0.80	1.75
151.80	931.7	15.12	2.76	3410.3	1368.7	0.79	1.74

C.3.3.12.4 Final Shear Strength Results

x_{dist} (in)	V_{ci} (kip)	V_{cw} (kip)	V_c (kip)	V_s (kip)	V_{n1} (kip)	V_{n2} (kip)	V_n (kip)
0.0	65.1	80.1	65.1	519.4	584.4	874.4	584.4
15.2	2151.0	120.8	120.8	120.9	241.6	890.5	241.6
30.4	1418.8	145.7	145.7	130.0	275.6	897.6	275.6
45.5	957	150.9	150.9	87.9	238.8	897.8	238.8
48.7	896	151.9	151.9	88.4	240.3	897.9	240.3
60.7	725	155.7	155.7	90.3	245.9	898.1	245.9
75.9	586	160.0	160.0	92.4	252.4	898.3	252.4
91.1	494	166.2	166.2	95.9	262.1	912.9	262.1
103.1	439	164.8	164.8	94.6	259.4	888.3	259.4
106.3	427	165.5	165.5	94.9	260.4	888.5	260.4
121.4	376	160.1	160.1	91.5	251.6	857.1	251.6
136.6	337	156.2	156.2	89.1	245.3	839.1	245.3
151.8	305	156.2	156.2	89.2	245.4	844.5	245.4

Appendix D

Database of Past Research on Shear Strength of Lightweight Concrete Beams

As discussed in Section 4.5.1, a literature review revealed 282 experiments on the shear strength of lightweight concrete beams containing mild longitudinal reinforcement. Of these, only 160 tests had sufficient data available to analyze their theoretical shear capacities using the 2010 AASHTO LRFD Bridge Design Specifications. Thus, the work by Kobayashi; Hoff, Hoiseth and Haverstad; Evans and Dongre; Kirmair; Swamy and Bandyopadhyay; Swamy and Lambert; and Jindal were not included in the analsysis. Likewise, the results from Brettle's research could not be used in the analysis of prestressed, lightweight concrete beams tested for shear. The inputs used to calculate theoretical shear strengths and compare to test results are presented in this appendix. Note that for the mildly-reinforced beams, input that is highlighted or italicized was not directly indicated by the authors, and thus was calculated using the available information.

D.1 Mild Reinforcement Database

D.1.1 Ahmad et al., Funahashi et al., and Hanson

Author	Specimen ID	Fine Agg. Type	γ_c (kcf)	f'_c (ksi)	A_c (in.^{2})	h_{beam} (in)	$I_{o\ beam}$ (in^4)	L_{beam} (ft)	b_v (in)
Ahmad, Xie, and Yu	LNN-1	sand	*0.116*	4.9	50	10.00	*417*	*2.92*	5
Ahmad, Xie, and Yu	LNN-2	sand	*0.116*	6.5	50	10.00	*417*	*4.33*	5
Ahmad, Xie, and Yu	LNN-3	sand	*0.116*	5.85	50	10.00	*417*	*5.75*	5
Ahmad, Xie, and Yu	LNW-1	sand	*0.116*	4.43	50	10.00	*417*	*2.92*	5
Ahmad, Xie, and Yu	LNW-2	sand	*0.116*	5.65	50	10.00	*417*	*4.33*	5
Ahmad, Xie, and Yu	LNW-3	sand	*0.116*	6.47	50	10.00	*417*	*5.75*	5
Ahmad, Xie, and Yu	LHN-1	sand	*0.128*	12.6	50	10.00	*417*	*2.92*	5
Ahmad, Xie, and Yu	LHN-2	sand	*0.128*	12.39	50	10.00	*417*	*4.33*	5
Ahmad, Xie, and Yu	LHN-3	sand	*0.128*	12.93	50	10.00	*417*	*5.75*	5
Ahmad, Xie, and Yu	LHW-1	sand	*0.128*	11.94	50	10.00	*417*	*2.80*	5
Ahmad, Xie, and Yu	LHW-2	sand	*0.128*	12.44	50	10.00	*417*	*4.10*	5
Ahmad, Xie, and Yu	LHW-3	sand	*0.128*	12.95	50	10.00	*417*	*5.40*	5
Ahmad, Xie, and Yu	LHW-3a	sand	*0.128*	12.79	50	10.00	*417*	*5.40*	5
Ahmad, Xie, and Yu	LHW-3b	sand	*0.128*	12.61	50	10.00	*417*	*5.40*	5
Ahmad, Xie, and Yu	LHW-4	sand	*0.128*	12.03	50	10.00	*417*	*6.70*	5
Funahashi et al.	V1.8	sand	0.107	4.9	124.0	15.75	*2562*	11.2	7.87
Funahashi et al.	V1.5	sand	0.101	6.5	124.0	15.75	*2562*	11.2	7.87
Funahashi et al.	V1.2	sand	0.082	4.8	124.0	15.75	*2562*	11.2	7.87
Funahashi et al.	V1.8d100	sand	0.113	5.5	829.5	42.13	*122698*	32.8	19.69
Funahashi et al.	V1.5d100	sand	0.097	4.9	829.5	42.13	*122698*	32.8	19.69
Hanson	9C	*sand*	0.106	7.27	72	12.00	*864*	7.5	6
Hanson	2A	*sand*	0.091	3.87	72	12.00	*864*	7.5	6
Hanson	2B	*sand*	0.098	5.63	72	12.00	*864*	7.5	6
Hanson	3A	*sand*	0.093	3.48	72	12.00	*864*	7.5	6
Hanson	3B	*sand*	0.098	4.31	72	12.00	*864*	7.5	6
Hanson	4A	*sand*	0.100	3.14	72	12.00	*864*	7.5	6
Hanson	4B	*sand*	0.102	5.15	72	12.00	*864*	7.5	6
Hanson	4C	*sand*	0.108	7.37	72	12.00	*864*	7.5	6
Hanson	4D	*sand*	0.113	8.59	72	12.00	*864*	7.5	6
Hanson	5A	*sand*	0.100	3.67	72	12.00	*864*	7.5	6
Hanson	5B	*sand*	0.104	5.04	72	12.00	*864*	7.5	6
Hanson	6A	*sand*	0.109	3.86	72	12.00	*864*	7.5	6
Hanson	6B	*sand*	0.111	5.13	72	12.00	*864*	7.5	6
Hanson	7A-X	*sand*	0.109	3.38	72	12.00	*864*	7.5	6
Hanson	7A	*sand*	0.110	4.46	72	12.00	*864*	7.5	6
Hanson	7B	*sand*	0.112	5.47	72	12.00	*864*	7.5	6
Hanson	2B2	sand	0.096	4.88	72	12.00	*864*	10.0	6
Hanson	3B2	sand	0.097	4.54	72	12.00	*864*	10.0	6
Hanson	4B2	sand	0.102	5.10	72	12.00	*864*	10.0	6
Hanson	5B2	sand	0.103	4.93	72	12.00	*864*	10.0	6
Hanson	6B2	sand	0.111	5.00	72	12.00	*864*	10.0	6
Hanson	7B2	sand	0.107	4.96	72	12.00	*864*	10.0	6
Hanson	10B2	sand	0.092	4.43	72	12.00	*864*	10.0	6
Hanson	13B2	sand	0.094	5.06	72	12.00	*864*	10.0	6
Hanson	2B3	sand	0.096	4.78	72	12.00	*864*	6.5	6
Hanson	6B3	sand	0.111	4.82	72	12.00	*864*	6.5	6
Hanson	7B3	sand	0.107	4.87	72	12.00	*864*	6.5	6
Hanson	13B3	sand	0.094	5.02	72	12.00	*864*	6.5	6
Hanson	7B1X	sand	0.107	4.68	72	12.00	*864*	6.5	6
Hanson	10B1	sand	0.092	4.86	72	12.00	*864*	6.5	6
Hanson	13B1	sand	0.094	4.94	72	12.00	*864*	6.5	6

Author	Specimen ID	b_{flange} (in)	y_{bot} (in)	y_{top} (in)	S (ft)	$x_{bearing}$ (in)	$A_{s\ bgt}$ (in.^{2})	f_y (ksi)	E_s (ksi)
Ahmad, Xie, and Yu	LNN-1	5	5	5	0.417	*9*	0.40	61	29000
Ahmad, Xie, and Yu	LNN-2	5	5	5	0.417	*9*	0.40	61	29000
Ahmad, Xie, and Yu	LNN-3	5	5	5	0.417	*9*	0.40	61	29000
Ahmad, Xie, and Yu	LNW-1	5	5	5	0.417	*9*	0.40	61	29000
Ahmad, Xie, and Yu	LNW-2	5	5	5	0.417	*9*	0.40	61	29000
Ahmad, Xie, and Yu	LNW-3	5	5	5	0.417	*9*	0.40	61	29000
Ahmad, Xie, and Yu	LHN-1	5	5	5	0.417	*9*	0.88	61	29000
Ahmad, Xie, and Yu	LHN-2	5	5	5	0.417	*9*	0.88	61	29000
Ahmad, Xie, and Yu	LHN-3	5	5	5	0.417	*9*	0.88	61	29000
Ahmad, Xie, and Yu	LHW-1	5	5	5	0.417	*9*	1.76	61	29000
Ahmad, Xie, and Yu	LHW-2	5	5	5	0.417	*9*	1.76	61	29000
Ahmad, Xie, and Yu	LHW-3	5	5	5	0.417	*9*	1.76	61	29000
Ahmad, Xie, and Yu	LHW-3a	5	5	5	0.417	*9*	1.76	61	29000
Ahmad, Xie, and Yu	LHW-3b	5	5	5	0.417	*9*	1.76	61	29000
Ahmad, Xie, and Yu	LHW-4	5	5	5	0.417	*9*	1.76	61	29000
Funahashi et al.	V1.8	7.87	7.875	7.875	0.656	9.84	*1.80*	55.3	29000
Funahashi et al.	V1.5	7.87	7.875	7.875	0.656	9.84	*1.80*	57.7	29000
Funahashi et al.	V1.2	7.87	7.875	7.875	0.656	9.84	*1.80*	57.7	29000
Funahashi et al.	V1.8d100	19.69	21.065	21.065	1.641	9.84	*7.44*	77.7	29000
Funahashi et al.	V1.5d100	19.69	21.065	21.065	1.641	9.84	*7.44*	77.7	29000
Hanson	9C	6	6	6	0.500	6	3.16	48.3	27550
Hanson	2A	6	6	6	0.500	6	1.575	48.3	27550
Hanson	2B	6	6	6	0.500	6	1.575	48.3	27550
Hanson	3A	6	6	6	0.500	6	1.575	48.3	27550
Hanson	3B	6	6	6	0.500	6	1.575	48.3	27550
Hanson	4A	6	6	6	0.500	6	1.575	48.3	27550
Hanson	4B	6	6	6	0.500	6	1.575	48.3	27550
Hanson	4C	6	6	6	0.500	6	3.16	48.3	27550
Hanson	4D	6	6	6	0.500	6	3.16	48.3	27550
Hanson	5A	6	6	6	0.500	6	1.575	48.3	27550
Hanson	5B	6	6	6	0.500	6	1.575	48.3	27550
Hanson	6A	6	6	6	0.500	6	1.575	48.3	27550
Hanson	6B	6	6	6	0.500	6	1.575	48.3	27550
Hanson	7A-X	6	6	6	0.500	6	1.575	48.3	27550
Hanson	7A	6	6	6	0.500	6	1.575	48.3	27550
Hanson	7B	6	6	6	0.500	6	1.575	48.3	27550
Hanson	2B2	6	6	6	0.500	6	*1.575*	48.1	27975
Hanson	3B2	6	6	6	0.500	6	*1.575*	48.1	27975
Hanson	4B2	6	6	6	0.500	6	*1.575*	48.1	27975
Hanson	5B2	6	6	6	0.500	6	*1.575*	48.1	27975
Hanson	6B2	6	6	6	0.500	6	*1.575*	48.1	27975
Hanson	7B2	6	6	6	0.500	6	*1.575*	48.1	27975
Hanson	10B2	6	6	6	0.500	6	*1.575*	48.1	27975
Hanson	13B2	6	6	6	0.500	6	*1.575*	48.1	27975
Hanson	2B3	6	6	6	0.500	6	*0.788*	48.1	27975
Hanson	6B3	6	6	6	0.500	6	*0.788*	48.1	27975
Hanson	7B3	6	6	6	0.500	6	*0.788*	48.1	27975
Hanson	13B3	6	6	6	0.500	6	*0.788*	48.1	27975
Hanson	7B1X	6	6	6	0.500	6	*1.575*	48.1	27975
Hanson	10B1	6	6	6	0.500	6	*1.575*	48.1	27975
Hanson	13B1	6	6	6	0.500	6	*1.575*	48.1	27975

Author	Specimen ID	A_v (in.^{2})	f_{yv} (ksi)	H	$x_{critical.\ assume}$ (ft)	f_{ct} (ksi)	a_g (in.)	E_c (ksi)	a/d
Ahmad, Xie, and Yu	LNN-1	0.000	47	*70*	0.50	0	0.50	*2867*	1
Ahmad, Xie, and Yu	LNN-2	0.000	47	*70*	1.00	0	0.50	*3303*	2
Ahmad, Xie, and Yu	LNN-3	0.000	47	*70*	1.00	0	0.50	*3133*	3
Ahmad, Xie, and Yu	LNW-1	0.098	47	*70*	0.50	0	0.50	*2726*	1
Ahmad, Xie, and Yu	LNW-2	0.098	47	*70*	1.00	0	0.50	*3079*	2
Ahmad, Xie, and Yu	LNW-3	0.098	47	*70*	1.00	0	0.50	*3295*	3
Ahmad, Xie, and Yu	LHN-1	0.000	47	*70*	0.50	0	0.50	*5389*	1
Ahmad, Xie, and Yu	LHN-2	0.000	47	*70*	1.00	0	0.50	*5344*	2
Ahmad, Xie, and Yu	LHN-3	0.000	47	*70*	1.00	0	0.50	*5460*	3
Ahmad, Xie, and Yu	LHW-1	0.098	47	*70*	0.50	0	0.50	*5246*	1
Ahmad, Xie, and Yu	LHW-2	0.098	47	*70*	1.00	0	0.50	*5355*	2
Ahmad, Xie, and Yu	LHW-3	0.098	47	*70*	1.00	0	0.50	*5464*	3
Ahmad, Xie, and Yu	LHW-3a	0.098	47	*70*	1.00	0	0.50	*5430*	3
Ahmad, Xie, and Yu	LHW-3b	0.098	47	*70*	1.00	0	0.50	*5392*	3
Ahmad, Xie, and Yu	LHW-4	0.098	47	*70*	1.00	0	0.50	*5266*	4
Funahashi et al.	V1.8	0	56.1	*70*	0.66	0	*0*	2596	2.50
Funahashi et al.	V1.5	0	52.5	*70*	0.66	0	*0*	2683	2.50
Funahashi et al.	V1.2	0	52.5	*70*	0.66	0	*0*	1827	2.50
Funahashi et al.	V1.8d100	0	55.1	*70*	1.76	0	*0*	3075	3.35
Funahashi et al.	V1.5d100	0	55.1	*70*	1.76	0	*0*	2480	2.85
Hanson	9C	0	0	*70*	0.50	0	*0.5*	2920	*2.14*
Hanson	2A	0	0	*70*	0.50	0	*0.375*	1600	*2.14*
Hanson	2B	0	0	*70*	0.50	0	*0.375*	1810	*2.14*
Hanson	3A	0	0	*70*	0.50	0	*0.375*	1870	*2.14*
Hanson	3B	0	0	*70*	0.50	0	*0.375*	1980	*2.14*
Hanson	4A	0	0	*70*	0.50	0	*0.375*	1530	*2.14*
Hanson	4B	0	0	*70*	0.50	0	*0.375*	1830	*2.14*
Hanson	4C	0	0	*70*	0.50	0	*0.5*	2090	*2.14*
Hanson	4D	0	0	*70*	0.50	0	*0.5*	2260	*2.14*
Hanson	5A	0	0	*70*	0.50	0	*0.375*	1900	*2.14*
Hanson	5B	0	0	*70*	0.50	0	*0.375*	2200	*2.14*
Hanson	6A	0	0	*70*	0.50	0	*0.375*	2250	*2.14*
Hanson	6B	0	0	*70*	0.50	0	*0.375*	2610	*2.14*
Hanson	7A-X	0	0	*70*	0.50	0	*0.375*	2020	*2.14*
Hanson	7A	0	0	*70*	0.50	0	*0.375*	2230	*2.14*
Hanson	7B	0	0	*70*	0.50	0	*0.375*	2540	*2.14*
Hanson	2B2	0	0	*70*	0.50	0	*0*	1620	*2.14*
Hanson	3B2	0	0	*70*	0.50	0	*0*	1870	*2.14*
Hanson	4B2	0	0	*70*	0.50	0	*0*	1800	*2.14*
Hanson	5B2	0	0	*70*	0.50	0	*0*	2210	*2.14*
Hanson	6B2	0	0	*70*	0.50	0	*0*	2680	*2.14*
Hanson	7B2	0	0	*70*	0.50	0	*0*	2180	*2.14*
Hanson	10B2	0	0	*70*	0.50	0	*0*	2040	*2.14*
Hanson	13B2	0	0	*70*	0.50	0	*0*	1920	*2.14*
Hanson	2B3	0	0	*70*	0.50	0	*0*	1600	*2.14*
Hanson	6B3	0	0	*70*	0.50	0	*0*	2780	*2.14*
Hanson	7B3	0	0	*70*	0.50	0	*0*	2130	*2.14*
Hanson	13B3	0	0	*70*	0.50	0	*0*	1940	*2.14*
Hanson	7B1X	0	0	*70*	0.50	0	*0*	2200	*2.14*
Hanson	10B1	0	0	*70*	0.50	0	*0*	2070	*2.14*
Hanson	13B1	0	0	*70*	0.50	0	*0*	1880	*2.14*

Author	Specimen ID	*Load Spacing* (ft)	$x_{bearing.roll}$ (in)	$A_{s\ top}$ (in^2)	d_{top} (in.)	A_{ct} ($in.^2$)	*s* (in.)	h_{flange} (in)	cg_s (in)
Ahmad, Xie, and Yu	LNN-1	0	9.0	0	0	*25*	1000000	10	*1.50*
Ahmad, Xie, and Yu	LNN-2	0	9.0	0	0	*25*	1000000	10	*1.50*
Ahmad, Xie, and Yu	LNN-3	0	9.0	0	0	*25*	1000000	10	*1.50*
Ahmad, Xie, and Yu	LNW-1	0	9.0	0.40	0	*25*	4	10	*5.00*
Ahmad, Xie, and Yu	LNW-2	0	9.0	0.40	0	*25*	4	10	*5.00*
Ahmad, Xie, and Yu	LNW-3	0	9.0	0.40	0	*25*	4	10	*5.00*
Ahmad, Xie, and Yu	LHN-1	0	9.0	0	0	*25*	1000000	10	*1.50*
Ahmad, Xie, and Yu	LHN-2	0	9.0	0	0	*25*	1000000	10	*1.50*
Ahmad, Xie, and Yu	LHN-3	0	9.0	0	0	*25*	1000000	10	*1.50*
Ahmad, Xie, and Yu	LHW-1	0	9.0	0.40	0	*25*	3.90	10	*3.37*
Ahmad, Xie, and Yu	LHW-2	0	9.0	0.40	0	*25*	3.90	10	*3.37*
Ahmad, Xie, and Yu	LHW-3	0	9.0	0.40	0	*25*	3.90	10	*3.37*
Ahmad, Xie, and Yu	LHW-3a	0	9.0	0.40	0	*25*	3.00	10	*3.37*
Ahmad, Xie, and Yu	LHW-3b	0	9.0	0.40	0	*25*	2.50	10	*3.37*
Ahmad, Xie, and Yu	LHW-4	0	9.0	0.40	0	*25*	3.90	10	*3.37*
Funahashi et al.	V1.8	3.28	9.8	1.20	0	*62.0*	1000000	15.8	*6.77*
Funahashi et al.	V1.5	3.28	9.8	1.20	0	*62.0*	1000000	15.8	*6.77*
Funahashi et al.	V1.2	3.28	9.8	1.20	0	*62.0*	1000000	15.8	*6.77*
Funahashi et al.	V1.8d100	8.20	9.8	2.98	0	*414.8*	1000000	42.1	*13.22*
Funahashi et al.	V1.5d100	8.20	9.8	2.98	0	*414.8*	1000000	42.1	*13.22*
Hanson	9C	2.17	6.0	0	0	*36*	1000000	12.0	*1.5*
Hanson	2A	2.17	6.0	0	0	*36*	1000000	12.0	*1.5*
Hanson	2B	2.17	6.0	0	0	*36*	1000000	12.0	*1.5*
Hanson	3A	2.17	6.0	0	0	*36*	1000000	12.0	*1.5*
Hanson	3B	2.17	6.0	0	0	*36*	1000000	12.0	*1.5*
Hanson	4A	2.17	6.0	0	0	*36*	1000000	12.0	*1.5*
Hanson	4B	2.17	6.0	0	0	*36*	1000000	12.0	*1.5*
Hanson	4C	2.17	6.0	0	0	*36*	1000000	12.0	*1.5*
Hanson	4D	2.17	6.0	0	0	*36*	1000000	12.0	*1.5*
Hanson	5A	2.17	6.0	0	0	*36*	1000000	12.0	*1.5*
Hanson	5B	2.17	6.0	0	0	*36*	1000000	12.0	*1.5*
Hanson	6A	2.17	6.0	0	0	*36*	1000000	12.0	*1.5*
Hanson	6B	2.17	6.0	0	0	*36*	1000000	12.0	*1.5*
Hanson	7A-X	2.17	6.0	0	0	*36*	1000000	12.0	*1.5*
Hanson	7A	2.17	6.0	0	0	*36*	1000000	12.0	*1.5*
Hanson	7B	2.17	6.0	0	0	*36*	1000000	12.0	*1.5*
Hanson	2B2	1.33	6.0	0	0	*36*	1000000	12.0	*1.5*
Hanson	3B2	1.33	6.0	0	0	*36*	1000000	12.0	*1.5*
Hanson	4B2	1.33	6.0	0	0	*36*	1000000	12.0	*1.5*
Hanson	5B2	1.33	6.0	0	0	*36*	1000000	12.0	*1.5*
Hanson	6B2	1.33	6.0	0	0	*36*	1000000	12.0	*1.5*
Hanson	7B2	1.33	6.0	0	0	*36*	1000000	12.0	*1.5*
Hanson	10B2	1.33	6.0	0	0	*36*	1000000	12.0	*1.5*
Hanson	13B2	1.33	6.0	0	0	*36*	1000000	12.0	*1.5*
Hanson	2B3	2.17	6.0	0	0	*36*	1000000	12.0	*1.5*
Hanson	6B3	2.17	6.0	0	0	*36*	1000000	12.0	*1.5*
Hanson	7B3	2.17	6.0	0	0	*36*	1000000	12.0	*1.5*
Hanson	13B3	2.17	6.0	0	0	*36*	1000000	12.0	*1.5*
Hanson	7B1X	2.17	6.0	0	0	*36*	1000000	12.0	*1.5*
Hanson	10B1	2.17	6.0	0	0	*36*	1000000	12.0	*1.5*
Hanson	13B1	2.17	6.0	0	0	*36*	1000000	12.0	*1.5*

Author	Specimen ID	$cg_{s.bot}$ (in)	$size_{long.rebar}$ (in)	V_{exp} (kip)
Ahmad, Xie, and Yu	LNN-1	*1.50*	4	23.8
Ahmad, Xie, and Yu	LNN-2	*1.50*	4	7.5
Ahmad, Xie, and Yu	LNN-3	*1.50*	4	5.1
Ahmad, Xie, and Yu	LNW-1	*1.50*	4	33.7
Ahmad, Xie, and Yu	LNW-2	*1.50*	4	18.9
Ahmad, Xie, and Yu	LNW-3	*1.50*	4	14.2
Ahmad, Xie, and Yu	LHN-1	*1.50*	4	42.4
Ahmad, Xie, and Yu	LHN-2	*1.50*	4	19.2
Ahmad, Xie, and Yu	LHN-3	*1.50*	4	9.8
Ahmad, Xie, and Yu	LHW-1	*2.20*	6	62.4
Ahmad, Xie, and Yu	LHW-2	*2.20*	6	30.5
Ahmad, Xie, and Yu	LHW-3	*2.20*	6	20.8
Ahmad, Xie, and Yu	LHW-3a	*2.20*	6	24.1
Ahmad, Xie, and Yu	LHW-3b	*2.20*	6	27.1
Ahmad, Xie, and Yu	LHW-4	*2.20*	6	21.3
Funahashi et al.	V1.8	*2.36*	7	19.8
Funahashi et al.	V1.5	*2.36*	7	13.8
Funahashi et al.	V1.2	*2.36*	7	13.3
Funahashi et al.	V1.8d100	*2.76*	11	50.0
Funahashi et al.	V1.5d100	*2.76*	11	134.5
Hanson	9C	*1.5*	8	25.4
Hanson	2A	*1.5*	8	18.5
Hanson	2B	*1.5*	8	21.6
Hanson	3A	*1.5*	8	9.9
Hanson	3B	*1.5*	8	11.0
Hanson	4A	*1.5*	8	12.4
Hanson	4B	*1.5*	8	18.8
Hanson	4C	*1.5*	8	24.6
Hanson	4D	*1.5*	8	26.8
Hanson	5A	*1.5*	8	10.9
Hanson	5B	*1.5*	8	11.0
Hanson	6A	*1.5*	8	10.0
Hanson	6B	*1.5*	8	15.8
Hanson	7A-X	*1.5*	8	12.7
Hanson	7A	*1.5*	8	19.9
Hanson	7B	*1.5*	8	19.7
Hanson	2B2	*1.5*	8	7.5
Hanson	3B2	*1.5*	8	8.0
Hanson	4B2	*1.5*	8	8.0
Hanson	5B2	*1.5*	8	9.9
Hanson	6B2	*1.5*	8	8.5
Hanson	7B2	*1.5*	8	11.0
Hanson	10B2	*1.5*	8	8.3
Hanson	13B2	*1.5*	8	8.6
Hanson	2B3	*1.5*	4	13.5
Hanson	6B3	*1.5*	4	9.5
Hanson	7B3	*1.5*	4	12.5
Hanson	13B3	*1.5*	4	13.0
Hanson	7B1X	*1.5*	8	17.8
Hanson	10B1	*1.5*	8	21.5
Hanson	13B1	*1.5*	8	20.0

D.1.2 Hanson, Ivey & Buth, Kawaguchi et al., and Murayama & Iwabuchi

Author	Specimen ID	Fine Agg. Type	γ_c (kcf)	f'_c (ksi)	A_{c_2} (in.^{2})	h_{beam} (in)	$I_{o\ beam}$ (in^4)	L_{beam} (ft)	b_v (in)
Hanson	3A4	sand	0.097	3.85	72	12.00	*864*	10.0	6
Hanson	4A4	sand	0.100	3.10	72	12.00	*864*	10.0	6
Hanson	10A4	sand	0.089	3.27	72	12.00	*864*	10.0	6
Hanson	2B4	sand	0.096	4.94	72	12.00	*864*	10.0	6
Hanson	3B4	sand	0.097	4.40	72	12.00	*864*	10.0	6
Hanson	4B4	sand	0.102	5.12	72	12.00	*864*	10.0	6
Hanson	6B4	sand	0.111	4.85	72	12.00	*864*	10.0	6
Hanson	10B4	sand	0.092	4.85	72	12.00	*864*	10.0	6
Hanson	13B4	sand	0.094	5.15	72	12.00	*864*	10.0	6
Hanson	10BW4	sand	0.092	4.53	72	12.00	*864*	10.0	6
Ivey and Buth	(1) 1 "4.62"	lwt	0.109	4.49	72	12.00	*864*	*8.00*	6
Ivey and Buth	(1) 2 "6.33"	lwt	0.106	4.5	72	12.00	*864*	*12.67*	6
Ivey and Buth	(1) 3 "8.00"	lwt	0.107	4.69	72	12.00	*864*	*18.33*	6
Ivey and Buth	(23) 1 "6.33"	lwt	0.106	4.04	72	12.00	*864*	*12.67*	6
Ivey and Buth	(23) 2 "6.33"	lwt	0.106	4.17	72	12.00	*864*	*12.67*	6
Ivey and Buth	(23) 3 "6.33"	lwt	0.106	4.16	72	12.00	*864*	*12.67*	6
Ivey and Buth	(23) 1S "6.33"	sand	0.125	3.73	72	12.00	*864*	*12.67*	6
Ivey and Buth	(23) 2S "6.33"	sand	0.126	3.87	72	12.00	*864*	*12.67*	6
Ivey and Buth	(23) 3S "6.33"	sand	0.125	4.06	72	12.00	*864*	*12.67*	6
Ivey and Buth	(27) 1 "4.62"	lwt	0.098	3.36	72	12.00	*864*	*8.00*	6
Ivey and Buth	(27) 2 "6.33"	lwt	0.099	3.71	72	12.00	*864*	*12.67*	6
Ivey and Buth	(27) 3 "8.00"	lwt	0.100	3.42	72	12.00	*864*	*18.33*	6
Ivey and Buth	(23) 4 "4.62"	lwt	0.108	3.56	38	9.00	*258*	*9.23*	4.25
Ivey and Buth	(23) 5 "6.33"	lwt	0.108	4.29	72	12.00	*864*	*12.67*	6
Ivey and Buth	(23) 6 "7.78"	lwt	0.108	3.82	113	15.00	*2109*	*15.57*	7.5
Ivey and Buth	(23) 7 "9.15"	lwt	0.108	3.76	160	18.00	*4311*	*18.30*	8.9
Ivey and Buth	(23) 8 "4.62"	lwt	0.096	3.03	72	12.00	*864*	*8.00*	6
Ivey and Buth	(23) 9 "4.62"	lwt	0.096	2.96	72	12.00	*864*	*8.00*	6
Ivey and Buth	(23) 10 "4.62"	lwt	0.096	3.25	72	12.00	*864*	*8.00*	6
Ivey and Buth	(23) 11 "4.62"	lwt	0.094	3.01	72	12.00	*864*	*8.00*	6
Ivey and Buth	(23) 12 "6.30"	lwt	0.094	3.27	72	12.00	*864*	*11.50*	6
Ivey and Buth	(23) 13 "7.00"	lwt	0.094	3.20	72	12.00	*864*	*15.00*	6
Ivey and Buth	(23) 14 "8.00"	lwt	0.094	2.78	72	12.00	*864*	*18.33*	6
Ivey and Buth	(23) 15 "6.33"	lwt	0.108	3.13	72	12.00	*864*	*12.67*	6
Ivey and Buth	(23) 16 "6.33"	lwt	0.107	2.78	72	12.00	*864*	*12.67*	6
Ivey and Buth	(23) 17 "6.33"	lwt	0.106	3.86	72	12.00	*864*	*12.67*	6
Kawaguchi et al.	A 1	sand	0.107	2.71	108.5	13.78	*1716*	9.843	7.87
Kawaguchi et al.	A 2	lwt	0.107	2.71	108.5	13.78	*1716*	9.843	7.87
Kawaguchi et al.	B 1	lwt	0.096	3.26	108.5	13.78	*1716*	9.843	7.87
Kawaguchi et al.	B 2	lwt	0.096	3.26	108.5	13.78	*1716*	9.843	7.87
Kawaguchi et al.	C 1	lwt	0.086	4.05	108.5	13.78	*1716*	9.843	7.87
Kawaguchi et al.	C 2	lwt	0.086	4.05	108.5	13.78	*1716*	9.843	7.87
Kawaguchi et al.	D 1	lwt	0.074	2.93	108.5	13.78	*1716*	9.843	7.87
Kawaguchi et al.	D 2	lwt	0.074	2.93	108.5	13.78	*1716*	9.843	7.87
Murayama and Iwabuchi	B1	sand	*0.119*	6.4	92.94	11.81	*1080*	6.6	7.87
Murayama and Iwabuchi	M1	sand	*0.119*	6.3	92.94	11.81	*1080*	6.6	7.87
Murayama and Iwabuchi	BS1	sand	*0.119*	7.2	92.94	11.81	*1080*	8.2	7.87
Murayama and Iwabuchi	BS2	sand	*0.119*	7.4	92.94	11.81	*1080*	8.2	7.87
Murayama and Iwabuchi	BS3	sand	*0.119*	7.4	92.94	11.81	*1080*	8.2	7.87
Murayama and Iwabuchi	BS4	sand	*0.119*	7.2	92.94	11.81	*1080*	8.2	7.87
Murayama and Iwabuchi	BS5	sand	*0.119*	7.4	92.94	11.81	*1080*	8.2	7.87
Murayama and Iwabuchi	BL1	sand	*0.119*	7.3	92.94	11.81	*1080*	8.2	7.87

Author	Specimen ID	b_{flange} (in)	y_{bot} (in)	y_{top} (in)	S (ft)	$x_{bearing}$ (in)	$A_{s\ bgt}$ (in.^{2})	f_y (ksi)	E_s (ksi)
Hanson	3A4	6	6	6	0.500	6	*0.788*	48.1	27975
Hanson	4A4	6	6	6	0.500	6	*0.788*	48.1	27975
Hanson	10A4	6	6	6	0.500	6	*0.788*	48.1	27975
Hanson	2B4	6	6	6	0.500	6	*0.788*	48.1	27975
Hanson	3B4	6	6	6	0.500	6	*0.788*	48.1	27975
Hanson	4B4	6	6	6	0.500	6	*0.788*	48.1	27975
Hanson	6B4	6	6	6	0.500	6	*0.788*	48.1	27975
Hanson	10B4	6	6	6	0.500	6	*0.788*	48.1	27975
Hanson	13B4	6	6	6	0.500	6	*0.788*	48.1	27975
Hanson	10BW4	6	6	6	0.500	6	*0.788*	48.1	27975
Ivey and Buth	(1) 1 "4.62"	6	6	6	0.500	*6*	0.800	60	*29000*
Ivey and Buth	(1) 2 "6.33"	6	6	6	0.500	*6*	0.800	60	*29000*
Ivey and Buth	(1) 3 "8.00"	6	6	6	0.500	*6*	0.800	60	*29000*
Ivey and Buth	(23) 1 "6.33"	6	6	6	0.500	*6*	0.600	60	*29000*
Ivey and Buth	(23) 2 "6.33"	6	6	6	0.500	*6*	0.800	60	*29000*
Ivey and Buth	(23) 3 "6.33"	6	6	6	0.500	*6*	0.93	60	*29000*
Ivey and Buth	(23) 1S "6.33"	6	6	6	0.500	*6*	0.6	60	*29000*
Ivey and Buth	(23) 2S "6.33"	6	6	6	0.500	*6*	0.8	60	*29000*
Ivey and Buth	(23) 3S "6.33"	6	6	6	0.500	*6*	0.93	60	*29000*
Ivey and Buth	(27) 1 "4.62"	6	6	6	0.500	*6*	0.8	60	*29000*
Ivey and Buth	(27) 2 "6.33"	6	6	6	0.500	*6*	0.8	60	*29000*
Ivey and Buth	(27) 3 "8.00"	6	6	6	0.500	*6*	0.8	60	*29000*
Ivey and Buth	(23) 4 "4.62"	4.25	4.50	4.50	0.354	*6*	0.40	60	*29000*
Ivey and Buth	(23) 5 "6.33"	6	6.00	6.00	0.500	*6*	0.80	60	*29000*
Ivey and Buth	(23) 6 "7.78"	7.5	7.50	7.50	0.625	*6*	1.24	60	*29000*
Ivey and Buth	(23) 7 "9.15"	8.87	9	9	0.739	*6*	1.76	60	*29000*
Ivey and Buth	(23) 8 "4.62"	6	6	6	0.500	*6*	0.60	60	*29000*
Ivey and Buth	(23) 9 "4.62"	6	6	6	0.500	*6*	0.80	60	*29000*
Ivey and Buth	(23) 10 "4.62"	6	6	6	0.500	*6*	0.93	60	*29000*
Ivey and Buth	(23) 11 "4.62"	6	6	6	0.500	*6*	1.32	60	*29000*
Ivey and Buth	(23) 12 "6.30"	6	6	6	0.500	*6*	1.32	60	*29000*
Ivey and Buth	(23) 13 "7.00"	6	6	6	0.500	*6*	1.32	60	*29000*
Ivey and Buth	(23) 14 "8.00"	6	6	6	0.500	*6*	1.32	60	*29000*
Ivey and Buth	(23) 15 "6.33"	6	6	6	0.500	*6*	0.6	60	*29000*
Ivey and Buth	(23) 16 "6.33"	6	6	6	0.500	*6*	0.8	60	*29000*
Ivey and Buth	(23) 17 "6.33"	6	6	6	0.500	*6*	0.93	60	*29000*
Kawaguchi et al.	A 1	7.87	6.89	6.89	0.656	11.81	1.571	134.9	*29000*
Kawaguchi et al.	A 2	7.87	6.89	6.89	0.656	11.81	1.571	134.9	*29000*
Kawaguchi et al.	B 1	7.87	6.89	6.89	0.656	11.81	1.571	134.9	*29000*
Kawaguchi et al.	B 2	7.87	6.89	6.89	0.656	11.81	1.571	134.9	*29000*
Kawaguchi et al.	C 1	7.87	6.89	6.89	0.656	11.81	1.571	134.9	*29000*
Kawaguchi et al.	C 2	7.87	6.89	6.89	0.656	11.81	1.571	134.9	*29000*
Kawaguchi et al.	D 1	7.87	6.89	6.89	0.656	11.81	1.571	134.9	*29000*
Kawaguchi et al.	D 2	7.87	6.89	6.89	0.656	11.81	1.571	134.9	*29000*
Murayama and Iwabuchi	B1	7.87	5.91	5.91	0.656	9.84	*1.2*	71.1	*29000*
Murayama and Iwabuchi	M1	7.87	5.91	5.91	0.656	9.84	*1.2*	71.1	*29000*
Murayama and Iwabuchi	BS1	7.87	5.91	5.91	0.656	9.84	*2.0*	71.1	*29000*
Murayama and Iwabuchi	BS2	7.87	5.91	5.91	0.656	9.84	*2.0*	71.1	*29000*
Murayama and Iwabuchi	BS3	7.87	5.91	5.91	0.656	9.84	*2.5*	71.1	*29000*
Murayama and Iwabuchi	BS4	7.87	5.91	5.91	0.656	9.84	*2.5*	71.1	*29000*
Murayama and Iwabuchi	BS5	7.87	5.91	5.91	0.656	9.84	*2.5*	71.1	*29000*
Murayama and Iwabuchi	BL1	7.87	5.91	5.91	0.656	9.84	*2.0*	71.1	*29000*

Author	Specimen ID	A_v (in.^{2})	f_{yv} (ksi)	H	$x_{critical.\ assume}$ (ft)	f_{ct} (ksi)	a_g (in.)	E_c (ksi)	a/d
Hanson	3A4	0	0	70	0.50	0	0	2000	2.14
Hanson	4A4	0	0	70	0.50	0	0	1540	2.14
Hanson	10A4	0	0	70	0.50	0	0	1900	2.14
Hanson	2B4	0	0	70	0.50	0	0	1690	2.14
Hanson	3B4	0	0	70	0.50	0	0	1800	2.14
Hanson	4B4	0	0	70	0.50	0	0	1800	2.14
Hanson	6B4	0	0	70	0.50	0	0	2700	2.14
Hanson	10B4	0	0	70	0.50	0	0	2060	2.14
Hanson	13B4	0	0	70	0.50	0	0	1970	2.14
Hanson	10BW4	0	0	70	0.50	0	0	2150	2.14
Ivey and Buth	(1) 1 "4.62"	0	0	70	0.50	0	0.5	2516	2
Ivey and Buth	(1) 2 "6.33"	0	0	70	0.50	0	0.5	2416	3.3
Ivey and Buth	(1) 3 "8.00"	0	0	70	0.50	0	0.5	2501	5.0
Ivey and Buth	(23) 1 "6.33"	0	0	70	0.50	0	0.5	2289	3.3
Ivey and Buth	(23) 2 "6.33"	0	0	70	0.50	0	0.5	2326	3.3
Ivey and Buth	(23) 3 "6.33"	0	0	70	0.50	0	0.5	2323	3.3
Ivey and Buth	(23) 1S "6.33"	0	0	70	0.50	0	0.5	2817	3.3
Ivey and Buth	(23) 2S "6.33"	0	0	70	0.50	0	0.5	2904	3.3
Ivey and Buth	(23) 3S "6.33"	0	0	70	0.50	0	0.5	2939	3.3
Ivey and Buth	(27) 1 "4.62"	0	0	70	0.50	0	0.5	1856	2
Ivey and Buth	(27) 2 "6.33"	0	0	70	0.50	0	0.5	1980	3.3
Ivey and Buth	(27) 3 "8.00"	0	0	70	0.50	0	0.5	1930	5.0
Ivey and Buth	(23) 4 "4.62"	0	0	70	0.38	0	0.5	2210	3.3
Ivey and Buth	(23) 5 "6.33"	0	0	70	0.50	0	0.5	2426	3.3
Ivey and Buth	(23) 6 "7.78"	0	0	70	0.63	0	0.5	2289	3.3
Ivey and Buth	(23) 7 "9.15"	0	0	70	0.75	0	0.5	2271	3.3
Ivey and Buth	(23) 8 "4.62"	0	0	70	0.50	0	0.5	1709	2
Ivey and Buth	(23) 9 "4.62"	0	0	70	0.50	0	0.5	1689	2
Ivey and Buth	(23) 10 "4.62"	0	0	70	0.50	0	0.5	1770	2
Ivey and Buth	(23) 11 "4.62"	0	0	70	0.50	0	0.5	1650	2
Ivey and Buth	(23) 12 "6.30"	0	0	70	0.50	0	0.5	1720	3
Ivey and Buth	(23) 13 "7.00"	0	0	70	0.50	0	0.5	1701	4
Ivey and Buth	(23) 14 "8.00"	0	0	70	0.50	0	0.5	1586	5.0
Ivey and Buth	(23) 15 "6.33"	0	0	70	0.50	0	0.5	2072	3.3
Ivey and Buth	(23) 16 "6.33"	0	0	70	0.50	0	0.5	1926	3.3
Ivey and Buth	(23) 17 "6.33"	0	0	70	0.50	0	0.5	2238	3.3
Kawaguchi et al.	A 1	0	53.4	70	0.57	0.296	0	1912	3.5
Kawaguchi et al.	A 2	0.09290535	53.4	70	0.57	0.296	0	1912	3.5
Kawaguchi et al.	B 1	0	53.4	70	0.57	0.287	0	1777	3.5
Kawaguchi et al.	B 2	0.09290535	53.4	70	0.57	0.287	0	1777	3.5
Kawaguchi et al.	C 1	0	53.4	70	0.57	0.318	0	1679	3.5
Kawaguchi et al.	C 2	0.09290535	53.4	70	0.57	0.318	0	1679	3.5
Kawaguchi et al.	D 1	0	53.4	70	0.57	0.287	0	1144	3.5
Kawaguchi et al.	D 2	0.09290535	53.4	70	0.57	0.287	0	1144	3.5
Murayama and Iwabuchi	B1	0	0	70	0.49	0.484	0	3433	2.5
Murayama and Iwabuchi	M1	0	0	70	0.49	0.488	0	3414	2.5
Murayama and Iwabuchi	BS1	0	0	70	0.49	0.522	0	3636	3.0
Murayama and Iwabuchi	BS2	0	0	70	0.49	0.518	0	3686	3.0
Murayama and Iwabuchi	BS3	0	0	70	0.49	0.512	0	3693	3.0
Murayama and Iwabuchi	BS4	0	0	70	0.49	0.502	0	3626	3.0
Murayama and Iwabuchi	BS5	0	0	70	0.49	0.488	0	3686	3.0
Murayama and Iwabuchi	BL1	0	0	70	0.49	0.532	0	3661	4.0

Author	Specimen ID	*Load Spacing* (ft)	$x_{bearing.roll}$ (in)	$A_{s\,top}$ (in^2)	d_{top} (in.)	A_{ct} ($in.^2$)	*s* (in.)	h_{flange} (in)	cg_s (in)
Hanson	3A4	1.33	6.0	0	0	*36*	1000000	12.0	*1.5*
Hanson	4A4	1.33	6.0	0	0	*36*	1000000	12.0	*1.5*
Hanson	10A4	1.33	6.0	0	0	*36*	1000000	12.0	*1.5*
Hanson	2B4	1.33	6.0	0	0	*36*	1000000	12.0	*1.5*
Hanson	3B4	1.33	6.0	0	0	*36*	1000000	12.0	*1.5*
Hanson	4B4	1.33	6.0	0	0	*36*	1000000	12.0	*1.5*
Hanson	6B4	1.33	6.0	0	0	*36*	1000000	12.0	*1.5*
Hanson	10B4	1.33	6.0	0	0	*36*	1000000	12.0	*1.5*
Hanson	13B4	1.33	6.0	0	0	*36*	1000000	12.0	*1.5*
Hanson	10BW4	1.33	6.0	0	0	*36*	1000000	12.0	*1.5*
Ivey and Buth	(1) 1 "4.62"	*3.50*	*6.0*	0	0	*36*	1000000	12.0	*1.5*
Ivey and Buth	(1) 2 "6.33"	*5.83*	*6.0*	0	0	*36*	1000000	12.0	*1.5*
Ivey and Buth	(1) 3 "8.00"	*8.67*	*6.0*	0	0	*36*	1000000	12.0	*1.5*
Ivey and Buth	(23) 1 "6.33"	*5.83*	*6.0*	0	0	*36*	1000000	12.0	*1.5*
Ivey and Buth	(23) 2 "6.33"	*5.83*	*6.0*	0	0	*36*	1000000	12.0	*1.5*
Ivey and Buth	(23) 3 "6.33"	*5.83*	*6.0*	0	0	*36*	1000000	12.0	*1.5*
Ivey and Buth	(23) 1S "6.33"	*5.83*	*6.0*	0	0	*36*	1000000	12.0	*1.5*
Ivey and Buth	(23) 2S "6.33"	*5.83*	*6.0*	0	0	*36*	1000000	12.0	*1.5*
Ivey and Buth	(23) 3S "6.33"	*5.83*	*6.0*	0	0	*36*	1000000	12.0	*1.5*
Ivey and Buth	(27) 1 "4.62"	*3.50*	*6.0*	0	0	*36*	1000000	12.0	*1.5*
Ivey and Buth	(27) 2 "6.33"	*5.83*	*6.0*	0	0	*36*	1000000	12.0	*1.5*
Ivey and Buth	(27) 3 "8.00"	*8.67*	*6.0*	0	0	*36*	1000000	12.0	*1.5*
Ivey and Buth	(23) 4 "4.62"	0	*6.0*	0	0	*19*	1000000	9.0	*2*
Ivey and Buth	(23) 5 "6.33"	0	*6.0*	0	0	*36*	1000000	12.0	*2*
Ivey and Buth	(23) 6 "7.78"	0	*6.0*	0	0	*56*	1000000	15.0	*2*
Ivey and Buth	(23) 7 "9.15"	0	*6.0*	0	0	*80*	1000000	18.0	*2*
Ivey and Buth	(23) 8 "4.62"	*3.50*	*6.0*	0	0	*36*	1000000	12.0	*1.5*
Ivey and Buth	(23) 9 "4.62"	*3.50*	*6.0*	0	0	*36*	1000000	12.0	*1.5*
Ivey and Buth	(23) 10 "4.62"	*3.50*	*6.0*	0	0	*36*	1000000	12.0	*1.5*
Ivey and Buth	(23) 11 "4.62"	*3.50*	*6.0*	0	0	*36*	1000000	12.0	*1.5*
Ivey and Buth	(23) 12 "6.30"	*5.25*	*6.0*	0	0	*36*	1000000	12.0	*1.5*
Ivey and Buth	(23) 13 "7.00"	*7.00*	*6.0*	0	0	*36*	1000000	12.0	*1.5*
Ivey and Buth	(23) 14 "8.00"	*8.67*	*6.0*	0	0	*36*	1000000	12.0	*1.5*
Ivey and Buth	(23) 15 "6.33"	*5.83*	*6.0*	0	0	*36*	1000000	12.0	*1.5*
Ivey and Buth	(23) 16 "6.33"	*5.83*	*6.0*	0	0	*36*	1000000	12.0	*1.5*
Ivey and Buth	(23) 17 "6.33"	*5.83*	*6.0*	0	0	*36*	1000000	12.0	*1.5*
Kawaguchi et al.	A 1	0.984	11.8	0.0982	1.97	*54.3*	1000000	13.8	*2.55*
Kawaguchi et al.	A 2	0.984	11.8	0.0982	1.97	*54.3*	7.87	13.8	*2.55*
Kawaguchi et al.	B 1	0.984	11.8	0.0982	1.97	*54.3*	1000000	13.8	*2.55*
Kawaguchi et al.	B 2	0.984	11.8	0.0982	1.97	*54.3*	7.87	13.8	*2.55*
Kawaguchi et al.	C 1	0.984	11.8	0.0982	1.97	*54.3*	1000000	13.8	*2.55*
Kawaguchi et al.	C 2	0.984	11.8	0.0982	1.97	*54.3*	7.87	13.8	*2.55*
Kawaguchi et al.	D 1	0.984	11.8	0.0982	1.97	*54.3*	1000000	13.8	*2.55*
Kawaguchi et al.	D 2	0.984	11.8	0.0982	1.97	*54.3*	7.87	13.8	*2.55*
Murayama and Iwabuchi	B1	0.820	9.8	0	0	*46.47*	1000000	11.8	*1.97*
Murayama and Iwabuchi	M1	0.820	9.8	0	0	*46.47*	1000000	11.8	*1.97*
Murayama and Iwabuchi	BS1	1.640	9.8	0	0	*46.47*	1000000	11.8	*1.97*
Murayama and Iwabuchi	BS2	1.640	9.8	0	0	*46.47*	1000000	11.8	*1.97*
Murayama and Iwabuchi	BS3	1.640	9.8	0	0	*46.47*	1000000	11.8	*1.97*
Murayama and Iwabuchi	BS4	1.640	9.8	0	0	*46.47*	1000000	11.8	*1.97*
Murayama and Iwabuchi	BS5	1.640	9.8	0	0	*46.47*	1000000	11.8	*1.97*
Murayama and Iwabuchi	BL1	0.0	9.8	0	0	*46.47*	1000000	11.8	*1.97*

Author	Specimen ID	$cg_{s.bot}$ (in)	$size_{long.rebar}$ (in)	V_{exp} (kip)
Hanson	3A4	*1.5*	4	6.0
Hanson	4A4	*1.5*	4	5.9
Hanson	10A4	*1.5*	4	6.5
Hanson	2B4	*1.5*	4	5.8
Hanson	3B4	*1.5*	4	5.8
Hanson	4B4	*1.5*	4	6.6
Hanson	6B4	*1.5*	4	6.5
Hanson	10B4	*1.5*	4	6.2
Hanson	13B4	*1.5*	4	6.6
Hanson	10BW4	*1.5*	4	5.8
Ivey and Buth	(1) 1 "4.62"	*1.5*	4	22.7
Ivey and Buth	(1) 2 "6.33"	*1.5*	4	8.8
Ivey and Buth	(1) 3 "8.00"	*1.5*	4	7.5
Ivey and Buth	(23) 1 "6.33"	*1.5*	4	8.1
Ivey and Buth	(23) 2 "6.33"	*1.5*	4	8.4
Ivey and Buth	(23) 3 "6.33"	*1.5*	5	9.2
Ivey and Buth	(23) 1S "6.33"	*1.5*	4	7.68
Ivey and Buth	(23) 2S "6.33"	*1.5*	4	8.9
Ivey and Buth	(23) 3S "6.33"	*1.5*	5	8.9
Ivey and Buth	(27) 1 "4.62"	*1.5*	4	16.4
Ivey and Buth	(27) 2 "6.33"	*1.5*	4	8.8
Ivey and Buth	(27) 3 "8.00"	*1.5*	4	6.2
Ivey and Buth	(23) 4 "4.62"	*2*	4	3.81
Ivey and Buth	(23) 5 "6.33"	*2*	4	8.20
Ivey and Buth	(23) 6 "7.78"	*2*	5	13.20
Ivey and Buth	(23) 7 "9.15"	*2*	6	17.00
Ivey and Buth	(23) 8 "4.62"	*1.5*	4	11.21
Ivey and Buth	(23) 9 "4.62"	*1.5*	4	14.10
Ivey and Buth	(23) 10 "4.62"	*1.5*	5	13.98
Ivey and Buth	(23) 11 "4.62"	*1.5*	6	18.85
Ivey and Buth	(23) 12 "6.30"	*1.5*	6	12.21
Ivey and Buth	(23) 13 "7.00"	*1.5*	6	8.62
Ivey and Buth	(23) 14 "8.00"	*1.5*	6	8.94
Ivey and Buth	(23) 15 "6.33"	*1.5*	4	7.54
Ivey and Buth	(23) 16 "6.33"	*1.5*	4	8.82
Ivey and Buth	(23) 17 "6.33"	*1.5*	5	8.95
Kawaguchi et al.	A 1	*1.97*	*8*	10.0
Kawaguchi et al.	A 2	*1.97*	*8*	19.7
Kawaguchi et al.	B 1	*1.97*	*8*	10.5
Kawaguchi et al.	B 2	*1.97*	*8*	19.3
Kawaguchi et al.	C 1	*1.97*	*8*	12.8
Kawaguchi et al.	C 2	*1.97*	*8*	21.5
Kawaguchi et al.	D 1	*1.97*	*8*	7.2
Kawaguchi et al.	D 2	*1.97*	*8*	17.3
Murayama and Iwabuchi	B1	*1.97*	*8*	11.48
Murayama and Iwabuchi	M1	*1.97*	*8*	12.03
Murayama and Iwabuchi	BS1	*1.97*	*10*	14.35
Murayama and Iwabuchi	BS2	*1.97*	*10*	12.92
Murayama and Iwabuchi	BS3	*1.97*	*11*	14.68
Murayama and Iwabuchi	BS4	*1.97*	*11*	13.14
Murayama and Iwabuchi	BS5	*1.97*	*11*	12.81
Murayama and Iwabuchi	BL1	*1.97*	*10*	6.62

D.1.3 Murayama & Iwabuchi, Nishibayashi et al., Salandra & Ahmad, and Walraven & Al-Zubi

Author	Specimen ID	Fine Agg. Type	γ_c (kcf)	f'_c (ksi)	A_{c_2} (in.^{2})	h_{beam} (in)	$I_{o\ beam}$ (in^4)	L_{beam} (ft)	b_v (in)
Murayama and Iwabuchi	BL2	sand	*0.119*	7.0	92.94	11.81	*1080*	8.2	7.87
Murayama and Iwabuchi	BL3	sand	*0.119*	7.0	92.94	11.81	*1080*	8.2	7.87
Murayama and Iwabuchi	BL4	sand	*0.119*	7.4	92.94	11.81	*1080*	8.2	7.87
Nishibayashi et al.	L-3-f-13-0	lwt	0.098	3.1	31	7.87	*160*	4.9	3.94
Nishibayashi et al.	L-3-f-13-0	lwt	0.098	3.1	31	7.87	*160*	4.9	3.94
Nishibayashi et al.	L-3-D13-0	lwt	0.098	3.2	31	7.87	*160*	4.9	3.94
Nishibayashi et al.	L-3-D13-0	lwt	0.098	3.2	31	7.87	*160*	4.9	3.94
Nishibayashi et al.	L-3-f-16-0	lwt	0.098	3.1	31	7.87	*160*	4.9	3.94
Nishibayashi et al.	L-3-f-16-0	lwt	0.098	3.1	31	7.87	*160*	4.9	3.94
Nishibayashi et al.	L-3-D16-0	lwt	0.098	3.7	31	7.87	*160*	4.9	3.94
Nishibayashi et al.	L-3-D16-0	lwt	0.098	3.7	31	7.87	*160*	4.9	3.94
Nishibayashi et al.	L-4-f-13-0	lwt	0.099	6.1	31	7.87	*160*	4.9	3.94
Nishibayashi et al.	L-4-f-13-0	lwt	0.099	6.1	31	7.87	*160*	4.9	3.94
Nishibayashi et al.	L-4-D13-0	lwt	0.099	6.1	31	7.87	*160*	4.9	3.94
Nishibayashi et al.	L-4-D13-0	lwt	0.099	6.1	31	7.87	*160*	4.9	3.94
Nishibayashi et al.	L-4-f-16-0	lwt	0.099	6.2	31	7.87	*160*	4.9	3.94
Nishibayashi et al.	L-4-f-16-0	lwt	0.099	6.2	31	7.87	*160*	4.9	3.94
Nishibayashi et al.	L-4-D16-0	lwt	0.099	6.3	31	7.87	*160*	4.9	3.94
Nishibayashi et al.	L-4-D16-0	lwt	0.099	6.3	31	7.87	*160*	4.9	3.94
Nishibayashi et al.	L-3-D16-5	lwt	0.098	3.7	31	7.87	*160*	4.9	3.94
Nishibayashi et al.	L-3-D16-5	lwt	0.098	3.7	31	7.87	*160*	4.9	3.94
Nishibayashi et al.	L-3-f-16-10	lwt	0.098	3.1	31	7.87	*160*	4.9	3.94
Nishibayashi et al.	L-3-f-16-10	lwt	0.098	3.1	31	7.87	*160*	4.9	3.94
Nishibayashi et al.	L-3-D16-10	lwt	0.098	3.7	31	7.87	*160*	4.9	3.94
Nishibayashi et al.	L-3-D16-10	lwt	0.098	3.7	31	7.87	*160*	4.9	3.94
Salandra and Ahmad	LR-0.52-NS	sand	*0.123*	8.0	32.0	8.00	*171*	6.0	4.00
Salandra and Ahmad	LR-1.56-NS	sand	*0.123*	8.2	32.0	8.00	*171*	6.0	4.00
Salandra and Ahmad	LR-2.59-NS	sand	*0.123*	8.2	32.0	8.00	*171*	6.0	4.00
Salandra and Ahmad	LR-3.63-NS	sand	*0.123*	8.0	32.0	8.00	*171*	6.0	4.00
Salandra and Ahmad	HR-0.52-NS	sand	*0.123*	10.2	32.0	8.00	*171*	6.0	4.00
Salandra and Ahmad	HR-1.56-NS	sand	*0.123*	10.4	32.0	8.00	*171*	6.0	4.00
Salandra and Ahmad	HR-2.59-NS	sand	*0.123*	10.2	32.0	8.00	*171*	6.0	4.00
Salandra and Ahmad	HR-3.63-NS	sand	*0.123*	10.5	32.0	8.00	*171*	6.0	4.00
Salandra and Ahmad	LR-0.52-WS	sand	*0.123*	8.0	32.0	8.00	*171*	6.0	4.00
Salandra and Ahmad	LR-1.56-WS	sand	*0.123*	8.2	32.0	8.00	*171*	6.0	4.00
Salandra and Ahmad	LR-2.59-WS	sand	*0.123*	8.2	32.0	8.00	*171*	6.0	4.00
Salandra and Ahmad	LR-3.63-WS	sand	*0.123*	8.0	32.0	8.00	*171*	6.0	4.00
Salandra and Ahmad	HR-0.52-WS	sand	*0.123*	10.2	32.0	8.00	*171*	6.0	4.00
Salandra and Ahmad	HR-1.56-WS	sand	*0.123*	10.4	32.0	8.00	*171*	6.0	4.00
Salandra and Ahmad	HR-2.59-WS	sand	*0.123*	10.2	32.0	8.00	*171*	6.0	4.00
Salandra and Ahmad	HR-3.63-WS	sand	*0.123*	10.5	32.0	8.00	*170.7*	6.0	4.00
Walraven and Al-Zubi	Lg30l	*sand*	0.121	2.889	279.0	31.50	37597	18.0	3.937
Walraven and Al-Zubi	Lr30l	*sand*	0.108	4.134	279.0	31.50	37597	18.0	3.937
Walraven and Al-Zubi	Ae30l	*sand*	0.131	3.445	279.0	31.50	37597	18.0	3.937
Walraven and Al-Zubi	Lg60l	*sand*	0.125	6.551	279.0	31.50	37597	18.0	3.937
Walraven and Al-Zubi	Lg60m	*sand*	0.125	6.998	279.0	31.50	37597	18.0	3.937
Walraven and Al-Zubi	Lg30m	*sand*	0.121	4.291	279.0	31.50	37597	18.0	3.937
Walraven and Al-Zubi	Lg30h	*sand*	0.121	3.807	279.0	31.50	37597	18.0	3.937
Walraven and Al-Zubi	Lr30m	*sand*	0.108	3.783	279.0	31.50	37597	18.0	3.937
Walraven and Al-Zubi	Lr30h	*sand*	0.108	3.807	279.0	31.50	37597	18.0	3.937
Walraven and Al-Zubi	Ae30m	*sand*	0.131	3.275	279.0	31.50	37597	18.0	3.937

Author	Specimen ID	b_{flange} (in)	y_{bot} (in)	y_{top} (in)	S (ft)	$x_{bearing}$ (in)	$A_{s\ bgt}$ (in.^{2})	f_y (ksi)	E_s (ksi)
Murayama and Iwabuchi	BL2	7.87	5.91	5.91	0.656	9.84	*2.0*	71.1	*29000*
Murayama and Iwabuchi	BL3	7.87	5.91	5.91	0.656	9.84	*2.5*	71.1	*29000*
Murayama and Iwabuchi	BL4	7.87	5.91	5.91	0.656	9.84	*2.5*	71.1	*29000*
Nishibayashi et al.	L-3-f-13-0	3.94	3.94	3.94	0.328	5.91	0.41	44.6	*29000*
Nishibayashi et al.	L-3-f-13-0	3.94	3.94	3.94	0.328	5.91	0.41	44.6	*29000*
Nishibayashi et al.	L-3-D13-0	3.94	3.94	3.94	0.328	5.91	0.39	58.3	*29000*
Nishibayashi et al.	L-3-D13-0	3.94	3.94	3.94	0.328	5.91	0.39	58.3	*29000*
Nishibayashi et al.	L-3-f-16-0	3.94	3.94	3.94	0.328	5.91	0.62	40.2	*29000*
Nishibayashi et al.	L-3-f-16-0	3.94	3.94	3.94	0.328	5.91	0.62	40.2	*29000*
Nishibayashi et al.	L-3-D16-0	3.94	3.94	3.94	0.328	5.91	0.61	51.8	*29000*
Nishibayashi et al.	L-3-D16-0	3.94	3.94	3.94	0.328	5.91	0.61	51.8	*29000*
Nishibayashi et al.	L-4-f-13-0	3.94	3.94	3.94	0.328	3.94	0.41	44.6	*29000*
Nishibayashi et al.	L-4-f-13-0	3.94	3.94	3.94	0.328	3.94	0.41	44.6	*29000*
Nishibayashi et al.	L-4-D13-0	3.94	3.94	3.94	0.328	3.94	0.39	58.3	*29000*
Nishibayashi et al.	L-4-D13-0	3.94	3.94	3.94	0.328	3.94	0.39	58.3	*29000*
Nishibayashi et al.	L-4-f-16-0	3.94	3.94	3.94	0.328	3.94	0.62	40.2	*29000*
Nishibayashi et al.	L-4-f-16-0	3.94	3.94	3.94	0.328	3.94	0.62	40.2	*29000*
Nishibayashi et al.	L-4-D16-0	3.94	3.94	3.94	0.328	3.94	0.61	51.8	*29000*
Nishibayashi et al.	L-4-D16-0	3.94	3.94	3.94	0.328	3.94	0.61	51.8	*29000*
Nishibayashi et al.	L-3-D16-5	3.94	3.94	3.94	0.328	5.91	0.61	51.8	*29000*
Nishibayashi et al.	L-3-D16-5	3.94	3.94	3.94	0.328	5.91	0.61	51.8	*29000*
Nishibayashi et al.	L-3-f-16-10	3.94	3.94	3.94	0.328	5.91	0.62	40.2	*29000*
Nishibayashi et al.	L-3-f-16-10	3.94	3.94	3.94	0.328	5.91	0.62	40.2	*29000*
Nishibayashi et al.	L-3-D16-10	3.94	3.94	3.94	0.328	5.91	0.61	51.8	*29000*
Nishibayashi et al.	L-3-D16-10	3.94	3.94	3.94	0.328	5.91	0.61	51.8	*29000*
Salandra and Ahmad	LR-0.52-NS	4.00	4.00	4.00	0.333	23.49	0.40	60.0	*29000*
Salandra and Ahmad	LR-1.56-NS	4.00	4.00	4.00	0.333	16.47	0.40	60.0	*29000*
Salandra and Ahmad	LR-2.59-NS	4.00	4.00	4.00	0.333	9.52	0.40	60.0	*29000*
Salandra and Ahmad	LR-3.63-NS	4.00	4.00	4.00	0.333	2.50	0.40	60.0	*29000*
Salandra and Ahmad	HR-0.52-NS	4.00	4.00	4.00	0.333	23.49	0.40	60.0	*29000*
Salandra and Ahmad	HR-1.56-NS	4.00	4.00	4.00	0.333	16.47	0.40	60.0	*29000*
Salandra and Ahmad	HR-2.59-NS	4.00	4.00	4.00	0.333	9.52	0.40	60.0	*29000*
Salandra and Ahmad	HR-3.63-NS	4.00	4.00	4.00	0.333	2.50	0.40	60.0	*29000*
Salandra and Ahmad	LR-0.52-WS	4.00	4.00	4.00	0.333	23.49	0.40	60.0	*29000*
Salandra and Ahmad	LR-1.56-WS	4.00	4.00	4.00	0.333	16.47	0.40	60.0	*29000*
Salandra and Ahmad	LR-2.59-WS	4.00	4.00	4.00	0.333	9.52	0.40	60.0	*29000*
Salandra and Ahmad	LR-3.63-WS	4.00	4.00	4.00	0.333	2.50	0.40	60.0	*29000*
Salandra and Ahmad	HR-0.52-WS	4.00	4.0	4.0	0.3	23.49	0.40	60.0	*29000*
Salandra and Ahmad	HR-1.56-WS	4.00	4.0	4.0	0.3	16.47	0.40	60.0	*29000*
Salandra and Ahmad	HR-2.59-WS	4.00	4.0	4.0	0.3	9.52	0.40	60.0	*29000*
Salandra and Ahmad	HR-3.63-WS	4.00	4.0	4.0	0.3	2.50	0.40	60.0	*29000*
Walraven and Al-Zubi	Lg30l	19.69	16.4	15.1	19.7	*10.00*	3.81	82.67	*29000*
Walraven and Al-Zubi	Lr30l	19.69	16.4	15.1	19.7	*10.00*	3.81	82.67	*29000*
Walraven and Al-Zubi	Ae30l	19.69	16.4	15.1	19.7	*10.00*	3.81	82.67	*29000*
Walraven and Al-Zubi	Lg60l	19.69	16.4	15.1	19.7	*10.00*	3.81	82.67	*29000*
Walraven and Al-Zubi	Lg60m	19.69	16.4	15.1	19.7	*10.00*	6.09	82.67	*29000*
Walraven and Al-Zubi	Lg30m	19.69	16.4	15.1	19.7	*10.00*	3.81	82.67	*29000*
Walraven and Al-Zubi	Lg30h	19.69	16.4	15.1	19.7	*10.00*	6.09	82.67	*29000*
Walraven and Al-Zubi	Lr30m	19.69	16.4	15.1	19.7	*10.00*	3.81	82.67	*29000*
Walraven and Al-Zubi	Lr30h	19.69	16.4	15.1	19.7	*10.00*	6.09	82.67	*29000*
Walraven and Al-Zubi	Ae30m	19.69	16.4	15.1	19.7	*10.00*	3.81	82.67	*29000*

Author	Specimen ID	A_v (in.^{2})	f_{yv} (ksi)	H	$x_{critical,\ assume}$ (ft)	f_{ct} (ksi)	a_g (in.)	E_c (ksi)	a/d
Murayama and Iwabuchi	BL2	0	0	*70*	0.49	0.478	*0*	*3589*	4.0
Murayama and Iwabuchi	BL3	0	0	*70*	0.49	0.526	*0*	*3575*	4.0
Murayama and Iwabuchi	BL4	0	0	*70*	0.49	0.529	*0*	*3693*	4.0
Nishibayashi et al.	L-3-f-13-0	0	49.2	*70*	0.33	0.247	0.8	2219	2.06
Nishibayashi et al.	L-3-f-13-0	0	49.2	*70*	0.33	0.247	0.8	2219	2.06
Nishibayashi et al.	L-3-D13-0	0	49.2	*70*	0.33	0.247	0.8	2276	2.06
Nishibayashi et al.	L-3-D13-0	0	49.2	*70*	0.33	0.247	0.8	2276	2.06
Nishibayashi et al.	L-3-f-16-0	0	49.2	*70*	0.33	0.247	0.8	2219	2.06
Nishibayashi et al.	L-3-f-16-0	0	49.2	*70*	0.33	0.247	0.8	2219	2.06
Nishibayashi et al.	L-3-D16-0	0	49.2	*70*	0.33	0.246	0.8	2375	2.06
Nishibayashi et al.	L-3-D16-0	0	49.2	*70*	0.33	0.246	0.8	2375	2.06
Nishibayashi et al.	L-4-f-13-0	0	49.2	*70*	0.33	0.375	0.8	2745	2.94
Nishibayashi et al.	L-4-f-13-0	0	49.2	*70*	0.33	0.375	0.8	2745	2.94
Nishibayashi et al.	L-4-D13-0	0	49.2	*70*	0.33	0.375	0.8	2745	2.94
Nishibayashi et al.	L-4-D13-0	0	49.2	*70*	0.33	0.375	0.8	2745	2.94
Nishibayashi et al.	L-4-f-16-0	0	49.2	*70*	0.33	0.398	0.8	2603	2.94
Nishibayashi et al.	L-4-f-16-0	0	49.2	*70*	0.33	0.398	0.8	2603	2.94
Nishibayashi et al.	L-4-D16-0	0	49.2	*70*	0.33	0.452	0.8	3030	2.94
Nishibayashi et al.	L-4-D16-0	0.000	49.2	*70*	0.33	0.452	0.8	3030	2.94
Nishibayashi et al.	L-3-D16-5	0.087	69.2	*70*	0.33	0	0.8	2375	2.06
Nishibayashi et al.	L-3-D16-5	0.087	69.2	*70*	0.33	0	0.8	2347	2.06
Nishibayashi et al.	L-3-f-16-10	0.087	69.2	*70*	0.33	0	0.8	2219	2.06
Nishibayashi et al.	L-3-f-16-10	0.087	69.2	*70*	0.33	0	0.8	2219	2.06
Nishibayashi et al.	L-3-D16-10	0.087	69.2	*70*	0.33	0	0.8	2375	2.06
Nishibayashi et al.	L-3-D16-10	0.087	69.2	*70*	0.33	0	0.8	2375	2.06
Salandra and Ahmad	LR-0.52-NS	0	60.0	*70*	0.33	0	0.50	*3992*	0.52
Salandra and Ahmad	LR-1.56-NS	0	60.0	*70*	0.33	0	0.50	*4052*	1.56
Salandra and Ahmad	LR-2.59-NS	0	60.0	*70*	0.33	0	0.50	*4052*	2.59
Salandra and Ahmad	LR-3.63-NS	0	60.0	*70*	0.33	0	0.50	*3992*	3.63
Salandra and Ahmad	HR-0.52-NS	0	60.0	*70*	0.33	0	0.50	*4519*	0.52
Salandra and Ahmad	HR-1.56-NS	0	60.0	*70*	0.33	0	0.50	*4565*	1.56
Salandra and Ahmad	HR-2.59-NS	0	60.0	*70*	0.33	0	0.50	*4521*	2.59
Salandra and Ahmad	HR-3.63-NS	0	60.0	*70*	0.33	0	0.50	*4593*	3.63
Salandra and Ahmad	LR-0.52-WS	0.098	60.0	*70*	0.33	0	0.50	*3992*	0.52
Salandra and Ahmad	LR-1.56-WS	0.098	60.0	*70*	0.33	0	0.50	*4052*	1.56
Salandra and Ahmad	LR-2.59-WS	0.098	60.0	*70*	0.33	0	0.50	*4052*	2.59
Salandra and Ahmad	LR-3.63-WS	0.098	60.0	*70*	0.33	0	0.50	*3992*	3.63
Salandra and Ahmad	HR-0.52-WS	0.098	60.0	*70*	0.33	0	0.50	*4519*	0.52
Salandra and Ahmad	HR-1.56-WS	0.098	60.0	*70*	0.33	0	0.50	*4565*	1.56
Salandra and Ahmad	HR-2.59-WS	0.098	60.0	*70*	0.33	0	0.50	*4521*	2.59
Salandra and Ahmad	HR-3.63-WS	0.098	60.0	*70*	0.33	0	0.50	*4593*	3.63
Walraven and Al-Zubi	Lg30l	0.156	83.40	*70*	1.31	0.244	*0*	*2360*	*2.2*
Walraven and Al-Zubi	Lr30l	0.156	83.40	*70*	1.31	0.354	*0*	*2377*	*2.2*
Walraven and Al-Zubi	Ae30l	0.156	83.40	*70*	1.31	0.299	*0*	*2897*	*2.2*
Walraven and Al-Zubi	Lg60l	0.243	89.92	*70*	1.31	0.429	*0*	*3735*	*2.2*
Walraven and Al-Zubi	Lg60m	0.243	89.92	*70*	1.31	0.460	*0*	*3860*	*2.3*
Walraven and Al-Zubi	Lg30m	0.243	89.92	*70*	1.31	0.383	*0*	*2877*	*2.2*
Walraven and Al-Zubi	Lg30h	0.243	89.92	*70*	1.31	0.352	*0*	*2710*	*2.3*
Walraven and Al-Zubi	Lr30m	0.243	89.92	*70*	1.31	0.339	*0*	*2274*	*2.2*
Walraven and Al-Zubi	Lr30h	0.243	89.92	*70*	1.31	0.336	*0*	*2281*	*2.3*
Walraven and Al-Zubi	Ae30m	0.243	89.92	*70*	1.31	0.302	*0*	*2825*	*2.2*

Author	Specimen ID	*Load Spacing* (ft)	$x_{bearing.roll}$ (in)	$A_{s\ top}$ (in^2)	d_{top} (in.)	A_{ct} ($in.^2$)	s (in.)	h_{flange} (in)	cg_s (in)
Murayama and Iwabuchi	BL2	0.0	9.8	0	0	*46.47*	1000000	11.8	*1.97*
Murayama and Iwabuchi	BL3	0.0	9.8	0	0	*46.47*	1000000	11.8	*1.97*
Murayama and Iwabuchi	BL4	0.0	9.8	0	0	*46.47*	1000000	11.8	*1.97*
Nishibayashi et al.	L-3-f-13-0	1.64	5.9	0.20	0.98	*15.5*	1000000	7.87	*3.03*
Nishibayashi et al.	L-3-f-13-0	1.64	5.9	0.20	0.98	*15.5*	1000000	7.87	*3.03*
Nishibayashi et al.	L-3-D13-0	1.64	5.9	0.20	0.98	*15.5*	1000000	7.87	*3.07*
Nishibayashi et al.	L-3-D13-0	1.64	5.9	0.20	0.98	*15.5*	1000000	7.87	*3.07*
Nishibayashi et al.	L-3-f-16-0	1.64	5.9	0.20	0.98	*15.5*	1000000	7.87	*2.55*
Nishibayashi et al.	L-3-f-16-0	1.64	5.9	0.20	0.98	*15.5*	1000000	7.87	*2.55*
Nishibayashi et al.	L-3-D16-0	1.64	5.9	0.20	0.98	*15.5*	1000000	7.87	*2.56*
Nishibayashi et al.	L-3-D16-0	1.64	5.9	0.20	0.98	*15.5*	1000000	7.87	*2.56*
Nishibayashi et al.	L-4-f-13-0	0.98	3.9	0.20	0.98	*15.5*	1000000	7.87	*3.03*
Nishibayashi et al.	L-4-f-13-0	0.98	3.9	0.20	0.98	*15.5*	1000000	7.87	*3.03*
Nishibayashi et al.	L-4-D13-0	0.98	3.9	0.20	0.98	*15.5*	1000000	7.87	*3.07*
Nishibayashi et al.	L-4-D13-0	0.98	3.9	0.20	0.98	*15.5*	1000000	7.87	*3.07*
Nishibayashi et al.	L-4-f-16-0	0.98	3.9	0.20	0.98	*15.5*	1000000	7.87	*2.55*
Nishibayashi et al.	L-4-f-16-0	0.98	3.9	0.20	0.98	*15.5*	1000000	7.87	*2.55*
Nishibayashi et al.	L-4-D16-0	0.98	3.9	0.20	0.98	*15.5*	1000000	7.87	*2.56*
Nishibayashi et al.	L-4-D16-0	0.98	3.9	0.20	0.98	*15.5*	1000000	7.87	*2.56*
Nishibayashi et al.	L-3-D16-5	1.64	5.9	0.20	0.98	*15.5*	2.0	7.87	*2.56*
Nishibayashi et al.	L-3-D16-5	1.64	5.9	0.20	0.98	*15.5*	2.0	7.87	*2.56*
Nishibayashi et al.	L-3-f-16-10	1.64	5.9	0.20	0.98	*15.5*	3.9	7.87	*2.55*
Nishibayashi et al.	L-3-f-16-10	1.64	5.9	0.20	0.98	*15.5*	3.9	7.87	*2.55*
Nishibayashi et al.	L-3-D16-10	1.64	5.9	0.20	0.98	*15.5*	3.9	7.87	*2.56*
Nishibayashi et al.	L-3-D16-10	1.64	5.9	0.20	0.98	*15.5*	3.9	7.87	*2.56*
Salandra and Ahmad	LR-0.52-NS	1.50	23.5	0	1.50	*16.0*	1000000	8.0	*1.25*
Salandra and Ahmad	LR-1.56-NS	1.50	16.5	0	1.50	*16.0*	1000000	8.0	*1.25*
Salandra and Ahmad	LR-2.59-NS	1.50	9.5	0	1.50	*16.0*	1000000	8.0	*1.25*
Salandra and Ahmad	LR-3.63-NS	1.50	2.5	0	1.50	*16.0*	1000000	8.0	*1.25*
Salandra and Ahmad	HR-0.52-NS	1.50	23.5	0	1.50	*16.0*	1000000	8.0	*1.25*
Salandra and Ahmad	HR-1.56-NS	1.50	16.5	0	1.50	*16.0*	1000000	8.0	*1.25*
Salandra and Ahmad	HR-2.59-NS	1.50	9.5	0	1.50	*16.0*	1000000	8.0	*1.25*
Salandra and Ahmad	HR-3.63-NS	1.50	2.5	0	1.50	*16.0*	1000000	8.0	*1.25*
Salandra and Ahmad	LR-0.52-WS	1.50	23.5	0.10	1.50	*16.0*	3.25	8.0	*2.28*
Salandra and Ahmad	LR-1.56-WS	1.50	16.5	0.10	1.50	*16.0*	3.25	8.0	*2.28*
Salandra and Ahmad	LR-2.59-WS	1.50	9.5	0.10	1.50	*16.0*	3.25	8.0	*2.28*
Salandra and Ahmad	LR-3.63-WS	1.50	2.5	0.10	1.50	*16.0*	3.25	8.0	*2.28*
Salandra and Ahmad	HR-0.52-WS	1.50	23.5	0.10	1.50	*16.0*	3.25	8.0	*2.28*
Salandra and Ahmad	HR-1.56-WS	1.50	16.5	0.10	1.50	*16.0*	3.25	8.0	*2.28*
Salandra and Ahmad	HR-2.59-WS	1.50	9.5	0.10	1.50	*16.0*	3.25	8.0	*2.28*
Salandra and Ahmad	HR-3.63-WS	1.50	2.5	0.10	1.50	*16.0*	3.25	8.0	*2.28*
Walraven and Al-Zubi	Lg30l	5.25	*10.0*	0.31	1.10	*131.8*	9.3	4.9	*3.92*
Walraven and Al-Zubi	Lr30l	5.25	*10.0*	0.31	1.10	*131.8*	9.3	4.9	*3.92*
Walraven and Al-Zubi	Ae30l	5.25	*10.0*	0.31	1.10	*131.8*	9.3	4.9	*3.92*
Walraven and Al-Zubi	Lg60l	5.25	*10.0*	0.31	1.10	*131.8*	9.4	4.9	*3.92*
Walraven and Al-Zubi	Lg60m	5.25	*10.0*	1.05	1.10	*131.8*	5.0	4.9	*3.92*
Walraven and Al-Zubi	Lg30m	5.25	*10.0*	0.31	1.10	*131.8*	7.0	4.9	*3.92*
Walraven and Al-Zubi	Lg30h	5.25	*10.0*	1.05	1.10	*131.8*	4.3	4.9	*3.92*
Walraven and Al-Zubi	Lr30m	5.25	*10.0*	0.31	1.10	*131.8*	7.0	4.9	*3.92*
Walraven and Al-Zubi	Lr30h	5.25	*10.0*	1.05	1.10	*131.8*	4.3	4.9	*3.92*
Walraven and Al-Zubi	Ae30m	5.25	*10.0*	0.31	1.10	*131.8*	7.0	4.9	*3.92*

Author	Specimen ID	$cg_{s.bot}$ (in)	$size_{long.rebar}$ (in)	V_{exp} (kip)
Murayama and Iwabuchi	BL2	*1.97*	*10*	6.40
Murayama and Iwabuchi	BL3	*1.97*	*11*	7.40
Murayama and Iwabuchi	BL4	*1.97*	*11*	7.07
Nishibayashi et al.	L-3-f-13-0	*1.18*	4	5.5
Nishibayashi et al.	L-3-f-13-0	*1.18*	4	5.8
Nishibayashi et al.	L-3-D13-0	*1.18*	4	4.2
Nishibayashi et al.	L-3-D13-0	*1.18*	4	3.8
Nishibayashi et al.	L-3-f-16-0	*1.18*	5	3.9
Nishibayashi et al.	L-3-f-16-0	*1.18*	5	6.4
Nishibayashi et al.	L-3-D16-0	*1.18*	5	4.1
Nishibayashi et al.	L-3-D16-0	*1.18*	5	4.1
Nishibayashi et al.	L-4-f-13-0	*1.18*	4	4.7
Nishibayashi et al.	L-4-f-13-0	*1.18*	4	4.5
Nishibayashi et al.	L-4-D13-0	*1.18*	4	3.5
Nishibayashi et al.	L-4-D13-0	*1.18*	4	4.3
Nishibayashi et al.	L-4-f-16-0	*1.18*	5	4.1
Nishibayashi et al.	L-4-f-16-0	*1.18*	5	4.1
Nishibayashi et al.	L-4-D16-0	*1.18*	5	4.3
Nishibayashi et al.	L-4-D16-0	*1.18*	5	4.4
Nishibayashi et al.	L-3-D16-5	*1.18*	5	10.9
Nishibayashi et al.	L-3-D16-5	*1.18*	5	10.1
Nishibayashi et al.	L-3-f-16-10	*1.18*	5	10.4
Nishibayashi et al.	L-3-f-16-10	*1.18*	5	10.4
Nishibayashi et al.	L-3-D16-10	*1.18*	5	8.6
Nishibayashi et al.	L-3-D16-10	*1.18*	5	8.9
Salandra and Ahmad	LR-0.52-NS	*1.25*	4	30.5
Salandra and Ahmad	LR-1.56-NS	*1.25*	4	17.0
Salandra and Ahmad	LR-2.59-NS	*1.25*	4	6.0
Salandra and Ahmad	LR-3.63-NS	*1.25*	4	4.9
Salandra and Ahmad	HR-0.52-NS	*1.25*	4	32.0
Salandra and Ahmad	HR-1.56-NS	*1.25*	4	16.3
Salandra and Ahmad	HR-2.59-NS	*1.25*	4	6.7
Salandra and Ahmad	HR-3.63-NS	*1.25*	4	4.5
Salandra and Ahmad	LR-0.52-WS	*1.25*	4	35.5
Salandra and Ahmad	LR-1.56-WS	*1.25*	4	18.5
Salandra and Ahmad	LR-2.59-WS	*1.25*	4	10.5
Salandra and Ahmad	LR-3.63-WS	*1.25*	4	7.3
Salandra and Ahmad	HR-0.52-WS	*1.25*	4	38.5
Salandra and Ahmad	HR-1.56-WS	*1.25*	4	16.5
Salandra and Ahmad	HR-2.59-WS	*1.25*	4	10.0
Salandra and Ahmad	HR-3.63-WS	*1.25*	4	6.0
Walraven and Al-Zubi	Lg30l	*1.59*	8	72.8
Walraven and Al-Zubi	Lr30l	*1.59*	8	74.2
Walraven and Al-Zubi	Ae30l	*1.59*	8	72.2
Walraven and Al-Zubi	Lg60l	*1.59*	8	116.2
Walraven and Al-Zubi	Lg60m	*1.59*	8	168.8
Walraven and Al-Zubi	Lg30m	*1.59*	8	116.9
Walraven and Al-Zubi	Lg30h	*1.59*	8	108.1
Walraven and Al-Zubi	Lr30m	*1.59*	8	103.6
Walraven and Al-Zubi	Lr30h	*1.59*	8	121.6
Walraven and Al-Zubi	Ae30m	*1.59*	8	102.7

D.1.4 Walraven & Al-Zubi and Malone

Author	Specimen ID	Fine Agg. Type	γ_c (kcf)	f'_c (ksi)	A_c (in.^{2})	h_{beam} (in)	$I_{o\ beam}$ (in^4)	L_{beam} (ft)	b_v (in)
Walraven and Al-Zubi	Ae30h	*sand*	0.131	3.058	279.0	31.50	37597	18.0	3.937
Malone	5-LWLA	sand	0.106	6.3	*196.2*	14.00	*3204.93*	11.0	14.02
Malone	6-LWLB	sand	0.106	6.2	*196.2*	14.00	*3204.93*	11.0	14.02
Malone	7-LWLC	sand	0.106	6.3	*196.2*	14.00	*3204.93*	11.0	14.02
Malone	8-LWLD	sand	0.106	6.4	*196.2*	14.00	*3204.93*	11.0	14.02
Malone	11-LWHD	sand	0.127	10.5	*196.2*	14.00	*3204.93*	11.0	14.02

Author	Specimen ID	b_{flange} (in)	y_{bot} (in)	y_{top} (in)	S (ft)	$x_{bearing}$ (in)	$A_{s\ bot}$ (in.^{2})	f_y (ksi)	E_s (ksi)
Walraven and Al-Zubi	Ae30h	19.69	16.4	15.1	19.7	*10.00*	6.09	82.67	*29000*
Malone	5-LWLA	14.02	7.0	7.0	1.2	6.0	3.95	60.0	*29000*
Malone	6-LWLB	14.02	7.0	7.0	1.2	6.0	3.95	60.0	*29000*
Malone	7-LWLC	14.02	7.0	7.0	1.2	6.0	4.00	60.0	*29000*
Malone	8-LWLD	14.02	7.0	7.0	1.2	6.0	4.00	60.0	*29000*
Malone	11-LWHD	14.02	7.0	7.0	1.2	6.0	4.00	60.0	*29000*

Author	Specimen ID	A_v (in.^{2})	f_{yv} (ksi)	H	$x_{critical.\ assume}$ (ft)	f_{ct} (ksi)	a_g (in.)	E_c (ksi)	a/d
Walraven and Al-Zubi	Ae30h	0.243	89.92	*70*	1.31	0.283	*0*	*2729*	*2.3*
Malone	5-LWLA	0.220	60.0	*70*	0.58	0.537	0.37	3110	*5.5*
Malone	6-LWLB	0.220	60.0	*70*	0.58	0.551	0.37	3110	*5.5*
Malone	7-LWLC	0.220	60.0	*70*	0.58	0.464	0.37	3110	*5.5*
Malone	8-LWLD	0.220	60.0	*70*	0.58	0.551	0.37	3110	*5.5*
Malone	11-LWHD	0.220	60.0	*70*	0.58	0.566	0.37	3800	*5.5*

Author	Specimen ID	*Load Spacing* (ft)	$x_{bearing.roll}$ (in)	$A_{s\ top}$ (in^2)	d_{top} (in.)	A_{ct} (in.^{2})	s (in.)	h_{flange} (in)	cg_s (in)
Walraven and Al-Zubi	Ae30h	5.25	*10.0*	1.05	1.10	*131.8*	4.3	4.9	*3.92*
Malone	5-LWLA	7.50	6.0	3.95	1.875	*98.1*	4	14.0	*7.01*
Malone	6-LWLB	7.50	6.0	3.95	1.875	*98.1*	6	14.0	*7.01*
Malone	7-LWLC	7.50	6.0	4.00	1.938	*98.1*	4	14.0	*7.01*
Malone	8-LWLD	7.50	6.0	4.00	1.938	*98.1*	6	14.0	*7.01*
Malone	11-LWHD	7.50	6.0	4.00	1.938	*98.1*	6	14.0	*7.01*

Author	Specimen ID	$cg_{s.bot}$ (in)	$size_{long.rebar}$ (in)	V_{exp} (kip)
Walraven and Al-Zubi	Ae30h	*1.59*	8	108.4
Malone	5-LWLA	*1.875*	8	73.7
Malone	6-LWLB	*1.875*	8	83.6
Malone	7-LWLC	*1.938*	9	80.3
Malone	8-LWLD	*1.938*	9	62.9
Malone	11-LWHD	*1.938*	9	89.0

D.2 Prestressed Database

Author	Specimen ID	t_{haunch} (in.)	t_{deck} (in.)	t_{struct} (in.)	$x_{bearing}$ (in)	A_{strand} (in^2)	φ_{strand} (in)	f_{pu} (ksi)	E_{ps} (ksi)	$A_{s\ bgt}$ (in.^{2})	f_y (ksi)	E_s (ksi)	A_v (in.^{2})	f_{yv} (ksi)	H (%)	HarpDist Ratio
Malone	PC6N	0	4.0	4.0	36	0.167	0.5	270	28500	1.20	70.0	29000	0	72.8	70	0
Malone	PC6S	0	4.0	4.0	36	0.167	0.5	270	28500	1.20	70.0	29000	0.22	72.8	70	0
Malone	PC10N	0	4.0	4.0	36	0.167	0.5	270	28500	2.37	70.0	29000	0	72.8	70	0
Malone	PC10S	0	4.0	4.0	36	0.167	0.5	270	28500	2.37	70.0	29000	0.22	72.8	70	0
Kahn et al.	G1A-East	0	11.5	11.5	6	0.2183	0.6	283	29000	0	0	29000	0.40	62.0	70	0
Kahn et al.	G1A-Center	0	11.5	11.5	137	0.2183	0.6	283	29000	0	0	29000	0.40	62.0	70	0
Kahn et al.	G1B-East	0	11.5	11.5	6	0.2183	0.6	283	29000	0	0	29000	0.40	62.0	70	0
Kahn et al.	G1B-Center	0	11.5	11.5	117	0.2183	0.6	283	29000	0	0	29000	0.40	62.0	70	0
Kahn et al.	G1C-East	0	11.5	11.5	6	0.2183	0.6	283	29000	0	0	29000	0.40	62.0	70	0
Kahn et al.	G2A-Center	0	11.5	11.5	137	0.2183	0.6	283	29000	0	0	29000	0.40	62.0	70	0
Kahn et al.	G2B-Center	0	11.5	11.5	117	0.2183	0.6	283	29000	0	0	29000	0.40	62.0	70	0
Dymond	web-shear	1.5	9	9.0	12	0.153	0.5	284	29040	0	0	29000	0.62	60.0	70	0.4603

Author	Specimen ID	$x_{critical.\ assume}$ (ft)	f_{ct} (ksi)	a_g (in.)	E_c (ksi)	E_{ci} (ksi)	$E_{c\ deck}$ (ksi)	$num_{strands}$	$num_{straight}$	a/d	$Load\ Spacing$ (ft)	$x_{bearing.roll}$ (in)	f_r (ksi)	b_{deck} (in.)	L_{span} (ft)
Malone	PC6N	1.92	0.464	0.37	2901	2287	5366	10	8	3.03	0	36	0.464	48	16.00
Malone	PC6S	1.92	0.479	0.37	2901	2287	5366	10	8	3.03	0	36	0.290	48	16.00
Malone	PC10N	1.92	0.566	0.37	3800	2998	5366	10	8	3.04	0	36	0.595	48	16.00
Malone	PC10S	1.92	0.537	0.37	3800	2998	5366	10	8	3.04	0	36	0.580	48	16.00
Kahn et al.	G1A-East	2.85	0	0.50	3720	3470	3349	10	8	2.02	0	6	1.010	19	38.00
Kahn et al.	G1A-Center	2.85	0	0.50	3720	3470	3350	10	8	1.84	0	146	1.010	19	15.42
Kahn et al.	G1B-East	2.85	0	0.50	3720	3470	3350	10	8	1.69	0	6	1.010	19	38.00
Kahn et al.	G1B-Center	2.85	0	0.50	3720	3470	3350	10	8	2.16	0	141	1.010	19	17.50
Kahn et al.	G1C-East	2.85	0	0.50	3690	3000	3350	10	8	1.91	0	6	0.796	19	42.00
Kahn et al.	G2A-Center	2.85	0	0.50	3880	3550	3360	10	8	1.84	0	146	1.204	19	15.42
Kahn et al.	G2B-Center	2.85	0	0.50	3880	3550	3360	10	8	2.16	0	141	1.204	19	17.50
Dymond	web-shear	3.81	0.796	0.75	3280	3600	2860	32	26	1.30	3	12	0.650	84	63.00

Author	Specimen ID	s (in.)	$A_{s\ top}$ (in.^{2})	$A_{ps\ bot}$ (in.^{2})	$A_{ps\ top}$ (in.^{2})	V_{exp} (kip)
Malone	PC6N	1000000	0.62	1.3	0.3	80.0
Malone	PC6S	20	0.62	1.3	0.3	116.9
Malone	PC10N	1000000	0.62	1.3	0.3	104.5
Malone	PC10S	20	0.62	1.3	0.3	120.0
Kahn et al.	G1A-East	7	0	1.746	0.437	362.8
Kahn et al.	G1A-Center	24	0	1.746	0.437	258.0
Kahn et al.	G1B-East	3.5	0	1.746	0.437	312.2
Kahn et al.	G1B-Center	24	0	1.746	0.437	234.1
Kahn et al.	G1C-East	7	0	1.746	0.437	289.2
Kahn et al.	G2A-Center	24	0	1.746	0.437	255.9
Kahn et al.	G2B-Center	24	0	1.746	0.437	246.3
Dymond	web-shear	7	0.61	3.98	0.92	658.1

Appendix E

Professional Factors and Reliability

E.1 Individual Results for Professional Factors

Table 4-24 in Section 4.5.1 summarizes the statistics for the individual professional factors for the database of all shear tests on lightweight concrete beams using the input and test results given in Appendices C and D. The individual professional factors for the three different shear design methods under consideration in this study appear in this section. Note that these professional factors assume that that the modification factor for lightweight concrete is *not* applied to the theoretical calculations. The italicized highlighting indicates that those specimens contained vertical stirrups. As discussed in Section 4.5.1, there were eight tests within the set of 160 mildly reinforced concrete beams that were excluded from the analysis due to either the relatively short shear spans or relatively large experimental-to-theoretical ratios. These tests have been struck through.

E.1.1 Professional Factors for Reinforced Concrete

Author	Specimen ID	$Exp/_{A.B5}$	$Exp/_{Gen}$	$Exp/_{Sim}$
~~Ahmad, Xie, and Yu~~	~~LNN-1~~	~~3.70~~	~~3.45~~	~~—~~
Ahmad, Xie, and Yu	LNN-2	1.20	1.13	—
Ahmad, Xie, and Yu	LNN-3	0.94	0.89	—
~~Ahmad, Xie, and Yu~~	~~LNW-1~~	~~1.74~~	~~1.81~~	~~1.48~~
Ahmad, Xie, and Yu	*LNW-2*	0.93	1.28	0.74
Ahmad, Xie, and Yu	*LNW-3*	0.68	1.06	0.55
~~Ahmad, Xie, and Yu~~	~~LHN-1~~	~~3.76~~	~~3.44~~	~~—~~
Ahmad, Xie, and Yu	LHN-2	1.95	1.79	—
Ahmad, Xie, and Yu	LHN-3	1.07	0.99	—
~~Ahmad, Xie, and Yu~~	~~LHW-1~~	~~2.53~~	~~2.62~~	~~2.51~~
Ahmad, Xie, and Yu	*LHW-2*	1.32	1.37	1.24
Ahmad, Xie, and Yu	*LHW-3*	0.95	1.00	0.84
Ahmad, Xie, and Yu	*LHW-3a*	0.98	1.03	0.81
Ahmad, Xie, and Yu	*LHW-3b*	1.00	1.06	0.79
Ahmad, Xie, and Yu	*LHW-4*	1.05	1.11	0.87
Funahashi et al.	V1.8	1.35	1.22	—
Funahashi et al.	V1.5	0.94	0.85	—
Funahashi et al.	V1.2	1.01	0.91	—
Funahashi et al.	V1.8d100	0.91	0.87	—
Funahashi et al.	V1.5d100	2.37	2.32	—
Hanson	9C	1.84	1.60	—
Hanson	2A	2.06	1.79	—
Hanson	2B	2.10	1.83	—
Hanson	3A	1.14	0.99	—
Hanson	3B	1.18	1.02	—
Hanson	4A	1.48	1.30	—
Hanson	4B	1.89	1.64	—
Hanson	4C	1.77	1.54	—
Hanson	4D	1.83	1.58	—
Hanson	5A	1.23	1.07	—
Hanson	5B	1.10	0.96	—
Hanson	6A	1.12	0.97	—
Hanson	6B	1.58	1.38	—
Hanson	7A-X	1.49	1.29	—
Hanson	7A	2.10	1.83	—
Hanson	7B	1.93	1.68	—
Hanson	2B2	1.01	0.88	—
Hanson	3B2	1.10	0.96	—
Hanson	4B2	1.06	0.92	—
Hanson	5B2	1.32	1.15	—
Hanson	6B2	1.13	0.98	—
Hanson	7B2	1.47	1.28	—
Hanson	10B2	1.15	1.00	—
Hanson	13B2	1.14	0.99	—
Hanson	2B3	1.78	1.60	—
Hanson	6B3	1.25	1.12	—
Hanson	7B3	1.64	1.47	—
Hanson	13B3	1.68	1.51	—

Author	Specimen ID	$^{Exp}/_{A.B5}$	$^{Exp}/_{Gen}$	$^{Exp}/_{Sim}$
Hanson	7B1X	1.97	1.76	—
Hanson	10B1	2.36	2.10	—
Hanson	13B1	2.18	1.94	—
Hanson	3A4	1.08	0.95	—
Hanson	4A4	1.14	1.00	—
Hanson	10A4	1.23	1.09	—
Hanson	2B4	0.94	0.91	—
Hanson	3B4	0.98	0.87	—
Hanson	4B4	1.06	0.94	—
Hanson	6B4	1.07	0.95	—
Hanson	10B4	1.02	0.90	—
Hanson	13B4	1.06	0.94	—
Hanson	10BW4	0.98	0.87	—
Ivey and Buth	(1) 1 "4.62"	2.75	2.45	—
Ivey and Buth	(1) 2 "6.33"	1.20	1.08	—
Ivey and Buth	(1) 3 "8.00"	1.13	1.02	—
Ivey and Buth	(23) 1 "6.33"	1.24	1.13	—
Ivey and Buth	(23) 2 "6.33"	1.18	1.06	—
Ivey and Buth	(23) 3 "6.33"	1.24	1.10	—
Ivey and Buth	(23) 1S "6.33"	1.22	1.10	—
Ivey and Buth	(23) 2S "6.33"	1.28	1.15	—
Ivey and Buth	(23) 3S "6.33"	1.21	1.07	—
Ivey and Buth	(27) 1 "4.62"	2.20	1.95	—
Ivey and Buth	(27) 2 "6.33"	1.29	1.15	—
Ivey and Buth	(27) 3 "8.00"	1.05	0.94	—
Ivey and Buth	(23) 4 "4.62"	0.64	0.58	—
Ivey and Buth	(23) 5 "6.33"	1.14	1.02	—
Ivey and Buth	(23) 6 "7.78"	1.28	1.13	—
Ivey and Buth	(23) 7 "9.15"	1.22	1.08	—
Ivey and Buth	(23) 8 "4.62"	1.70	1.52	—
Ivey and Buth	(23) 9 "4.62"	1.98	1.75	—
Ivey and Buth	(23) 10 "4.62"	1.83	1.61	—
Ivey and Buth	(23) 11 "4.62"	2.30	2.01	—
Ivey and Buth	(23) 12 "6.30"	1.59	1.38	—
Ivey and Buth	(23) 13 "7.00"	1.21	1.05	—
Ivey and Buth	(23) 14 "8.00"	1.40	1.21	—
Ivey and Buth	(23) 15 "6.33"	1.28	1.16	—
Ivey and Buth	(23) 16 "6.33"	1.43	1.27	—
Ivey and Buth	(23) 17 "6.33"	1.24	1.10	—
Kawaguchi et al.	*A 1*	1.32	1.19	—
Kawaguchi et al.	*A 2*	2.43	2.16	1.31
Kawaguchi et al.	*B 1*	1.28	1.14	—
Kawaguchi et al.	*B 2*	0.98	1.16	1.22
Kawaguchi et al.	*C 1*	1.41	1.25	—
Kawaguchi et al.	*C 2*	1.03	1.20	1.28
Kawaguchi et al.	*D 1*	0.92	0.82	—
Kawaguchi et al.	*D 2*	0.90	1.07	1.13
Murayama and Iwabuchi	B1	1.09	0.97	—
Murayama and Iwabuchi	M1	1.15	1.02	—
Murayama and Iwabuchi	BS1	1.20	1.06	—
Murayama and Iwabuchi	BS2	1.07	0.94	—

Author	Specimen ID	$^{Exp}/_{A.B5}$	$^{Exp}/_{Gen}$	$^{Exp}/_{Sim}$
Murayama and Iwabuchi	BS3	1.21	1.06	—
Murayama and Iwabuchi	BS4	1.10	0.97	—
Murayama and Iwabuchi	BS5	1.06	0.93	—
Murayama and Iwabuchi	BL1	0.59	0.51	—
Murayama and Iwabuchi	BL2	0.57	0.50	—
Murayama and Iwabuchi	BL3	0.64	0.55	—
Murayama and Iwabuchi	BL4	0.59	0.51	—
Nishibayashi et al.	L-3-ϕ-13-0	1.51	1.45	—
Nishibayashi et al.	L-3-ϕ-13-0	1.61	1.55	—
Nishibayashi et al.	L-3-D13-0	1.18	1.13	—
Nishibayashi et al.	L-3-D13-0	1.07	1.03	—
Nishibayashi et al.	L-3-ϕ-16-0	1.00	0.95	—
Nishibayashi et al.	L-3-ϕ-16-0	1.63	1.55	—
Nishibayashi et al.	L-3-D16-0	1.00	0.96	—
Nishibayashi et al.	L-3-D16-0	1.01	0.96	—
Nishibayashi et al.	L-4-ϕ-13-0	1.06	1.04	—
Nishibayashi et al.	L-4-ϕ-13-0	1.03	1.02	—
Nishibayashi et al.	L-4-D13-0	0.81	0.81	—
Nishibayashi et al.	L-4-D13-0	1.00	0.99	—
Nishibayashi et al.	L-4-ϕ-16-0	0.86	0.82	—
Nishibayashi et al.	L-4-ϕ-16-0	0.85	0.82	—
Nishibayashi et al.	L-4-D16-0	0.91	0.87	—
Nishibayashi et al.	L-4-D16-0	0.92	0.89	—
Nishibayashi et al.	*L-3-D16-5*	0.50	0.50	0.51
Nishibayashi et al.	*L-3-D16-5*	0.47	0.47	0.48
Nishibayashi et al.	*L-3-ϕ-16-10*	0.69	0.74	0.88
Nishibayashi et al.	*L-3-ϕ-16-10*	0.69	0.74	0.88
Nishibayashi et al.	*L-3-D16-10*	0.57	0.61	0.72
Nishibayashi et al.	*L-3-D16-10*	0.58	0.63	0.74
~~Salandra and Ahmad~~	~~LR-0.52-NS~~	—	—	—
Salandra and Ahmad	LR-1.56-NS	3.17	3.04	—
Salandra and Ahmad	LR-2.59-NS	1.25	1.21	—
Salandra and Ahmad	LR-3.63-NS	1.12	1.10	—
~~Salandra and Ahmad~~	~~HR-0.52-NS~~	—	—	—
Salandra and Ahmad	HR-1.56-NS	2.75	2.66	—
Salandra and Ahmad	HR-2.59-NS	1.28	1.24	—
Salandra and Ahmad	HR-3.63-NS	0.92	0.91	—
~~Salandra and Ahmad~~	~~LR-0.52-WS~~	—	—	—
Salandra and Ahmad	*LR-1.56-WS*	0.89	1.15	0.67
Salandra and Ahmad	*LR-2.59-WS*	0.51	0.74	0.38
Salandra and Ahmad	*LR-3.63-WS*	0.35	0.57	0.26
~~Salandra and Ahmad~~	~~HR-0.52-WS~~	—	—	—
Salandra and Ahmad	*HR-1.56-WS*	0.76	1.00	0.58
Salandra and Ahmad	*HR-2.59-WS*	0.46	0.69	0.35
Salandra and Ahmad	*HR-3.63-WS*	0.27	0.46	0.21
Walraven and Al-Zubi	*Lg30l*	1.05	1.06	1.14
Walraven and Al-Zubi	*Lr30l*	1.04	1.05	1.11
Walraven and Al-Zubi	*Ae30l*	1.03	1.04	1.10
Walraven and Al-Zubi	*Lg60l*	1.45	1.52	1.56
Walraven and Al-Zubi	*Lg60m*	1.29	1.32	1.35
Walraven and Al-Zubi	*Lg30m*	1.22	1.32	1.29

Author	Specimen ID	$^{Exp}/_{A.B5}$	$^{Exp}/_{Gen}$	$^{Exp}/_{Sim}$
Walraven and Al-Zubi	*Lg30h*	0.97	0.97	0.96
Walraven and Al-Zubi	*Lr30m*	1.09	1.18	1.16
Walraven and Al-Zubi	*Lr30h*	1.09	1.09	1.08
Walraven and Al-Zubi	*Ae30m*	1.10	1.18	1.16
Walraven and Al-Zubi	*Ae30h*	1.22	1.22	1.20
Malone	*5-LWLA*	0.89	0.93	1.19
Malone	*6-LWLB*	1.22	1.28	1.70
Malone	*7-LWLC*	0.97	1.02	1.64
Malone	*8-LWLD*	0.91	0.96	1.28
Malone	*11-LWHD*	1.16	1.22	1.56

E.1.2 Professional Factors for Prestressed Concrete

Author	Specimen ID	$^{Exp}/_{A.B5}$	$^{Exp}/_{Gen}$	$^{Exp}/_{Sim}$
Malone	*PC6N*	1.37	1.70	—
Malone	*PC6S*	1.56	1.56	1.41
Malone	*PC10N*	1.60	1.92	—
Malone	*PC10S*	1.48	1.45	1.29
Kahn et al.	*G1A-East*	1.46	2.35	1.08
Kahn et al.	*G1A-Center*	1.86	1.92	1.39
Kahn et al.	*G1B-East*	0.71	1.17	0.54
Kahn et al.	*G1B-Center*	1.80	1.89	1.25
Kahn et al.	*G1C-East*	1.18	1.86	0.86
Kahn et al.	*G2A-Center*	1.82	1.88	1.36
Kahn et al.	*G2B-Center*	1.87	1.96	1.29
Dymond et al.	*web-shear*	1.25	1.55	0.98
current study	*T2.8.Typ.1*	1.63	1.74	1.07
current study	*T2.8.Typ.2*	1.48	1.57	0.94
current study	*T2.8.Min.1*	1.97	2.10	1.35
current study	*T2.8.Min.2*	1.66	1.78	1.11
current study	*BT.8.Typ.1*	1.60	1.70	1.34
current study	*BT.8.Typ.2*	1.44	1.49	1.22
current study	*BT.10.Typ.1*	1.78	1.83	1.49
current study	*BT.10.Typ.2*	1.57	1.62	1.28
current study	*BT.10.Min.1*	2.05	2.04	1.95
current study	*BT.10.Min.2*	1.60	1.58	1.54

E.2 Reliability Programs

The two figures in this section show the programs used to perform the reliability calculations that result in the recommended resistance factors for the shear capacity of sand-lightweight concrete beams. Details of the calculations are discussed in Section 4.5.2.2.

```
Rel = | R_NCHRP ← R_HS20·r
      | φ_A.B5_1 ← φ_A.B5
      | φ_Gen_1 ← φ_Gen
      | φ_Sim_1 ← φ_Sim
      | for i ∈ 1..3
      |     φ_A.B5_i ← φ_A.B5_1 + 0.05·(i − 1)
      |     φ_Gen_i ← φ_Gen_1 + 0.05·(i − 1)
      |     φ_Sim_i ← φ_Sim_1 + 0.05·(i − 1)
      | R_lwc ← R_NCHRP − 0.24DC_NCHRP
      | R_u ← 0.90R_lwc
      | for i ∈ 1..3
      |     R_n.A.B5_i ← R_u / φ_A.B5_i
      |     R_n.Gen_i ← R_u / φ_Gen_i
      |     R_n.Sim_i ← R_u / φ_Sim_i
      | for i ∈ 1..1
```

Figure E-1. Main program used to determine the reliability index for the beams in this study.

for $i \in 1..1$

$\lambda_{R.A.B5} \leftarrow \lambda_{FM.lwc} \cdot \lambda_{P.A.B5}$

$\lambda_{R.Gen} \leftarrow \lambda_{FM.lwc} \cdot \lambda_{P.Gen}$

$\lambda_{R.Sim} \leftarrow \lambda_{FM.lwc} \cdot \lambda_{P.Sim}$

for $i \in 1..1$

$CoV_{R.A.B5} \leftarrow \sqrt{CoV_{FM.lwc}^{2} + CoV_{P.A.B5}^{2}}$

$CoV_{R.Gen} \leftarrow \sqrt{CoV_{FM.lwc}^{2} + CoV_{P.Gen}^{2}}$

$CoV_{R.Sim} \leftarrow \sqrt{CoV_{FM.lwc}^{2} + CoV_{P.Sim}^{2}}$

for $i \in 1..3$

$\beta_{A.B5_i} \leftarrow \left(\beta\left(R_{n.A.B5_i}, \lambda_{R.A.B5}, CoV_{R.A.B5}, \mu_{Q.lwc}, \sigma_{Q.lwc}\right)^{T}\right)_{1}$

$\beta_{Gen_i} \leftarrow \left(\beta\left(R_{n.Gen_i}, \lambda_{R.Gen}, CoV_{R.Gen}, \mu_{Q.lwc}, \sigma_{Q.lwc}\right)^{T}\right)_{1}$

$\beta_{Sim_i} \leftarrow \left(\beta\left(R_{n.Sim_i}, \lambda_{R.Sim}, CoV_{R.Sim}, \mu_{Q.lwc}, \sigma_{Q.lwc}\right)^{T}\right)_{1}$

for $i \in 1..3$

$ans_{i,1} \leftarrow \phi_{A.B5_i}$

$ans_{i,2} \leftarrow \dfrac{R_{n.A.B5_i}}{kip}$

$ans_{i,3} \leftarrow \beta_{A.B5_i}$

$ans_{i,4} \leftarrow \phi_{Gen_i}$

$ans_{i,5} \leftarrow \dfrac{R_{n.Gen_i}}{kip}$

$ans_{i,6} \leftarrow \beta_{Gen_i}$

$ans_{i,7} \leftarrow \phi_{Sim_i}$

Figure E-1(cont.). Main program used to determine the reliability index for the beams in this study.

$$\text{ans}_{i,7} \leftarrow \phi_{Sim_i}$$

$$\text{ans}_{i,8} \leftarrow \frac{R_{n.Sim_i}}{kip}$$

$$\text{ans}_{i,9} \leftarrow \beta_{Sim_i}$$

ans

Figure E-1(cont.). Main program used to determine the reliability index for the beams in this study.

$$\beta = \left| \begin{array}{l} \left(\sigma_{ln.R}\ \mu_R\ \mu_{ln.R}\ r_{star}\ q_{star}\ \sigma_{R.equiv}\ \mu_{R.equiv}\ \sigma_{Q.equiv}\ \mu_{Q.equiv}\right) \\ \mu_R \leftarrow \lambda_R \cdot R_n \\ \sigma_{ln.R} \leftarrow \sqrt{\ln\left(1 + CoV_R^{\,2}\right)} \\ \mu_{ln.R} \leftarrow \left(\ln\left(\frac{\mu_R}{kip}\right) - 0.5\sigma_{ln.R}^{\,2}\right) \cdot kip \\ r_{star} \leftarrow \frac{1}{2}\left(\mu_R + \mu_Q\right) \\ q_{star} \leftarrow r_{star} \\ \beta_{calc} \leftarrow \text{"NG"} \\ \text{while } \beta_{calc} = \text{"NG"} \\ \quad \left| \begin{array}{l} \text{iterations} \leftarrow \text{iterations} + 1 \\ \sigma_{R.equiv} \leftarrow r_{star} \cdot \sigma_{ln.R} \\ \mu_{R.equiv} \leftarrow r_{star} \cdot \left(1 - \ln\left(\frac{r_{star}}{kip}\right) + \frac{\mu_{ln.R}}{kip}\right) \\ \sigma_{Q.equiv} \leftarrow \sigma_Q \\ \mu_{Q.equiv} \leftarrow \mu_Q \\ z_{star_1} \leftarrow \frac{r_{star} - \mu_{R.equiv}}{\sigma_{R.equiv}} \end{array} \right. \end{array} \right.$$

Figure E-2. Subroutine to the main program in Figure E-1, follows the Rackwitz-Fiessler procedure.

$$z_{star_1} \leftarrow \frac{r_{star} - \mu_{R.equiv}}{\sigma_{R.equiv}}$$

$$z_{star_2} \leftarrow \frac{q_{star} - \mu_Q}{\sigma_Q}$$

$$G_1 \leftarrow -\sigma_{R.equiv}$$

$$G_2 \leftarrow \sigma_Q$$

$$\rho \leftarrow \begin{pmatrix} 1 & 0 \\ 0 & 1 \end{pmatrix}$$

$$\beta_{old} \leftarrow \beta$$

$$\beta \leftarrow \frac{G^T \cdot z_{star}}{\sqrt{G^T \cdot \rho \cdot G}}$$

$$\beta_{calc} \leftarrow \text{"OK"} \quad \text{if} \left(\left| \beta - \beta_{old} \right| \le 0.005 \wedge \left| r_{star} - r_{star.old} \right| \le 0.05\text{kip} \right)$$

otherwise

$$\alpha \leftarrow \frac{\rho \cdot G}{\sqrt{G^T \cdot \rho \cdot G}}$$

$$z_{star_1} \leftarrow \beta \cdot \alpha_1$$

$$r_{star.old} \leftarrow r_{star}$$

$$r_{star} \leftarrow z_{star_1} \cdot \sigma_{R.equiv} + \mu_{R.equiv}$$

$$q_{star} \leftarrow r_{star}$$

$$\begin{pmatrix} \beta & \frac{r_{star}}{\text{kip}} & \text{iterations} \end{pmatrix}$$

Figure E-2 (cont.) Subroutine to the main program in Figure E-1, follows the Rackwitz-Fiessler procedure.